



Instytut Chemii Organicznej
Polskiej Akademii Nauk

Diketopyrrolopyrrole-based fluorescent probes for cations

G. Dinesh Kumar M.Sc.

A monothematic series of publications with a commentary presented to the Scientific Council of the Institute of Organic Chemistry of the Polish Academy of Sciences in order to obtain a doctorate in chemical sciences

Promotor: prof. dr hab. Daniel T. Gryko

Warszawa 2022

Praca doktorska wykonana w ramach projektu:



**INNOWACYJNA
GOSPODARKA**
NARODOWA STRATEGIA SPÓJNOŚCI



UNIA EUROPEJSKA
EUROPEJSKI FUNDUSZ
ROZWOJU REGIONALNEGO



“New generation of fluorescent probes for stimulated emission depletion microscopy”

Realizowanego w ramach programu **TEAM**

Fundacji na rzecz Nauki Polskiej

Numer grantu: POIR.04.04.00-00-3CF4/16-00-TEAM/2016-3/22

Acknowledgements:

First and foremost, I would like to express my sincerest thanks to my supervisor Prof. Daniel T. Gryko, who I'm so grateful for giving me the opportunity to work in his research group. I'm incredibly grateful to have had such an understanding, kind and supportive supervisor throughout my PhD, from whom I've learnt so much. Again, I thank him for his guidance, encouragement, support, and patience throughout the years.

Secondly, I would like to thank all current and past members of the Daniel Gryko group for their support, friendly working environment, comments, and friendship. Special thanks to Dr. Olena Vakuliuk, Dr. Mariusz Tasior, Dr. David Young, and Kateryna Vygranenko for their invaluable support. In particular, I would like to thank Olena Vakuliuk once more for her friendship, guidance and company in the lab for over the years.

Again, I would like to give special thanks to Dr. David Young for the proofreading of this thesis.

I also thank all my collaborators, especially Dr. Marzena Banasiewicz for photophysical characterization of many compounds and Dr. Antoni Wrzosek for great support and guidance in bio-imaging studies.

Additionally, I would like to thank the FNP-TEAM for funding my PhD.

I want to thank my close friends Lakshmi Kantha, Girish, Sudheendra Rao, and G. Santhosh Kumar who have supported and encouraged me throughout the years. I also thank Prof. Satish Patil (IISc, Bangalore), Dr. Madhusudhana Reddy, and Dr. Puttaraju for their kind support, advices, and encouragement.

Finally, I dedicate this thesis to my family, whose love and strength I'm forever grateful for. To my parents, my sister and my wife, I thank them for their encouragement, support and love, which without them, this dissertation would not be possible.

Again, I sincerely thank you all.

Abstract in English

In the past decade, there has been a considerable growth in applying fluorescence technique to cellular imaging. This technique provides unique advantages such as high sensitivity, low cytotoxicity, low cost and non-invasiveness, and makes it a promising tool. Among the wide range of applications of fluorescence technique, sensing of various cations is one of the most important and active areas.

The main objective of my PhD dissertation was the design and synthesis of new generation of fluorescent probes and investigation of their optical properties and bioimaging applications. I have started with extending the novel synthetic methodology for the synthesis of fully asymmetrical diketopyrrolopyrroles developed in our laboratory. Condensation between aromatic nitriles and pyrrolidin-2-one leads to 1,4-diketopyrrolo[4,3-c]pyrrole (DPP) derivatives possessing two different C-aryl substituents. The first part of this Thesis explored how the direct linkage of molecular recognition unit to DPP core can affect the optical properties. Taking advantage of the new methodology, I have designed and synthesized new class of diketopyrrolopyrrole sensors directly from nitriles possessing (aza)crown ethers leading to macrocycle-dye hybrids. Their strong interaction with cations possessing Lewis acid character such as Li^+ , Mg^{2+} and Zn^{2+} leads to significant changes of optical properties, hence to the new fluorescent probes.

In the second part of my work, I synthesized novel highly sensitive potassium probes with the strategic placement of a recognition crown ether unit at most conjugated position of the second aryl substituent of diketopyrrolopyrrole core. These D-A-D' hybrid fluorophores exhibits very high fluorescence quantum yields ($\Phi_{\text{fl}} = 0.8-0.9\%$) even in CH_3CN . An additional lariat alkoxy group at *ortho* position to aza-18-crown-6 induces strong coordination to K^+ with 80 nm blue-shift of fluorescence. The incorporation of PPh_3^+ group enables the probe to be selectively accumulated in mitochondria of cardiac H9C2 cells and it makes it possible to observe the fast efflux/influx of mitochondrial K^+ upon stimulation with nigericin.

In the final part of my thesis, I designed and synthesized diketopyrrolopyrrole-based novel highly sensitive fluorescent zinc sensors directly from pyridine-derived nitriles

possessing dipicolylamine as a zinc recognition unit. The obtained DPP sensors showed favorable photophysical properties including strong bathochromic shifts ($\approx 80\text{nm}$) of fluorescence upon complexation with Zn^{2+} and high fluorescence quantum yields. The probes decorated with PPh_3^+ and morpholine units are selectively localized in mitochondria and lysosomes of cardiac H9C2 cells respectively.

Abstract in Polish

W ostatniej dekadzie nastąpił znaczny wzrost zainteresowania technikami fluorescencyjnymi w obrazowaniu komórkowym. Oferują one wiele korzyści, takich jak wysoka czułość, niska cytotoksyczność, niski koszt i nieinwazyjność, co czyni je obiecującym narzędziem w biologii molekularnej i medycynie. Wśród szerokiego zakresu ich zastosowań jednym z najważniejszych i najbardziej aktywnych obszarów jest wykrywanie różnych kationów.

Głównym celem mojej rozprawy doktorskiej było zaprojektowanie i synteza nowej generacji sond fluorescencyjnych, a także badanie ich właściwości optycznych oraz zastosowanie praktyczne otrzymanych barwników w bioobrazowaniu. Pracę rozpocząłem od rozszerzenia zakresu stosowalności opracowanej w naszym laboratorium nowatorskiej metodologii syntezy asymetrycznych diketopirolopiroli. Kondensacja nitryli aromatycznych i pirolidyn-2-onu prowadzi do pochodnych 1,4-diketopirolo[4,3-c]pirolu (DPP) posiadających dwa różne podstawniki C-arylowe. W pierwszej części pracy zbadałem, w jaki sposób bezpośrednie połączenie jednostki rozpoznania molekularnego z rdzeniem DPP może wpływać na właściwości optyczne. Wykorzystując nową metodologię, zaprojektowałem i zsyntetyzowałem nową klasę sond opartych o rdzeń diketopirolopirolu bezpośrednio z nitryli zawierających (aza)etery koronowe. Silne oddziaływanie otrzymanych hybryd makrocycl-barwnik z kationami o charakterze kwasowym, takimi jak Li^+ , Mg^{2+} i Zn^{2+} ma znaczący wpływ na właściwości optyczne barwników, a więc potwierdza możliwość ich stosowania jako sond fluorescencyjnych.

W drugiej części mojej pracy zsyntetyzowałem nowe, wysoce czułe sondy potasowe umieszczając jednostkę rozpoznania molekularnego kationów w najbardziej sprzężonej z chromoforem pozycji podstawnika arylowego. Otrzymane hybrydowe fluorofory typu D-A-D' wykazują bardzo wysokie wydajności kwantowe fluorescencji ($\Phi_{\text{fl}} = 0,8-0,9\%$), nawet w acetonitrylu. Dodatkowa grupa alkoksylowa w pozycji *orto*- do aza-18-korony-6 indukuje silną koordynację K^+ z przesunięciem fluorescencji o 80 nm w kierunku hipsochromowym. Przyłączenie grupy PPh_3^+ umożliwia selektywną akumulację sondy w mitochondriach komórek sercowych H9C2 oraz obserwację szybkiego wypływu/napływu mitochondrialnego K^+ po stymulacji nigerycyną.

W końcowej części pracy zaprojektowałem i zsyntetyzowałem oparte na diketopirolopirolu nowatorskie, wysoce czułe, fluorescencyjne sondy na kationy cynku, wychodząc bezpośrednio z nitrylowych pochodnych pirydyny posiadających dipikoliloaminę jako jednostkę rozpoznawania. Uzyskane sondy oparte o rdzeń DPP wykazywały korzystne właściwości fotofizyczne, w tym silne przesunięcia batochromowe fluorescencji ($\approx 80\text{nm}$) po kompleksowaniu z Zn^{2+} oraz wysokie wydajności kwantowe fluorescencji. Sondy udekorowane jednostkami PPh_3^+ i morfoliną są selektywnie zlokalizowane odpowiednio w mitochondriach i lizosomach komórek sercowych H9C2.

Table of Contents:

List of publications.....	13
Participation in conferences and seminars.....	15
Short CV	17
1. Introduction.....	19
1.1. Introduction to fluorescence.....	19
1.2. Fluorescence sensing.....	20
1.3. Metal cation sensing.....	21
1.4. Mechanism of signal transduction.....	22
1.4.1. Fluorescence resonance energy transfer (FRET).....	22
1.4.2. Photo-induced intramolecular charge transfer (ICT).....	23
1.4.3. Photo-induced electron transfer (PET).....	24
2. Diketopyrrolopyrroles (DPPs).....	26
3. New developments.....	27
4. Aims and objectives.....	29
5. Results and discussions.....	30
5.1. DPP-based chemosensors possessing macrocyclic units.....	30
5.2. DPP-based K ⁺ sensitive probes.....	33
5.3. DPP-based Zn ²⁺ sensitive probes.....	35
6. Comparison and conclusions.....	38
7. References.....	42
8. Original publications.....	49
9. Declarations of the authors of publications.....	291

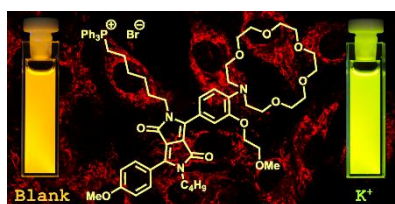
Reprints of publications included part of the doctoral dissertation.

List of Publications for the Doctoral Dissertation:

1. **G. Dinesh Kumar**, M. Banasiewicz, D. Jacquemin, D. T. Gryko, *Chem. Asian J.* **2021**, *16*, 355–362, DOI: 10.1002/asia.202001376. „Switch-on Diketopyrrolopyrrole-Based Chemosensors for Cations Possessing Lewis Acid Character” IF₂₀₂₂= 4.839



2. **G. Dinesh Kumar**, M. Banasiewicz, A. Wrzosek, R. P. Kampa, M. H. E. Bousquet, D. Kusy, D. Jacquemin, A. Szewczyk, D. T. Gryko, *Chem. Commun.*, **2022**, *58*, 4500–4503, DOI: 10.1039/d2cc00324d. „Probing the flux of mitochondrial potassium using an azacrown-diketopyrrolopyrrole based highly sensitive probe” IF₂₀₂₂= 6.065



3. **G. Dinesh Kumar**, M. Banasiewicz, A. Wrzosek, O. O’Mari, M. Zochowska, V. I. Vullev, D. Jacquemin, A. Szewczyk, D. T. Gryko, *Org. Biomol. Chem.*, **2022**, *20*, 7439–7447, DOI: <https://doi.org/10.1039/D2OB01296K>. „A sensitive zinc probe operating via enhancement of excited-state intramolecular charge transfer” IF₂₀₂₂= 3.890



Participation in conferences and seminars

1. 19th International Symposium on Novel Aromatic Compounds (ISNA 2022), 3–8 July, 2022, Warsaw, Poland. Poster title: “A highly sensitive mitochondria-targeting potassium probe based on azacrown-diketopyrrolopyrrole.”
2. 9th MITOCHONDRION on-line conference, 27th January, 2021, Warsaw, Poland. Title of talk “A Diketopyrrolopyrrole-based Fluorescent Potassium Sensors for Mitochondria Targeting.”

Short CV:

I was born on 15th March 1989, in Chimakalahalli, Karnataka, India. In 2006, I started my Bachelor's Degree at the University of Bangalore, India and at the same University I completed a Master's Degree in organic chemistry in 2014. After working in a pharmaceutical company for one year as a research chemist, I joined Prof. Satish Patil's organic electronics research group at the Indian Institute of Science, Bangalore as a research assistant. There I worked on the "design and synthesis of donor-acceptor π -conjugated-based aggregation induced emission materials for OLED applications."

In 2018, I joined Prof. Daniel Gryko's group at the Institute of Organic Chemistry, Polish Academy of Sciences working towards the Foundation for Polish Science grant "New generation of fluorescent probes for stimulated emission depletion microscopy", Grant Agreement nr: POIR.04.04.00-00-3CF4/16-00-TEAM/2016-3/22. Towards this end, I researched diketopyrrolopyrrole based fluorescent probes for the detection of metal cations and their bio-imaging applications. This has culminated in the publication of three papers, a poster presentation and an oral presentation.

1. Introduction

1.1. Introduction to fluorescence

Over the past several decades the phenomenon of photoluminescence has received much attention in the field of biological science. Photoluminescence is the emission of light from excited electronic states of a molecule, first created by the absorption of light. Based on the nature of the excited state, photoluminescence is divided into fluorescence and phosphorescence. Fluorescence is the photoluminescence from a singlet electronic excited state to the ground state where the spin state of the electron does not change. The fluorescence lifetime, the time between excitation and emission, is in the order of nanoseconds. Phosphorescence differs in the fact that emission is from a triplet electronic excited state and relaxation involves the change of electron spin. Due to this spin change, phosphorescence lifetimes are typically in milliseconds or seconds.

In 1845, John Frederick William Herschel reported the first observation of fluorescence from a quinine sulfate solution when it was exposed to a UV light source or the sun.¹ Later, in 1852, George Gabriel Stokes named this phenomenon as “fluorescence” in honor of the fluorescent mineral fluorspar. Stokes also discovered that emission occurs at

longer wavelengths than absorption. This relationship now bears his name and the ‘Stokes Shift’ is counted as one of the most positive characteristics of fluorescent molecular sensors.² In 1935, Alexander Jablonski illustrated the processes that occur between the absorption and emission of light using a diagram, now known as a Jablonski diagram (Figure-1).³

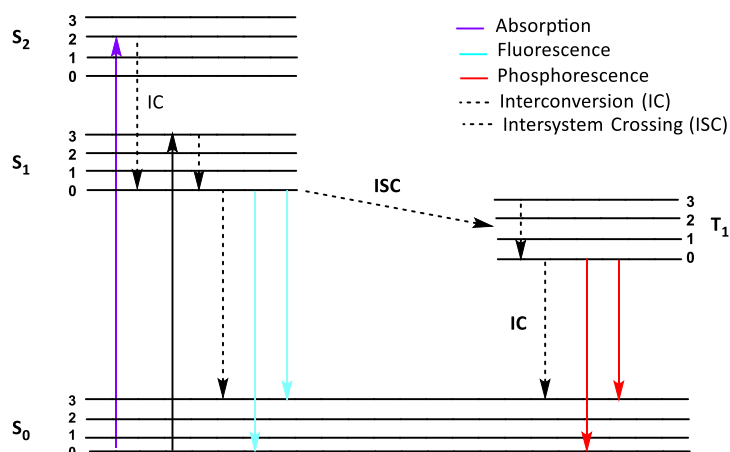


Figure-1: Jablonski diagram showing photon absorption and emission processes. The straight arrows indicate radiative processes and dotted arrows indicate nonradiative processes.

These diagrams often depict the ground state S₀, the first and second singlet excited electronic states S₁ and S₂ as well as the first triplet excited electronic state T₁. Each state can exist in various vibrational energy levels, due to the variety of nuclear geometries, represented by the numbers 0, 1, 2 and 3. According to the Frank-Condon principle, the transitions of electrons between states occurs in a much shorter time (10⁻¹⁵

¹⁵ s) than the displacement of the nuclei (10^{-12} s) and therefore can be represented as vertical lines. Jablonski diagrams provide a theoretical basis for the development of fluorescence and are often used as the starting point for discussing light absorption and emission. As the mechanism of fluorescence became more widely understood, it has received more and more attention and developed into a field of study in its own right.

In recent decades, advances in fluorescent technology has made great strides, and has yielded increasingly fascinating discoveries for diverse fields in biological sciences. Fluorescence spectroscopy is considered to be one of the most important research tools in biochemistry and biophysics. Presently, fluorescence is a dominant methodology widely used in a great number of research domains, including biotechnology, medical diagnostics, genetic analysis, DNA sequencing, flow cytometry, and forensic analysis among others. Due to the high sensitivity of fluorescence detection, there has been a remarkable growth in the use of fluorescence for cellular imaging, which renders fluorescence techniques promising tools to replace radioactive tracers for most biochemical measurements, avoiding the high expense and difficulties of handling such unstable isotopes. Moreover, fluorescence imaging has the resolution to effectively reveal the localization of intracellular molecules.

1.2. Fluorescence sensing

Fluorescence sensing of chemical and biological analytes is an active research field.⁴⁻⁸ The efforts devoted to this subject were initially driven by the desire to eliminate the use of radioactive tracers, which are costly to use and dispose of. Nowadays, the high sensitivity of fluorescence sensing techniques is another important reason for the increased attention. Fluorescence sensing also meets the need for rapid and low-cost determination methods for a wide range of chemical, biochemical, clinical, and environmental processes.

Fluorescence sensing requires a change in a spectral property, such as fluorescence intensity, emission spectrum, excitation spectrum, fluorescence lifetime, anisotropy, or Φ_{fl} with concomitant environmental changes around the fluorophore through a binding event to an analyte. The most popular fluorescence sensing approach is the fluorescence intensity-based strategy, that is, the fluorescence intensity of the probe changes in response to an analyte. A great number of this type of sensor have been developed for pH, cations, anions, DNA, RNA, ATP, enzymes, amino acids, glucose, etc.⁹⁻¹⁶ An additional advantage of fluorescence sensing is that detection of analytes can be performed *via* time resolved measurements.

As illustrated in Figure-2, fluorescent probe design strategies mostly include three main features; (1) a recognition moiety with high selectivity for the analyte of interest; (2) a fluorophore with sufficient brightness and spectral properties in some form; (3) a suitable linker that connects the two former moieties allowing for signal transduction.^{9, 15, 17} There are generally four types of reaction mechanisms between fluorescent probes

and the corresponding analytes: (1) complexation; (2) formation or cleavage of a covalent bond; (3) redox reaction; and (4) protonation-deprotonation.¹⁵

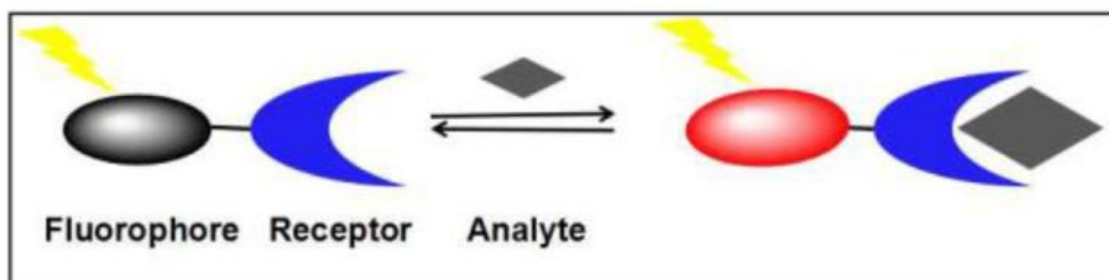


Figure-2: Schematic representation of the mechanism of fluorescent probe. Fluorescence emission is turned-on upon binding with analyte.

1.3. Metal cation sensing

Metal cations are essential for sustaining every form of life because they play a vital role in many chemical, biological, and environmental processes. Based on a physiological viewpoint, metal cations can be broadly classified into two pools: (1) essential metal cations (Li^+ , Na^+ , K^+ , Mg^{2+} , Ca^{2+} , Zn^{2+} , $\text{Fe}^{2+}/^{3+}$, etc.) which play a key role in many biological processes, including intra- and intercellular communication, in the regulation of DNA transcription, proper functioning of nerve cells, the transport of oxygen, in photosynthesis and electron transfer processes; and (2) nonessential or toxic metal cations (Hg^{2+} , Cd^{2+} , As^{3+} , Pb^{2+} , $\text{Cr}^{3+/6+}$, Ni^{2+} , Co^{2+} , etc.) which have a serious impact on the environment and health. In medicine, it is important to control the serum levels of lithium in patients under treatment for manic depression, and potassium in the case of high blood pressure. Due to their importance in many areas, the chemistry of cation complexation has played an important role in the origin of the field of molecular sensors.

Great efforts have been dedicated towards the development of fluorescent probes for various metal cations. The research on metal cation sensing has come a long way since Pederson's pioneering discovery of crown ethers and their ability to form complexes with metal cations.¹⁸ After Pedersen's first report on the cation-complexation of crown ethers in 1967, a tremendous amount of subsequent work was performed to create more complex structures to bind a variety of metal cations.¹⁹ Among various metal cations, alkali and alkaline earth metal cations, especially Li^+ , Na^+ , K^+ , Mg^{2+} , and Ca^{2+} have attracted significant attention because of their well-known biological significance.¹⁹⁻²⁵ With the discovery of the important roles of transition metal cations play in a diverse array of biological and environmental processes, more recent attention has been focused on developing sensors for transition metal cations, such as Cr^{3+} ,²⁶ Fe^{3+} ,²⁷ Co^{2+} ,²⁸ Ni^{2+} ,²⁹ Cu^{2+} ,³⁰ Zn^{2+} ,³¹⁻³² Cd^{2+} ,³³ and Hg^{2+} .³³

Complexation is the most widely used strategy for the development of fluorescent sensors for various metal cations by virtue of their strong binding affinities with electronegative heteroatoms such as N, O, and S.³⁴ There are some general principles

for probes based on this strategy: (1) an appropriate ring/cavity size for a given metal cation, e.g., crown ethers with different ring sizes bind different alkali metal cations; (2) suitable ligands forming five- or six-membered chelate ring complexes with metal cations, such as probes with an DPA (dipicolylamine) unit complexing Zn^{2+} ; and (3) soft-hard acid-base principle, for instance, soft sulfur-containing receptors exhibit high affinities for soft metal cations such as Ag^+ and Hg^{2+} .

1.4. Mechanism of signal transduction

The signaling moiety acts as signal transducer and is responsible for the conversion of the recognition event into a change in the photophysical properties of the fluorescent probe. This happens because the chemical and structural properties of the excited state are very different from the ones of the ground state and various processes such as fluorescence resonance energy transfer (FRET), photo-induced electron transfer (PET), internal charge transfer (ICT), energy transfer (ET), aggregation induced emission (AIE), excimer and exciplex formation can occur in the excited state.

1.4.1 Fluorescence resonance energy transfer (FRET)

A non-radiative process results from interaction between different fluorophore couples wherein the transfer of resonance energy occurs from a donor fluorophore (D-F) excited state to an acceptor fluorophore (A-F) ground state and emission may subsequently arise from the acceptor centre through non-radiative “dipole–dipole coupling” (Figure-3).³⁵ The basic necessity for the FRET process is an appropriate overlap of the emission spectrum of donor (D) with the absorption spectrum of acceptor (A). A higher spectral overlap leads to a better FRET depending on the distance between donor and acceptor which should lie between 10 to 100 Å for an efficient process. FRET also depends on the virtual orientation of dipole moments of the donor absorption and acceptor emission.³⁶ The FRET mechanism is generally used to design fluorescent ratiometric sensors capable of displaying large pseudo Stokes shifts. In metal-complex based FRET fluorescent probes, both the donor-fluorophore (D-F) and acceptor-fluorophore (A-F) are linked to the metal ion bound receptor/ionophore. However, the possibility of another receptor site for metal ion binding enables the entire metal-complex to serve as a FRET probe (Figure-3). It is worth mentioning that usually charge transfer inactive Zn(II) and Cd(II) are pre-bound metal ions in complex based probes so that a non-radiative FRET can be observed. However, occasionally other metal ion (d^1 – d^9) based complexes are also fluorescent and can serve as FRET sensors.

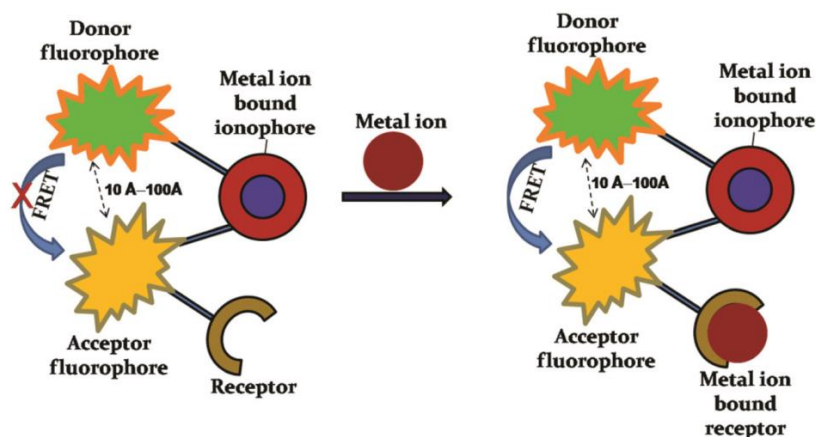
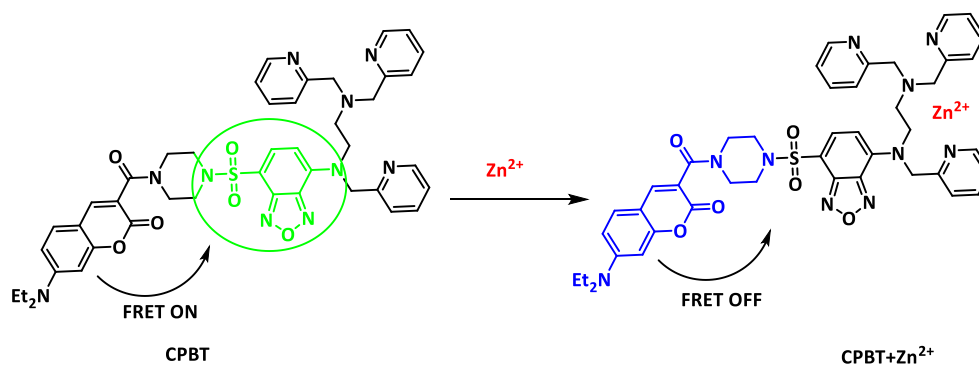


Figure-3: Metal-complex based fluorescent probes for metal ion sensing *via* FRET mechanism.

Scheme-1 shows FRET-based fluorescent probe CPBT for Zn^{2+} , which is a combination of a coumarin moiety acting as the fluorescence donor and 4-amine-7-sulfamoylbenzo[*c*][1,2,5]-oxadiazole (ASBD) as the acceptor.³⁷ The emission spectrum of coumarin overlaps well with the absorption spectrum of ASBD with strong emission at 560 nm and weak emission at 480 nm. After Zn^{2+} binding, the absorption spectrum of ASBD moiety shows a large blue-shift due to the decreased Intramolecular charge transfer (ICT) effect, which leads to a dramatic decrease in the spatial-overlap and FRET efficiency. Consequently, by increasing the concentration of Zn^{2+} , the emission intensity at 560 nm significantly decreased and fluorescence emission at 480 nm increased.



Scheme-1: Schematic illustration of mechanism of FRET probe CPBT.

1.4.2 Photo-induced Intramolecular Charge Transfer (ICT)

ICT processes from a donor to an acceptor in a single molecule have also been used as the basis of the sensing mechanism for macrocyclic fluorescent probes for cations. In this process, fluorescence effects depend on the combination of electron-donating groups and electron-accepting groups in a conjugated π -system that combines the fluorophore and the acceptor. After light excitation, the redistribution of electron cloud density from the electron donor to the electron acceptor produces a dipole moment in the molecule. When an analyte is added, the dipole distance can be increased or

decreased depending on the property of the analyte and the electronic relationship between the acceptor and the fluorophore. The reduced dipole moment will cause a blue-shift in the fluorescence emission spectrum (ICT) pathway to be suppressed, which makes the excited state more unstable than the ground state when reacting with the analyte. Conversely, the increased dipole distance will cause a red-shift in the emission spectrum and the strength of the ICT process is enhanced, which results in the excited state being more stable relative to the ground state after analyte binding (Figure-4).³⁸

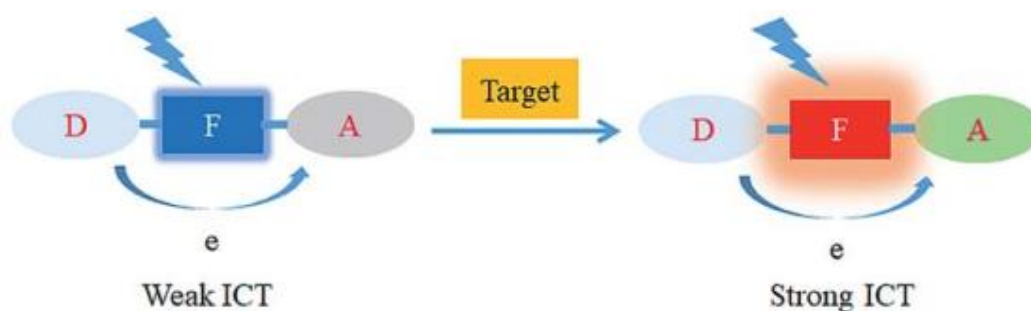
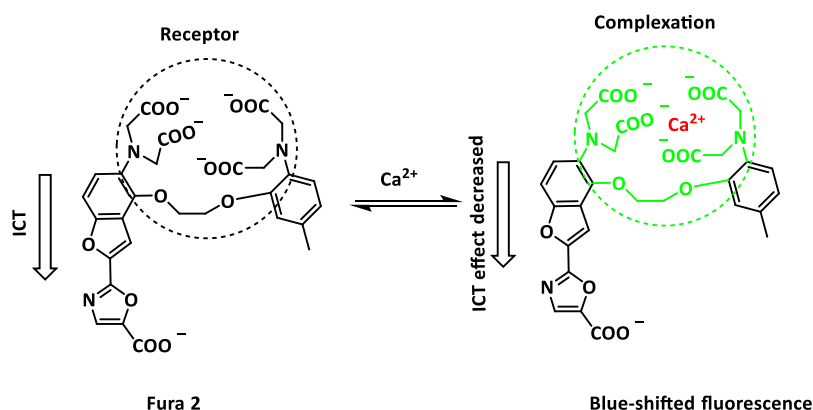


Figure-4: Metal-complex based fluorescent probes for metal ion sensing *via* an ICT mechanism.

To date, many fluorophores have been designed and reported utilizing the ICT mechanism. Scheme-2 shows a typical example of an ICT-based probe, Fura 2.³⁹ Upon complexing with Ca^{2+} , Fura 2 exhibits a remarkable blue-shifted fluorescence and increased fluorescence intensity.



Scheme-2: Schematic illustration of mechanism of ICT probe Fura 2.

1.4.3 Photo-induced Electron Transfer (PET)

In PET probes, the analyte recognition moiety (the receptor) is often connected to a fluorophore *via* a spacer, rendering the receptor and the fluorophore electronically isolated, which essentially differs from ICT-based probes. The electronegative element, usually a nitrogen atom, embraced in the receptor moiety has a high-energy lone pair of electrons, which can transfer an electron to the fluorophore in the excited state, resulting in fluorescence quenching. Upon complexing metal cations, the reduction potential of the receptor is enhanced and, thus, the HOMO of the receptor becomes lower in energy than that of the fluorophore. As a result, the PET process from the

receptor to the fluorophore is restricted, and consequently fluorescence quenching of the fluorophore is reduced, leading to increased fluorescence intensity of the fluorophore.^{9,40} Therefore, the PET mechanism has potential to be explored to develop fluorescence “turn-on” sensors.

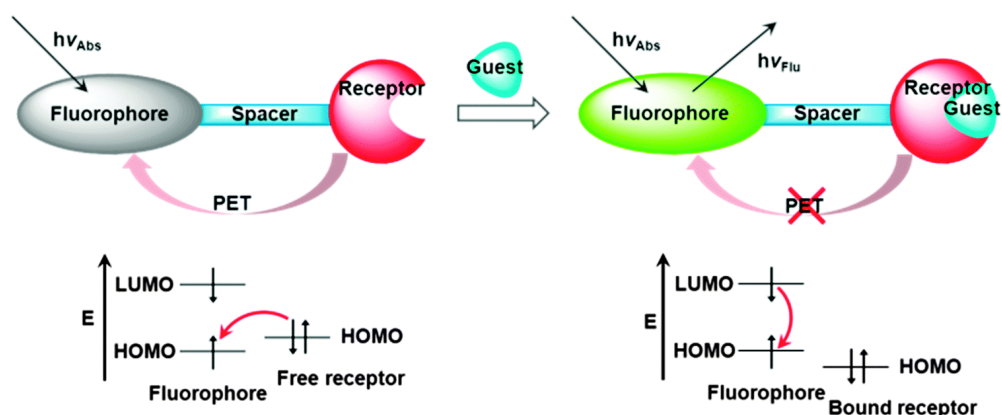
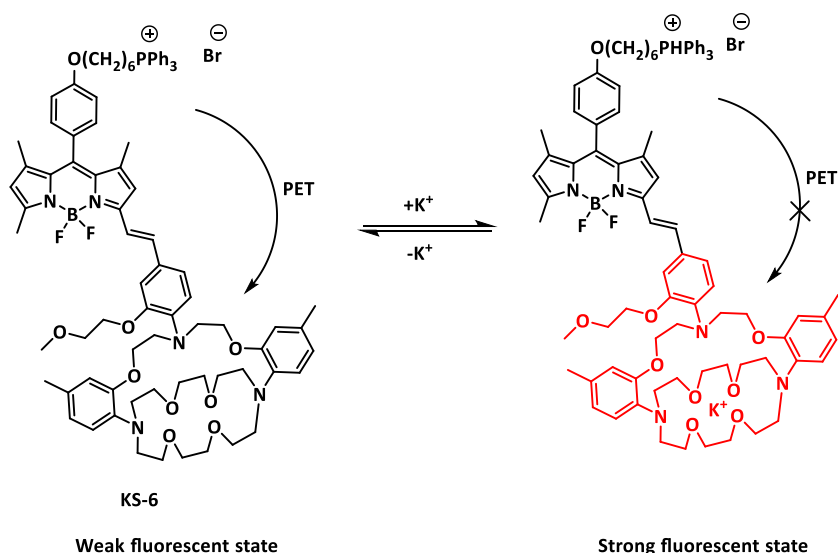


Figure-5: Metal-complex based fluorescent probes for metal ion sensing *via* PET mechanism.

Scheme-3 shows a typical example of a PET probe, in this case a BODIPY based K^+ sensor.⁴¹ In the absence of K^+ , KS-6 fluorescence emission is relatively weak because of the PET process from the receptor moiety to the BODIPY fluorophore. However, upon binding with K^+ ions, the fluorescence of the fluorophore is increased 130-fold at 572 nm due to prohibition of the PET process and shows strong transduction to K^+ concentrations ranging from 30 to 500 mM. KS-6 has been applied for selective imaging of the K^+ efflux/influx in mitochondria living cells.^{41, 42} Due to the advantages of fluorescence “turn-on” sensors in cell imaging applications, probes utilizing the PET mechanism have become more numerous than others and have been attracting more and more attention in developing various fluorescent probes for metal cations.



Scheme-3: Schematic illustration of PET probe, BODIPY KS-6.

2. Diketopyrrolopyrroles (DPPs)

In the past two decades, a wide variety of fluorescent probes with different recognition moieties have been designed and synthesized, which were based on the most versatile fluorophores, including fluorescein, coumarin, cyanine, boron-dipyrromethene (BODIPY), rhodamine, and 1,8-naphthalimide, etc., which are applied in many applications including cation, anion and biological relevant molecules detection, food analysis, medical diagnosis, environmental monitoring, and many other applications.

Diketopyrrolopyrroles (DPPs) were first discovered by Farmum *et al.* in 1974 as a by-product of the classical Reformatsky reaction between benzonitrile and ethyl bromoacetate (Figure-6).⁴³ Due to poor yields, the discovery of DPPs went largely unnoticed until 1983, when Iqbal *et al.*⁴⁴ reported the synthesis of DPP *via* a new one-step route, using benzonitrile and diethyl succinate in the presence of base. This revised synthesis increased the yield to 60-70%, encouraging the commercialization of DPPs for use as a pigment in inks, varnishes and paints due to their easy functionalization, bright red color, high thermal stability, and excellent photophysical properties.⁴⁵ Since expiration of the key patent in 2003, they underwent transformation from high-quality pigments to the most popular dyes for optoelectronic applications including organic field-effect transistors (OFETs), organic photovoltaics (OPVs), organic light emitting diodes (OLEDs), dye sensitized solar cells (DSSCs) and perovskite solar cells.⁴⁶ Further striking innovations include the development of DPP-based singlet fission,⁴⁷ organic sensorimotor synapse,⁴⁸ and circularly polarized luminescence.⁴⁹

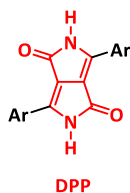
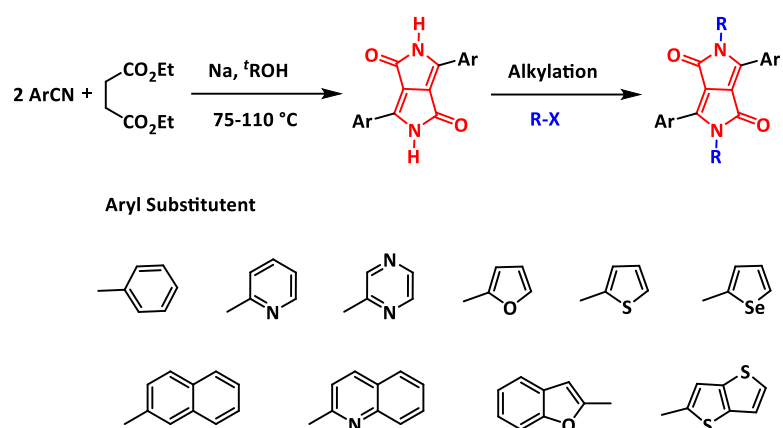


Figure-6: Structure of diketopyrrolopyrrole (DPP) where Ar represents aryl groups.

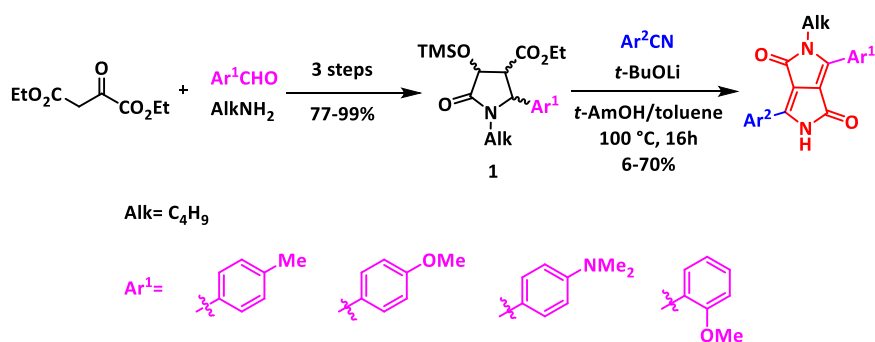
The synthesis of the DPP core generally occurs *via* a condensation reaction between one equivalent of diethyl succinate and two equivalents of an aromatic nitrile, under basic conditions.⁴⁵ The DPP core is electron deficient due to the two amide groups present in the ring and, through incorporation of electron rich moieties such as benzene or thiophene, as flanking groups on either side of the DPP core, the absorption and emission able to be tuned in the bathochromic direction. It is well known that unsubstituted DPPs are highly insoluble due to intermolecular hydrogen bonding between N-H and O atoms. In order to improve the solubility, it is necessary to functionalize the lactam N-H position, usually by means of alkylation (Scheme-4).



Scheme-4: Classical nitrile-succinate method for the synthesis of DPP *via* condensation.

3. New developments

In recent years there has been a growing interest in the synthesis of asymmetrically substituted DPPs, in which the DPP core is flanked by two different aryl groups and two various substituents on the nitrogen atoms. This breaks the symmetry of final molecule and improves solubility in non-chlorinated solvents. There have been various reported examples of asymmetrical DPPs possessing a wide variety of aryl substituents, mostly relying on the use of analogs of 4,5-dihydro-5-oxo-2-arylpyrrole-3-carboxylate developed in Ciba-Geigy laboratories.⁵⁰ Although this synthetic method allows for the formation of free-NH DPPs, which can be mono-alkylated non-selectively, the yields of such transformations are low which limits the substrate scope especially for highly electron-rich and sterically bulky nitriles. To overcome this problem, in 2020, Gryko and co-workers developed an efficient method for the programmed synthesis of asymmetrical DPPs (Scheme-5).⁵¹ In order to increase the stability and solubility of the intermediate pyrrolidone in *t*-AmOH, a trimethylsilane (TMS) protected hydroxyl group was introduced in pyrrolidone **1** which could then be used in condensation reactions with nitriles providing asymmetrical DPPs incorporating two different aryl groups and selective incorporation of a single alkylated lactam product in good yields.



Scheme-5: The method for synthesis of asymmetrical DPPs developed by Gryko and co-workers.⁵¹

With this new methodology authors have been able to transform nitriles, which failed to produce diketopyrrolopyrroles in classical succinate method, into asymmetrical DPPs. This is especially true for electron-rich nitriles derived from benzene, carbazole,

naphtho[2,3-*b*]furan and sterically hindered nitriles such as 2-bromobenzonitrile, 2-methoxybenzonitrile, 8-methoxy-4-cyanoquinoline, and 9-cyanoacridine. Furthermore, electron-donating substituents such as 4-dimethyl-aminophenyl, 3-indolyl, and even 2-methoxyphenyl, which are both electron-donating and sterically hindered moieties can be easily incorporated into DPPs with good yields. This programmed method for the synthesis of diketopyrrolopyrroles enables freedom to incorporate an almost unrestricted variety of substituents around the heterocyclic core.

During the past decade, DPP dyes have shown incredible potential as fluorescent probes for applications in biological systems. So far, many research groups have designed and synthesized DPP based fluorescent probes for the detection of metal cations and anions.^{45,52} Among various anions, fluoride ions have the highest affinity to protons and are capable of deprotonating hydrogen-containing polar moieties, such as O-H and N-H groups. In 2010, Tian and co-workers developed the first DPP based fluorescent probes for the detection of fluoride ions.⁵³ They synthesized mono-N-alkylated DPP chemosensor **2** (Figure-7) for the detection of fluoride ions through colorimetric and ratiometric fluorescence signalling. Upon addition of F⁻ ions, the color of the solution showed significant change from orange to red and a fluorescence change from yellow to red was observed due to deprotonation of the N-unsubstituted amide group of DPP. In 2013, Wang and co-workers reported the first DPP based fluorescent Zn²⁺ chemosensor **3** (Figure-7) by attaching zinc chelator *N,N*-di(pyridine-2-ylmethyl)amine (DPA) to the phenyl rings at positions 3 and 6 of the DPP core. This moiety shows strong Zn²⁺ complexation with a concurrent large emission enhancement and 70 nm blue-shift response appearing through PeT and ICT mechanisms. Those probes were used for detecting Zn²⁺ ions inside living cells.⁵⁴ More recently, Wang, Sessler and co-workers reported DPP-based Zn²⁺ sensors **4** and **5** (Figure-7) by functionalizing the N2 position with a zinc-sensing unit comprised of a methoxy derivative of *N,N*-di-(2-picolyl)ethylenediamine (MeO-DPEN) and a mitochondria targeting PPh₃⁺ or lysosome-targeting morpholine group at the N5 position, respectively. In these cases, signaling was based on PeT processes.⁵⁵ They proved that changing the position of zinc chelator unit to the N-position of the lactam induces a 77-fold fluorescence enhancement upon the addition of Zn²⁺ and were applied to imaging lysosomal Zn²⁺ in prostate cancer cells.

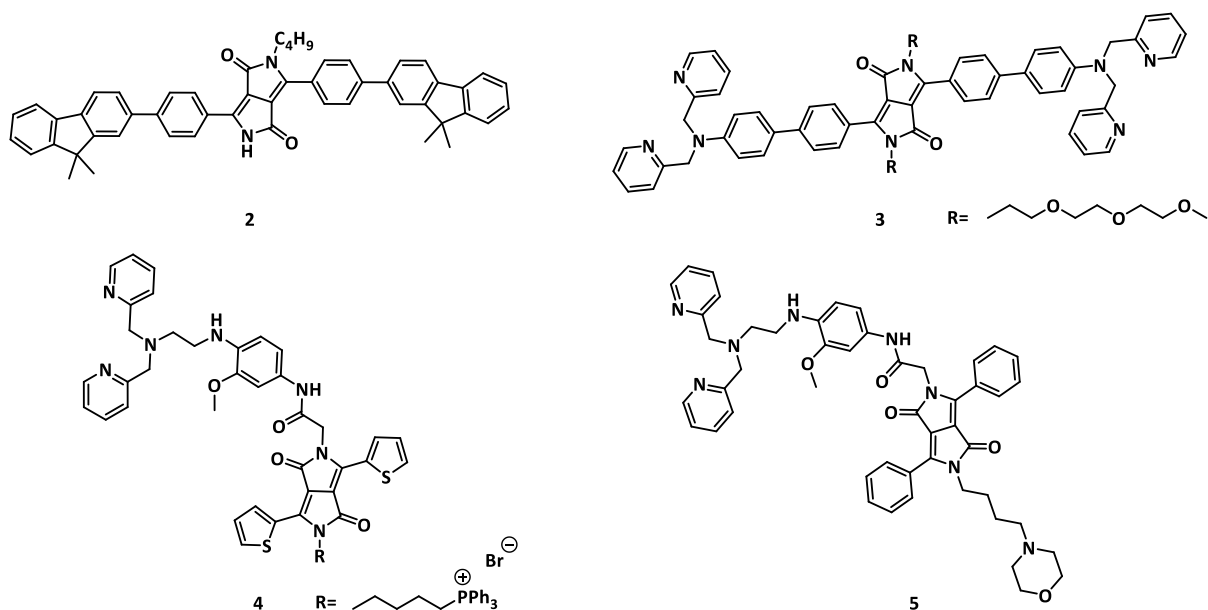


Figure-7: Reported DPP-based fluorescent sensors.

4. Aims and Objectives

Until now, there has only been limited research focused on DPPs designed for detection of metal cations especially for biologically important alkali metal ions including lithium (Li^+), sodium (Na^+), potassium (K^+) and alkaline earth metal ions magnesium (Mg^{2+}) and calcium (Ca^{2+}). Although there have been reports of DPPs designed for zinc (Zn^{2+}) detection, the vast majority of them are based on the photo-induced electron transfer (PET) mechanism. These reported DPP zinc probes have absorption and emission maxima below 600 nm, however, which limits their biological applications in the therapeutic window. Moreover, these probes exhibited low fluorescence quantum yields, even after zinc complexation, and were not organelle-specific, which often results in the detection of the subcellular Zn^{2+} decreasing resolution. While a large number of DPP-based fluorescent probes have been developed for detection of metal cations, the vast majority of them possess poor water solubility and biocompatibility combined with a low Φ_{fl} and low photostability. Therefore, when designing the next generation of fluorescent probes for imaging metal ions in living cellular systems they must meet the above mentioned key properties along with high optical brightness values which can lower the amount of dye needed for cellular applications, minimizing the potential for altering endogenous cellular distribution, and have visible-light excitation in order to minimize sample damage and reduce autofluorescence.

The aim of my project was to investigate ways of overcoming the above limitations by designing and synthesizing new diketopyrrolopyrrole-based fluorescent probes which are not only highly selective and sensitive for the detection of metal cations such as Li^+ , K^+ and Zn^{2+} , but also have good solubility in polar solvents, bathochromically shifted emission, high fluorescence quantum yield, hydrophilicity and cell permeability.

The rationale behind the use of diketopyrrolopyrrole as a fluorophore was two-fold. First of all they have appreciable photophysical properties to start with (see above) which can be modulated by alteration of C-aryl substituents. Moreover I would like to exploit the newly developed programmed method for the synthesis of fully asymmetrical diketopyrrolopyrroles⁵¹ which gives full freedom to incorporate an unrestricted variety of substituents regulating all essential features i.e., cation recognition unit, solubility, functional targeting group for a specific organelle in biological systems and modulation of the fluorescence by donor-acceptor architecture. Therefore, I decided to construct highly sensitive and selective probes comprised of two different electron-donating or electron-withdrawing peripheral aryl groups, only one of which would contain the cation recognition unit, and strong electron-accepting DPP core in the middle. Given that the rationale behind my PhD-Thesis was to design and synthesize the targeted fluorescent probes, biological targeting groups will also play an important role to accumulate in specific organelles and increase the solubility in polar solvents for molecular biology cell studies. Finally, all the novel DPP probes may induce better compatibility with the cells to detect changes in concentrations of metal cations (K^+ , Zn^{2+}) in specific localization in living cells.

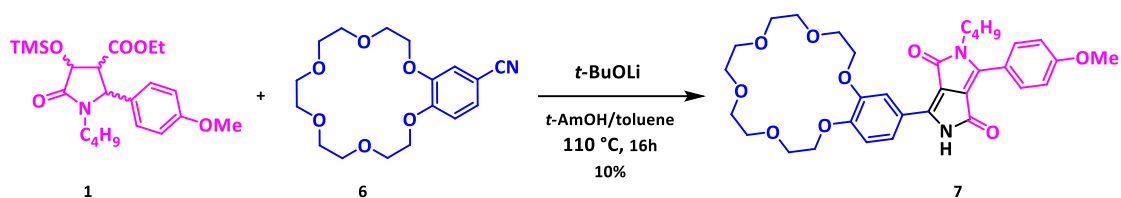
5. Result and discussion

5.1 Diketopyrrolopyrrole-based Chemosensors Possessing Macrocyclic Units

Crown ethers are flexible macrocyclic compounds consisting of multiple oligo-ethylene oxides in a cyclic array and were first discovered by Pedersen in 1967.¹⁸ These crown ethers and their aza-crown analogues have been a popular receptors for alkali and alkaline earth metal cations owing to their strong binding ability between metal ions and electron rich donor atoms through electrostatic ion-dipole interactions. The most common types of crown ethers are 15-crown-5, 18-crown-6 and 1-aza-18-crown-6 which are widely used in the design of fluorescence based sensor systems.⁵⁶ The predominant design of such probes is based on photo-induced electron transfer (PET) and the probes typically comprise both a fluorophore and a recognition unit linked *via* a methylene group or longer electronically isolating bridge. However, a limited number of studies have been conducted on the photophysical consequences of directly linking the fluorophore core with a molecular recognition unit. Such fluorescent sensors operate *via* intramolecular charge transfer (ICT) which leads to a strong push-pull electron system. If the dye is polarized, the cation binding to electron-donating group affects the push-pull electronic character of the fluorophore, weakens or strengthens the ICT and leads to changes in emission such as blue- or red-shifts.⁵⁷ On the other hand, DPPs have rarely been used as fluorophores to study the recognition of metal cations and to the best of my knowledge, there is no single example on DPP-based fluorescent probe for detection of alkali metal ions such as Li^+ , Na^+ , K^+ and all existing examples designed for Zn^{2+} detection rely on the PET mechanism. Therefore, I decided to explore the direct linkage of intramolecular charge transfer (ICT) mechanism to construct more

efficient probes based on the DPP chromophore directly from nitriles possessing macrocyclic units.

In the first part of my study (Paper 1), I prepared a series of nitriles bearing crown ether moieties directly fused to a peripheral aryl group of DPP of different ring sizes including 18-crown-6, 15-crown-5 and 21-crown-7 (chosen as Na⁺/K⁺ ionophores). Initially I attempted condensation of these nitriles under classical DPP synthesis conditions in presence of diethyl succinate. Unfortunately, these reactions were unsuccessful and did not produce the desired symmetrical DPPs. Taking advantage of the recently developed new methodology for synthesis of fully asymmetrical DPPs to overcome the problem of low reactivity of nitrile which relies on the condensation of nitrile with key intermediate pyrrolidin-2-one **1**.⁵¹ I decided to apply these conditions for condensation of nitrile **6** bearing benzo-18-crown-6 scaffold, with pyrrolidin-2-one **1**. This reaction was successful and produced the first ever macrocyclic hybrid dye DPP **7** possessing crown ether unit in low yield (Scheme-6).



Scheme-6: Synthesis of asymmetrical benzo-crown DPP **7**

After confirming the molecular structure of DPP **7** by ¹H-NMR and HR-MS, the methodology was extended to synthesize a library of DPPs possessing benzo crown ethers differing in crown size. The optical studies performed at the Institute of Physics, PAS (Warsaw), revealed that fluorescence quantum yields are in the range of 0.8-0.96 but disappointingly fluorescence titration studies displayed weak selectivity for Na⁺ and K⁺ even in large excess. Although the size of these crown ethers are known to be compatible for complexation with the radii of Na⁺ and K⁺ ions, no significant changes in the emission were observed.

Previously, our group had developed a rare example of a non-fluorescent DPP dye possessing 2-dialkylaminopyridine substituents on both sides of the DPP core. I decided to utilize this finding to look for a highly prized “switch-on” fluorescent sensor. For this purpose, suitable nitriles were prepared by attaching azacrown ethers *via* nucleophilic aromatic substitution at position 2 of a 4-cyano pyridine. The resulting nitriles were subsequently used for DPP synthesis *via* condensation of nitrile using same conditions to Scheme-6. The incorporation of pyridine containing crown ethers on DPP core leads to A'-A-D architectures with improved yields of up to 30%. In contrast to the typical DPPs, which are known to be highly fluorescent, these new pyridine DPPs (**8-10**, Figure-8) bearing azacrown ether units at the *meta* position turned out to be very weak emissive (Φ_{fl} = 0.01-0.03%) compared to benzocrown DPP **7**. The quantum chemical calculations performed by Prof. Denis Jacquemin (Nantes, France) revealed that the triplet T₂ state is located very close in energy to the S₁ with a small energy gap which

leads to efficient intersystem crossing (ISC). Thus, the presence of an accessible triplet state quenches the emission in **8-10**.

As predicted, the addition of sodium and potassium salts (1000 eq.) to DPPs **8**, **9** and **10** (Figure-8) possessing 2-dialkylaminopyridin-4-yl (where alkyl is a crown ether) showed moderate fluorescence enhancement with a range of 0.06-0.14% fluorescence quantum yields in acetonitrile and the emission is bathochromically shifted by 9 nm. The photophysical studies of all three DPPs **8**, **9** & **10** displayed significant bathochromic shift of both absorption and emission compared to benzo crown DPP **7** when coordinated to cations possessing Lewis acid character such as Li^+ , Mg^{2+} and Zn^{2+} with strong fluorescence enhancement ≈ 20 to 30 times in presence 1000 eq. of each salt. Both probes **8** and **10** possessed Φ_{fl} of ≈ 0.2 -0.3% in acetonitrile in the presence of 1000 eq. of Li^+ , Mg^{2+} and Zn^{2+} , while the emissions were red-shifted from 550 to 630 nm (≈ 80 nm) going beyond the 600 nm into IR to NIR region.

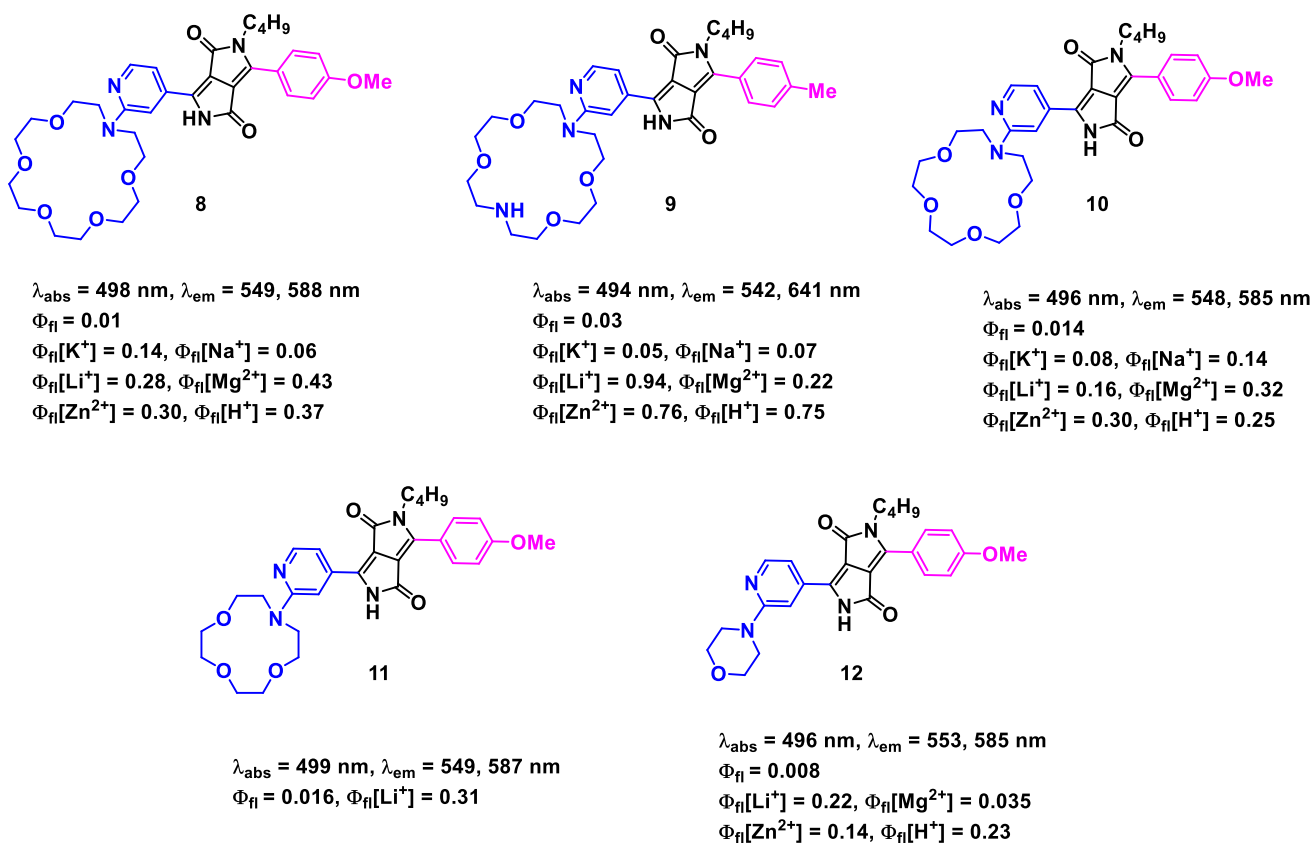


Figure-8: Structures, optical properties of new fluorescent chemosensors (**8-12**) in acetonitrile.

The same trend was observed for protonation with benzenesulfonic acid. Probe **9** displayed very high emission quantum yield upon Li^+ binding ($\Phi_{\text{fl}} = 0.94$ & 34 times) and Zn^{2+} ($\Phi_{\text{fl}} = 0.76$ & 25 times). Finally, probe **12** (Figure-8) which lacks a macrocyclic ring, showed 30-fold fluorescence enhancement with large bathochromic shift of 120 nm in the presence of 1000 eq. of Li^+ . This clearly indicates that interaction of lithium with the 2-dialkylaminopyridine unit is responsible for the striking effect.

In conclusion, by using new, efficient, programmed method for the synthesis of DPPs,⁵¹ it is possible to obtain D-A-D and A'-A-D type DPP based fluorescent chemosensors bearing macrocyclic units directly from nitriles. As I hoped, this new class of chemosensors showed strong fluorescence intensity and bathochromic shift of emission upon complexation with metal cations especially for Li⁺, Mg²⁺ and Zn²⁺. Also, experimental results indicate that these macrocyclic hybrid dyes exhibit moderate fluorescence enhancement in the presence of Na⁺ and K⁺. These results open the door for me to design and synthesize highly selective and sensitive fluorescent probes for bioimaging applications in living cells as "turn-on" sensors.

5.2 DPP-based K⁺ sensitive probes

Potassium ions play diverse roles in a number of biological functions especially in mitochondrial metabolic processes. Moreover, the significance of potassium channels in mitochondria plays indispensable functions in cell proliferation, cell growth, muscle contraction and nerve transmission. On the other hand, an unbalance in the potassium levels in the human body leads to many diseases. Hence, considering the importance of an intracellular and extracellular potassium concentration changes in living cells and taking into consideration of the results of my first project, I aimed to prepare highly sensitive mitochondria targeting potassium probes directly linked to a DPP fluorophore operating *via* the intramolecular charge transfer (ICT) mechanism. The obvious consequence of this fact is that the direct linking an amine-bearing recognition unit with a chromophore leads to a strongly polarized dye. Changing the electron-donating or electron-withdrawing properties in push-pull donor-acceptor systems influences the intramolecular charge transfer (ICT) and leads to increasing or decreasing of HOMO-LUMO gap.³⁸ To the best of my knowledge, there are no examples of DPP based fluorophores used to study K⁺ concentration changes in mitochondria. For this reason in my second project I planned to synthesize K⁺ probes possessing phenylaza-18-crown-6 as a key receptor due to its high selectivity and sensitivity for K⁺ over Na⁺ in biologically relevant conditions. Consequently, I chose an asymmetrical DPP in my molecular design strategy so that I decided to place the basic nitrogen atom at the most conjugated position of the aryl substituent, so that the fluorescence will be sensitive to the binding event. The efficient stepwise DPP synthesis allowed me to prepare 4-bromo-phenyl asymmetrical DPP derivatives bearing additional alkoxy group at an *ortho* position to bromine. The resulting dyes were used for Buchwald-Hartwig amination with 1-aza-18-crown-6 to obtain K⁺-probes **13**, **14** and **15** (Figure-9). In order to increase the K⁺ binding constant an additional lariat ether at a position adjacent to the aza-18-crown-6 moiety was added in probe **15**. This new programmed method for DPP synthesis selectively gives mono-alkylation at N2-position with NH-free at N5-position. This NH-free position is crucial for my design since I planned to attach the mitochondria targeting lipophilic triphenylphosphonium group which was done by means of alkylation with long alkyl chain 1, 6-dibromohexane which was subsequently reacted to form a triphenylphosphonium salt to give mitochondria probe **16** in 25% yield (Figure-9). Probe **16** represents the first DPP-based mitochondria targeting potassium probe to date. As expected, all four probes displayed good solubility in both polar and non-polar solvents.

The photophysical studies of the new fluorescent probes were broadly investigated at the Institute of Physics, PAS. Simultaneously the bioimaging experiments were performed in Nencki Institute of Experimental Biology, PAS (Warsaw).

Photophysical studies of the new D-A-D' hybrid fluorophores displayed a good combination of favorable properties including strong absorption of green light (500-530 nm) and strong emission of yellow light (560-590 nm), and very high fluorescence quantum yields (0.8-0.9%) in both CH₃CN and toluene. The probes **13-16** (Figure-9) bearing additional alkoxy substituents adjacent to crown ether moiety are very sensitive to K⁺ which leads to hypsochromic shifts of emission from 580 to 520 nm in the presence of just 1 equivalent of K⁺. Discouragingly, all four probes failed to give fluorescence changes in water and in HEPES buffer. In the absence of additional alkoxy group probe **13** displayed no essential changes in the emission even in presence of huge excess of K⁺. Probe **16** displayed the highest fluorescence enhancement in the presence of 5 eq. of K⁺ in CH₃CN.

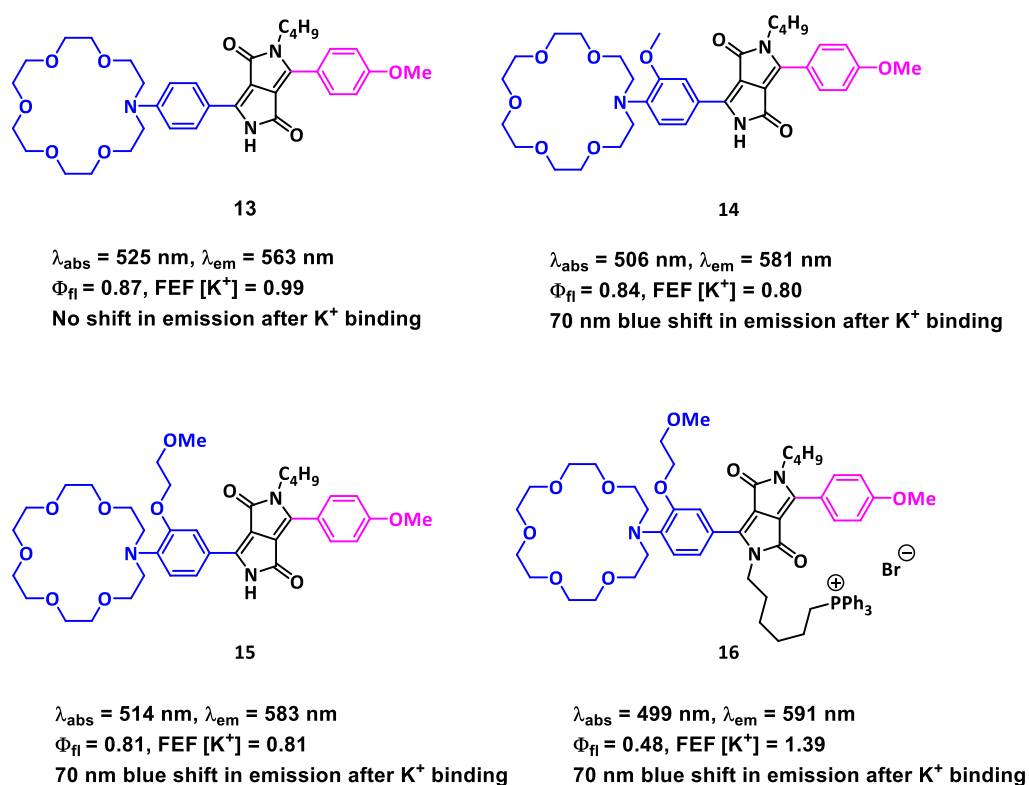


Figure-9: Structures, optical properties of new fluorescent K⁺ probes **13-16** in acetonitrile.

As a result, probe **16** was selected for bioimaging studies and investigated by myself together with Dr. Antoni Wrzosek in the group of Prof. Adam Szewczyk (Nencki Institute of Experimental Biology, Warsaw). The conducted fluorescence microscopy experiments showed probe **16** localized selectively in mitochondria of cardiac H9C2 cells which was confirmed by co-localization with MitoTracker™ Green. As probe **16** possesses a lipophilic cation, it accumulated in the mitochondria at very low concentrations (150-500 nM) after incubation with cardiac H9C2 cells. Also, modulation in the mitochondrial K⁺ concentration under stimulation in the presence of potassium

ionophore valinomycin and nigericin were visible *via* changes of fluorescence. Importantly, this sensing of mitochondrial K⁺ flux in live cells could be observed at two different excitation wavelengths (green and red emission channels). With these results I have demonstrated that probe comprising of the DPP chromophore bridged with phenylaza-18-crown-6 lariat ether and quaternary phosphonium moiety is a promising K⁺ sensor for intracellular imaging studies in mitochondria. To the best of my knowledge, probe **16** represents the first ever DPP-based mitochondria-targeting fluorescent K⁺ sensor to date.

5.3 DPP-based Zn²⁺ sensitive probes

In the final part of my experimental work I decided on an approach to design, synthesize and study the photophysical properties as well as the intracellular imaging of diketopyrrolopyrrole-based zinc sensors directly obtained from nitriles possessing zinc chelator units. As described for the potassium probe, the development of a probe that is specific for the zinc cation is challenging as it needs to be sensitive and selective. Since zinc's biological significance has led to its intense study and its involvement in important roles in a wide range of biological processes, it is becoming increasingly important to determine zinc in living organisms.

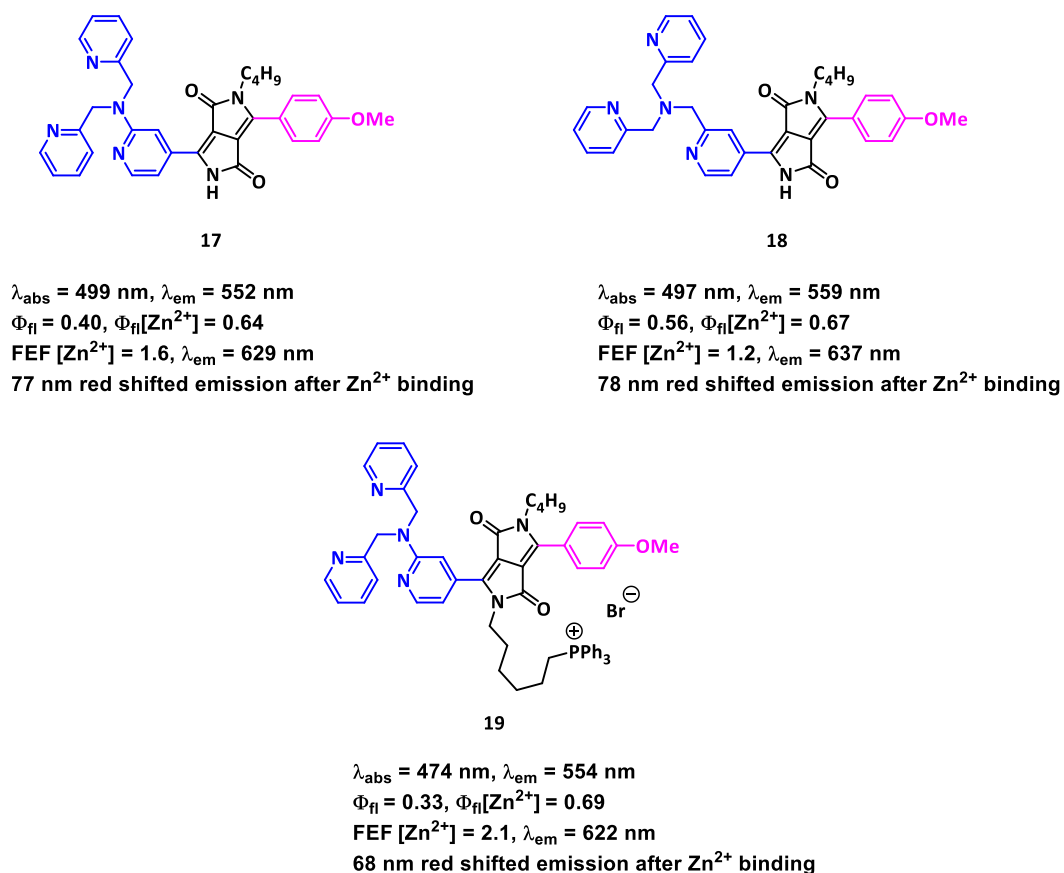
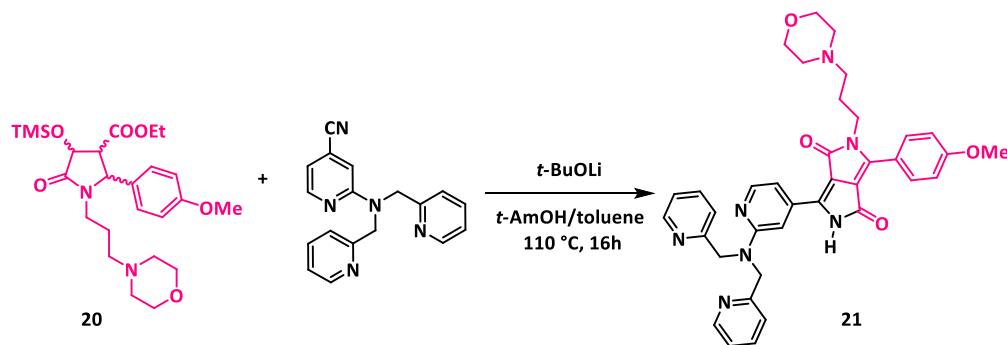


Figure-10: Structures, optical properties of new fluorescent Zn²⁺ probes **17-19** in acetonitrile.

Although DPP and a large number of different fluorophore-based zinc chemosensors have been extensively investigated and studied,^{54-55&58-59} limited attention has been dedicated to direct linking of the DPP fluorophore with the recognition unit for the zinc cation. Since di-(2-picolyl)amine (DPA) is the most commonly used zinc chelator as its strong binding affinity over other metal cations, I decided to attach DPA unit at position 2 of a peripheral pyridine ring, so that the basic nitrogen of the pyridine also actively participates in the binding event along with DPA. Knowing from my first project that hydrophilic nitriles are compatible with DPP synthesis, I prepared two starting materials possessing a DPA unit either directly attached or *via* a methylene spacer at the 2-position of a pyridine-4-carbonitrile and they were used for the final condensation with pyrrolidin-2-one **1** using the developed methodology leading to A'-A-D architecture zinc probes **17** and **18** (Figure-10). Subsequently, I modified the structure of these probes to include triphenylphosphine cation (PPh₃⁺), with the idea to transform them into mitochondrial probe **19** (Figure-10) in overall 27% yield.

In addition, a propylmorpholine group was chosen to be present at the N2 position of the final molecule as a lysosome targeting group as, due to its basic nature, it easily accumulates in acidic lysosomes. Hence, I synthesized the key intermediate pyrrolidin-2-one **20** using the previously developed method by multicomponent reaction of 4-methoxybenzaldehyde with 3-aminopropylmorpholine and diethyl oxaloacetate followed by reduction and TMS protection in overall 43% yield.⁵¹ In analogy to the previous probes **17** and **18**, I prepared two lysosome targeting probes **21** and **22** *via* condensation of nitrile with pyrrolidin-2-one **20** using the developed conditions (Scheme-7 & Figure-11).



Scheme-7: Exemplary synthesis of asymmetrical, lysosome-targeting DPP **21**

Altogether, a set of five zinc probes have been prepared and the optical properties and bioimaging studies of all five probes were extensively studied in Institute of Physics, PAS and Nencki Institute of Experimental Biology, PAS (Warsaw).

All probes except **19** absorb at $\approx 500\text{ nm}$ and emit at $550\text{-}560\text{ nm}$. Probes **17** and **18** display moderate fluorescence quantum yields (0.4 & 0.6%) in CH_3CN and obviously the fluorescence quantum yields are usually not too high for lysosomal probes, although probes **21** & **22** have $\Phi_{\text{fl}} = 0.09$ and 0.12% respectively. Interestingly, a strong hypsochromic shift of absorption was observed for probe **19** with $\Phi_{\text{fl}} = 0.33\%$. As

predicted, electronically conjugated polarized DPPs **17**, **18** & **19** are very sensitive to the zinc cation and display strong ≈ 80 nm red-shifts of emission (yellow to orange-red) upon addition of 1 equivalent of zinc (Figure-10). It is worth mentioning that upon zinc complexation the emission of these probes shifts beyond 600 nm which is almost invisible to the naked-eye.

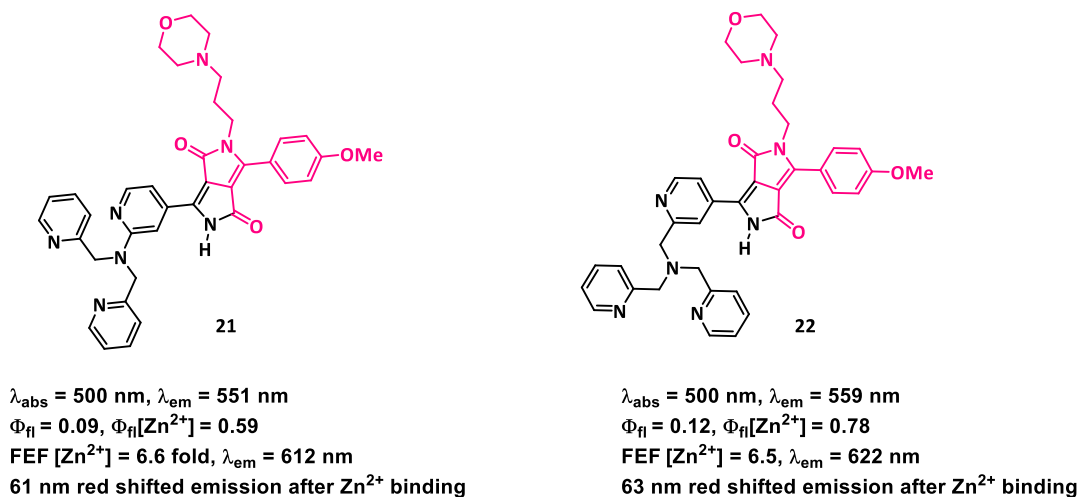


Figure-11: Structures, optical properties of new fluorescent Zn^{2+} probes (**21-22**) in acetonitrile.

As shown in the Figure-11 probes **21** and **22** bearing morpholine units displayed the highest fluorescence intensity increase (6-fold) with concurrent 50-60 nm red-shift of emission after zinc complexation with high fluorescence quantum yields in CH_3CN (≈ 0.6 - 0.8%). The other notable findings are as follows; (a) these probes also react with Cd^{2+} but they are silent to other divalent cations of biological importance such as Mg^{2+} and Ca^{2+} ; (b) protonation of these probes with Brønsted acid shifts the emission beyond 700 nm.

Cell studies were conducted by Dr. Antoni Wrzosek and myself in the group of Prof. Adam Szewczyk (Nencki Institute of Experimental Biology, Warsaw). As predicted the staining experiments of probe **19** bearing PPh_3^+ revealed that it was selectively accumulated in mitochondria (confirmed co-localization with MitoTrackerTM Green). On the other hand the probe **22** selectively localized in lysosomes which was confirmed by co-localization with LysoTrackerTM. The observed photophysical response of studied DPPs and their ability to act as probes were possible due to the installing vital substituents implementing all important features, i.e., cation recognition unit, functional targeting group, solubility and donor-acceptor architecture. This in turn was only possible, thanks to the previously developed programmed synthesis of diketopyrrolopyrroles.⁵¹

6. Comparison and Conclusions

At the beginning of my PhD I designed and synthesized library of quadrupolar (D'-A-D) and dipolar (A'-A-D) type diketopyrrolopyrrole-based chemosensors for cations possessing Lewis acid character and their optical properties were investigated. Detailed literature studies revealed that there are not too many chemosensors possessing DPP as fluorophore. Therefore, I decided to cross-compare my compounds with other chemosensors possessing either crown ethers or 2-aminopyridine moieties. The structures and key optical properties of chemosensors **23-27** are presented on Figure-12. The comparison of cation sensitivity and fluorescence enhancement of dyes **8-12** with known probes **23-27** revealed that my compounds possess more beneficial properties. Diketopyrrolopyrroles (DPPs) are known to be used as organic dyes but have now, for the first time been successfully applied for detection of cations possessing Lewis acid character such as Li^+ , Mg^{2+} and Zn^{2+} . In particular the comparison with 3,6-dibutylbenzodipyrido[3,2-*a*:2'3'-*c*]phenazine **23** which has a low Φ_{fl} and emits in the green region with slight red-shift of emission upon addition of Li^+ is interesting.⁶⁰ On the other hand chemosensors possessing a crown ether directly fused with a coumarin fluorophore (**24**) showed emission in the blue region with hypsochromic shift of fluorescence upon Li^+ complexation.⁶¹ Merugu and co-workers reported a zinc chemosensor based on an aminopyridine Schiff base (**25**) which has a weak fluorescence enhancement with 30 nm red-shifted emission upon binding with zinc.⁶² Wang and Yu developed a BINOL-based fluorescent sensor **26** for Zn^{2+} which showed weak 7.6-fold fluorescent intensity enhancement and bathochromically shifted emission by 50 nm.⁶³ One of the classical compounds from the point of Li^+ sensors is **27**, bearing an azacrown ether and possessing emission maximum beyond 600 nm after binding to Li^+ ions, but its fluorescence enhancement is low (15-fold).⁶⁴

In conclusion, my probes **8-12** possessing 2-dialkylaminopyridine are more sensitive to Li^+ , Mg^{2+} and Zn^{2+} with higher fluorescence quantum yields and displayed strong fluorescence enhancements of up to 45 fold. They also have bathochromically shifted both absorption and emission upon complexation with both acid and cations possessing Lewis acid character. Since the DPP core has never been utilized before to construct chemosensors, especially for Li^+ , it is impossible to directly compare the optical behavior of compounds **8-12** with data for analogous compounds. Still, they are very favorable compared with chemosensors of similar sensing units and these findings brings DPP to the fore in the design of new generations of sensors.

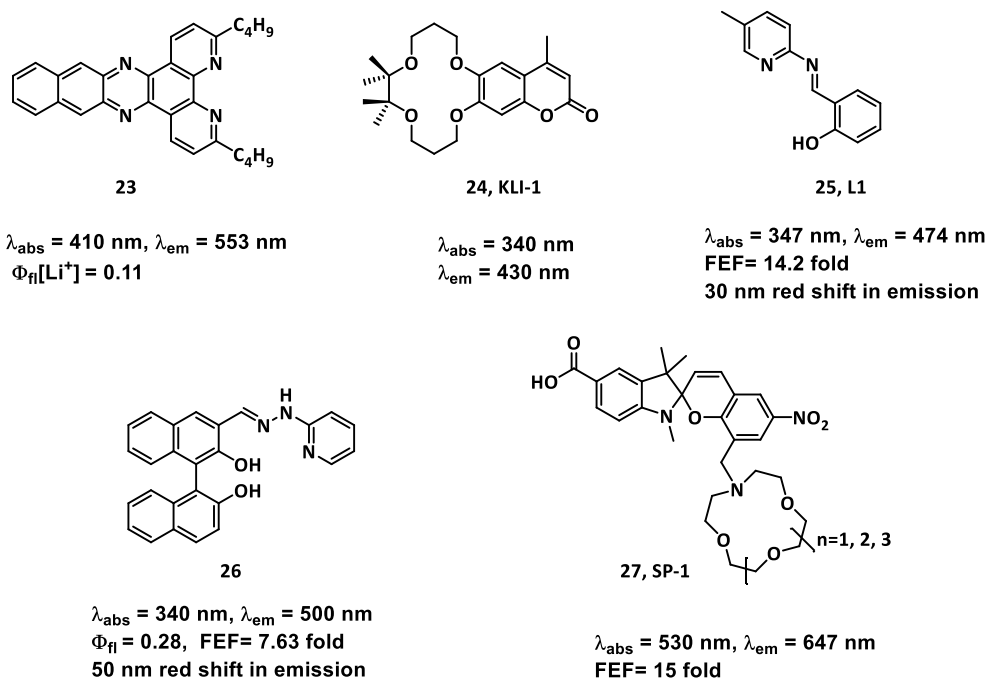


Figure-12: Photophysical results for structurally related chemosensors for Li^+ , Mg^{2+} and Zn^{2+} .

In the main part of my work I designed and synthesized a set of DPP-based fluorescent K^+ sensors and their optical properties and biological applications were investigated. Fluorescent K^+ sensors **28-32**, well known from literature^{22e, 23q,j,o,m} were compared with my new DPP K^+ sensors **13-16**. Holdt and co-workers synthesized **28** and proved that the presence of an additional 2-methoxyethoxy lariat group at the *ortho* position of the crown ether moiety is crucial to increase the binding constant. Probe **28** had low fluorescence quantum yields with weak fluorescence enhancement after complexation with K^+ .²² Furthermore, Borisov and co-workers developed set of BODIPY based red- to NIR emitting K^+ sensors with moderate quantum yields.^{23j} Recently, Tian and co-workers reported a library of K^+ sensors **29, 31, 32** (Figure-13) and they have displayed blue-shift of absorption and very low Φ_{fl} upon K^+ complexation. Moreover, they have comparable changes in fluorescence properties upon addition of K^+ and probe **32** was used for monitoring the K^+ fluxes in mitochondria under stimulations by adding nigericin ionophore.

In summary I have synthesized set of DPP-based K^+ sensors possessing high fluorescence quantum yields (0.8-0.90%). I have shown that there is the possibility to fine tune the photophysical properties of DPP-based K^+ sensors and an addition of just 1 equivalent of potassium salt leads to hypsochromic shift of emission from 580 nm to 520 nm. The incorporation of mitochondria targeting group PPh_3^+ allowed to study changes in concentration of mitochondrial K^+ by adding nigericin and valinomycin at two different excitation wavelengths with increase and decrease in emission intensity. The dual excitation wavelength of the probe **16** is advantageous.

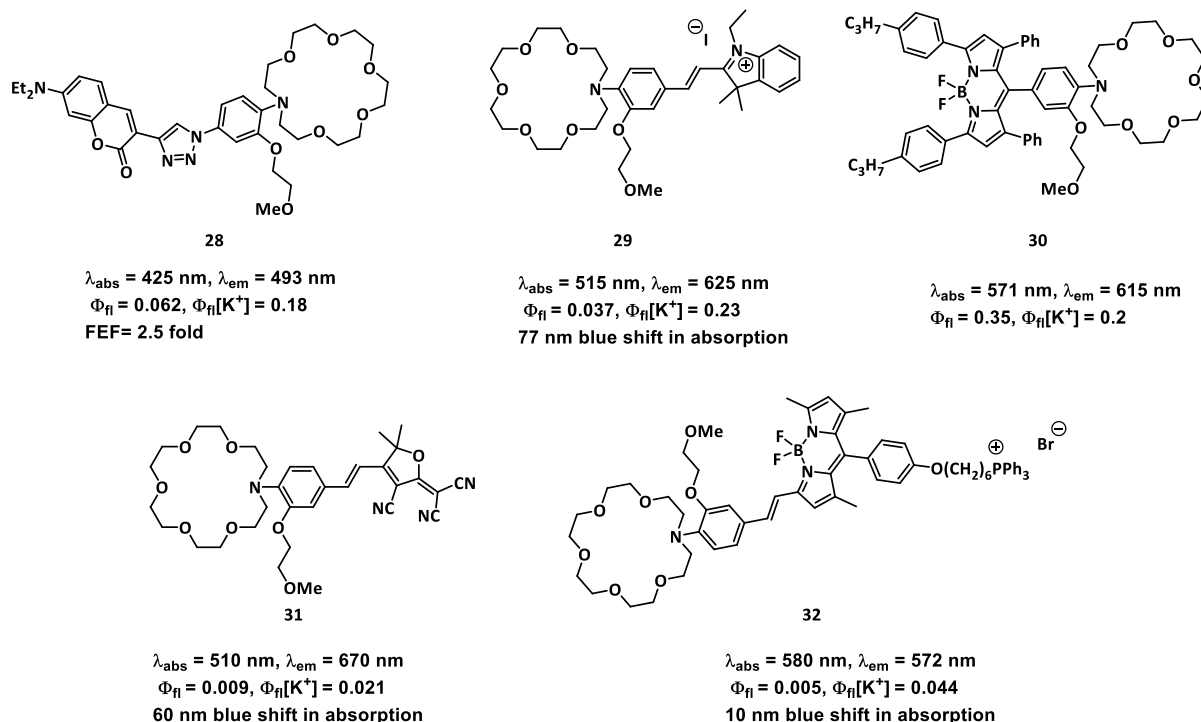


Figure-13: Photophysical results for structurally related fluorescent K^+ sensors.

Finally, I designed and synthesized DPP-based zinc sensors directly from nitriles possessing zinc recognition DPA unit and their photophysical properties and bioimaging studies were investigated. A few DPP-based fluorescent zinc sensors **33-35** (Figure-14) are well known from literature^{54,55}. Therefore, I decided to cross compare these known sensors **33-35** with my zinc probes **17-19** and **20-21**. Wang and co-workers reported the first DPP based fluorescent Zn^{2+} chemosensor **33** and proved a strong Zn^{2+} complexation with 25-fold fluorescent enhancement and 70 nm blue-shift of emission.⁵⁴ Recently, Du *et al.* synthesized mitochondrial zinc probe **34** by changing the zinc chelator to the N2 position and it possessed low fluorescence quantum yield and 77-fold fluorescence enhancement in zinc complexation form, but mitochondrial targeting group PPh_3^+ exhibited a negligible effect on the optical properties of the DPP fluorophore.^{55a} Very recently, the Wang and Sessler groups reported a series of lysosomal zinc probes by attaching alkyl morpholine group at N5 position and these probes display rather low quantum yields and moderate fluorescence enhancement after bound with zinc.^{55b} In all the above probes authors were not able to shift the emission bathochromically to biological window beyond 600 nm.

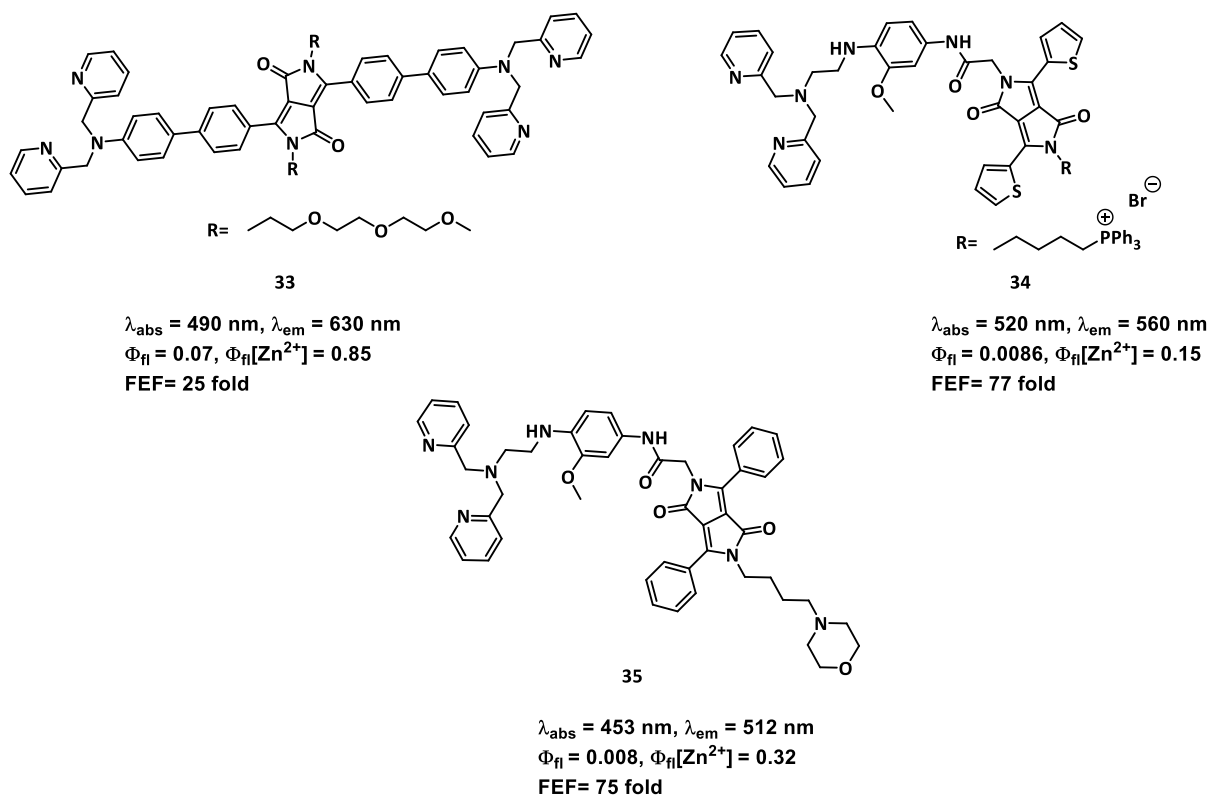


Figure-14: Photophysical results for structurally related fluorescent Zn^{2+} sensors.

In conclusion, I have shown that my probes which contain sensing moieties directly conjugated to fluorophore cores display strong bathochromic shifts of fluorescence moving beyond 600 nm with large fluorescence quantum yields and high emission intensity when they bind to zinc. Addition of just 1 equivalent of zinc changes the fluorescence from yellow to orange-red color. Moreover, in the absence of zinc my compounds possessed nearly 200 fold higher fluorescence quantum yields than previously reported analogous lysoDPP probes. I also proved that direct linking of a zinc chelator to DPP fluorophore in a dipolar architecture opens the pathway towards modulating intramolecular charge transfer *via* increase in the electron-withdrawing properties of pyridyl substituent upon zinc coordination, which eventually leads to strong red-shift of emission. These characteristics in combination with strong orange-red emission (600-700 nm) mean these new DPP-based zinc probes are promising for bioimaging applications.

7. References

1. a) Herschel, J. F. W., *Philos. Trans. R. Soc.*, **1845**, *135*, 143-145; b) Herschel, J. F. W., *Philos. Trans. R. Soc.*, **1845**, *135*, 147-153.
2. Stokes, G. G., *Philos. Trans. R. Soc.*, **1852**, *142*, 463-562.
3. Jabłoński, A., *Z. Physik*, **1935**, *94*, 38-46.
4. de Silva, A. P.; Fox, D. B.; Moody, T. S.; Weir, S. M., *Trends Biotechnol*, **2001**, *19*, 29-34.
5. Rich, R. L.; Myszka, D. G., *J. Mol. Recognit.*, **2002**, *15*, 352-376.
6. Cammann, K., *Phys. Chem. Chem. Phys.*, **2003**, *5*, 5159-5168.
7. Badugu, R., *J. Fluoresc.*, **2005**, *15*, 71-83.
8. Wang, X.-D.; Wolfbeis, O. S., *Anal. Chem.*, **2012**, *85*, 487-508.
9. de Silva, A. P.; Gunaratne, H. Q. N.; Gunnlaugsson, T.; Huxley, A. J. M.; McCoy, C. P.; Rademacher, J. T.; Rice, T. E., *Chem. Rev.*, **1997**, *97*, 1515-1566.
10. Nolan, E. M.; Lippard, S. J., *Chem. Rev.*, **2008**, *108*, 3443-3480.
11. Duke, R. M.; Veale, E. B.; Pfeffer, F. M.; Kruger, P. E.; Gunnlaugsson, T., *Chem. Soc. Rev.*, **2010**, *39*, 3936-3953.
12. Chen, X.; Pradhan, T.; Wang, F.; Kim, J. S.; Yoon, J., *Chem. Rev.*, **2011**, *112*, 1910-1956.
13. Hargrove, A. E.; Nieto, S.; Zhang, T.; Sessler, J. L.; Anslyn, E. V., *Chem. Rev.*, **2011**, *111*, 6603-6782.
14. Boens, N.; Leen, V.; Dehaen, W., *Chem. Soc. Rev.*, **2012**, *41*, 1130-1172.
15. Li, X.; Gao, X.; Shi, W.; Ma, H., *Chem. Rev.*, **2013**, *114*, 590-659.
16. a) Yin, J.; Hu, Y.; Yoon, J., *Chem. Rev.*, **2015**, *44*, 4619-4644; b) Wu, D.; Sedgwick, A. C.; Gunnlaugsson, T.; Akkaya, E. U.; Yoon, J.; James, T. D., *Chem. Rev.*, **2017**, *46*, 7105-7123.
17. Shi, W.; Ma, H., *Chem. Commun.*, **2012**, *48*, 8732-8744.
18. a) Pedersen, C. J., *J. Am. Chem. Soc.*, **1967**, *89*, 7017-7036; b) Cram, D., *Science*, **1988**, *240*, 760-767; c) Pedersen, C. J., *Science*, **1988**, *241*, 536-540.
19. a) Tsien, R. Y., *Nature*, **1981**, *290*, 527-528; b) Minta, A.; Kao, J. P.; Tsien, R. Y., *J. Biol. Chem.*, **1989**, *264*, 8171-8178; c) Minta, A.; Tsien, R. Y., *J. Biol. Chem.*, **1989**, *264*, 19449-19457; d) de Silva, A. P.; Gunaratne, H. Q. N.; Gunnlaugsson, T.; Nieuwenhuizen, M., *Chem. Commun.*, **1996**, 1967-1968; e) Miyawaki, A.; Llopis, J.; Heim, R.; McCaffery, J. M.; Adams, J. A.; Ikura, M.; Tsien, R. Y., *Nature*, **1997**, *388*, 882-887; f) He, H.; Mortellaro, M. A.; Leiner, M. J. P.; Young, S. T.; Fraatz, R. J.; Tusa, J. K., *Anal. Chem.*, **2002**, *75*, 549-555; g) He, H.; Mortellaro, M. A.; Leiner, M. J. P.; Fraatz, R. J.; Tusa, J. K., *J. Am. Chem. Soc.*, **2003**, *125*, 1468-1469.
20. a) Obare, S. O.; Murphy, C. J., *Inorg. Chem.*, **2001**, *40*, 6080-6082; b) Citterio, D.; Takeda, J.; Kosugi, M.; Hisamoto, H.; Sasaki, S.; Komatsu, H.; Suzuki, K., *Anal. Chem.*, **2007**, *79*, 1237-1242; c) Heng, S.; Nguyen, M. -C.; Kostecki, R.; Monro, T. M.; Abell, A. D., *RSC Adv.*, **2013**, *3*, 8308-8317; d) Stubing, D. B.; Heng, S.; Abell, A. D., *Org. Biomol. Chem.*, **2016**, *14*, 3752-3757; e) Hangarge, R. V.; La, D. D.; Boguslavsky, M.; Jones, L. A.; Kim, Y. S.; Bhosale, S. V., *ChemistrySelect*, **2017**, *2*, 11487-11491; f) Li, E.; Kang, J.; Ye, P.; Zhang, W.; Cheng, F.; Yin, C., *J. Mater. Chem. B*, **2019**, *7*, 903-907.
21. a) Martin, V. V.; Rothe, A.; Diwu, Z.; Gee, K. R., *Bioorg. Med. Chem. Lett.*, **2004**, *14*, 5313-5316; b) Martin, V. V.; Rothe, A.; Gee, K. R., *Bioorg. Med. Chem. Lett.*, **2005**, *15*, 1851-1855; c) Domaille, D. W.; Que, E. L.; Chang, C. J., *Nat. Chem. Biol.*, **2008**, *4*, 168-175; d) Gunnlaugsson, T.; Nieuwenhuizen, M.; Richard, L.; Thoss, V., *Tetrahedron Lett.*, **2001**, *42*, 4725-4728; e) Gokel, G. W.; Leevy, W. M.; Weber, M. E., *Chem. Rev.*, **2004**, *104*, 2723-2750; f) Gao, G.; Cao, Y.; Liu, W.; Li, D.; Zhou, W.; Liu, J., *Anal. Methods*, **2017**, *9*, 5570-5579.

22. a) Martin, V. V.; Rothe, A.; Diwu, Z.; Gee, K. R., *Bioorg. Med. Chem. Lett.*, **2004**, *14*, 5313–5316; b) Kim, M. K.; Lim, C. S.; Hong, J. T.; Han, J. H.; Jang, H.-Y.; Kim, H. M.; Cho, B. R., *Angew. Chem., Int. Ed.*, **2010**, *49*, 364–367; c) Sarkar, A. R.; Heo, C. H.; Park, M. Y.; Lee, H. W.; Kim, H. M., *Chem. Commun.*, **2014**, *50*, 1309–1312; d) Ast, S.; Muller, H.; Flehr, R.; Klamroth, T.; Walz, B.; Holdt, H. –J., *Chem. Commun.*, **2011**, *47*, 4685–4687; e) Ast, S.; Schwarze, T.; Muller, H.; Sukhanov, A.; Michaelis, S.; Wegener, J.; Wolfbeis, O. S.; Korzdorfer, T.; Durkop, A.; Holdt, H. –J., *Chem. Eur. J.*, **2013**, *19*, 14911 –14917; f) Schwarze, T.; Muller, H.; Ast, S.; Steinbruck, D.; Eidner, S.; Geibler, F.; Kumke, M. U.; Holdt, H. –J., *Chem. Commun.*, **2014**, *50*, 14167–14170; g) Schwarze, T.; Muller, H.; Schmidt, D.; Reimer, J.; Holdt, H. –J., *Chem. Eur. J.*, **2017**, *23*, 7255 –7263; h) Schwarze, T.; Reimer, J.; Reimer, J.; John, L.; Holdt, H. –J.; Wessig, P., *Chem. Eur. J.*, **2019**, *25*, 12412–12422.
23. a) He, H.; Mortellaro, M.A.; Leiner, M.J.P.; Fraatz, R.J.; Tusa, J.K., *J. Am. Chem. Soc.*, **2003**, *125*, 1468–1469; b) Padmawar, P.; Yao, X.; Bloch, O.; Manley, G. T.; Verkman, A. S., *Nat. Methods.*, **2005**, *2*, 825–827; c) Namkung, W.; Padmawar, P.; Mills, A. D.; Verkman, A. S., *J. Am. Chem. Soc.*, **2008**, *130*, 7794–7795; d) Hirata, T.; Terai, T.; Komatsu, T.; Hanaoka, K.; Nagano, T., *Bioorg. Med. Chem. Lett.*, **2011**, *21*, 6090–6093; e) Zhou, X.; Su, F.; Gao, W.; Tian, Y.; Youngbull, C.; Johnson, R. H.; Meldrum, D. R. *Biomaterials*, **2011**, *32*, 8574–8583; f) Zhou, X.; Su, F.; Tian, Y.; Youngbull, C.; Johnson, R. H.; Meldrum, D. R. *J. Am. Chem. Soc.*, **2011**, *133*, 18530–18533; g) Sui, B.; Yue, X.; Tichy, M.G.; Liu, T.; Belfield, K.D., *Eur. J. Org. Chem.*, **2015**, 1189–1192; h) Kong, X.; Su, F.; Zhang, L.; Yaron, J.; Lee, F.; Shi, Z.; Tian, Y.; Meldrum, D.R., *Angew. Chem. Int. Ed.*, **2015**, *54*, 12053–12057; i) Sui, B.; Yue, X.; Kim, B.; Belfield, K.D., *ACS Appl. Mater. Interfaces*, **2015**, *7*, 17565–17568; j) Müller, B.J.; Borisov, S.M.; Klimant, I., *Adv. Funct. Mater.* **2016**, *26*, 7697–7707; k) Hirata, T.; Terai, T.; Yamamura, H.; Shimonishi, M.; Komatsu, T.; Hanaoka, K.; Ueno, T.; Imaizumi, Y.; Nagano, T.; Urano, Y., *Anal. Chem.*, **2016**, *88*, 2693–2700; l) Bandara, H. M. D.; Hua, Z.; Zhang, M.; Pauff, S. M.; Miller, S. C.; Davie, E. A. C.; Kobertz, W. R., *J. Org. Chem.*, **2017**, *82*, 8199–8205; m) Ning, J.; Tian, Y., *Sens. Actuators B*, **2020**, *307*, 127659; n) Song, G.; Jiang, D.; Wang, L.; Ning, J.; Sun, X.; Su, F.; Chen, M.; Tian, Y., *Chem. Commun.*, **2020**, *56*, 5405–5408; o) Ning, J.; Lin, X.; Su, F.; Sun, A.; Liu, H.; Luo, J.; Wang, L.; Tian, Y., *Anal. Bioanal. Chem.*, **2020**, *412*, 6947–6957; p) Wang, Z.; Detomasi, T. C.; Chang, C. J., *Chem. Sci.*, **2021**, *12*, 1720–1729; q) Song, G.; Sun, R.; Du, J.; Chen, M.; Tian, Y., *Chem. Commun.*, **2017**, *53*, 5602–5605.
24. a) Rusakov, D. A.; Fine, A., *Neuron*, **2003**, *37*, 287–297; b) Suzuki, Y.; Komatsu, H.; Ikeda, T.; Saito, N.; Araki, S.; Citterio, D.; Hisamoto, H.; Kitamura, Y.; Kubota, T.; Nakagawa, J.; Oka, K.; Suzuki, K., *Anal. Chem.*, **2002**, *74*, 1423–1428; c) Csordás, G.; Hajnóczky, G., *J. Biol. Chem.*, **2003**, *278*, 42273–42282; d) Leite, M. F.; Thrower, E. C.; Echevarria, W.; Koulen, P.; Hirata, K.; Bennett, A. M.; Ehrlich, B. E.; Nathanson, M. H., *Proc. Natl. Acad. Sci.*, **2003**, *100*, 2975–2980; e) Behanna, H. A.; Stupp, S. I., *Chem. Commun.*, **2005**, 4845–4847; f) Komatsu, H.; Miki, T.; Citterio, D.; Kubota, T.; Shindo, Y.; Kitamura, Y.; Oka, K.; Suzuki, K., *J. Am. Chem. Soc.*, **2005**, *127*, 10798–10799; g) Kim, H. M.; Kim, B. R.; Hong, J. H.; Park, J.-S.; Lee, K. J.; Cho, B. R., *Angew. Chem. Int. Ed.*, **2007**, *46*, 7445–7448; h) Kim, H. M.; Kim, B. R.; An, M. J.; Hong, J. H.; Lee, K. J.; Cho, B. R., *Chem. Eur. J.*, **2008**, *14*, 2075–2083; i) Dong, X.; Yang, Y.; Sun, J.; Liu, Z.; Liu, B.-F. *Chem. Commun.*, **2009**, 3883–3885; j) Kamiya, M.; Johnsson, K., *Anal. Chem.*, **2010**, *82*, 6472–6479; k) Egawa, T.; Hanaoka, K.; Koide, Y.; Ujita, S.; Takahashi, N.; Ikegaya, Y.; Matsuki, N.; Terai, T.; Ueno, T.; Komatsu, T.; Nagano, T., *J. Am. Chem. Soc.*, **2011**, *133*, 14157–14159; l) Matsui, A.; Umezawa, K.; Shindo, Y.; Fujii, T.; Citterio, D.; Oka, K.; Suzuki, K.,

- Chem. Commun.*, **2011**, *47*, 10407-10409; m) Liu, Q.; Bian, W.; Shi, H.; Fan, L.; Shuang, S.; Dong, C.; Choi, M. M. F., *Org. Biomol. Chem.*, **2013**, *11*, 503-508; n) Liu, Z.; Jing, X.; Zhang, S.; Tian, Y., *Anal. Chem.*, **2019**, *19*, 2488-2497.
25. a) Komatsu, H.; Iwasawa, N.; Citterio, D.; Suzuki, Y.; Kubota, T.; Tokuno, K.; Kitamura, Y.; Oka, K.; Suzuki, K., *J. Am. Chem. Soc.*, **2004**, *126*, 16353-16360; b) Farruggia, G.; Iotti, S.; Prodi, L.; Montalti, M.; Zaccheroni, N.; Savage, P. B.; Trapani, V.; Sale, P.; Wolf, F. I., *J. Am. Chem. Soc.*, **2005**, *128*, 344-350; c) Kim, H. M.; Jung, C.; Kim, B. R.; Jung, S.-Y.; Hong, J. H.; Ko, Y.-G.; Lee, K. J.; Cho, B. R., *Angew. Chem. Int. Ed.*, **2007**, *46*, 3460-3463; d) Kim, H. M.; Yang, P. R.; Seo, M. S.; Yi, J.-S.; Hong, J. H.; Jeon, S.-J.; Ko, Y.-G.; Lee, K. J.; Cho, B. R., *J. Org. Chem.*, **2007**, *72*, 2088-2096; e) Jin, J.; Desai, B. N.; Navarro, B.; Donovan, A.; Andrews, N. C.; Clapham, D. E., *Science*, **2008**, *322*, 756-760; f) Marraccini, C.; Farruggia, G.; Lombardo, M.; Prodi, L.; Sgarzi, M.; Trapani, V.; Trombini, C.; Wolf, F. I.; Zaccheroni, N.; Iotti, S., *Chem. Sci.*, **2012**, *3*, 727-734; g) Liu, M.; Yu, X.; Li, M.; Liao, N.; Bi, A.; Jiang, Y.; Liu, S.; Gong, Z.; Zeng, W., *RSC Adv.*, **2018**, *8*, 12573-12587.
26. a) Mao, J.; Wang, L.; Dou, W.; Tang, X.; Yan, Y.; Liu, W., *Org. Lett.*, **2007**, *9*, 4567-4570; b) Huang, K.; Yang, H.; Zhou, Z.; Yu, M.; Li, F.; Gao, X.; Yi, T.; Huang, C., *Org. Lett.*, **2008**, *10*, 2557-2560; c) Zhou, Z.; Yu, M.; Yang, H.; Huang, K.; Li, F.; Yi, T.; Huang, C., *Chem. Commun.*, **2008**, 3387-3389; d) He, X.; Wu, C.; Qian, Y.; Li, Y.; Zhang, L.; Ding, F.; Chen, H.; Shen, J., *Analyst*, **2019**, *144*, 3807-3816.
27. Sahoo, S. K.; Crisponi, G., *Molecules*, **2019**, *24*, 3267.
28. a) Maity, D.; Govindaraju, T., *Inorg. Chem.*, **2011**, *50*, 11282-11284; b) Zhen, S. J.; Guo, F. L.; Chen, L. Q.; Li, Y. F.; Zhang, Q.; Huang, C. Z., *Chem. Commun.*, **2011**, *47*, 2562-2564; c) Shiraiishi, Y.; Matsunaga, Y.; Hirai, T., *Chem. Commun.*, **2012**, *48*, 5485-5487
29. a) Dodani, S. C.; He, Q.; Chang, C. J., *J. Am. Chem. Soc.*, **2009**, *131*, 18020-18021; b) Banerjee, A.; Sahana, A.; Guha, S.; Lohar, S.; Hauli, I.; Mukhopadhyay, S. K.; Sanmartín Matalobos, J.; Das, D. *Inorg. Chem.*, **2012**, *51*, 5699-5704; c) Kang, M. Y.; Lim, C. S.; Kim, H. S.; Seo, E. W.; Kim, H. M.; Kwon, O.; Cho, B. R., *Chem. Eur. J.*, **2012**, *18*, 1953-1960; d) Song, Y.; Tao, J.; Wang, Y.; Cai, Z.; Fang, X.; Wang, S.; Xu, H., *Inorg. Chim. Acta*, **2021**, *516*, 120099; e) Wang, X.; Liu, C.; Zhu, H.; Cheng, S.; Zhang, Y.; Su, M.; Rong, X.; Yu, M.; Sheng, W.; Zhu, B., *Sens. Actuators B*, **2022**, *369*, 132300.
30. a) Royzen, M.; Dai, Z.; Canary, J. W., *J. Am. Chem. Soc.*, **2005**, *127*, 1612-1613; b) Xiang, Y.; Tong, A.; Jin, P.; Ju, Y., *Org. Lett.*, **2006**, *8*, 2863-2866; c) Zhao, Y.; Zhang, X.-B.; Han, Z.-X.; Qiao, L.; Li, C.-Y.; Jian, L.-X.; Shen, G.-L.; Yu, R.-Q., *Anal. Chem.*, **2009**, *81*, 7022-7030; d) Goswami, S.; Sen, D.; Das, N. K., *Org. Lett.*, **2010**, *12*, 856-859; e) Li, P.; Duan, X.; Chen, Z.; Liu, Y.; Xie, T.; Fang, L.; Li, X.; Yin, M.; Tang, B., *Chem. Commun.*, **2011**, *47*, 7755-7757.
31. a) Nolan, E. M.; Jaworski, J.; Okamoto, K.-I.; Hayashi, Y.; Sheng, M.; Lippard, S. J., *J. Am. Chem. Soc.*, **2005**, *127*, 16812-16823; b) Atilgan, S.; Ozdemir, T.; Akkaya, E. U., *Org. Lett.*, **2008**, *10*, 4065-4067; c) Sivaraman, G.; Anand, T.; Chellappa, D. *Analyst*, **2012**, *137*, 5881-5884; d) Zhang, Z.; Wang, F.-W.; Wang, S.-Q.; Ge, F.; Zhao, B.-X.; Miao, J.-Y., *Org. Biomol. Chem.*, **2012**, *10*, 8640-8644; e) Xue, L.; Li, G.; Yu, C.; Jiang, H., *Chem. Eur. J.*, **2012**, *18*, 1050-1054; f) Masanta, G.; Lim, C. S.; Kim, H. J.; Han, J. H.; Kim, H. M.; Cho, B. R., *J. Am. Chem. Soc.*, **2011**, *133*, 5698-5700; g) Roopa; Kumar, N.; Bhalla, V.; Kumar, M., *Chem. Commun.*, **2015**, *51*, 15614-15628; h) Zastrow, M. L.; Radford, R. J.; Chyan, W.; Anderson, C. T.; Zhang, D. Y.; Loas, A.; Tzounopoulos, T.; Lippard, S. J., *ACS Sens.*, **2016**, *1*, 32-39; i) Komatsu, K.; Urano, Y.; Kojima, H.; Nagano, T., *J. Am. Chem. Soc.*, **2007**, *129*, 13447-13454; j) Lee, J. H.; Lee, J. H.; Jung, S. H.; Hyun, T. K.; Feng, M.; Kim, J.-Y.; Lee, J.-

- H.; Lee, H.; Kim, J. S.; Kang, C.; Kwon, K.-Y.; Jung, J. H., *Chem. Commun.*, **2015**, *51*, 7463–7465.
32. a) Sreenath, K.; Yuan, Z.; Allen, J. R.; Davidson, M. W.; Zhu, L., *Chem. Eur. J.*, **2015**, *21*, 867–874; b) Su, H. Z.; Chen, X. B.; Fang, W. H., *Anal. Chem.*, **2014**, *86*, 891–899; c) Sumalekshmy, S.; Henary, M. M.; Siegel, N.; Lawson, P. V.; Wu, Y. Schmidt, K.; Bredas, J.-L.; Perry, J. W.; Fahrni, C. J., *J. Am. Chem. Soc.*, **2007**, *129*, 11888–11889; d) Chen, X. – Y.; Shi, J.; Li, Y. –M.; Wang, F. –L.; Wu, X.; Guo, Q. –X.; Liu, L., *Org. Lett.*, **2009**, *19*, 4426–4429; e) Fang, L.; Watinkson, M., *Chem. Sci.*, **2020**, *11*, 11366–11379; f) Woodroffe, C. C.; Lippard, S. J., *J. Am. Chem. Soc.*, **2003**, *125*, 11458–11459; g) You, Y.; Lee, S.; Kim, T.; Ohkubo, K.; Chae, W.-S.; Fukuzumi, S.; Jhon, G.-J.; Nam, W.; Lippard, S. J., *J. Am. Chem. Soc.*, **2011**, *133*, 18328–18342; h) Wong, B. A.; Friedle, S.; Lippard, S. J., *J. Am. Chem. Soc.*, **2009**, *131*, 7142–7152; i) Du, P.; Lippard, S. J. *Inorg. Chem.*, **2010**, *49*, 10753–10755.
33. Chen, S. –Y.; Li, Z.; Li, K.; Yu, X. –Q., *Coord. Chem. Rev.*, **2021**, *429*, 213691.
34. Callan, J. F.; de Silva, A. P.; Magri, D. C., *Tetrahedron*, **2005**, *61*, 8551–8588.
35. Deng, R.; Wang, J.; Chen, R.; Huang, W.; Liu, X., *J. Am. Chem. Soc.*, **2016**, *138*, 15972–15979.
36. Junager, N. P. L.; Kongsted, J.; Astakhova, K., *Sensors*, **2016**, *16*, 1173.
37. Xu, H.; Zhu, C.; Chen, Y.; Bai, Y.; Han, Z.; Yao, S.; Jiao, Y.; Yuan, H.; He, W.; Guo, Z., *Chem. Sci.*, **2020**, *11*, 11037–11041.
38. a) Valeur, B.; Leray, I., *Coord. Chem. Rev.*, **2000**, *205*, 3–40; b) Gryniewicz, G.; Poenie, M.; Tsien, R. Y. *J. Biol. Chem.* **1985**, *260*, 3440–3450.
39. a) Gryniewicz, G.; Poenie, M.; Tsien, R. Y., *J. Biol. Chem.*, **1985**, *260*, 3440–3450; b) Tsien, R. Y., *Trends Neurosci.*, **1988**, *11*, 419–424.
40. a) Nolan, E. M.; Lippard, S. J., *Acc. Chem. Res.*, **2008**, *42*, 193–203; b) Wong, J.K.H.; Todd, M.H.; Rutledge, P.J., *Molecules*, **2017**, *22*, 200.
41. Kong, X.; Su, F.; Zhang, L.; Yaron, J.; Lee, F.; Shi, Z.; Tian, Y.; Meldrum, D.R., *Angew. Chem. Int. Ed.*, **2015**, *54*, 12053–12057.
42. a) Sui, B.; Yue, X.; Kim, B.; Belfield, K. D., *ACS Appl. Mater. Interfaces*, **2015**, *7*, 17565–17568; b) Ning, J.; Tian, Y., *Sens. Actuators B*, **2020**, *307*, 127659; c) Song, G.; Jiang, D.; Wang, L.; Ning, J.; Sun, X.; Su, F.; Chen, M.; Tian, Y., *Chem. Commun.*, **2020**, *56*, 5405–5408.
43. Farnum, D. G.; Mehta, G.; Moore, G. G. I.; Siegal, F. P., *Tetrahedron Lett.*, **1974**, *29*, 2549–2552.
44. A) Rochat, A. C.; Cassar, L.; Iqbal, A., (Ciba-Geigy AG), *Eur. Pat. Appl.* 94911, **1983**; b) Iqbal, A.; Jost, M.; Kirchmayr, R.; Rochat, A. C, *Bull. SOC. Chim. Belg.*, **1988**, *97*, 615–644.
45. Grzybowski, M.; Gryko, D. T., *Adv. Opt. Mater.*, **2015**, *3*, 280–320.
46. a) Liu, Q.; Bottle, S. E.; Sonar, P., *Adv. Mater.*, **2019**, *32*, 1903882; b) Molina, D.; Álvaro-Martins, M. J.; Sastre-Santos, Á., *J. Mater. Chem. C*, **2021**, *9*, 16078–16109; c) Yi, Z.; Wang, S.; Liu, Y., *Adv. Mater.*, **2015**, *27*, 3589–3606; d) Tang, A.; Zhan, C.; Yao, J.; Zhou, E., *Adv. Mater.*, **2017**, *29*, 1600013; e) Liu, Q.; Chavhan, S.; Zhang, H.; Sun, H.; Brock, A. J.; Manzhos, S.; Chen, Y.; Feron, K.; Bottle, S. E.; McMurtrie, J. C.; Jou, J.-H.; Chen, H.-S.; Nagar, M. R.; Hu, W.; Noh, Y.-Y.; Zhen, Y.; Sonar, P., *Adv. Electron. Mater.*, **2021**, *7*, 2000804; f) Shukla, A.; McGregor, S. K. M.; Wawrzinek, R.; Saggarr, S.; Moore, E. G.; Lo, S.-C.; Namdas, E. B., *Adv. Funct. Mater.*, **2021**, *31*, 2009817; g) Leventis, A.; Royackers, J.; Rapidis, A. G.; Goodeal, N.; Corpinot, M. K.; Frost, J. M.; Bucar, D. –K.; Blunt, M. O.; Cacialli, F.; Bronstein, H., *J. Am. Chem. Soc.*, **2018**, *140*, 1622–1626.
47. a) Mauck, C. M.; Hartnett, P. E.; Margulies, E. A.; Ma, L.; Miller, C. E.; Schatz, G. C.; Marks, T. J.; Wasielewski, M. R., *J. Am. Chem. Soc.*, **2016**, *138*, 11749–11761; b) Ye, C.; Mallick,

- S.; Hertzog, M.; Kowalewski, M.; Börjesson, K., *J. Am. Chem. Soc.*, **2021**, *143*, 19, 7501–7508; c) Papadopoulos, I.; Álvaro-Martins, M. J.; Molina, D.; McCosker, P. M.; Keller, P. A.; Clark, T.; Sastre-Santos, Á.; Guldi, D. M., *Adv. Energy Mater.*, **2020**, *10*, 2001496; d) Masoomi-Godarzi, S.; Liu, M.; Tachibana, Y.; Goerigk, L.; Ghiggino, K. P.; Smith, T. A.; Jones, D. J., *Adv. Energy Mater.*, **2018**, *8*, 1801720; e) Krishnapriya, K. C.; Roy, P.; Puttaraju, B.; Salzner, U.; Musser, A. J.; Jain, M.; Dasgupta, J.; Patil, S., *Nat. Commun.*, **2019**, *10*, 1-8.
48. Lee, Y.; Oh, J. Y.; Xu, W.; Kim, O.; Kim, T. R.; Kang, J.; Kim, Y.; Son, D.; Tok, J. B.-H.; Park, M. J.; Bao, Z.; Lee, T.-W., *Sci. Adv.*, **2018**, *4*, eaat7387.
49. Dhbaibi, K.; Favereau, L.; Srebro-Hooper, M.; Jean, M.; Vanthuyne, N.; Zinna, F.; Jamoussi, B.; Bari, L. D.; Autschbach, J.; Crassous, J., *Chem. Sci.*, **2018**, *9*, 735-742.
50. a) Pfenninger, J.; Iqbal, A.; Rochat, A. C.; Wallquist, O., (Ciba-Geigy AG), *Eur. Pat. Appl.* 184982, **1986**; b) Potrawa, T.; Langhals, H., *Chem. Ber.*, **1987**, *120*, 1075-1078; c) Morton, C. J. H.; Riggs, R. L.; Smith, D. M.; Lightfoot, P.; Slawin, A. M. Z.; MacLean, E. J., *Tetrahedron*, **2002**, *58*, 5547-5565; d) Stas, S.; Balandier, J.-Y.; Lemaure, V.; Fenwick, O.; Tregnago, G.; Quist, F.; Cacialli, F.; Cornil, J.; Geerts, Y. H., *Dyes Pigm.*, **2013**, *97*, 198–208; e) Ding, S.; Ni, Z.; Hu, M.; Qiu, G.; Li, J.; Ye, J.; Zhang, X.; Liu, F.; Dong, H.; Hu, W., *Macromol. Rapid Commun.*, **2018**, *39*, 1800225; f) Jiang, Z.; Ni, Z.; Wang, H.; Wang, Z.; Zhang, J.; Qiu, G.; Fang, J.; Zhang, Y.; Dong, H.; Lu, K.; Hu, W.; Wei, Z., *Polym. Chem.*, **2017**, *8*, 5603–5610; g) Qiu, G.; Jiang, Z.; Ni, Z.; Wang, H.; Dong, H.; Zhang, J.; Zhang, X.; Shu, Z.; Lu, K.; Zhen, Y.; Wei, Z.; Hu, W., *J. Mater. Chem. C*, **2017**, *5*, 566–572; h) Wang, X.; Jiang, B.; Du, C.; Ren, X.; Duan, Z.; Wang, H., *New J. Chem.*, **2019**, *43*, 16411–16420.
51. Pieczykolan, M.; Sadowski, B.; Gryko, D. T., *Angew. Chem. Int. Ed.*, **2020**, *59*, 7528–7535.
52. a) Li, W.; Wang, L.; Tang, H.; Cao, D., *Dyes Pigm.* **2019**, *162*, 934-950; b) Auwalu, M. A.; Cheng, S., *Chemosensors*, **2021**, *9*, 44.
53. Qu, Y.; Hua, J.; Tian, H., *Org. Lett.*, **2010**, *12*, 3320-3323.
54. a) Zhang, G. J.; Li, H. Y.; Bi, S. M.; Song, L. F.; Lu, Y. X.; Zhang, L.; Yua, J. J.; Wang, L. M., *Analyst*, **2013**, *138*, 6163–6170; b) Zhang, G. J.; Bi, S. M.; Song, L. F.; Wang, F.; Yu, J. J.; Wang, L. M., *Dyes Pigm.*, **2013**, *99*, 779–786.
55. a) Du, C. C.; Fu, S. B.; Ren, X. L.; Wang, X. H.; Wang, Z.; Zhou, J.; Wang, H. Y., *New J. Chem.*, **2018**, *42*, 3493–3502; b) Du, C. C.; Fu, S. B.; Wang, X. H.; Sedgwick, A. C.; Zhen, W.; Li, M.; Li, X.; Zhou, J.; Wang, Z.; Wang, H. Y.; Sessler, J. L., *Chem. Sci.*, **2019**, *10*, 5699-5704.
56. Li, J.; Yim, D.; Jang, W. -D.; Yoon, J., *Chem. Soc. Rev.*, **2017**, *46*, 2437-2458.
57. Lee, M. H.; Kim, J. S.; Sessler, J. L., *Chem. Soc. Rev.*, **2015**, *44*, 4185–4191.
58. a) Ning, P.; Jiang, J. C.; Li, L. C.; Wang, S. X.; Yu, H. Z.; Feng, Y.; Zhu, M.Z.; Zhang, B. C.; Yin, H.; Guo, Q. X.; Meng, X. M., *Biosens. Bioelectron.*, **2016**, *77*, 921–927; b) Zastrow, M. L.; Radford, R. J.; Chyan, W.; Anderson, C. T.; Zhang, D. Y.; Loas, A.; Tzounopoulos, T.; Lippard, S. J., *ACS Sens.*, **2016**, *1*, 32–39; c) Komatsu, K.; Urano, Y.; Kojima, H.; Nagano, T., *J. Am. Chem.Soc.*, **2007**, *129*, 13447–13454; d) Lee, J. H.; Lee, J. H.; Jung, S. H.; Hyun, T. K.; Feng, M.; Kim, J.-Y.; Lee, J.-H.; Lee, H.; Kim, J. S.; Kang, C.; Kwon, K.-Y.; Jung, J. H., *Chem. Commun.*, **2015**, *51*, 7463–7465; e) Sreenath, K.; Yuan, Z.; Allen, J. R.; Davidson, M. W.; Zhu, L., *Chem. Eur. J.*, **2015**, *21*, 867–874; f) Su, H.Z.; Chen, X. B.; Fang, W. H.; *Anal. Chem.*, **2014**, *86*, 891–899.
59. a) Zhu, S.; Zhang, J.; Janjanam, J.; Vegesna, G.; Luo, F.-T.; Tiwari, A.; Liu, H., *J. Mater. Chem. B*, **2013**, *1*, 1722–1728; b) Xue, L.; Li, G.; Yu, C.; Jiang, H., *Chem. Eur. J.*, **2012**, *18*, 1050-1054; c) Masanta, G.; Lim, C. S.; Kim, H. J.; Han, J. H.; Kim, H. M.; Cho, B. R., *J. Am. Chem. Soc.*, **2011**, *133*, 5698-5700; d) Peng, S.; He, Q.; Vargas-Zúñiga, G. I.; Qin, L.

- Hwang, I.; Kim, S. K.; Heo, N. J.; Lee, C.-H.; Dutta, R.; Sessler, J. L., *Chem. Soc. Rev.*, **2020**, *49*, 865-907; e) Kanegae, A.; Takata, Y.; Takashima, I.; Uchinomiya, S.; Kawagoe, R.; Usui, K.; Yamashita, A.; Wongkongkatep, J.; Sugimoto, M.; Ojida, A., *Commun. Chem.*, **2021**, *4*, 104; f) Lim, N. C.; Brückner, C., *Chem. Commun.*, **2004**, 1094–1095.
60. Obare, S. O.; Murphy, C. J., *Inorg. Chem.*, **2001**, *40*, 6080–6082.
61. Citterio, D.; Takeda, J.; Kosugi, M.; Hisamoto, H.; Sasaki, S.; Komatsu, H.; Suzuki, K., *Anal. Chem.*, **2007**, *79*, 1237-1242.
62. Gupta, V. K.; Singh, A. K.; Kumawat, L. K.; Mergu, N., *Sens. Actuators B*, **2016**, 468-482.
63. Jiao, S. -Y.; Peng, L. -L.; Li, K.; Xie, Y. -M.; Ao, M. -Z.; Wang, X.; Yu, X. -Q., *Analyst*, **2013**, *138*, 5762-5768.
64. Stubing, D. B.; Heng, S.; Abell, A. D., *Org. Biomol. Chem.*, **2016**, *14*, 3752-3757.

7. Original publications

Switch-On Diketopyrrolopyrrole-Based Chemosensors for Cations Possessing Lewis Acid Character

 G. Dinesh Kumar,^[a] Marzena Banasiewicz,^[b] Denis Jacquemin,^{*,[c]} and Daniel T. Gryko^{*,[a]}

Abstract: For the first time diketopyrrolopyrroles (DPPs) have been synthesized directly from nitriles possessing (aza)crown ethers leading to macrocycle-dye hybrids. Depending on the nature of the linkage between DPP and macrocyclic ring, various coordination effects are found. The strong interaction of the cations possessing Lewis acid character such as Li⁺, Mg²⁺ and Zn²⁺ with 2-aminopyridin-4-yl-DPPs, leading to a bathochromic shift of both emission and absorption, as well as to strong enhancement of fluorescence was rationalized in terms of strong binding of these cations to the N=C–NR₂

functionality. The same effect has been observed for protonation. Depending on the size and the structure of the macrocyclic ring the complexation of cations by aza-crown ethers plays an important but secondary role. The interaction of Na⁺ and K⁺ with 2-aminopyridin-4-yl-DPPs leads to moderate enhancement of fluorescence due to the aza-crown ethers binding. The very weak fluorescence of DPP bearing 2-dialkylamino-pyridine-4-yl substituents is due to the closely lying T₂ state and the resulting intersystem crossing.

Introduction

Detection and binding of metal cations has come a long way since Pedersen's pioneering discovery of crown ethers.^[1] These macrocycles, and their aza-crown ether analogues, are ideal recognition components for monitoring alkali metal cations and consequently they have been widely used as receptors in fluorescent probes. The predominant design of such probes is based on photoinduced electron transfer (PET) and the probes typically comprise both a fluorophore and a recognition unit linked through a methylene unit or longer electronically isolating bridge.^[2,3] Independent optimizations of fluorophores^[4] and macrocyclic ethers and cryptands have enabled selective sensing of K⁺,^[5] Na⁺,^[6] and Li⁺^[7] with high specificity.^[8] More advanced options for studying these cations in biological samples including two-photon absorption have been proposed as well.^[9]

On the other hand, markedly less is known about the photophysical consequences of directly linking a fluorophore with the recognition unit.^[10] Such probes are sometimes based on photoinduced charge transfer (PCT). If a dye is polarized, the binding of cation to electron-donating group causes reducing the electron-donating character of this group, resulting in emission blue-shift. Valeur and co-workers studied 3-

carboxamido-coumarins possessing crown ethers on the amide group and showed that decrease in the HOMO-LUMO gap is observed leading to a bathochromic shift of emission upon complexation.^[11]

This article interrogates how the linkage of an (aza)crown unit with a chromophore through aryl substituents, along with the type of macrocyclic ring, affects the fluorescence response. We employ derivatives of diketopyrrolopyrroles (DPPs), which belong to a class of organic dyes with great potential for photonic and electronic applications.^[12] Although, the synthesis of DPPs is well advanced,^[13,14] to the best of our knowledge, DPPs have rarely been used as fluorophores to study the recognition of metal cations, and all existing examples we are aware of rely on PET.^[15]

Results and Discussion

In order to investigate the effect of an alkali ion binding site directly connected to a fluorophore we decided to design probes with either a crown ether moiety directly fused, or an azacrown moiety attached *via* a nitrogen atom, to an aryl group of a DPP dye. For the former case, crown ethers of differing sizes including 18-crown-6, 15-crown-5 and 21-crown-7 were chosen as Na⁺/K⁺-ionophores to ascertain the effect alkali binding strength has on the fluorescent properties. In the case of the latter, we have previously identified that when 2-dialkylaminopyridine substituents are attached to a DPP core, a rare example of a non-fluorescent DPP dye can be formed, making azacrown ethers built from this amino group a great place to start in the search for desirable 'switch-on' fluorescent sensors.^[16] We reasoned that recovery of fluorescence in the presence of a particular analyte from this dark mode can be possible. As these DPPs possess a dialkylamino group at the *meta* position relative to the bond with the DPP core the coupling is expected to be weak. The electronic coupling between donors and acceptors linked by benzene rings varies

[a] G. D. Kumar, Prof. D. T. Gryko
 Institute of Organic Chemistry
 Polish Academy of Sciences
 Kasprzaka 44/52, 01-224 Warsaw (Poland)
 E-mail: dtgryko@icho.edu.pl

[b] Dr. M. Banasiewicz
 Institute of Physics
 Polish Academy of Sciences
 Al. Lotników 32/46, 02-668 Warsaw (Poland)

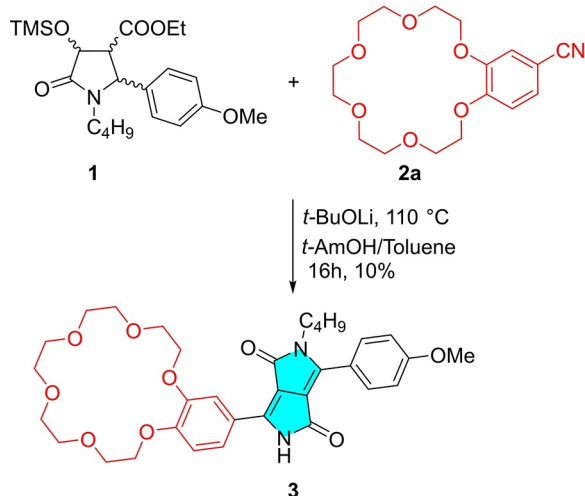
[c] Prof. D. Jacquemin
 CEISAM UMR 6230, CNRS, Université de Nantes
 44000 Nantes (France)
 E-mail: Denis.Jacquemin@univ-nantes.fr

Supporting information for this article is available on the WWW under <https://doi.org/10.1002/asia.202001376>

depending on their relative positions; *ortho* and *para* configurations ensure strong electronic coupling, whereas *meta* does not.^[17]

The required nitriles were either synthesized following literature procedures^[18] or from 2-fluoro-4-cyanopyridine and an appropriate azacrown ether *via* nucleophilic aromatic substitution in decent yields (see the ESI for details). Initially we attempted to use the classical DPP synthesis and nitriles **2a–2g** were condensed with diisopropyl succinate. These reactions failed to give the desired symmetric diketopyrrolopyrroles. Given that analogous 3,4-dimethoxybenzonitrile and 2-morpholine-4-cyanopyridine react smoothly^[16,19] the origin of this failure is rather unclear. We have recently developed a new technique which overcomes the problem of low nitrile reactivity which relies on the condensation of a nitrile with a pyrrolidin-2-one **1**.^[20] The reaction of benzo-18-crown-6 nitrile **2a**, with pyrrolidin-2-one **1** proceeded smoothly under these conditions to give unsymmetrical DPP **3** in a low yield of 10% (Scheme 1). After determining the chemical structure of DPP **3** the methodology was extended to benzo-15-crown-5 DPP **4** (5% yield) and benzo-21-crown-7 DPP **5** (20% yield). The pyridine-2-aza-crown ether DPPs **6**, **7** and **8** were obtained in 13%, 18% and 22% yield respectively (Figure 1). The increase in yields observed for the pyridine-substituted DPPs compared to the benzo-crown ether DPPs is attributed to the CN group being located at the strongly activating 4-position of a pyridine ring.

Photophysical studies of unsymmetrical DPPs **3–8** were performed in CH₃CN. DPPs **3–5** bearing benzo-18-crown-6, benzo-15-crown-5 and benzo-21-crown-7 units, respectively, have absorption maximum at 499 nm i.e. bathochromically shifted by 5 nm compared to an analogous DPP possessing a 3-bromo-4-methoxyphenyl substituent (Figure 2).^[20] This, in addition to the same λ_{em}^{max} highlights that the presence of an alkoxy group at position 3 of the benzene ring has almost no influence on the electronic properties of DPPs. The fluorescence quantum yields of DPPs **3–5** are 96%, 86% and 80% respectively, which corresponds well with analogous DPPs, that are known to be highly emissive.^[15,20]



Scheme 1. Exemplary synthesis of diketopyrrolopyrrole **3**.

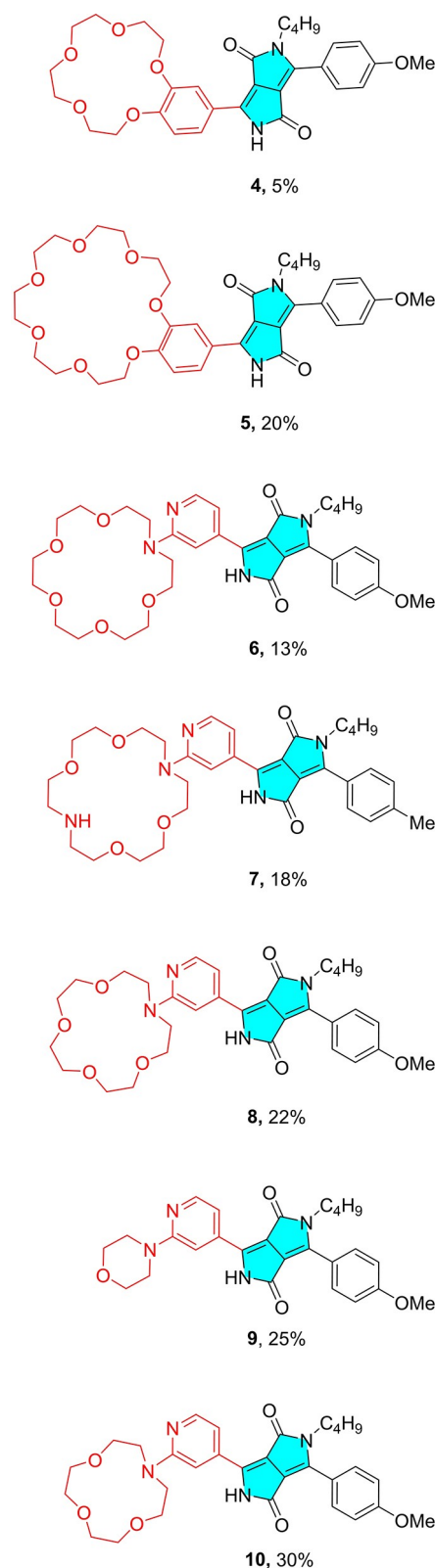


Figure 1. The structures of the synthesized diketopyrrolopyrroles **4–10**.

The absorption of DPPs **6–8** bearing pyridine-aza-crown ether scaffolds showed identical absorption maxima (around 494–498 nm) compared to their analogue i.e. 2-butyl-3-(4-

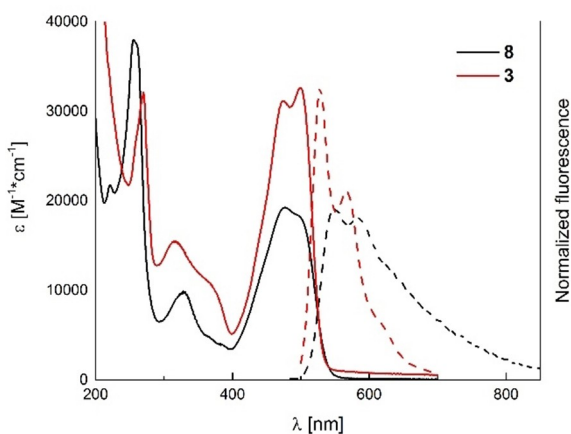


Figure 2. Absorption (solid) and emission (dotted) spectra of dyes **3** (red line) and **8** (black line) measured in acetonitrile.

methoxyphenyl)-6-(pyridin-4-yl)-diketopyrrolopyrrole (Figure 2, Table 1).^[20]

Interestingly, the same is true for emission maxima, there is a hypsochromic shift of the emission maxima by 10 nm although weak fluorescence and broad signals in the case of DPPs **6–8** causes uncertainties in the comparison.^[20] The

Table 1. Photophysical properties of DPPs **3–10** measured in acetonitrile.

DPP	$\lambda_{\text{abs}}^{\text{max}}$ [nm]	$\lambda_{\text{em}}^{\text{max}}$ [nm]	$\phi^{[a]}$ [%]
3	499	528, 567	96
4	499	528, 567	86
5	499	528, 566	80
6	498	549, 588	1.0
7	494	542, 641	3.0
8	496	548, 585	1.4
9	496	553, 585	0.8
10	499	549, 587	1.6

[a] Rh6G in EtOH as a standard.

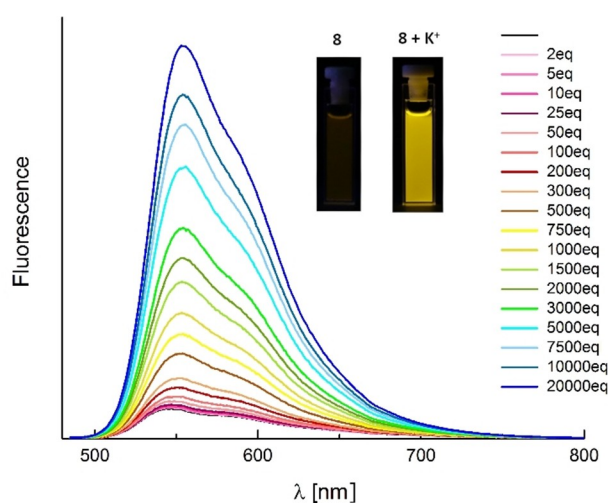


Figure 3. The effect of KBF_4 addition on the emission spectra of DPP **8** measured in acetonitrile.

fluorescence quantum yields of DPPs **6–8** in CH_3CN are extremely low compared to their analogue possessing a simple pyridin-4-yl substituent but remain on the same level as its symmetric analogue described by us earlier (Table 1).^[16,20]

To validate the metal cation sensing capabilities, complexation studies were performed with all six crown-DPPs (see Figures 3 and 4 and ESI). We noticed a fundamental difference in the behavior of crown-DPPs **3–5** vs. **6–8**.

Initially, we performed titration experiments with benzocrown DPPs **3–5** in CH_3CN with addition of 0–20000 eq. of Li^+ , Na^+ and K^+ . The emission of DPPs **3–5** do not undergo any notable changes in the presence of LiClO_4 , KPF_6 or NaClO_4 (Figures S2–S16). There is 10–15% decrease in the emission intensity in the presence of 10,000 eq. regardless of the size of the macrocycle and the type of cation. There is no doubt that sodium and potassium complexation occurs, since the size of the crown ethers is known to be compatible with the radii of Na^+ and K^+ ions.^[21] The complexation, however, does not seem to markedly alter the electronic structure of the DPPs.

On the other hand, in DPPs **6–8** possessing 2-dialkylamino-pyridin-4-yl substituents (where alkyl is a crown ether) the fluorescence increases in the presence of both sodium and potassium salts (Figure 3, Tables 2 and 3 and ESI). The fluorescence of DPP **6** increases by the factor of 7 in the presence of 1000 eq. of Na^+ , however an increased concentration of K^+ (1000 eq.) results in a 13-fold fluorescence enhancement which is bathochromically shifted by 9 nm. DPP **8** showed a reversed fluorescence response in the presence of 1000 eq. Na^+ (7-fold) and 1000 eq. K^+ (4-fold) which is related to smaller size of the macrocycle. Much weaker fluorescence response has been registered for DPP **7**. This is undoubtedly related to the lack of compatibility originating from too large size of the macrocycle in the case of Na^+ and the presence of additional nitrogen atom in the case of K^+ . The most striking difference, however, is the effect of the addition of LiClO_4 to solutions of dyes **6–8** (Tables 2–3, Figures 4–5). In all cases there is significant bathochromic shift of both absorption and

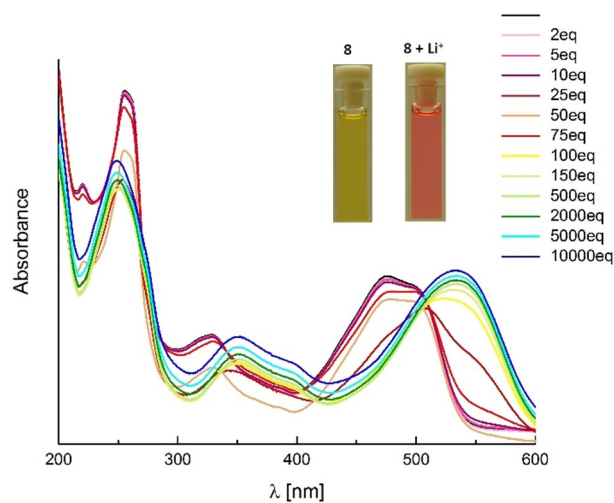


Figure 4. The effect of LiClO_4 addition on the absorption spectra of DPP **8** measured in acetonitrile.

Table 2. Enhancement of fluorescence of DPPs 6–10 in the presence of 1000 eq. of various salts or in the presence of 5 eq. PhSO₃H in acetonitrile.

DPP	LiClO ₄	NaClO ₄	KPF ₆	Mg(ClO ₄) ₂	Zn(ClO ₄) ₂	PhSO ₃ H
6	22.5	7	13	45	28	30
7	34	2.3	1.5	8	25	26
8	10	7	4	22	22	16
9	30	nd	nd	4	17	26.5
10	19	nd	nd	nd	nd	nd

nd – non-determined.

Table 3. The fluorescence quantum yields of DPPs 3–10 in the presence of 1000 eq. of various salts or in the presence of 5 eq. PhSO₃H, measured in acetonitrile.

DPP	LiClO ₄	NaClO ₄	KPF ₆	Mg(ClO ₄) ₂	Zn(ClO ₄) ₂	PhSO ₃ H
3	90	91	90	nd	nd	nd
4	81	80	79	nd	nd	nd
5	76	74	75	nd	nd	nd
6	28	6.0	14	43	30	37
7	94	7.1	4.9	22	76	75
8	16	14	7.8	32	30	25
9	22	nd	nd	3.5	14	23
10	31	nd	nd	nd	nd	nd

[a] Rh6G in EtOH as a standard. nd – non-determined.

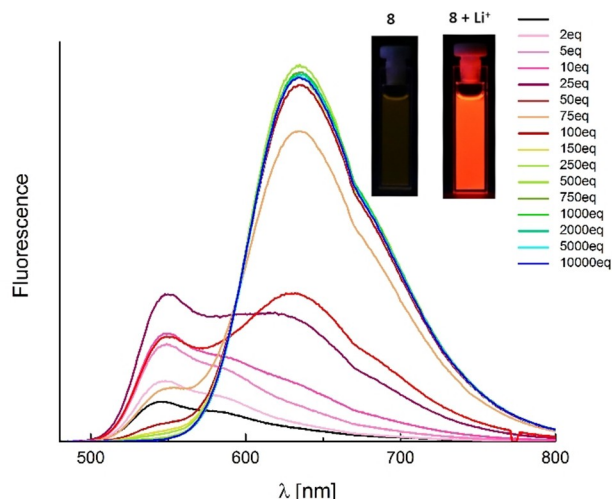


Figure 5. The effect of LiClO₄ addition on the emission spectra of DPP 8 measured in acetonitrile.

emission. The bathochromic shift of absorption means that the addition of lithium salts changes the electronic structure of DPPs 6–8. The interaction of DPPs 6–8 with Li⁺ was investigated by titration. The fluorescence intensity of DPP 6 increased 22.5 times in presence of 1000 eq. Li⁺ and red shifted by 80 nm (see ESI), whereas the fluorescence enhancement of DPP 8 was 10-fold under the same conditions. Interestingly, the strongest fluorescence enhancement was observed for DPP 7 (34 times in the presence of 1000 eq. of Li⁺).

Given that neither benzo-18-crown-6 nor benzo-15-crown-5 are truly compatible with lithium cations, the working hypothesis was that the interaction of lithium with the 2-dialkylamino-pyridine unit is responsible for this striking effect. The fact that DPP bearing the least fitting 1,10-diaza-18-crown-6 gave the

strongest enhancement seems to corroborate this hypothesis. To validate this assumption analogous diketopyrrolopyrroles 9 and 10 possessing either 2-morpholino-4-pyridyl or 2-(1-aza-12-crown-4)-4-pyridyl as substituents were synthesized and their photophysics were investigated (Figure 1). 1-Aza-12-crown-4 is well known for its strong Li⁺ binding and it is utilized in majority of lithium probes.^[7]

DPPs 9 and 10 turned out to possess almost identical absorption/emission characteristics compared to DPPs 6–8 (Table 1). Addition of LiClO₄ gave identical changes to both absorption and emission as compared with these macrocyclic dyes. In the case of DPP 9 the strong, almost 30-fold fluorescence enhancement which was markedly bathochromically shifted by 117 nm in the presence of 1000 eq. of Li⁺ was registered. Interestingly, a weaker response has been observed for DPP 10 (Table 1). These data give evidence that the absorption and emission changes of DPPs 6–10 in the presence of lithium cation should be attributed to its interaction with 2-dialkylaminopyridine moiety. This provides evidence that Li⁺ interacts strongly with the amidine type functionality giving rise to significant perturbation of the electronic structure. This is not unprecedented since apparent basicity of DBU is increased in the presence of LiBr.^[22,23] Murphy and Okada discovered that 1,10-phenanthroline interacts with LiClO₄ giving rise to drastic changes of optoelectronic properties as result of complexation.^[7d,24] Similar observations were also made for macrocyclic ligand possessing two 1,10-phenanthroline moieties.^[25] Indeed complexation properties of lithium cation towards nitrogen chelating ligands are broadly used in directed *ortho*-lithiation methodology (Li⁺-TMEDA complex).^[26]

The change of emission of DPPs 6–10 in the presence of Li⁺ roughly corresponds to the effect of protonation of analogous, symmetrical DPP possessing two 2-morpholino-4-pyridyl substituents.^[16] It is noteworthy that lithium ion sensors^[7,27] are

sought for monitoring ion transport in lithium ion batteries^[28] and for biomedical applications.^[29]

These studies inclined us to investigate the effects of Brønsted and Lewis acids on the absorption and emission of DPPs 6–10. The benzenesulfonic acid, magnesium perchlorate and zinc perchlorate were selected for this study. The addition of already small amounts (1–5 eq.) of PhSO₃H, Mg(ClO₄)₂ and Zn(ClO₄)₂ induced comparable changes to the effect observed for larger excess of LiClO₄. Both the absorption and emission were markedly bathochromically shifted and the fluorescence quantum yield enhancement was in the range of 4 to 45 (Figures S15–S53, Tables 2–3). These results corroborate the reasoning stated above: not the specific interaction of given metal cation with macrocyclic units but interaction of H⁺ or cations displaying Lewis acid properties with 2-dialkylaminopyridine moiety is responsible for changes in electronic properties of DPPs, which are reflected by enhancement of Φ . Indeed the magnitude of change in the presence of 1 equiv. of salts/PhSO₃H strongly depends on the strength of an acid. Still, the effect of the size and the character of the macrocyclic ring is substantial. The difference in the enhancement of emission of between DPPs 6 and 7 in the presence of Mg(ClO₄)₂ is ca. 5.5, reflecting the well-known fact that Mg²⁺ has stronger binding to crown ethers possessing less nitrogen atoms. If 15-crown-5 is present (DPP 8) no differentiation between Mg²⁺ and Zn²⁺ is observed (Tables 2–3). Finally, lack of macrocyclic units (DPPs 6–8 → DPP 9) decreases the fluorescence response for both these cations.

To gain additional insights into the nature of the excited states of the various compounds, we used Time-Dependent Density Functional Theory calculations relying on a well-known protocol (i.e., PCM(LR+cLR)-TD-M06-2X/6-311+G(2d,p), see details in the experimental Section).^[30] We used a simplified structures for the sake of computational effort: the crown ethers were replaced by methyl groups, as we do not focus on the complexation with cations in this theoretical part (Figure S1). Theory reveals a bright π - π^* low-lying S₁ state for all dyes with relatively mild geometric relaxation in the excited state, as expected for DPP derivatives. The 0–0 wavelengths that have been determined are 519 nm, 525 nm, 520 nm and 531 nm for our models of 3/4/5, 6/8, 7, and 9, respectively. These values do compare very well both qualitatively and quantitatively with the experimental values of the absorption/emission crossing points (see above), indicating that the chosen method is suited for the dyes under investigation. The density difference plots determined for these compounds are displayed in Figure 6. In all compounds, the excited-state is mainly localized on the DPP core. As expected, the methoxy groups on the side act as very mild donor groups, whereas the nitrogen of the pyridine is mostly an acceptor (in 6–9). In contrast, the nitrogen of the crown ether attached in the *meta* position in 6–9 isn't involved in the excitation process. This shows that although a conjugated moiety is used to connect the sensing group to the fluorophore, the direct electronic communication remains rather limited.

A striking effect that needs to be understood is the large difference in the emission quantum yields between 3–5, and 6–

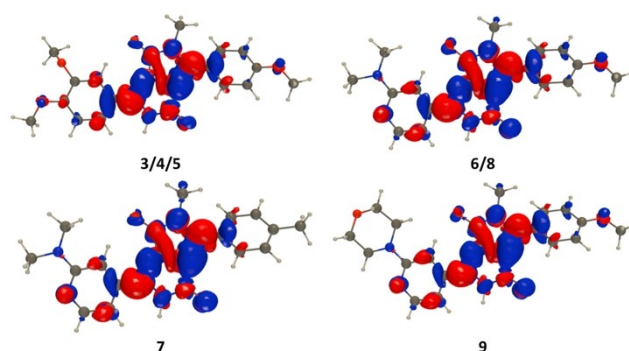


Figure 6. Representation of the difference of total electronic densities between the lowest excited state and the ground state. The blue and red lobes represent decrease and increase of density upon excitation, respectively.

9 (Table 1), the former group exhibiting much higher emission yields. We first suspected the appearance of a TICT quenching state due to the presence of the *N,N*-dialkyl groups in the second series. However, performing a scan by rotating the morpholine group with respect to the pyridyl from 0° to 90° in 9 revealed only one minimum at the LR+cLR-TD-M06-2X level, corresponding to the structure displayed in Figure 6. This result is the logical consequence of the rather passive role of the nitrogen of the morpholine in the structure. Next, we envisaged the possibility of intersystem crossing (ISC). In 3/4/5, there is only one triplet state below the bright S₁ at the optimal geometry of the fluorescent state, but this triplet is very distant energetically, the S₁-T₁ gap being 1.40 eV. The second triplet is 0.36 eV above S₁ for 3/4/5 and is therefore not accessible. Clearly ISC is very improbable in those DPPs. In strong contrast in 6/8 (7), a second triplet becomes very close to S₁ with a S₁-T₂ gap being 0.02 (0.08) eV, so that an ISC from S₁ to T₂ can be envisaged. We computed a SOC coupling of ca. 0.1–0.2 cm⁻¹ for that ISC process, typical values in organic compounds without heavy atoms. We therefore interpret the quenching of the emission in 6–9, as being related to the presence of an accessible triplet state, rather than a TICT phenomenon.

Conclusion

In this study we identified a new class of sensing fluorophores possessing electronically linked 2-dialkylaminopyridine and diketopyrrolopyrrole moieties. Both the protonation and the interaction with cations possessing Lewis acid character such as Li⁺, Mg²⁺ and Zn²⁺ trigger strong fluorescence enhancement. The detection process harnesses the unique property of diketopyrrolopyrroles bearing 2-dialkylaminopyridine i.e. exceptionally weak fluorescence which can be enhanced *via* forming the complexes. The compatibility between given cation and the azacrown ether plays secondary but important role modulating to the emission enhancement. Placing dialkylamino groups at the *meta* position of the pyridin-4-yl substituent ensures electronic coupling with the principal DPP chromophore core that is sufficiently strong to make S–T gaps very small leading

to intersystem crossing, hence fluorescence quenching. This feature combined with fluorescence recovery upon interaction with lithium, magnesium and zinc cations makes these DPPs ideally suited as a new generation of sensors. The successful development of this sensing mode expands the field of sought after "turn-on" sensors to include DPP and is anticipated to drive further advances investigations into similar systems.

Experimental Section

All reagents and solvents were purchased from commercial sources and were used as received unless otherwise noted. Reagent grade solvents (CH_2Cl_2 , hexanes) were distilled prior to use. Transformations with moisture- and oxygen-sensitive compounds were performed under a stream of argon. The reaction progress was monitored by means of thin-layer chromatography (TLC), which was performed on aluminum foil plates, covered with silica gel 60 F254. Product purifications were done by means of column chromatography with Kieselgel 60. The identity and purity of prepared compounds were proved by ^1H NMR and ^{13}C NMR, as well as by mass spectrometry (via EI-MS or ESI-MS). HRMS (ESI-TOF) and HRMS (EI): double-focusing magnetic sector instruments with EBE geometry were utilized. NMR spectra were measured on 400 or 500 MHz instruments. Chemical shifts (δ , ppm) were determined with tetramethylsilane (TMS) as the internal reference; J values are given in Hz. All melting points for crystalline products were measured with an automated melting point apparatus and are given without correction.

2-Butyl-3-(4-methoxyphenyl)-6-(decahydro benzohexaoxacyclooctadecan-18-yl)-2,5-dihydropyrrolo[3,4-c]pyrrole-1,4-dione (3).

In flame dried Schlenk flask under argon atmosphere $t\text{BuOLi}$ (4 equiv. 1.42 g, 17.8 mmol) was placed, followed by decahydrobenzohexaoxacyclooctadecan-18-carbonitrile **2a** (1 equiv. 1.5 g, 4.4 mmol). Schlenk flask was placed in preheated oil bath (110°C), next compound **1** (1 equiv. 1.82 g, 4.4 mmol) dissolved in *tert*-amyl alcohol (4 mL) and toluene (2 mL) was added dropwise over an hour. After completion of addition reaction mixture was stirred at same temperature for next 16 h. After cooling to room temperature reaction mixture was diluted with DCM (100 mL) and extracted with water (100 mL), water phase was one more time washed with DCM (50 mL). The combined organic phases were dried with Na_2SO_4 , filtered and concentrated in vacuum. The resulting crude compound was chromatographed on silica gel (DCM/MeOH = 9:1) and crystallization from DCM/hexanes allowed to obtain product **3** as shiny red crystals in 10% yield, 200 mg, m.p. = 221°C . ^1H NMR (500 MHz, CDCl_3) δ 9.9 (s, 1H), 8.2 (s, 1H), 7.83 (s, 1H), 7.81 (d, J = 8.8 Hz, 2H), 7.03 (d, J = 8.5 Hz, 2H), 6.9 (d, J = 8.5 Hz, 1H), 4.29–4.22 (m, 4H), 3.97 (t, J = 8.3 Hz, 2H), 3.83–3.79 (m, 7H), 3.75–3.69 (m, 11H), 1.63 (p, J = 15.5 Hz, 2H), 1.45 (t, J = 14.4 Hz, 1H), 1.3 (sextet, J = 18.5 Hz, 2H), 0.88 (t, J = 7.5 Hz, 3H). ^{13}C NMR (126 MHz, CDCl_3) δ 163.7, 162.7, 161.6, 152.0, 148.9, 146.8, 144.6, 130.6, 121.5, 121.0, 120.8, 114.3, 113.0, 112.8, 110.1, 108.4, 70.9, 70.8, 70.7, 70.5, 69.4, 69.3, 68.9, 55.5, 41.9, 31.6, 20.0, 13.6. HRMS (ESI, m/z): [M + H]⁺ + Calcd. for $\text{C}_{33}\text{H}_{40}\text{N}_2\text{O}_9$: 608.6880; found, 631.2637[M + Na].

2-Butyl-3-(4-methoxyphenyl)-6-(octahydro bezopentaoxacyclooctadecan-15-yl)-2,5-dihydropyrrolo[3,4-c]pyrrole-1,4-dione (4).

DPP **4** was obtained following both the procedure and the purification described above for DPP **3** as red crystals in 5% yield, 180 mg, m.p. = 223°C . ^1H NMR (500 MHz, CDCl_3) δ 9.91 (s, 1H), 8.15 (s, 1H), 7.85 (s, 1H), 7.8 (d, J = 6.9 Hz, 2H), 7.03 (d, J = 6.7 Hz, 2H), 6.8 (d, J = 7.2 Hz, 1H), 4.23 (d, J = 15.8 Hz, 4H), 3.9 (d, J = 26.9 Hz, 6H), 3.78 (d, J = 14.1 Hz, 14H), 1.76 (s, 2H), 1.61 (s, 2H), 1.29 (d, J = 6.3 Hz, 3H), 0.88 (t, J = 7.5 Hz, 3H). ^{13}C NMR (126 MHz, CDCl_3) δ 163.7, 162.7,

161.7, 146.8, 144.5, 130.7, 121.8, 121.2, 120.8, 114.3, 113.0, 112.8, 110.1, 108.5, 70.9, 70.3, 69.2, 55.4, 41.9, 31.6, 20.0, 13.6. HRMS (ESI, m/z): [M + H]⁺ + Calcd. for $\text{C}_{31}\text{H}_{36}\text{N}_2\text{O}_8$: 564.6350; found, 587.2369[M + Na].

2-Butyl-3-(4-methoxyphenyl)-6-(2,3,5,6,8,9,11,12,14,15,17,18-decahydro-1,4,7,10,13,16,19-benzoheptaoxacycloheptacosin-21-yl)-2,5-dihydropyrrolo[3,4-c]pyrrole-1,4-dione (5).

DPP **5** was obtained following both the procedure and the purification described above for DPP **3** as red crystals in 20% yield, 400 mg, m.p. = 185 – 187°C . ^1H NMR (500 MHz, CDCl_3) δ 10.0 (s, 1H), 8.17 (s, 1H), 7.8 (d, J = 8.6 Hz, 3H), 7.03 (d, J = 8.8 Hz, 2H), 6.9 (d, J = 8.5 Hz, 1H), 4.29–4.22 (m, 4H), 3.97 (t, J = 9.0 Hz, 4H), 3.83–3.79 (m, 8H), 3.75–3.69 (m, 18H), 1.63 (p, J = 15.5 Hz, 2H), 1.3 (sextet, J = 18.5 Hz, 2H), 0.88 (t, J = 7.5 Hz, 3H). ^{13}C NMR (126 MHz, CDCl_3) δ 163.7, 162.7, 161.7, 151.9, 148.9, 147.0, 144.5, 130.6, 121.5, 121.1, 120.7, 114.3, 113.1, 112.9, 110.0, 108.4, 71.3, 71.2, 71.1, 70.8, 70.6, 70.5, 69.5, 69.2, 69.1, 55.5, 41.9, 31.6, 20.0, 13.6. HRMS (ESI, m/z): [M + H]⁺ + Calcd. for $\text{C}_{35}\text{H}_{44}\text{N}_2\text{O}_{10}$: 652.7410; found, 675.2910[M + Na].

2-Butyl-3-(4-methoxyphenyl)-6-(1,4,7,10,13-pentaoxa-16-azacyclooctadecane,16-(2-pyridine-4-yl)-2,5-dihydropyrrolo[3,4-c]pyrrole-1,4-dione (6).

DPP **6** was obtained following both the procedure and the purification described above for DPP **3** as red crystals in 13% yield, 250 mg, m.p. = 229°C . ^1H NMR (500 MHz, CDCl_3) δ 9.89 (s, 1H), 8.26 (d, J = 5.2 Hz, 1H), 7.86 (d, J = 8.8 Hz, 2H), 7.47 (d, J = 12 Hz, 2H), 7.04 (d, J = 8.5 Hz, 2H), 3.91–3.83 (m, 10H), 3.75 (t, J = 11.3 Hz, 4H), 3.68–3.60 (m, 17H), 1.77 (s, 2H), 1.63 (q, J = 30 Hz, 2H), 1.3 (q, J = 18.5 Hz, 2H), 0.88 (t, J = 14.6 Hz, 3H). ^{13}C NMR (126 MHz, CDCl_3) δ 162.8, 162.7, 162.2, 158.8, 149.6, 148.9, 142.4, 135.2, 130.8, 120.3, 114.4, 111.6, 110.1, 108.7, 103.6, 70.6, 70.5, 70.4, 69.2, 55.5, 49.9, 42.0, 31.5, 19.9, 13.6. HRMS (ESI, m/z): [M + H]⁺ + Calcd. for $\text{C}_{34}\text{H}_{44}\text{N}_4\text{O}_8$: 637.7460; found, 637.3237.

2-Butyl-3-(*p*-tolyl)-6-(1,4,10,13-tetraoxa-7,16-diazacyclooctadecane, 16-(2-pyridine-4-yl)-2,5-dihydropyrrolo[3,4-c]pyrrole-1,4-dione (7).

DPP **7** was obtained following both the procedure and the purification described above for DPP **3** as red crystals in 18% yield, 150 mg, m.p. = 115 – 118°C . ^1H NMR (500 MHz, CDCl_3) δ 8.25 (d, J = 5.3 Hz, 1H), 7.70 (d, J = 8.09 Hz, 2H), 7.511 (s, 1H), 7.34 (d, J = 8.0 Hz, 2H), 7.24 (s, 1H), 3.86–3.57 (m, 27H), 3.07 (s, 4H), 2.43 (s, 3H), 1.58 (p, J = 31 Hz, 2H), 1.25 (q, J = 29.5 Hz, 2H), 0.85 (t, J = 14.7 Hz, 3H). ^{13}C NMR (126 MHz, CDCl_3) δ 163.0, 162.7, 158.9, 149.8, 149.1, 143.2, 142.2, 135.5, 129.7, 128.8, 125.1, 111.6, 110.6, 104.0, 70.1, 69.7, 69.0, 49.4, 48.2, 41.9, 31.5, 21.7, 19.9, 13.6. HRMS (ESI, m/z): [M + H]⁺ + Calcd. for $\text{C}_{34}\text{H}_{45}\text{N}_5\text{O}_6$: 620.7630; found, 620.3440.

2-Butyl-3-(4-methoxyphenyl)-6-(1,4,7,10-tetraoxa-13-azacyclo-pentadecane,13-(2-pyridine-4-yl)-2,5-dihydropyrrolo[3,4-c]pyrrole-1,4-dione (8).

DPP **8** was obtained following both the procedure and the purification described above for DPP **3** as red crystals in 22% yield, 400 mg, m.p. = 251°C . ^1H NMR (500 MHz, CDCl_3) δ 10.01 (s, 1H), 8.25 (d, J = 5.2 Hz, 1H), 7.85 (d, J = 8.7 Hz, 2H), 7.61 (s, 1H), 7.22 (d, J = 4.9 Hz, 1H), 7.04 (d, J = 8.5 Hz, 2H), 3.9 (s, 3H), 3.82 (m, 10H), 3.65 (d, J = 14.6 Hz, 13H), 1.80 (s, 1H), 1.64 (p, J = 30.2 Hz, 2H), 1.30 (sextet, J = 37.0 Hz, 2H), 0.88 (t, J = 14.7 Hz, 3H). ^{13}C NMR (126 MHz, CDCl_3) δ 163.1, 162.8, 162.2, 158.7, 150.1, 148.9, 142.3, 135.3, 130.9, 120.2, 114.4, 111.5, 110.0, 107.9, 104.0, 71.2, 71.1, 68.9, 55.5, 51.3, 42.0, 31.5, 19.9, 13.6. HRMS (ESI, m/z): [M + H]⁺ + Calcd. for $\text{C}_{32}\text{H}_{40}\text{N}_4\text{O}_7$: 593.6930; found, 593.2975.

2-Butyl-3-(4-methoxyphenyl)-6-(2-morpholino-pyridine-4-yl)-2,5-dihydropyrrolo[3,4-c]pyrrole-1,4-dione (9).

DPP **4** was obtained following both the procedure and the purification described above for DPP **3** as red crystals in 25% yield, 600 mg, m.p. = 285 – 287°C . ^1H NMR (500 MHz, CDCl_3) δ 8.25 (s, 1H), 7.96 (d, J = 8.5 Hz, 3H), 7.39 (s, 1H), 7.15 (d, J = 8.5 Hz, 2H), 3.86–4.06 (m, 13H), 1.71 (q, J = 30 Hz, 2H), 1.36 (q, J = 18.5 Hz, 2H), 0.88 (t, J = 14.6 Hz, 3H). ^{13}C NMR

(126 MHz, CDCl₃) δ 165.3, 163.5, 141.1, 132.7, 117.9, 117.8, 116.2, 110.9, 109.5, 109.4, 65.7, 55.9, 46.1, 43.4, 31.2, 19.9, 13.3. HRMS (ESI, m/z): [M + H]⁺ Calcd. for C₂₆H₂₈N₄O₄: 460.5340; found, 461.2175.

2-Butyl-3-(4-methoxyphenyl)-6-(1,4,7-Trioxa-10-azacyclododecane, 10-(2-pyridine-4-yl)-2,5-dihydropyrrolo[3,4-c]pyrrole-1,4-dione (10). DPP **10** was obtained following both the procedure and the purification described above for DPP **3** as red crystals in 30% yield, 600 mg, m.p. = 274 °C. ¹H NMR (500 MHz, CDCl₃) δ 10.5 (s, 1H), 8.25 (d, *J* = 5.1 Hz, 1H), 7.82 (d, *J* = 8.6 Hz, 2H), 7.61 (s, 1H), 7.29 (d, *J* = 4.2 Hz, 1H), 6.98 (d, *J* = 8.1 Hz, 2H), 3.9 (s, 3H), 3.85–3.74 (m, 10H), 3.65–3.57 (m, 8H), 1.61 (p, *J* = 30.3 Hz, 2H), 1.30 (sextet, *J* = 29.6 Hz, 2H), 0.88 (t, *J* = 14.7 Hz, 3H). ¹³C NMR (126 MHz, CDCl₃) δ 163.3, 162.7, 162.2, 159.1, 150.1, 148.7, 142.5, 135.3, 130.9, 120.2, 114.3, 111.4, 110.0, 108.4, 104.2, 71.4, 70.1, 70.0, 69.9, 69.7, 55.5, 50.7, 42.0, 31.5, 19.9, 13.6. HRMS (ESI, m/z): [M + H]⁺ Calcd. for C₃₀H₃₆N₄O₆: 548.6400; found, 549.2689.

Optical Measurements

UV/Vis absorption spectra were recorded on PerkinElmer Lambda 35 Spectrometer. Fluorescence spectra were recorded on FLS1000, Edinburgh Instruments. All linear optical studies were performed with freshly prepared air-equilibrated solutions at room temperature (298 K). Acetonitrile was spectrophotometric grade and was used without further purification. Quartz cells (10 mm) were used for the measurements of absorption and emission spectra. As a standard, Rh6G (Φ_r = 0.94 in EtOH) was used to determine fluorescence quantum yields.

Computational Studies

Simplified structures of the dyes for which the flexible crown ether was replaced by Me groups were used. This is justified by the very similar experimental properties of **3** and **4** (**5** and **7**). We use a computational strategy relying on TD-DFT combined with the popular Polarizable Continuum Model (PCM)^[31] for simulating solvent effects. All calculations were achieved with the Gaussian16.A03 program,^[32] with improved self-consistent field (10⁻¹⁰ a.u.) and geometry optimization (10⁻⁵ a.u.) thresholds. The DFT and TD-DFT calculations use Truhlar's M06-2X meta-GGA hybrid functional,^[33] a choice justified as this functional tends to provide consistent (high correlation) energies with respect to experimental data. Following an approach,^[30] the 6-31 + G(d) atomic basis set was selected for geometries and vibrations whereas the 6-311 + G(2d,p) basis set is chosen for obtaining total and transition energies. We have optimized the structures and computed the vibrational frequencies for both the ground and excited states, and no imaginary frequency was found in the latter step. All our TD-DFT energies rely on the LR+cLR solvation model,^[34] so as to be as general as possible in the modelling of environmental effects. The TDA approach was applied for the computation of the Singlet-Triplet gaps. Eventually the spin-orbit coupling elements were computed with the ORCA code^[35] using the same M06-2X hybrid functional. We used the ZORA Hamiltonian, the def2-TVP basis set and the CPCM(SMD) solvent model for the calculations.

Acknowledgements

The authors would like to thank the Foundation for Polish Science (TEAM POIR.04.04.00-00-3CF4/16-00), the National Science Centre, Poland, (QuantERA programme, project 2017/25/Z/ST2/03038) and Global Research Laboratory Program (2014 K1 A1 A2064569)

through the National Research Foundation (NRF) funded by Ministry of Science, ICT & Future Planning (Korea). We thank Dr. David C. Young for amending the manuscript. DJ is indebted to the CCIPL computational center installed in Nantes for generous allocation of computational time.

Conflict of Interest

The authors declare no conflict of interest.

Keywords: Dyes/Pigments · Lactams · Heterocycles · Donor-acceptor systems · Fluorescence

- [1] C. J. Pedersen, *J. Am. Chem. Soc.* **1967**, *89*, 2495.
- [2] a) J. Yin, Y. Hua, J. Yoon, *Chem. Soc. Rev.* **2015**, *44*, 4619; b) A. Romieu, *Org. Biomol. Chem.* **2015**, *13*, 1294–1306; c) P. D. Wadhavane, M. Á. Izquierdo, D. Lutters, M. I. Burguete, M. J. Marín, D. A. Russell, F. Galindo, S. V. Luis, *Org. Biomol. Chem.* **2014**, *12*, 823–831; d) J. Li, D. Yim, W.-D. Jang, J. Yoon, *Chem. Soc. Rev.* **2017**, *46*, 2437; e) J. K.-H. Wong, M. H. Todd, P. J. Rutledge, *Molecules* **2017**, *22*, 200.
- [3] X. Kong, F. Su, L. Zhang, J. Yaron, F. Lee, Z. Shi, Y. Tian, D. R. Meldrum, *Angew. Chem. Int. Ed.* **2015**, *54*, 12053–12057; *Angew. Chem.* **2015**, *127*, 12221–12225.
- [4] a) Y. Fu, N. S. Finney, *RSC Adv.* **2018**, *8*, 29051–29061; b) F. D. Moliner, N. Kielland, R. Lavilla, M. Vendrell, *Angew. Chem. Int. Ed.* **2017**, *56*, 3758–3769; *Angew. Chem.* **2017**, *129*, 3812–3823; c) J. Zhou, H. Ma, *Chem. Sci.* **2016**, *7*, 6309–6315; d) Y. M. Poronik, V. Hugues, M. Blanchard-Desce, D. T. Gryko, *Chem. Eur. J.* **2012**, *18*, 9258–9266.
- [5] a) S. Ast, H. Müller, R. Flehr, T. Klamroth, B. Walz, H.-J. Holdt, *Chem. Commun.* **2011**, *47*, 4685–4687; b) S. Ast, T. Schwarze, H. Müller, A. Sukhanov, S. Michaelis, J. Wegener, O. S. Wolfbeis, T. Körzdörfer, A. Dürkop, H. J. Holdt, *Chem. Eur. J.* **2013**, *19*, 14911–14917; c) P. Padmawar, X. Yao, O. Bloch, G. T. Manley, A. Verkman, *Nat. Methods* **2005**, *2*, 825–827; d) X. Zhou, F. Su, Y. Tian, C. Youngbull, R. H. Johnson, D. R. Meldrum, *J. Am. Chem. Soc.* **2011**, *133*, 18530–18533.
- [6] a) J. D. Blakemore, R. Chitta, F. D'Souza, *Tetrahedron Lett.* **2007**, *48*, 1977–1982; b) T. Ueno, T. Nagano, *Nat. Methods* **2011**, *8*, 642–645; c) P. Nandhikonda, M. P. Begaye, M. D. Heagy, *Tetrahedron Lett.* **2009**, *50*, 2459–2461; d) S. Kenmoku, Y. Urano, K. Kanda, H. Kojima, K. Kikuchi, T. Nagano, *Tetrahedron* **2004**, *60*, 11067–11073.
- [7] a) S. H. Kim, J. W. Kim, J. H. Kim, K. N. Koh, S. W. Kang, *Dyes Pigm.* **2000**, *46*, 49–53; b) E. Hirayama, T. Sugiyama, H. Hisamoto, K. Suzuki, *Anal. Chem.* **2000**, *72*, 465; c) C. R. Chenthamarakshan, A. Ajayaghosh, *Tetrahedron Lett.* **1998**, *39*, 1795; d) K. Hiratani, M. Nomoto, H. Sugihara, T. Okada, *Analyst* **1992**, *117*, 1491.
- [8] a) C. Deo, S. H. Sheu, J. Seo, D. E. Clapham, L. D. Lavis, *J. Am. Chem. Soc.* **2019**, *141*, 13734–13738; b) S. K. Kim, G. I. Vargas-Zúñiga, B. P. Hay, N. J. Young, L. H. Delmau, C. Masselin, C.-H. Lee, J. S. Kim, V. M. Lynch, B. A. Moyer, J. L. Sessler, *J. Am. Chem. Soc.* **2012**, *134*, 1782–1792.
- [9] a) H. M. Kim, B. R. Cho, *Chem. Rev.* **2015**, *115*, 5014–5055; b) A. R. Sarkar, C. H. Heo, M. Y. Park, H. W. Lee, H. M. Kim, *Chem. Commun.* **2014**, *50*, 1309–1312; c) Y. M. Poronik, G. Clermont, M. Blanchard-Desce, D. T. Gryko, *J. Org. Chem.* **2013**, *78*, 11721–11732.
- [10] a) R. Grossley, Z. Goolamali, P. G. Sammes, *J. Chem. Soc. Perkin Trans. 1* **1994**, *2*, 1615; b) J. Bourson, M.-N. Borrel, B. Valeur, *Anal. Chim. Acta* **1992**, *257*, 189; c) J. Bourson, J. Pouget, B. Valeur, *J. Phys. Chem.* **1993**, *97*, 4552; d) J. Bourson, F. Badaoui, B. Valeur, *J. Fluoresc.* **1994**, *4*, 275; e) G. A. Smith, T. R. Hesketh, J. C. Metcalfe, *Biochem. J.* **1988**, *250*, 227; f) G. Gryniewicz, M. Poenie, R. Y. Tsien, *J. Biol. Chem.* **1985**, *260*, 3440; g) C.-T. Chen, W.-P. Huang, *J. Am. Chem. Soc.* **2002**, *124*, 6246–6247.
- [11] a) B. Valeur, I. Leray, *Coord. Chem. Rev.* **2000**, *205*, 3–40; b) J.-L. Habib Jiwan, C. Branger, J.-P. Soumillion, B. Valeur, *J. Photochem. Photobiol. A* **1998**, *116*, 127.
- [12] a) A. Tang, C. Zhan, J. Yao, E. Zhou, *Adv. Mater.* **2017**, *29*, 1600013; b) C. Zhao, Y. Guo, Y. Zhang, N. Yan, S. You, W. Li, *J. Mater. Chem. A* **2019**, *7*, 10174–10199; c) A. Punzi, F. Nicoletta, G. Marzano, C. G. Fortuna, J. Dagar, T. M. Brown, G. M. Farinola, *Eur. J. Org. Chem.* **2016**, *19*, 3233–3242; d) Y. Patil, T. Jadhav, B. Dhokale, R. Misra, *Asian J. Org. Chem.*

- 2016, 5, 1008–1914; e) P. Josse, C. Dalinot, Y. Jiang, S. Dabos-Seignon, J. Roncali, P. Blanchard, C. Cabanetos, *J. Mater. Chem. A* **2016**, 4, 250–256; f) E. Q. Guo, P. H. Ren, Y. L. Zhang, H. C. Zhang, W. J. Yang, *Chem. Commun.* **2009**, 5859–5861; g) H. Ftouni, F. Bolze, H. de Rocquigny, J.-F. Nicoud, *Bioconjugate Chem.* **2013**, 24, 942–950; h) M. Grzybowski, V. Hugues, M. Blanchard-Desce, D. T. Gryko, *Chem. Eur. J.* **2014**, 20, 12493–12501; i) T. He, Y. Gao, S. Sreejith, X. Tian, L. Liu, Y. Wang, H. Joshi, S. Z. F. Phua, S. Yao, X. Lin, Y. Zhao, A. C. Grimsdale, H. Sun, *Adv. Opt. Mater.* **2016**, 4, 746–755; j) A. Purc, B. Koszarna, I. Iachina, D. H. Friese, M. Tasiar, K. Sobczyk, T. Pędziński, J. Brewer, D. T. Gryko, *Org. Chem. Front.* **2017**, 4, 724–736; k) M. Kaur, D. H. Choi, *Chem. Soc. Rev.* **2015**, 44, 58–77; l) Y. Sato, R. Bertermann, M. Taki, C. Lambert, S. Yamaguchi, T. B. Marder, *Chem. Sci.* **2019**, 10, 5405–5422; m) A. Purc, E. M. Espinoza, R. Nazir, J. J. Romero, K. Skonieczny, A. Jeżewski, J. M. Larsen, D. T. Gryko, V. I. Vullev, *J. Am. Chem. Soc.* **2016**, 138, 12826–12832; n) M. Krzeszewski, E. M. Espinoza, C. Červinka, J. B. Derr, J. A. Clark, D. Borchardt, G. J. O. Beran, D. T. Gryko, V. I. Vullev, *Angew. Chem. Int. Ed.* **2018**, 57, 12365–12369. *Angew. Chem.* **2018**, 130, 12545–12549.
- [13] a) D. G. Farnum, G. Mehta, G. G. I. Moore, F. P. Siegal, *Tetrahedron Lett.* **1974**, 29, 2549; b) S. Shimizu, *Chem. Commun.* **2019**, 55, 8722–8743; c) S. Ogi, N. Fukaya, B. Arifin, B. Skjelstad, Y. Hijikata, S. Yamaguchi, *Chem. Eur. J.* **2019**, 25, 7303–7307; d) B. Gole, V. Stepanenko, S. Rager, M. Grüne, D. D. Medina, T. Bein, F. Würthner, F. Beuerle, *Angew. Chem. Int. Ed.* **2018**, 57, 846–850; *Angew. Chem.* **2018**, 130, 856–860; e) B. Soberats, M. Hecht, F. Würthner, *Angew. Chem. Int. Ed.* **2017**, 56, 10771–10774; *Angew. Chem.* **2017**, 129, 10911–10914; f) S. Shimizu, T. Iino, A. Saeki, S. Seki, N. Kobayashi, *Chem. Eur. J.* **2015**, 21, 2893; g) K. Skonieczny, I. Papadopoulos, D. Thiel, K. Gutkowski, P. Haines, P. M. McCosker, A. D. Laurent, P. A. Keller, T. Clark, D. Jacquemin, D. M. Guldi, D. T. Gryko, *Angew. Chem. Int. Ed.* **2020**, 59, 16104–16113.
- [14] a) J. C. Bijleveld, B. P. Karsten, S. G. Mathijssen, M. M. Wienk, D. M. de Leeuw, R. A. Janssen, *J. Mater. Chem.* **2011**, 21, 1600; b) S. Wood, J. Wade, M. Shahid, E. Collado-Fregoso, D. D. Bradley, J. R. Durrant, M. Heeney, J.-S. Kim, *Energy Environ. Sci.* **2015**, 8, 3222; c) J.-L. Wang, Z. Wu, J.-S. Miao, K.-K. Liu, Z.-F. Chang, R.-B. Zhang, H.-B. Wu, Y. Cao, *Chem. Mater.* **2015**, 27, 4338; d) H. Bronstein, Z. Chen, R. S. Ashraf, W. Zhang, J. Du, J. R. Durrant, P. S. Tuladhar, K. Song, S. E. Watkins, Y. Geerts, M. M. Wienk, R. A. J. Janssen, T. Anthopoulos, H. Sirringhaus, M. Heeney, I. McCulloch, *J. Am. Chem. Soc.* **2011**, 133, 3272; e) D. C. Young, M. Tasiar, A. D. Laurent, Ł. Dobrzycki, M. K. Cyrański, N. Tkachenko, D. Jacquemin, D. T. Gryko, *J. Mater. Chem. C* **2020**, 8, 7708–7717; f) J. W. Jung, F. Liu, T. P. Russell, W. H. Jo, *Chem. Commun.* **2013**, 49, 8495.
- [15] a) M. Grzybowski, D. T. Gryko, *Adv. Opt. Mater.* **2015**, 3, 280–320; b) C. Du, S. Fu, X. Wang, A. C. Sedgwick, W. Zhen, M. Li, X. Li, J. Zhou, Z. Wang, H. Wang, J. L. Sessler, *Chem. Sci.* **2019**, 10, 5699–5704.
- [16] A. Purc, M. Banasiewicz, E. Glodkowska-Mrowka, D. T. Gryko, *J. Mater. Chem. C* **2016**, 4, 2877–2885.
- [17] A. L. Thompson, T.-S. Ahn, K. R. J. Thomas, S. Thayumanavan, T. J. Martinez, C. J. Bardeen, *J. Am. Chem. Soc.* **2005**, 127, 16348–16349.
- [18] Y. Zhang, Y. Ouyang, Z. Luo, S. Dong, *Eur. J. Org. Chem.* **2019**, 4741–4744.
- [19] M. Grzybowski, E. Glodkowska-Mrowka, T. Stoklosa, D. T. Gryko, *Org. Lett.* **2012**, 14, 2670–2673.
- [20] M. Pieczykolan, B. Sadowski, D. T. Gryko, *Angew. Chem. Int. Ed.* **2020**, 59, 7528–7535.
- [21] Y. Inoue, in *Cation Binding by Macrocycles: Complexation of Cationic Species by Crown Ethers*, G. W. Gokel (Eds), **1990**, Marcel Dekker, New York.
- [22] K. Hiratani, *J. Chem. Soc. Chem. Commun.* **1987**, 960–961.
- [23] D. Seebach, A. Thaler, D. Blaser, S. Y. Ko, *Helv. Chim. Acta* **1991**, 74, 1102.
- [24] a) H. Sugihara, K. Hiratani, *J. Synth. Org. Chem. Jpn.* **1994**, 52, 530; b) H. Sugihara, T. Okada, K. Hiratani, *Anal. Sci.* **1993**, 9, 593; c) S. O. Obare, C. J. Murphy, *Inorg. Chem.* **2001**, 40, 6080–6082.
- [25] S. Tsuchiya, Y. Nakatani, R. Ibrahim, S. Ogawa, *J. Am. Chem. Soc.* **2002**, 124, 4936–4937.
- [26] V. Snieckus, *Chem. Rev.* **1990**, 90, 879–933.
- [27] a) M. Kamenica, R. R. Kothur, A. Willows, B. A. Patel, P. J. Cragg, *Sensors* **2017**, 17, 2430; b) D. B. Stubing, S. Heng, A. D. Abell, *Org. Biomol. Chem.* **2016**, 14, 3752.
- [28] W. H. Meyer, *Adv. Mater.* **1998**, 10, 439.
- [29] P. E. Keck, S. L. McElroy, S. M. Strakowski, C. A. J. Soutullo, *Clin. Psychiat.* **2000**, 61, 33.
- [30] D. Jacquemin, A. Planchat, C. Adamo, B. Mennucci, *J. Chem. Theory Comput.* **2012**, 8, 2359–2372.
- [31] J. Tomasi, B. Mennucci, R. Cammi, *Chem. Rev.* **2005**, 105, 2999–3094.
- [32] M. J. Frisch, G. W. Trucks, H. B. Schlegel, G. E. Scuseria, M. A. Robb, J. R. Cheeseman, G. Scalmani, V. Barone, G. A. Petersson, H. Nakatsuji, X. Li, M. Caricato, A. V. Marenich, J. Bloino, B. G. Janesko, R. Gomperts, B. Mennucci, H. P. Hratchian, J. V. Ortiz, A. F. Izmaylov, J. L. Sonnenberg, Williams, F. Ding, F. Lipparini, F. Egidi, J. Goings, B. Peng, A. Petrone, T. Henderson, D. Ranasinghe, V. G. Zakrzewski, J. Gao, N. Rega, G. Zheng, W. Liang, M. Hada, M. Ehara, K. Toyota, R. Fukuda, J. Hasegawa, M. Ishida, T. Nakajima, Y. Honda, O. Kitao, H. Nakai, T. Vreven, K. Throssell, J. A. Montgomery Jr., J. E. Peralta, F. Ogliaro, M. J. Bearpark, J. J. Heyd, E. N. Brothers, K. N. Kudin, V. N. Staroverov, T. A. Keith, R. Kobayashi, J. Normand, K. Raghavachari, A. P. Rendell, J. C. Burant, S. S. Iyengar, J. Tomasi, M. Cossi, J. M. Millam, M. Klene, C. Adamo, R. Cammi, J. W. Ochterski, R. L. Martin, K. Morokuma, O. Farkas, J. B. Foresman, D. J. Fox, *Gaussian 16 Rev. B.01*, Wallingford, CT, **2016**.
- [33] Y. Zhao, D. G. Truhlar, *Theor. Chem. Acc.* **2008**, 120, 215–241.
- [34] P. M. Vêrité, C. A. Guido, D. Jacquemin, *Phys. Chem. Chem. Phys.* **2019**, 21, 2307–2317.
- [35] F. Neese, *WIREs Comput. Mol. Sci.* **2018**, 8, e1327.

Manuscript received: December 1, 2020
Revised manuscript received: January 9, 2021
Accepted manuscript online: January 12, 2021
Version of record online: January 25, 2021

CHEMISTRY

AN ASIAN JOURNAL

Supporting Information

Switch-On Diketopyrrolopyrrole-Based Chemosensors for Cations Possessing Lewis Acid Character

G. Dinesh Kumar, Marzena Banasiewicz, Denis Jacquemin,* and Daniel T. Gryko*

Author Contributions

D.K. Investigation:Lead; Visualization:Supporting; Writing – original draft:Equal; Writing – review & editing:Supporting

M.B. Data curation:Equal; Investigation:Lead; Writing – original draft:Supporting; Writing – review & editing:Supporting

D.J. Investigation:Lead; Visualization:Equal; Writing – original draft:Equal; Writing – review & editing:Equal

Table of contents

Section S1	General Information	S2
Section S2	Experimental procedures	S3
Section S3	Absorption and emission spectra	S5
Section S4	^1H NMR and ^{13}C NMR Spectra	S31
Section S5	References	S54

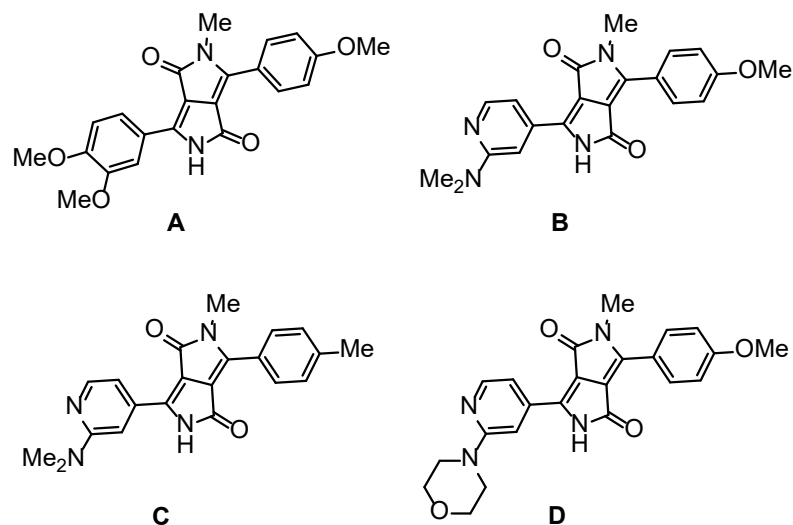


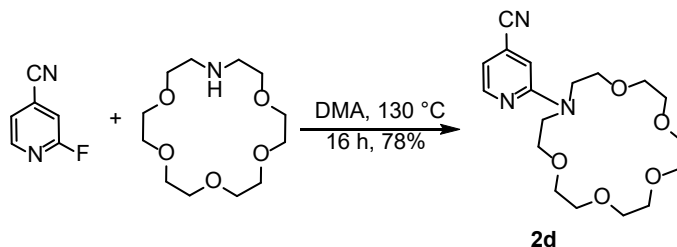
Fig S1. Structures used in computational studies.

Section S1: General Information

All chemicals are from commercial sources and were used as received, unless otherwise noted. All reported NMR spectra were recorded on Bruker 500 MHz and Varian 500 MHz spectrometers. Chemical shifts (δ ; ppm) for ^1H and ^{13}C NMR spectra were determined with TMS or residual solvent signals as the internal reference. J values are given in Hz. Spectroscopic-grade solvents were used in all fluorescence/absorption-spectroscopy measurements. Mass spectra were obtained with EI ion source and the EBE double focusing geometry mass analyzer or spectrometer equipped with electro-spray ion source with Q-TOF type mass analyzer. The synthesis of compounds 2a, 2b, 2c¹ and 2g² have been described previously.

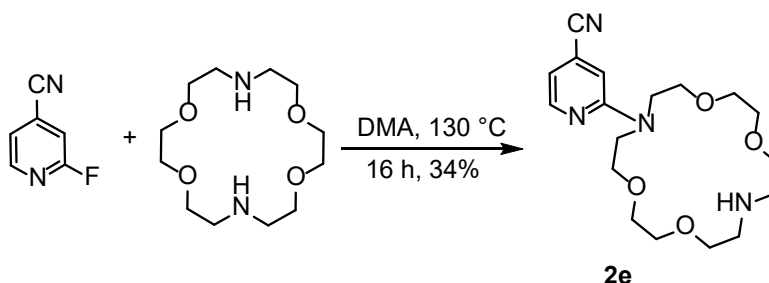
Section S2: Experimental Procedures

1,4,7,10,13-Pentaoxa-16-azacyclooctadecane, 16-(2-pyridine)-4-nitrile (2d)



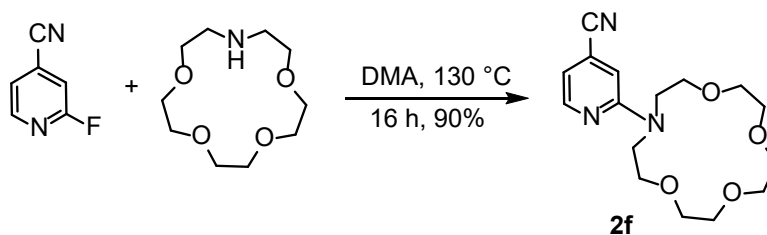
A mixture commercially available 2-fluoro-4-cyanopyridine (500 mg, 4 mmol), 1-Aza-18-crown-6 (1.1 g, 4 mmol) in 5 ml of deoxygenated N,N-dimethylacetamide was heated (130 °C) under argon for overnight. Then reaction mixture was cooled to room temperature, diluted with water (100 mL) and extracted with EtOAc (2x100 mL). The organic phase dried over anhydrous Na₂SO₄ and filtered. The solvent was removed under reduced pressure and the resulting colorless oil was chromatographed on silica gel (hexane/EtOAc = 1: 1) to obtain 78 % yield, 1.17 g. ¹H NMR (500 MHz, CDCl₃) δ 8.15 (d, *J* = 2.4 Hz, 1H), 6.80 (s, 1H), 6.66 (d, *J* = 2.3 Hz, 1H), 3.79 (t, *J* = 8.0 Hz, 4H), 3.72 (t, *J* = 12.0 Hz, 4H), 3.66 (s, 16H). ¹³C NMR (126 MHz, CDCl₃) δ 157.7, 148.9, 120.7, 117.6, 111.6, 108.3, 70.7, 70.6, 68.9, 49.5. HRMS (ESI, *m/z*): [M+H]⁺ Calcd. for C₁₈H₂₇N₃O₅: 366.4300; found, 388.4300[M+Na].

1,4,10,13-Tetraoxa-7,16-diazacyclooctadecane, 16-(2-pyridine)-4-nitrile (2e)



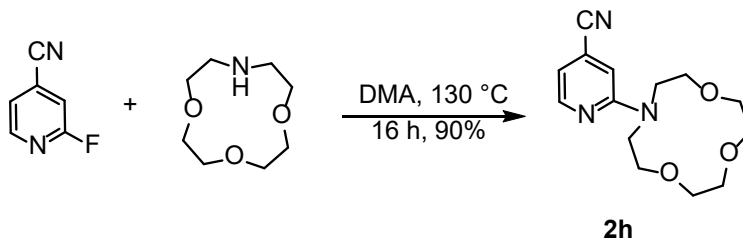
A mixture commercially available 2-fluoro-4-cyanopyridine (500 mg, 4mmol), 1, 10-Diaza-18-crown-6 (1.08 g, 4mmol) in 5 ml of deoxygenated N,N-dimethylacetamide was heated (130 °C) under argon for overnight. Then reaction mixture was cooled to room temperature, diluted with water (100 mL) and extracted with EtOAc (2x100 mL). The organic phase dried over anhydrous Na₂SO₄ and filtered. The solvent was removed under reduced pressure and the resulting colorless oil was chromatographed on silica gel (hexane/EtOAc = 1: 1) to obtain 34 % yield, 500 mg. ¹H NMR (500 MHz, CDCl₃) δ 8.09 (d, *J* = 4.8 Hz, 1H), 6.61 (s, 1H), 6.57 (d, *J* = 4.8 Hz, 1H), 3.85 (m, 8H), 3.73 (t, *J* = 10.8 Hz, 4H), 3.67 (s, 8H), 3.18 (t, *J* = 8 Hz, 4H). ¹³C NMR (126 MHz, CDCl₃) δ 157.4, 149.0, 120.7, 117.3, 111.8, 107.5, 69.9, 69.4, 68.8, 65.3, 48.6, 47.3 HRMS (ESI, *m/z*): [M+H]⁺ Calcd. for C₁₈H₂₈N₄O₄: 365.4460; found, 387.4360[M+Na].

1,4,7,10-Tetraoxa-13-azacyclopentadecane, 13-(2-pyridine)-4-nitrile (2f)



A mixture commercially available 2-fluoro-4-cyanopyridine (500 mg, 4mmol), 1-Aza-15-crown-5 (900 mg, 4mmol) in 5 ml of deoxygenated N,N-dimethylacetamide was heated (130 °C) under argon for overnight. Then reaction mixture was cooled to room temperature, diluted with water (100 mL) and extracted with EtOAc (2x100 mL). The organic phase dried over anhydrous Na₂SO₄ and filtered. The solvent was removed under reduced pressure and the resulting colorless oil was chromatographed on silica gel (hexane/EtOAc = 1: 1) to obtain 90 % yield, 1.2 g. ¹H NMR (500 MHz, CDCl₃) δ 8.15 (d, *J* = 2.4 Hz, 1H), 6.84 (s, 1H), 6.66 (d, *J* = 2.3 Hz, 1H), 3.79 (t, *J* = 8.0 Hz, 4H), 3.72 (t, *J* = 12.0 Hz, 4H), 3.66 (s, 12H). ¹³C NMR (126 MHz, CDCl₃) δ 157.7, 148.9, 120.7, 117.6, 111.6, 108.3, 70.1, 69.8, 51.2. HRMS (ESI, *m/z*): [M+H]⁺ Calcd. for C₁₆H₂₃N₃O₄: 322.3770; found, 344.3770[M+Na].

1,4,7-Trioxa-10-azacyclododecane, 10-(2-pyridine)-4-nitrile (2h)



A mixture commercially available 2-fluoro-4-cyanopyridine (500 mg, 4 mmol), 1-Aza-12-crown-4 (700 mg, 4 mmol) in 5 ml of deoxygenated N,N-dimethylacetamide was heated (130 °C) under argon for overnight. Then reaction mixture was cooled to room temperature, diluted with water (100 mL) and extracted with EtOAc (2x100 mL). The organic phase dried over anhydrous Na₂SO₄ and filtered. The solvent was removed under reduced pressure and the resulting colorless oil was chromatographed on silica gel (hexane/EtOAc = 1: 1) to obtain 90 % yield, 1.17 g. ¹H NMR (600 MHz, CDCl₃) δ 8.19 (dd, *J* = 5.8 Hz, 1H), 6.94 (s, 1H), 6.66 (dd, *J* = 6.1 Hz, 1H), 3.89 (t, *J* = 9.9 Hz, 4H), 3.70 (t, *J* = 9.80 Hz, 4H), 3.66 (m, 8H). ¹³C NMR (126 MHz, CDCl₃) δ 158.5, 148.6, 120.7, 117.8, 111.9, 109.6, 71.3, 69.7, 69.5, 51.2. HRMS (ESI, *m/z*): [M+H]⁺ Calcd. for C₁₄H₁₉N₃O₃: 277.3240; found, 278.1540[M+H].

Section S3: Absorption and emission spectra

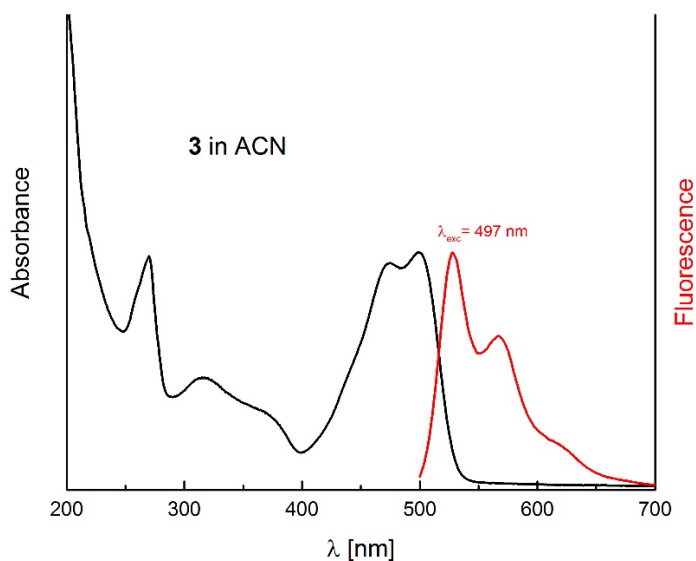


Fig. S2. The absorption and emission spectra of DPP **3** in acetonitrile.

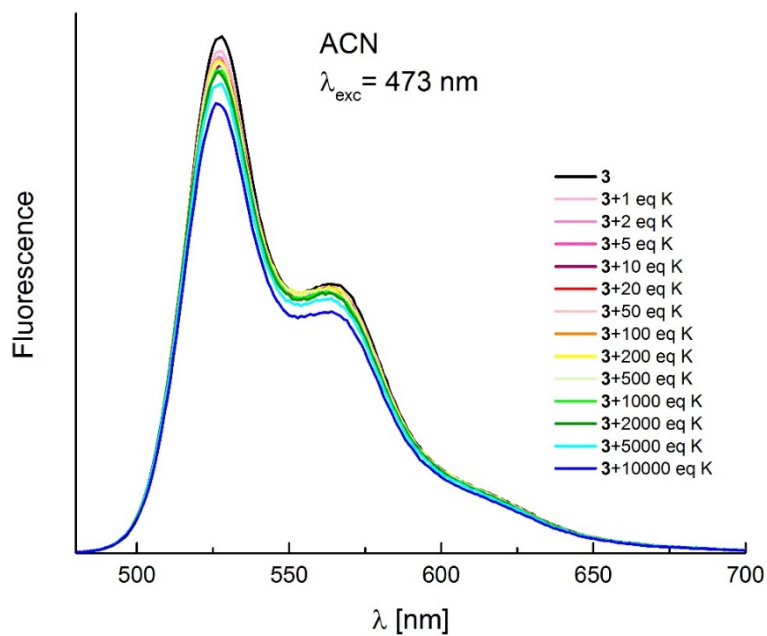


Fig. S3. The effect of KBF_4 addition on the emission spectra of DPP **3** measured in ACN.

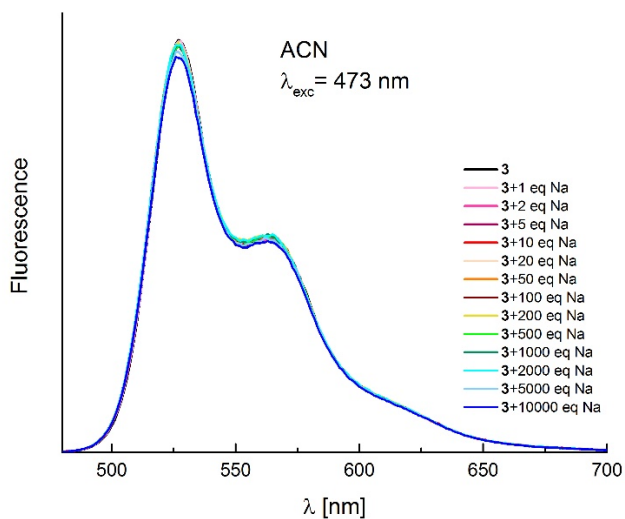


Fig. S4. The effect of NaClO₄ addition on the emission spectra of DPP **3** measured in ACN.

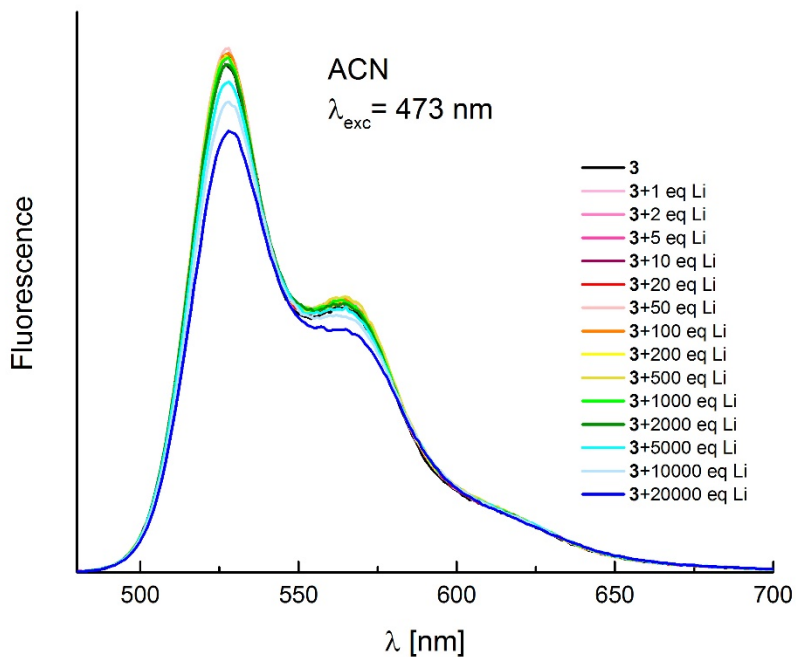


Fig. S5. The effect of LiClO₄ addition on the emission spectra of DPP **3** measured in ACN.

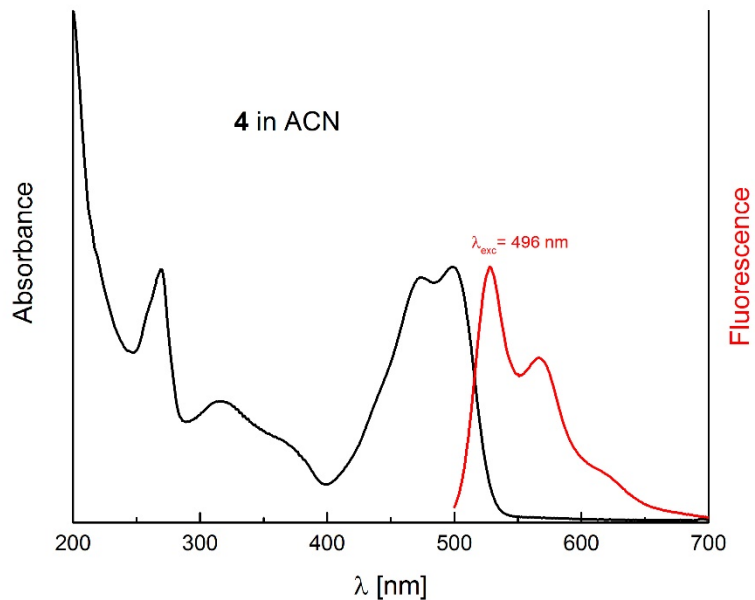


Fig. S6. The absorption and emission spectra of DPP **4** in acetonitrile.

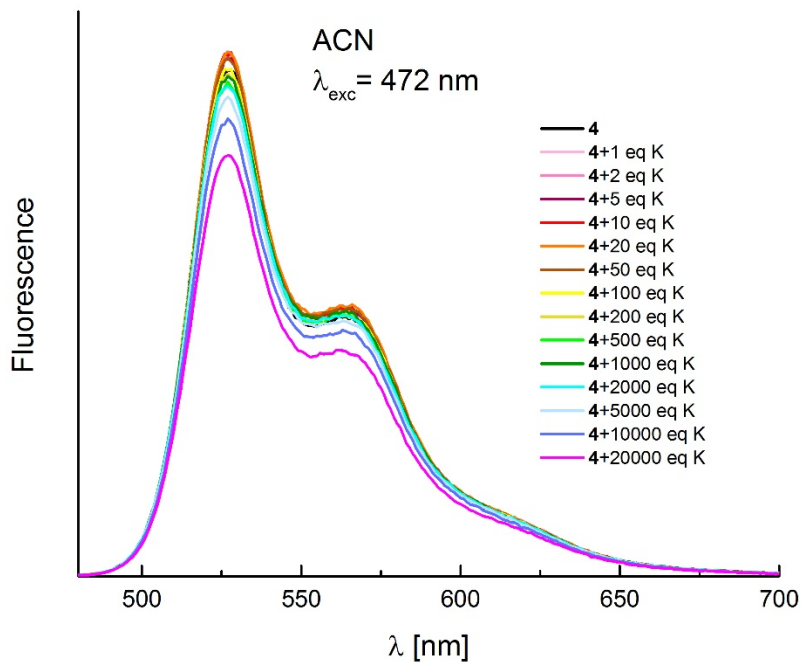


Fig. S7. The effect of KBF_4 addition on the emission spectra of DPP **4** measured in ACN.

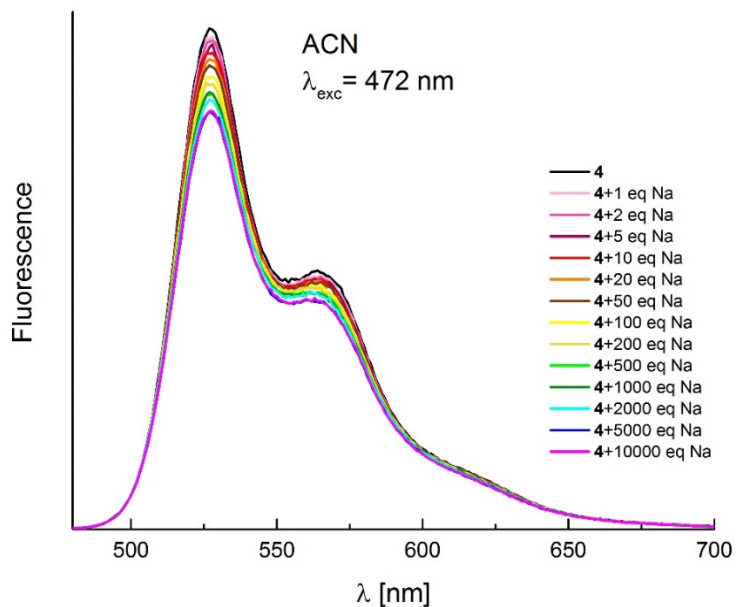


Fig. S8. The effect of NaClO₄ addition on the emission spectra of DPP **4** measured in ACN.

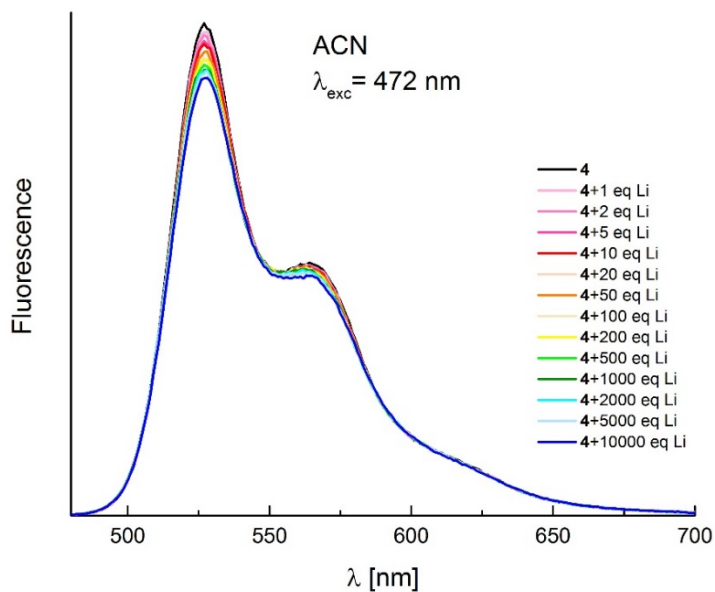


Fig. S9. The effect of LiClO₄ addition on the emission spectra of DPP **4** measured in ACN.

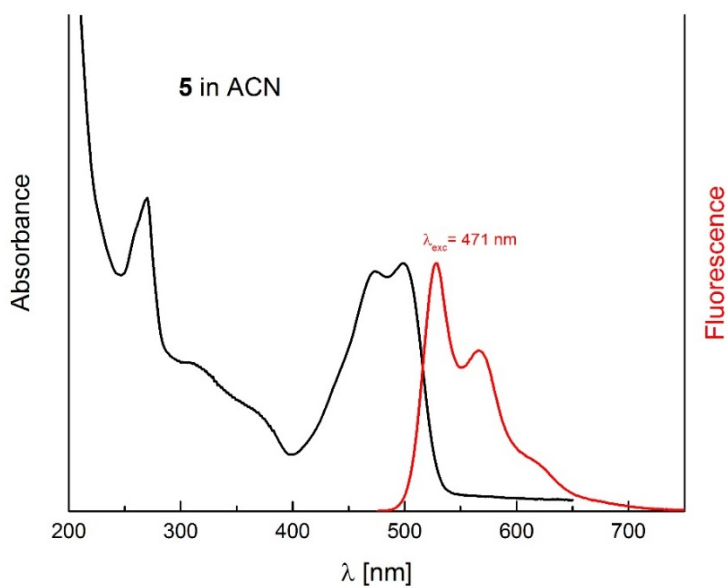


Fig. S10. The absorption and emission spectra of DPP 5 in acetonitrile.

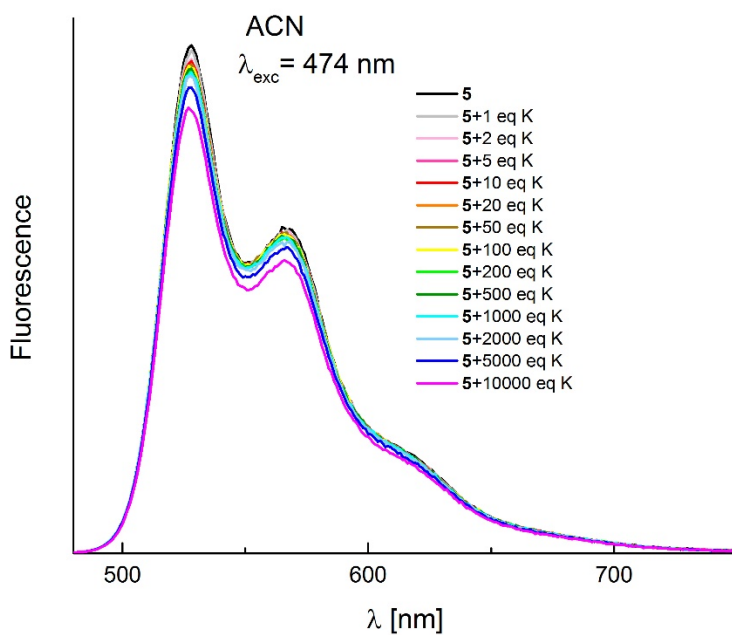


Fig. S11. The effect of KBF_4 addition on the emission spectra of DPP 5 measured in ACN.

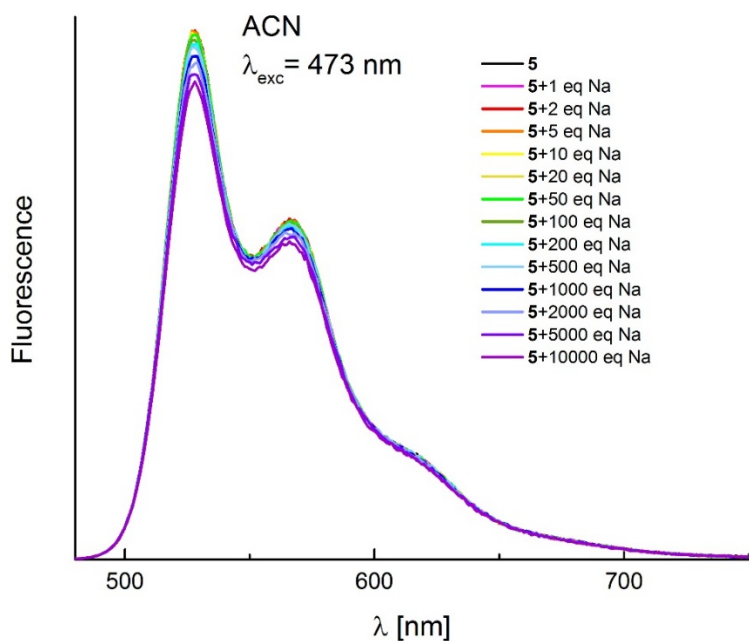


Fig. S12. The effect of NaClO₄ addition on the emission spectra of DPP 5 measured in ACN.

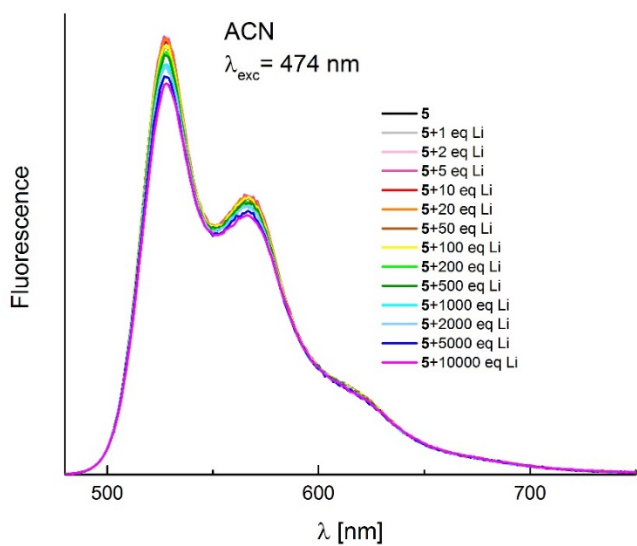


Fig. S13. The effect of LiClO₄ addition on the emission spectra of DPP 5 measured in ACN.

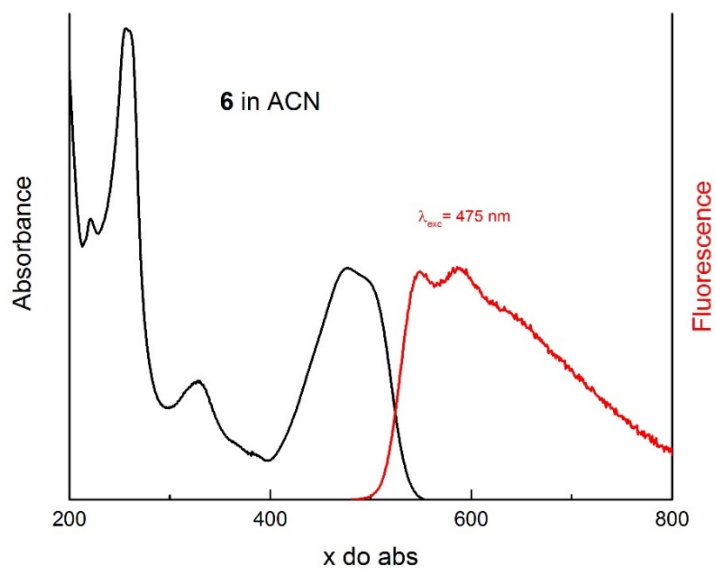


Fig. S14. The absorption and emission spectra of DPP **6** in acetonitrile.

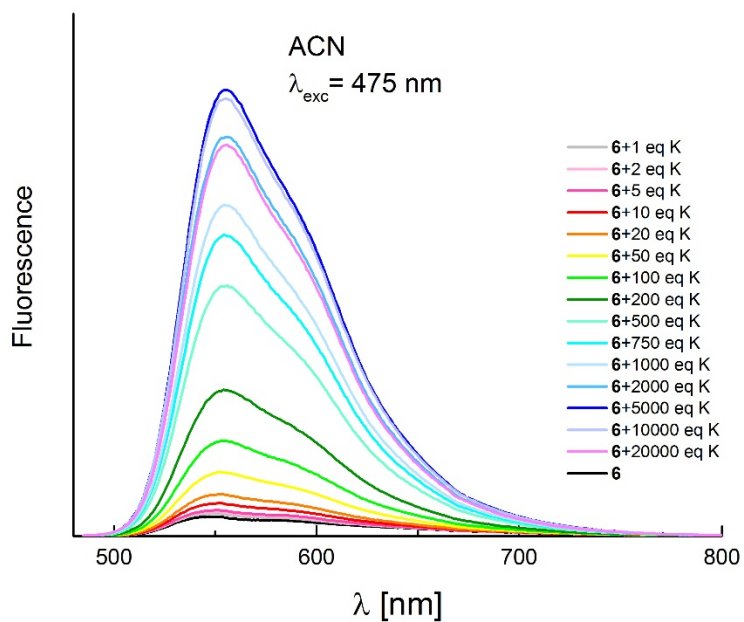


Fig. S15. The effect of KBF_4 addition on the emission spectra of DPP **6** measured in ACN.

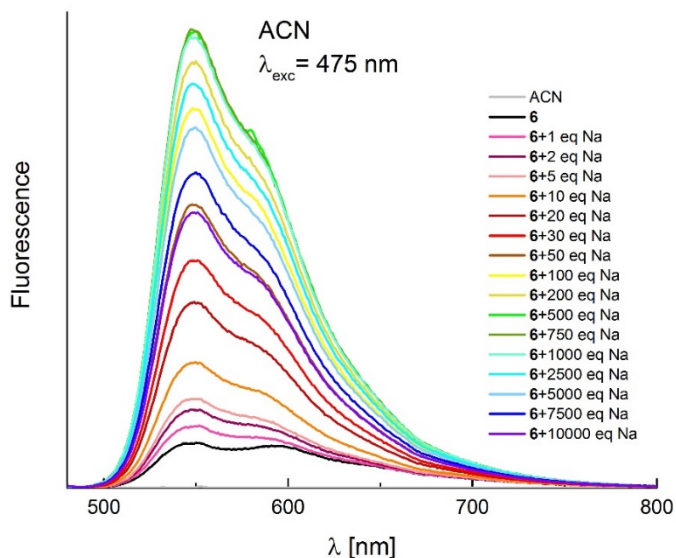


Fig. S16. The effect of NaClO_4 addition on the emission spectra of DPP 6 measured in ACN.

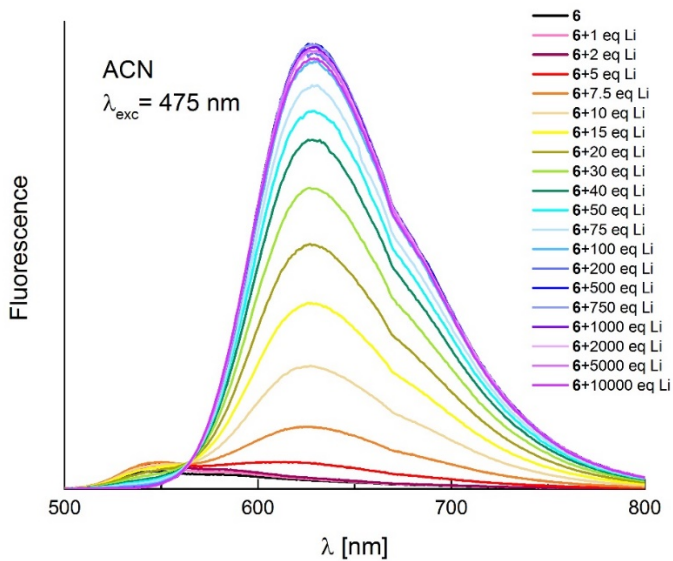


Fig. S17. The effect of LiClO_4 addition on the emission spectra of DPP 6 measured in ACN.

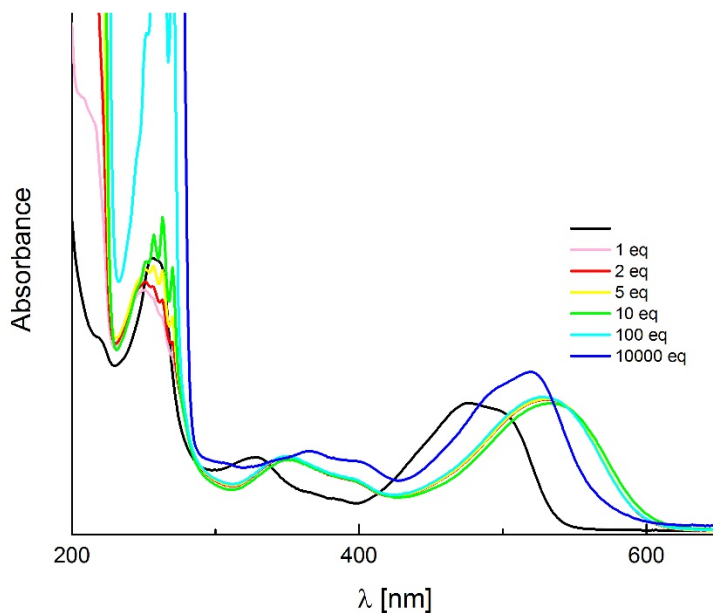


Fig. S18. The effect of PhSO₃H addition on the absorption spectra of DPP 6 measured in ACN.

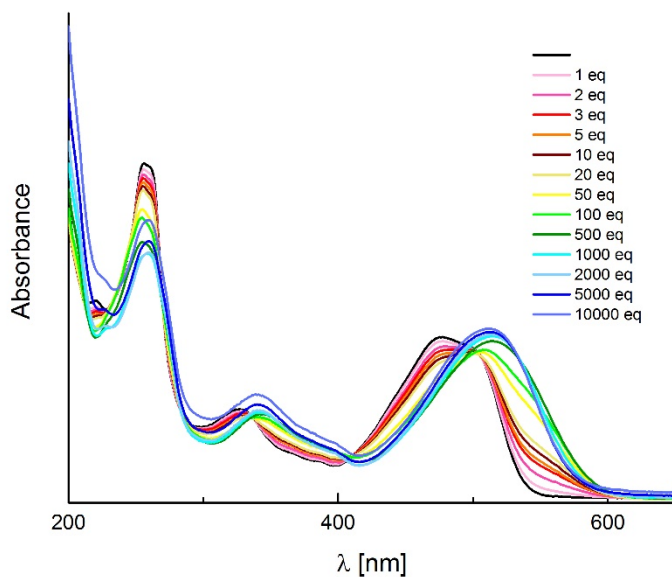


Fig. S19. The effect of Mg(ClO₄)₂ addition on the absorption spectra of DPP 6 measured in ACN.

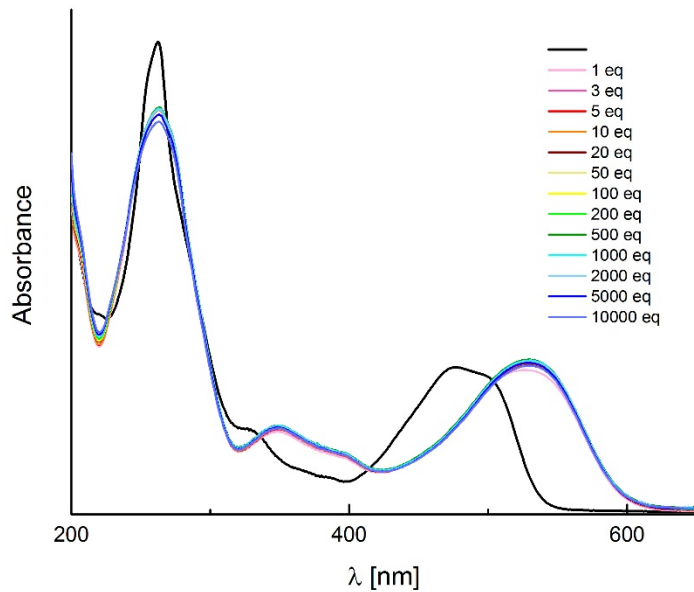


Fig. S20. The effect of $\text{Zn}(\text{ClO}_4)_2$ addition on the absorption spectra of DPP 6 measured in ACN.

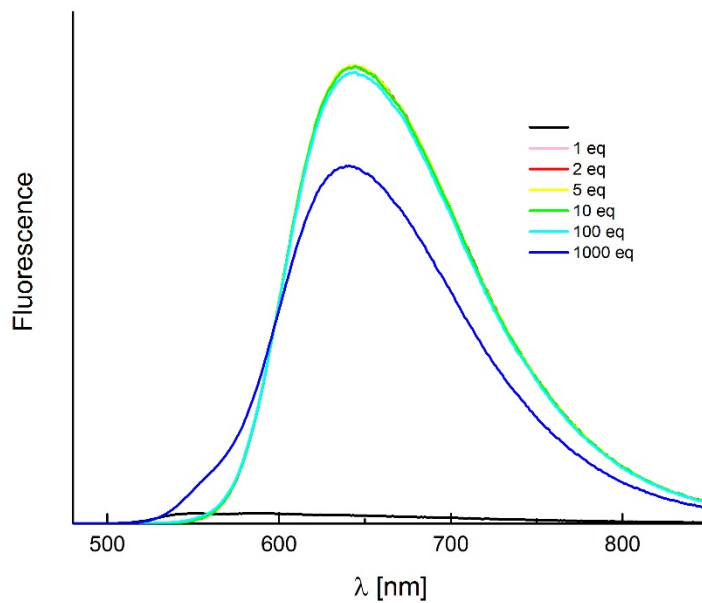


Fig. S21. The effect of PhSO_3H addition on the emission spectra of DPP 6 measured in ACN.

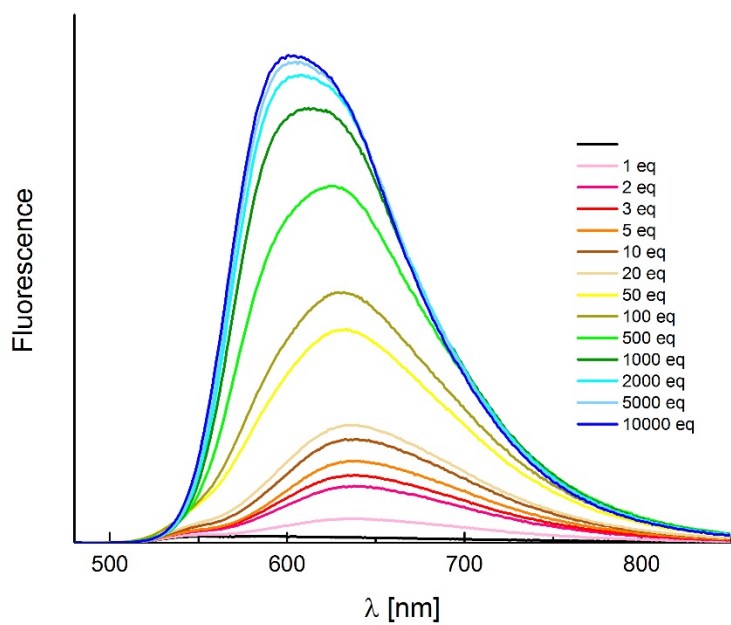


Fig. S22. The effect of $\text{Mg}(\text{ClO}_4)_2$ addition on the emission spectra of DPP 6 measured in ACN.

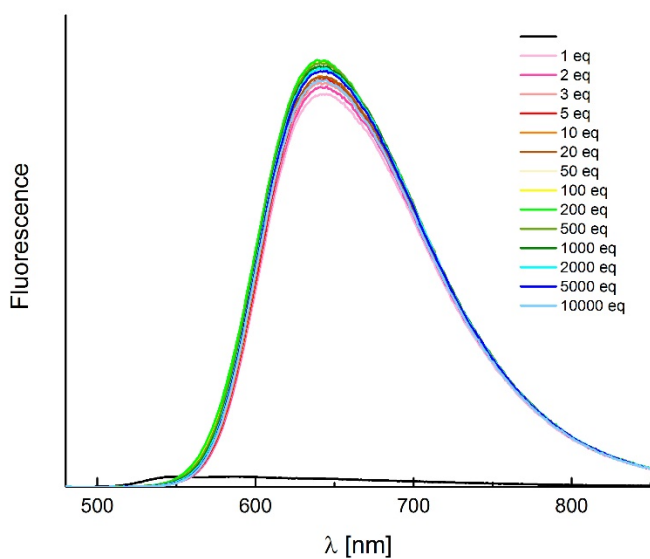


Fig. S23. The effect of $\text{Zn}(\text{ClO}_4)_2$ addition on the emission spectra of DPP 6 measured in ACN.

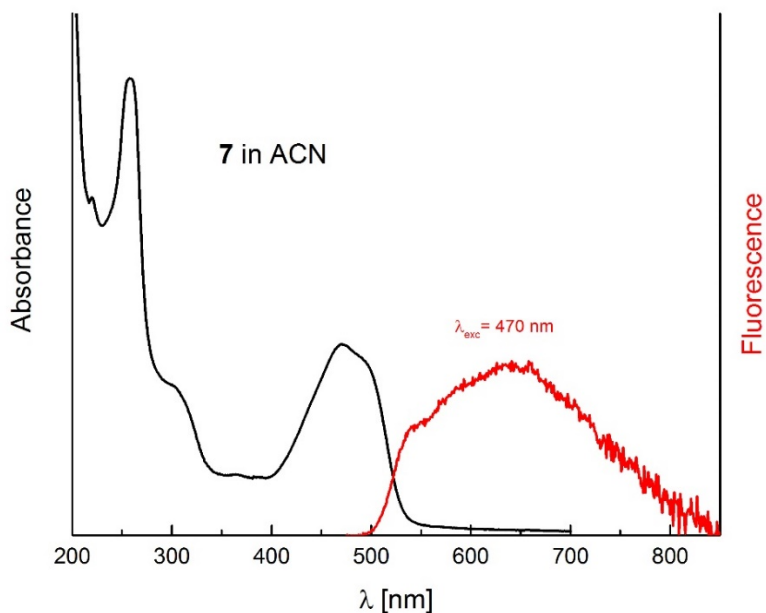


Fig. S24. The absorption and emission spectra of DPP **7** in acetonitrile.

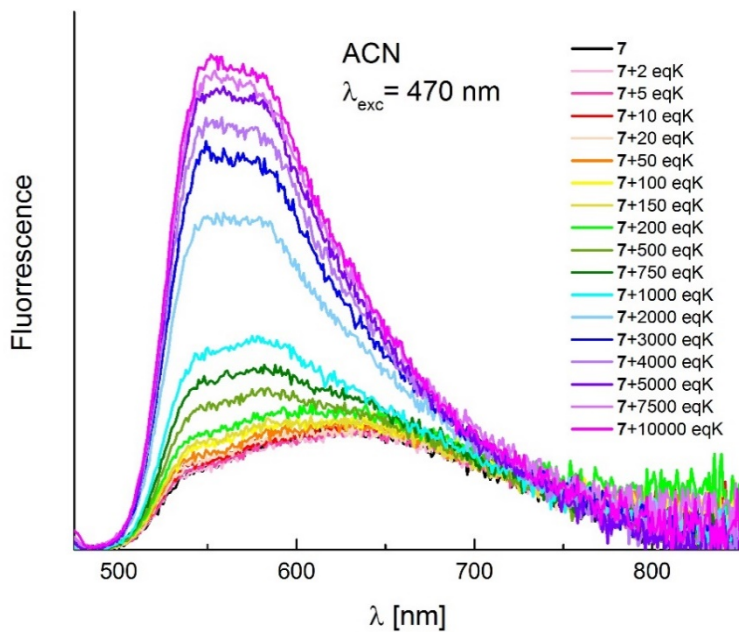


Fig. S25. The effect of KBF_4 addition on the emission spectra of DPP **7** measured in ACN.

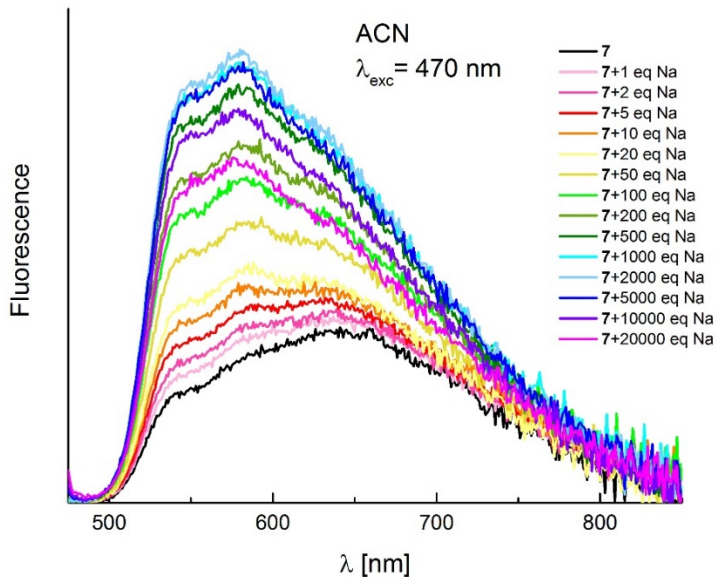


Fig. S26. The effect of NaClO_4 addition on the emission spectra of DPP **7** measured in ACN.

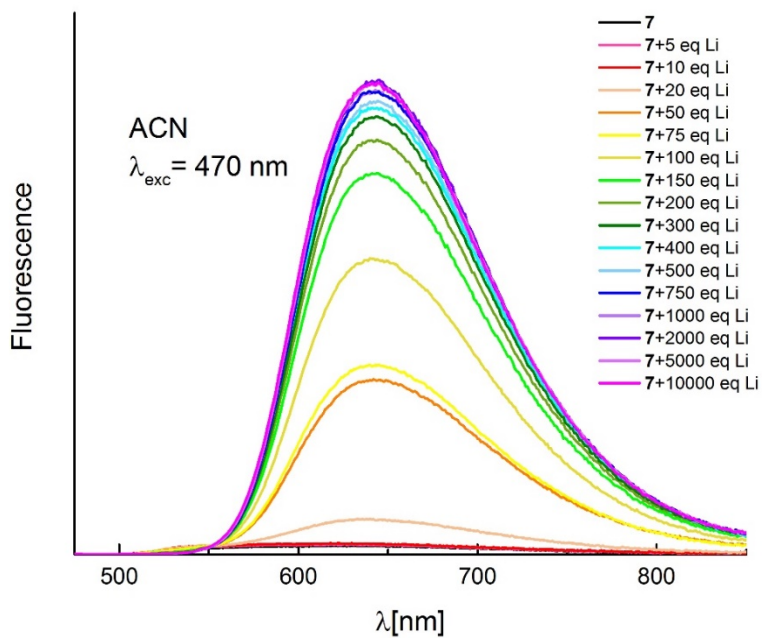


Fig. S27. The effect of LiClO_4 addition on the emission spectra of DPP **7** measured in ACN.

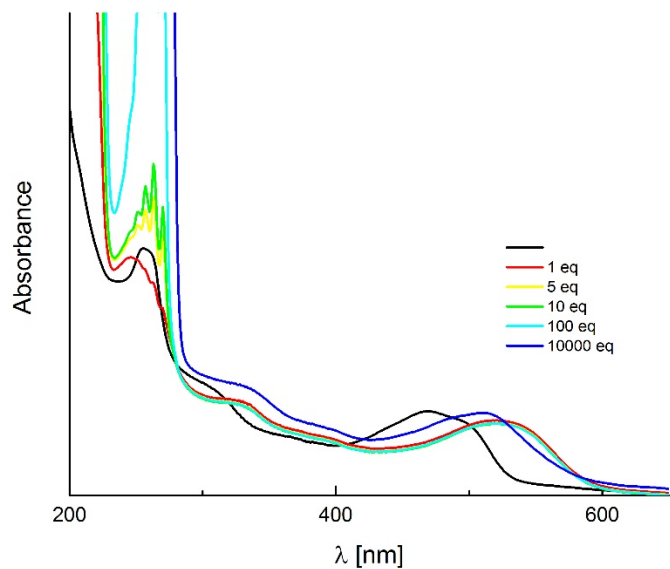


Fig. S28. The effect of PhSO₃H addition on the absorption spectra of DPP 7 measured in ACN.

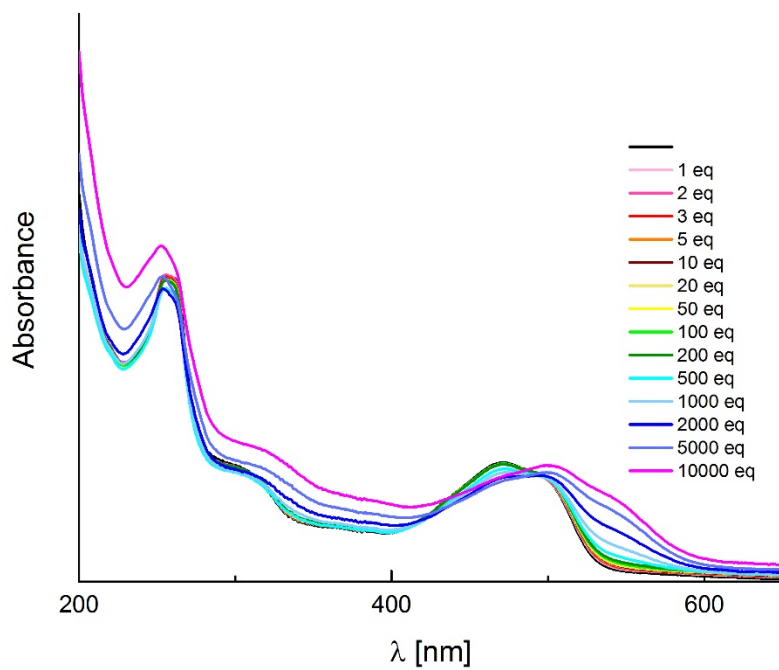


Fig. S29. The effect of Mg(ClO₄)₂ addition on the absorption spectra of DPP 7 measured in ACN.

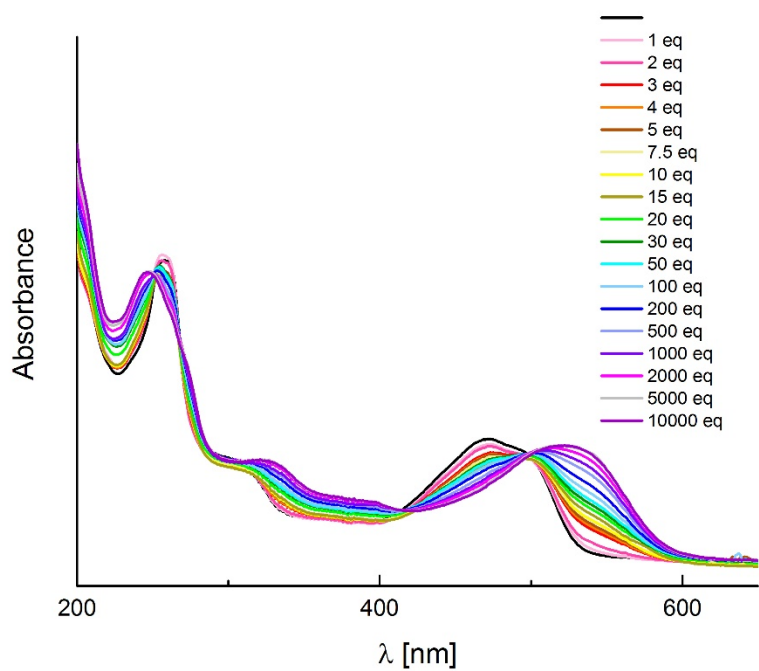


Fig. S30. The effect of $Zn(ClO_4)_2$ addition on the absorption spectra of DPP 7 measured in ACN.

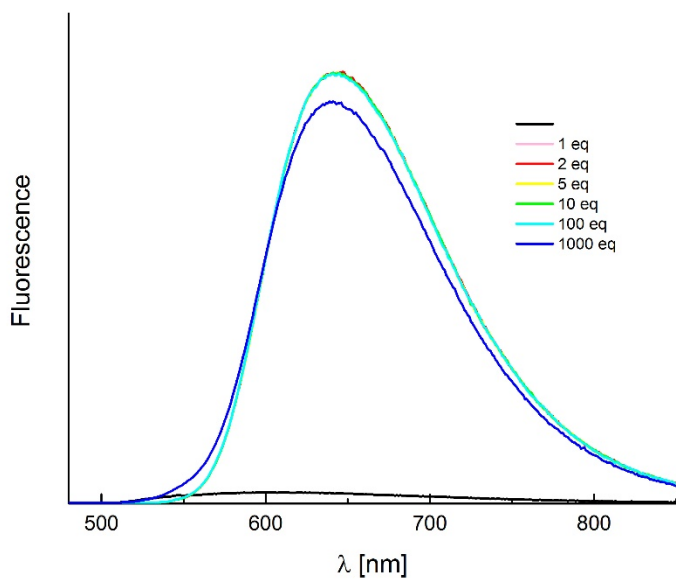


Fig. S31. The effect of $PhSO_3H$ addition on the emission spectra of DPP 7 measured in ACN.

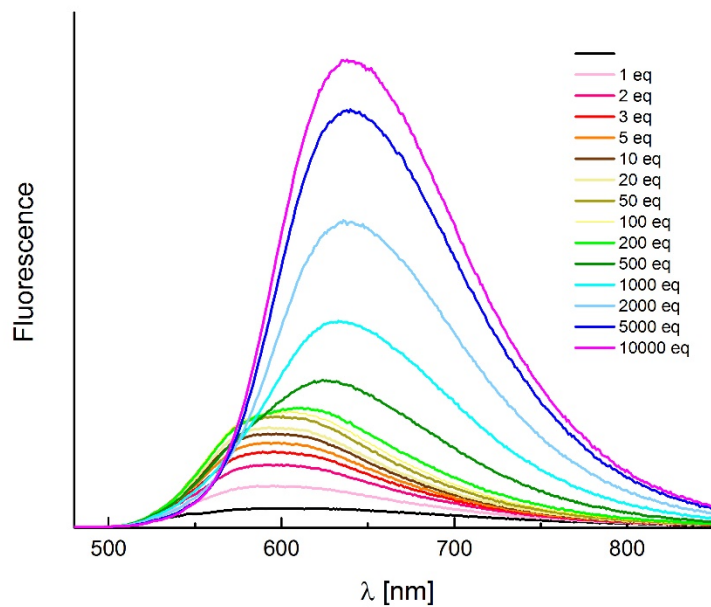


Fig. S32. The effect of Mg(ClO₄)₂ addition on the emission spectra of DPP 7 measured in ACN.

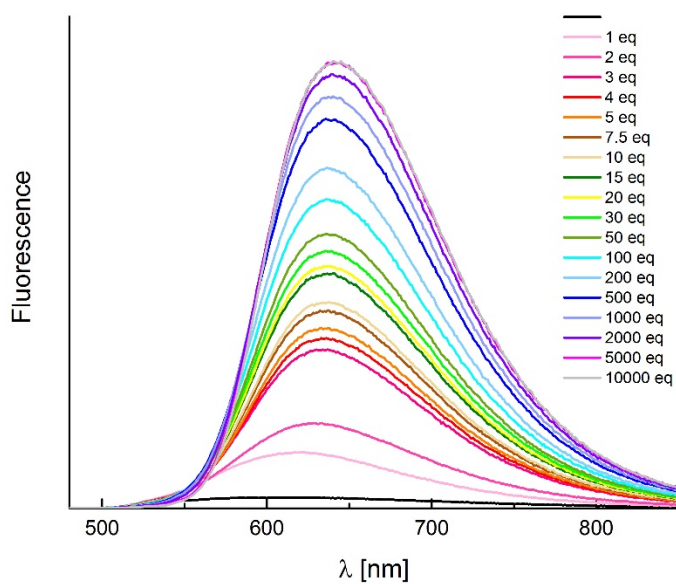


Fig. S33. The effect of Zn(ClO₄)₂ addition on the emission spectra of DPP 7 measured in ACN.

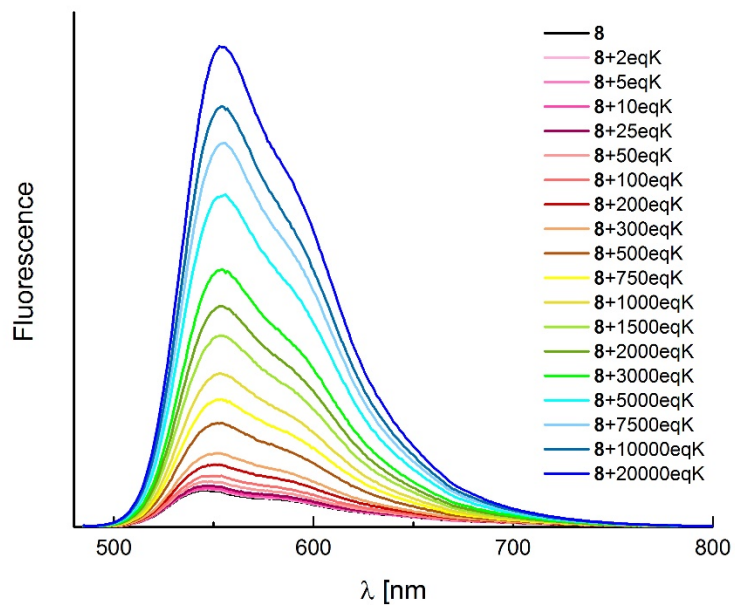


Fig. S34. The effect of KBF₄ addition on the emission spectra of DPP **8** measured in ACN.

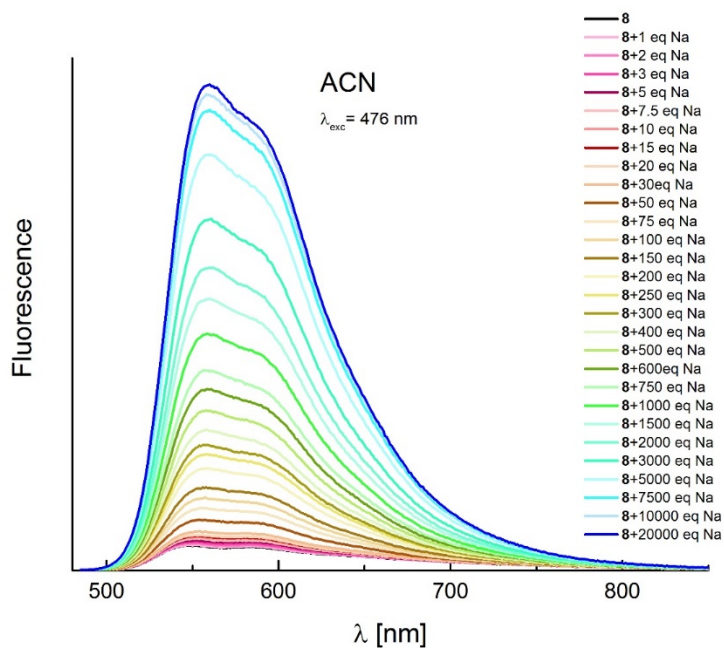


Fig. S35. The effect of NaClO₄ addition on the emission spectra of DPP **8** measured in ACN.

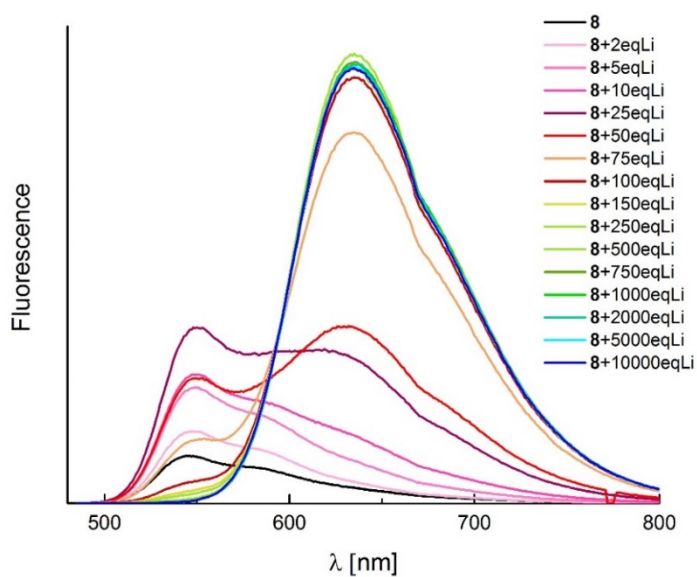


Fig. S36. The effect of LiClO₄ addition on the emission spectra of DPP 8 measured in ACN.

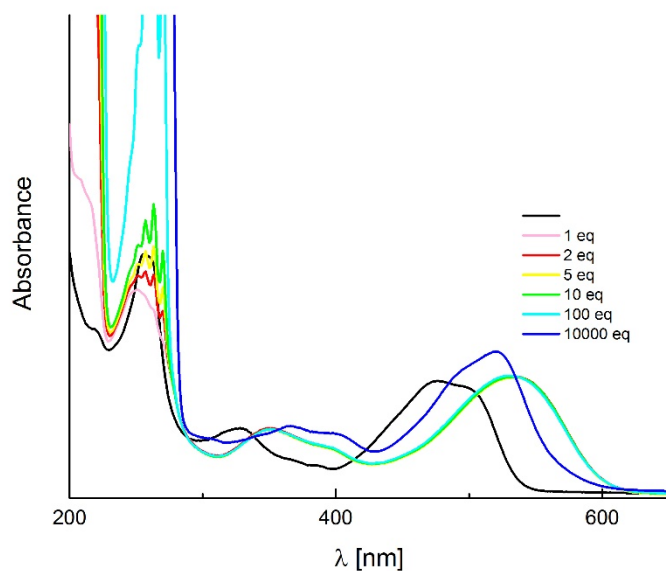


Fig. S37. The effect of PhSO₃H addition on the absorption spectra of DPP 8 measured in ACN.

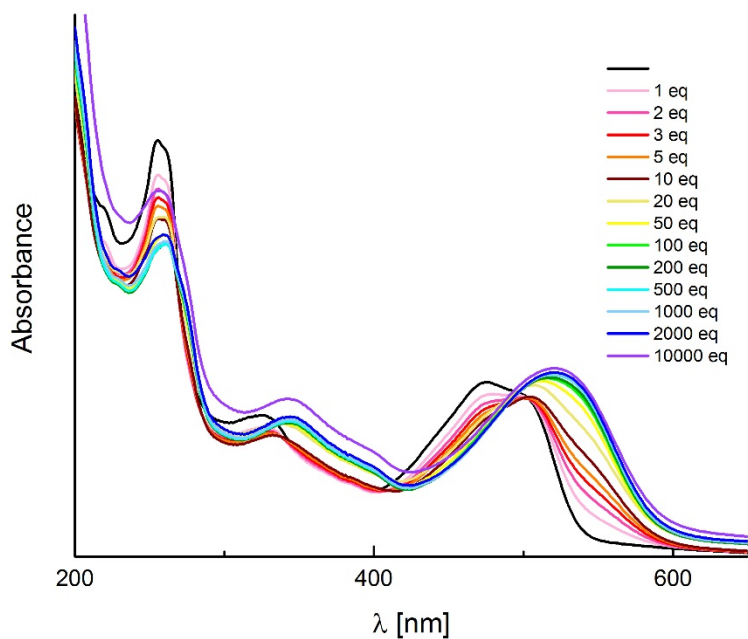


Fig. S38. The effect of $\text{Mg}(\text{ClO}_4)_2$ addition on the absorption spectra of DPP 8 measured in ACN.

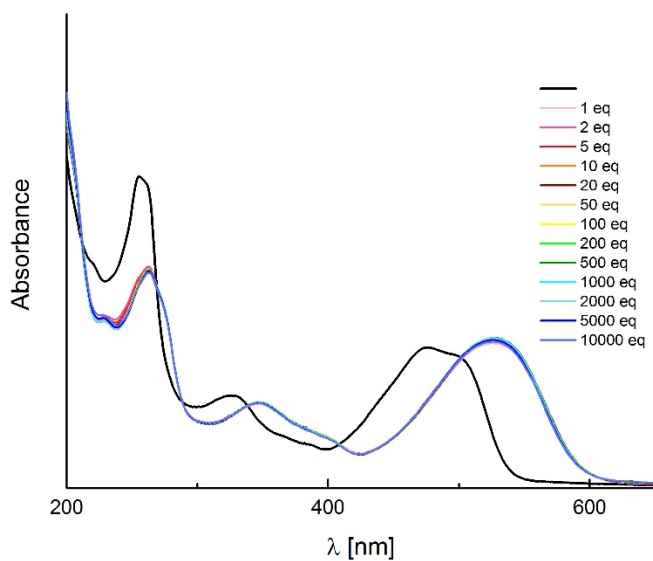


Fig. S39. The effect of $\text{Zn}(\text{ClO}_4)_2$ addition on the absorption spectra of DPP 8 measured in ACN.

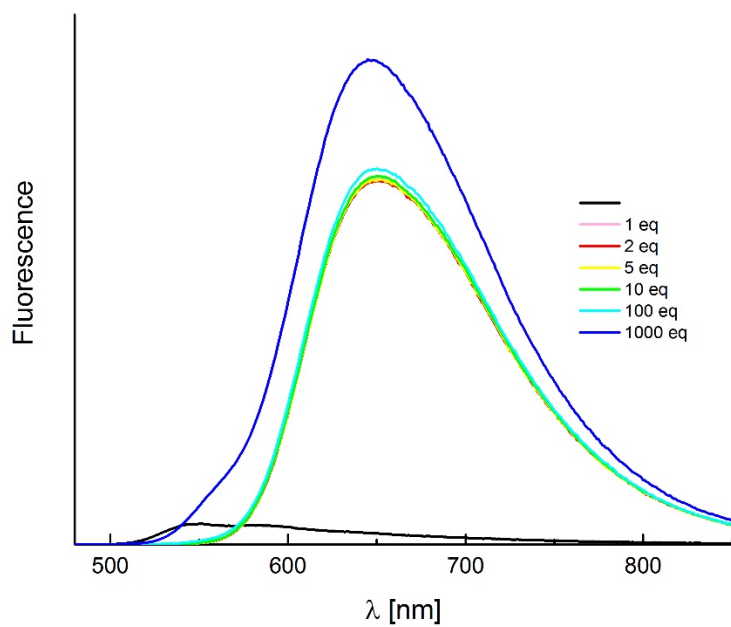


Fig. S40. The effect of PhSO_3H addition on the emission spectra of DPP 8 measured in ACN.

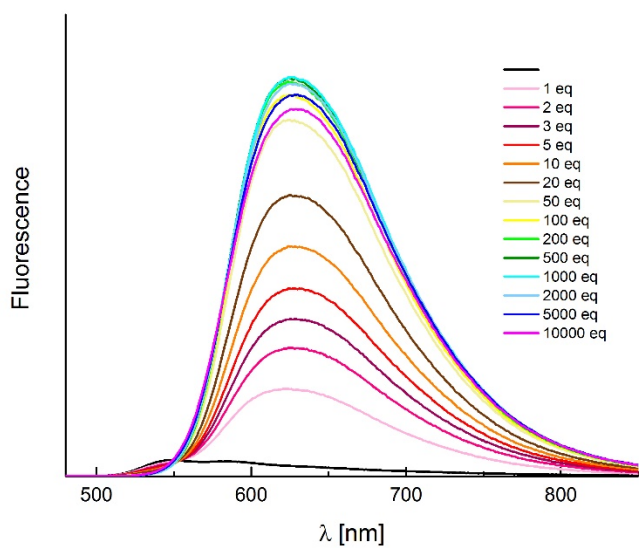


Fig. S42. The effect of $\text{Mg}(\text{ClO}_4)_2$ addition on the emission spectra of DPP 8 measured in ACN.

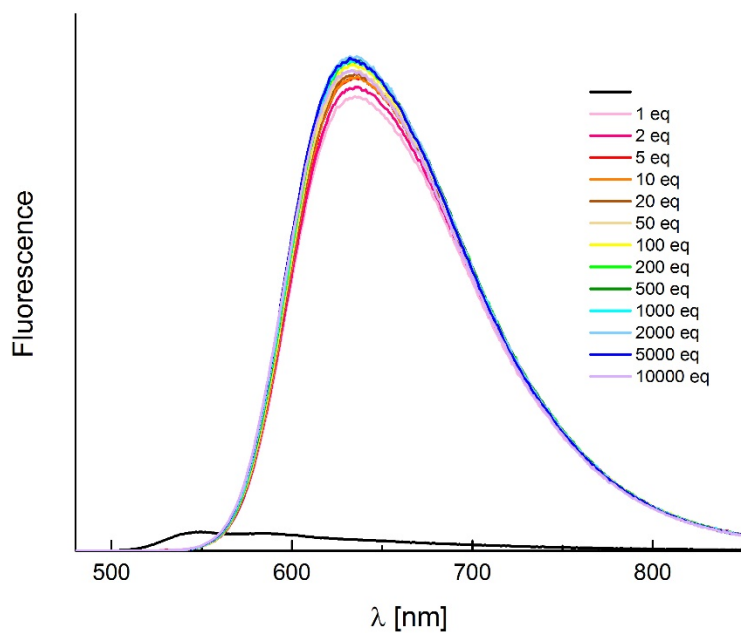


Fig. S43. The effect of $\text{Zn}(\text{ClO}_4)_2$ addition on the emission spectra of DPP **8** measured in ACN.

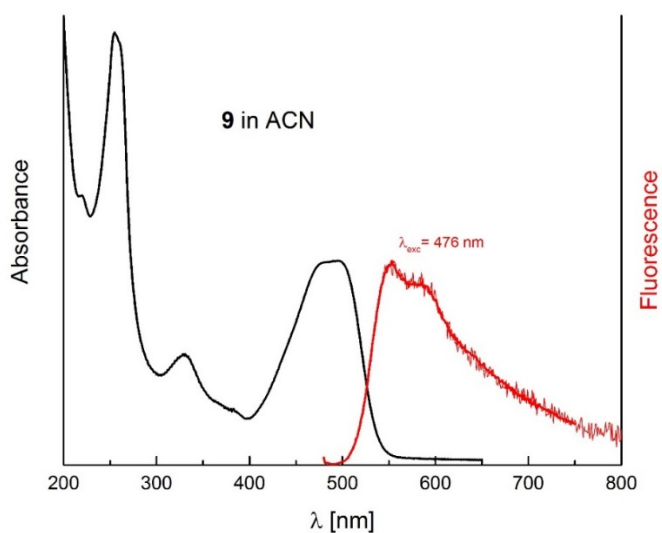


Fig. S44. The absorption and emission spectra of DPP **9** in acetonitrile.

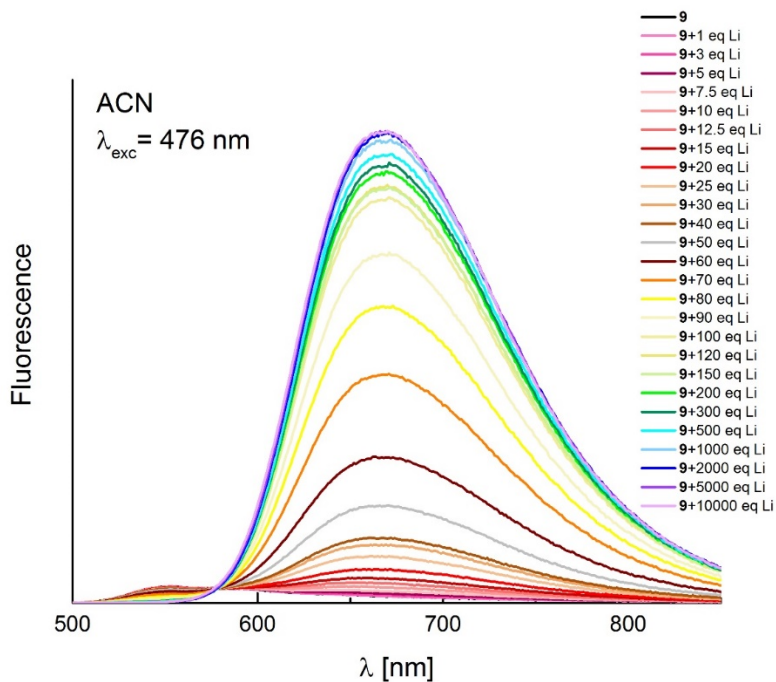


Fig. S45. The effect of LiClO₄ addition on the emission spectra of DPP 9 measured in ACN.

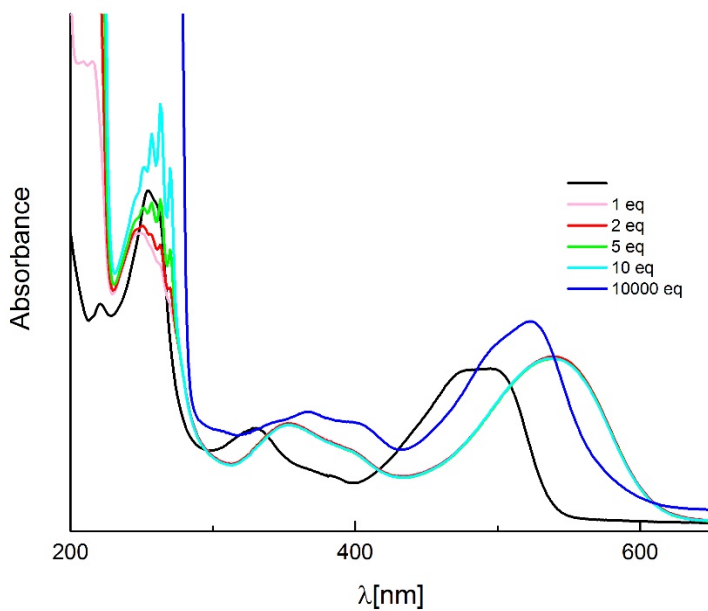


Fig. S46. The effect of PhSO₃H addition on the absorption spectra of DPP 9 measured in ACN.

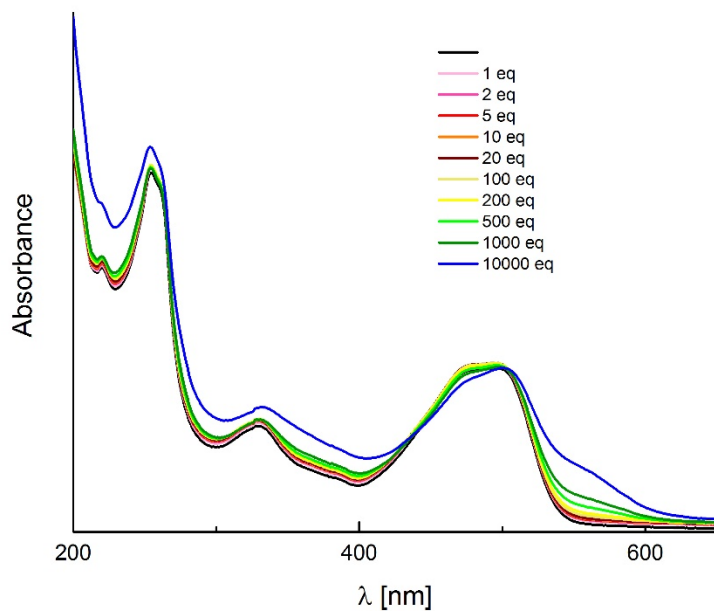


Fig. S47. The effect of $\text{Mg}(\text{ClO}_4)_2$ addition on the absorption spectra of DPP 9 measured in ACN.

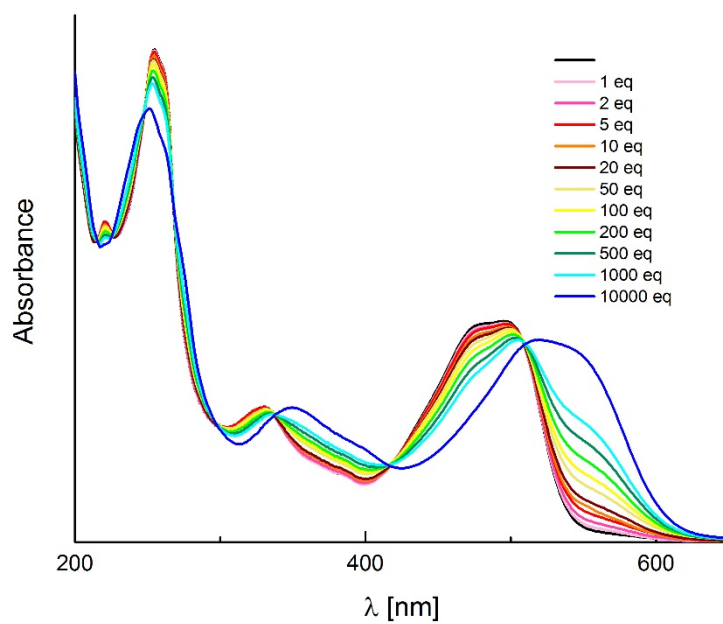


Fig. S48. The effect of $\text{Zn}(\text{ClO}_4)_2$ addition on the absorption spectra of DPP 9 measured in ACN.

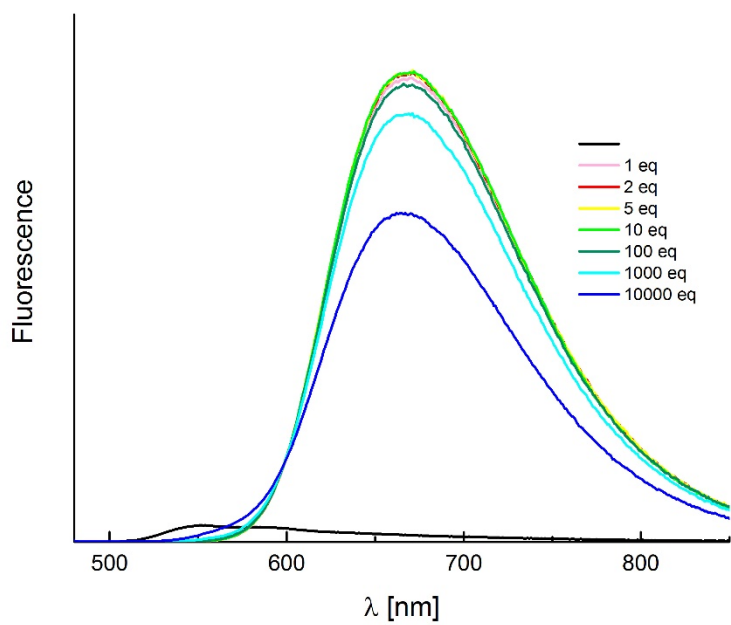


Fig. S49. The effect of PhSO₃H addition on the emission spectra of DPP 9 measured in ACN.

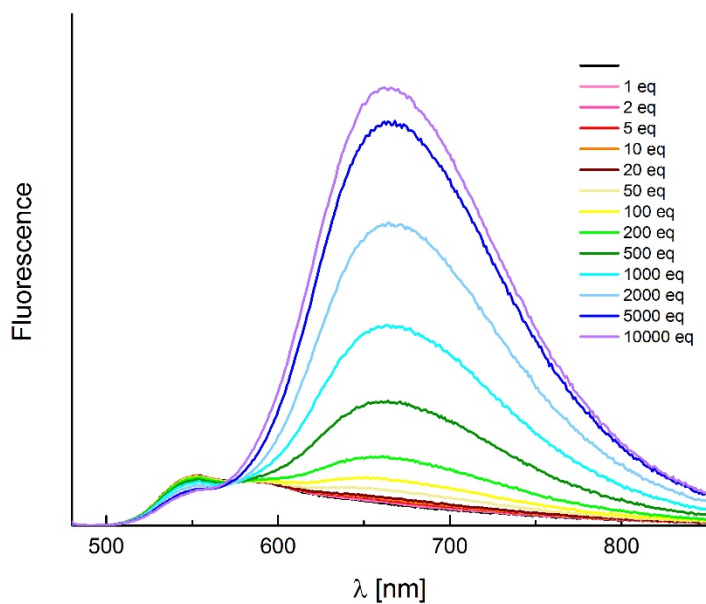


Fig. S50. The effect of Mg(ClO₄)₂ addition on the emission spectra of DPP 9 measured in ACN.

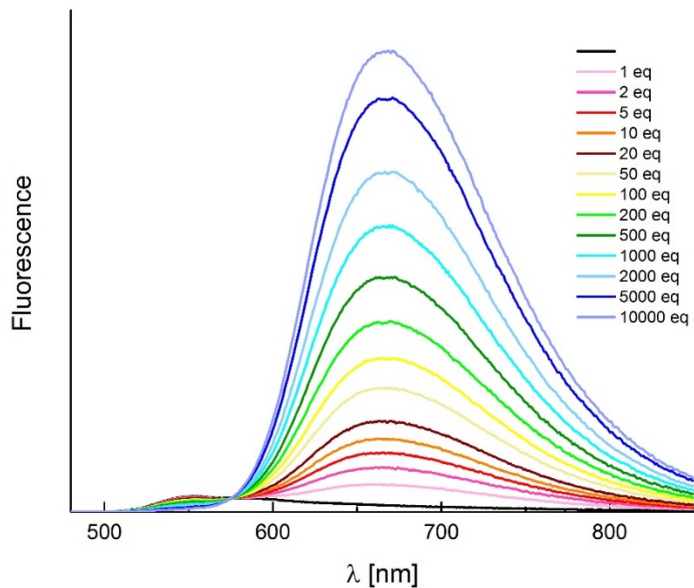


Fig. S51. The effect of $\text{Zn}(\text{ClO}_4)_2$ addition on the emission spectra of DPP **9** measured in ACN.

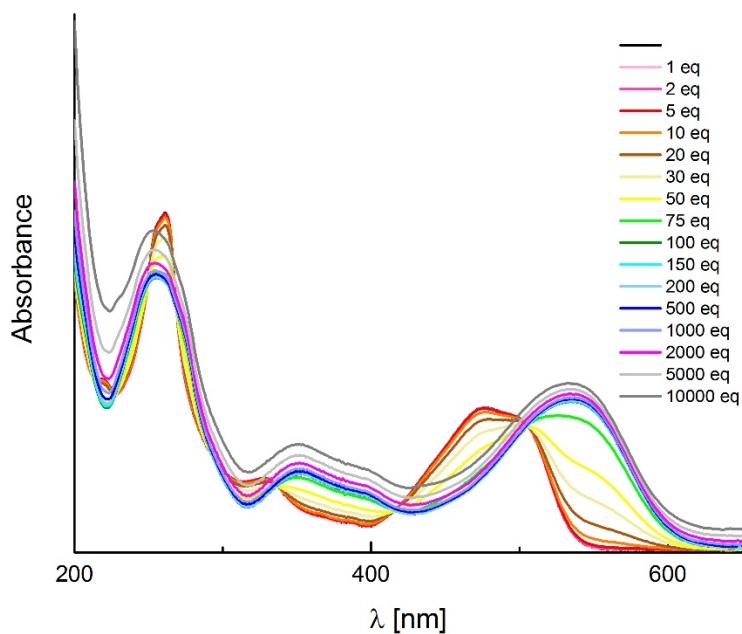


Fig. S52. The effect of LiClO_4 addition on the emission spectra of DPP **10** measured in ACN.

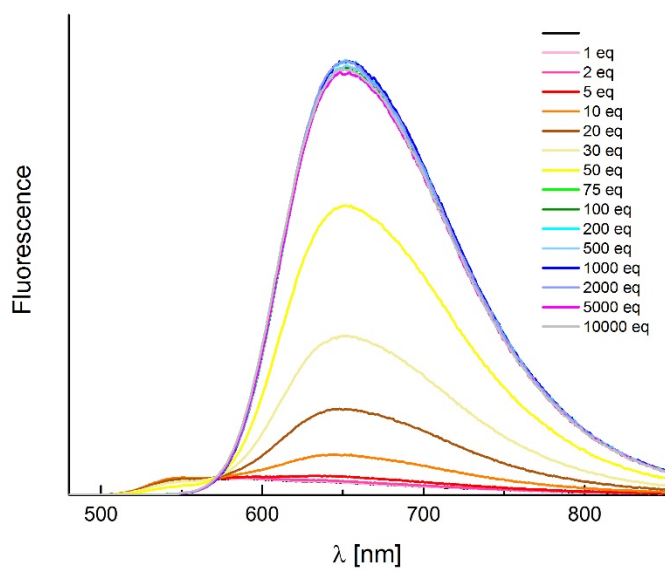
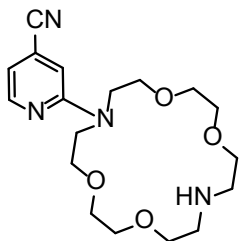
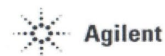
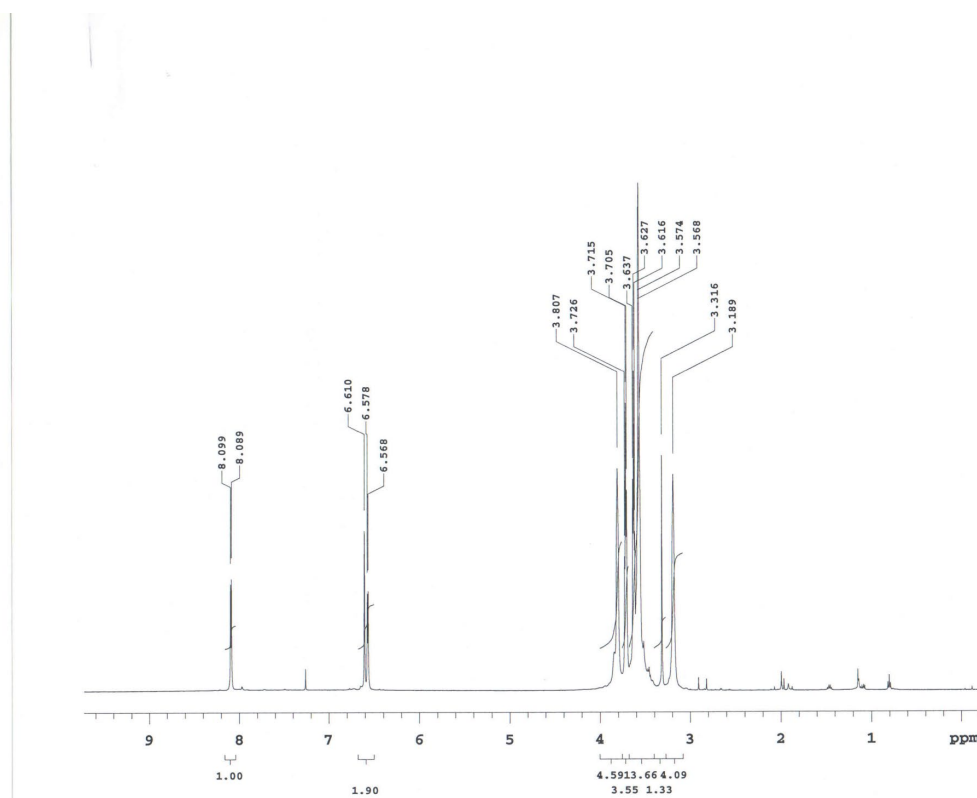


Fig. S53. The effect of LiClO₄ addition on the emission spectra of DPP **10** measured in ACN.

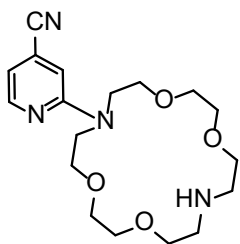
Section S4: ¹H NMR and ¹³C NMR Spectra



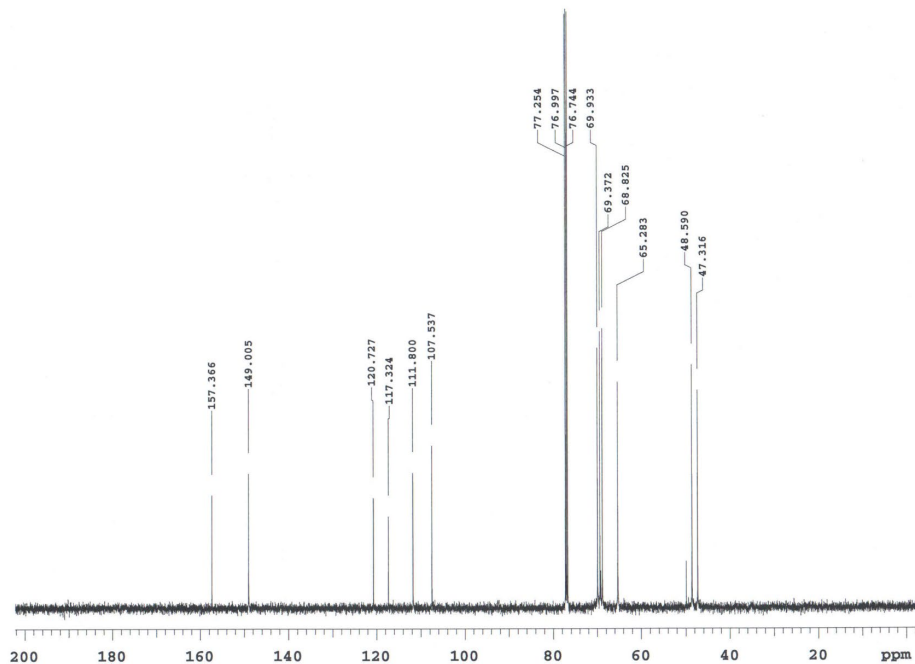
2e



D.Kumar
 resp10/Var500/GDK-115/GDK-115-H1
 Sample Name:
 GDK-115
 Data Collected on:
 Varian-NMR-vnmrs500
 Archive directory:
 Sample directory:
 Fidfile: PROTON
 Pulse Sequence: PROTON (s2pul)
 Solvent: cdcl3
 Data collected on: Apr 6 2020
 Temp. 25.0 C / 298.1 K
 Operator: vmmr1
 Relax. delay 1.000 sec
 Pulse 19.8 degrees
 Acq. time 4.000 sec
 Width 8012.8 Hz
 16 repetitions
 OBSERVE H1, 499.8247786 MHz
 DATA PROCESSING
 FT size 65536



2e



D.Kumar
resp10/Var500/GDK-115/GDK-115-C1
3

Sample Name:
GDK-115
Data Collected on:
Varian-NMR-vnmrs500
Archive directory:

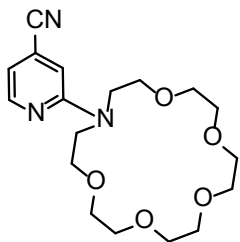
Sample directory:

FidFile: CARBON

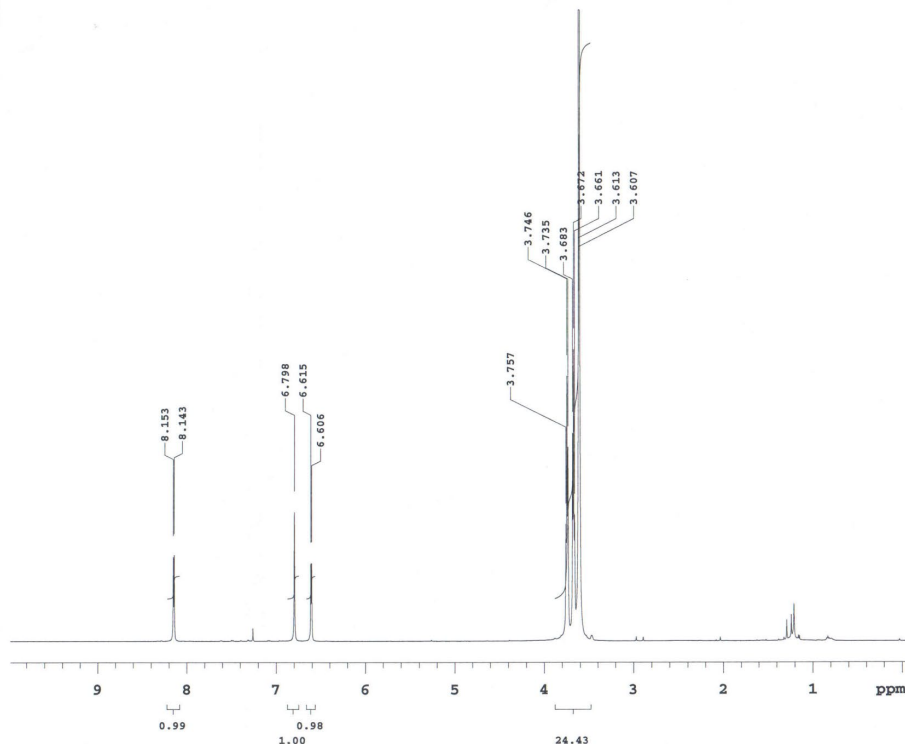
Pulse Sequence: CARBON (s2pul)
Solvent: cdcl3
Data collected on: Apr 6 2020

Temp. 25.0 C / 298.1 K
Operator: vnmr1

Relax. delay 0.500 sec
Pulse 30.0 degrees
Acq. time 1.200 sec
Width 37878.8 Hz
112 repetitions
OBSERVE C13, 125.6810703 MHz
DECOUPLE H1, 499.8272777 MHz
Power 36 dB
continuously on
WALTZ-16 modulated
DATA PROCESSING
Line broadening 1.0 Hz
Ft size 131072



2d



D.Kumar
zesp10/Var500/GDK-168/GDK-168-H1

Sample Name:
GDK-168
Data Collected on:
Varian-NMR-vmr5500
Archive directory:

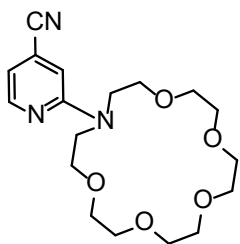
Sample directory:

FidFile: PROTON

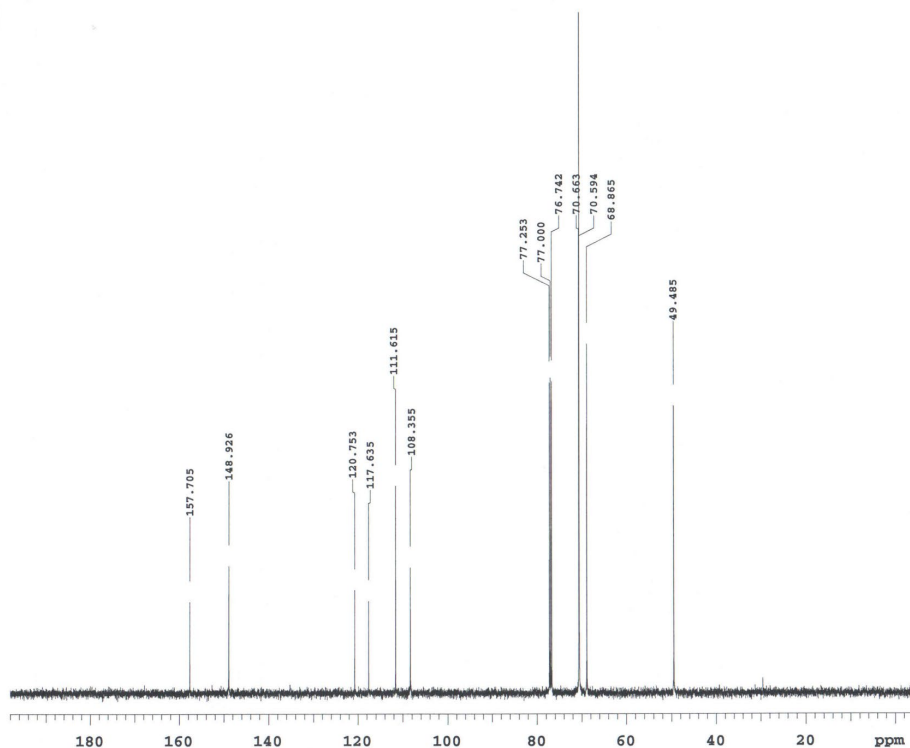
Pulse Sequence: PROTON (s2pul)
Solvent: cdcl3
Data collected on: Apr 6 2020

Temp. 25.0 C / 298.1 K
Operator: vmr1

Relax. delay 1.000 sec
Pulse 19.8 degrees
Acq. time 4.000 sec
Width 8012.8 Hz
16 repetitions
OBSERVE H1, 499.8247786 MHz
DATA PROCESSING
FT size 65536



2d



D.Kumar
zesp10/Var500/GDK-168/GDK-168-C1
3

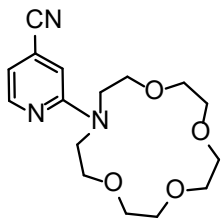
Sample Name:
GDK-168
Data Collected on:
Varian-NMR-vmms500
Archive directory:

Sample directory:
FidFile: CARBON

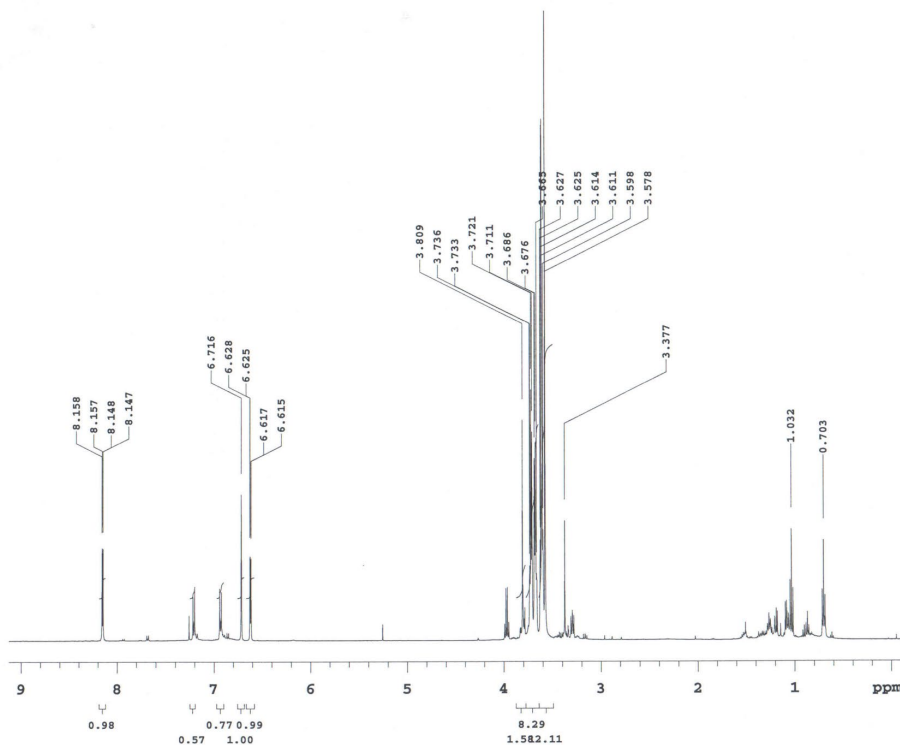
Pulse Sequence: CARBON (s2pu1)
Solvent: cdcl3
Data collected on: Apr 6 2020

Temp. 25.0 C / 298.1 K
Operator: vmr1

Relax. delay 0.500 sec
Pulse 30.0 degrees
Acq. time 1.200 sec
Width 37878.8 Hz
64 repetitions
OBSERVE C13, 125.6810549 MHz
DECOUPLE H1, 499.8272777 MHz
Power 36 dB
continuously on
WALTZ-16 modulated
DATA PROCESSING
Line broadening 1.0 Hz
FT size 131072



2f



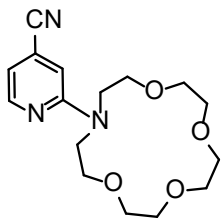
D.Kumar
zesp10/Var500/GDK-189/GDK-189-H1

Sample Name: GDK-189
Data Collected on: Varian-NMR-vnmrs500
Archive directory:
Sample directory:
FidFile: PROTON

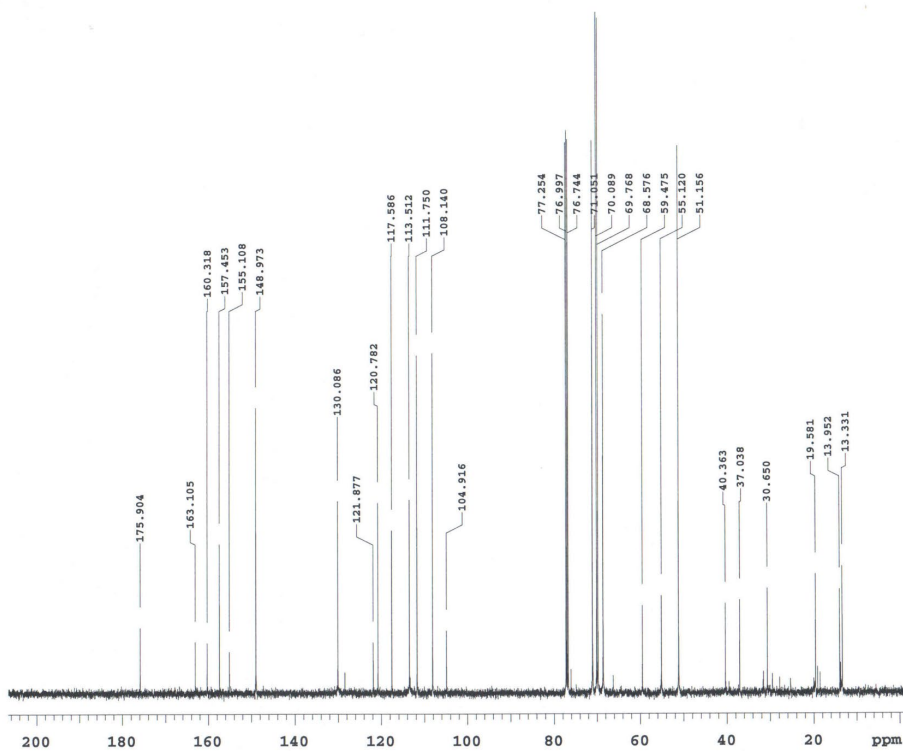
Pulse Sequence: PROTON (s2pul)
Solvent: cdcl3
Data collected on: Apr 6 2020

Temp. 25.0 C / 298.1 K
Operator: vnmr1

Relax. delay 1.000 sec
Pulse 19.8 degrees
Acq. time 4.000 sec
Width 8012.8 Hz
16 repetitions
OBSERVE H1, 499.8247786 MHz
DATA PROCESSING
FT size 65536



2f



D.Kumar
zesp10/Var500/GDK-189/GDK-189-C1
3

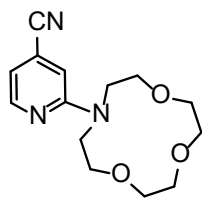
Sample Name:
GDK-189
Data Collected on:
Varian-NMR-vnmr500
Archive directory:

Sample directory:
FidFile: CARBON

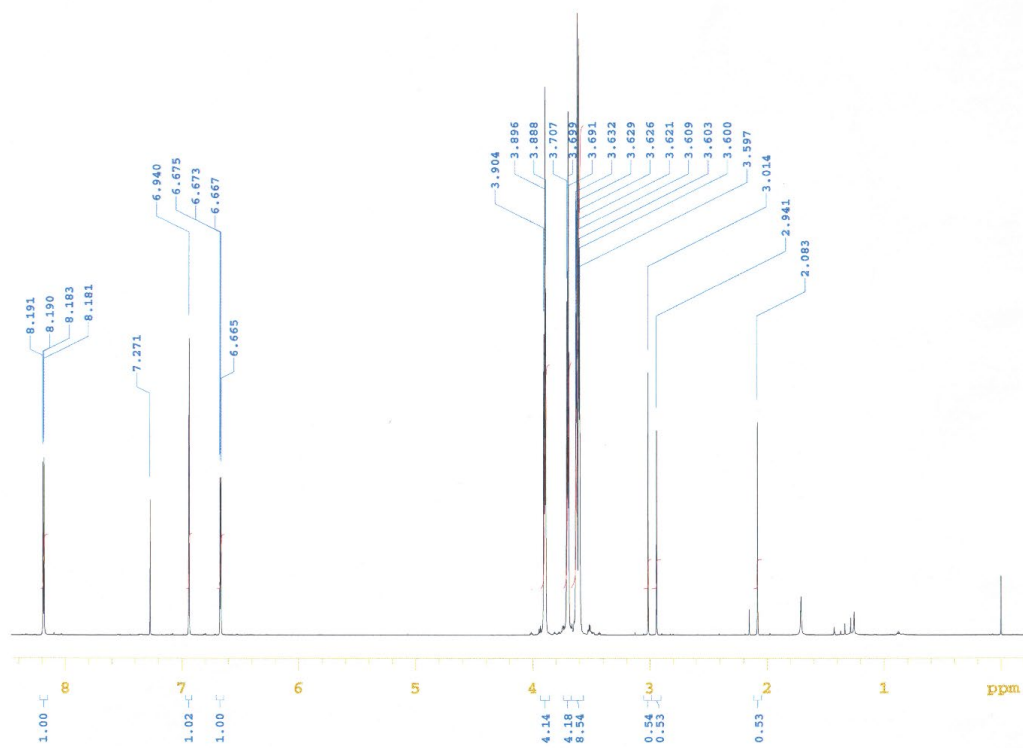
Pulse Sequence: CARBON (s2pul)
Solvent: cdcl3
Data collected on: Apr 6 2020

Temp. 25.0 C / 298.1 K
Operator: vnmr1

Relax. delay 0.500 sec
Pulse 30.0 degrees
Acq. time 1.200 sec
Width 37878.8 Hz
224 repetitions
OBSERVE C13, 125.6810564 MHz
DECOUPLE H1, 499.8272777 MHz
Power 35 dB
continuously on
WALTZ-16 modulated
DATA PROCESSING
Line broadening 1.0 Hz
FT size 131072



2h



D. Kumar

zep10/Var600/GDK-302/GDK-302

Sample Name: GDK-302
 Data Collected on: Varian-NMR-vmrs600
 Archive directory:

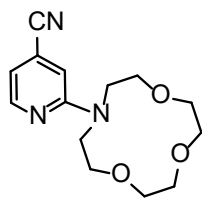
Sample directory:

FidFile: PROTON

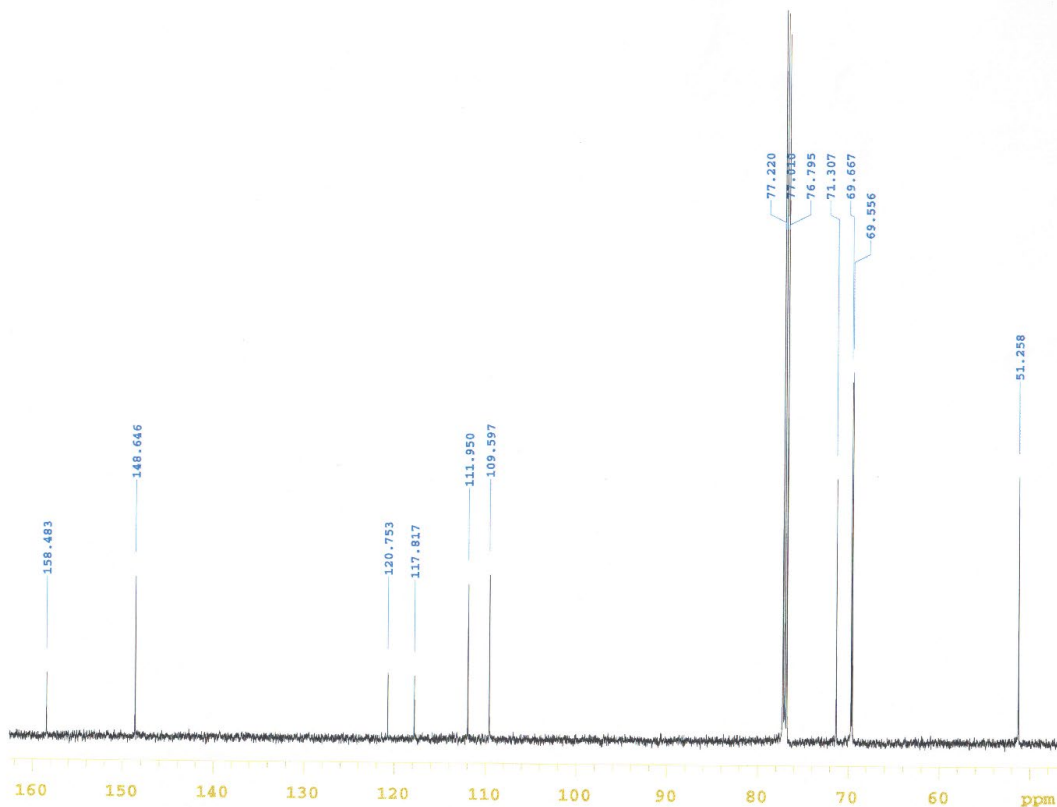
Pulse Sequence: PROTON (s2pul)
 Solvent: cdcl3
 Data collected on: Dec 9 2021

Solvent: cdcl3
 Temp. 25.0 C / 298.1 K
 Operator: vmr1
 VMRS-600 "Varian-NMR"

Relax. delay 1.000 sec
 Pulse 30.0 degrees
 Acq. time 4.000 sec
 Width 8333.3 Hz
 32 repetitions
 OBSERVE H1, 599.8350609 MHz
 DATA PROCESSING
 FT size 131072



2h



D. Kumar

zesp10/Var600/GDK-302/GDK-303

Sample Name: GDK-302
 Data Collected on: Varian-NMR-vmr600
 Archive directory:

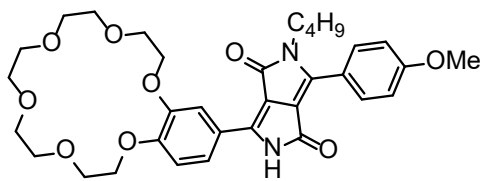
Sample directory:

Fidfile: CARBON

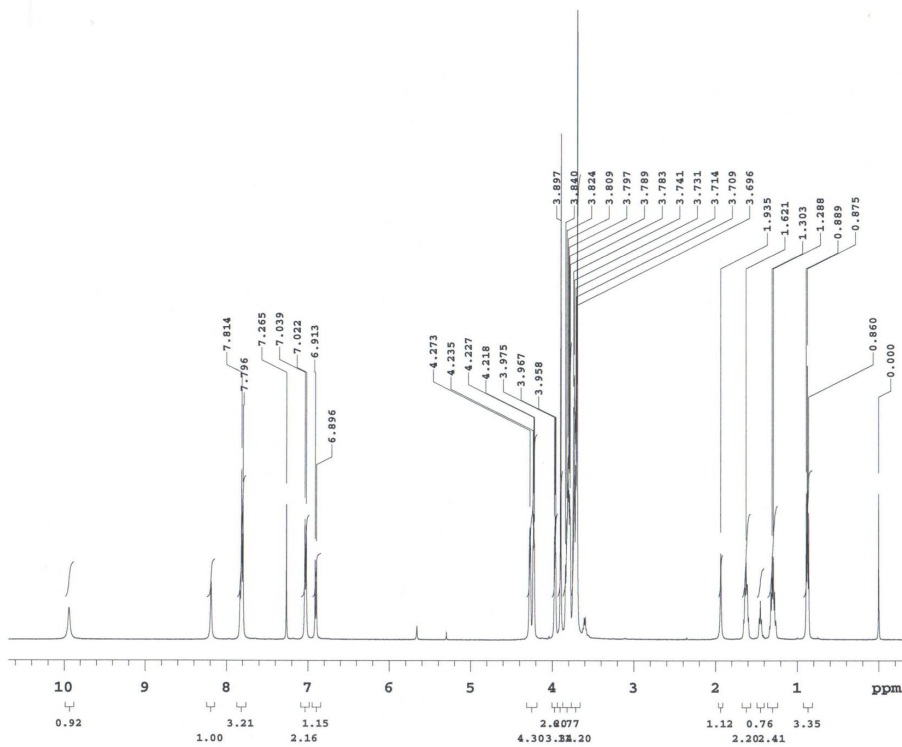
Pulse Sequence: CARBON (s2pu)
 Solvent: cdcl3
 Data collected on: Dec 9 20:

Solvent: cdcl3
 Temp. 25.0 C / 298.1 K
 Operator: vmr1
 VMRS-600 "Varian-NMR"

Relax. delay 0.500 sec
 Pulse 30.0 degrees
 Acq. time 1.200 sec
 Width 37878.8 Hz
 480 repetitions
 OBSERVE C13, 150.8286494 MHz;
 DECOUPLE H1, 599.8380734 MHz;
 Power 34 dB
 continuously on
 WALTZ-16 modulated
 DATA PROCESSING
 Line broadening 2.0 Hz
 FT size 131072



3



Dinesh Kumar
 resp10/Var500/GiDK-188/GiDK-188-
 H1

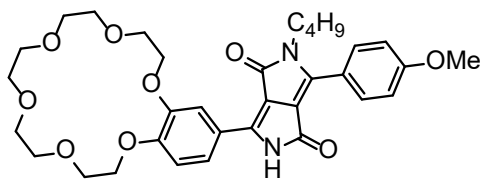
Sample Name:
 GiDK-188
 Data Collected on:
 Varian-NMR-vmmr500
 Archive directory:

Sample directory:
 Fidfile: PROTON

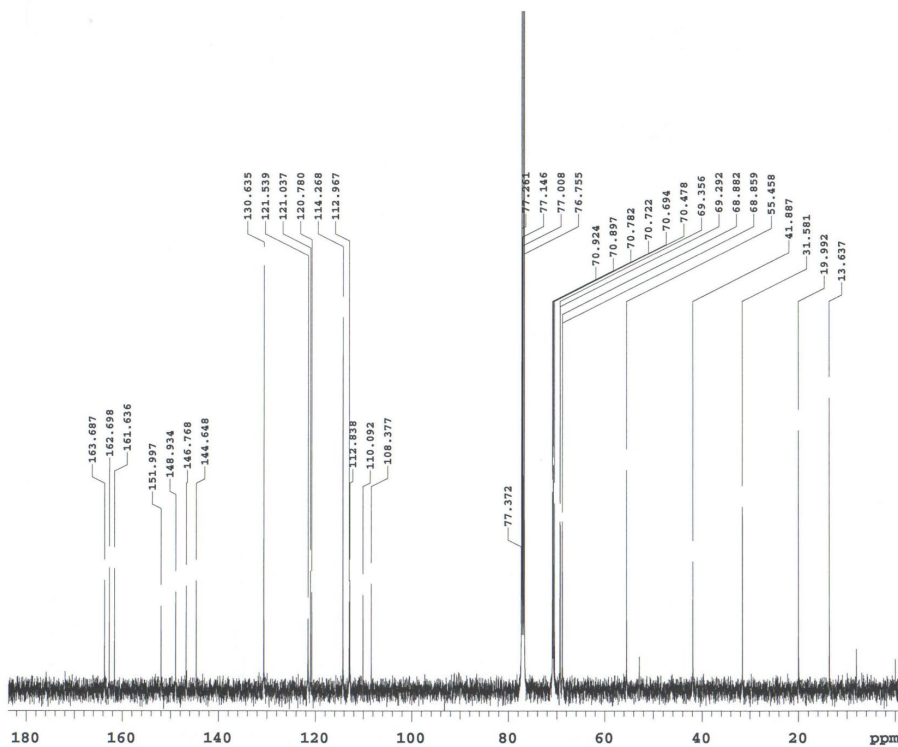
Pulse Sequence: PROTON (s2pul)
 Solvent: cdcl3
 Data collected on: Feb 6 2020

Temp. 25.0 C / 298.1 K
 Operator: vmmr1

Relax. delay 1.000 sec
 Pulse 45.0 degrees
 Acq. time 4.000 sec
 Width 8012.8 Hz
 32 repetitions
 OBSERVE H1, 499.8247754 MHz
 DATA PROCESSING
 FT size 65536



3



Dinesh Kumar
zesp10/Var500/GiDK-188/GiDK-188-C13

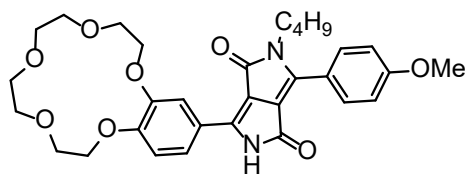
Sample Name: GiDK-188
Data Collected on: Varian-NMR-vnmr500
Archive directory:

Sample directory:
FidFile: CARBON

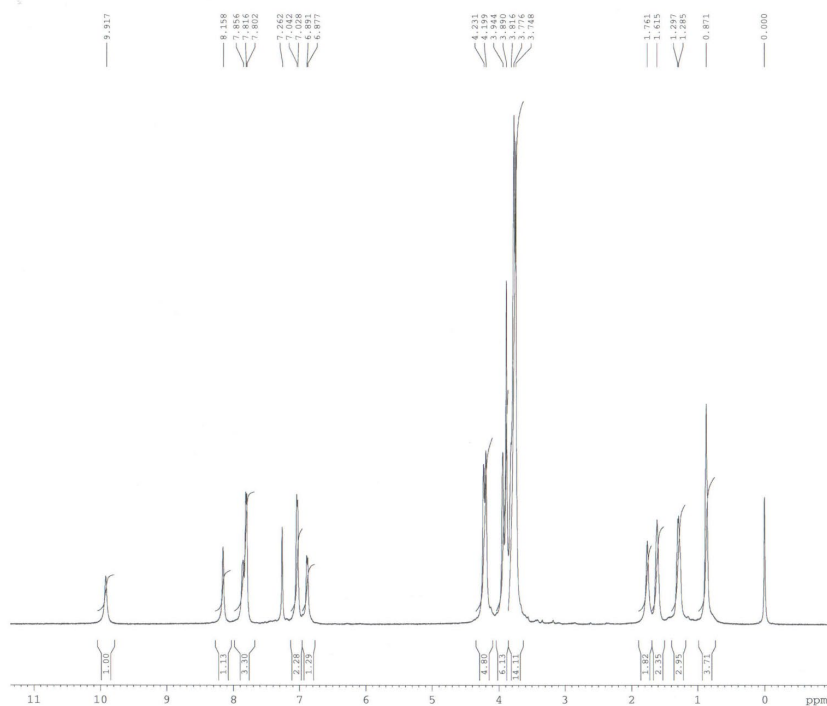
Pulse Sequence: CARBON (s2pul)
Solvent: cdcl3
Data collected on: Feb 6 2020

Temp. 25.0 C / 298.1 K
Operator: vnmr1

Relax. delay 0.500 sec
Pulse 30.0 degrees
Acq. time 1.200 sec
Width 37878.8 Hz
1600 repetitions
OBSERVE C13, 125.6810405 MHz
DECOUPLE H1, 499.8272777 MHz
Power 36 dB
continuously on
WALTZ-16 modulated
DATA PROCESSING
Line broadening 1.0 Hz
FT size 131072



4

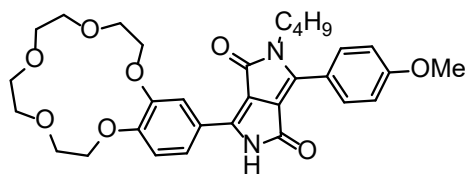


Current Data Parameters
 NAME GDK-167-DPP-pure
 EXPNO 1
 PROCNO 1

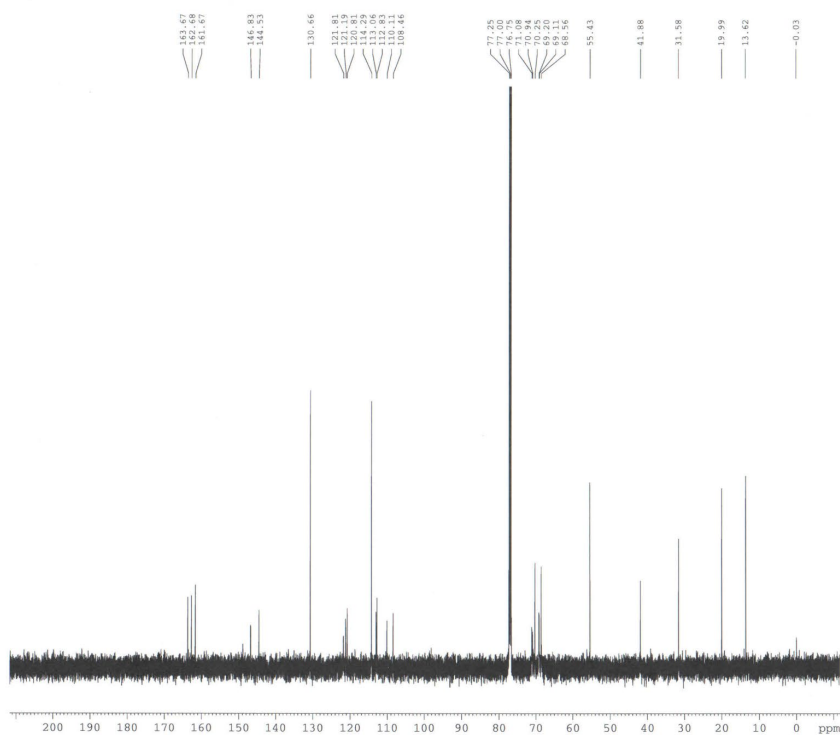
F2 - Acquisition Parameters
 Date_ 20200121
 Time 13.40
 INSTRUM DRX
 PROBHD 5 mm TBI 1H/13
 PULPROG zgpg30
 TD 65536
 SOLVENT CDCl3
 NS 32
 DS 0
 SWH 10330.578 Hz
 FIDRES 0.157632 Hz
 AQ 3.1719923 sec
 RG 143.7
 DW 48.400 usec
 DE 6.78 usec
 TE 303.0 K
 D1 1.00000000 sec
 TDO 1

===== CHANNEL f1 =====
 NUCL1 1H
 P1 2.50 usec
 PL1 0.00 dB
 SFO1 500.1330885 MHz

F2 - Processing parameters
 SI 32768
 SF 500.1300222 MHz
 WDW no
 SSB 0
 LB 0.00 Hz
 GB 0
 PC 1.00



4



```

Current Data Parameters
NAME      GDK-167-DPP-pure
EXPNO    2
PROCNO   1

F2 - Acquisition Parameters
Date_    20200121
Time     11.58
INSTRUM  DEX
PROBHD   5 mm TBI 1H/13
PULPROG  zgpg2
TD        65536
SOLVENT  CDCl3
NS        5000
DS        4
SWH       32679.738 Hz
FIDRES    0.499653 Hz
AQ         1.0027508 sec
RG         32768
SW         15.300 usec
DE         7.10 usec
TE         303.0 K
D1         1.00000000 sec
d11        0.03000000 sec
DELTA     0.89999998 sec
TDO        4

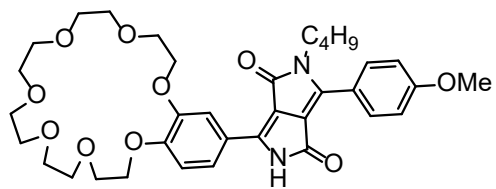
===== CHANNEL f1 =====
NUC1      13C
P1         5.00 usec
PL1        -3.00 dB
SFO1      125.7703643 MHz

===== CHANNEL f2 =====
CYPRG2    waltz16
NUC2       1H
PCPD2     98.00 usec
PL2        3.00 dB
PL12       23.00 dB
PL13       32.00 dB
SFO2      500.1320005 MHz

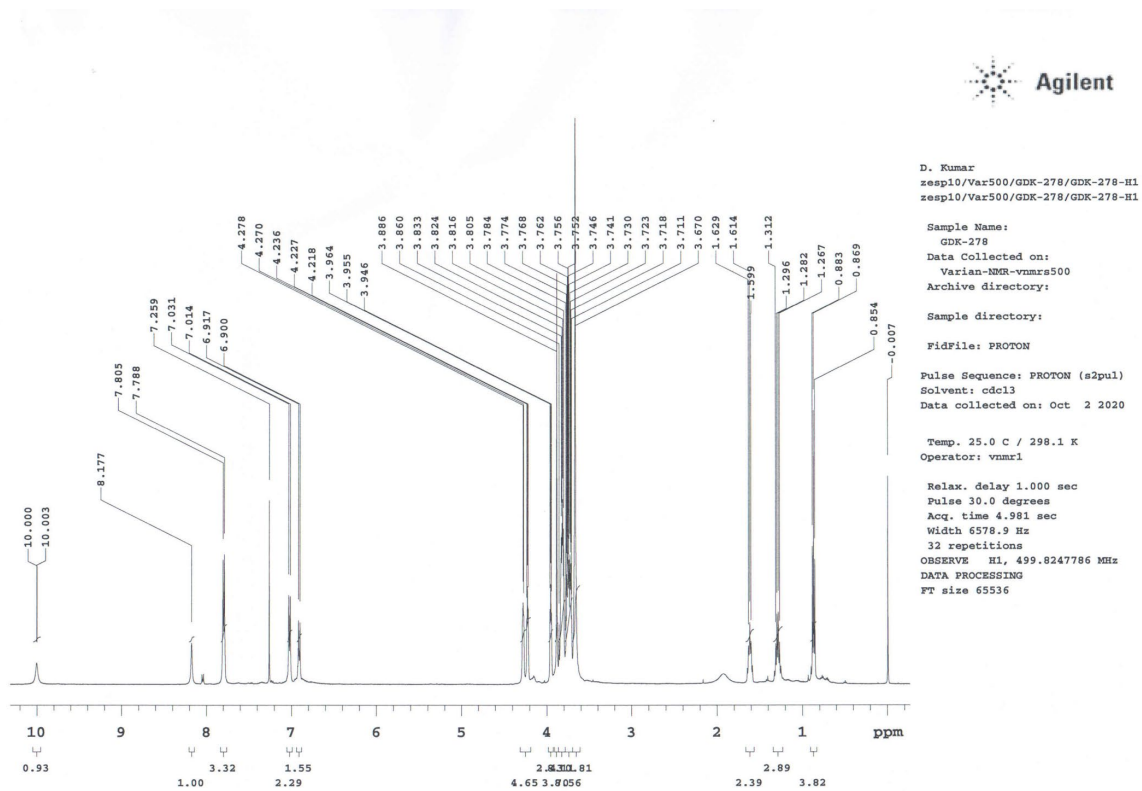
F1 - Acquisition parameters
ND0        2
TD         128
SFO1      500.132 MHz
FIDRES     7.812500 Hz
SW         1.999 ppm
PRMODE     QF

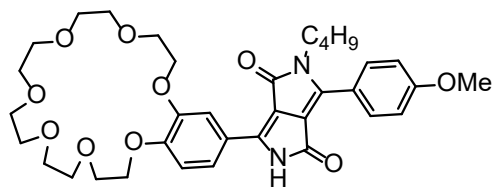
F2 - Processing parameters
SI         262144
SF         125.7577937 MHz
WDW        RM
SSB        0
LB         0.50 Hz
GB         0
PC         1.40

F1 - Processing parameters
SI         1024
MC2        QF
SFO1      500.1300000 MHz
WDW        SINE
SSB        0
LB         0.30 Hz
GB         0.1
  
```

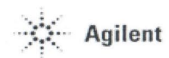
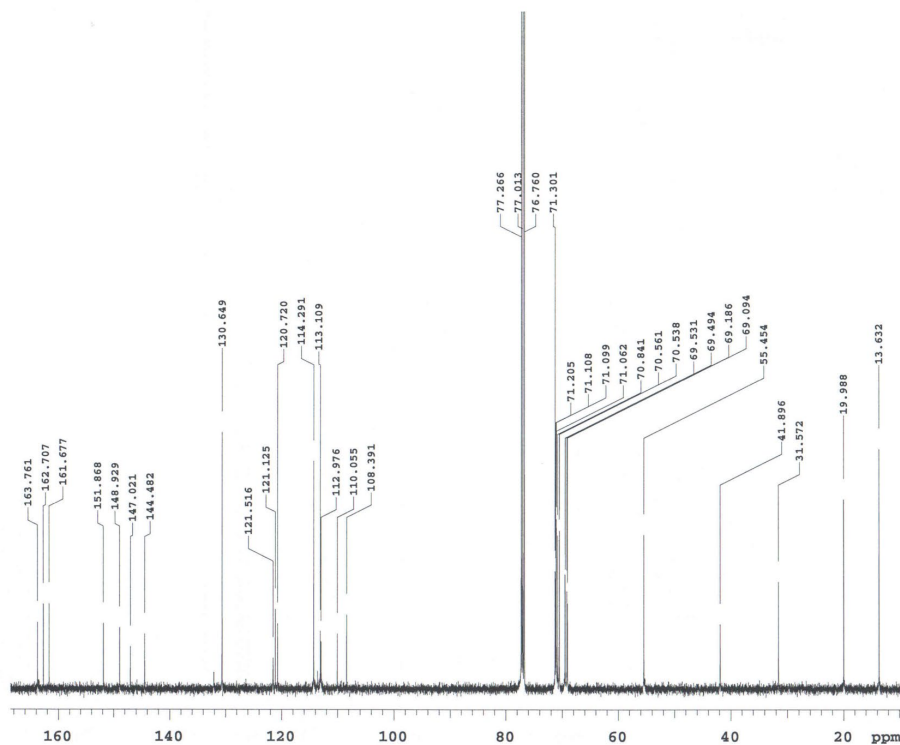


5





5



D. Kumar
zesp10/Var500/GDK-278/GDK-278-C1
3

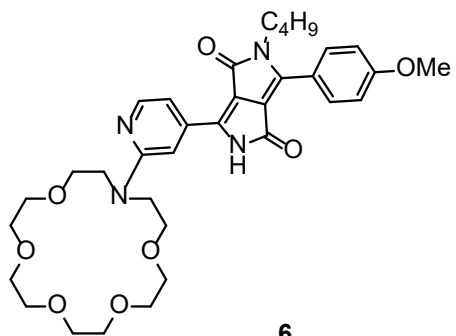
Sample Name:
GDK-278
Data Collected on:
Varian-NMR-vmr500
Archive directory:

Sample directory:
FidFile: CARBON

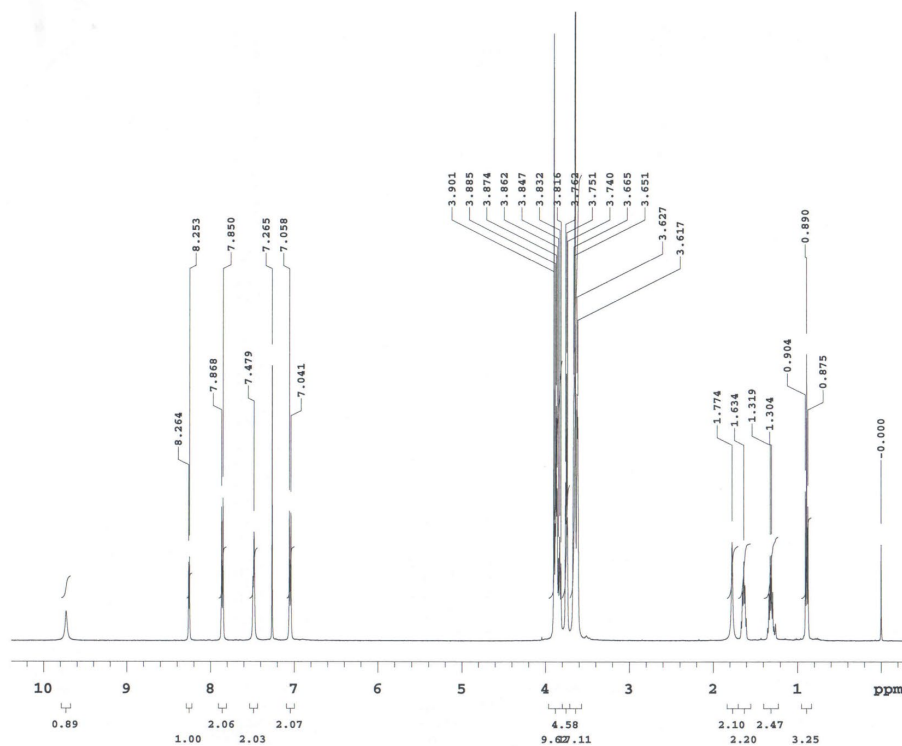
Pulse Sequence: CARBON (s2pul)
Solvent: cdcl3
Data collected on: Oct 2 2020

Temp. 25.0 C / 298.1 K
Operator: vmr1

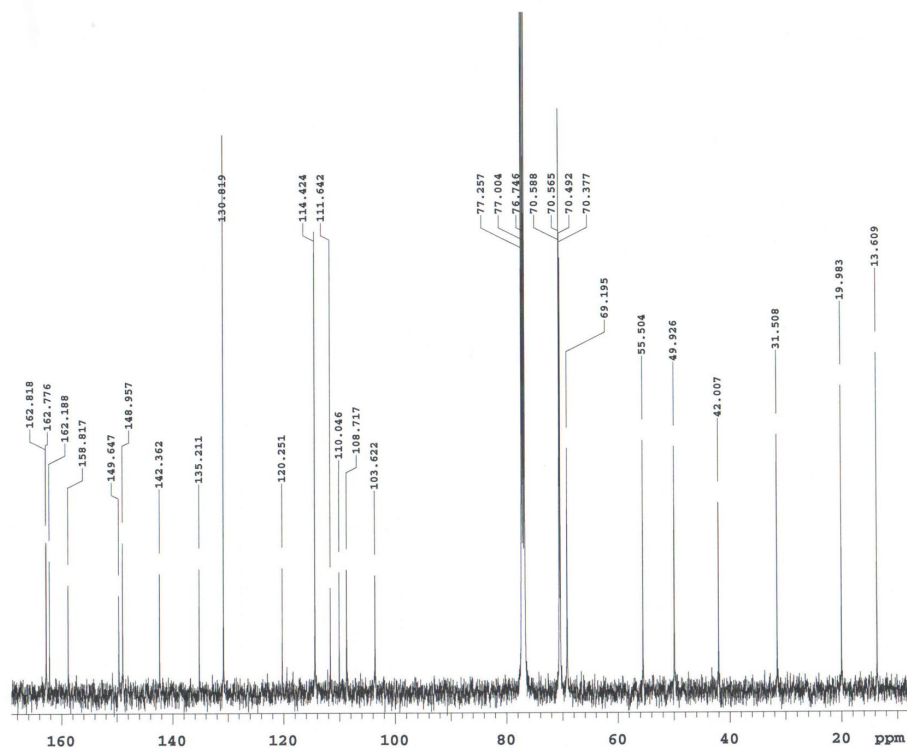
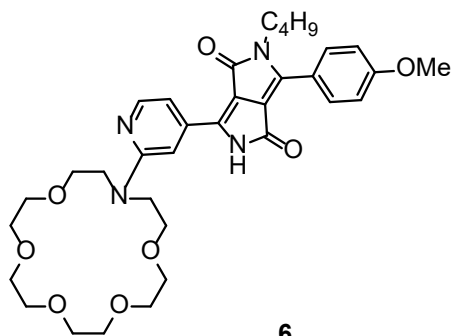
Relax. delay 0.500 sec
Pulse 30.0 degrees
Acq. time 1.200 sec
Width 37878.8 Hz
2416 repetitions
OBSERVE C13, 125.6810405 MHz
DECOUPLE H1, 499.8272777 MHz
Power 36 dB
continuously on
WALTZ-16 modulated
DATA PROCESSING
Line broadening 0.5 Hz
FT size 131072



6



Dinesh Kumar
 resp10/Var500/GDK-168-DPP/GDK-16
 8-DPP-H1
 Sample Name:
 GDK-168-DPP
 Data Collected on:
 Varian-NMR-vnmrs500
 Archive directory:
 Sample directory:
 Fidfile: PROTON
 Pulse Sequence: PROTON (s2pul)
 Solvent: cdcl3
 Data collected on: Nov 21 2019
 Temp. 25.0 C / 298.1 K
 Operator: vmm1
 Relax. delay 1.000 sec
 Pulse 45.0 degrees
 Acq. time 3.618 sec
 Width 9058.0 Hz
 32 repetitions
 OBSERVE H1, 499.8247749 MHz
 DATA PROCESSING
 FT size 65536



Dinesh Kumar
 zesp10/Var500/GDK-168-DPP/GDK-16
 8-DPP-C13

Sample Name:
 GDK-168-DPP
 Data Collected on:
 Varian-NMR-vnmrs500
 Archive directory:

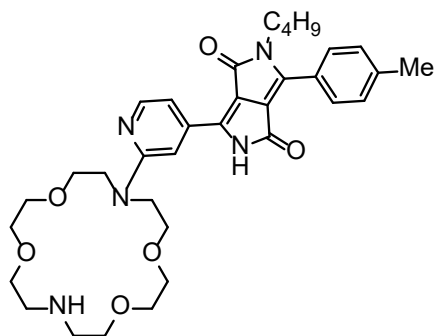
Sample directory:

FidFile: CARBON

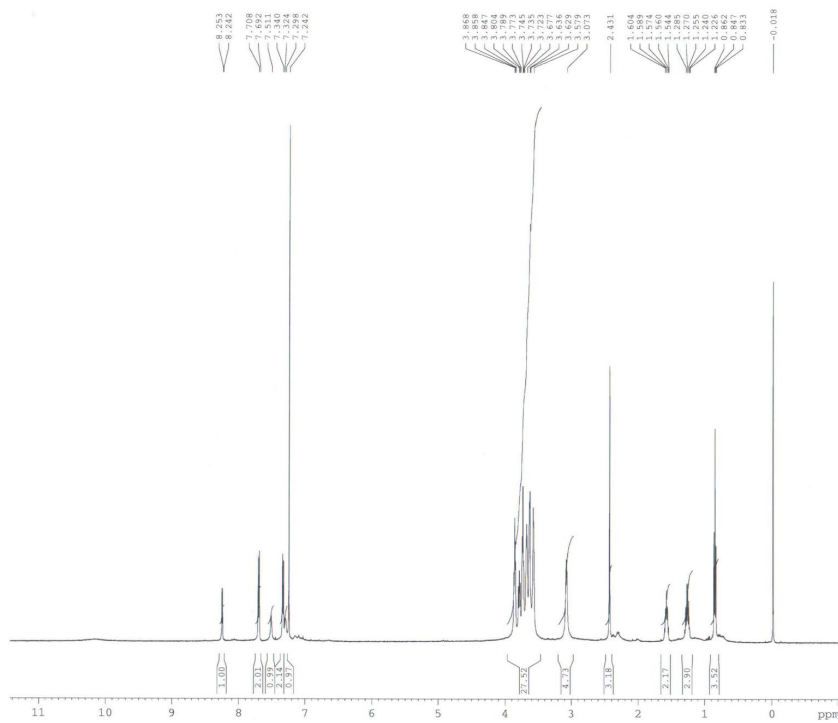
Pulse Sequence: CARBON (s2pul)
 Solvent: cdcl3
 Data collected on: Nov 21 2019

Temp. 25.0 C / 298.1 K
 Operator: vnmr1

Relax. delay 0.500 sec
 Pulse 30.0 degrees
 Acq. time 1.200 sec
 Width 37878.8 Hz
 2032 repetitions
 OBSERVE C13, 125.6810405 MHz
 DECOUPLE H1, 499.8272777 MHz
 Power 36 dB
 continuously on
 WALTZ-16 modulated
 DATA PROCESSING
 Line broadening 2.0 Hz
 FT size 131072



7



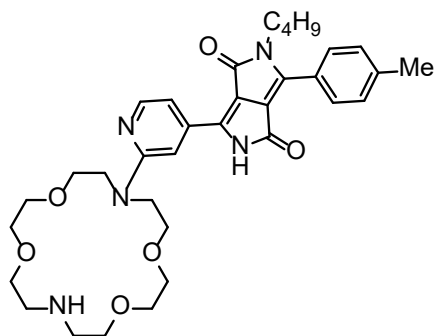
```

Current Data Parameters
NAME          GDK-117
EXPNO         1
PROCNO        1

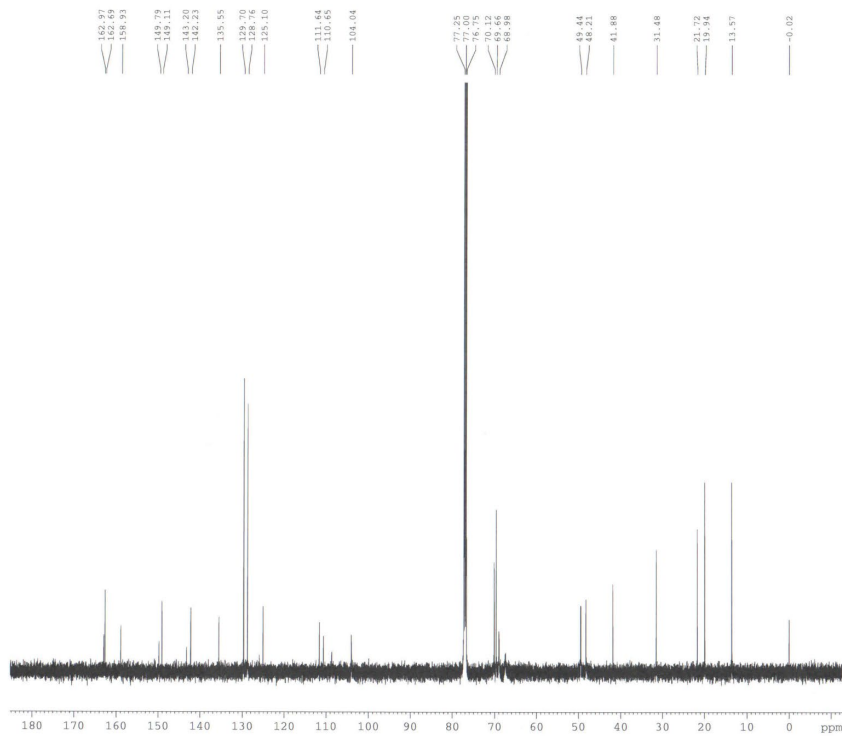
F2 - Acquisition Parameters
Date_         20190131
Time          11.59
INSTRUM       DSK
PROBHD        5 mm TBI 1H/13
PULPROG       zg30
TD            65536
SOLVENT       CDCl3
NS            32
DS            0
SWH           10330.578 Hz
FIDRES        0.157632 Hz
AQ            3.1719923 sec
RG            322.5
DW            48.400 usec
DE            6.78 usec
TE            301.0 K
D1            1.00000000 sec
TDO           1

===== CHANNEL f1 =====
NUC1          1H
P1            8.20 usec
PL1           5.00 dB
SFO1          500.1330885 MHz

F2 - Processing parameters
SI            32768
SF            500.1300326 MHz
WDW           no
SSB           0
LB            0.00 Hz
GB            0
PC            1.00
  
```



7



```

Current Data Parameters
NAME      GDK-117
EXPNO    2
PROCNO   1

F2 - Acquisition Parameters
Date_    20190111
Time     12.29
INSTRUM  DSK
PROBHD   5 mm TBI 1H/13
PULPROG  zgpg
TD        65536
SOLVENT  CDCl3
NS        32501
DS        4
SWH       32679.738 Hz
FIDRES    0.498653 Hz
AQ        1.0027508 sec
RG        32768
DW        15.300 usec
DE        7.10 usec
TE        303.0 K
D1        1.00000000 sec
d11       0.03000000 sec
DELTA     0.89999998 sec
TD0       4

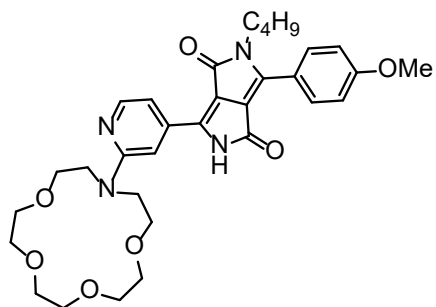
***** CHANNEL f1 *****
NUC1      13C
P1        5.00 usec
PL1       -1.00 dB
SFO1      125.7703643 MHz

***** CHANNEL f2 *****
CPDPRG2   waltz16
NUC2      1H
PCPD2     98.00 usec
PL2        1.00 dB
PL12       23.00 dB
PL13       32.00 dB
SFO2      500.1320005 MHz

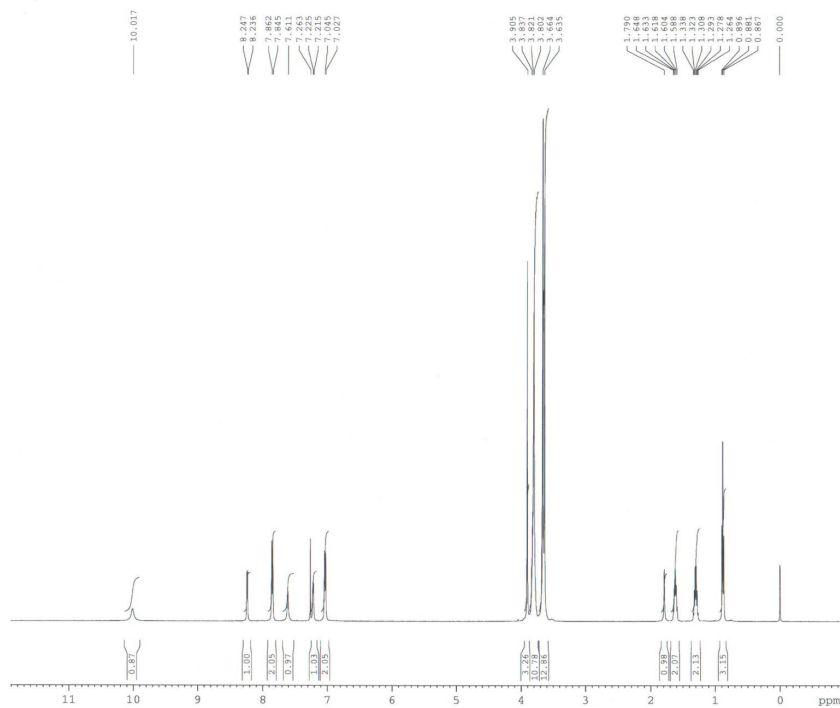
F1 - Acquisition parameters
ND0       128
SFO1      500.132 MHz
FIDRES    7.812500 Hz
SW        1.999 ppm
PUMODE    QF

F2 - Processing parameters
SI         262144
SF         125.7577927 MHz
WMW        8
SGB        0.50 Hz
GB         0
PC         1.40

F1 - Processing parameters
SI         1024
MC2        QF
SF         500.1300000 MHz
WMW        8
SGB        0.30 Hz
GB         0.1
  
```



8

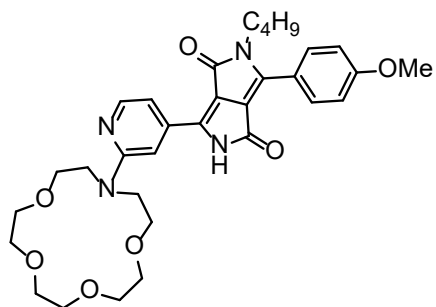


Current Data Parameters
 NAME GDK-190
 EXPNO 1
 PROCNO 1

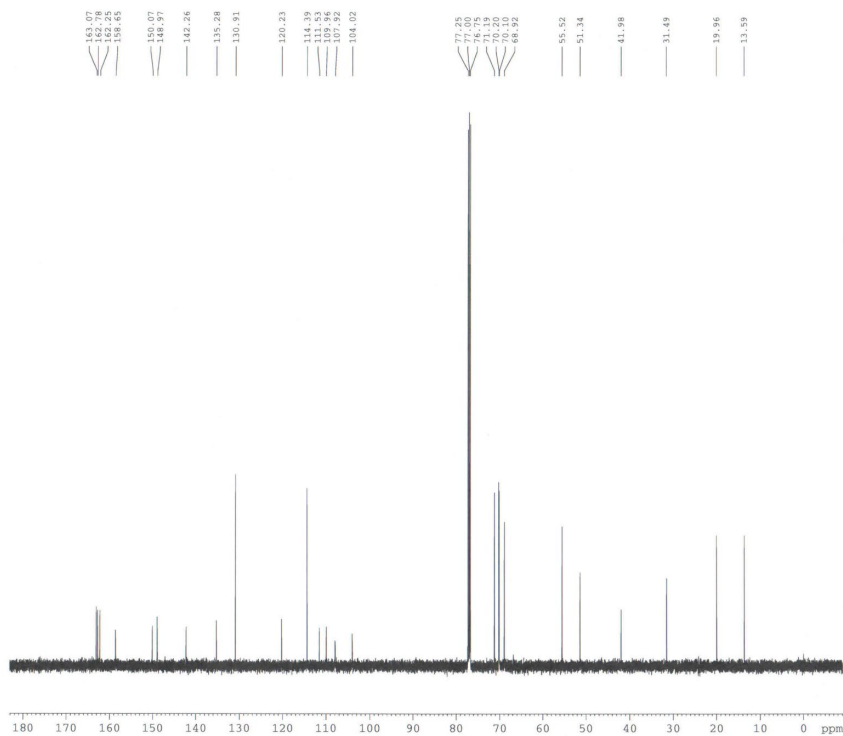
F2 - Acquisition Parameters
 Date_ 20200213
 Time 11.30
 INSTRUM DRX
 PROBHD 5 mm TBI 1H/13
 PULPROG zg
 TD 65536
 SOLVENT CDCl3
 NS 32
 DS 0
 SWH 10330.578 Hz
 FIDRES 0.157632 Hz
 AQ 3.1719923 sec
 RG 114
 DW 48.400 usec
 DE 6.78 usec
 TE 303.0 K
 D1 1.0000000 sec
 TDO 1

===== CHANNEL f1 =====
 NUC1 1H
 P1 2.50 usec
 PL1 0.00 dB
 SFO1 500.1330885 MHz

F2 - Processing parameters
 SI 32768
 SF 500.1300221 MHz
 WDW no
 SSB 0
 LB 0.00 Hz
 GB 0
 PC 1.00



8



```

Current Data Parameters
NAME      GDR-190
EXPNO     2
PROCNO    1

F2 - Acquisition Parameters
Date_     20200213
Time      12.16
INSTRUM   D00
PROBHD    5 mm TBI 1H/13
PULPROG   zgpg
TD         65536
SOLVENT   CDCl3
NS         3000
DS         4
SWH        32679.739 Hz
FIDRES     0.498653 Hz
AQ         1.0027508 sec
RG         32768
DW         15.300 usec
DE         7.10 usec
TE         303.0 K
D1         1.0000000 sec
d11        0.3300000 sec
DELTA      0.8999999 sec
TDO        1

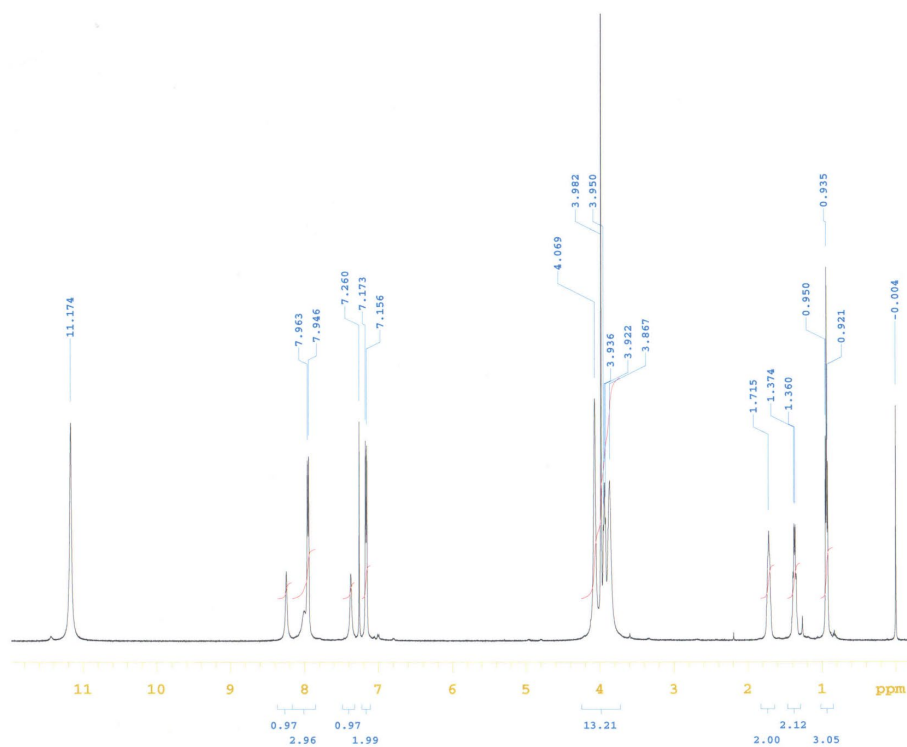
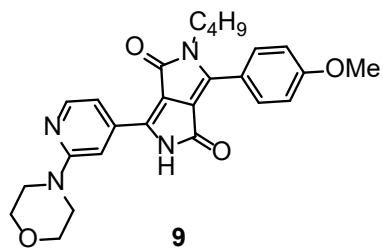
===== CHANNEL f1 =====
NUC1       13C
P1         5.00 usec
PL1        -3.00 dB
SFO1       125.7703641 MHz

===== CHANNEL f2 =====
CPDPRG2   waltz16
NUC2       1H
PCPD2     98.00 usec
PL2        3.00 dB
PL12       23.00 dB
PL13       32.00 dB
SFO2       500.1320005 MHz

F1 - Acquisition parameters
RG        1
TD        128
SFO1      500.132 MHz
FIDRES    7.812500 Hz
SW        1.999 ppm
FWhMODE   QF

F2 - Processing parameters
SI         262144
SF         125.7577937 MHz
WDW        EM
SSB        0
LB         0.50 Hz
GB         0
PC         1.40

F1 - Processing parameters
SI         1024
NUC2       13C
SF         500.1300000 MHz
WDW        EM
SSB        0
LB         0.30 Hz
GB         0.1
  
```



D.Kumar
resp10/Var500/GDK-279/GDK-279-H1

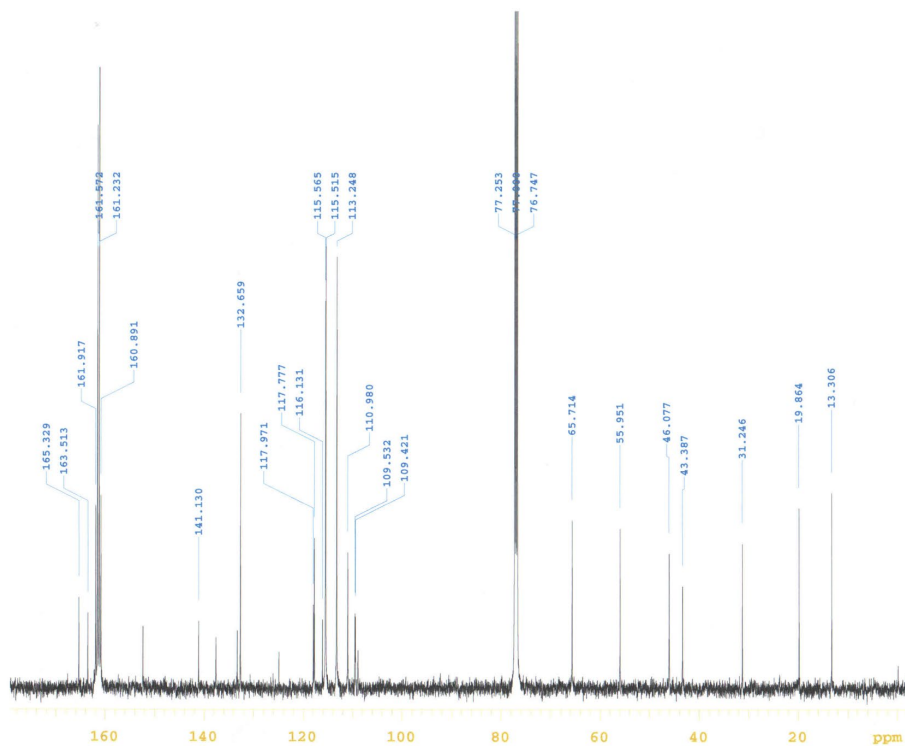
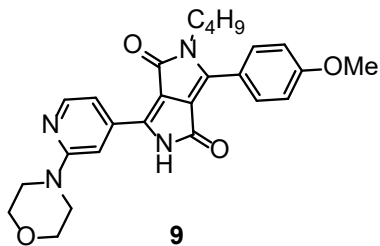
Sample Name:
GDK-279
Data Collected on:
Varian-NMR-vnmrs500
Archive directory:

Sample directory:

FidFile: PROTON
Pulse Sequence: PROTON (s2pul)
Solvent: cdcl3
Data collected on: Sep 29 2020

Temp. 25.0 C / 298.1 K
Operator: vnmr1

Relax. delay 1.000 sec
Pulse 45.0 degrees
Acq. time 4.000 sec
Width 8012.8 Hz
16 repetitions
OBSERVE H1, 499.8247786 MHz
DATA PROCESSING
FT size 65536



D.Kumar
 resp10/Var500/GDK-279/GDK-279-C1
 3

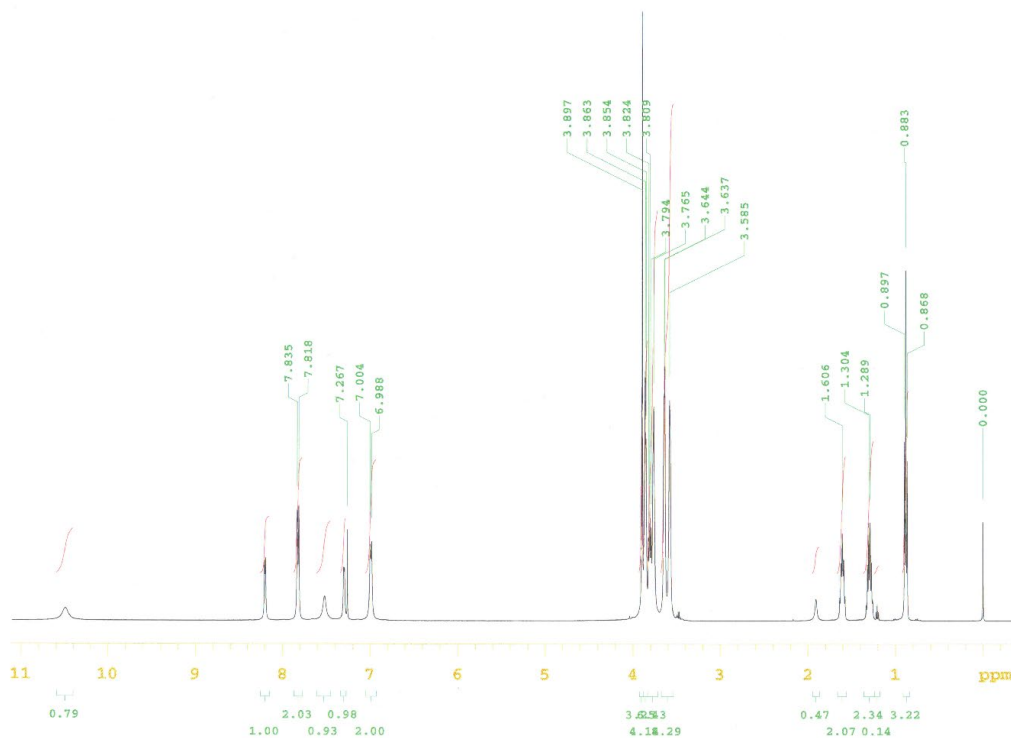
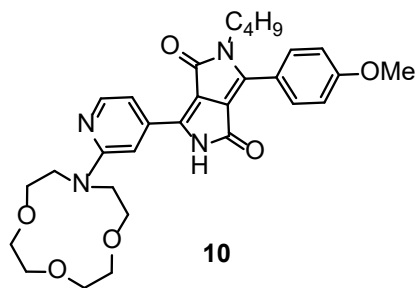
Sample Name:
 GDK-279
 Data Collected on:
 Varian-NMR-vnmrs500
 Archive directory:

Sample directory:
 FidFile: CARBON

Pulse Sequence: CARBON (s2pul)
 Solvent: cdcl3
 Data collected on: Sep 29 2020

Temp. 25.0 C / 298.1 K
 Operator: vnmr1

Relax. delay 0.500 sec
 Pulse 30.0 degrees
 Acq. time 1.200 sec
 Width 37878.8 Hz
 2928 repetitions
 OBSERVE C13, 125.6810306 MHz
 DECOUPLE H1, 499.8272777 MHz
 Power 36 dB
 continuously on
 WALTZ-16 modulated
 DATA PROCESSING
 Line broadening 2.0 Hz
 FT size 131072



D. Kumar
zesp10/Var500/GDK-303/GDK-303-H1

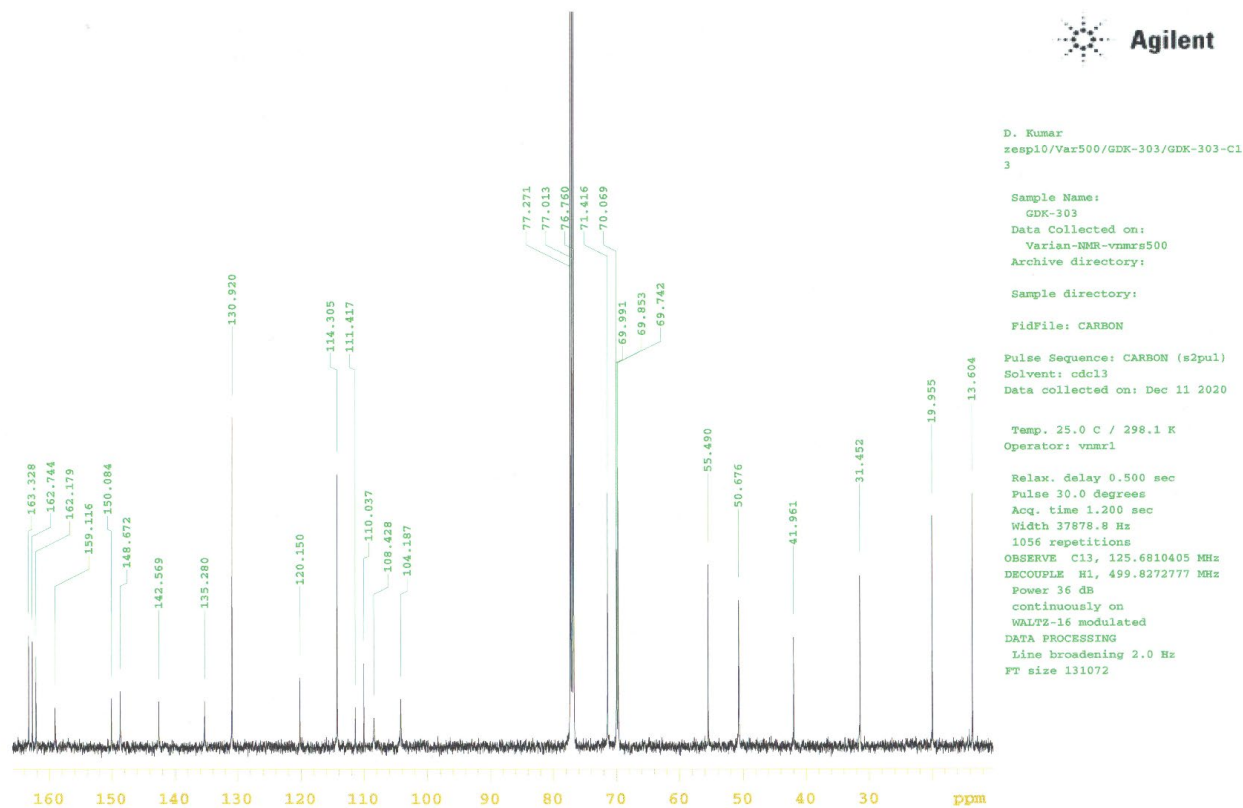
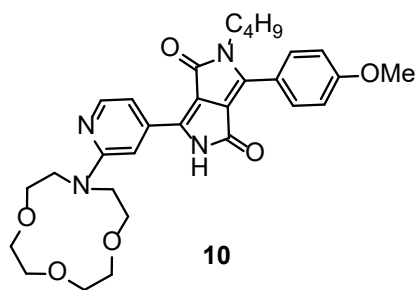
Sample Name:
GDK-303
Data Collected on:
Varian-NMR-vmr500
Archive directory:

Sample directory:
FidFile: PROTON

Pulse Sequence: PROTON (s2pul)
Solvent: cdcl3
Data collected on: Dec 11 2020

Temp. 25.0 C / 298.1 K
Operator: vmr1

Relax. delay 1.000 sec
Pulse 45.0 degrees
Acq. time 4.000 sec
Width 8012.9 Hz
64 repetitions
OBSERVE H1, 499.8247752 MHz
DATA PROCESSING
FT size 65536



Section S5: References

1. Y. Zhang, Y. Ouyang, Z. Luo, S. Dong. *Eur. J. Org. Chem.* **2019**, 4741-4744.
2. A. Purc, M. Banasiewicz, E. Glodkowska-Mrowka, D. T.Gryko, *J. Mater. Chem. C*, **2016**, 4, 2877 – 2885.


 Cite this: *Chem. Commun.*, 2022, 58, 4500

 Received 17th January 2022,
 Accepted 9th March 2022

DOI: 10.1039/d2cc00324d

rsc.li/chemcomm

Probing the flux of mitochondrial potassium using an azacrown-diketopyrrolopyrrole based highly sensitive probe†

 G. Dinesh Kumar,^a Marzena Banasiewicz,^b Antoni Wrzosek,^c Rafal P. Kampa,^{id c} Manon H. E. Bousquet,^{id d} Damian Kusy,^a Denis Jacquemin,^{id *d} Adam Szewczyk^{*c} and Daniel T. Gryko^{id *a}

The diketopyrrolopyrrole bearing an aza-18-crown-6 as a binding unit as well as a PPh₃⁺ group is highly sensitive towards K⁺ and localizes selectively in mitochondria of cardiac H9C2 cells. Fast efflux/influx of mitochondrial K⁺ can be observed upon stimulation with nigericin.

The concentration of potassium plays an important role in mitochondrial metabolic processes.¹ In particular, the potassium channels in mitochondria are involved in many physiological functions, such as cell proliferation, growth and apoptosis.^{2,3} Consequently, many mitochondrial targeting potassium probes have been developed over the years.^{4–7} Both the lipophilic triphenylphosphonium (TPP⁺) moiety,^{2b,c,5} quaternary ammonium salts^{6,8} and triarylsulfonium salts⁹ have been found to promote selective mitochondrial localization for fluorescent probes.

As far as potassium recognition is concerned, probes are predominantly based on quenching an electron-transfer.¹⁰ In the alternative and rarely employed strategy, upon binding of a cation to the electron-donating group, the photoinduced intramolecular charge transfer (ICT) is modified due to reduction in the electron-donating character, resulting in a blue-shift of the absorption and/or emission.¹¹ Taking advantage of recent synthetic breakthroughs related to diketopyrrolopyrroles (DPPs),^{12,13} we decided to apply these principles to the construction of a probe for K⁺ accumulating in mitochondria. Through this, we wanted to investigate what the effect of K⁺ binding^{14,15} by a moiety directly linked to a DPP

fluorophore on the resultant photophysical properties will be and how this could be applied to the intracellular imaging of biological samples.

Given that DPPs possess a strong electron-accepting core, we decided to utilize two different electron-donating peripheral aryl groups, only one of which contains a macrocyclic potassium recognition unit. Thus, we designed asymmetrical DPP bearing phenylaza-18-crown-6 as a key receptor due to its high selectivity and sensitivity for K⁺ over Na⁺ in biologically relevant conditions.¹⁶ The key structural element is positioning the basic nitrogen atom in the most conjugated position of the aryl substituent, so that the fluorescence will be sensitive to the binding event. In order to increase the K⁺ cation binding constant, an additional lariat ether (MeOCH₂CH₂O) at a position adjacent to the aza-18-crown-6 moiety¹⁷ was added as well.

The synthetic approach used to prepare DPP **1** and targeted probe **2** (Fig. 1) is based on our previously developed strategy¹² towards the synthesis of asymmetrical DPPs and it is shown in the ESI†.

The photophysical properties of DPPs **1** and **2** were studied in toluene and MeCN as prototypical non-polar and polar solvents (Table 1, Fig. S1 and S10, ESI†). From a structural point of view these DPPs represent D–A–D' systems where the azacrownphenyl is a strongly electron-donating group, the 4-MeOC₆H₄ is a weakly electron-donating substituent, and the DPP core is electron-deficient. DPPs **1** and **2** absorb at approx. 530 nm and emit at 540–580 nm in toluene. Interestingly, adding a triphenylphosphonium moiety strongly affects the photophysical properties shifting the absorption hypsochromically and emission bathochromically to 590 nm (Table 1). The photostability of DPP **2** in both acetonitrile and in H₂O turned out to be poor (see ESI† for details).

For DPP **1** and **2** the addition of just one equivalent of K⁺ shifts the emission hypsochromically from 580 to 525 nm (Fig. 2, Table 2, Fig. S6 and S13, ESI†). The addition of benzenesulfonic acid yields the same trend (Fig. S9 and S14, ESI†). Hypochromic shifts of absorption were observed for

^a Institute of Organic Chemistry, Polish Academy of Sciences, Kasprzaka 44/52, 01-224 Warsaw, Poland. E-mail: dtgryko@icho.edu.pl

^b Institute of Physics, Polish Academy of Sciences, Al. Lotników 32/46, 02-668 Warsaw, Poland

^c Nencki Institute of Experimental Biology of Polish Academy of Sciences, Pasteur 3, 02-093 Warsaw, Poland. E-mail: a.szewczyk@nencki.gov.pl

^d University of Nantes, CNRS, CEISAM, UMR-6230, F-4400 Nantes, France. E-mail: Denis.Jacquemin@univ-nantes.fr

† Electronic supplementary information (ESI) available: NMR, UV/vis and fluorescence spectra; fluorescence imaging; and computational details. See DOI: 10.1039/d2cc00324d

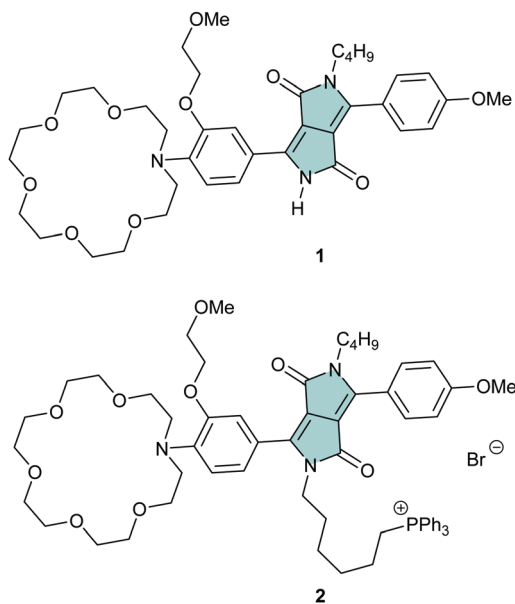


Fig. 1 The structures of DPPs **1** and **2**.

Table 1 Photophysical properties of DPPs in toluene and CH₃CN

Dye	Solvent	$\lambda_{\text{abs}}^{\text{max}}$ (nm)	$\lambda_{\text{em}}^{\text{max}}$ (nm)	Φ_{f}^a
1	PhMe	530	569	0.77
	MeCN	514	583	0.81
2	PhMe	519	592	0.80
	MeCN	499	591	0.48

^a Determined using Rhodamine 6G in EtOH.

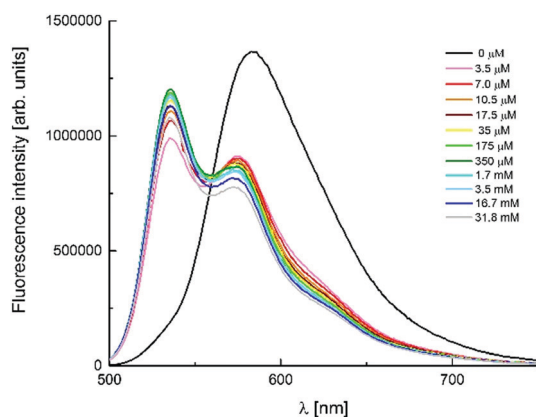


Fig. 2 The effect of KPF₆ addition on the emission spectra of DPP **1** measured in acetonitrile.

DPP **2** and **1** upon addition of K⁺ and benzenesulfonic acid (Fig. S2, S5 and S11, S12, ESI[†]). Furthermore, the selectivity of DPP **2** was also tested for other metal cations relevant to the cellular environment. Upon addition of Na⁺ and Mg²⁺, no significant fluorescence changes were observed (Table 2, Fig. S3, S7 and S4, S8, ESI[†]). Interestingly, decorating the DPP with a phosphonium salt chain

modulates the effect: the change of emission is also hypsochromic but weaker and hyperchromic (Fig. S13, ESI[†]). These effects are obviously related to complexation of K⁺ by azacrown ether and to protonation of the basic nitrogen atom in azacrown ether. In both cases, there is a decrease in the strength of the polarization since the electron-donating moiety (either *via* protonation or *via* complexation with K⁺) becomes weaker due to the involvement of the lone electron pair.

Excitation of the solution of DPP **2** in MeCN at 473 nm gave broad intense emission with λ_{max} at 590 nm but after addition of 100 eq. of KPF₆ its intensity increases, and a vibronic structure appears ($\lambda_{\text{em}} = 536$ nm). On the other hand excitation at 559 nm leads to much weaker emission, which essentially disappears after K⁺ complexation (resulting from hypsochromic shift of absorption upon complexation, see Fig. 3).

Interestingly the analogous studies in water (containing 1% of DMSO) and in HEPES buffer (pH = 7.4) gave different results. The addition of KCl to the aqueous solution of DPPs **1** and **2** did not lead to a marked hypsochromic shift of fluorescence. Analogous results were observed when the study was performed in HEPES buffer.

Having in hand the dye **2** possessing both a mitochondrion anchor and potassium recognition unit, we performed studies of its localization in cardiac cells. The conducted fluorescence microscopy experiments showed the subcellular distribution of dye **2** in the cardiac H9C2 cell line. Incubation with DPP **2** produces a staining pattern corresponding to the dye localized in the mitochondria, after only a short loading time of incubation (15–30 min) (Fig. 4).

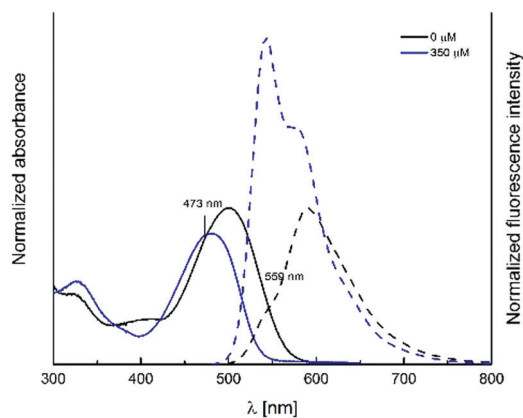
The staining of mitochondria was confirmed by the co-localization with MitoTracker™ Green with large Pearson's and Mander's coefficients (see ESI[†]). As DPP **2** is a cation, it accumulates in the mitochondrial matrix (negatively charged) after incubation with the cardiac H9C2 cells at very low concentrations (150–500 nM). DPP **1**, which lacks the TPP⁺ functionality, stains cardiac H9C2 cells in a nonselective manner, with no apparent accumulation in the mitochondria (Fig. 4).

To monitor the mitochondrial K⁺ concentration change under simulation, H9C2 cells which had been incubated for 30 min with dye **2**, were treated with the potassium ionophore valinomycin and nigericin, an ionophore that exchanges K⁺ for H⁺ across most biologic membranes inducing intracellular K⁺ efflux across the membrane.¹⁸ The cells were then excited at both 473 nm and 559 nm (Fig. S45, ESI[†]) with sequential detection for green and red emission.

The changes of mitochondrial K⁺ concentration were indicated by fluorescence intensity measurements at the excitation wavelength of 473 nm (detection in the green emission channel) and the excitation wavelength of 559 nm (detection in the red emission channel) (Fig. 5A–C). When control cells were excited at 473 nm (excitation of both dye **2** and its potassium complex), fluorescence was detected in both the green and red channels (Fig. 5A–C). The presence of nigericin and valinomycin at the concentration 10 μ M and 30 μ M in the incubation medium (FluoroBrite) caused a lowering of the intracellular K⁺ concentration from about 120 mM to the level of 5 mM

Table 2 Changes of fluorescence of DPPs **1** and **2** in the presence of 5 eq. various salts in CH₃CN

Dye	KPF ₆ (5 eq.)		PhSO ₃ H (5 eq.)		NaClO ₄ (5 eq.)		Mg(ClO ₄) ₂ (5 eq.)	
	Enhancement of fluorescence	λ_{em} (nm)	Enhancement of fluorescence	λ_{em} (nm)	Enhancement of fluorescence	λ_{em} (nm)	Enhancement of fluorescence	λ_{em} (nm)
1	0.81	536	0.72	550	0.90	578/538	0.94	583/541
2	1.39	543	1.53	553				

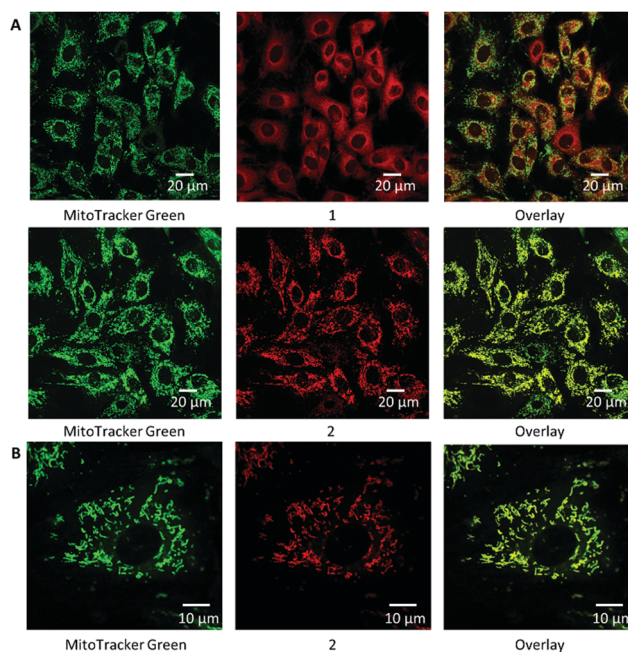
**Fig. 3** Absorption (solid line) and normalized fluorescence (dotted line) spectra of DPP **2** measured in CH₃CN in the absence and in the presence of KPF₆ (100 eq.) recorded with excitation at 473 nm. Legend specifies colors of lines.

(non-complexed dye prevails in mitochondria, Fig. 5A–C). The changes in K⁺ concentration in the cells could be detected since at $\lambda_{exc} = 473$ nm a sharp decrease of the fluorescence intensity was observed, whereas at $\lambda_{exc} = 559$ nm (selective for free base – Fig. 3) a marked increase of emission in the red channel was found.

The addition of only nigericin to the cell culture loaded with dye **2** also caused substantial changes in the fluorescence intensity for the 473 nm and 559 nm excitation wavelengths (Fig. S46, ESI[†]). The addition of only valinomycin to the cell culture loaded with dye **2** caused substantial changes in the fluorescence intensity for the 473 nm and 559 nm excitation wavelengths as well (Fig. S47, ESI[†]). In the presence of valinomycin, the fluorescence is somehow diffused. It was possible to calculate the ratio of the fluorescence intensity at both excitation wavelengths, which allows for the measurement of the K⁺ changes independent from the dye **2** concentration (Fig. S48, ESI[†]).

Data presented in Fig. S51 (ESI[†]) show that both tested crown-diketopyrrolopyrroles could not induce an apoptotic response of the Ea.hy 926 cells in comparison to the control conditions.

The discrepancy between the results in cells and in aqueous solutions of DPPs **1** and **2** is puzzling. On the other hand, Ahn and co-workers observed contrasting behavior of benzocoumarins in water vs. cells in terms of fluorescence intensity,¹⁹ which underlines the uniqueness of the cellular environment.

**Fig. 4** Intracellular localization of DPPs **1** and **2** as detected using confocal fluorescence microscopy. (A) The fluorescence of MitoTracker™ Green was recorded with 473 nm excitation wavelength, and the fluorescence of the DPPs **2** and **1** was recorded with 559 nm excitation wavelength and emission range 610–750 nm. Overlay picture recorded simultaneously for two fluorophores in living H9C2 cells. (B) Pictures were recorded with higher magnification (3x) for a better resolution to see a single cell chosen from the above larger field of view for DPP **2**.

In this study we found that if a suitable azacrown ether is appended as an electron-donating unit in a diketopyrrolopyrrole, it responds to the presence of a potassium cation with a marked hypsochromic shift of fluorescence. The DPP possessing both a quaternary phosphonium moiety as the mitochondrial targeting unit, as well as an aza-18-crown-6, responds to the mitochondrial K⁺ concentration change with an increase and decrease in emission intensity at two different excitation wavelengths. The probe **2** has a comparable performance to recently described K⁺-probes possessing the same aza-18-crown-6 binding unit accompanied by a lariat –OCH₂CH₂OMe group.¹⁰ Its different response to K⁺ in CH₃CN, H₂O and in cells is a shortcoming. On the other hand, the ability of selective excitation of the probe lacking a complexed metal cation is an advantage. These findings may serve as a blueprint to construct more sensitive mitochondria-targeting fluorescent potassium sensors.

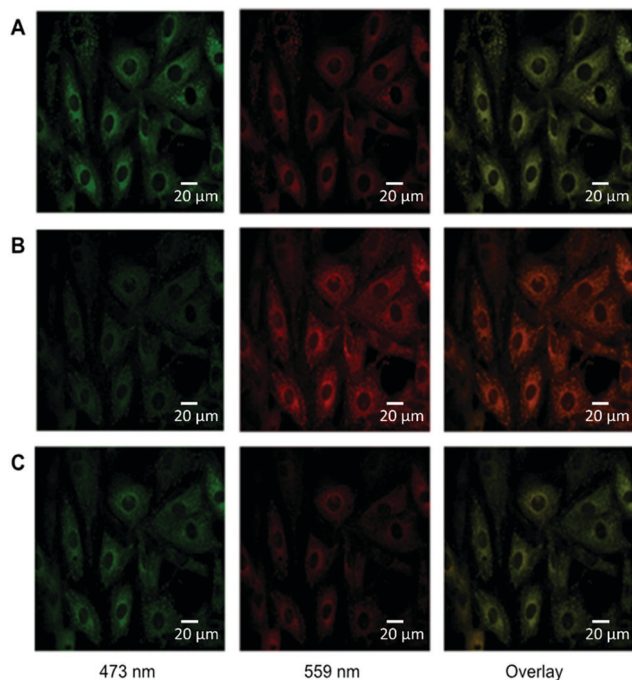


Fig. 5 Changes in the fluorescence of DPP **2** in the different intracellular K^+ concentrations caused by nigericin and valinomycin. (A) Fluorescence at the control condition without nigericin and valinomycin (intracellular K^+ concentration about 120 mM). (B) Changes in the fluorescence intensity in the presence of nigericin (10 μ M) and valinomycin (30 μ M) when the intracellular K^+ concentration was lowered to 5 mM. (C) Changes in the fluorescence intensity in the presence of nigericin (10 μ M) and valinomycin (30 μ M) when the intracellular K^+ concentration was increased to 200 mM.

Conceptualization: D. T. G., G. D. K.; **investigation:** G. D. K., M. B., A. W., M. H. E. B., D. K.; **supervision:** D. T. G., A. S., D. J.; **visualization:** G. D. K., M. B., A. W., D. K.; **writing – original draft:** G. D. K., D. J., A. W.; **writing – review & editing:** D. T. G., M. B., A. S., D. J.

This work was financially supported by the Foundation for Polish Science (TEAM POIR.04.04.00-00-3CF4/16-00). We also thank the National Science Centre, Poland, under QuantERA programme, project 2017/25/Z/ST2/03038. This project that has received funding from the European Union's Horizon 2020 research and innovation programme under the Marie Skłodowska-Curie grant agreement No 101007804 (Micro4Nano). MHEB and DJ are indebted to the CCIPL mesocenter installed in Nantes for the very generous allocation of computational time. Imaging experiments were supported by Nencki Institute of Experimental Biology, Polish Academy of Sciences.

Conflicts of interest

There are no conflicts to declare.

Notes and references

- 1 V. Checchetto, E. Teardo, L. Carraretto, L. Leanza and I. Szabó, *Biochim. Biophys. Acta, Bioenerg.*, 2016, **1857**, 1258–1266.

- 2 (a) Q. Hu, M. Gao, G. Feng and B. Liu, *Angew. Chem., Int. Ed.*, 2014, **53**, 14225–14229; (b) C. W. T. Leung, Y. Hong, S. Chen, E. Zhao, J. W. Y. Lam and B. Z. Tang, *J. Am. Chem. Soc.*, 2013, **135**, 62–65; (c) Roopa, N. Kumar, V. Bhalla and M. Kumar, *Chem. Commun.*, 2015, **51**, 15614–15628.
- 3 (a) D. Urrego, A. P. Tomczak, F. Zahed, W. Stuhmer and L. A. Pardo, *Philos. Trans. R. Soc., B*, 2014, **369**, 20130094; (b) I. Szabó, L. Leanza, E. Gulbins and M. Zoratti, *Pfluegers Arch.*, 2012, **463**, 231–246; (c) D. Malinska, S. R. Mirandola and W. S. Kunz, *FEBS Lett.*, 2010, **584**, 2043–2048; (d) V. Pétrilli, S. Papin, C. Dostert, A. Mayor, F. Martinon and J. Tschopp, *Cell Death Differ.*, 2007, **14**, 1583–1589; (e) D. Rotko, W. S. Kunz, A. Szewczyk and B. Kulawiak, *Int. J. Biochem. Cell Biol.*, 2020, **125**, 105792; (f) A. Wrzosek, B. Augustynek, M. Żochowska and A. Szewczyk, *Biomolecules*, 2020, **10**, 1200.
- 4 (a) X. Kong, F. Su, L. Zhang, J. Yaron, F. Lee, Z. Shi, Y. Tian and D. R. Meldrum, *Angew. Chem., Int. Ed.*, 2015, **54**, 12053–12057; (b) G. Song, D. Jiang, L. Wang, J. Ning, X. Sun, F. Su, M. Chen and Y. Tian, *Chem. Commun.*, 2020, **56**, 5405–5408.
- 5 (a) Q. Hu, M. Gao, G. Feng and B. Liu, *Angew. Chem., Int. Ed.*, 2014, **53**, 14225–14229; (b) H. Ogasawara, Y. Tanaka, M. Taki and S. Yamaguchi, *Chem. Sci.*, 2021, **12**, 7902–7907.
- 6 (a) W. Yang, P. S. Chan, M. S. Chan, K. F. Li, P. K. Lo, N. K. Mak, K. W. Cheah and M. S. Wong, *Chem. Commun.*, 2013, **49**, 3428–3430; (b) M. Grzybowski, E. Glodkowska-Mrowka, V. Hugues, W. Brutkowski, M. Blanchard-Desce and D. T. Gryko, *Chem. – Eur. J.*, 2015, **21**, 9101–9110; (c) S. Samanta, Y. He, A. Sharma, J. Kim, W. Pan, Z. Yang, J. Li, W. Yan, L. Liu, J. Qu and J. S. Kim, *Chem*, 2019, **5**, 1697–1726.
- 7 Z. Xu and L. Xu, *Chem. Commun.*, 2016, **52**, 1094–1119, DOI: 10.1039/c5cc09248e.
- 8 L. Long, M. Huang, N. Wang, Y. Wu, K. Wang, A. Gong, Z. Zhang and J. L. Sessler, *J. Am. Chem. Soc.*, 2018, **140**, 1870–1875.
- 9 T. Zhao, Z. Wan, K. Sambath, S. Yu, M. N. Uddin, Y. Zhang and K. D. Belfield, *Chem. – Eur. J.*, 2021, **27**, 247–251.
- 10 K. Sambath, X. Liu, Z. Wan, L. Hutnik, K. D. Belfield and Y. Zhang, *ChemPhotoChem*, 2021, **5**, 317–325.
- 11 (a) R. Grossley, Z. Goolamali and P. G. Sammes, *J. Chem. Soc., Perkin Trans. 2*, 1994, 1615–1623; (b) B. Valeur and I. Leray, *Coord. Chem. Rev.*, 2000, **205**, 3–40; (c) J. Bourson, J. Pouget and B. Valeur, *J. Phys. Chem.*, 1993, **97**, 4552–4557; (d) J. Bourson, F. Badaoui and B. Valeur, *J. Fluoresc.*, 1994, **4**, 275–277; (e) G. A. Smith, T. R. Hesketh and J. C. Metcalfe, *Biochem. J.*, 1988, **250**, 227–232; (f) G. Gryniewicz, M. Poenie and R. Y. Tsien, *J. Biol. Chem.*, 1985, **260**, 3440–3450; (g) Z. Zhang, F. Li, C. He, H. Ma, Y. Feng, Y. Zhang and M. Zhang, *Sens. Actuators, B*, 2018, **255**, 1878–1883.
- 12 M. Pieczykolan, B. Sadowski and D. T. Gryko, *Angew. Chem., Int. Ed.*, 2020, **59**, 7528–7535.
- 13 D. C. Young, M. Tasiar, A. D. Laurent, Ł. Dobrzycki, N. Tkachenko, D. Jacquemin and D. T. Gryko, *J. Mater. Chem. C*, 2020, **8**, 7708–7717, DOI: 10.1039/D0TC01202E.
- 14 (a) S. Ast, T. Schwarze, H. Müller, A. Sukhanov, S. Michaelis, J. Wegener, O. S. Wolfbeis, T. Körzdörfer, A. Dürkop and H. J. Holdt, *Chem. – Eur. J.*, 2013, **19**, 14911–14917; (b) Z. Wang, T. C. Detomasi and C. J. Chang, *Chem. Sci.*, 2021, **12**, 1720–1729.
- 15 B. J. Müller, S. M. Borisov and I. Klimant, *Adv. Funct. Mater.*, 2016, **26**, 7697–7707, DOI: 10.1002/adfm.201603822.
- 16 (a) R. A. Schultz, B. D. White, D. M. Dishone, K. A. Arnold and G. W. Gokel, *J. Am. Chem. Soc.*, 1985, **107**, 6659–6668; (b) G. W. Gokel, L. J. Barbour, R. Ferdani and J. Hu, *Acc. Chem. Res.*, 2002, **35**, 878–886.
- 17 (a) S. Ast, H. M03CBller, R. Flehr, T. Klamroth, B. Walz and H.-J. Holdt, *Chem. Commun.*, 2011, **47**, 4685–4687; (b) P. Padmawar, X. Yao, O. Bloch, G. T. Manley and A. Verkman, *Nat. Methods*, 2005, **2**, 825–827; (c) X. Zhou, F. Su, Y. Tian, C. Youngbull, R. H. Johnson and D. R. Meldrum, *J. Am. Chem. Soc.*, 2011, **133**, 18530–18533.
- 18 P. T. Kang, C.-L. Chen, P. Lin, W. M. Chilian and Y.-R. Chen, *Basic Res. Cardiol.*, 2017, **112**, 36, DOI: 10.1007/s00395-017-0626-1.
- 19 Y. J. Reo, Y. W. Jun, S. W. Cho, J. Jeon, H. Roh, S. Singha, M. Dai, S. Sarkar, H. R. Kim, S. Kim, Y. Jin, Y. L. Jung, Y. J. Yang, C. Ban, J. Joo and K. H. Ahn, *Chem. Commun.*, 2020, **56**, 10556–10559.

Supporting Information

Probing flux of mitochondrial potassium using an azacrown-diketopyrrolopyrrole based highly sensitive probe

G. Dinesh Kumar,^a Marzena Banasiewicz,^b Antoni Wrzosek,^c Rafal P. Kampa,^c Manon H. E. Bousquet,^d Damian Kusy,^a Denis Jacquemin,^{*d} Adam Szewczyk,^{*c} and Daniel T. Gryko^{*a}

^a Institute of Organic Chemistry, Polish Academy of Sciences, Kasprzaka 44/52, 01-224 Warsaw, Poland. E-mail: dtgryko@icho.edu.pl

^b Institute of Physics, Polish Academy of Sciences, Al. Lotników 32/46, 02-668 Warsaw, Poland.

^c Nencki Institute of Experimental Biology of Polish Academy of Sciences, Pasteur 3, 02-093 Warsaw, Poland. E-mail: a.szewczyk@nencki.gov.pl.

^d CEISAM UMR 6230, CNRS, Université de Nantes, 44000 Nantes, France. E-mail :Denis.Jacquemin@univ-nantes.fr

Table of contents

Section S1	General Information.....	S2
Section S2	Synthesis.....	S3
Section S3	Experimental procedure.....	S7
Section S4	Photophysical studies.....	S13
Section S5	Absorption and emission spectra.....	S15
Section S6	Imaging.....	S36
Section S7	Confocal fluorescence microscopy images.....	S38
Section S8	Theoretical calculations.....	S45
Section S9	¹H & ¹³C- NMR and MS spectra.....	S48
Section S10	References.....	S88

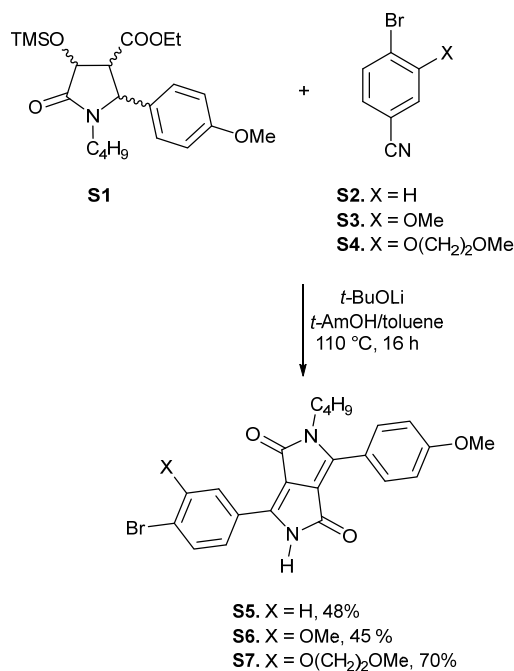
Section S1: General Information

All reagents and solvents were purchased from commercial sources and were used as received unless otherwise noted. Reagent grade solvents (CH_2Cl_2 , hexanes) were distilled prior to use. Transformations with moisture- and oxygen-sensitive compounds were performed under a stream of argon. The reaction progress was monitored by means of thin-layer chromatography (TLC), which was performed on Kieselgel 60. The identity and purity of prepared compounds were proved by ^1H NMR and ^{13}C NMR as well as by mass spectrometry (via EI-MS or ESI-MS). HRMS (ESI-TOF) and HRMS (EI): double-focusing magnetic sector instruments with EBE geometry were utilized. NMR spectra were measured on 400 or 500 or 600 MHz instruments. Chemical shifts (δ , ppm) were determined with tetramethylsilane (TMS) as the internal reference; J values are given in Hz. All melting points for crystalline products were measured with an automated melting point apparatus and are given without correction.

UV/Vis absorption spectra were recorded on a PerkinElmer Lambda 35 Spectrometer. Fluorescence spectra were recorded on a FLS1000 of Edinburgh Instruments. All linear optical studies were performed with freshly prepared air-equilibrated solutions at room temperature (298 K). Acetonitrile was spectrophotometric grade and was used without further purification. Quartz cells (10 mm) were used for the measurements of absorption and emission spectra. As a standard, Rh6G ($\Phi_{\text{fl}} = 0.94$ in EtOH) was used to determine fluorescence quantum yields.

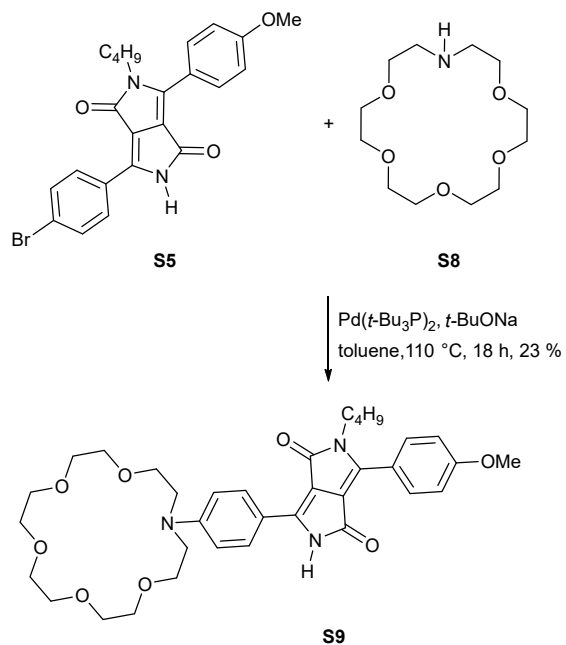
Section S2: Synthesis

The synthetic strategy used to prepare DPP-based probes is based on the synthesis of asymmetrical DPPs incorporating a single bromoaryl substituent followed by Buchwald-Hartwig amination with a corresponding azacrown ether. Hence, DPP **S5** was prepared from 4-bromobenzonitrile (**S2**) and pyrrolidin-2-one **S1** following our previously developed strategy in 48% yield (Scheme S1). Subsequently the desired crown-DPP **S9** was obtained by Buchwald-Hartwig amination with 1-aza-18-crown-6 (**S8**) in 23 % yield (Scheme S2).



Scheme S1. The synthesis of diketopyrrolopyrroles **S5-S7**.

It is well known that the presence of an additional alkoxy group at an ortho position relative to an 18-azacrown-6 moiety increases the binding constant with K⁺ as well as its selectivity versus this cation. In order to exploit this beneficial property, following similar synthetic procedures we designed DPPs **S10** and **S12** possessing MeO and MeOCH₂CH₂O groups, respectively. We also designed DPP **S11** possessing a 15-azacrown-5 macrocycle as a model. The synthesis of these three DPPs was achieved following the aforementioned pathway, i.e., synthesis of unsymmetrical bromophenyl-DPPs **S6** and **S7** followed by optimized Buchwald-Hartwig amination with 1-aza-18-crown-6 or 1-aza-15-crown-5 to provide crown DPPs **S10** and **S11** in 15% and 50% yield respectively (Scheme S1, Fig. S1). Nitrile **S4**, obtained in two steps from 4-bromo-3-methoxy benzonitrile, was reacted with pyrrolidin-2-one **S1** forming DPP **S7** in high yield (70%). The latter dye was used for amination with 1-aza-18-crown-6 (**S8**) to afford DPP **1** in 18% yield (Scheme S1, Fig. S1).



Scheme S2. The synthesis of DPP **S9** via Buchwald-Hartwig amination.

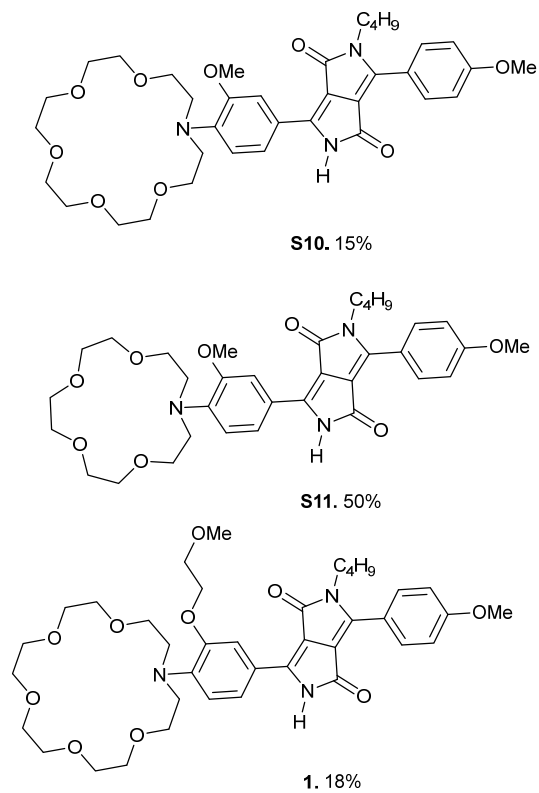
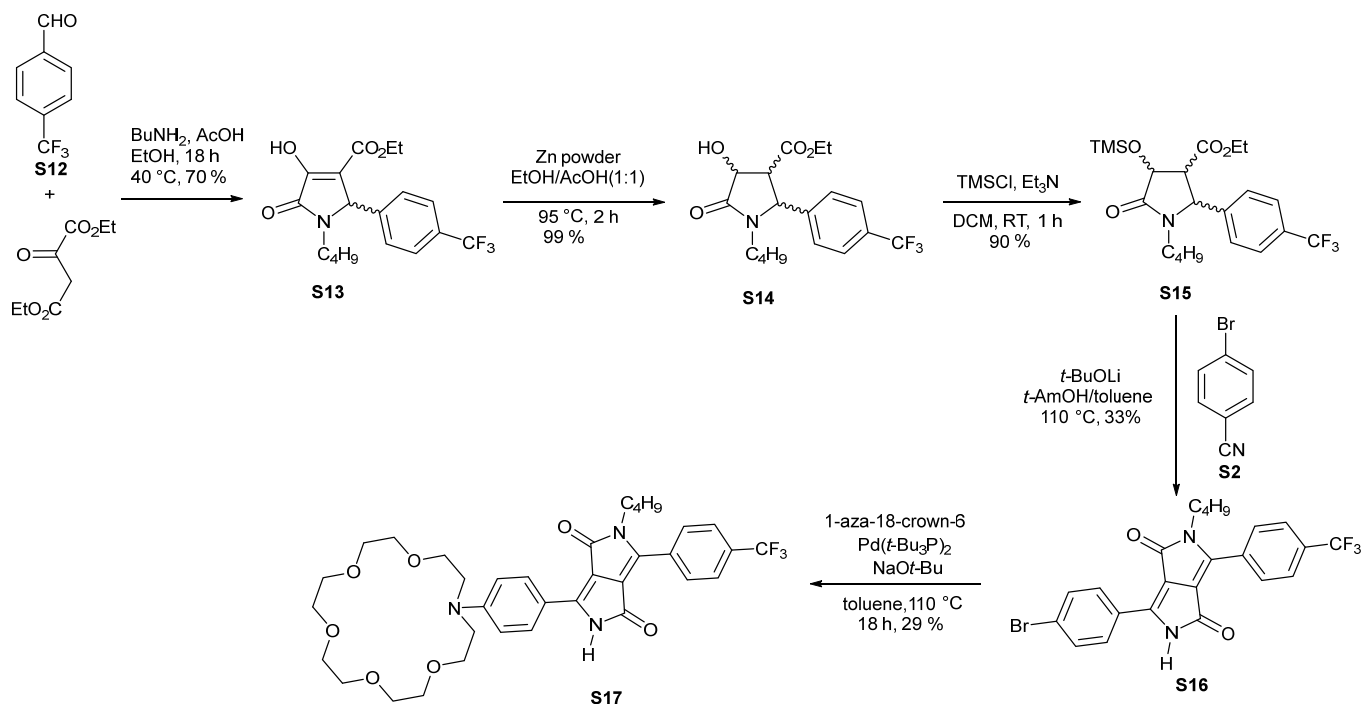


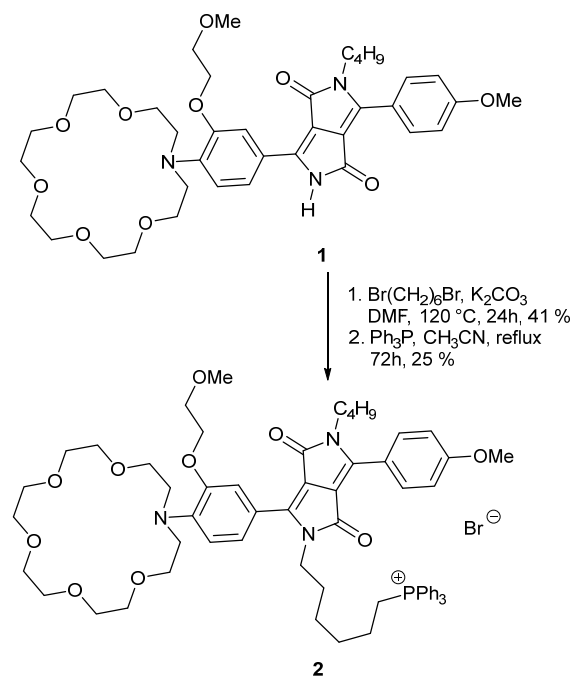
Fig. S1. The structures of crown-DPPs **S10-S11** and **1**.

The photophysical properties of unsymmetrically substituted DPPs strongly depend on the nature of both aryl substituents. Previously, it was found that the replacement of 4-MeOC₆H₄ with 4-CF₃C₆H₄ can render DPPs' fluorescence inert to changes in solvent polarity. This provided us with motivation to prepare analogues of DPPs **S9-S11** and **1** possessing 4-trifluoromethylphenyl substituents at position 2. The 4-trifluoromethylphenyl pyrrolidin-2-one **S15** was synthesized following the general procedure developed by us. The multicomponent reaction of 4-trifluoromethylbenzaldehyde with butylamine and diethyl oxalacetate afforded pyrrolidone **S13** (Scheme S3). Subsequent reduction gave lactam **S14** which was finally protected with TMS to give **S15** in 62% overall yield. The condensation of pyrrolidone **S15** with 4-bromobenzonitrile followed by Buchwald-Hartwig amination with 1-aza-18-crown-6 (**S8**) led to the formation of DPP **S17** in 29% yield.



Scheme S3. Synthesis of diketopyrrolopyrrole **17**.

Finally DPP **1** was transformed into DPP **2** possessing a triphenylphosphonium salt using standard procedures (Scheme S4).

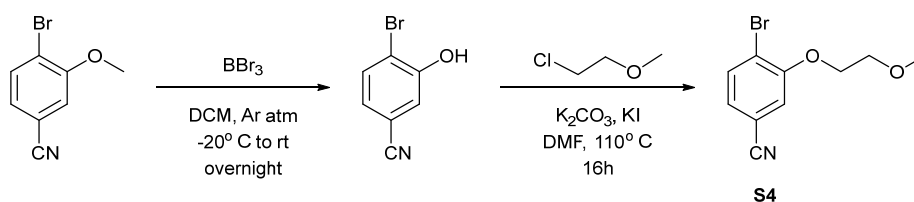


Scheme S4. The transformation of DPP **1** into mitochondrion probe **2**.

Section S3: Experimental Procedure

All reagents and solvents were purchased from commercial sources and were used as received unless otherwise noted. Reagent grade solvents (DCM, hexanes) were distilled prior to use. Transformations with moisture- and oxygen-sensitive compounds were performed under a stream of argon. The reaction progress was monitored by means of thin-layer chromatography (TLC), which was performed on Kieselgel 60. The identity and purity of prepared compounds were proved by ^1H NMR and ^{13}C NMR, ^{19}F NMR as well as by mass spectrometry (via EI-MS or ESI-MS). HRMS (ESI-TOF) and HRMS (EI): double-focusing magnetic sector instruments with EBE geometry were utilized. NMR spectra were measured on 400 or 500 or 600 MHz instruments. Chemical shifts (δ , ppm) were determined with tetramethylsilane (TMS) as the internal reference; J values are given in Hz. All melting points for crystalline products were measured with an automated melting point apparatus and are given without correction. Pyrrolidone **S1** was obtained following the literature procedure.¹

Synthesis of 4-bromo-3-(2-methoxyethoxy)benzonitrile (**S4**)



4-bromo-3-hydroxybenzonitrile was synthesized according to following known literature procedure.²

A suspension of 4-bromo-3-hydroxybenzonitrile (0.8 g, 4 mmol), chloroethyl methyl ether (0.37 mL, 4 mmol), KI (0.33 g, 2 mmol) and K_2CO_3 (0.84 g, 6 mmol) in 20 mL DMF was heated at 110°C for 16 h. Then reaction mixture was cooled to room temperature and dissolved in 100 mL ethyl acetate and 50 mL water. Organic phase was separated and washed with 50 mL sat. NaCl , dried over Na_2SO_4 . The solvent was evaporated to afford as brown solid in 97 % yield, 1.0 g. m.p. = 184°C . ^1H NMR (500 MHz, CDCl_3) δ 7.65 (d, $J = 8.1$ Hz, 1H), 7.14 (m, 2H), 4.21 (t, $J = 4.9$ Hz, 2H), 3.82 (t, $J = 4.6$ Hz, 2H), 3.48 (s, 3H). ^{13}C NMR (126 MHz, CDCl_3) δ 155.8, 134.3, 125.5, 118.5, 118.1, 116.0, 112.1, 70.6, 69.4, 59.5. HRMS (EI, m/z): $[\text{M}^{+\bullet}]$ Calcd. for $\text{C}_{10}\text{H}_{10}\text{BrNO}_2$: 254.9895; found, 254.9904.

General procedure for the synthesis of DPP derivatives **S5-S7**:

In flame dried Schlenk flask, a mixture of appropriate nitrile (1 eq.) and lithium *tert*-butoxide (4 eq.) was heated to 110°C under argon. To this solid mixture, *tert*-amyl alcohol (5 mL) was added in one portion followed by dropwise addition of pyrrolidone **S1** (1 eq.) dissolved in dry toluene (3 mL). The resulting dark solution was left to stir at this temperature for overnight. After cooling to room temperature reaction mixture was diluted with water (100 mL) and extracted with DCM

(100 mL), water phase was one more time washed with DCM (50 mL). The combined organic phases were dried over Na₂SO₄, filtered and concentrated in vacuum. The resulting crude compound was chromatographed on silica gel (DCM/MeOH = 9: 1) and crystallization from DCM/n-hexanes allowed to obtain the desired DPP product.

2-Butyl-3-(4-methoxyphenyl)-6-(4-bromophenyl)-2,5-dihydropyrrolo[3,4-c]pyrrole-1,4-dione (S5).

4-Bromobenzonitrile (**S2**, 1.0 g, 5.5 mmol), lithium *tert*-butoxide (1.8 g, 22 mmol) and pyrrolidone **S1** (2.2 g, 5.5 mmol) in combined solvent were used to obtain **S5** as red crystals in 48 % yield, 1.2 g. m.p. = 290 °C. ¹H NMR (500 MHz, CDCl₃) δ 10.68 (s, 1H), 8.15 (d, *J* = 8.0 Hz, 2H), 7.82 (d, *J* = 8.5 Hz, 2H), 7.47 (d, *J* = 8.1 Hz, 2H), 6.95 (d, *J* = 8.5 Hz, 2H), 3.92 (s, 3H), 3.78 (t, *J* = 7.6 Hz, 2H), 1.65 (quint, *J* = 7.1 Hz, 2H), 1.32 (m, 2H), 0.90 (t, *J* = 7.3 Hz, 3H). ¹³C NMR (126 MHz, CDCl₃) δ 163.5, 162.7, 162.1, 148.9, 142.6, 132.1, 131.0, 129.4, 126.8, 125.8, 120.2, 114.1, 55.5, 42.2, 31.5, 20.05, 13.6. HRMS (ESI, *m/z*): [M+Na]⁺ Calcd. for C₂₃H₂₁BrN₂O₃Na: 475.3360; found, 475.3380.

2-Butyl-3-(4-methoxyphenyl)-6-(4-bromo-3-methoxyphenyl)-2,5-dihydropyrrolo[3,4-c]pyrrole-1,4-dione (S6).

4-Bromo-3-methoxybenzonitrile (**S3**, 1.0 g, 4.7 mmol), lithium *tert*-butoxide (1.5 g, 18.8 mmol) and pyrrolidone **S1** (1.92 g, 4.7 mmol) in combined solvent were used to obtain **S6** as orange-red crystals in 45 % yield, 1.0 g. m.p. = 292 °C. ¹H NMR (600 MHz, CDCl₃) δ 10.87 (s, 1H), 8.07 (s, 1H), 7.80 (d, *J* = 8.8 Hz, 2H), 7.69 (d, *J* = 8.2 Hz, 1H), 7.18 (d, *J* = 7.3 Hz, 1H), 7.08 (d, *J* = 8.8 Hz, 2H), 4.04 (s, 3H), 3.94 (s, 3H), 3.85 (t, *J* = 7.9 Hz, 2H), 1.65 (quint, *J* = 7.5 Hz, 2H), 1.32 (m, 2H), 0.90 (t, *J* = 7.3 Hz, 3H). ¹³C NMR (150 MHz, CDCl₃) δ 163.3, 163.2, 159.9, 159.6, 156.7, 154.0, 134.2, 131.3, 127.3, 119.9, 119.1, 116.9, 115.5, 114.9, 113.6, 111.1, 56.5, 55.6, 42.6, 31.3, 19.8, 13.4. HRMS (ESI, *m/z*): [M+Na]⁺ Calcd. For C₂₄H₂₃BrN₂O₄Na: 505.0739; found, 505.0726.

2-Butyl-3-(4-methoxyphenyl)-6-(4-bromo-3-methoxyethoxyphenyl)-2,5-dihydropyrrolo[3,4-c]pyrrole-1,4-dione (S7).

4-Bromo-3-methoxyethoxybenzonitrile (**S4**, 1.0 g, 3.9 mmol), lithium *tert*-butoxide (1.25 g, 15.6 mmol) and pyrrolidone **S1** (1.6 g, 3.9 mmol) in combined solvent were used to obtain **S7** as orange-red crystals in 70 % yield, 1.4 g. m.p. = 284 °C. ¹H NMR (600 MHz, CDCl₃) δ 8.12 (s, 1H), 7.80 (d, *J* = 9.0 Hz, 2H), 7.69 (d, *J* = 8.2 Hz, 1H), 7.38 (d, *J* = 9.9 Hz, 1H), 7.08 (d, *J* = 8.8 Hz, 2H), 4.40 (t, *J* = 4.5 Hz, 2H), 4.02 (t, *J* = 4.4 Hz, 2H), 3.92 (s, 3H), 3.86 (t, *J* = 7.8 Hz, 2H), 3.62 (s, 3H), 3.57 (s, 1H), 1.65 (quint, *J* = 7.5 Hz, 2H), 1.32 (m, 2H), 0.90 (t, *J* = 7.4 Hz, 3H). ¹³C NMR (150 MHz, CDCl₃) δ 163.3, 159.9, 159.7, 155.7, 153.7, 134.3, 131.3, 127.3, 119.9, 119.2, 117.0, 115.5, 114.8, 113.6, 112.1, 108.8, 70.7, 68.4, 59.3, 55.6, 42.5, 31.3, 19.8, 13.4. HRMS (ESI, *m/z*): [M+H]⁺ Calcd. for C₂₆H₂₆BrN₂O₅: 525.1025; found, 525.1008.

2-Butyl-3-(4-trifluoromethylphenyl)-6-(4-bromophenyl)-2,5-dihydropyrrolo[3,4-c]pyrrole-1, 4-dione (S16).

4-Bromobenzonitrile (**S2**, 1.0 g, 5.5 mmol), lithium *tert*-butoxide (1.75 g, 22 mmol) and pyrrolidone **S15** (2.5 g, 5.5 mmol) in combined solvent were used to obtain **S16** as red crystals in 33 % yield, 900 mg. m.p. = 283 °C. ¹H NMR (500 MHz, CDCl₃) δ 9.27 (s, 1H), 8.16 (d, *J* = 8.7 Hz, 2H), 7.92 (d, *J* = 8.1 Hz, 2H), 7.82 (d, *J* = 8.4 Hz, 2H), 7.64 (d, *J* = 8.7 Hz, 2H), 3.82 (t, *J* = 7.7 Hz, 2H), 1.60 (quint, *J* = 7.6 Hz, 2H), 1.28 (m, 2H), 0.88 (t, *J* = 7.4 Hz, 3H). ¹³C NMR (126 MHz, CDCl₃) δ 162.7, 162.2, 146.2, 144.5, 132.6, 131.3, 129.2, 129.1, 129.0, 127.2, 126.1, 125.9, 125.9, 111.7, 110.0, 42.0, 31.6, 20.0, 13.6. HRMS (ESI, *m/z*): [M+H]⁺ Calcd. for C₂₃H₁₇BrF₃N₂O₂: 489.0426; found, 489.0413.

General procedure for Buchwald-Hartwig amination of DPP derivatives **S9-S11** and **1**:

A mixture of appropriate DPP (1 eq.), 1-aza-18-crown-6 (2 eq.), sodium *tert*-butoxide (4 eq.) and bis(*tri-tert*-butylphosphine)palladium(0) (0.05 eq.) were placed in a dried Schenk flask under argon atmosphere followed by 10 mL dry toluene were added. The reaction mixture was stirred at 110 °C for 18 h. After cooling to room temperature, reaction mixture was diluted with water (100 mL) and extracted with DCM (100 mL), aqueous phase was one more time washed with DCM (50 mL). The combined organic phases were dried over Na₂SO₄, filtered and concentrated in vacuum. The crude product was purified by column chromatography over silica gel using a step gradient of MeOH in DCM as eluent (from 0% to 10%). Crystallization from DCM/hexanes allowed to obtain desired product.

2-Butyl-3-(4-methoxyphenyl)-6-(1,4,7,10,13-pentaoxa-16-azacyclooctadecane,16-(4-phenyl)-2,5-dihydropyrrolo[3,4-*c*]pyrrole-1, 4-dione (S9).

DPP (**S5**, 0.25 g, 0.55 mmol), 1-aza-18-crown-6 (**S8**, 0.29 g, 1.1 mmol), sodium *tert*-butoxide (0.21 g, 2.2 mmol), and bis(*tri-tert*-butylphosphine)palladium(0) (15 mg, 0.05 mmol) in 10 mL of dry toluene were used to obtain product **S9** as a red crystals in 23 % yield, 80 mg. m.p. = 208 °C. ¹H NMR (500 MHz, CDCl₃) δ 9.35 (s, 1H), 8.27 (d, *J* = 7.8 Hz, 2H), 7.8 (s, 2H), 7.03 (d, *J* = 8.6 Hz, 2H), 6.80 (s, 2H), 3.87 (s, 3H), 3.73-3.65 (m, 26H), 1.63 (quint, *J* = 7.3 Hz, 2H), 1.3 (m, 2H), 0.88 (t, *J* = 7.3 Hz, 3H). ¹³C NMR (126 MHz, CDCl₃) δ 163.7, 162.4, 161.3, 161.2, 150.8, 145.2, 144.4, 144.3, 130.5, 130.2, 121.2, 115.3, 114.2, 111.6, 110.0, 106.5, 70.9, 70.8, 70.7, 68.5, 55.4, 51.5, 41.9, 31.7, 20.0, 13.7. HRMS (ESI, *m/z*): [M+Na]⁺ Calcd. for C₃₅H₄₅N₃O₈Na: 658.3104; found, 658.3085.

2-Butyl-3-(4-methoxyphenyl)-6-(1,4,7,10,13-pentaoxa-16-azacyclooctadecane,16-(2-methoxyphenyl-4-yl)-2,5-dihydropyrrolo[3,4-*c*]pyrrole-1, 4-dione (S10).

DPP (**S6**, 0.25 g, 0.51 mmol), 1-aza-18-crown-6 (**S8**, 0.22 g, 1.03 mmol), sodium *tert*-butoxide (0.16 g, 2.06 mmol), and bis(*tri-tert*-butylphosphine)palladium(0) (20 mg, 0.05 mmol) in 10 mL of dry toluene were used to obtain **S10** as red crystals in 15 % yield, 50 mg. m.p. = 188 °C. ¹H NMR (500 MHz, CDCl₃) δ 9.46 (s, 1H), 8.17 (s, 1H), 7.79 (d, *J* = 8.2 Hz, 2H), 7.7 (s, 1H), 7.05 (d, *J* = 8.6 Hz, 2H), 6.99 (s, 1H), 3.89 (s, 6H), 3.7-3.61 (m, 26H), 1.63 (quint, *J* = 7.0 Hz, 2H), 1.3 (m, 2H), 0.88 (t, *J* = 7.4 Hz, 3H). ¹³C NMR (126 MHz, CDCl₃) δ 163.7, 162.6, 161.5, 151.0, 145.6, 144.8, 143.7, 130.5,

121.0, 117.7, 114.3, 112.0, 110.1, 70.7, 70.2, 69.9, 69.2, 55.9, 52.6, 41.8, 31.6, 20.0, 13.7. HRMS (EI, m/z): [M⁺] Calcd. for C₃₆H₄₇N₃O₉: 665.3312; found, 665.3304.

2-Butyl-3-(4-methoxyphenyl)-6-(1,4,7,10-tetraoxa-13-azacyclopentadecane,16-(2-methoxyphenyl-4-yl)-2,5-dihydropyrrolo[3,4-c]pyrrole-1, 4-dione (S11).

DPP (S6, 0.25 g, 5.1 mmol), 1-aza-15-crown-5 (0.23 g, 10.3 mmol), sodium *tert*-butoxide (0.2 g, 20.4 mmol), and bis(*tri-tert*-butylphosphine)palladium(0) (15 mg, 0.05 mmol) in 10 mL of dry toluene were used to obtain S11 as red crystals in 50 % yield, 160 mg. m.p. = 210 °C. ¹H NMR (600 MHz, CDCl₃) δ 9.82 (s, 1H), 8.17 (s, 1H), 7.79 (s, 1H), 7.77 (d, *J* = 8.3 Hz, 2H), 7.03 (d, *J* = 8.6 Hz, 2H), 6.99 (d, *J* = 8.2 Hz, 1H), 3.92 (m, 6H), 3.89-3.80 (s, 6H), 3.73-3.64 (m, 13H), 3.2 (t, *J* = 8.9 Hz, 2H), 1.61 (quint, *J* = 7.0 Hz, 2H), 1.3 (m, 2H), 0.86 (t, *J* = 7.2 Hz, 3H). ¹³C NMR (150 MHz, CDCl₃) δ 163.9, 162.5, 161.4, 150.7, 145.2, 143.6, 130.5, 130.4, 121.7, 121.1, 119.1, 117.1, 114.2, 112.0, 110.2, 107.4, 71.0, 70.4, 70.0, 69.7, 69.6, 69.1, 65.2, 55.9, 55.4, 53.5, 47.7, 41.7, 31.6, 20.0, 13.6. HRMS (ESI, m/z): [M+Na]⁺ Calcd. for C₃₄H₄₃N₃O₈Na: 644.2948; found, 644.2941.

2-Butyl-3-(4-methoxyphenyl)-6-(1,4,7,10,13-Pentaoxa-16-azacyclooctadecane,16-(2-methoxyethoxyphenyl-4-yl)-2,5-dihydropyrrolo[3,4-c]pyrrole-1, 4-dione (1).

DPP (S7, 0.5 g, 0.94 mmol), 1-aza-18-crown-6 (S8, 0.5 g, 1.9 mmol), sodium *tert*-butoxide (0.37 g, 3.8 mmol), and bis(*tri-tert*-butylphosphine)palladium(0) (25 mg, 0.05 mmol) in 10 mL of dry toluene were used to obtain 1 as red crystals in 18 % yield, 120 mg. m.p. = 182 °C. ¹H NMR (500 MHz, CDCl₃) δ 8.19 (s, 1H), 7.79 (d, *J* = 8.6 Hz, 2H), 7.03 (d, *J* = 8.8 Hz, 4H), 3.82 (t, *J* = 7.8 Hz, 2H), 3.68-3.59 (m, 29H), 3.38 (s, 6H), 1.63 (quint, *J* = 7.2 Hz, 2H), 1.3 (m, 2H), 0.88 (t, *J* = 7.2 Hz, 3H). ¹³C NMR (126 MHz, CDCl₃) δ 163.7, 162.7, 161.6, 149.6, 145.3, 144.8, 130.6, 129.4, 121.7, 121.6, 120.9, 115.6, 114.5, 114.3, 114.1, 113.0, 110.2, 71.1, 70.8, 70.2, 69.6, 69.4, 69.3, 69.2, 69.1, 69.0, 68.9, 67.5, 58.9, 55.5, 52.8, 41.8, 31.6, 20.0, 13.7. HRMS (ESI, m/z): [M+H]⁺ Calcd. for C₃₈H₅₂N₃O₁₀: 710.3653; found, 710.3666.

2-Butyl-3-(4-trifluoromethylphenyl)-6-(1,4,7,10,13-pentaoxa-16-azacyclooctadecane,16-(4-phenyl)-2,5-dihydropyrrolo[3,4-c]pyrrole-1,4-dione (S17).

DPP (S16, 0.1 g, 0.2 mmol), 1-aza-18-crown-6 (S8, 0.11 g, 0.4 mmol), sodium *tert*-butoxide (0.08 g, 0.8 mmol), and bis(*tri-tert*-butylphosphine)palladium(0) (5 mg, 0.05 mmol) in 10 mL of dry toluene were used to obtain S17 as red crystals in 29 % yield, 50 mg. m.p. = 205 °C. ¹H NMR (500 MHz, CDCl₃) δ 10.05 (s, 1H), 8.32 (s, 2H), 7.92 (d, *J* = 8.0 Hz, 2H), 7.75 (d, *J* = 8.5 Hz, 2H), 6.76 (d, *J* = 9.0 Hz, 2H), 3.83 (t, *J* = 7.0 Hz, 2H), 3.73-3.65 (m, 24H), 1.63 (quint, *J* = 7.5 Hz, 2H), 1.3 (m, 2H), 0.88 (t, *J* = 7.5 Hz, 3H). ¹³C NMR (126 MHz, CDCl₃) δ 164.3, 161.9, 151.5, 147.6, 141.0, 132.3, 131.5, 131.2, 131.1, 130.9, 130.8, 129.0, 128.9, 128.8, 125.6, 125.5, 125.0, 124.8, 122.8, 114.9, 112.4, 111.8, 111.7, 106.2, 70.8, 70.7, 68.5, 51.5, 41.9, 31.7, 20.0, 13.7. HRMS (ESI, m/z): [M+Na]⁺ Calcd. for C₃₅H₄₂F₃N₃O₇Na: 696.2873; found, 696.2889.

Preparation of mitochondrial probe (2):

A suspension of unsymmetrical DPP **1** (100 mg, 0.14 mmol) and K₂CO₃ (40 mg, 0.28 mmol) in dry DMF (5 mL) was stirred at 120 °C under argon atmosphere for 5 min. Then 1, 6-dibromohexane (0.22 mL, 1.4 mmol) was added and the mixture was stirred at 120 °C under argon for 24 h. Thereafter, the mixture was cooled down to room temperature and water (50 mL) was added. The product was extracted with DCM three times. The combined organic layers were dried over anhydrous Na₂SO₄, filtered and the solvent was evaporated under reduced pressure. The product was purified by column chromatography over silica gel using a step gradient of MeOH in DCM as eluent (from 0% to 10%). Compound was obtained as an orange red semi solid in 41% yield, 50 mg. HRMS (ESI, m/z): [M+Na]⁺ Calcd. for C₄₄H₆₂BrN₃O₁₀Na: 894.3516; found, 894.3496.

Alkylated crude compound of **1** (50 mg, 0.06 mmol) and triphenylphosphine (0.15 g, 0.57 mmol) were added into a flask containing 5 mL of acetonitrile. The mixture was refluxed for 72 h. After removal of solvent in vacuo, the remaining solid was purified by column chromatography with gradient solvent from CH₂Cl₂ to CH₂Cl₂/MeOH (v/v = 9/1). Compound **2** was obtained as orange-red crystals by recrystallization from diethyl ether in 25% yield, 15 mg. m.p. = 94 °C. ¹H NMR (600 MHz, CD₃CN): δ 7.86-7.62 (m, 15H), 7.46 (dd, *J* = 6.6 Hz, 2H), 7.24 (dd, *J* = 8.4 Hz, 2H), 7.09 (d, *J* = 9.0 Hz, 1H), 6.99 (d, *J* = 8.4 Hz, 2H), 4.01 (t, *J* = 6.6 Hz, 2H), 3.85-3.40 (m, 28H), 2.81 (t, *J* = 7.8 Hz, 2H), 2.54 (t, *J* = 7.2 Hz, 2H), 1.39-1.27 (m, 19H), 0.88 (t, *J* = 6.6 Hz, 3H). ¹³C NMR (126 MHz, CDCl₃) δ 173.8, 163.4, 162.9, 153.0, 148.7, 139.6, 138.2, 136.1, 135.8, 134.7, 134.6, 133.2, 132.9, 131.7, 131.2, 130.6, 125.8, 125.1, 119.8, 116.2, 115.2, 114.8, 70.5, 70.1, 65.1, 59.3, 56.3, 42.1, 36.9, 35.6, 35.2, 35.1, 34.4, 32.6, 32.1, 31.8, 31.6, 30.6, 30.5, 30.3, 30.2, 30.1, 29.9, 29.6, 29.4, 26.6, 26.3, 23.4, 22.7, 22.3, 20.5, 14.4, 13.9.; HRMS (ESI, m/z): [M+H]⁺ Calcd. for C₆₂H₇₈N₃O₁₀P⁺: 1055.5425; found, 1055.5405.

Ethyl-1-butyl-4-hydroxy-5-oxo-2-(4-Trifluoromethylphenyl)-2,5-dihydro-1H-pyrrole-3-carboxylate (S13).

A 250 mL round-bottom flask equipped with a magnetic stirring bar, was charged with ethanol (100 mL), 4-trifluoromethyl benzaldehyde **S12** (7.3 mL, 53 mmol) and *n*-butylamine (5.25 mL, 53 mmol), reaction mixture was kept at room temperature, with constant stirring for 15 minutes. Next diethyl oxalacetate (10.0 g, 53 mmol) was added in one portion, followed by dropwise addition of acetic acid (6.1 mL, 106 mmol). Reaction mixture was heat up to 40 °C, and vigorously stirred overnight. Then reaction mixture was cooled to room temperature and diluted with water (200 mL), and extracted with DCM (200mL×2). Organic phase was dried over anhydrous Na₂SO₄, filtered and concentrated in vacuo. Yellowish solid was recrystallized from EtOAc to obtain product **S13** as white crystals 70 %, 14.0 g. m.p. = 198-199 °C. ¹H NMR (600 MHz, CDCl₃) δ 9.02 (s, 1H), 7.61 (d, *J* = 8.2 Hz, 2H), 7.30 (d, *J* = 8.0 Hz, 2H), 5.14 (s, 1H), 4.13 (q, *J* = 7.1 Hz, 2H), 3.78 (m, 1H), 2.63 (m, 1H), 1.48 – 1.41 (m, 2H), 1.28 – 1.22 (m, 2H), 1.12 (t, *J* = 7.1 Hz, 3H), 0.86 (t, *J* = 7.4 Hz, 3H); ¹³C NMR (151 MHz, CDCl₃) δ 164.8, 163.6, 157.7, 139.3, 131.2, 128.1, 125.8, 122.9, 112.4, 61.2, 60.0, 40.3, 30.3, 19.9, 13.9, 13.6. ¹⁹F NMR (470 MHz, CDCl₃) δ -62.71. HRMS (ESI, m/z): [M+Na]⁺ Calcd. for C₁₈H₂₀F₃NO₄Na: 394.3562; found, 394.3520.

Ethyl-1-butyl-4-hydroxy-2-(4-Trifluoromethylphenyl)-5-oxopyrrolidine-3-carboxylate (S14).

Compound **S13** (14.0 g, 37.7 mmol) was dissolved in 150 mL mixture of EtOH/AcOH (1:1) and zinc powder (15.0 g, 226.2 mmol) was added and reaction mixture vigorously stirred at 95 °C for 1h. A second portion of zinc powder (15.0 g, 226.2 mmol) was added and stirring was continued at 95 °C until completion of the reaction. After cooling to room temperature reaction mixture was diluted with EtOAc (100 mL) the excess of zinc and the inorganic salts were filtered off. The filtrate was then diluted with water (150 mL). The aqueous layer was extracted with EtOAc (100 mL), and the combined organic phases were washed with saturated NaHCO₃ solution until neutral and finally dried over Na₂SO₄, filtered and concentrated in vacuo to obtain liquid product **S14** as mixture of diastereoisomers in 85% yield, 11.9 g. Careful analysis of ¹H NMR spectra of crude **S14** showed the ratio 2:1 of major isomer **S14** with the all-trans configuration in relation to the rest three minor compounds.

Crude compound (11.9 g, 31.9 mmol) was dissolved in dry EtOH (75 mL), freshly powdered K₂CO₃ (11.2 g, 68.5 mmol) was added in one portion. Reaction mixture was stirred at room temperature for 30 minutes. Next reaction mixture was diluted with EtOAc (100 mL) the excess of inorganic salts were filtered off. The filtrate was then washed with water (100 mL x 2), organic phase was dried over Na₂SO₄, filtered and concentrated in vacuum to obtain yellowish liquid product in 99.5 %, 11.8 g. ¹H NMR spectra showed 10:1 ratio of major isomer **S14a** with the all-trans configuration in relation to the rest two minor compounds. ¹H NMR (500 MHz, CDCl₃) δ 7.63 (d, *J* = 8.0 Hz, 2H), 7.44 (d, *J* = 8.0 Hz, 2H), 4.75 (d, *J* = 7.5 Hz, 1H), 4.65 (d, *J* = 8.0 Hz, 1H), 4.15 (m, 2H), 3.7-3.65 (m, 1H), 3.03 (t, *J* = 8.5 Hz, 1H), 2.45 (quint, *J* = 7.5 Hz, 1H), 1.32-1.11 (m, 8H), 0.79 (t, *J* = 7.5 Hz, 3H); ¹³C NMR (126 MHz, CDCl₃) δ 173.6, 171.1, 142.3, 131.1, 129.4, 129.0, 126.1, 125.3, 72.1, 61.6, 55.9, 40.6, 28.5, 19.9, 13.9, 13.6. HRMS (EI, m/z): [M⁺] Calcd. for C₁₈H₂₂F₃NO₄: 373.3722; found, 373.1507.

Ethyl-1-butyl-2-(4-trifluoromethylphenyl)-5-oxo-4-((trimethylsilyl)oxy)pyrrolidine-3-carboxylate (S15).

To cooled to ~0 °C solution of **S14a** (11.8 g, 31.6 mmol) in dry DCM (100 mL), dry Et₃N (8.0 mL, 56.8 mmol) was added, next TMSCl (6.0 mL, 47.4 mmol) was added drop wise. After addition cooling bath was removed, and reaction mixture was allowed to reach room temperature and stirring was continued at room temperature for 1.5 h. Next reaction mixture was diluted with water (100 mL), phases were separated and organic phase was dried over anhydrous Na₂SO₄, filtered and concentrated in vacuo gives 90% yield, 12.8 g of product **S15** without chromatographic purification. ¹H NMR spectra showed 10:1 ratio of major isomer **S15** with the all-trans configuration in relation to the rest two minor compounds, used for next reaction without further purification. ¹H NMR (500 MHz, CDCl₃) δ 7.63 (d, *J* = 8.0 Hz, 2H), 7.40 (d, *J* = 8.0 Hz, 2H), 4.70 (d, *J* = 7.5 Hz, 1H), 4.56 (d, *J* = 8.0 Hz, 1H), 4.16 (m, 2H), 3.69-3.63 (m, 1H), 2.91 (t, *J*

= 7.5 Hz, 1H), 2.52 (m, 1H), 1.39 – 1.31 (m, 4H), 1.24-1.17 (m, 3H), 0.81 (t, $J = 11.5$ Hz, 3H), 0.21 (s, 9H). ^{13}C NMR (101 MHz, CDCl_3) δ 171.6, 171.1, 142.5, 131.0, 130.7, 129.3, 127.7, 125.9, 73.1, 61.5, 60.5, 56.6, 45.7, 40.6, 28.6, 19.8, 14.0, 13.6, 0.1. HRMS (EI m/z): [$\text{M}^{+\bullet}$] Calcd. for $\text{C}_{21}\text{H}_{30}\text{F}_3\text{NO}_4\text{Si}$: 445.5542; found, 445.5510.

Section S4: Photophysical studies

The photophysical properties of DPPs **S7**, **S9-S11** and **S17** were studied in toluene and MeCN as prototypical non-polar and polar solvents (Table S1, Figures in ESI). From a structural point of view these DPPs represent D-A-D' systems where the azacrownphenyl is a strongly electron-donating group, the 4-MeOC₆H₄ is a weakly electron-donating substituent, and the DPP core is electron-deficient. DPPs **S7**, **S9-S11** and **S17** absorb at approx. 530 nm and emit at 540-580 nm in toluene. There is a small but noticeable hypsochromic shift of absorption in CH₃CN as compared to toluene (506-525 nm). Simultaneously emission shifts bathochromically to ~580 nm. Replacing MeOC₆H₄ with 4-CF₃C₆H₄ effectively increases the strength of the acceptor in the donor-acceptor system, by going from a quadrupolar-like D-A-D' structure to a dipolar like D-A-A' architecture. This should lead to a bathochromic shift of absorption and emission which is indeed observed experimentally (**S17** vs. **S9**: abs. 540 nm vs. 530 nm, em. 578 nm vs. 555 nm in toluene, Table S1). Solvatochromic trends are the same as for DPPs **S9-S11**. Interestingly, adding a triphenylphosphonium moiety strongly affects the photophysical properties shifting absorption hypsochromically and emission bathochromically to 590 nm. At the same time, the emission maxima does not show any solvent polarity effects (Table S1).

In all cases the fluorescence quantum yields are very high (80-90%) and the difference between toluene and CH₃CN is trifling in spite of the nature of the considered transitions. This observation is in strong contrast to solvatochromic behavior of 6-(3,5-bis(trifluoromethyl)phenyl)-2-butyl-3-(4-(dimethylamino)phenyl)-2,5-dihydropyrrolo[3,4-c]pyrrole-1,4-dione which showed very bright emission in toluene that almost totally quenched in CH₃CN.

Table 1. Photophysical properties of DPPs in toluene and CH₃CN.

Compound	solvent	^{max} λ _{abs} [nm]	^{max} λ _{ems} [nm]	Stokes shift [cm ⁻¹]	Φ _f ^a
S7	toluene	508	540	1200	0.77
	CH ₃ CN	498	538	1400	0.66
S9	toluene	529	555	900	0.78
	CH ₃ CN	525	563	1300	0.87
S10	toluene	528	566	1300	0.88
	CH ₃ CN	506	581	2500	0.84
S11	toluene	531	564	1100	0.85
	CH ₃ CN	519	582	2100	0.86
1	toluene	530	569	1300	0.77
	CH ₃ CN	514	583	2300	0.81
S17	toluene	540	578	1200	0.88
	CH ₃ CN	530	599	2200	0.87
2	toluene	519	592	2400	0.80
	CH ₃ CN	499	591	3100	0.48

^aDetermined using Rhodamine 6G in EtOH.**Table S2.** Changes of fluorescence of DPPs **S7**, **S9-S11** and **S17** in the presence of 5 eq. KPF₆ and PhSO₃H in CH₃CN.

DPP	KPF ₆ (5 eq.)		PhSO ₃ H (5 eq.)	
	Enhancement of fluorescence	λ _{em} (nm)	Enhancement of fluorescence	λ _{em} (nm)
S7	1.02	536	1.01	537
S9	0.99	564	0.55	550
S10	0.80	536	0.83	550
S11	0.96	582/536	0.65	551
S17	1.02	596	0.49	536

Having the fundamental photophysical properties measured, we moved on to investigation of the influence of both K⁺ cations and protonation on the absorption and emission of DPPs **S7**, **S9-S11** and **S17** (Table S2). The influence of KPF₆ addition on the fluorescence of these DPPs strongly depends on the presence of the additional alkoxy substituents. In their absence (DPPs **S9** and **S17**) there is essentially no effect even in the presence of a huge excess of KPF₆ (Fig. S9 & S34). In contrast, for DPP **S10** which bears MeO substituent that assist coordination, the effect is spectacular and the addition of just one equivalent of K⁺ shifts emission hypsochromically from 580 to 525 nm (Fig. 3). Decreasing the size of macrocycle to 15-crown-5 (DPP **S11**, too small to accommodate K⁺) makes the response a very weak one, and hundreds of equivalents of KPF₆ are necessary to induce comparable changes (Fig. 4). The addition of benzenesulfonic acid yields the same trend, however, there is no difference in strength of the bathochromic shift between

DPPs bearing differently sized crowns (Figs. S3, S5, S10, S13, S16, S19, S21, S26, S30, S33, S35, S38, S40). The presence of auxiliary alkoxy groups does not help in obtaining a more marked response to benzenesulfonic acid either.

Section S5: Absorption and emission spectra

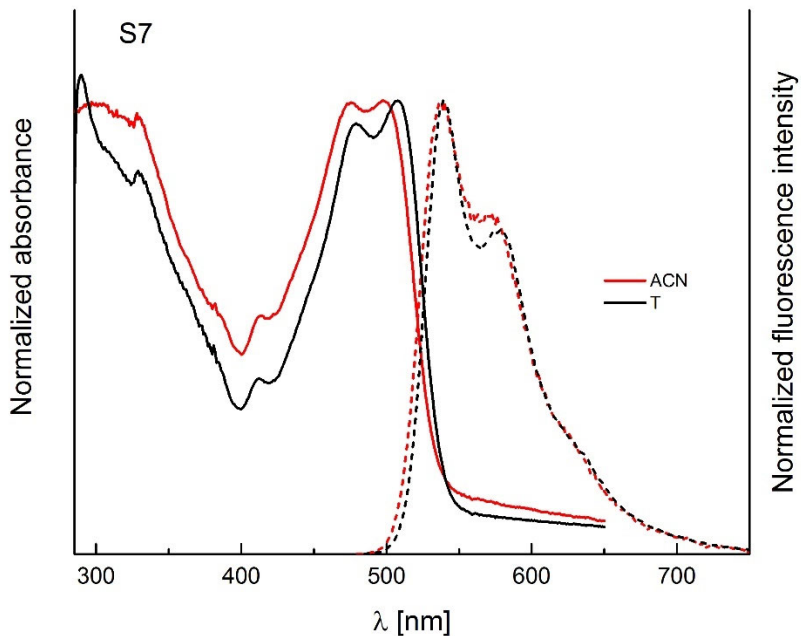


Fig. S1. The absorption and emission spectra of DPP **S7** in acetonitrile and in toluene.

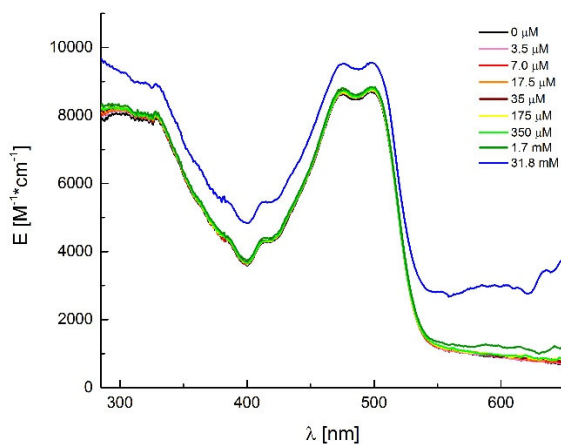


Fig. S2. The effect of KPF₆ addition on the absorption spectra of DPP **S7** measured in CH₃CN.

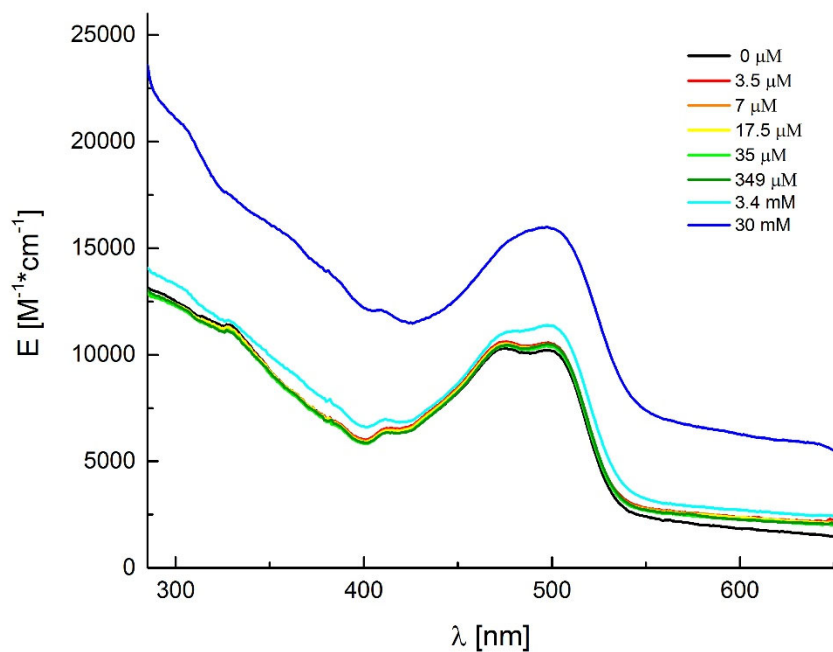


Fig. S3. The effect of BENZENESULFONIC ACID addition on the absorption spectra of DPP **S7** measured in CH_3CN .

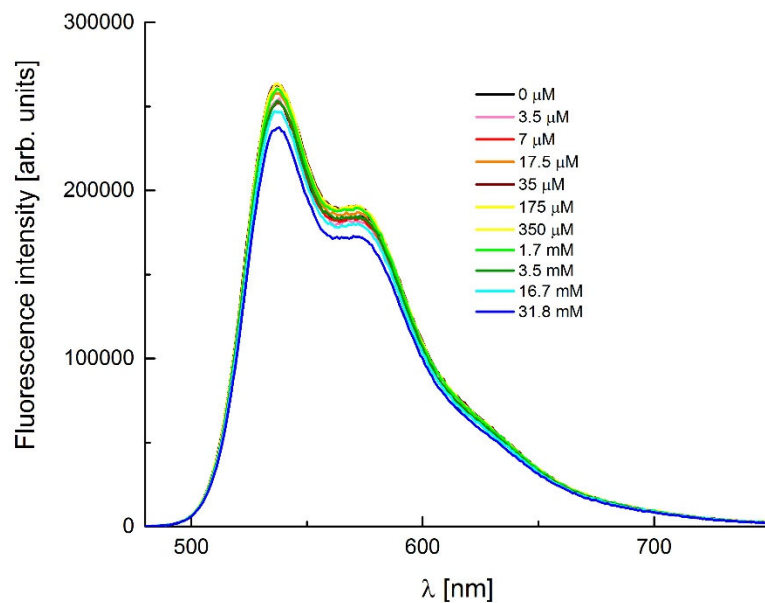


Fig. S4. The effect of KPF_6 addition on the emission spectra of DPP **S7** measured in CH_3CN .

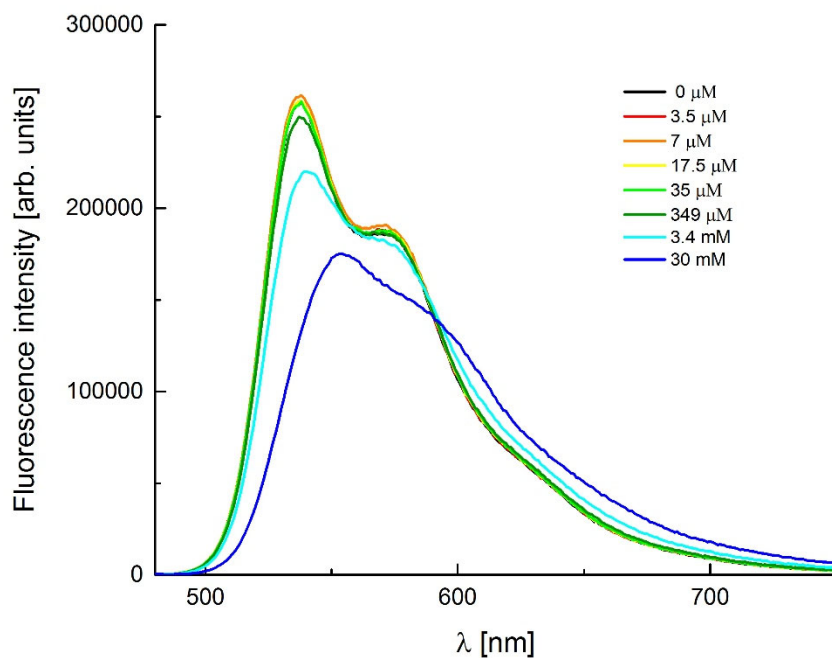


Fig. S5. The effect of BENZENESULFONIC ACID addition on the emission spectra of DPP S7 measured in CH₃CN.

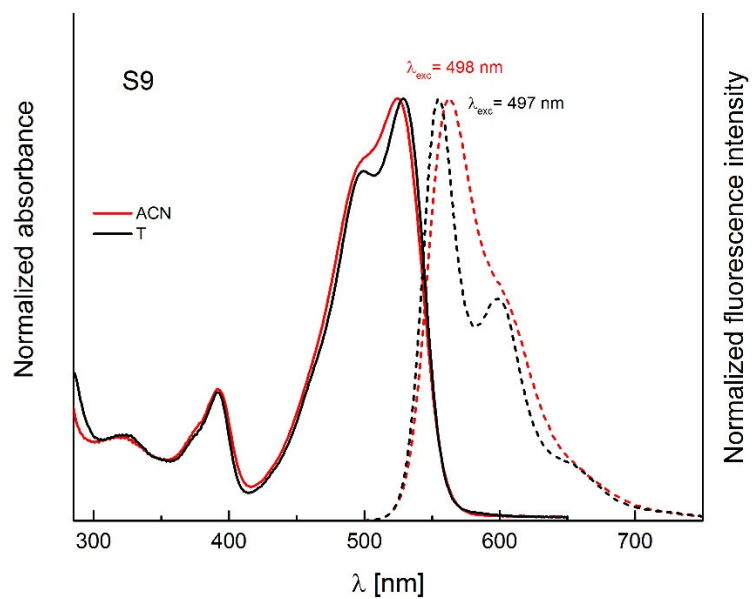


Fig. S6. The absorption and emission spectra of DPP S9 in acetonitrile and in toluene.

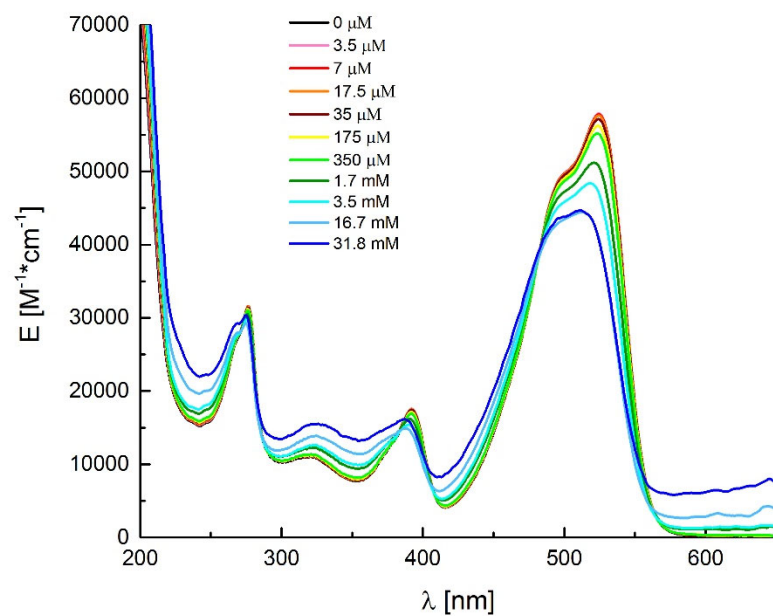


Fig. S7. The effect of KPF₆ addition on the absorption spectra of DPP S9 measured in CH₃CN.

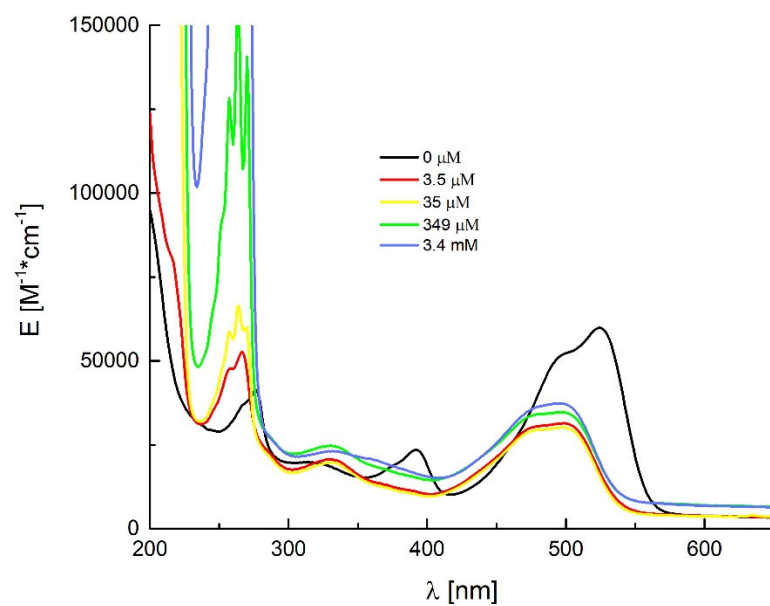


Fig. S8. The effect of BENZENESULFONIC ACID addition on the absorption spectra of DPP S9 measured in CH₃CN.

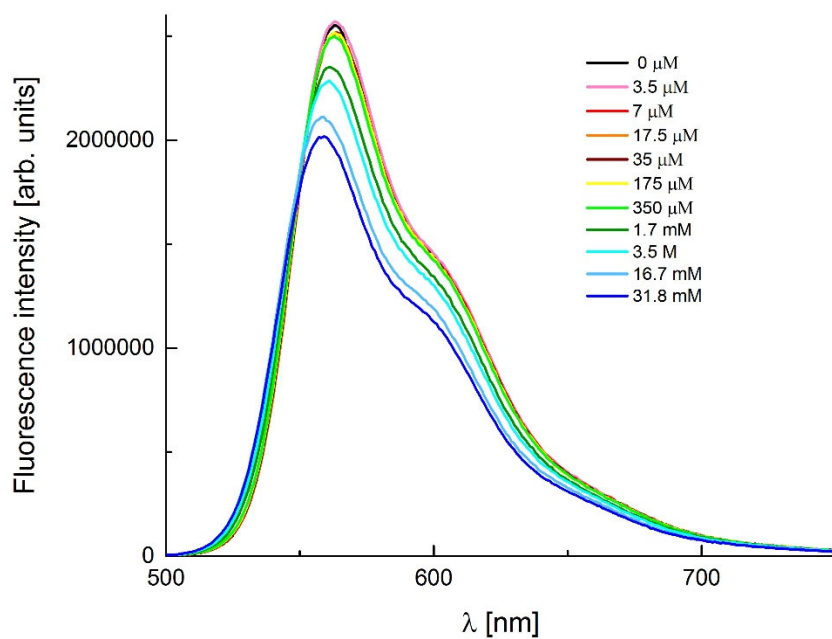


Fig. S9. The effect of KPF₆ addition on the emission spectra of DPP S9 measured in CH₃CN.

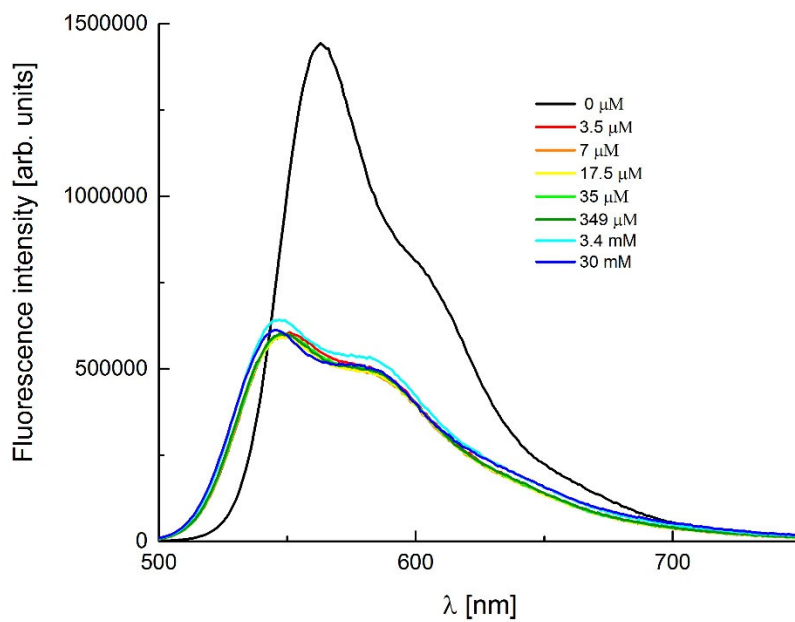


Fig. S10. The effect of BENZENESULFONIC ACID addition on the emission spectra of DPP S9 measured in CH₃CN.

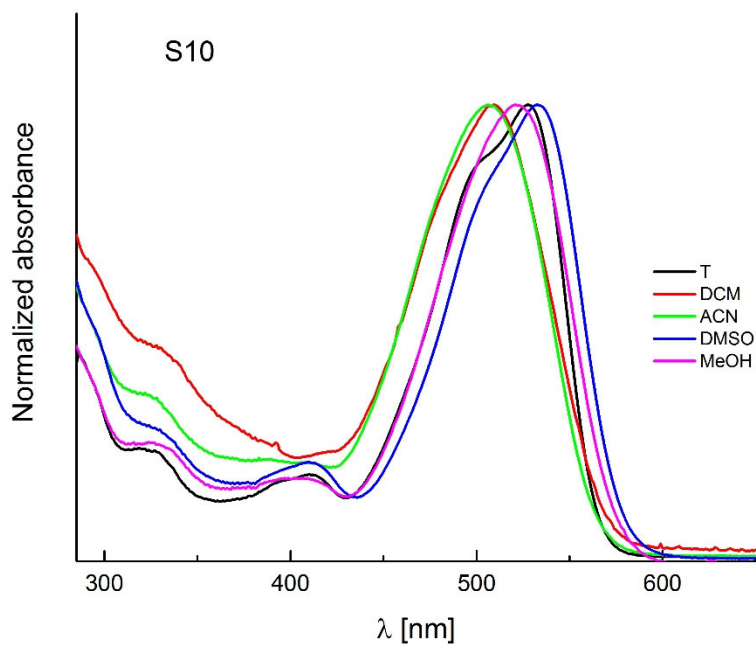


Fig. S11. The absorption and emission spectra of DPP **S10** in various solvents.

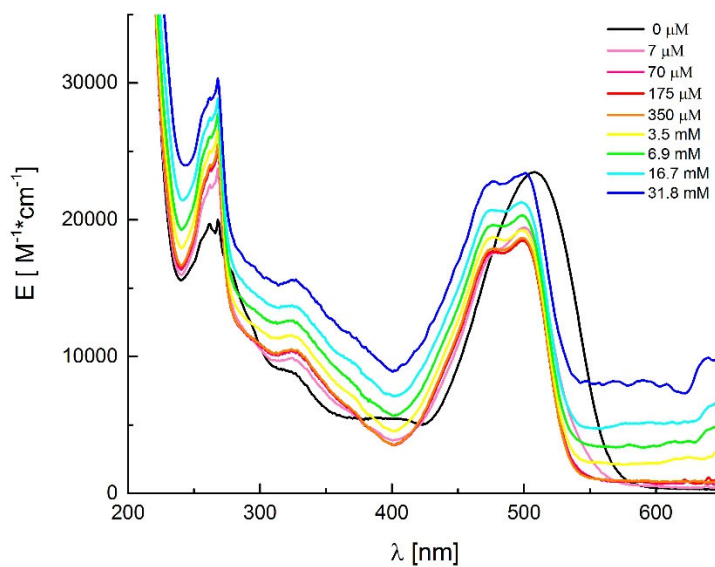


Fig. S12. The effect of KPF₆ addition on the absorption spectra of DPP **S10** measured in CH₃CN.

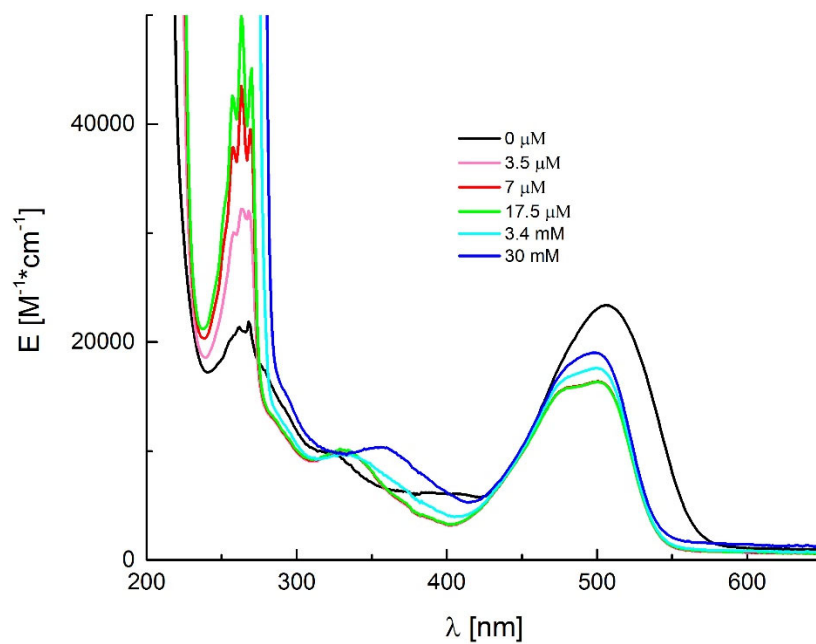


Fig. S13. The effect of BENZENESULFONIC ACID addition on the absorption spectra of DPP S10 measured in CH₃CN.

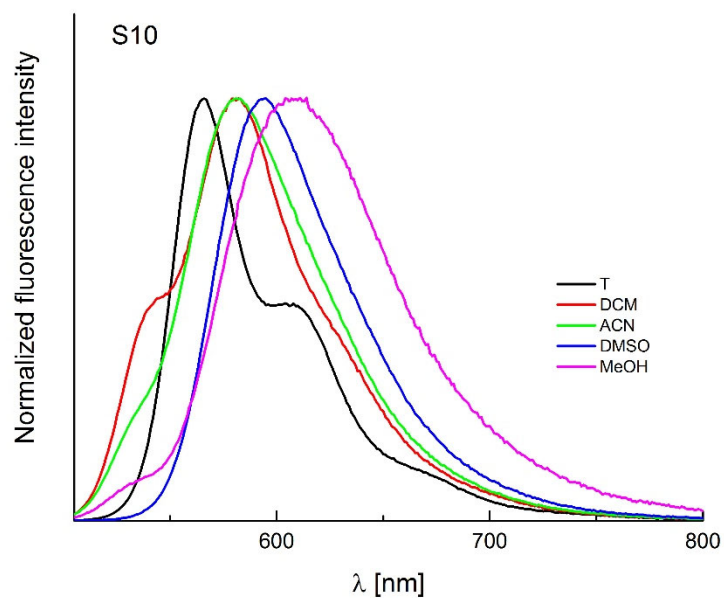


Fig. S14. The emission spectra of DPP S10 in various solvents.

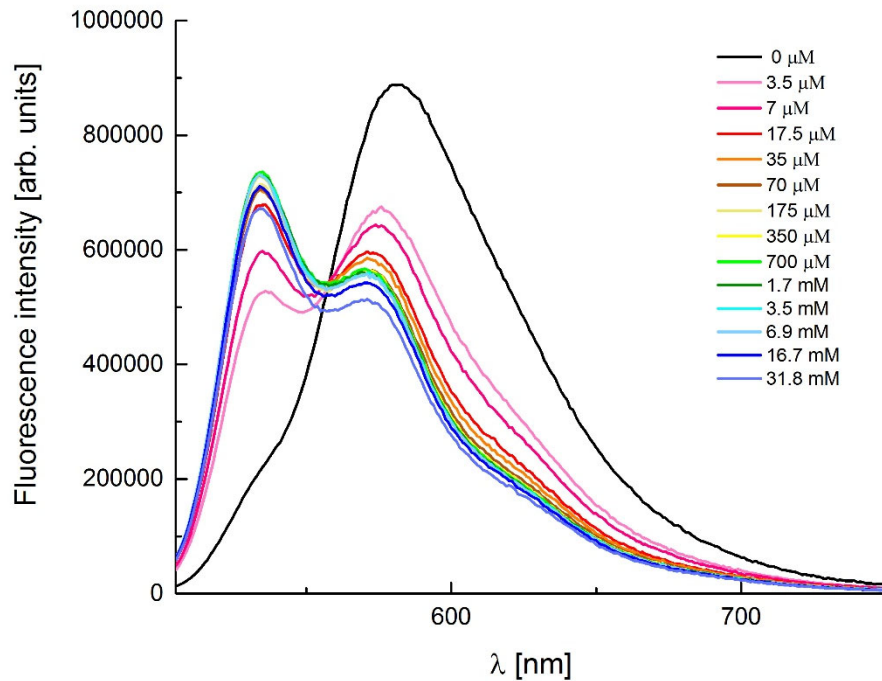


Fig. S15. The effect of KPF₆ addition on the emission spectra of DPP S10 measured in CH₃CN.

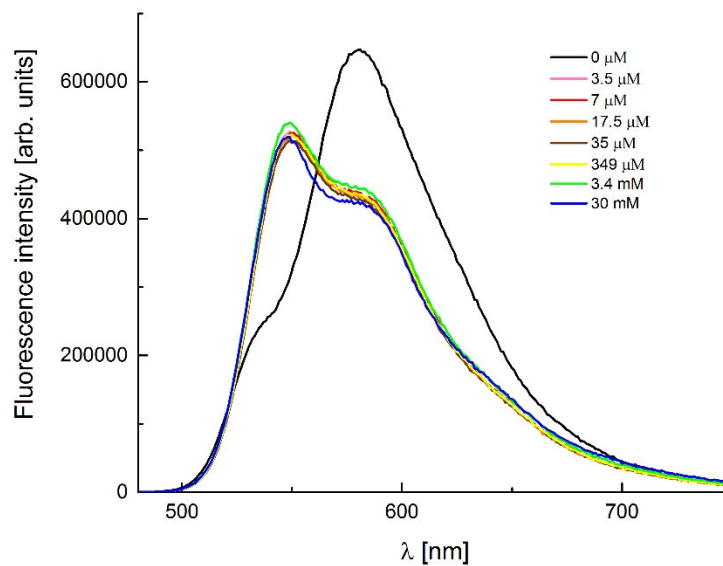


Fig. S16. The effect of BENZENESULFONIC ACID addition on the emission spectra of DPP S10 measured in CH₃CN.

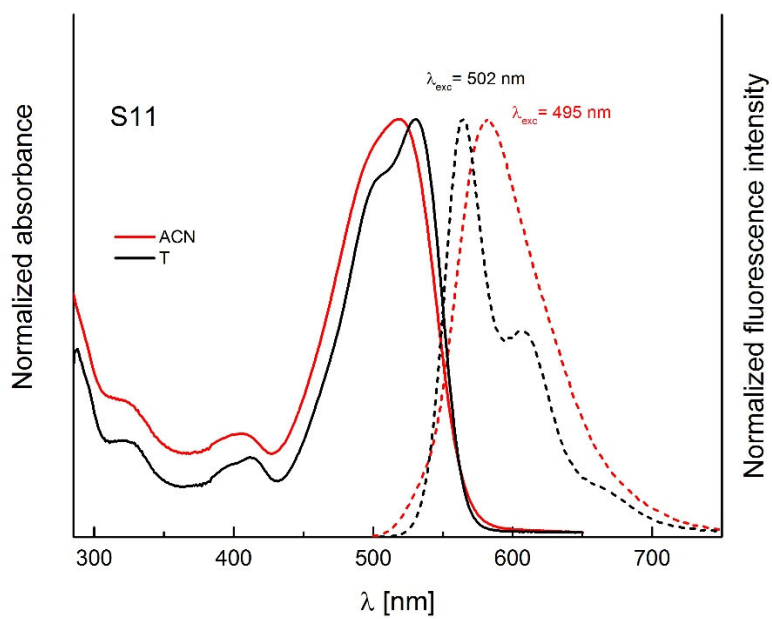


Fig. S17. The absorption and emission spectra of DPP **S11** in acetonitrile and in toluene.

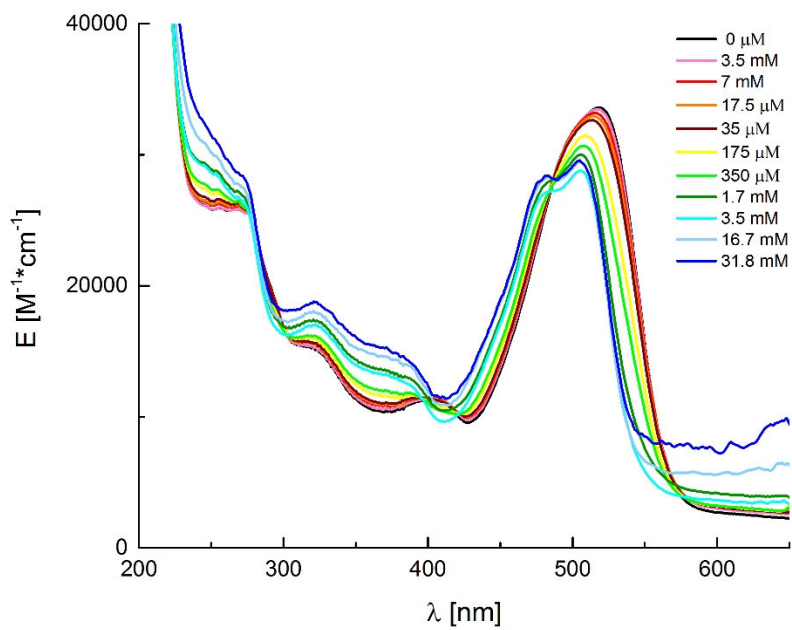


Fig. S18. The effect of KPF₆ addition on the absorption spectra of DPP **S11** measured in CH₃CN.

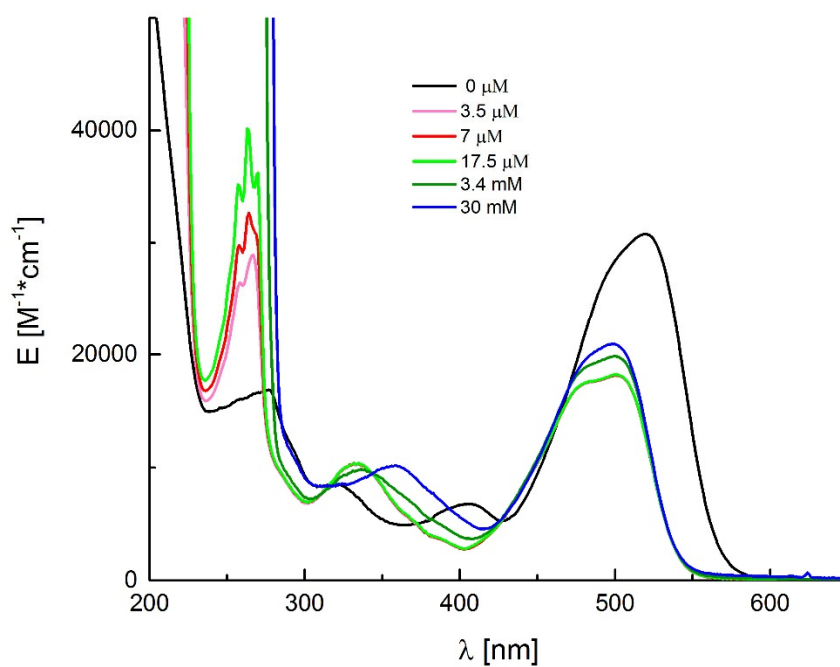


Fig. S19. The effect of BENZENESULFONIC ACID addition on the absorption spectra of DPP **S11** measured in CH_3CN .

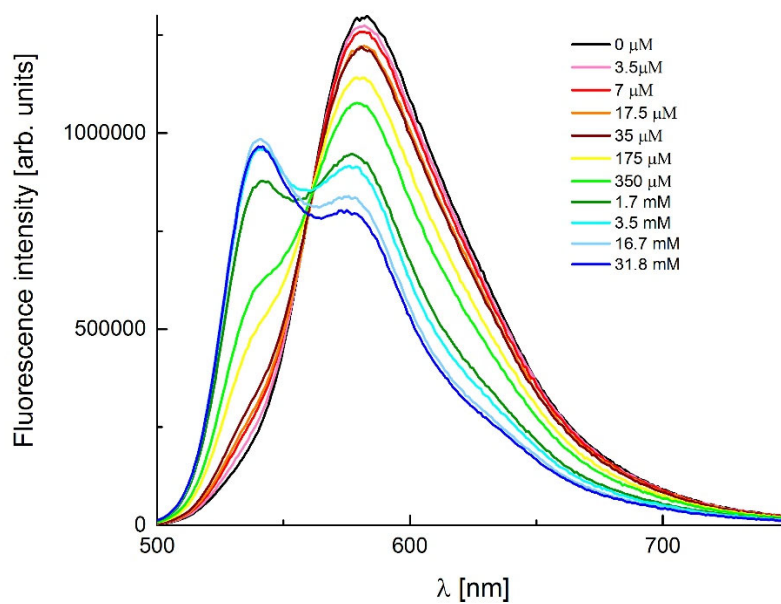


Fig. S20. The effect of KPF_6 addition on the emission spectra of DPP **S11** measured in CH_3CN .

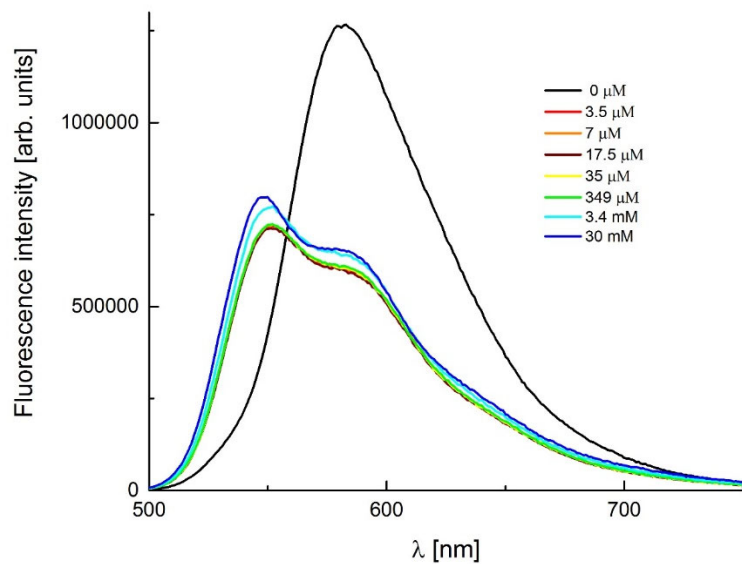


Fig. S21. The effect of BENZENESULFONIC ACID addition on the emission spectra of DPP **S11** measured in CH_3CN .

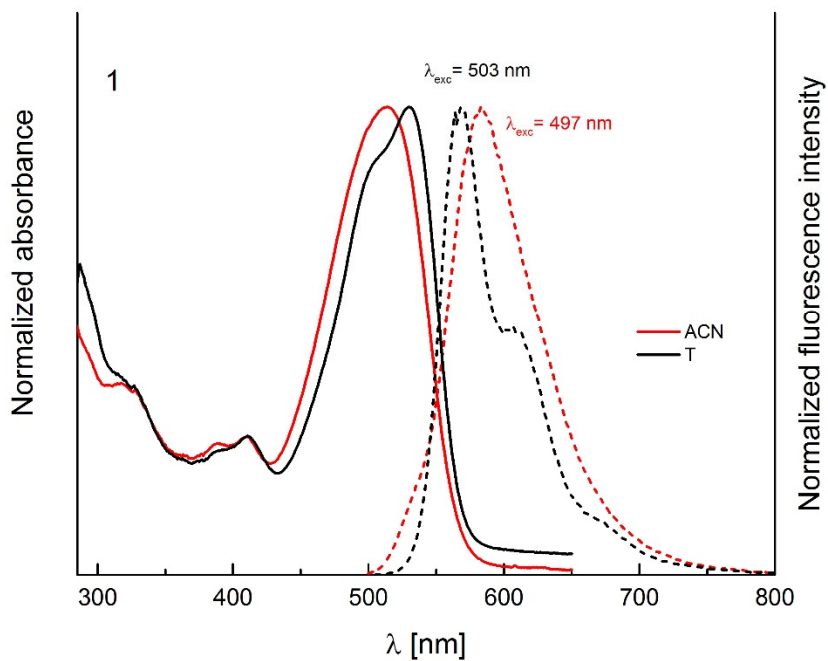


Fig. S22. The absorption and emission spectra of DPP **1** in acetonitrile and in toluene.

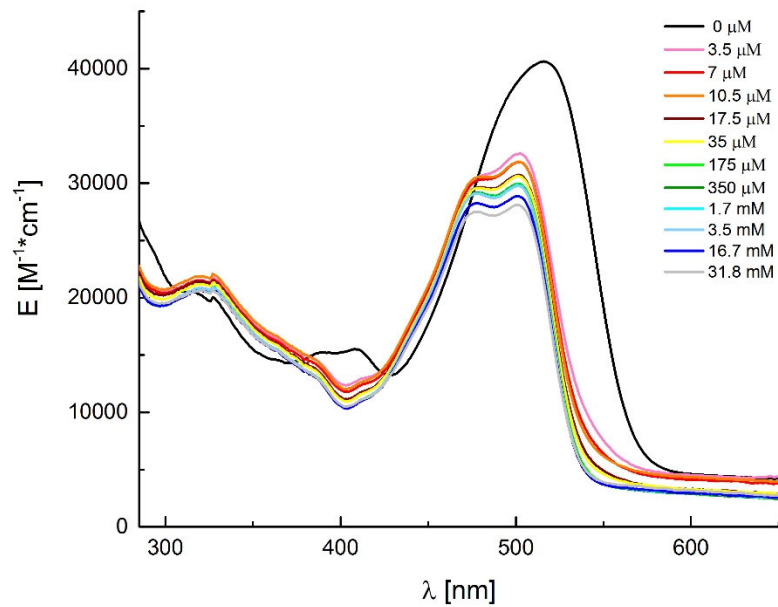


Fig. S23. The effect of KPF₆ addition on the absorption spectra of DPP **1** measured in CH₃CN.

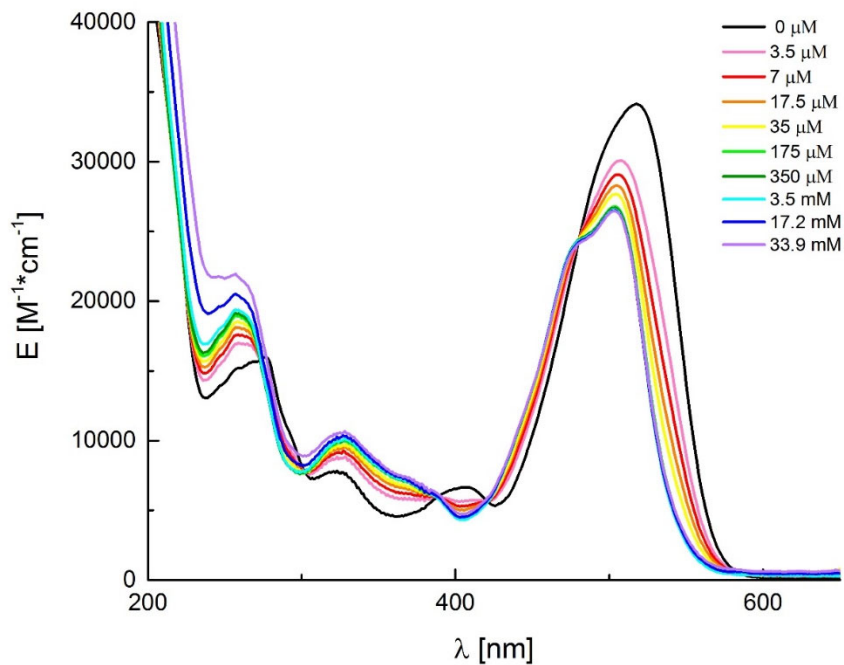


Fig. S24. The effect of sodium perchlorate addition on the absorption spectra of DPP **1** measured in CH₃CN.

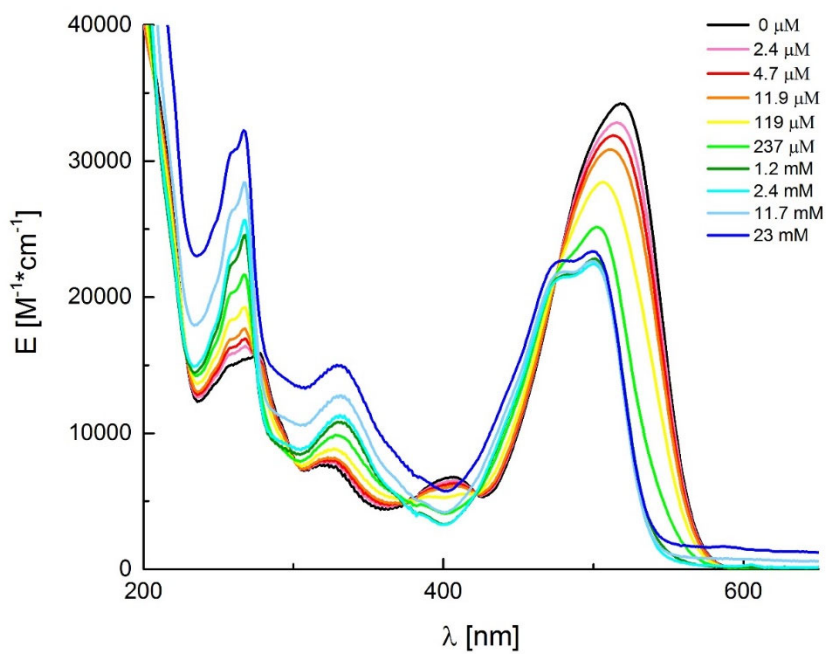


Fig. S25. The effect of magnesium perchlorate addition on the absorption spectra of DPP **1** measured in CH₃CN.

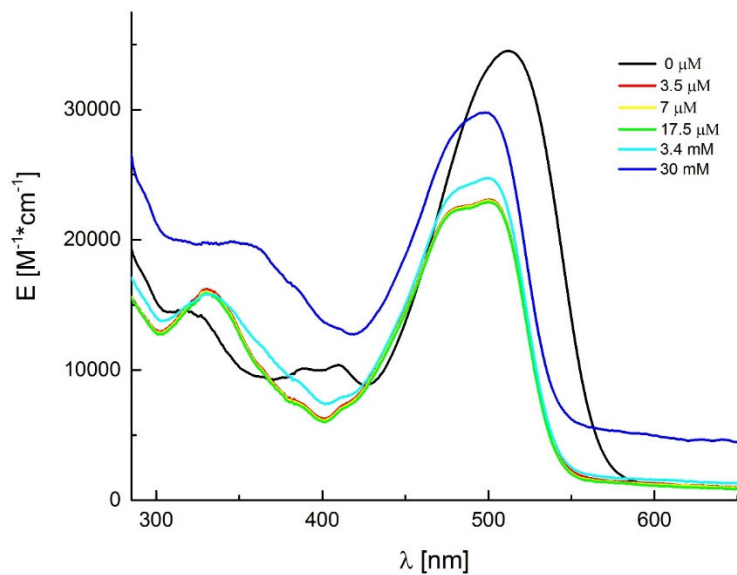


Fig. S26. The effect of benzenesulfonic acid addition on the absorption spectra of DPP **1** measured in CH₃CN.

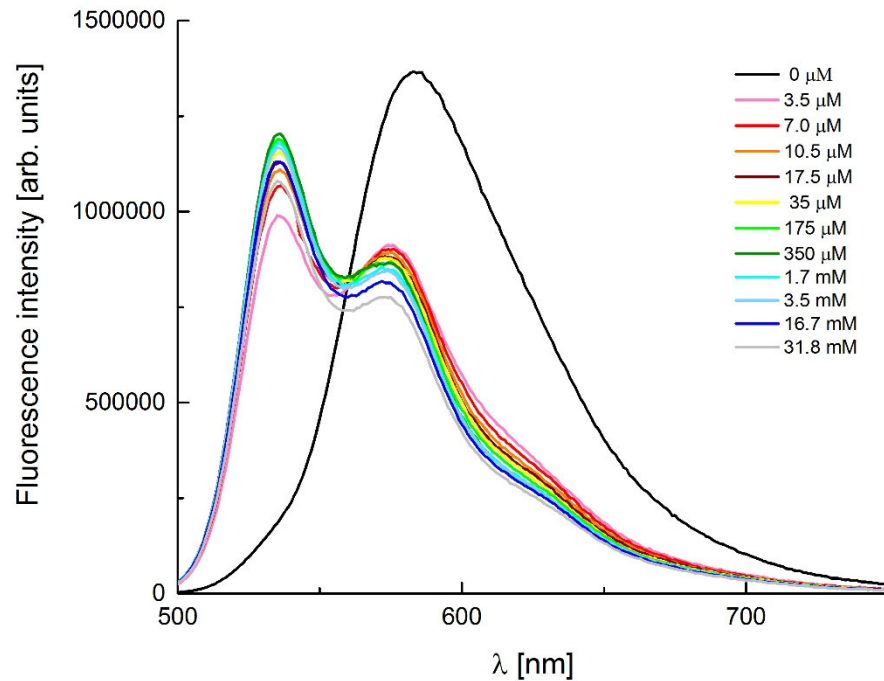


Fig. S27. The effect of KPF₆ addition on the emission spectra of DPP 1 measured in CH₃CN.

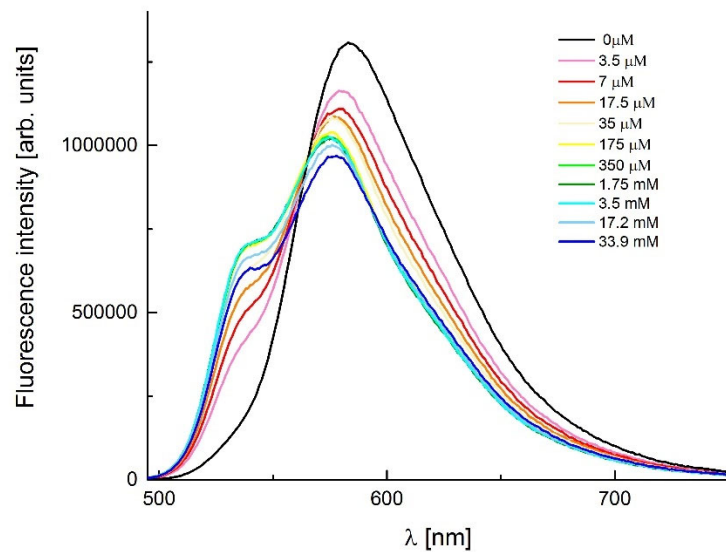


Fig. S28. The effect of sodium perchlorate addition on the emission spectra of DPP 1 measured in CH₃CN.

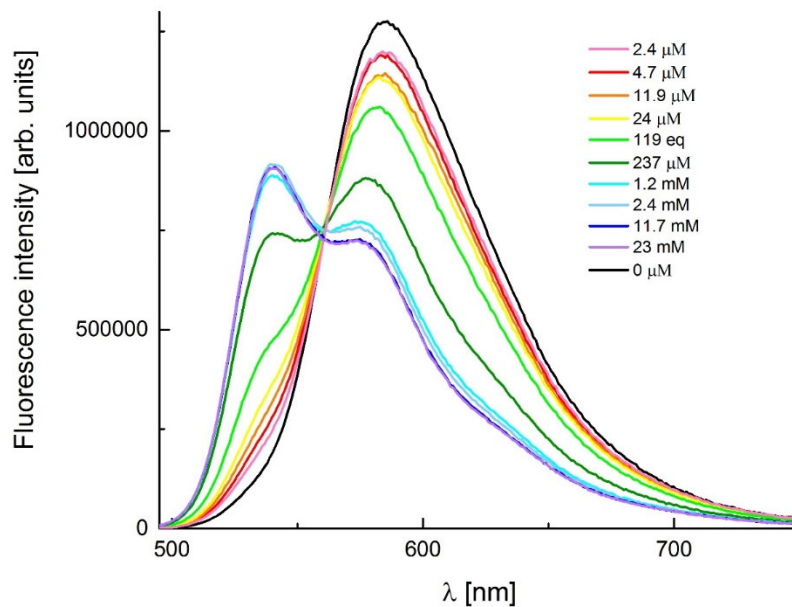


Fig. S29. The effect of magnesium perchlorate addition on the emission spectra of DPP **1** measured in CH₃CN.

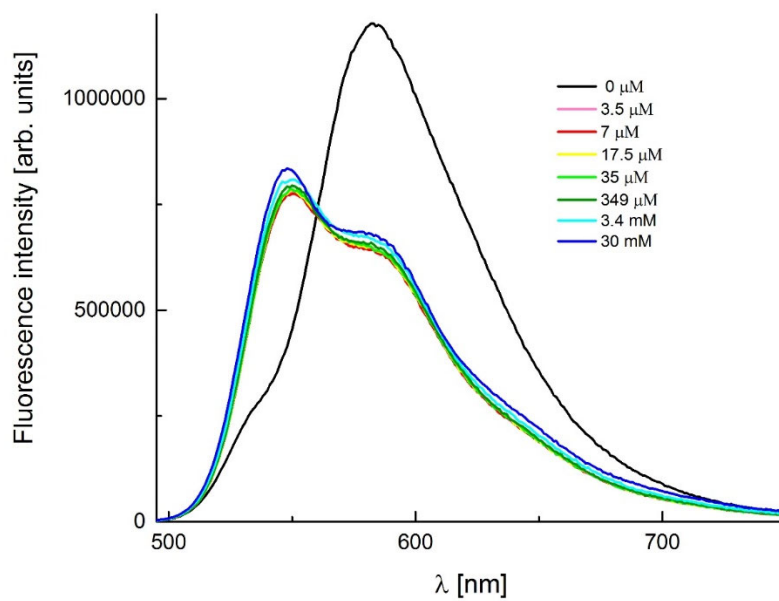


Fig. S30. The effect of BENZENESULFONIC ACID addition on the emission spectra of DPP **1** measured in CH₃CN.

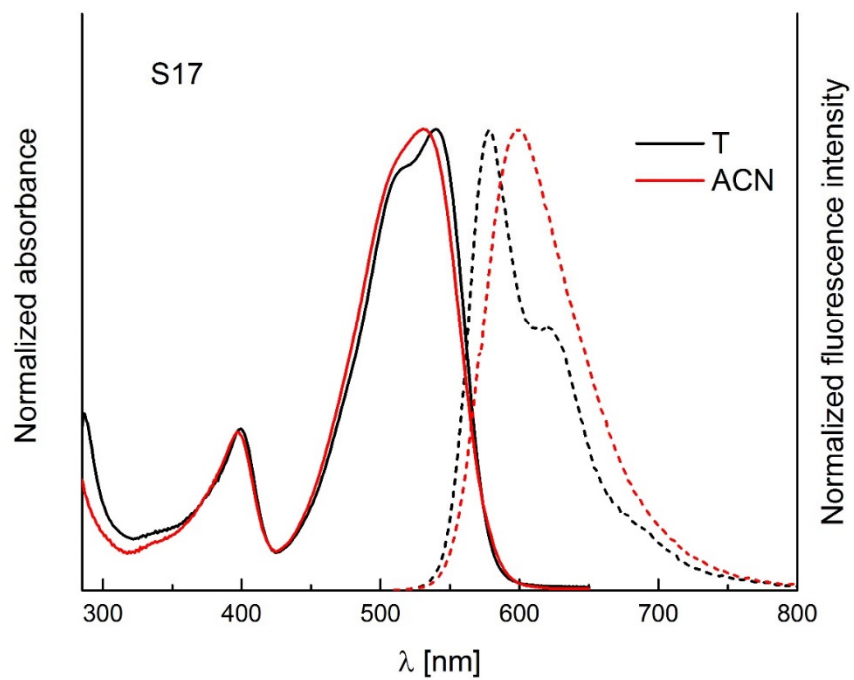


Fig. S31. The absorption and emission spectra of DPP **S17** in acetonitrile and in toluene.

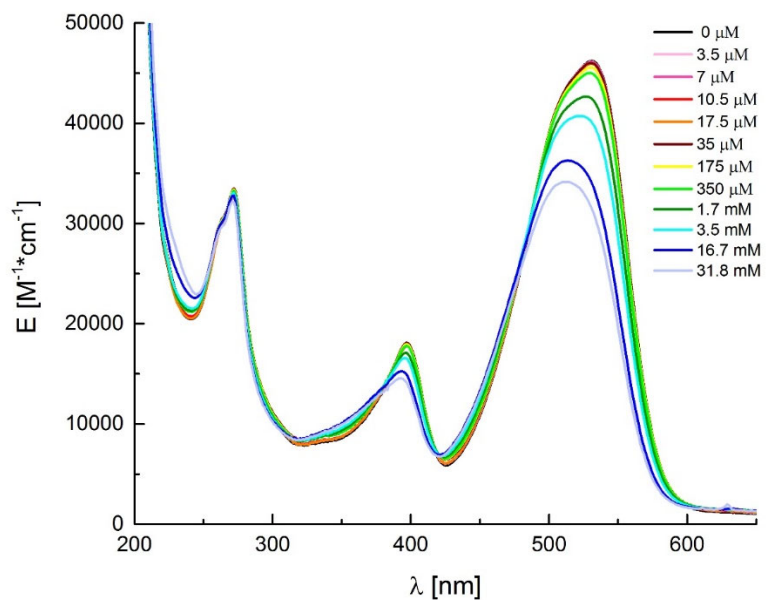


Fig. S32. The effect of KPF₆ addition on the absorption spectra of DPP **S17** measured in CH₃CN.

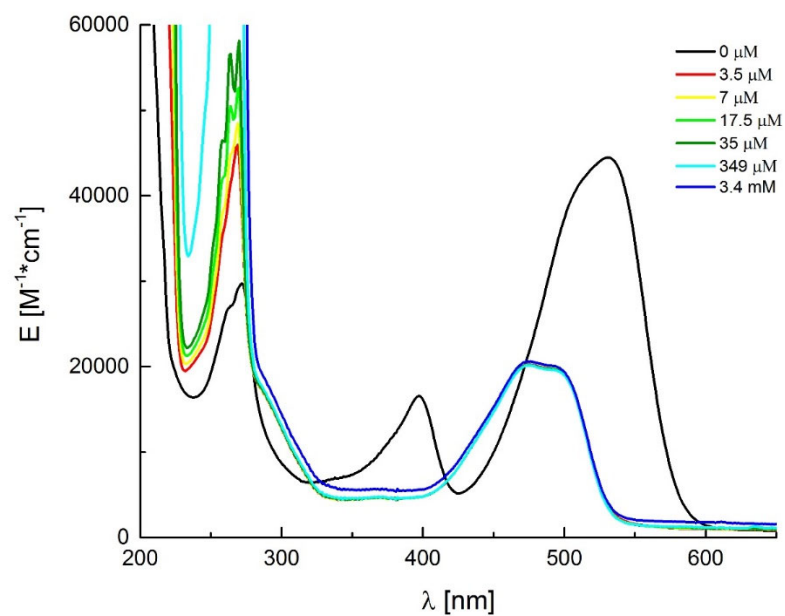


Fig. S33. The effect of BENZENESULFONIC ACID addition on the absorption spectra of DPP **S17** measured in CH_3CN .

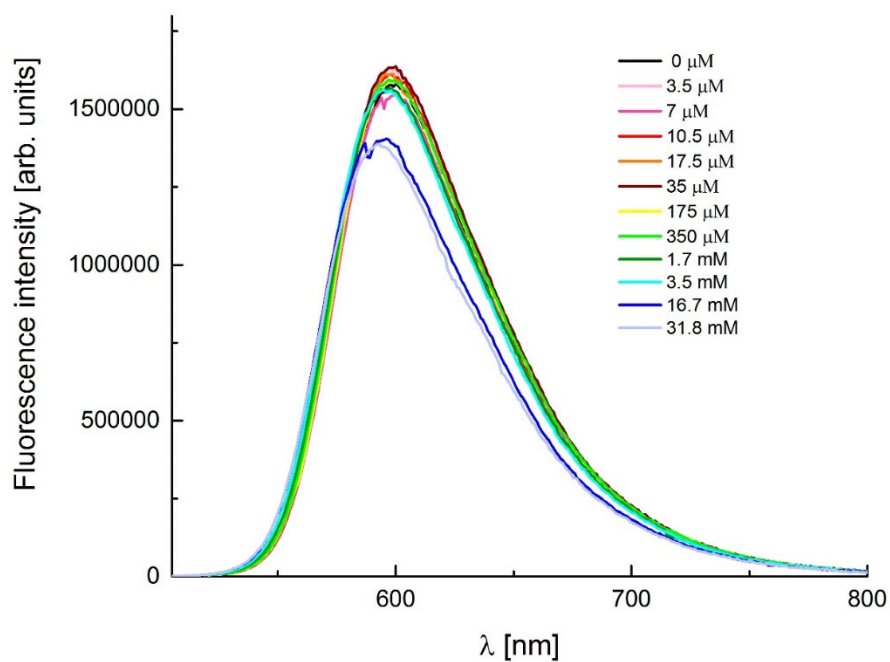


Fig. S34. The effect of KPF_6 addition on the emission spectra of DPP **S17** measured in CH_3CN .

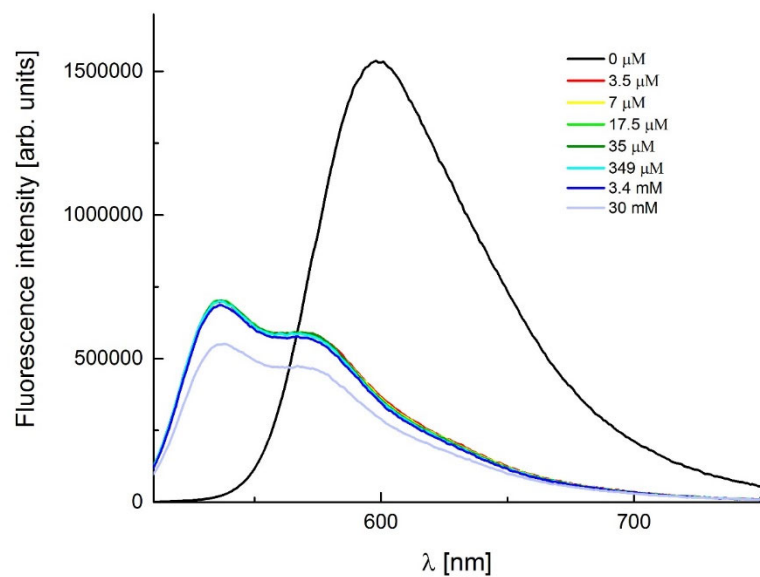


Fig. S35. The effect of BENZENESULFONIC ACID addition on the emission spectra of DPP S17 measured in CH₃CN.

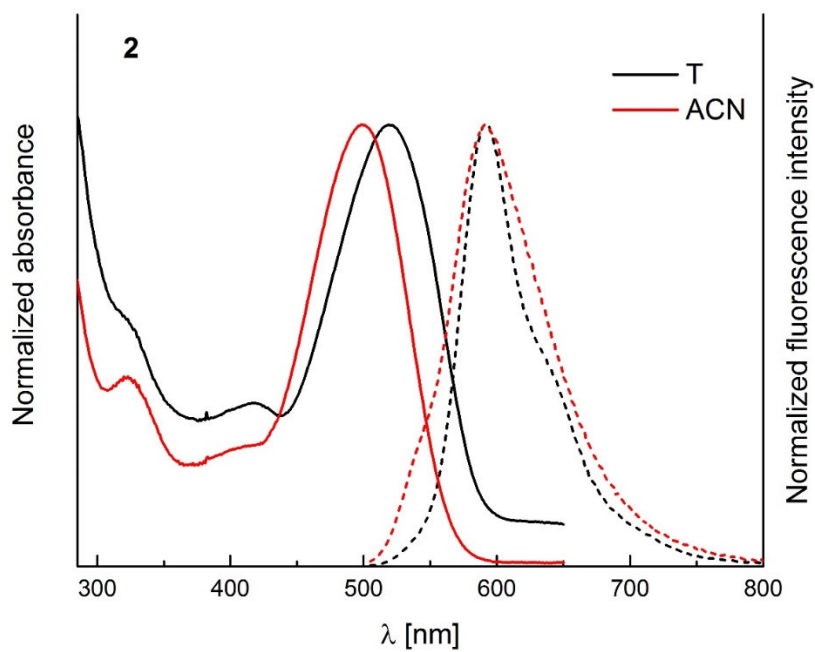


Fig. S36. The absorption and emission spectra of DPP 2 in acetonitrile and in toluene.

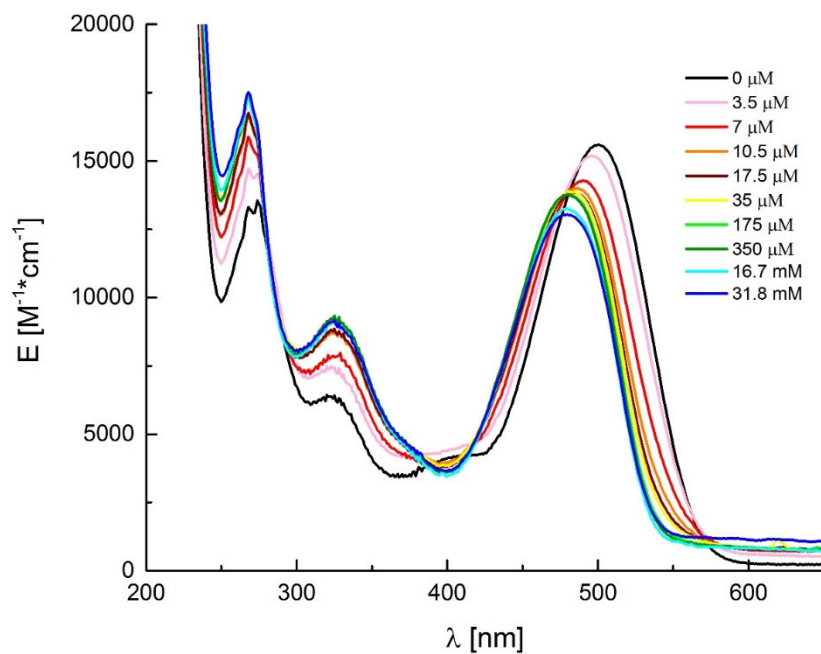


Fig. S37. The effect of KPF₆ addition on the absorption spectra of DPP 2 measured in CH₃CN.

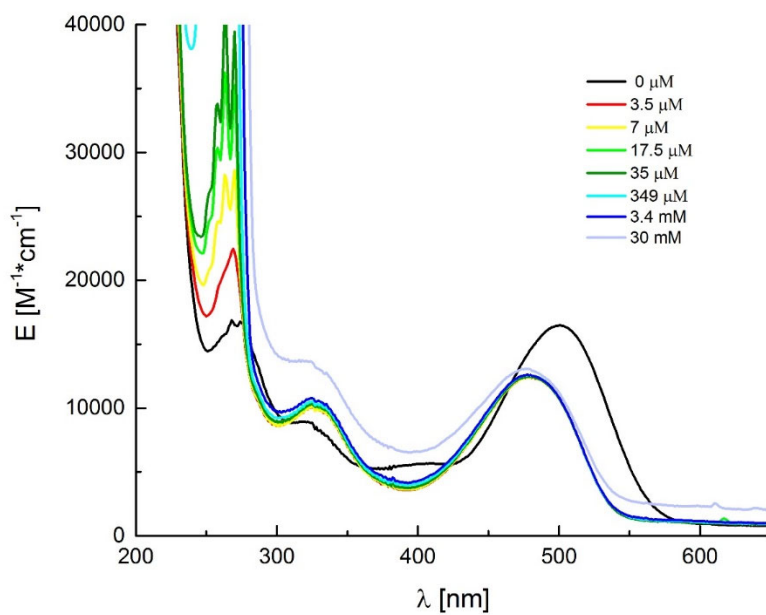


Fig. S38. The effect of BENZENESULFONIC ACID addition on the absorption spectra of DPP 2 measured in CH₃CN.

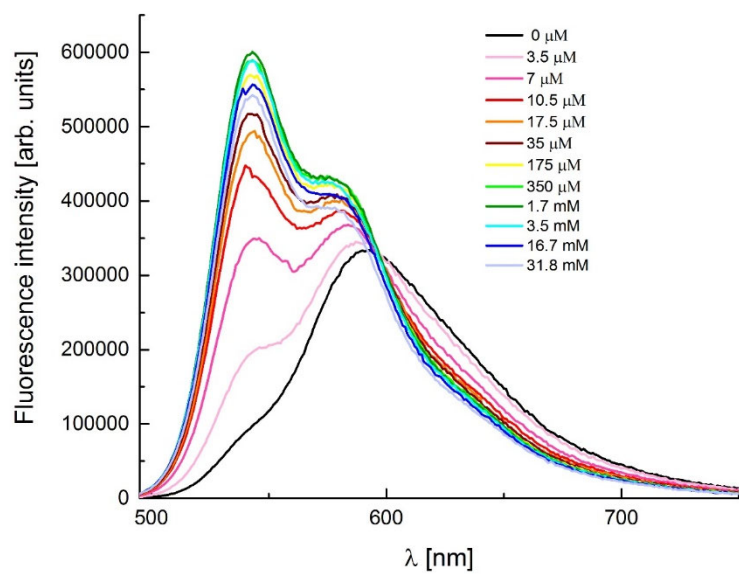


Fig. S39. The effect of KPF₆ addition on the emission spectra of DPP 2 measured in CH₃CN.

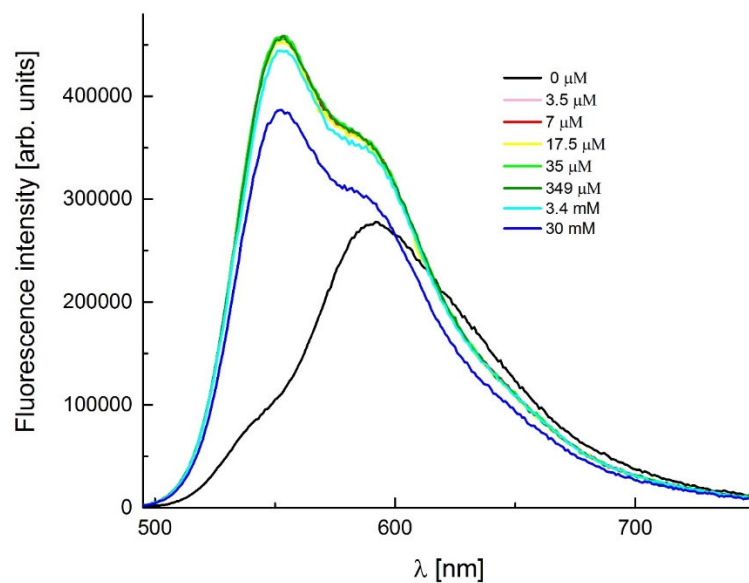


Fig. S40. The effect of BENZENESULFONIC ACID addition on the emission spectra of DPP 2 measured in CH₃CN.

Photostability measurements

Photostability of DPP **2** was determined through the variation in absorption of each sample at the appropriate absorption maximum wavelength (λ_{abs}) with respect to irradiation time. Toluene was selected as the solvent. Concentrations giving similar optical densities ($A \approx 1$) were used. Quartz cells of samples were irradiated with a 300 W Xe lamp (Asahi spectra MAX-350, light power: 0.115 W/cm^2) for 180 min at $25 \text{ }^\circ\text{C}$ equipped with a UV/vis mirror module through a glass fiber. The absorption spectra were measured at appropriate times during the irradiation. BODIPY (difluoro{2-[1-(3,5-dimethyl-2*H*-pyrrol-2-ylidene-*N*)ethyl]-3,5-dimethyl-1*H*-pyrrolato-*N*}boron), DPP (2,5-dimethyl-3,6-bis(3,4-dimethoxyphenyl)pyrrolo[3,4-*c*]pyrrole-1,4(2*H*,5*H*)-dione) and Alexa Fluor 555 were used as references.

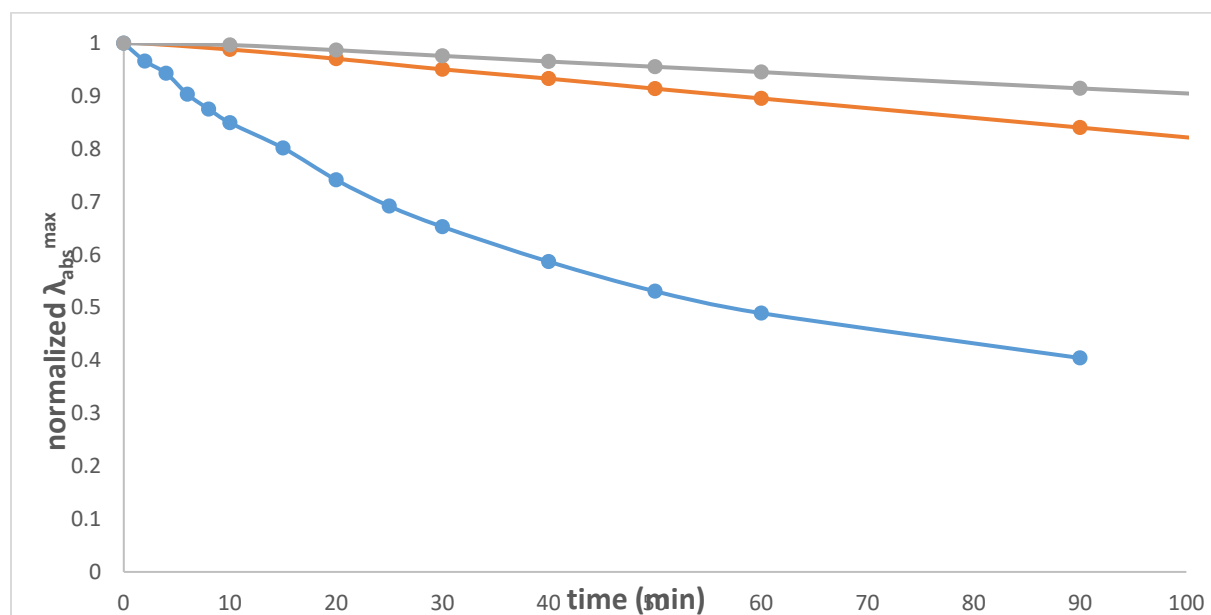


Fig. S41. Photostability of DPP **2** measured in CH_3CN (DPP **2** – blue line, BODIPY 493/503 – gray line, DPP (2,5-dioctyl-3,6-bis(3,4,5-trimethoxyphenyl)pyrrolo[3,4-*c*]pyrrole-1,4(2*H*,5*H*)-dione – orange line).

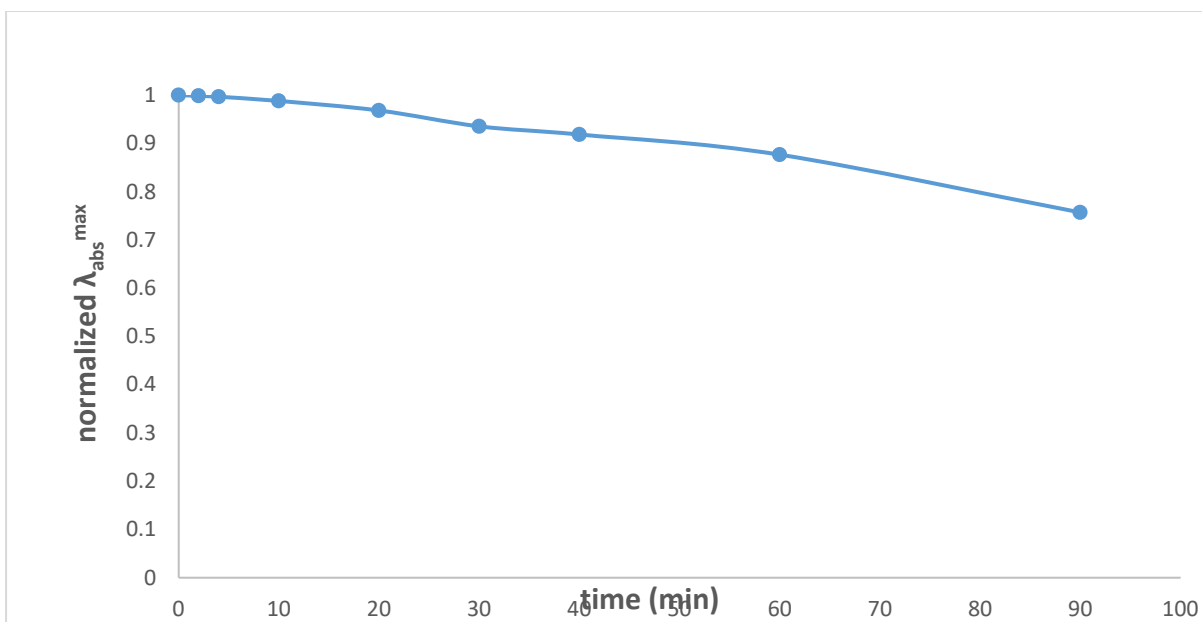


Fig. S42. Photostability of DPP 2 measured in water (containing 10% of DMSO).

Section S6: IMAGING

Cell culture conditions. The rat embryonic cardiomyoblast-derived H9C2 and endothelial EA.hy 926 cell lines were cultured at 37 °C in a humidified atmosphere containing 5% CO₂ in DMEM supplemented with 10% foetal bovine serum, 2 mM glutamine, 100 U/ml penicillin, and 100 µg/ml streptomycin.

Fluorescence localization of crown-diketopyrrolopyrroles within the cells. The cardiac H9C2 cells were loaded with fluorophores in DMEM medium supplemented with 10% foetal bovine serum, 2 mM glutamine, 100 U/ml penicillin, and 100 µg/ml streptomycin at 37 °C in a humidified atmosphere containing 5% CO₂ for 15 to 30 minutes with the crown-diketopyrrolopyrroles compounds at the final concentration ranging from 200 to 500 nM. The final concentration of the MitoTracker™ Green FM was 150 nM. Both fluorophores were dissolved in DMSO. Before measurements, the incubation medium was replaced with FluoroBrite™ DMEM. The measurements were performed with use of Olympus IX83 confocal microscope with the water objective 60x UPLSAPO 60XW. Registered data were transferred to the ImageJ and analyzed for presentation.

The research was carried out on "live" unfixed cells. The given run of the experiment, the control, the administration of valinomycin and naringenin, and the change of the incubation medium to 200 mM KCl were performed on the same cells. The research was carried out on "live" unfixed cells. The given run of the experiment, the control, the administration of valinomycin and

naringenin, and the change of the incubation medium to 200 mM KCl were performed on the same Petri dish.

H9C2 cells, which had been incubated for 30 minutes with DPP 2 at 37°C at 5% CO₂, were washed with incubation medium (FloroBrite) and measurements were made under control conditions Fig A. Then valinomycin and nigericin were added to the control medium to a final concentration of 30 μM and 10 μM respectively and after 5 min of incubation the measurements were performed for 5 mM KCl conditions. After that, the incubation medium was changed to a medium containing 200 mM KCl with appropriate concentrations of valinomycin and nigericin. And the fluorescence intensity was measured for 200 mM KCl conditions. Measurements performed only in the presence of valinomycin transport only potassium ions, which in the case of the cell membrane would do the job. However, in the case of mitochondria, the process is more complicated. Administration of valinomycin alone would change only the electrical potential ΔΨ of the inner mitochondrial membrane which would lead to activation of the respiratory chain and an increase in pH. The addition of nigericin reduces the transmembrane ΔpH (Kang, Chen et al. 2017).

Kang, P. T., C. L. Chen, P. Lin, W. M. Chilian and Y. R. Chen (2017). "Impairment of pH gradient and membrane potential mediates redox dysfunction in the mitochondria of the post-ischemic heart." *Basic Res Cardiol* 112(4): 36.

The number of cells used for the measurement is usually 100,000 if we take into account their volume (assuming that they are a sphere) $\frac{4}{3}\pi r^3$ (radius of the cell 50 μm) then compared to the volume of 2 ml of incubation medium, if the concentration on both sides of the biological membrane is equalized, the concentration will be close to the value of 5 mM as it is in incubation medium.

mean from both samples	B3-A	YG2-A	B3-A/YG2-A
Probe	5,77E+05	1,57E+05	3,81E+00
Probe_valinomycin_nigericin	4,44E+05	1,72E+05	2,56E+00
Probe_valinomycin_nigericin	6,14E+05	1,09E+05	5,65E+00
Control	18052	4170	4,32901679
Pearson r (B3 vs YG2):	-0,82		

In response to this comment the measurements were performed using a flow cytometer and the results confirmed those obtained for the confocal microscopy measurements. Only the extreme values of potassium ions were used to define the limit of changes in the value of the fluorescence intensity ratio for green and red colors. Further studies with potassium titration are planned, but require a separate approach to demonstrate the biological usefulness of a given fluorescent probe.

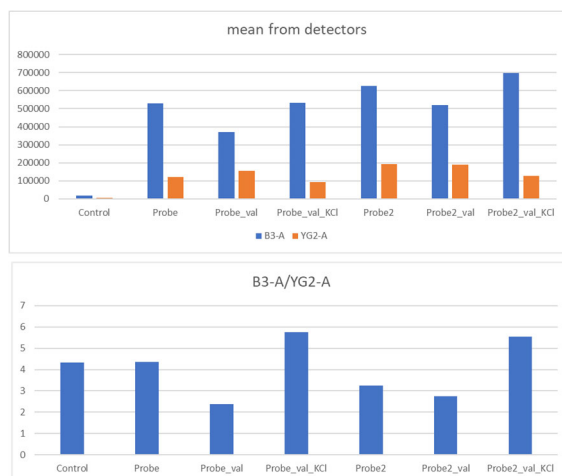


Figure 43. Measurements made using flow cytometry for different KCl concentrations. Probe_val is for valinomycin and nigericin. Data from two experiments.

In order to determine the viability of cells under the influence of the tested crown-diketopyrrolopyrroles, an annexin V-based apoptosis and necrosis test (RealTime-Glo™ Annexin V Apoptosis and Necrosis Assay, Promega) was performed, allowing the simultaneous examination of the effect of the substances on the induction of apoptotic and necrotic cell death.

Section S7: Confocal fluorescence microscopy images

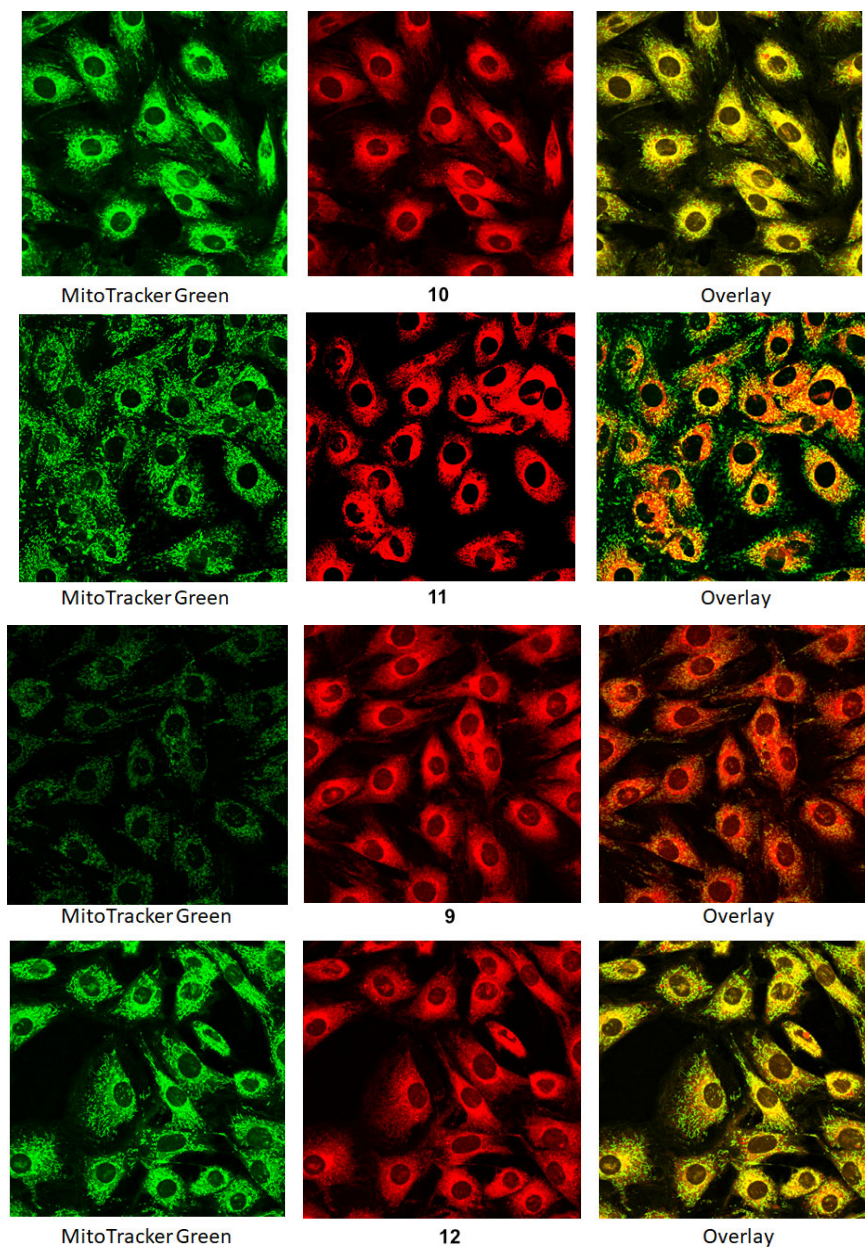


Fig. S44. Intracellular localization of **S10**, **S11**, **S9** and **1** compounds as detected using confocal fluorescence microscopy.

The fluorescence of MitoTracker™ Green (green) as a well-established marker for mitochondria, and the fluorescence of the **S10**, **S11**, **S9** and **S12** (red) compounds were recorded with 559 nm excitation wavelength and emission range 610–750 nm. Overlay picture recorded simultaneously for two fluorophore in living H9C2 cells line.

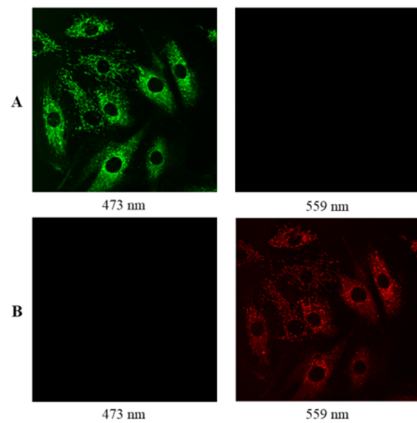


Fig. S45. Separation of the fluorescence emission wavelength with excitation with laser line 473 nm (A) and 559 nm (B). Detection channels were set for fluorescence green and red light respectively.

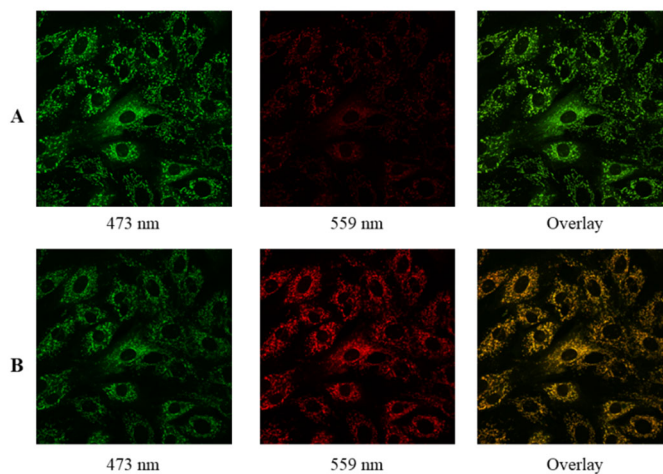


Fig. S46. Changes in the fluorescence of the **2** compound in the different intracellular K^+ concentration caused by nigericin. A control condition. B in the presence of nigericin (10 μM).

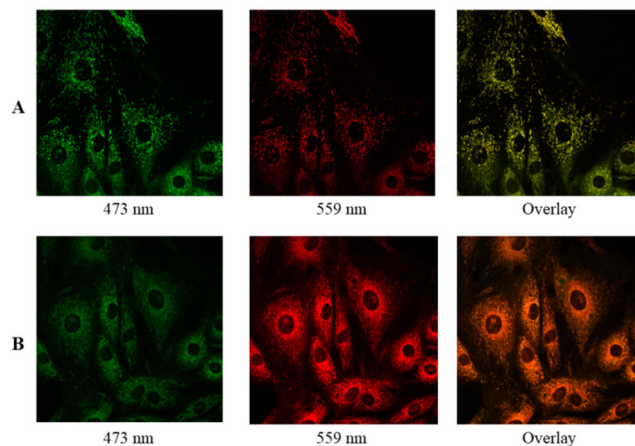


Fig. S47. Changes in the fluorescence of the **2** compound in the different intracellular K^+ concentration caused by valinomycin. A control condition. B in the presence of valinomycin (30 μ M).

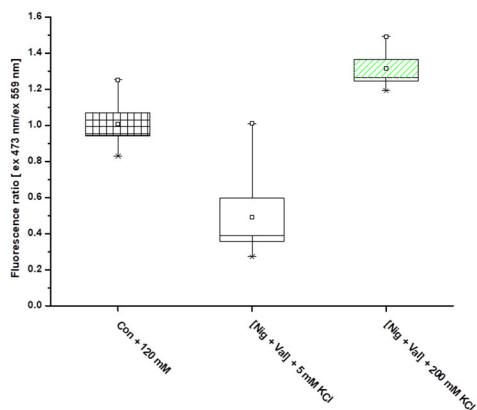


Fig. S48. Changes in the ratio (473 nm/559 nm) of the fluorescence intensity at the different excitation wavelength as measured with use of ImageJ. The ratio is statistically different for each conditions as measured in paired sample t Test at the level 0.05.

Penetration into the cell depends on a number of factors and under our conditions, after many trials, we decided to load the cells with the dye in the presence of Pluronic 127 detergent and FBS in the incubation medium. This is due to the fact that research on living cells is taken into account and the dye entering the cell accumulates in the inner mitochondrial membrane and

mitochondria. Too rapid accumulation could damage the performance of the mitochondrial activity system and produce undesirable results. It turned out that the penetration of the dye into the cell without FBS in the environment is extremely fast, but it is easier to control the charge level of the cell in the presence of FBS by changing the time of loading. In our opinion, it is more important to obtain a stable dye balance. In the ratiometric measurements of fluorescence the level of dyes loading is less important.

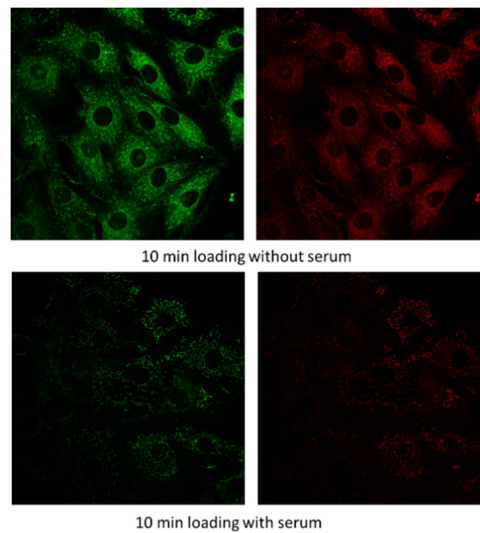


Figure 49. Different level loading of dye 6 in the presence and absence of serum.

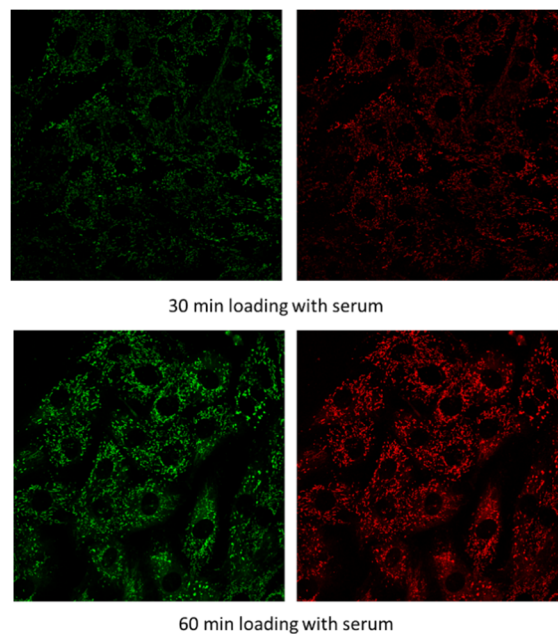


Figure 50. Different time loading of dye 6 in the presence of serum in incubation medium.

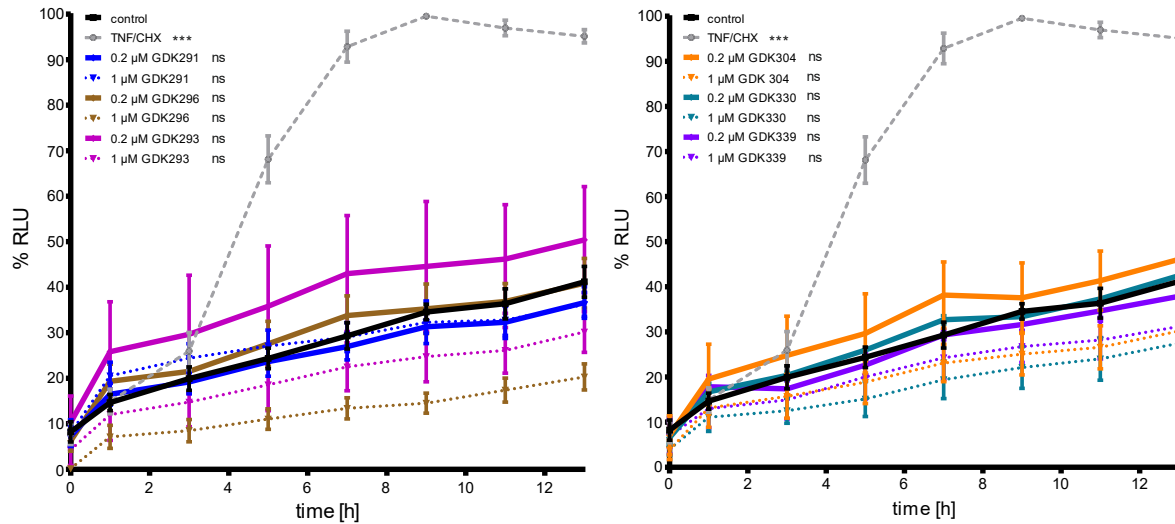
Pearson's correlation coefficient and Mander's overlap coefficient (MOC).

For pair of two signal channels Mitotracker Green and DPP **1** Pearson's Coefficient: $r=0.597$, Manders' Coefficients (original): $M1=0.997$ (fraction of Mitotracker Green overlapping DPP **1**), $M2=0.763$ (fraction of DPP **1** overlapping Mitotracker Green).

For pair of two signal channels Mitotracker Green and DPP **2** Pearson's Coefficient: $r=0.793$, Manders' Coefficients (original): $M1=0.888$ (fraction of Mitotracker Green overlapping DPP **2**) $M2=0.993$ (fraction of DPP **2** overlapping Mitotracker Green).

For pair of two signal channels: Mitotracker Green and DPP **2** (B) Pearson's Coefficient: $r=0.788$, Manders' Coefficients (original): $M1=0.944$ (fraction of Mitotracker Green overlapping DPP **2**), $M2=0.968$ (fraction of DPP **2** overlapping Mitotracker Green).

A APOPTOSIS



B NECROSIS

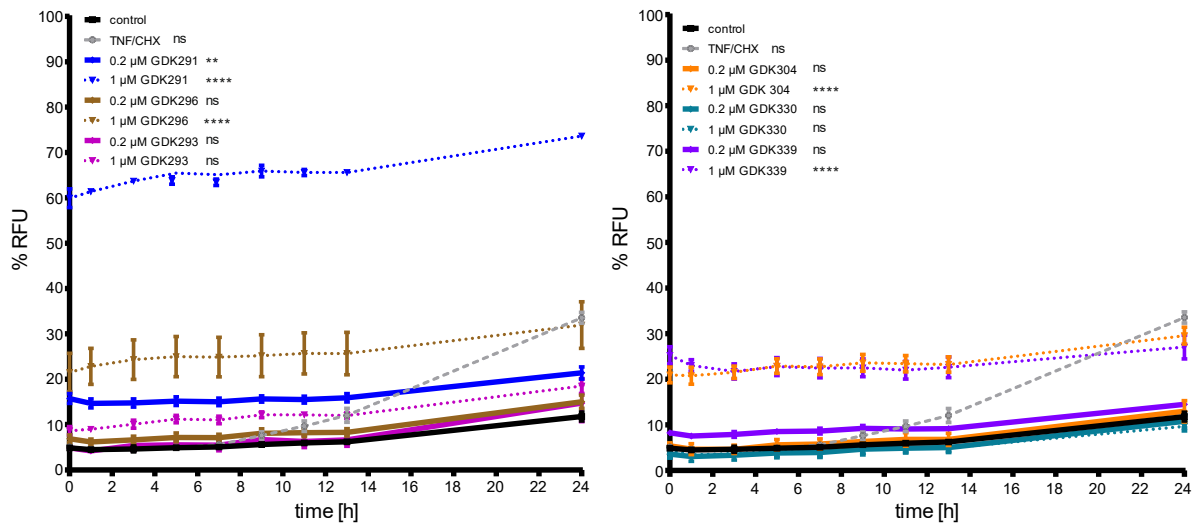


Fig. S51. Effect of crown-diketopyrrolopyrroles on apoptosis and necrosis of the EA.hy 926 cells.

Change in luminescence as a measure of apoptosis (A) and fluorescence (B) over the time. Statistical significance relative to the control was determined by two-way ANOVA with Tukey's test for $n = 3$ ($p < 0.0001$ (****); $p > 0.05$ (ns)).

Section S8: Theoretical calculations

Methods

For the calculations, the selected protocol follows one that has been extensively described and tested before,^[3] and is only briefly outlined below. In this approach, the ground and excited state geometries are optimized at the PCM^[4]-(TD-)M06-2X^[5] 6-31+G(d) level, the vibrational frequencies are obtained at the exact same level of theory, the total and transition energies are determined at CC2/*aug-cc-pVTZ* level, and the solvent corrections (here acetonitrile) on these CC2 energies are included at the PCM(LR+cLR^[6])-TD-M06-2X/6-311+G(2d,p) level. All (TD)-DFT calculations have been performed with the Gaussian16.A03 program,^[7] whereas the CC2 calculations have been achieved with Turbomole 7.3,^[8] applying the RI density fitting approach. This approach allows to obtain 0-0 energies that correspond to the crossing point between the measured absorption and emission curves. Finally, the vibronic calculations shown in the ESI were performed with the FCClasses code within the TD approach and the vertical-gradient vibronic model. Temperature effects were considered (298 K) and a broadening function was used (Gaussian, HWMH: 200 cm⁻¹).^[9]

Studies

To gain further insights into the photophysics of these DPPs, we conducted a computational study. In the performed computations, we used model compounds (denoted with an added **M**, Fig. S20) in which the crown ether groups were replaced by NMe₂ moieties. This decision was justified by computational savings as well as the non-conjugated nature of the crown ether. We computed the 0-0 energies to be 2.24, 2.24, and 2.17 eV for **9M**, **10M**, and **17M** respectively. These values can be rightfully compared to the experimental absorption-fluorescence crossing point, which has the values 2.28, 2.28, and 2.20 eV. Naturally, the selected level of theory can restore the experimental values with high accuracy. In addition, as can be seen in Fig. 48 for **9M**, the shape of the absorption spectrum with the presence of two maxima is globally reproduced when vibronic calculations are made.

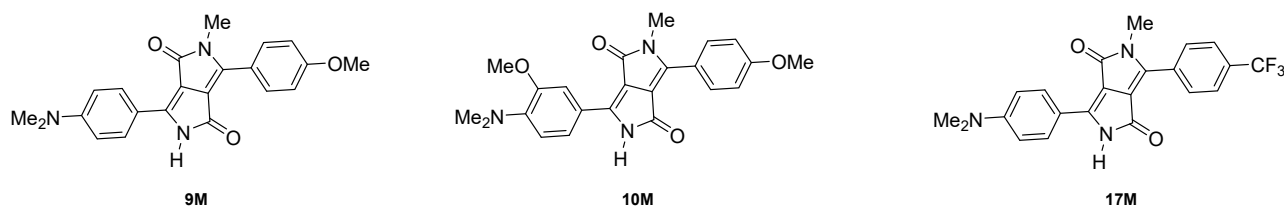


Fig. S52. Structures used in computational studies

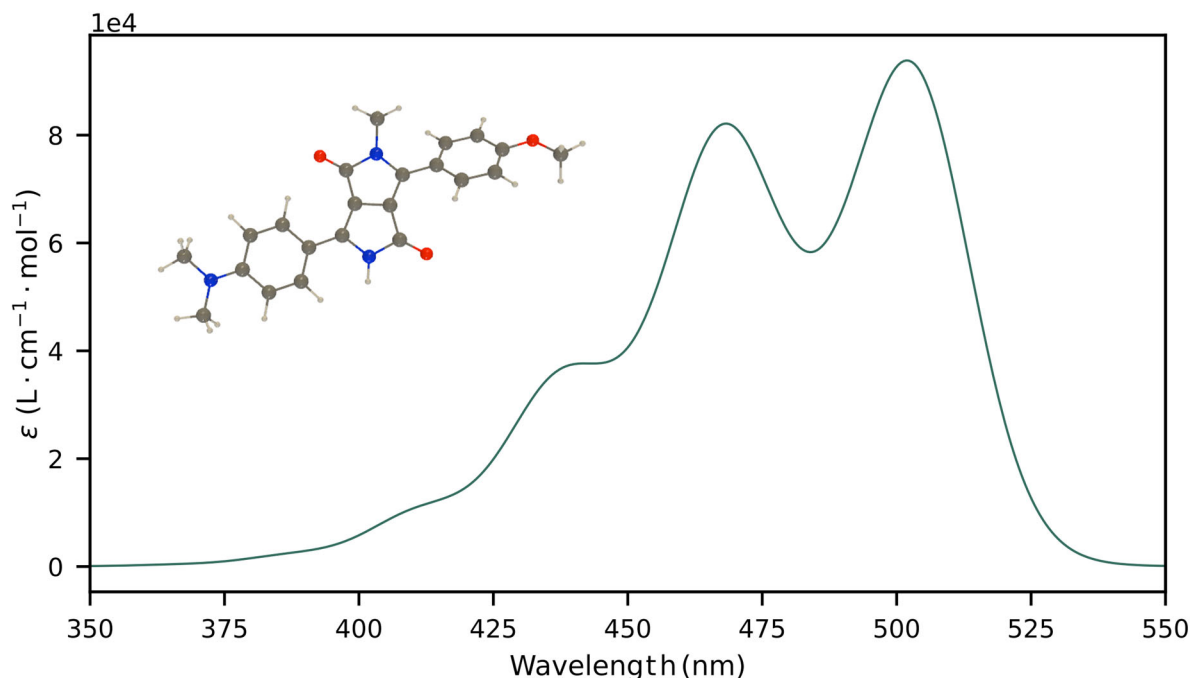


Fig. S53. Vibrationally-resolved absorption spectrum of **9M** calculated with PCM-TD-M06-2X/6-31+G(d), using the TD-VG vibronic model.

Plots displaying density differences for the three dyes are presented in Figure S22. In **9M**, the 4-Me₂NC₆H₄ is nearly coplanar with the DPP with a twist of only 6° as compared to a value of 33° for the 4-MeOC₆H₄. As can be further seen in Figure 5, the amino group, which is perfectly coplanar in both ground and excited states with the benzene ring, acts as the main donor. The DPP unit acts as the acceptor, while the methoxy group has a weak impact. When adding the secondary OMe (in **10M**), the steric clash between the two donating groups induces a twist of the NMe₂ as compared to the phenyl (40° in the ground, and 35° in the excited state). The latter however remains coplanar with the DPP as in **9M**. Nevertheless, the twist of the NMe₂ in **10M** makes it slightly less donating than in **9M**, though the topologies remain vastly similar, as consistent with the D-A-D' architecture. We note that the non-planarity of NMe₂ in **10M** hints at a more flexible structure, thus likely able to accommodate complexation. When one turns to **17M**, the pattern significantly changes with a clearer charge-transfer character, as well as the CF₃-bearing ring acting as the acceptor in a D-A-A' structure. The above noted differences are reflected in the excited-state dipole moments that attain 7.8, 6.4, and 16.5 D in **9M**, **10M**, and **17M**, respectively. It is noted experimentally that these series of dyes are especially emissive. To explain this, let us first note that TD-DFT yields very large oscillator strengths for the S₁→S₀ transition (ca. 1.0 for all three compounds), which is indicative of a very large radiative constant. At the same time TD-DFT reveals that, at the optimal S₁ geometry, there is only a triplet available

below the S_1 , but the gap is hugged between the singlet and triplet (> 1.2 eV), which is clearly detrimental for ISC to occur. These two facts are consistent with a bright emission.

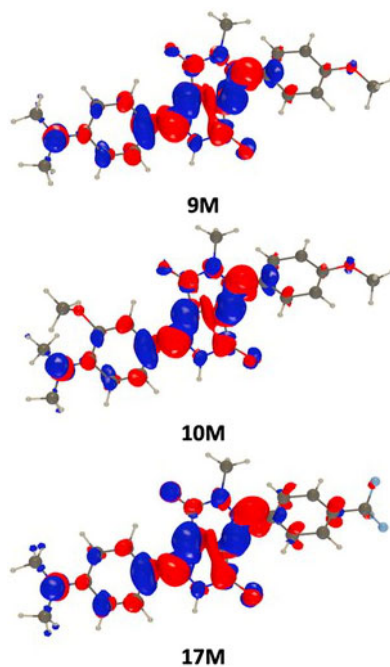


Fig. S54. Density difference plot for the model dyes of **9M**, **10M**, and **17M**. The blueberry and crimson lobed indicate regions of decreased and increase of density upon absorption. Contour threshold 1×10^{-3} .

As a simple way to model complexation, we have used a structure in which **10M** has been protonated. In this case, the CT character is lost (see Figure S23), consistent with the blueshift and the stronger vibrationally resolved character of the experimental band after complexation (Figure 4).

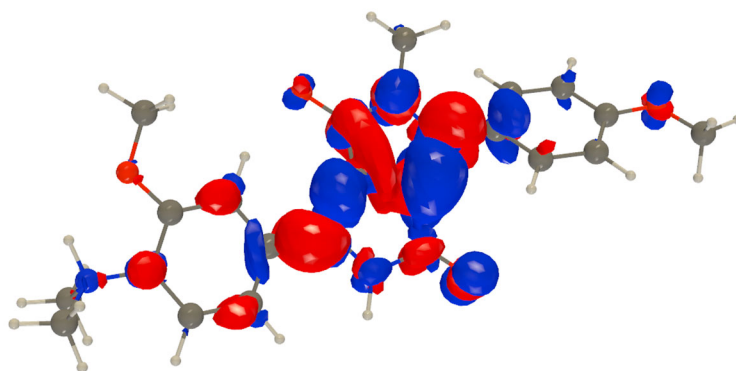
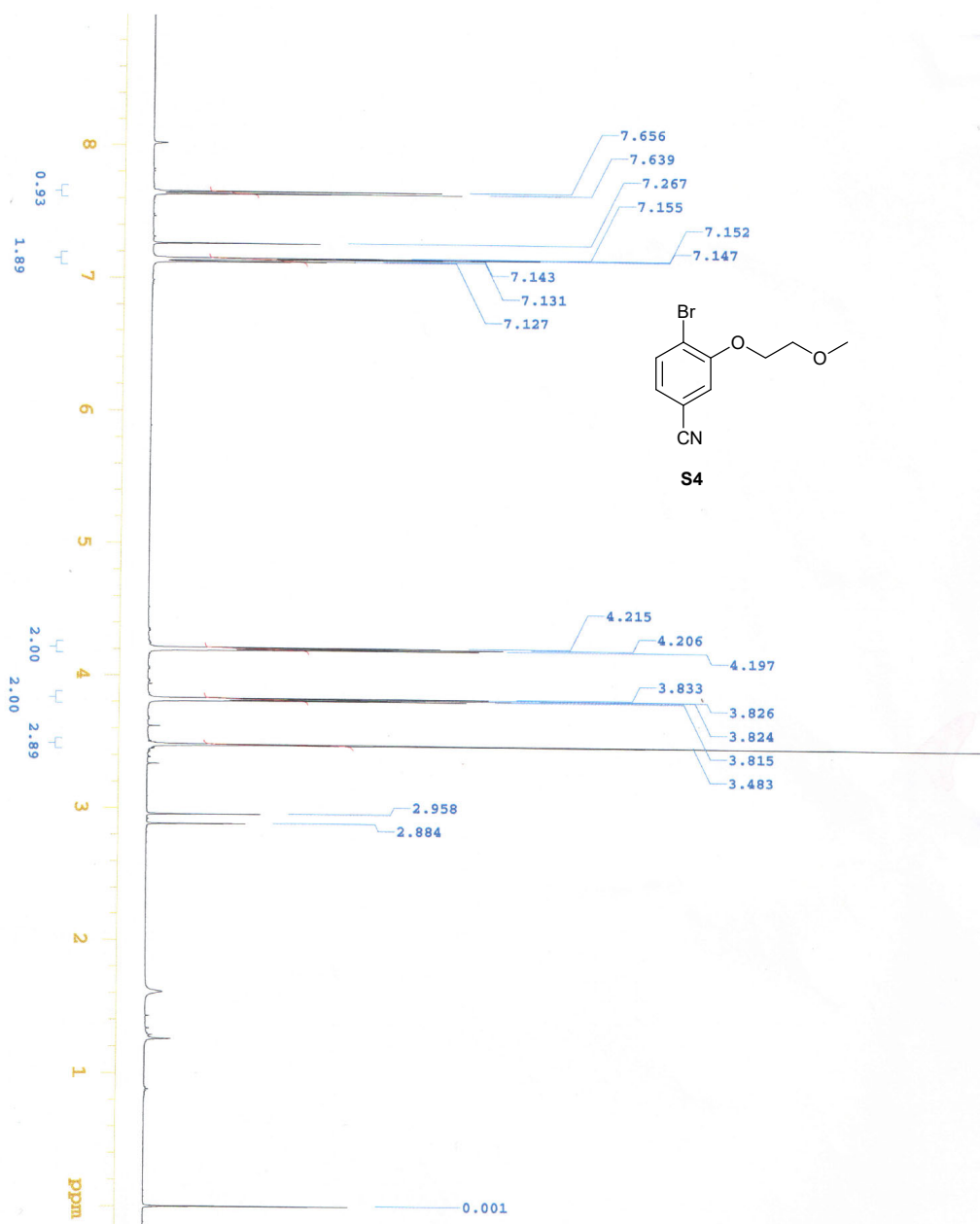
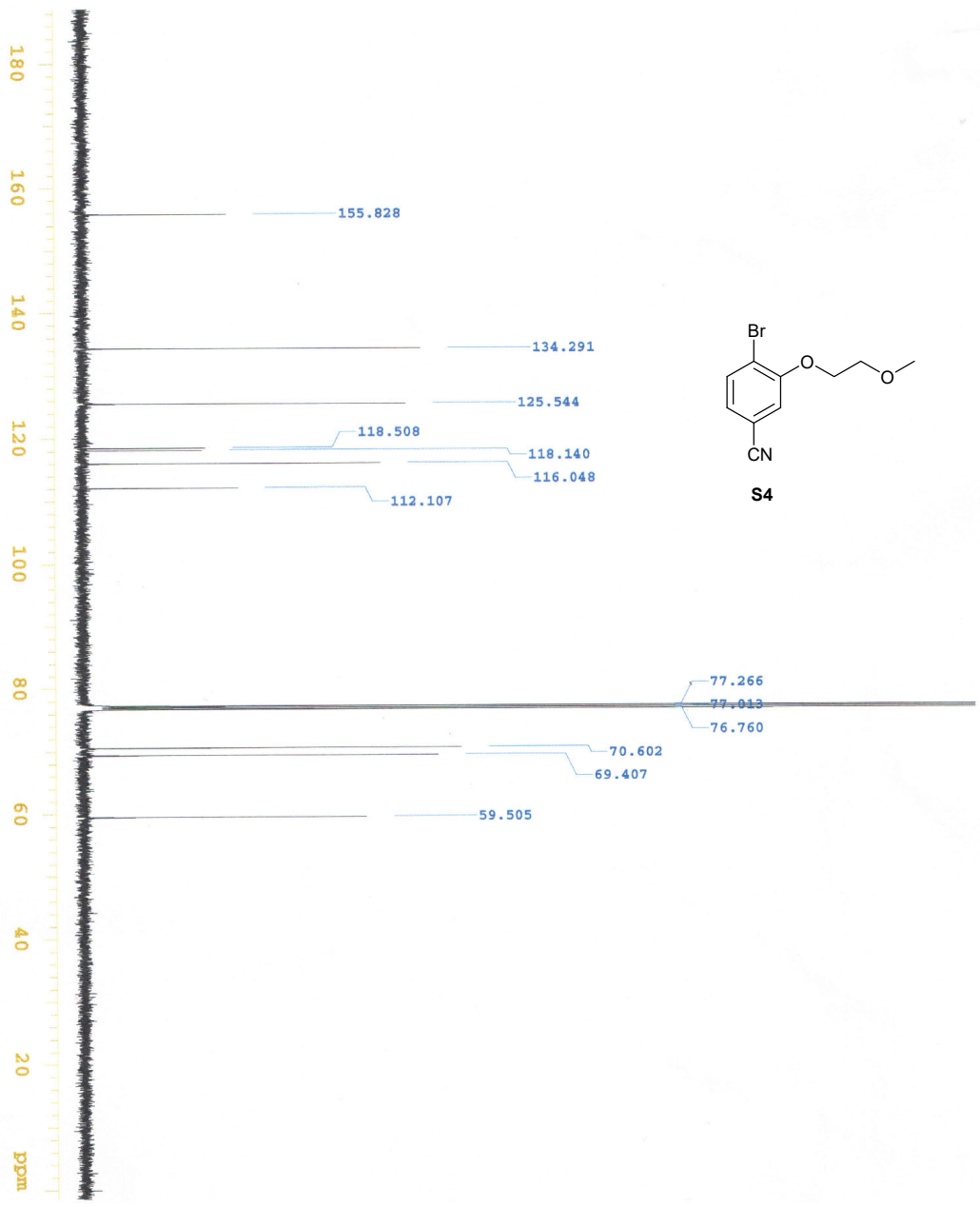
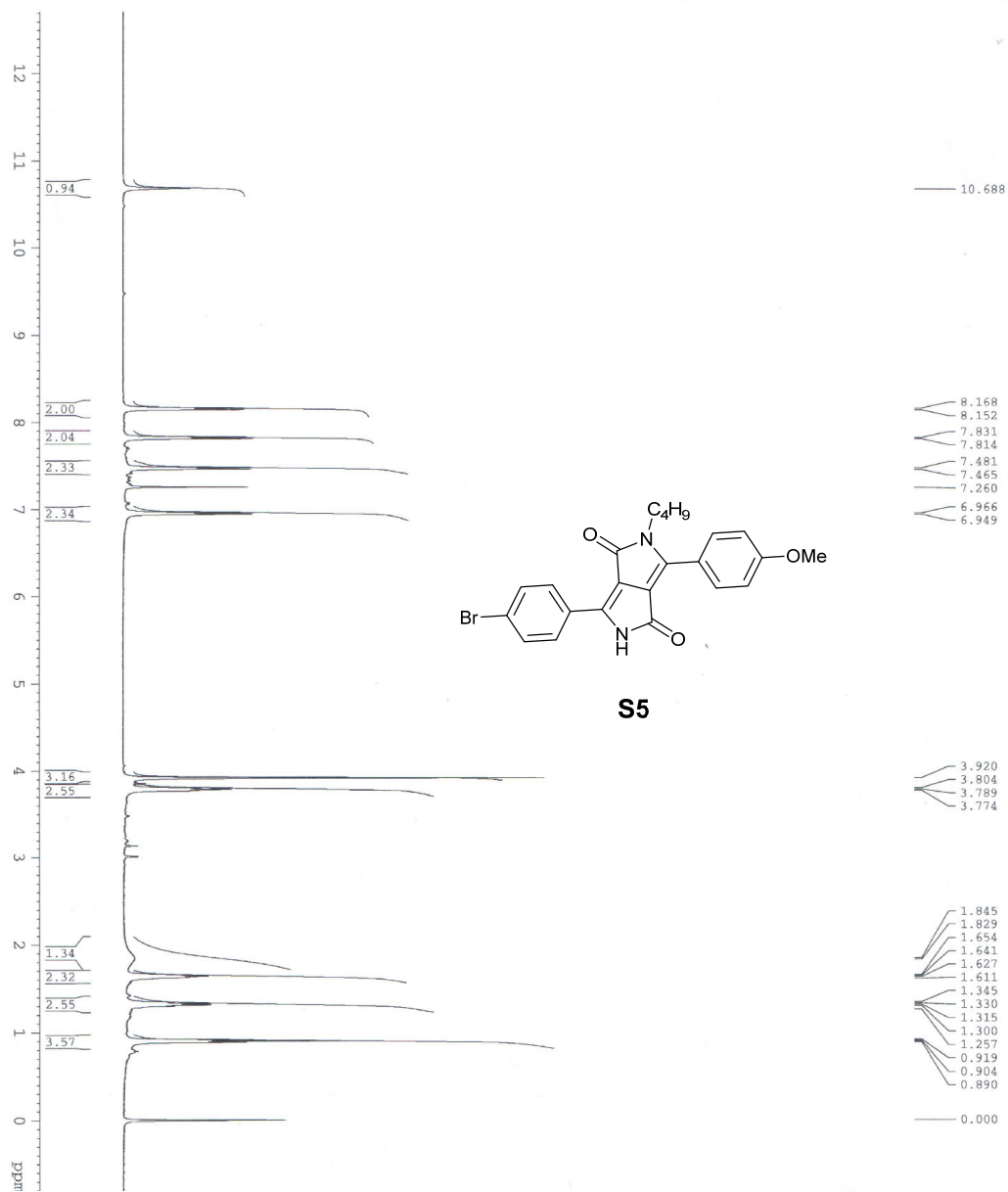


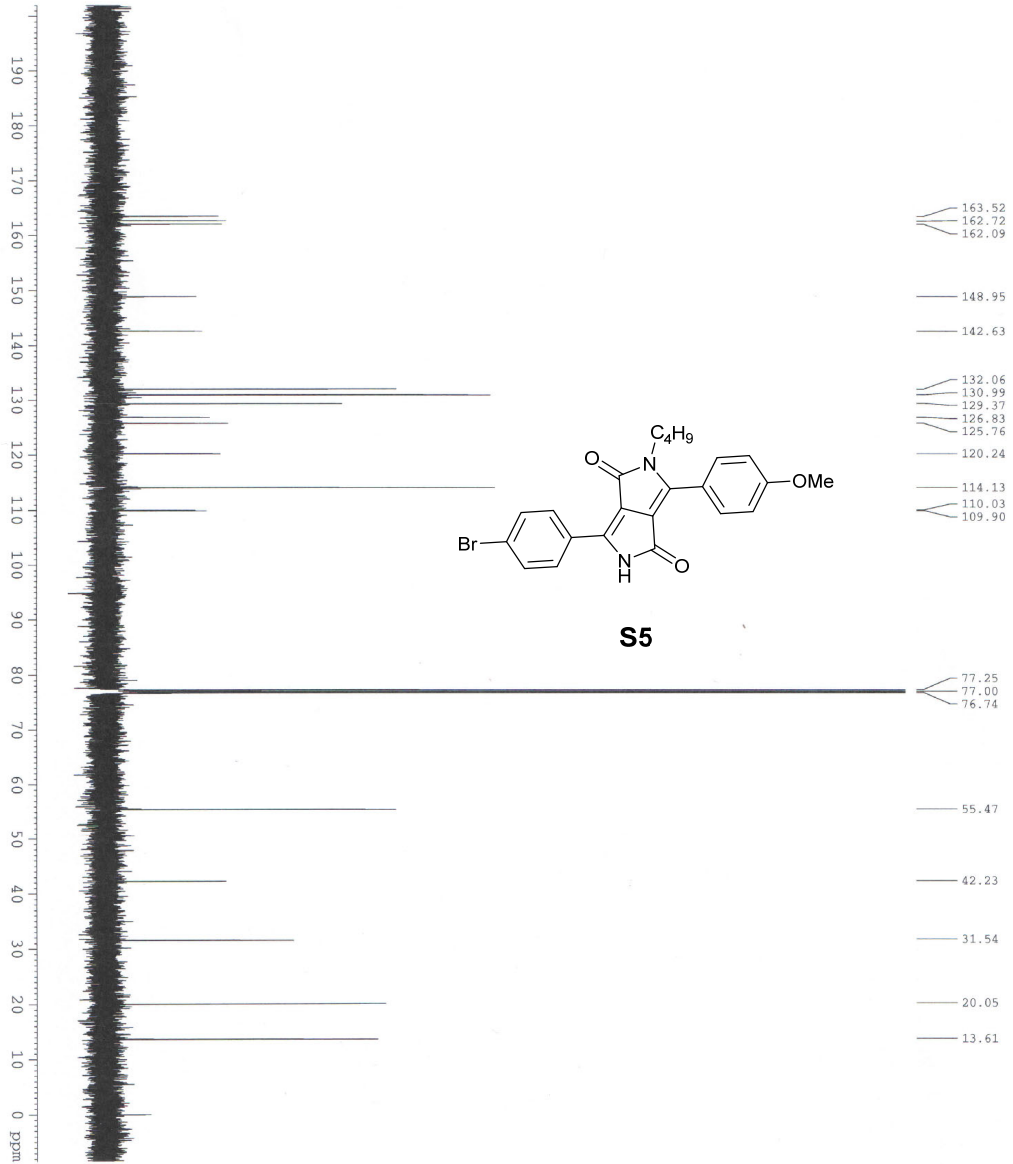
Fig. S55. Density difference plot for the model dyes of **10M+H⁺** Contour threshold 1×10^{-3} .

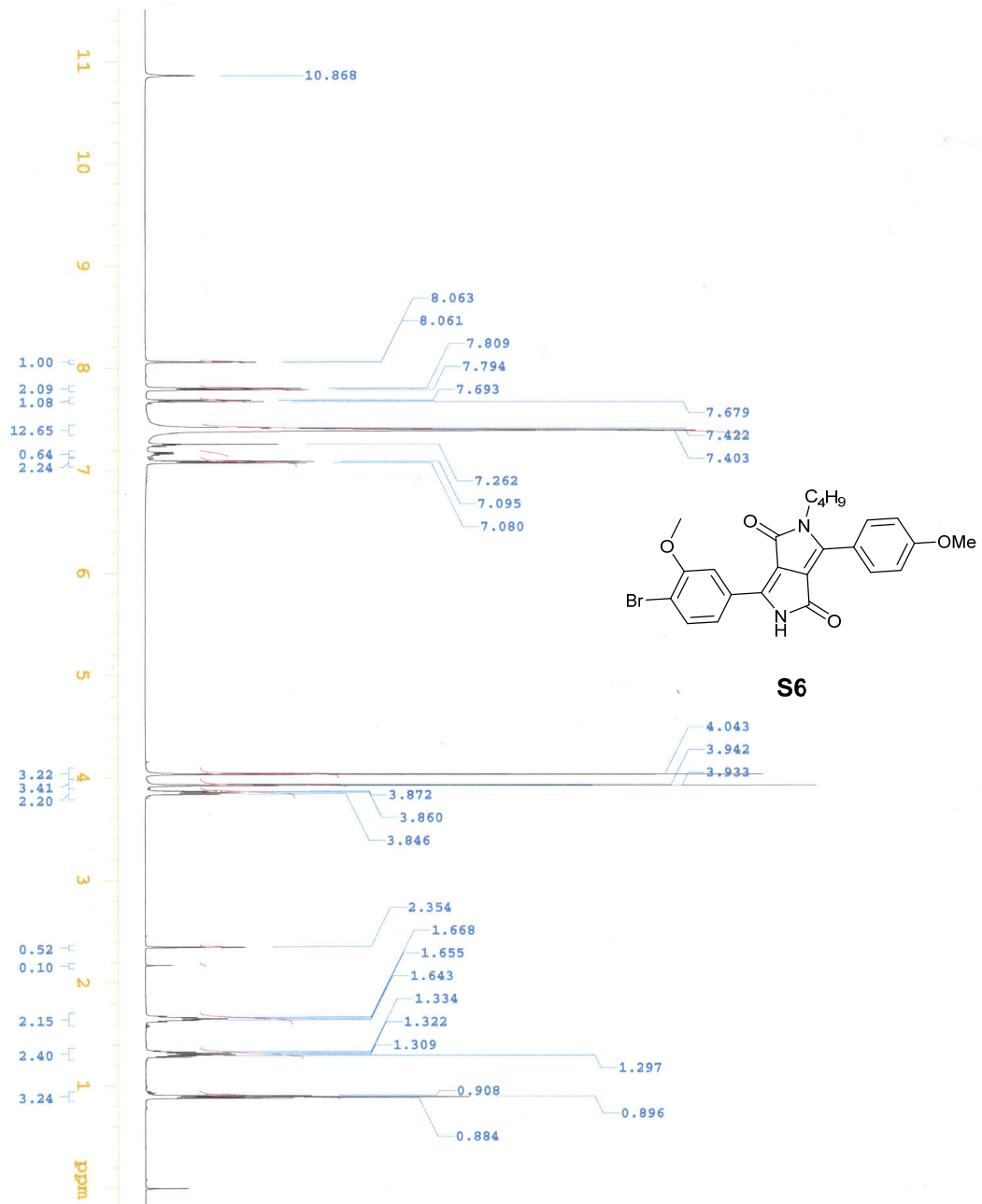
Section S9: ^1H NMR and ^{13}C NMR Spectra

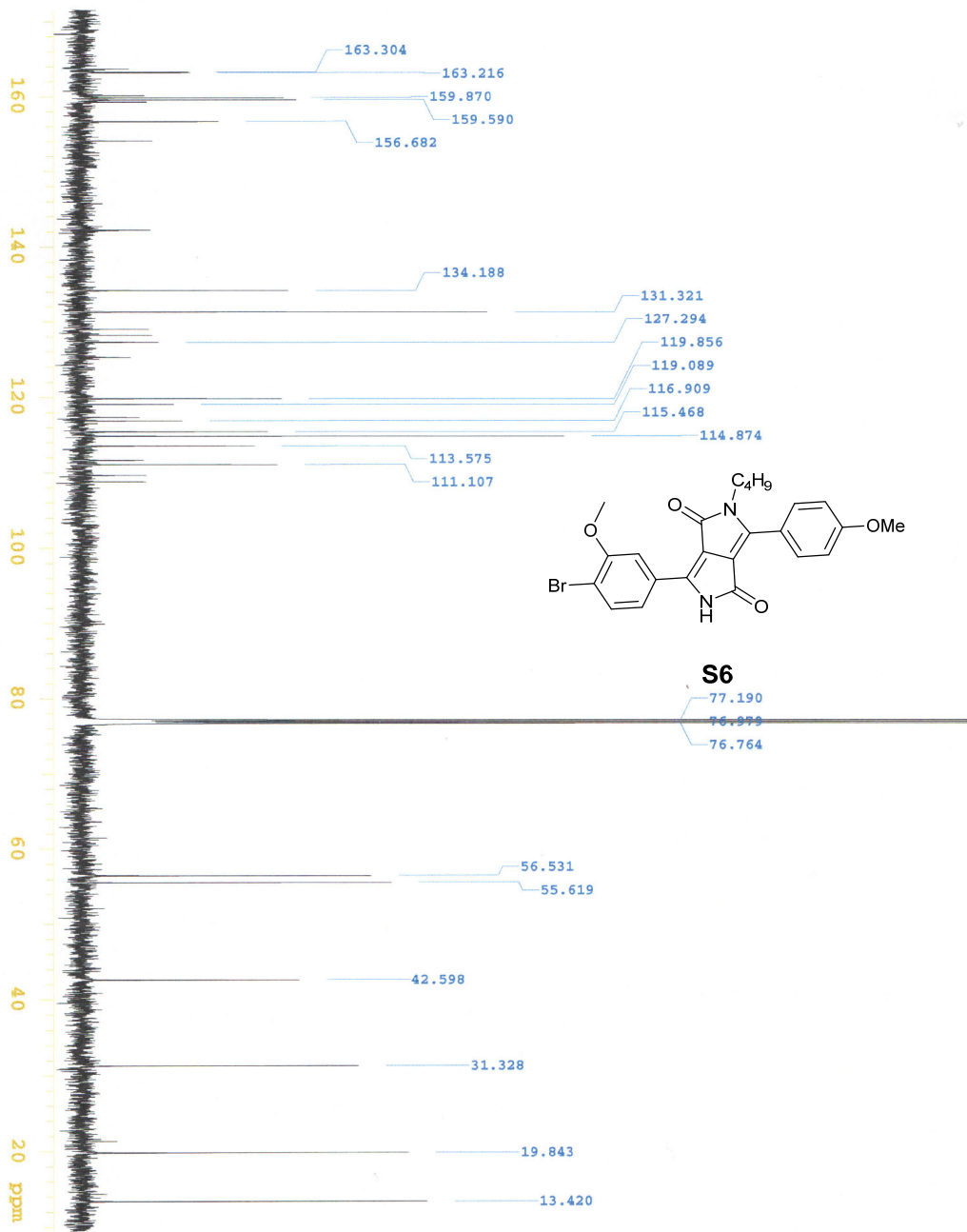


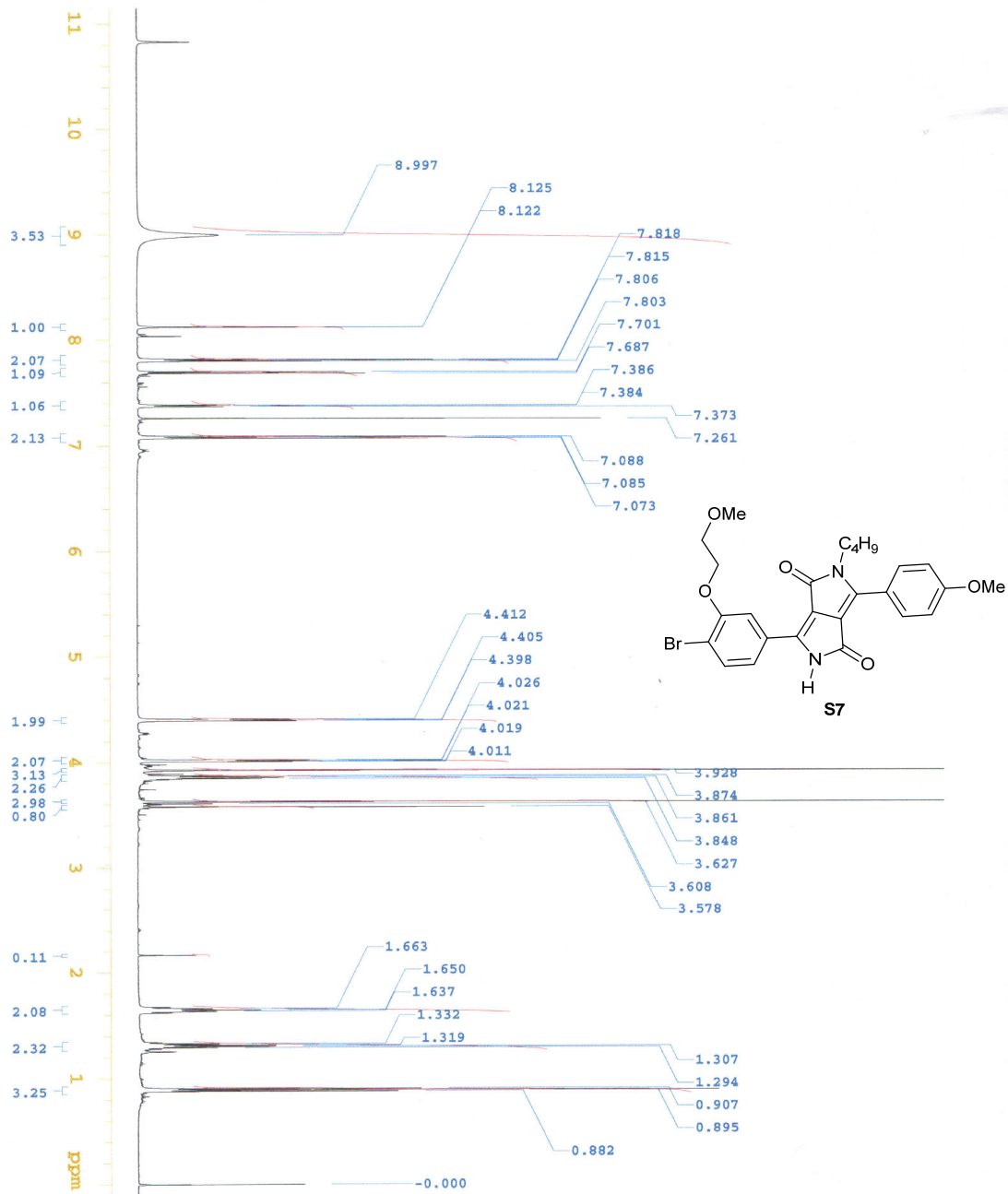


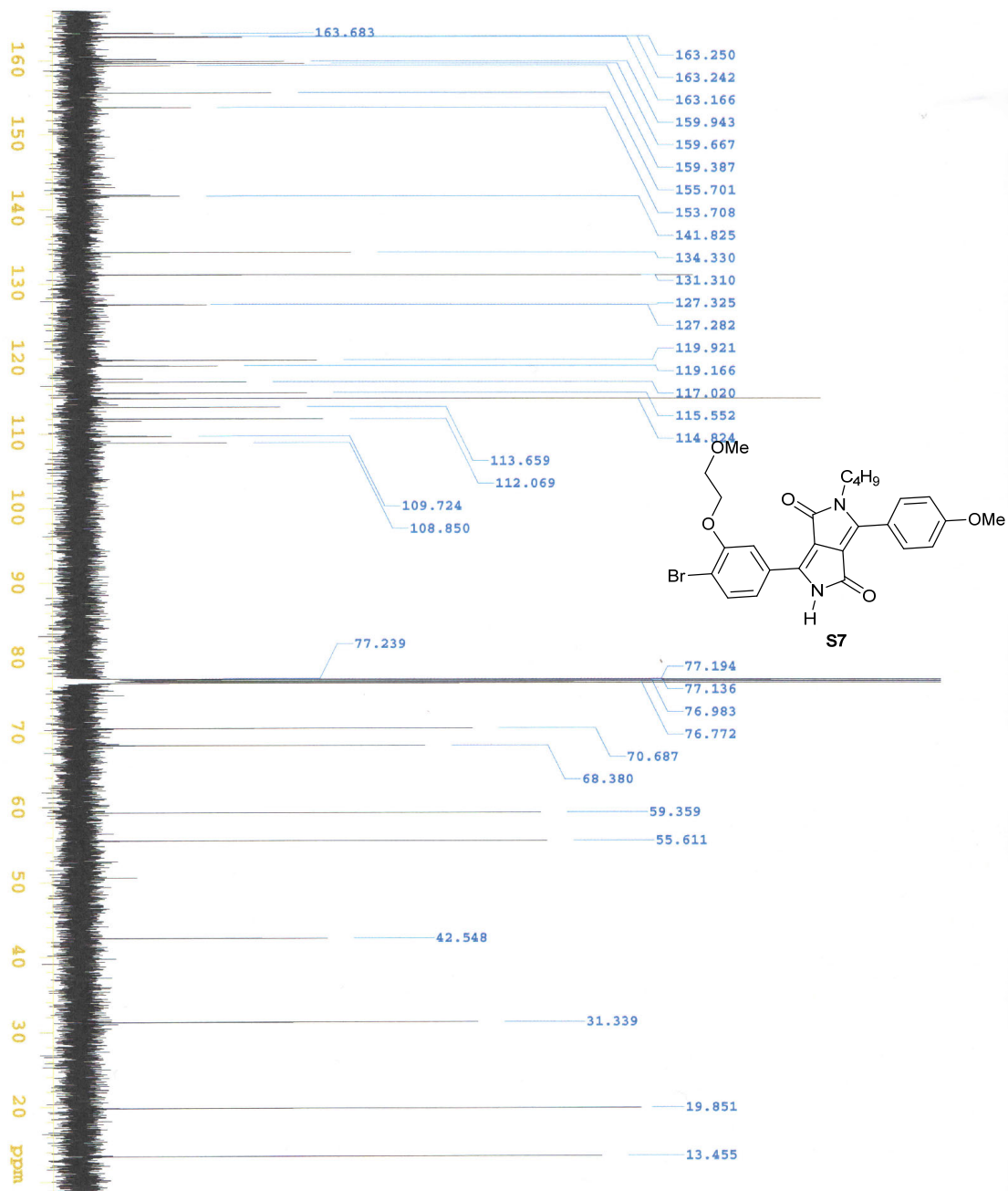


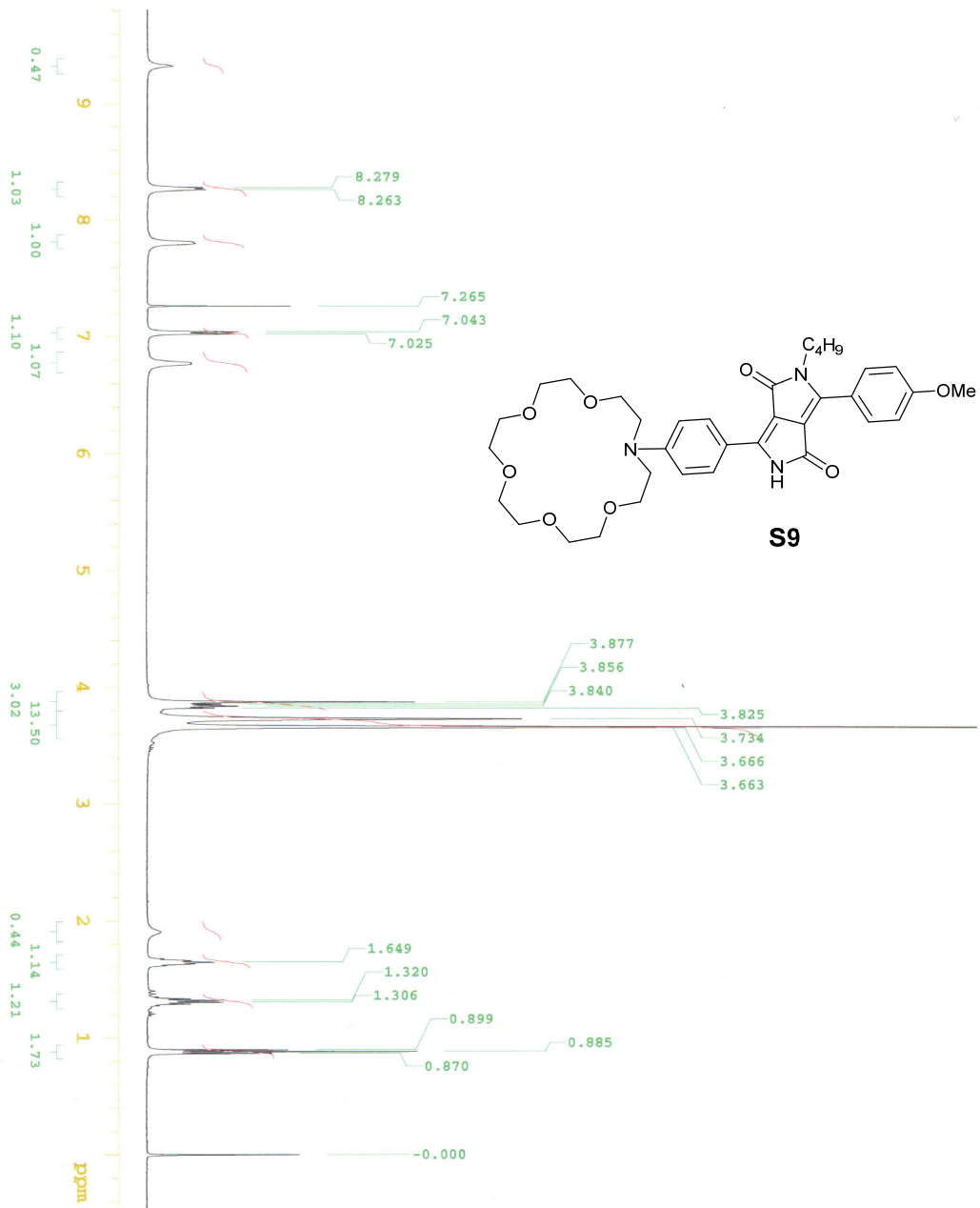


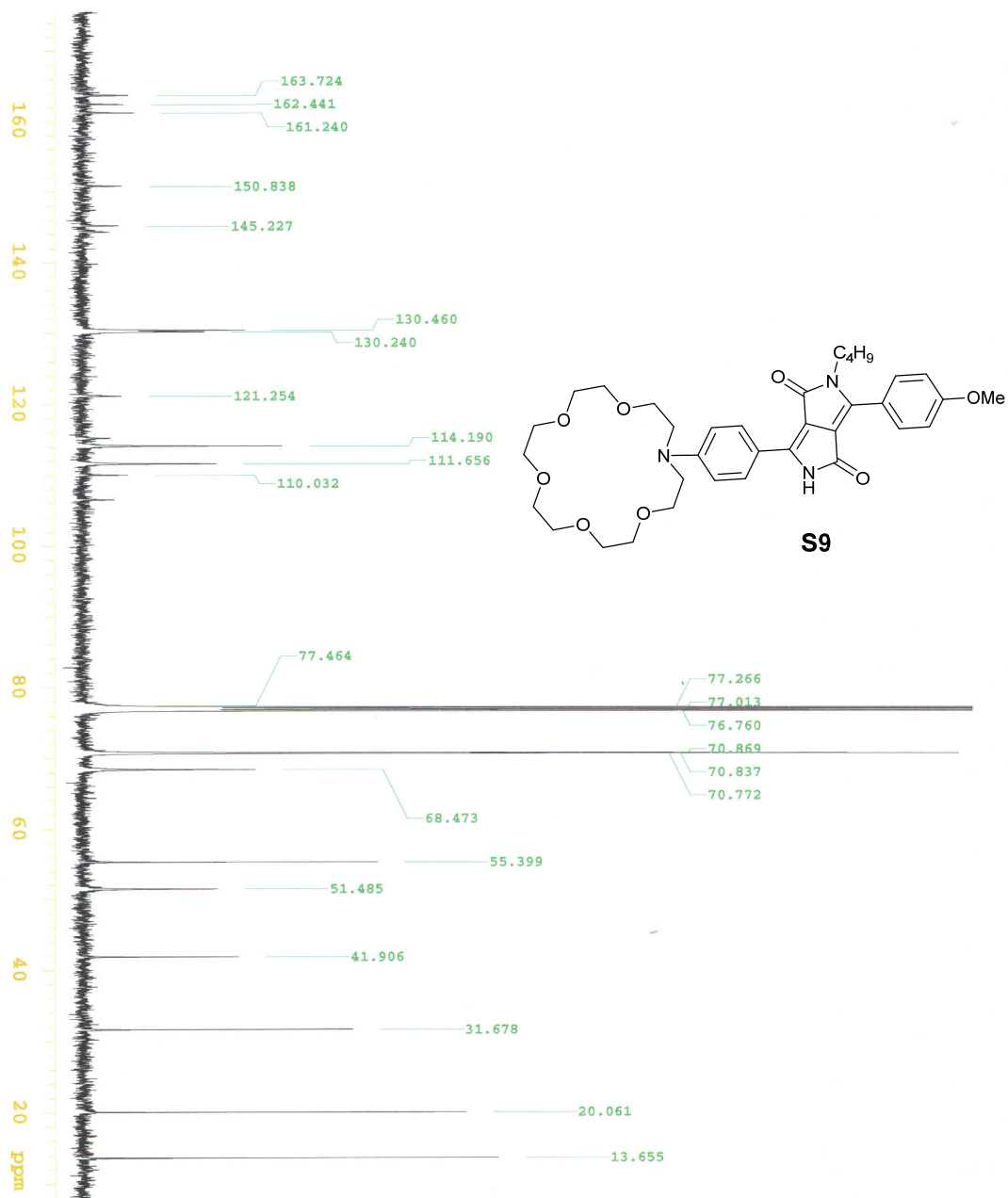


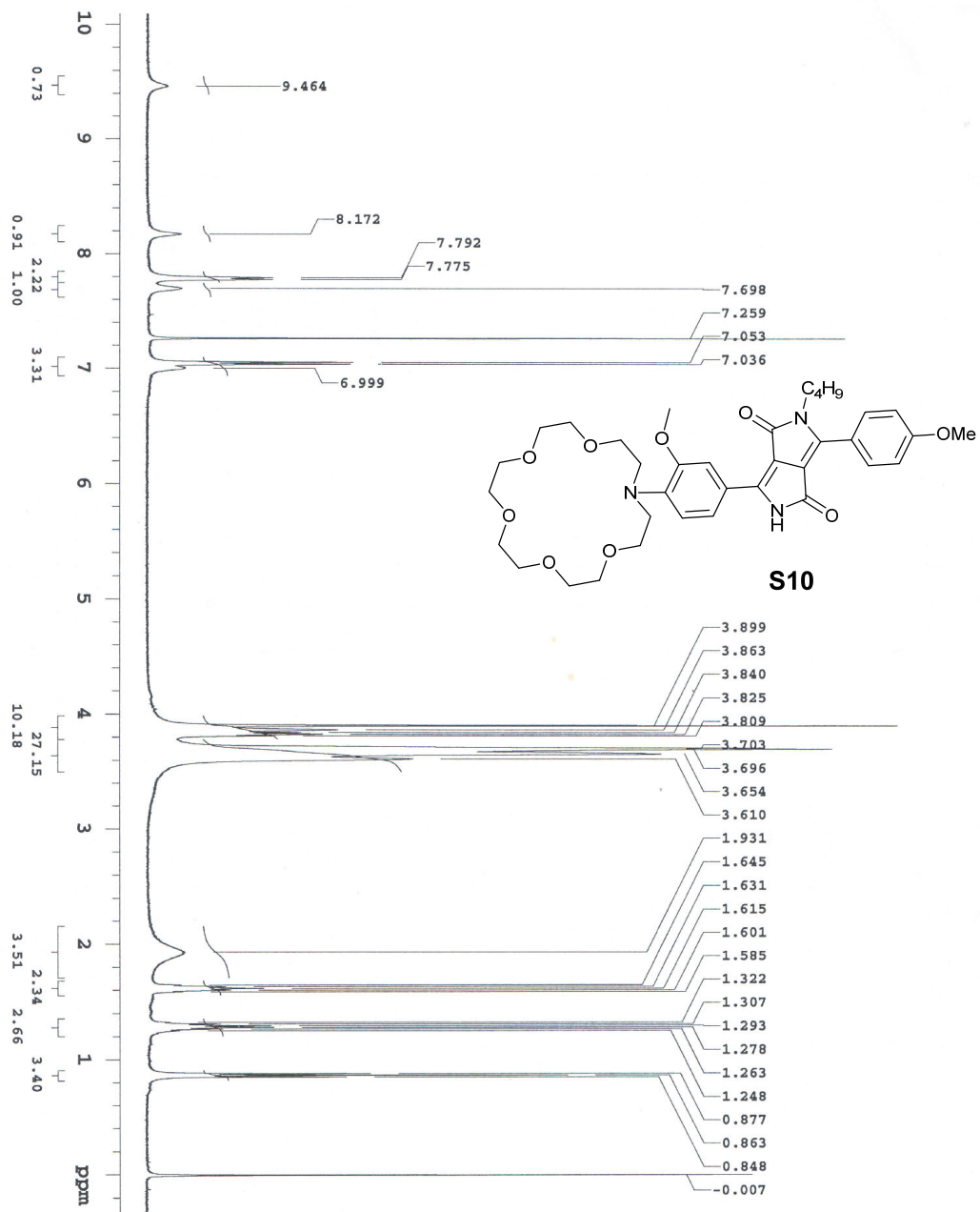


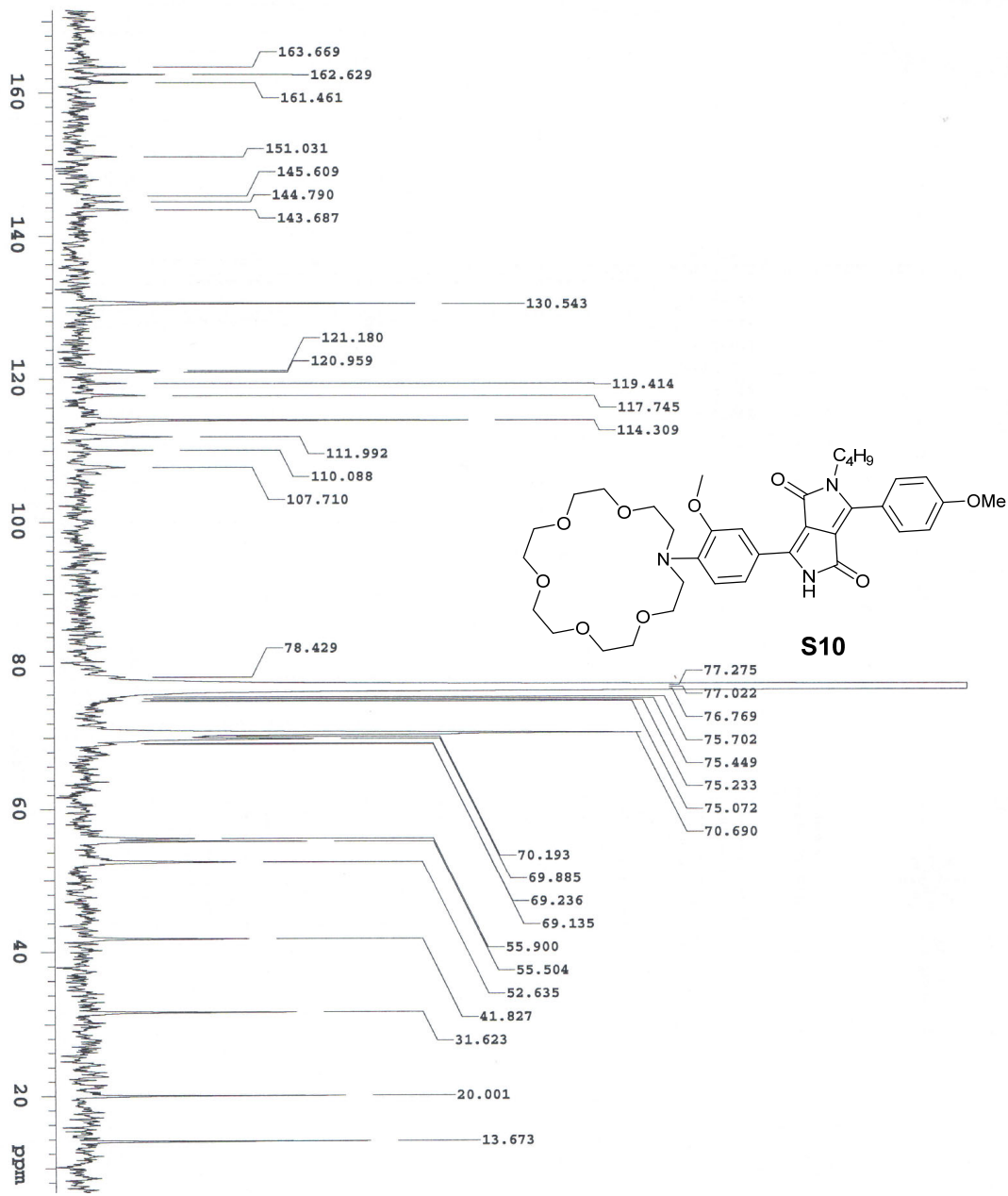


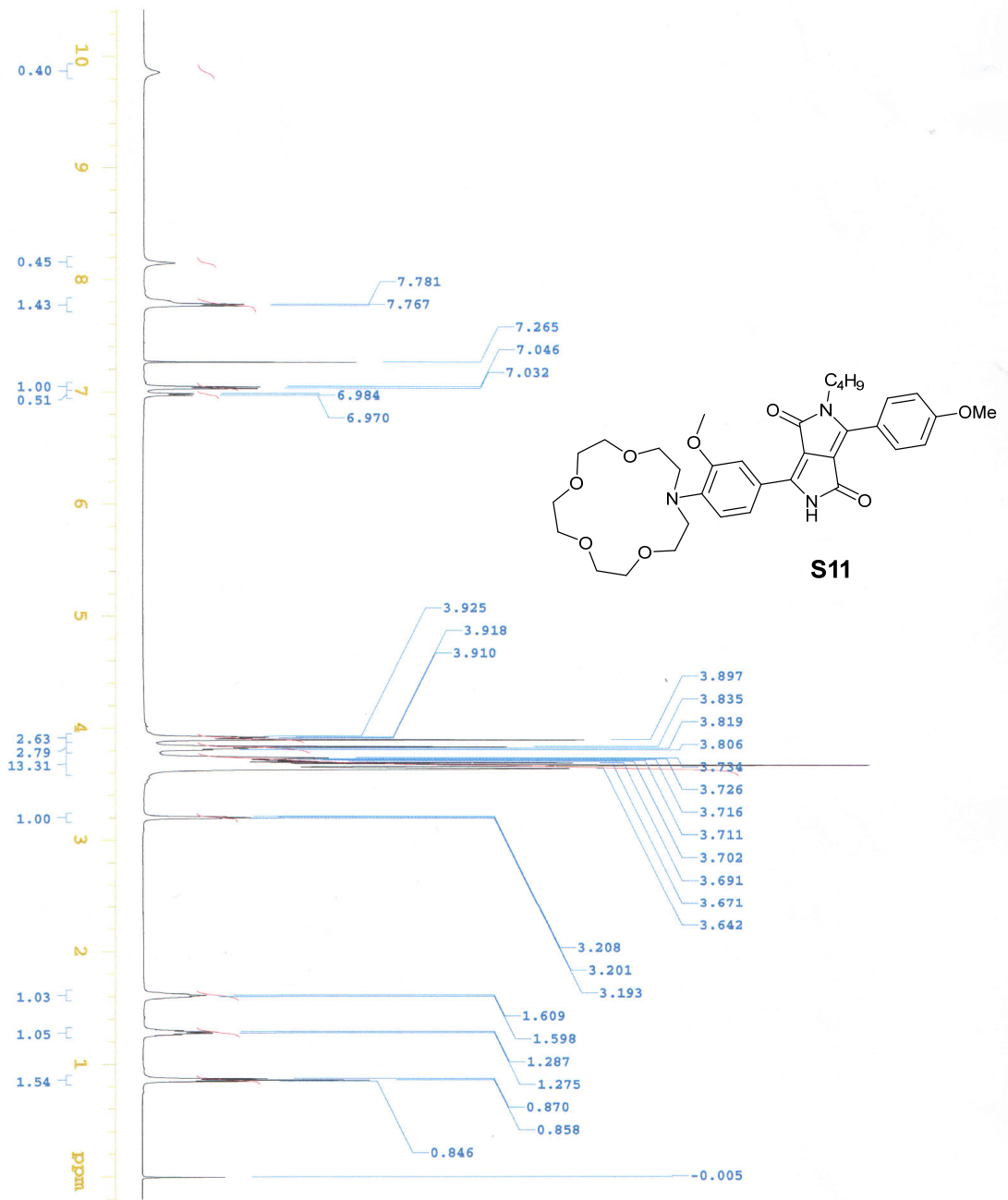


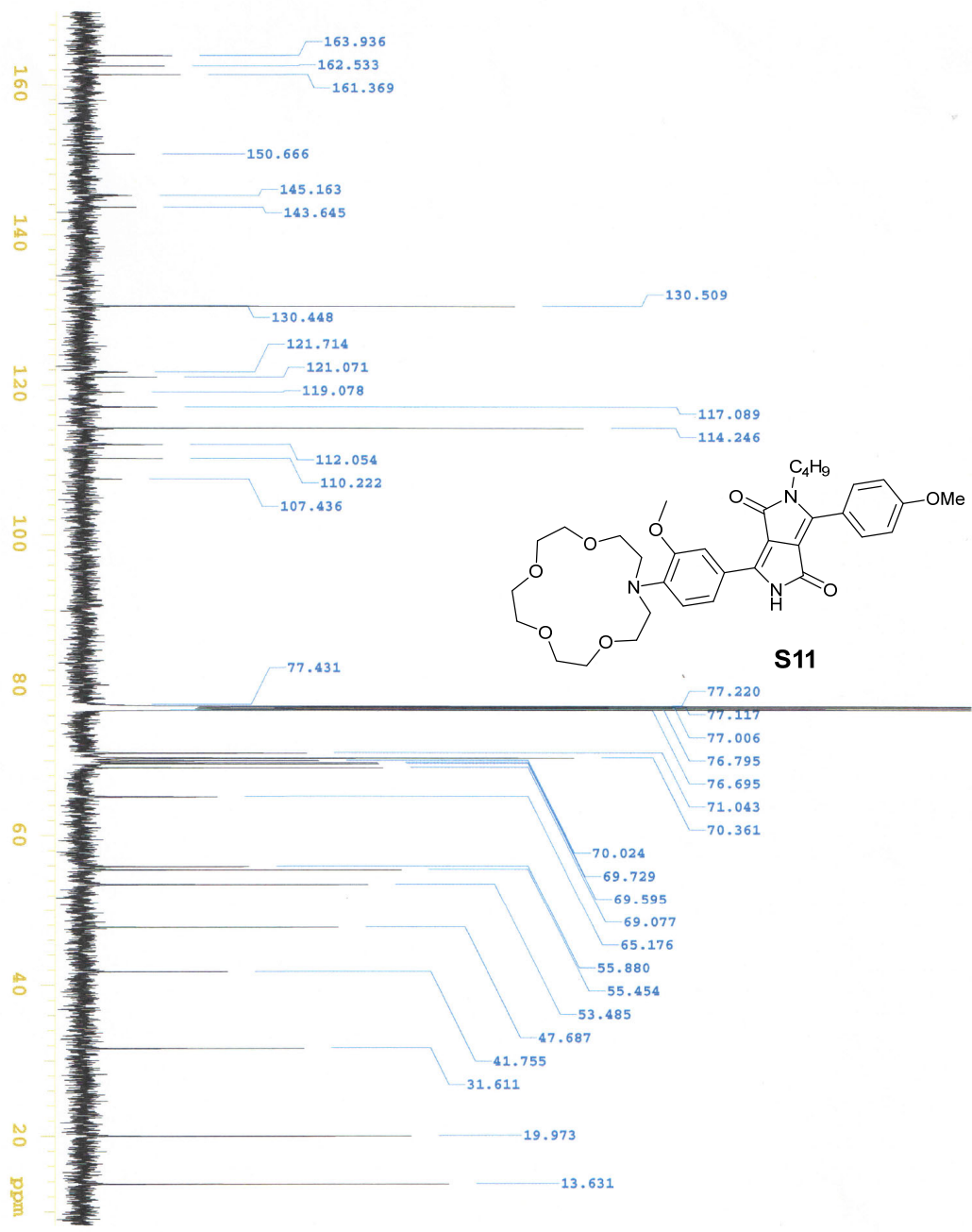


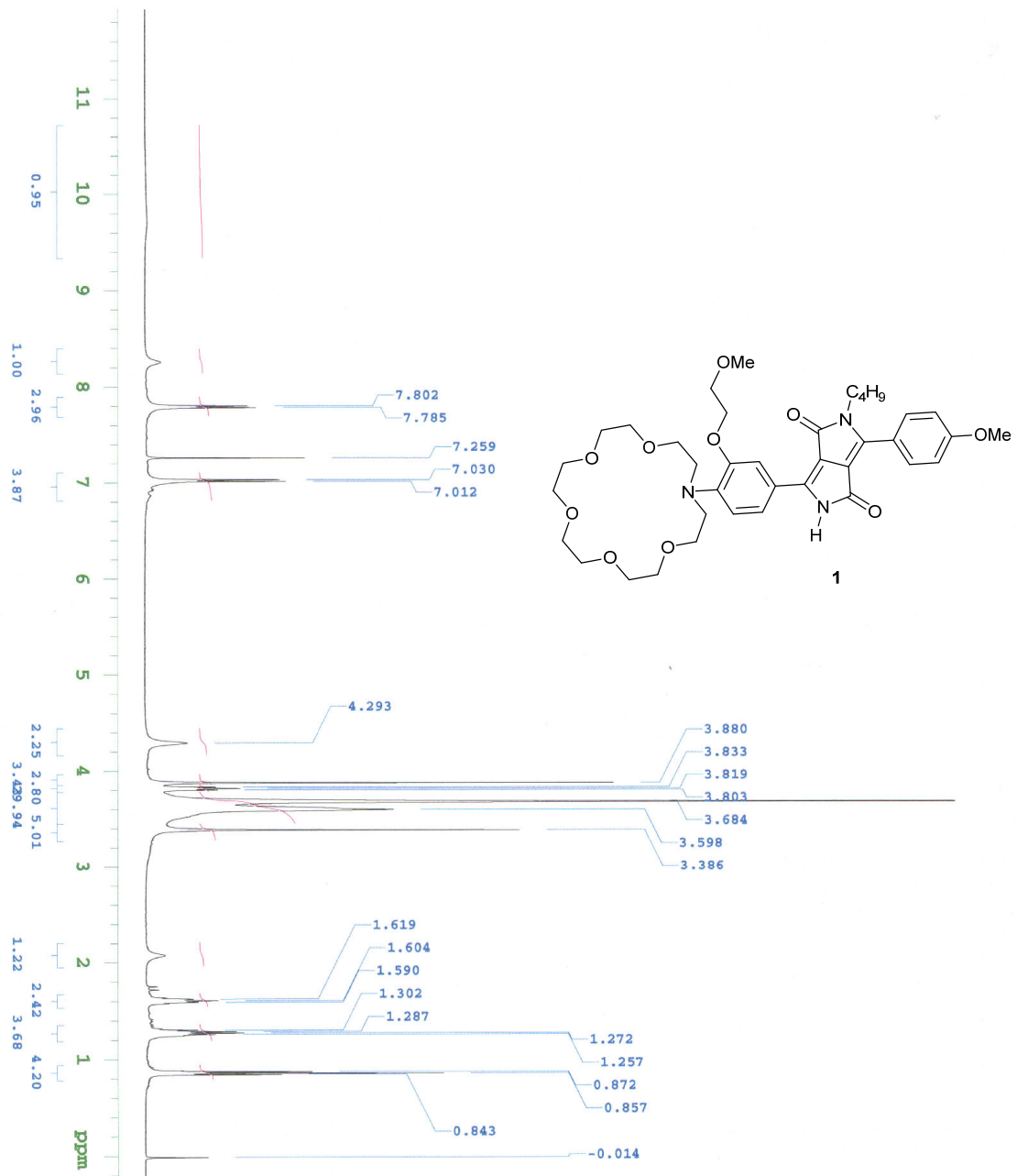


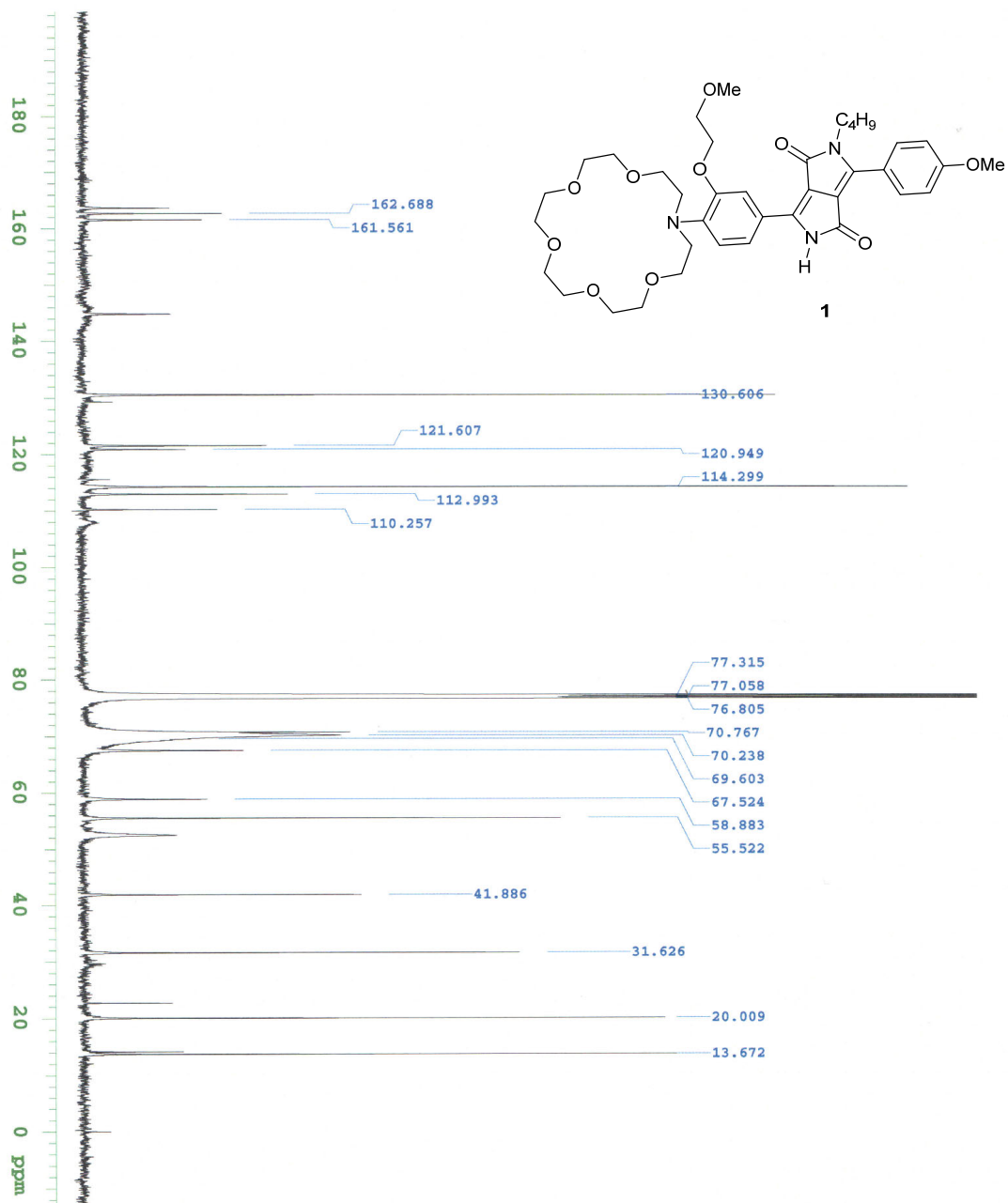


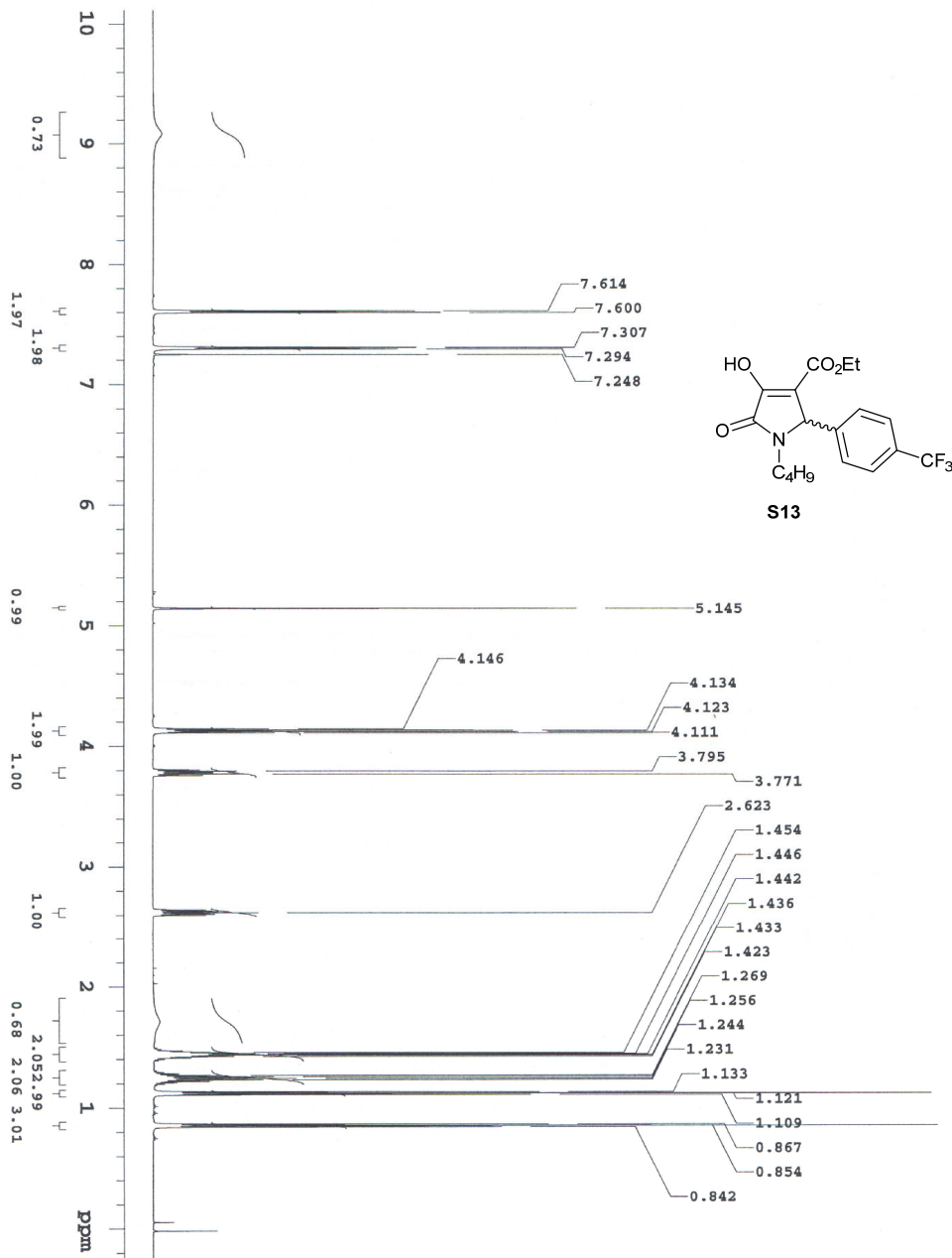


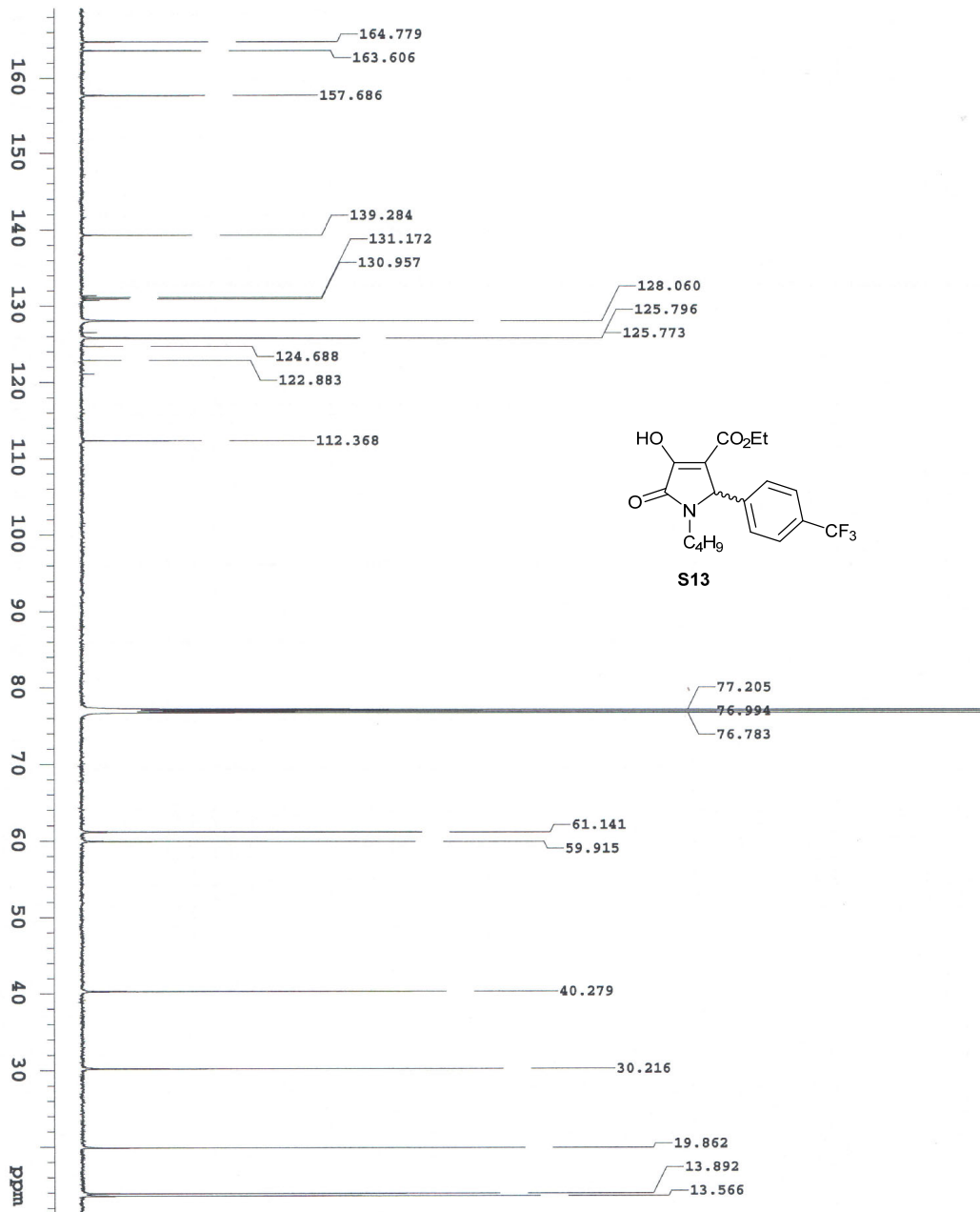


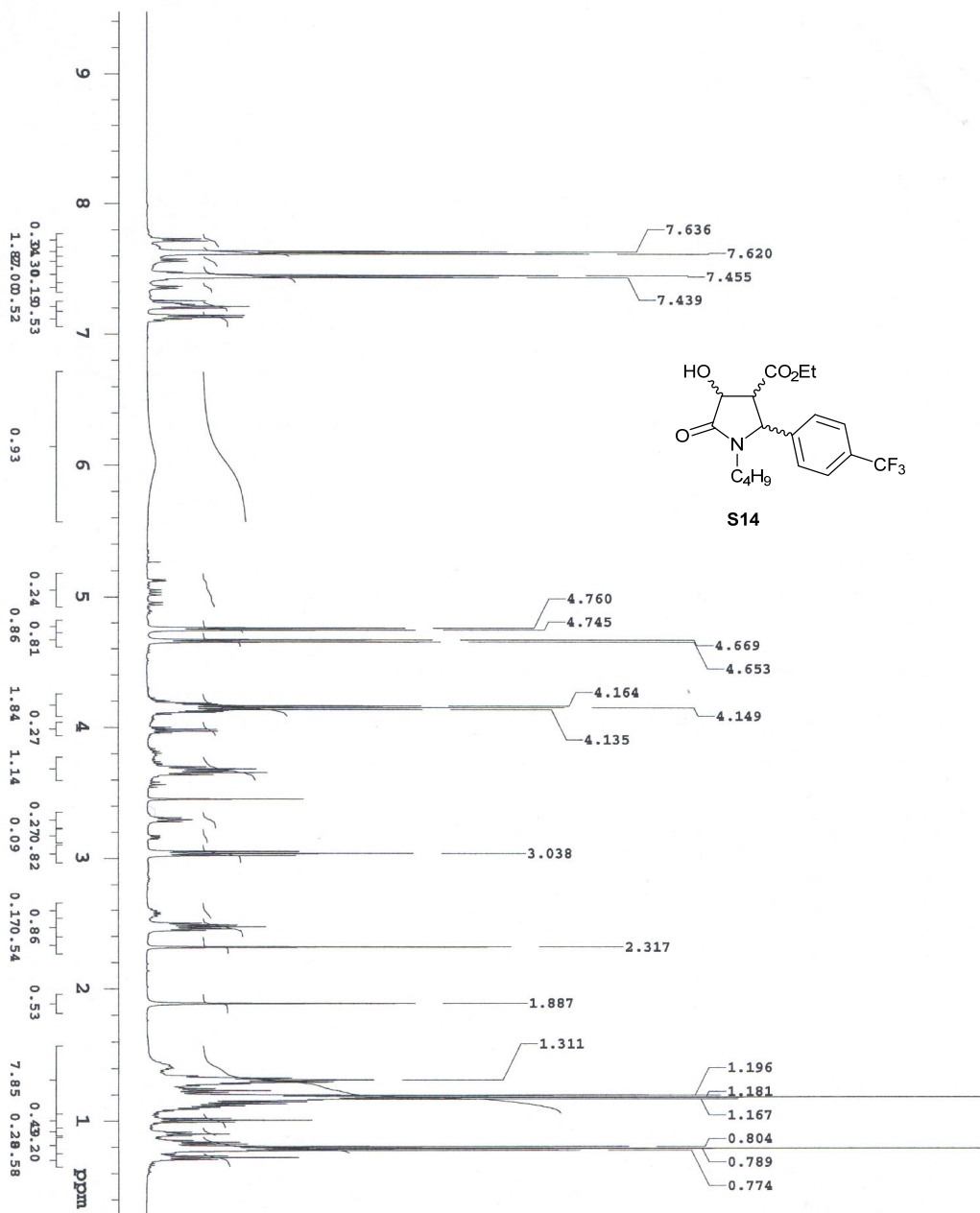


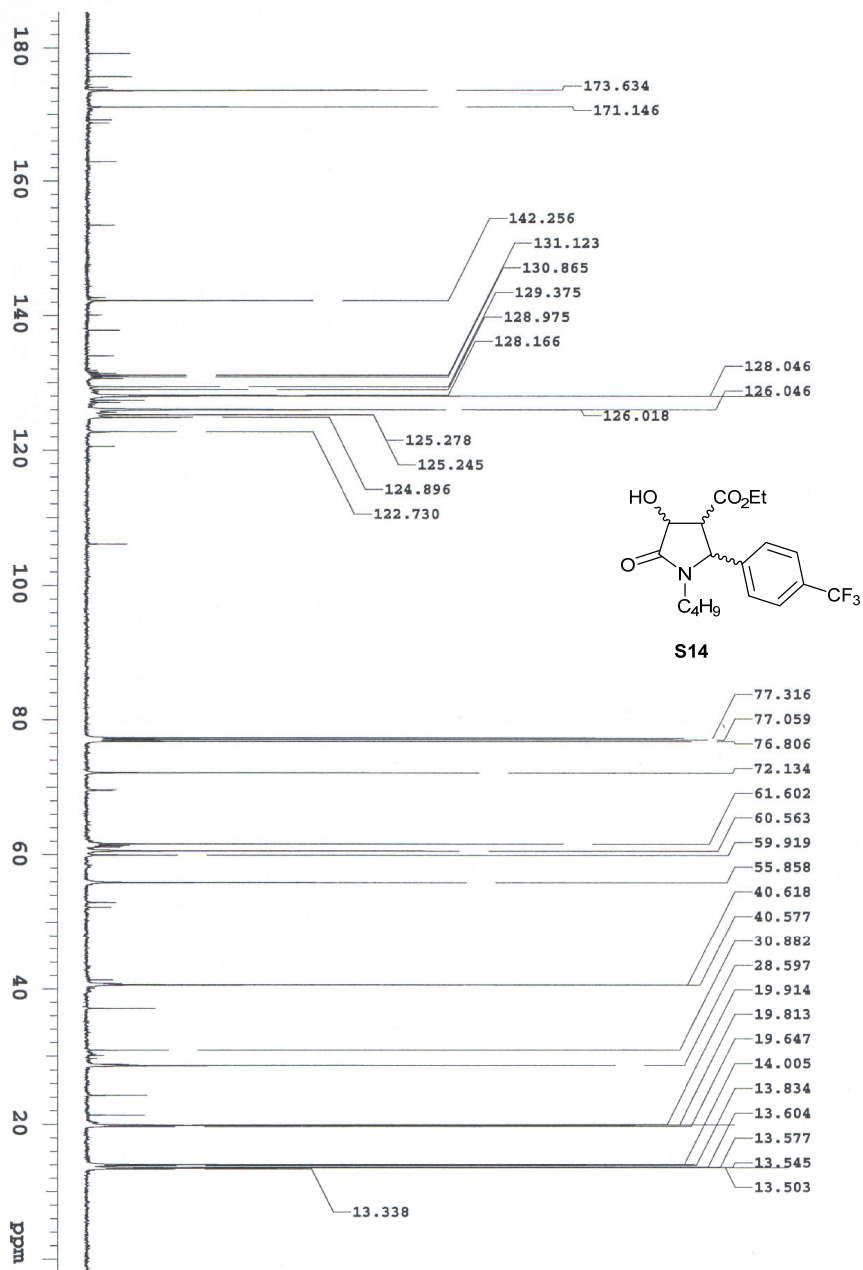


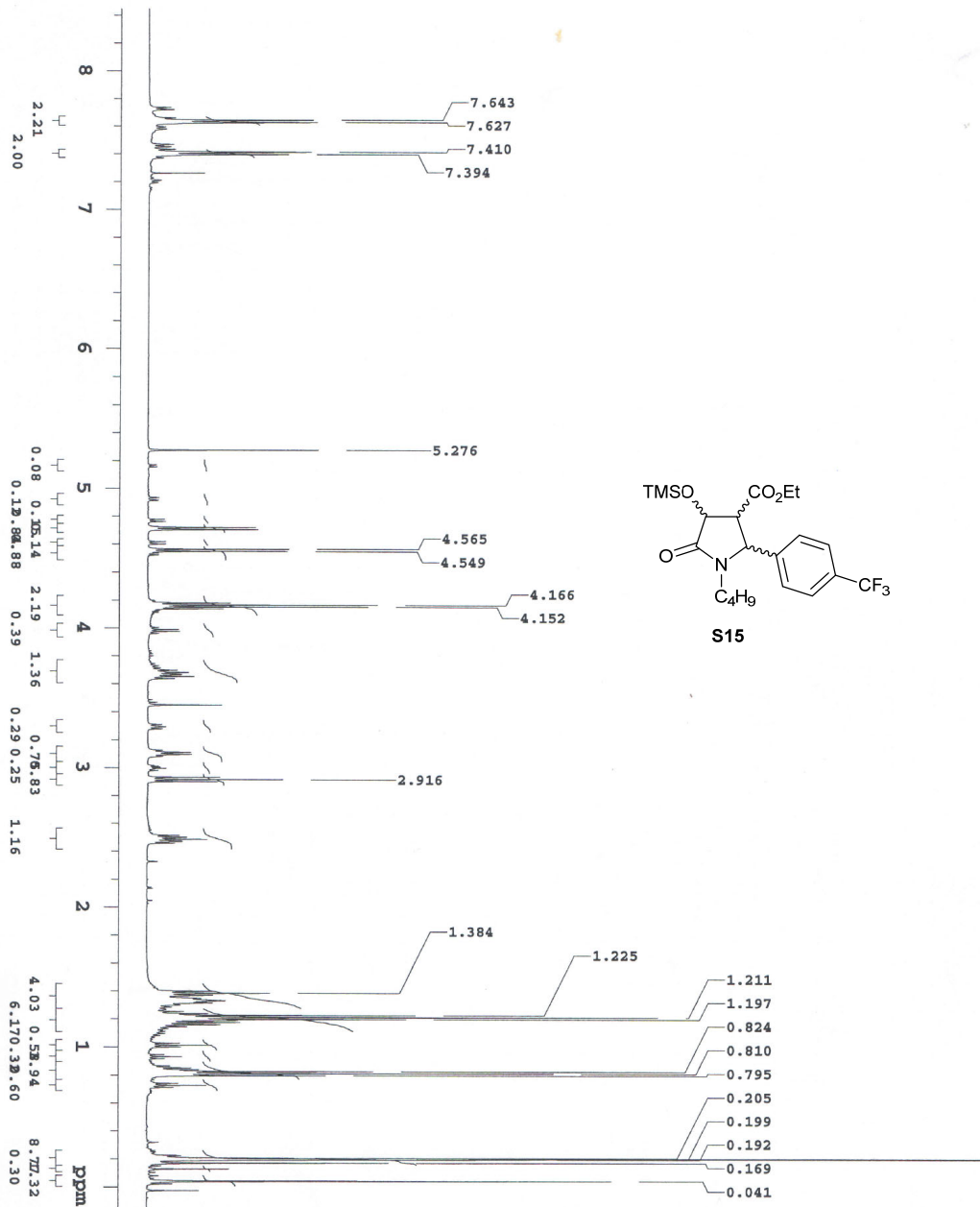


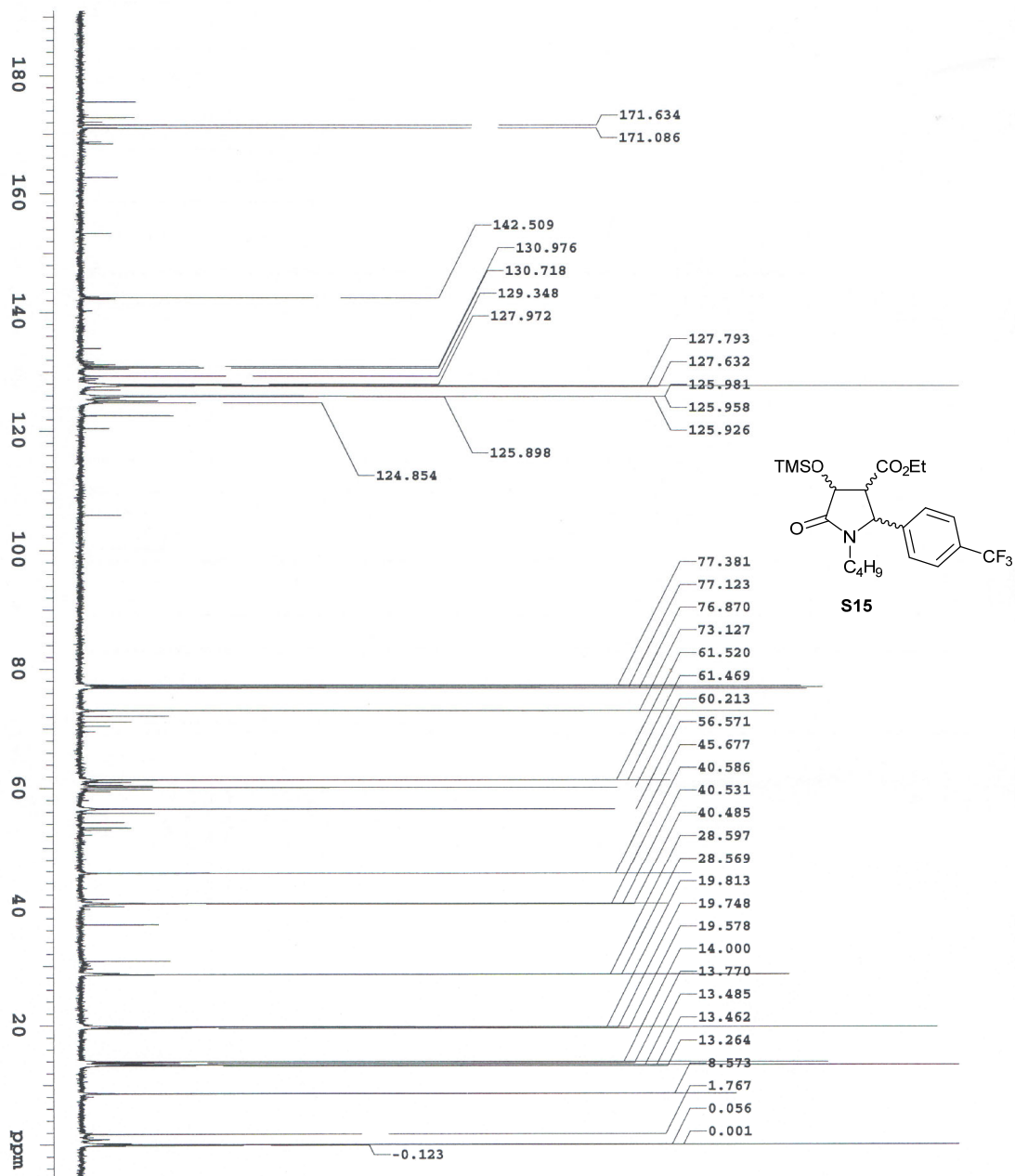


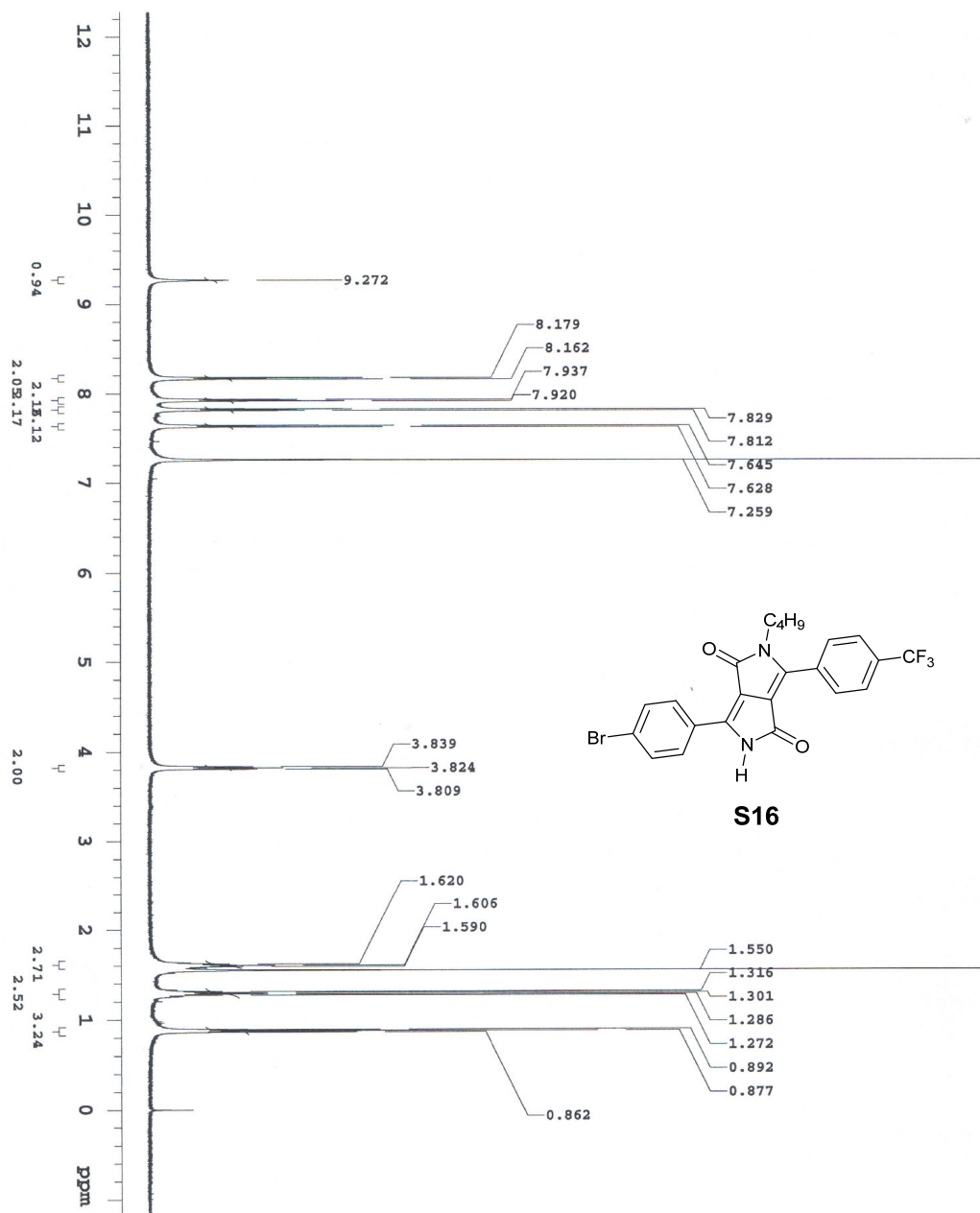


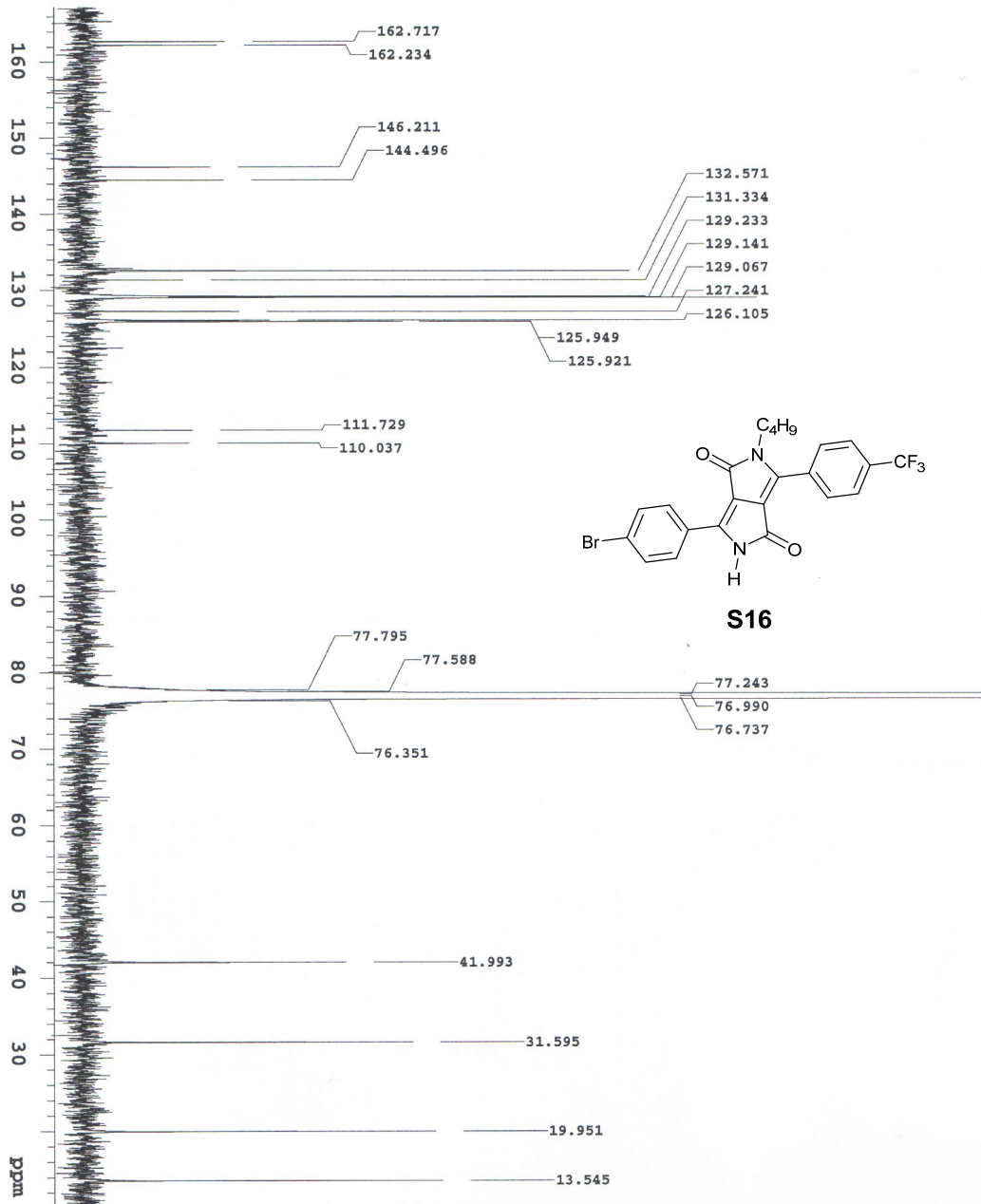


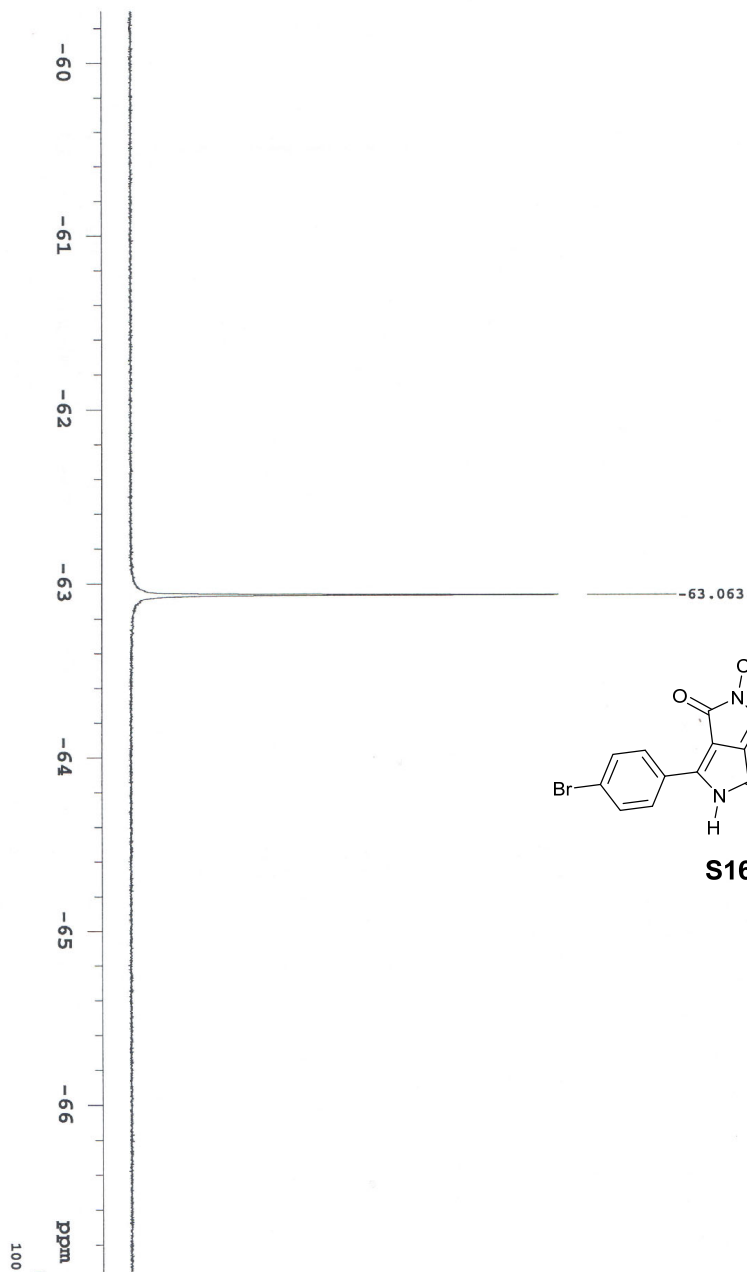


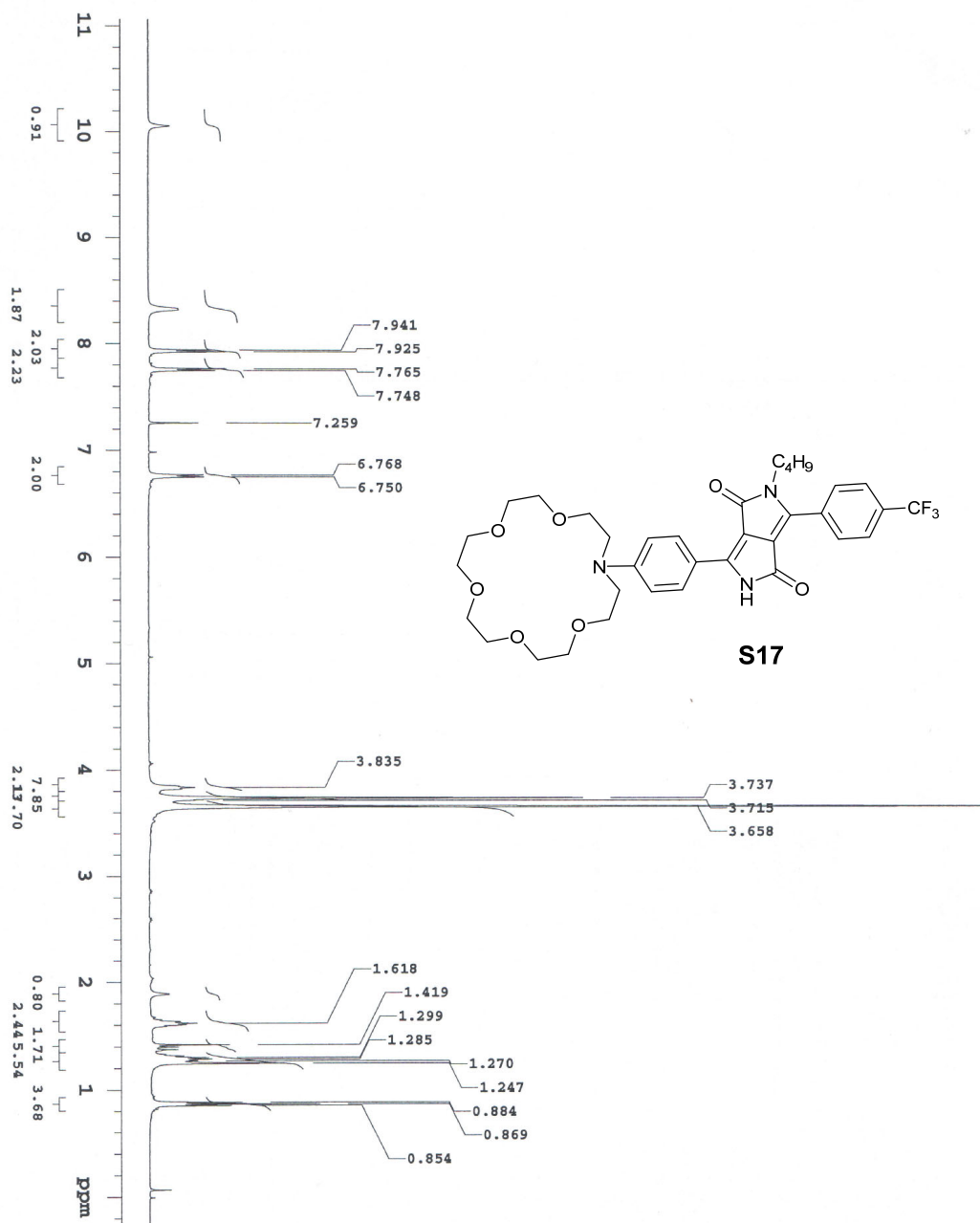


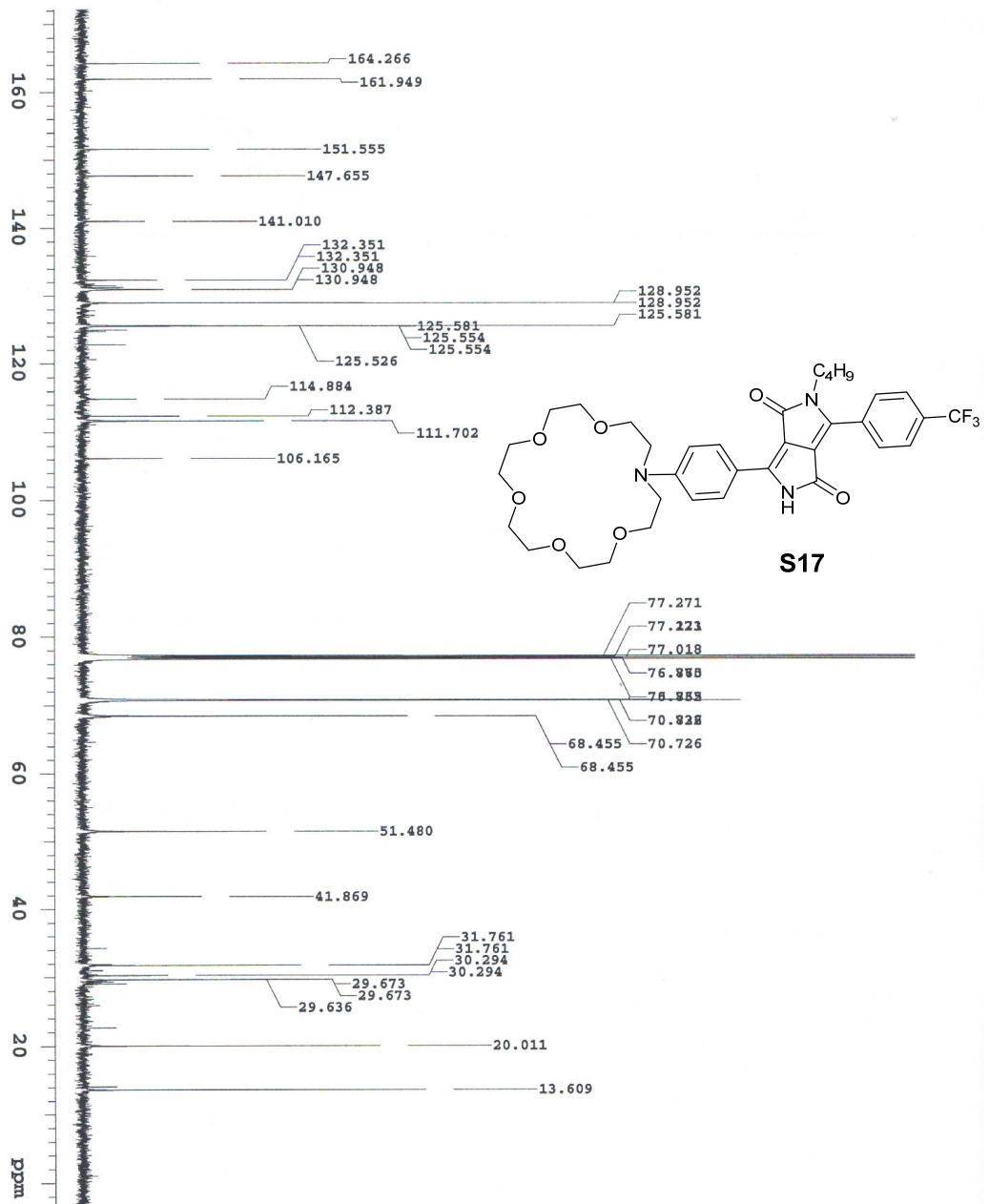


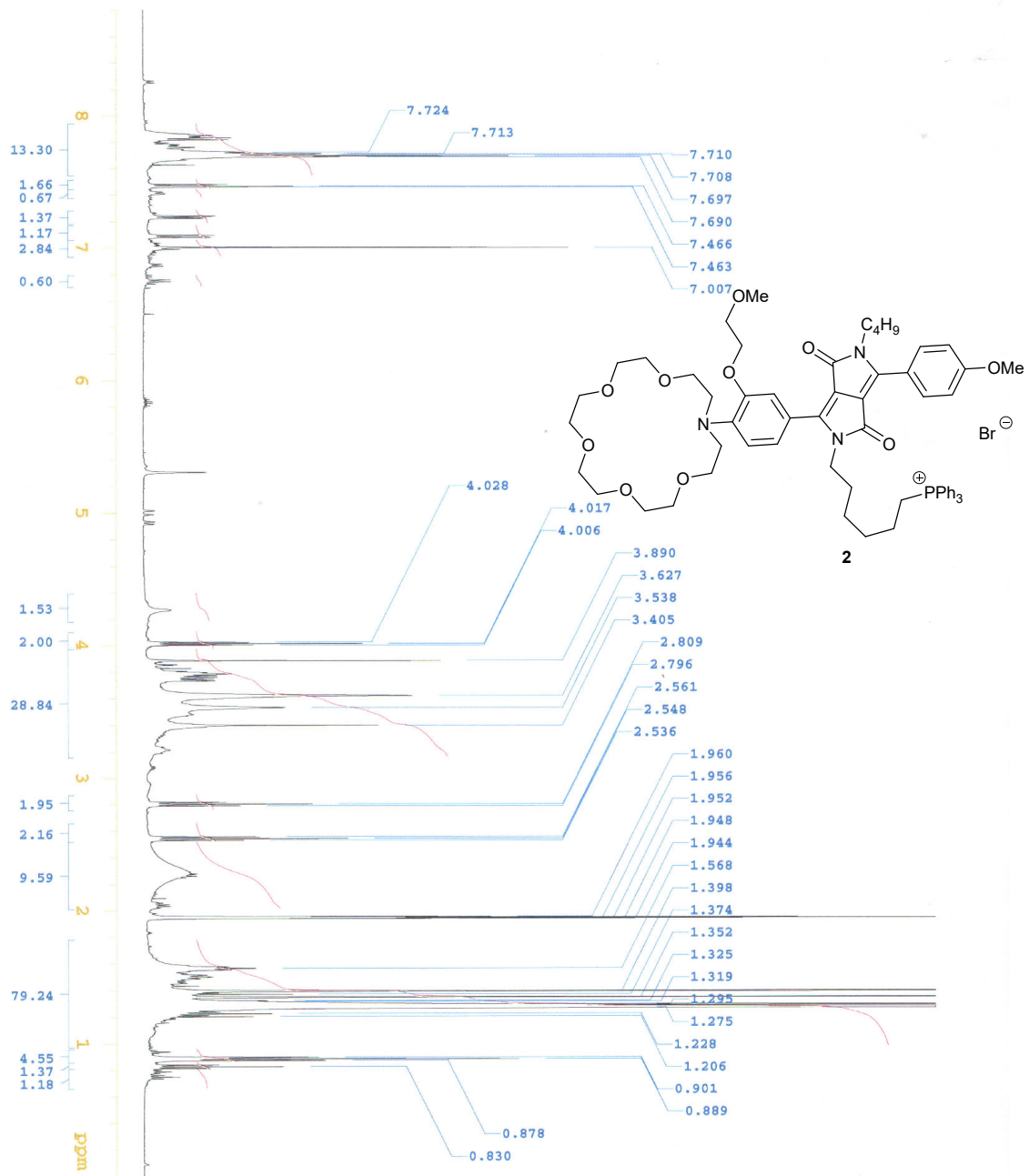


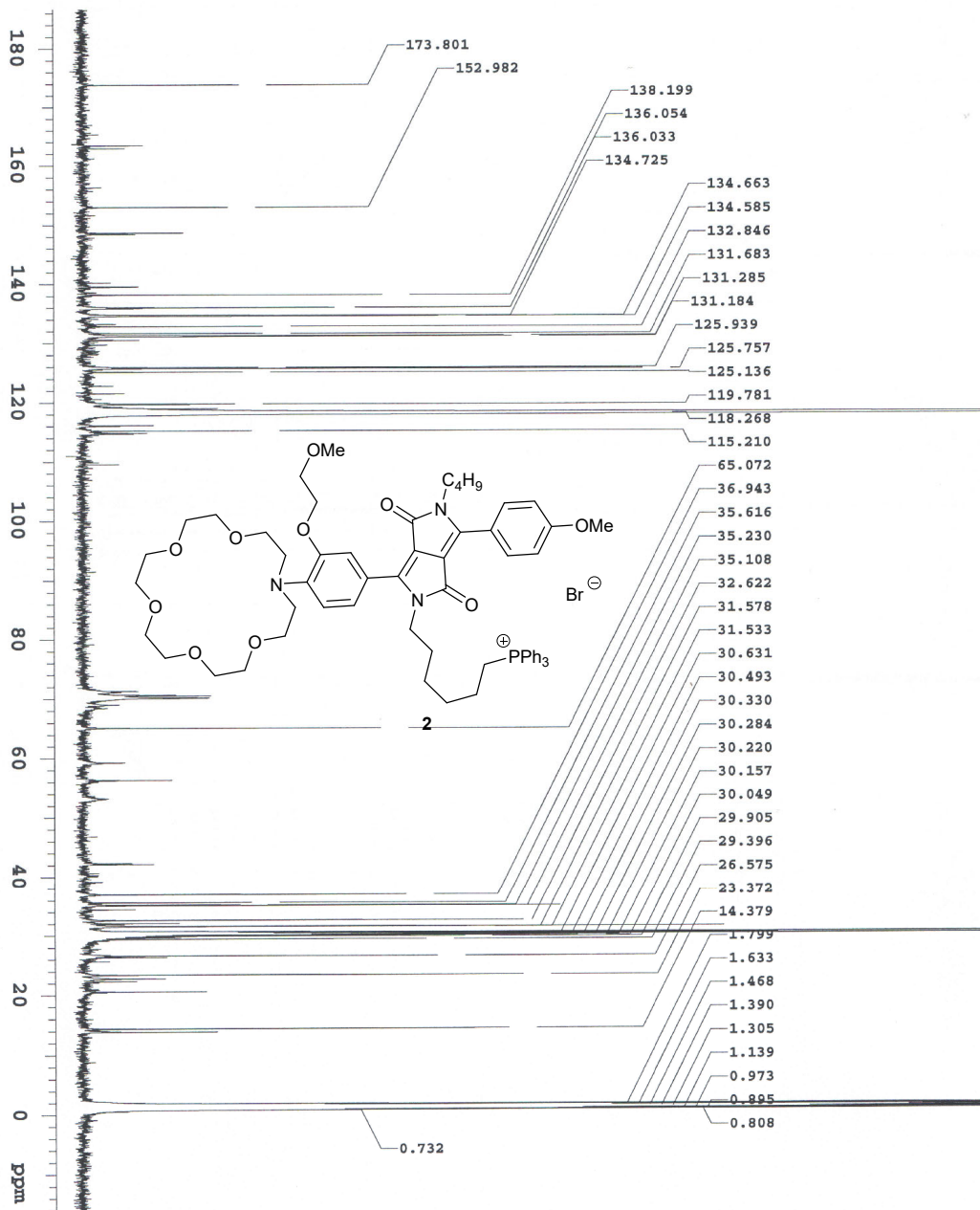












MS spectra

Elemental Composition Report

Single Mass Analysis

Tolerance = 20.0 PPM / DBE: min = -1.5, max = 50.0

Selected filters: None

Monoisotopic Mass, Odd and Even Electron Ions

31 formula(e) evaluated with 1 results within limits (up to 50 best isotopic matches for each mass)

Elements Used:

C: 0-70 H: 0-100 N: 0-2 O: 0-3 Br: 1-1

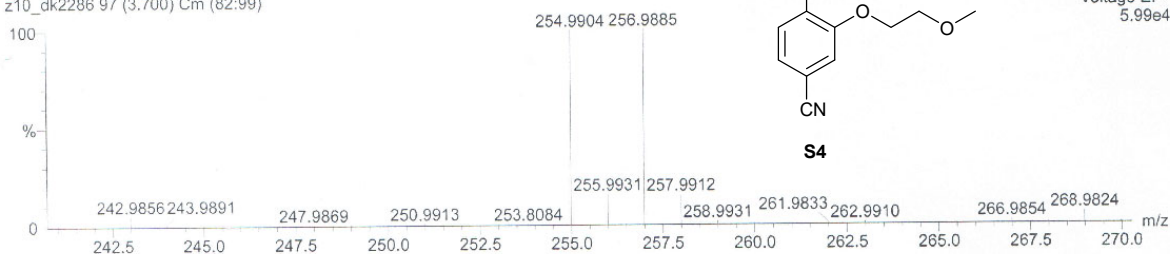
D. Kumar

GDK-300

z10_dk2286 97 (3.700) Cm (82:99)

AUTOSPEC

04-Dec-2020 11:48:06
Operator: Malgorzata Grela
Voltage EI+
5.99e4



Minimum: -1.5
Maximum: 5.0 20.0 50.0

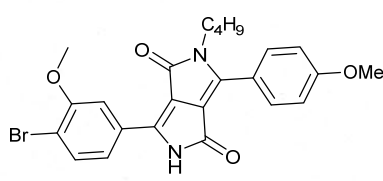
Mass	Calc. Mass	mDa	PPM	DBE	i-FIT	Formula
254.9904	254.9895	0.9	3.5	6.0	248.2	C10 H10 N O2 Br

Mass	Calc. Mass	mDa	PPM	DBE	Formula	I-FIT	I-FIT Norm	Fit Conf %	C	H	N	O	Na	Br
505.0726	505.0742	-1.6	-3.2	33.5	C37 H10 N2 Na	416.0	13.734	0.00	37	10	2	1	1	
	505.0742	-1.6	-3.2	9.5	C25 H31 O Br2	402.5	0.218	80.43	25	31		1		2
	505.0739	-1.3	-2.6	13.5	C24 H23 N2 O4 Na Br	403.9	1.634	19.52	24	23	2	4	1	1
	505.0718	0.8	1.6	6.5	C23 H32 O Na Br2	409.9	7.635	0.05	23	32		1	1	2

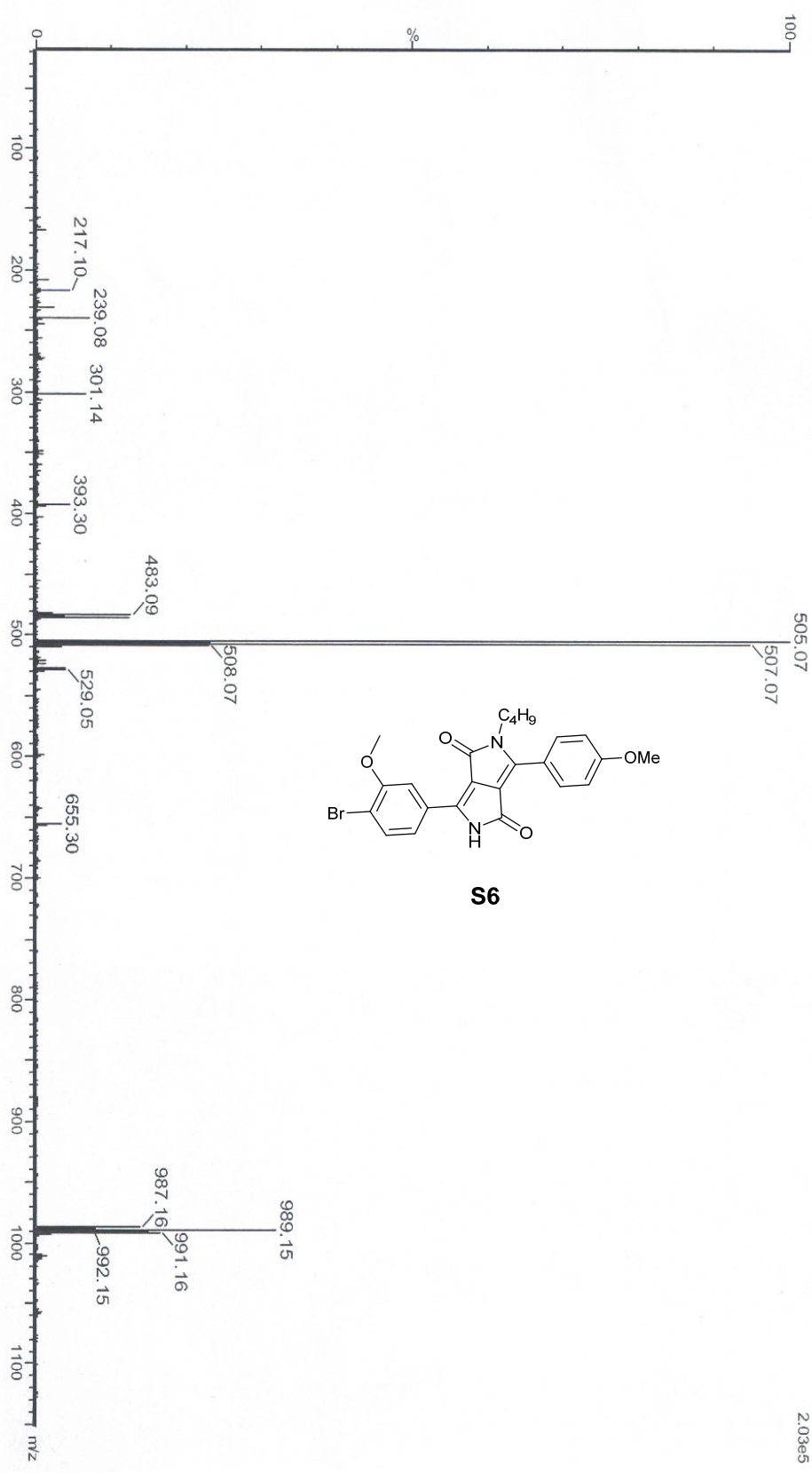
OV-959

z10_dk716 11 (0.243) Cm(8:20-(2:4+40:47))

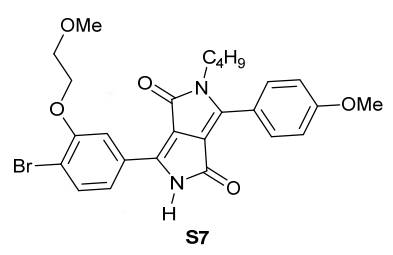
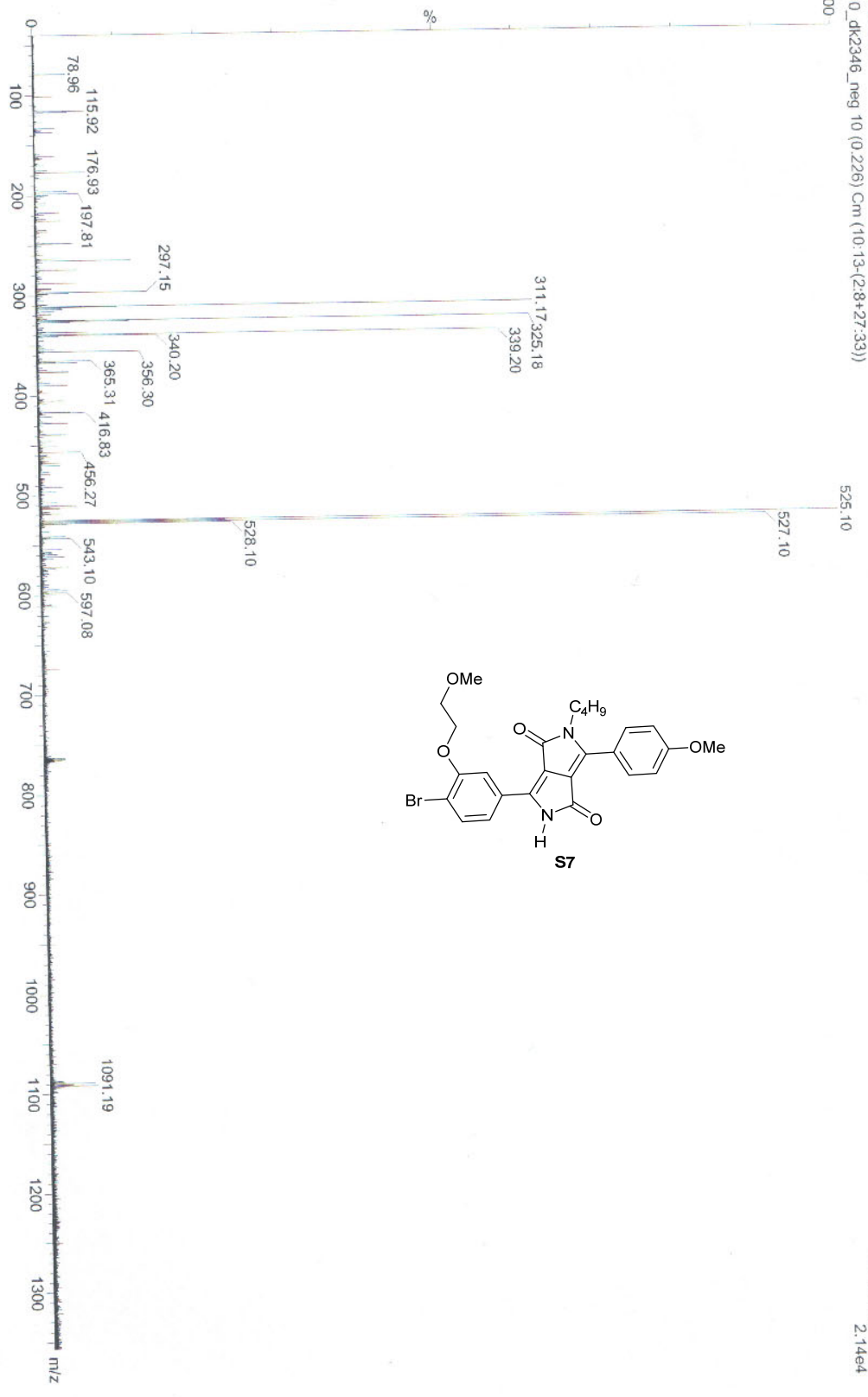
1: TOF MS ES+
2.03e5



S6



GDK-301
z10_dk2346_neg 10 (0.226) Cm (10-13-(2.8+27.33))
100



1: TOF MS ES-
2.14e4

Elemental Composition Report

Single Mass Analysis

Tolerance = 15.0 PPM / DBE: min = -1.5, max = 50.0

Selected filters: None

Monoisotopic Mass, Odd and Even Electron Ions

28 formula(e) evaluated with 1 results within limits (up to 50 best isotopic matches for each mass)

Elements Used:

C: 0-70 H: 0-100 N: 0-3 O: 9-9

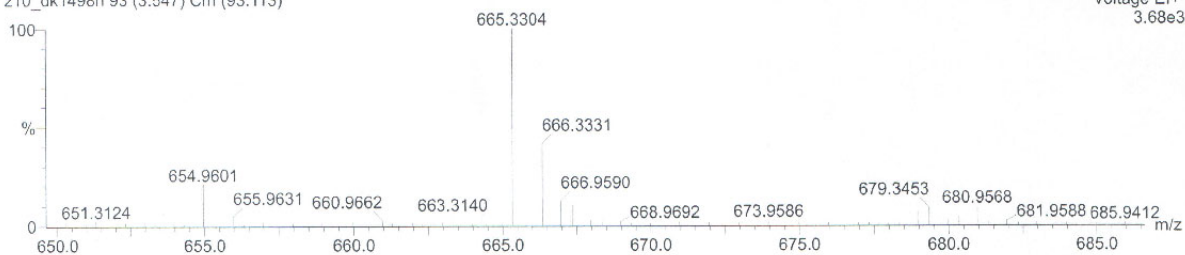
D. Kumar

GDK-273

z10_dk1498h 93 (3.547) Cm (93:113)

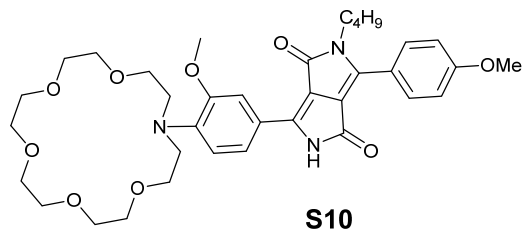
AUTOSPEC

17-Sep-2020 11:42:39
Operator: Malgorzata Grela
Voltage EI+
3.68e3



Minimum: -1.5
Maximum: 5.0 15.0 50.0

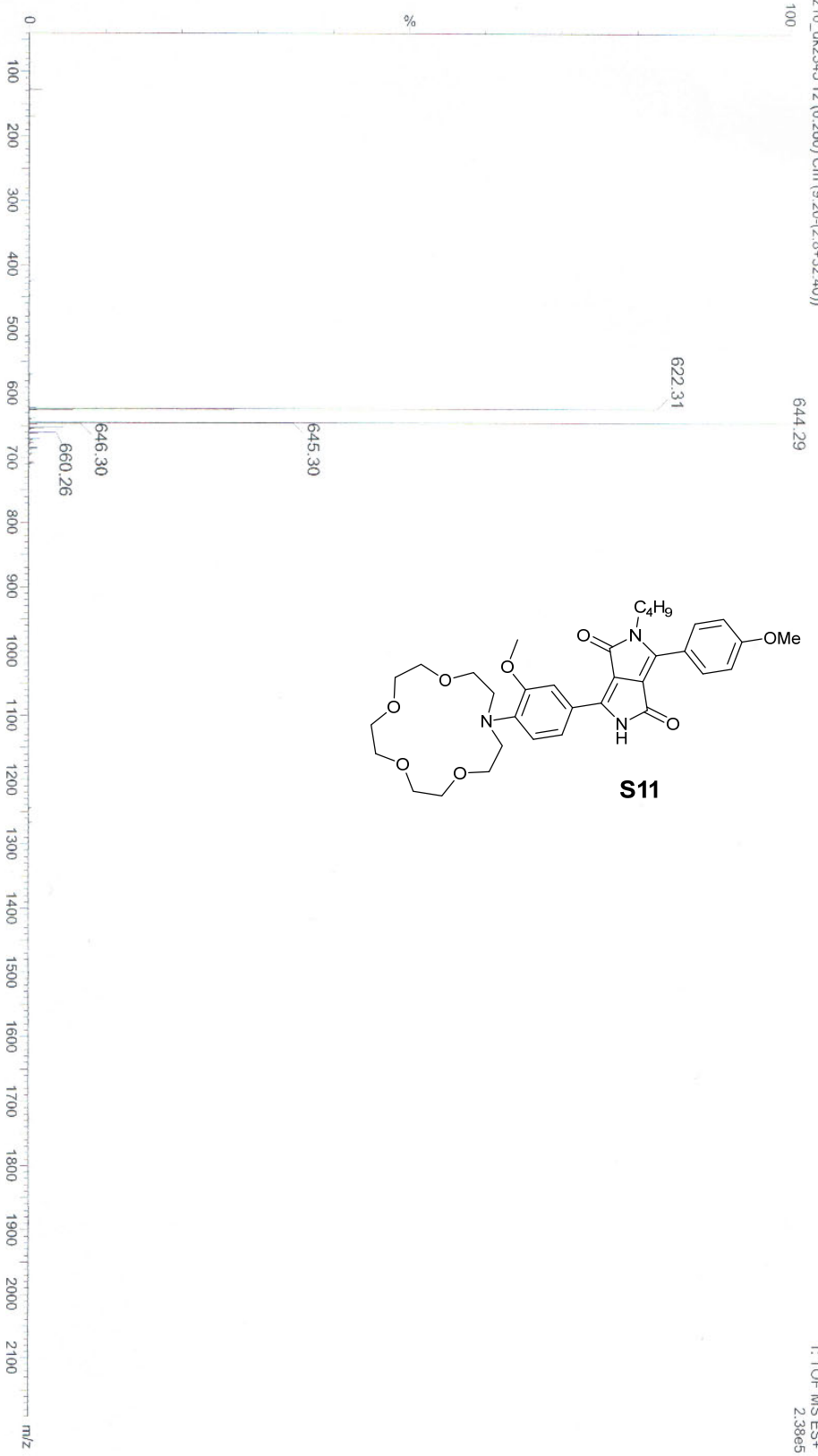
Mass	Calc. Mass	mDa	PPM	DBE	i-FIT	Formula
665.3304	665.3312	-0.8	-1.2	15.0	1.2	C36 H47 N3 O9



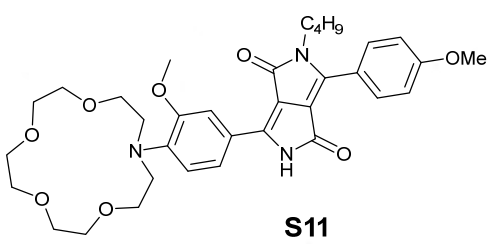
GDK-293

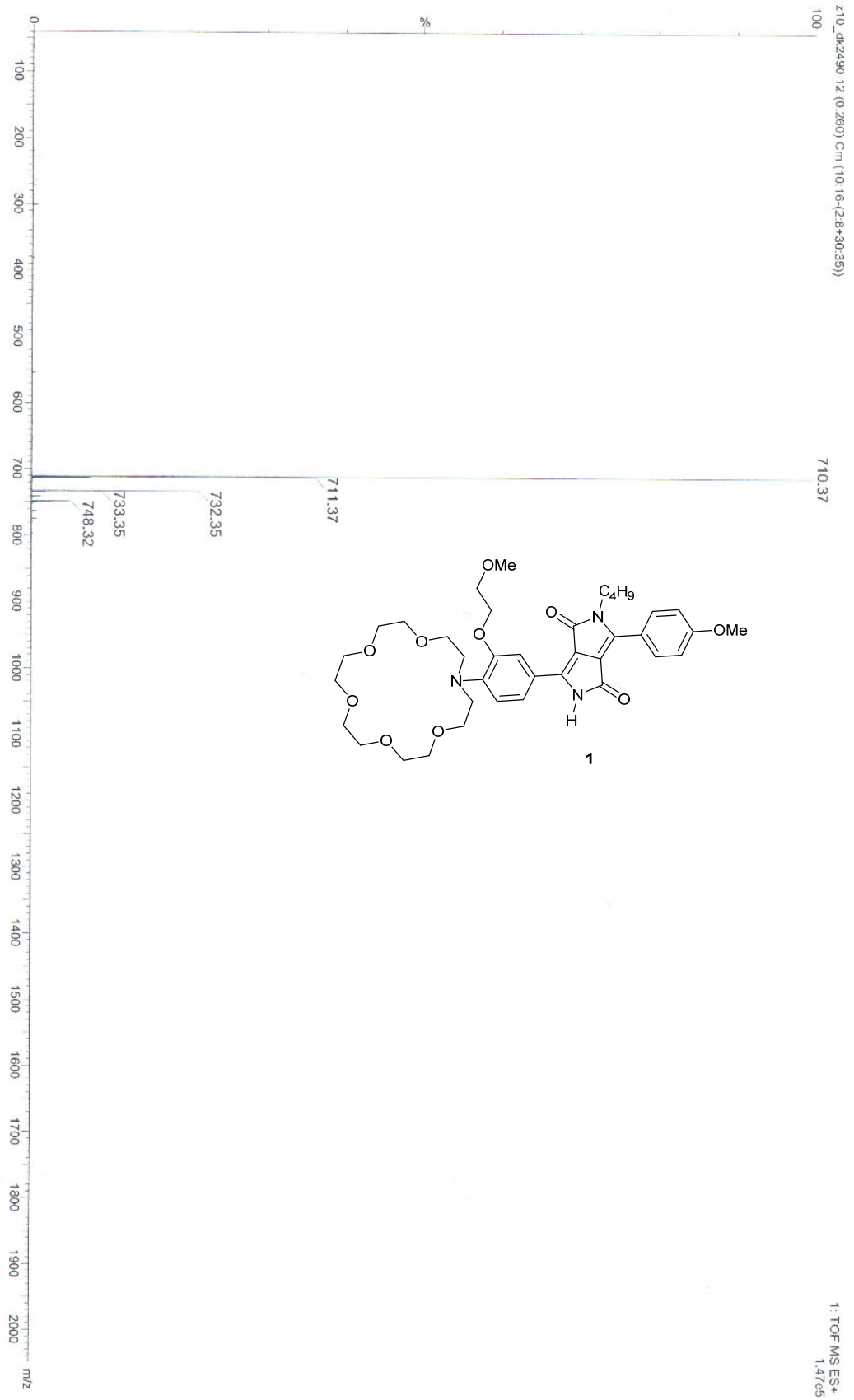
Z10_DK2345 12 (0.260) Cm (9:20-(2:8+32:40))

100



1: TOF MS ES+
2.38e5





Single Mass Analysis

Tolerance = 15.0 PPM / DBE: min = -1.5, max = 50.0

Selected filters: None

Monoisotopic Mass, Odd and Even Electron Ions

42 formula(e) evaluated with 1 results within limits (up to 50 best isotopic matches for each mass)

Elements Used:

C: 0-70 H: 0-100 N: 0-1 O: 0-4 F: 3-3

K. Dinesh

GDK0344-10

z10_kd0708h 142 (5.415) Cm (136:142)

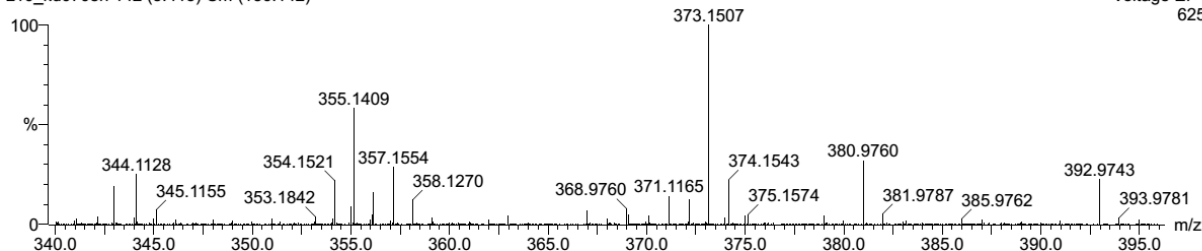
AUTOSPEC

31-Mar-2021 15:06:39

Operator: Marian Olejnik

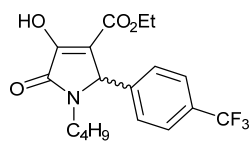
Voltage EI+

625



Minimum: -1.5
Maximum: 5.0 15.0 50.0

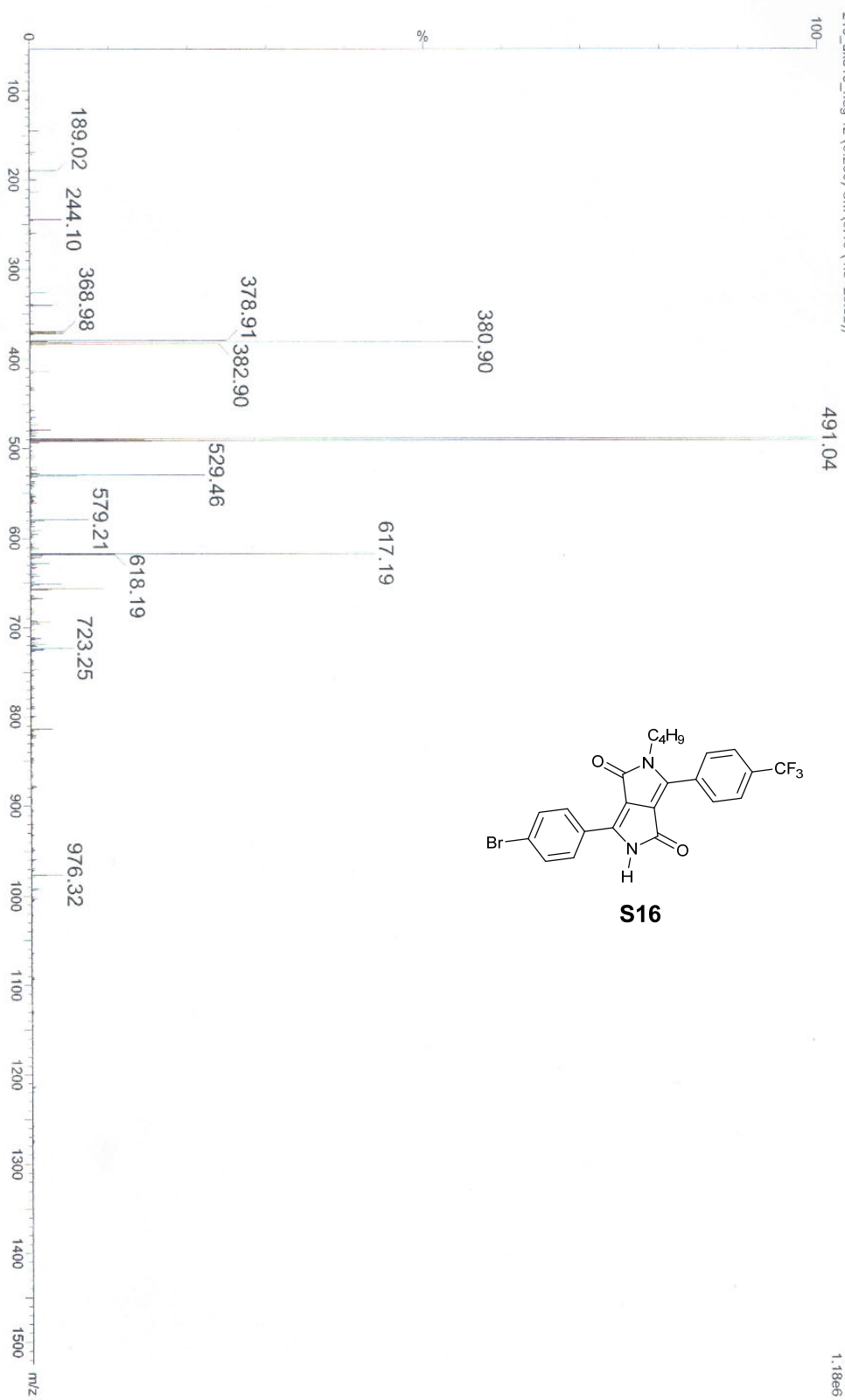
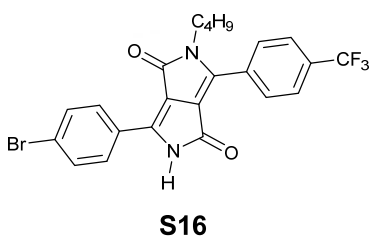
Mass	Calc. Mass	mDa	PPM	DBE	i-FIT	Formula
373.1507	373.1501	0.6	1.6	7.0	2.9	C18 H22 N O4 F3



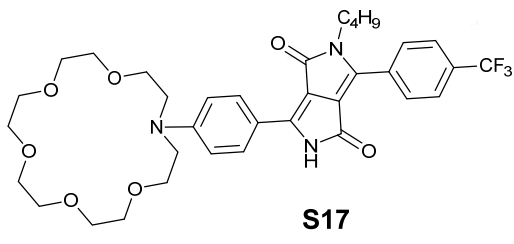
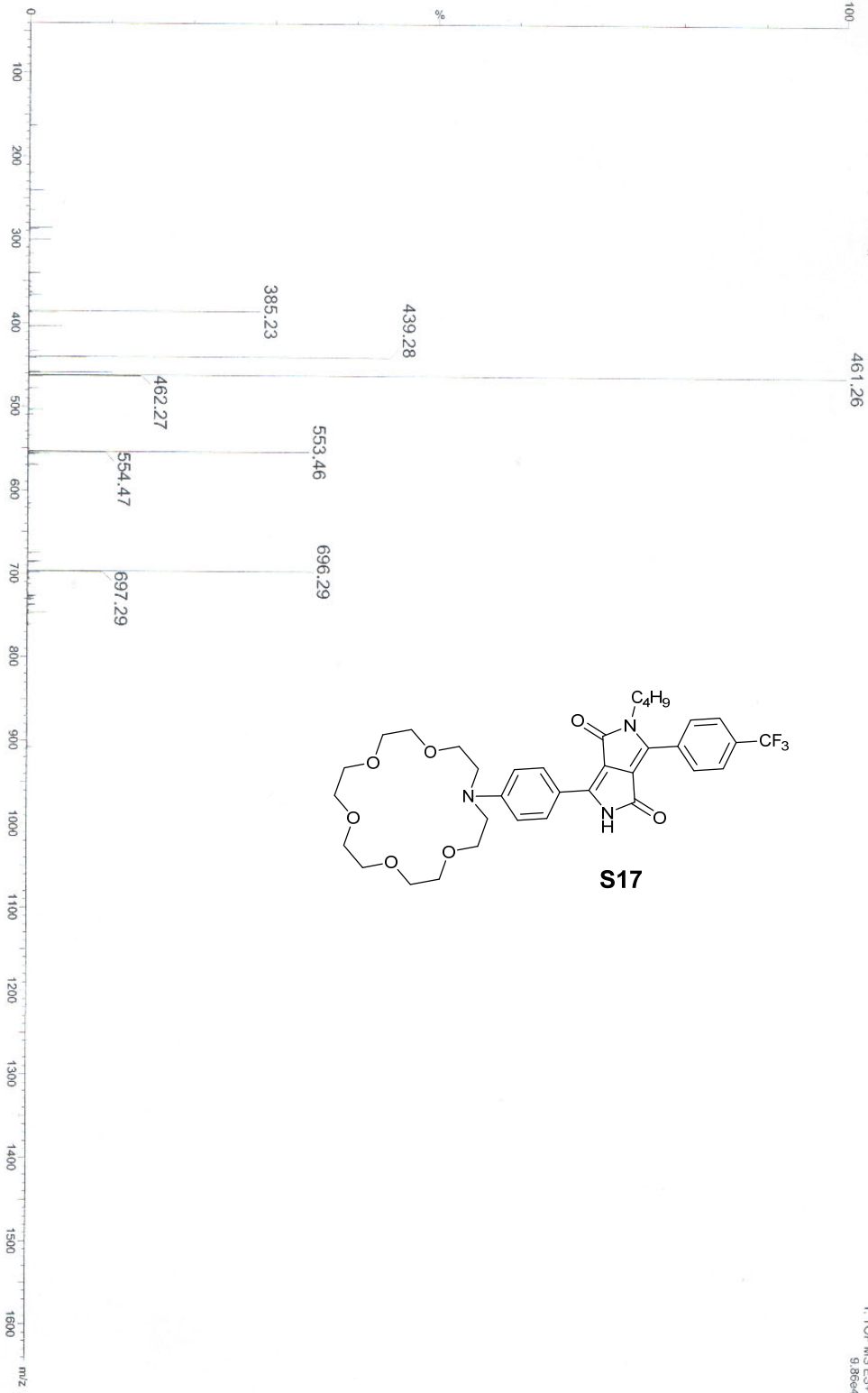
S13

z10_dk319_neg 12 (0.280) Cm (9:16-(4:8+29:32))

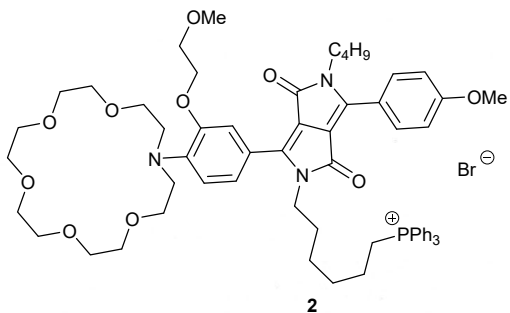
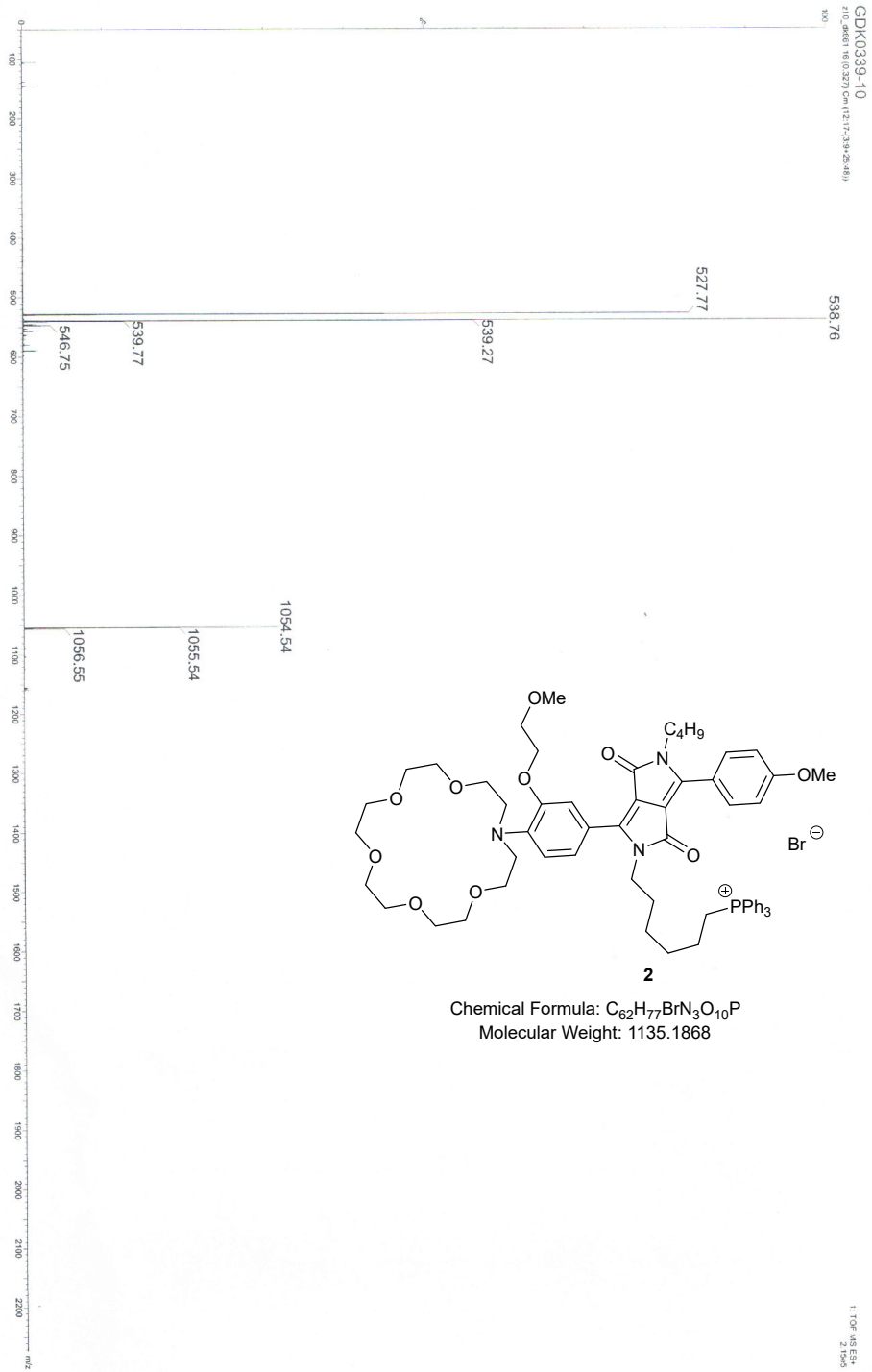
1: TOF MS ES-
1.18e6



z10_dk379b_17 (0.364) Cm (17:22:26+40:42)



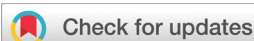
1. TOF MS ES+
9.86e4



Chemical Formula: C₆₂H₇₇BrN₃O₁₀P
 Molecular Weight: 1135.1868

Section S7: References

1. M. Pieczykolan, B. Sadowski and D. T. Gryko, *Angew. Chem. Int. Ed.*, 2020, **59**, 7528-7535.
2. Q. Hu, J. Kunde, N. Hanke and R. W. Hartmann, *Eur. J. Med. Chem.*, 2015, **96**, 139-150.
3. D. Jacquemin, I. Duchemin, X. Blasé, *J. Chem. Theory Comput.* **2015**, *11*, 5340-5359.
4. J. Tomasi, B. Mennucci, R. Cammi, *Chem. Rev.* **2005**, *105*, 2999-3094.
5. Y. Zhao, D. G. Truhlar, *Theor. Chem. Acc.* **2008**, *120*, 215-241.
6. P. M. Vérité, C. A. Guido, D. Jacquemin, *Phys. Chem. Chem. Phys.* **2019**, *21*, 2307-2317.
7. M. J. Frisch, G. W. Trucks, H. B. Schlegel, G. E. Scuseria, M. A. Robb, J. R. Cheeseman, G. Scalmani, V. Barone, G. A. Petersson, H. Nakatsuji, X. Li, M. Caricato, A. V. Marenich, J. Bloino, B. G. Janesko, R. Gomperts, B. Mennucci, H. P. Hratchian, J. V. Ortiz, A. F. Izmaylov, J. L. Sonnenberg, Williams, F. Ding, F. Lipparini, F. Egidi, J. Goings, B. Peng, A. Petrone, T. Henderson, D. Ranasinghe, V. G. Zakrzewski, J. Gao, N. Rega, G. Zheng, W. Liang, M. Hada, M. Ehara, K. Toyota, R. Fukuda, J. Hasegawa, M. Ishida, T. Nakajima, Y. Honda, O. Kitao, H. Nakai, T. Vreven, K. Throssell, J. A. Montgomery Jr., J. E. Peralta, F. Ogliaro, M. J. Bearpark, J. J. Heyd, E. N. Brothers, K. N. Kudin, V. N. Staroverov, T. A. Keith, R. Kobayashi, J. Normand, K. Raghavachari, A. P. Rendell, J. C. Burant, S. S. Iyengar, J. Tomasi, M. Cossi, J. M. Millam, M. Klene, C. Adamo, R. Cammi, J. W. Ochterski, R. L. Martin, K. Morokuma, O. Farkas, J. B. Foresman, D. J. Fox, *Gaussian 16 Rev. B.01*, Wallingford, CT, **2016**.
8. TURBOMOLE V6.2 2010, a development of University of Karlsruhe and Forschungszentrum Karlsruhe GmbH, 1989-2007, TURBOMOLE GmbH, since 2007; available from <http://www.turbomole.com>.
9. a) J. Cerezo, F. Santoro, FCClasses 3.0, <http://www.pi.iccom.cnr.it/fcclasses>; b) F. Santoro, R. Improta, A. Lami, J. Bloino, V. Barone, *J. Chem. Phys.* **2007**, *126*, 084509; c) F. Santoro, D. Jacquemin, *Wires Comput. Mol. Sci.* **2016**, *6*, 460-486.
- 1.



Cite this: DOI: 10.1039/d2ob01296k

A sensitive zinc probe operating *via* enhancement of excited-state intramolecular charge transfer†

G. Dinesh Kumar,^a Marzena Banasiewicz,^b Antoni Wrzosek,^c Omar O'Mari,^d Monika Zochowska,^c Valentine I. Vullev,^e Denis Jacquemin,^{*e} Adam Szewczyk^{*c} and Daniel T. Gryko^{*a}

Novel highly sensitive fluorescent probes for zinc cations based on the diketopyrrolopyrrole scaffold were designed and synthesized. Large bathochromic shifts (≈ 80 nm) of fluorescence are observed when the Zn^{2+} -recognition unit (di-(2-picoyl)amine) is bridged with the fluorophore possessing an additional pyridine unit able to participate in the coordination process. This effect originates from the dipolar architecture and the increasing electron-withdrawing properties of the diketopyrrolopyrrole core upon addition of the cation. The new, greenish-yellow emitting probes, which operate *via* modulation of intramolecular charge transfer, are very sensitive to the presence of Zn^{2+} . Introduction of a morpholine unit in the diketopyrrolopyrrole structure induces a selective six-fold increase of the emission intensity upon zinc coordination. Importantly, the presence of other divalent biologically relevant metal cations has negligible effects and typically even at a 100-fold higher concentration of Mg^{2+}/Zn^{2+} , the effect is comparable. Computational studies rationalize the strong bathochromic shift upon Zn^{2+} -complexation. Decorating the probes with the triphenylphosphonium cation and morpholine unit enables selective localization in the mitochondria and the lysosome of cardiac H9C2 cells, respectively.

Received 19th July 2022.
Accepted 1st September 2022
DOI: 10.1039/d2ob01296k

rsc.li/obc

Introduction

Zinc cations (Zn^{2+}) are the second most abundant transition-metal ions in the human body.¹ They are responsible for the structural integrity of over 3000 human proteins and play important roles in a wide range of biological processes such as brain activity, immune function, gene transcription, carbon-dioxide transport and mammalian reproduction.¹ Zinc deficiency usually leads to a range of diseases and disorders including immune dysfunction and susceptibility to infection, diabetes, Alzheimer's disease, and prostate disease.² Therefore, the development of highly sensitive and selective

fluorescent probes for detecting and monitoring Zn^{2+} in biological systems is crucial for functional studies.

In eukaryotic organisms, Zn^{2+} is present in various subcellular organelles and it plays a particularly important role in mitochondria and lysosomes.³ While mitochondria are the "power plants" of the cells, lysosomes are membrane-bound dynamic organelles responsible for terminal catabolic digestion and degradation of macromolecules by hydrolytic enzymes. The lysosomal functions are closely linked to other cell processes such as plasma membrane repair and providing metabolic building blocks.⁴

Over the years, a large panel of molecular fluorescence sensors based on different fluorophores, such as quinoline, coumarins, fluorescein, naphthalene, BODIPY, and anthracene, have been designed and synthesized for measuring Zn^{2+} both *in vitro* and *in vivo*.^{5,6} These fluorescent probes usually comprise chromophores with motifs for the selective binding of Zn^{2+} ions attached to them. The ion binding alters the emission quantum yields of the chromophores *via* intramolecular charge transfer (ICT), energy transfer (EnT), including electron-exchange (*i.e.*, Dexter) EnT and Förster resonance EnT (FRET), and chelation-enhanced fluorescence.⁷

When aiming towards a sensitive and selective probe for Zn^{2+} , a fluorophore compatible with programmed synthesis so that all the required functionalities and substituents are readily installed at the periphery is ideal. In this regard, we

^aInstitute of Organic Chemistry, Polish Academy of Sciences, Kasprzaka 44/52, 01-224 Warsaw, Poland. E-mail: dtgryko@icho.edu.pl

^bInstitute of Physics, Polish Academy of Sciences, Al. Lotników 32/46, 02-668 Warsaw, Poland

^cNencki Institute of Experimental Biology, Polish Academy of Sciences, Pasteur 3, 02-093 Warsaw, Poland. E-mail: a.szewczyk@nencki.gov.pl

^dDepartment of Bioengineering, University of California, Riverside, 900 University Ave., Riverside, CA 92521, USA. E-mail: vullev@ucr.edu

^eNantes University, CNRS, CEISAM, UMR-6230, F-4400 Nantes, France. E-mail: Denis.Jacquemin@univ-nantes.fr

† Electronic supplementary information (ESI) available: NMR, UV/vis and fluorescence spectra; fluorescence imaging; and computational details. See DOI: <https://doi.org/10.1039/d2ob01296k>

chose to base our studies on diketopyrrolopyrroles (DPPs),^{8–11} as the programmed synthesis of these allows for control over all four substituents. This ability has made it an attractive target for exploration, as evident from the recent emergence of applications of DPPs as chemosensors.¹² Recent work from the groups of Wang and Sessler demonstrates the utility of DPP in fluorescence molecular sensors for zinc ions and acidic media.^{13,14} These sensors comprise a chelator for Zn²⁺, *i.e.*, di-(2-picolyl)amine (DPA), and a tertiary amine, *i.e.*, *N*-morpholinyl, linked to DPP. In the absence of Zn²⁺ and at physiological pH, these amines linked to the amide nitrogen of DPP quench its fluorescence *via* photoinduced electron transfer (PET) to the fluorophore. Binding Zn²⁺ to the ion-chelating amine, or protonating the morpholine, suppresses their electron-donating capabilities, makes PET thermodynamically unfeasible, and allows the DPP fluorescence to recover, which is the sensing principle of these conjugates.

We believed that the polarizable DPP fluorophore is even more suitable for ICT-based probes. Along these lines, the primary goal of the present study is to develop a diketopyrrolopyrrole-based Zn²⁺-probe operating upon the ICT principle. In contrast to the overwhelming number of studies on PET-sensors and FRET-probes, the direct linking of the fluorophore with the recognition unit has not been extensively explored for Zn²⁺-imaging.¹⁵ In particular, we sought to achieve naked-eye visible effects beyond 600 nm.

Results and discussion

Design and synthesis

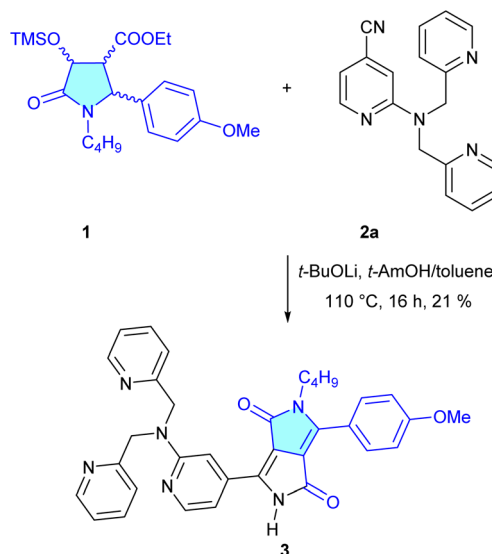
The fundamental idea was to prepare DPPs with an acceptor–acceptor–donor (A'–A–D) architecture where pyridine is an electron-withdrawing moiety conjugated with an electron-deficient DPP core, whereas 4-MeOC₆H₄ is a weakly electron-donating substituent. Di-(2-picolyl)amine (DPA) as a zinc chelator was introduced by de Silva,¹⁶ because it is able to afford excellent selectivity for Zn²⁺ over Na⁺, K⁺, Mg²⁺, Ca²⁺ and other metal cations.¹⁷ Our design encompasses molecular architectures where DPA coordination properties are enhanced by linking it to a third pyridine ring. In this approach, the basic nitrogen atom of the pyridine, which is part of the fluorophore, actively participates in the coordination of Zn²⁺. The DPA moiety was either directly bridged with pyridine or linked *via* a CH₂ spacer. This change typically affects the efficiency of the ICT of the chemosensor.¹⁸ This elaborate design is made possible by taking advantage of a programmed method for the synthesis of diketopyrrolopyrroles which gives the freedom to incorporate an almost unrestricted panel of substituents around the heterocyclic core.

The required nitrile **2a** was prepared from 2-fluoro-4-cyanopyridine *via* nucleophilic aromatic substitution with di-(2-picolyl)amine. Simultaneously, nitrile **2b** was synthesized from the corresponding aldehyde employing reductive amination following a literature procedure¹⁹ (see the ESI† for details). To obtain the desired probes, we employed our novel synthetic

strategy relying on condensation of nitrile with pyrrolidin-2-ones.²⁰ Hence, DPP **3** was prepared from the reaction of 2-(bis(pyridin-2-ylmethyl)amino)isonicotinonitrile (**2a**) with pyrrolidin-2-one **1** in 21% yield (Scheme 1). DPP **4** was obtained in an analogous way from nitrile **2b**, again in 21% yield (Fig. 1). It has to be emphasized that nitriles **2a** and **2b** could not be transformed directly into symmetrical DPPs *via* condensation with diethyl succinate.

Morpholine, due to its basicity, is frequently used as a targeting group for imaging acidic lysosomes in living cells.²¹ Consequently, in order to achieve the above-described goals, we prepared analogs of DPP **4** possessing propylmorpholine substituents at the N2 position.

Using our previously developed strategy,²⁰ pyrrolidin-2-one **7**, possessing a morpholine unit, was synthesized by the multi-component reaction of 4-methoxybenzaldehyde with 3-amino-propylmorpholine and diethyl oxaloacetate followed by reduction and TMS-protection giving pyrrolidone **7** in an overall 43% yield (Scheme 2). The condensation of pyrrolidinone **7** with 2-(bis(pyridin-2-ylmethyl)amino)isonicotinonitrile (**2a**) afforded DPP **8** in 14% yield (Scheme 2). Following the same strategy, nitrile **2b** was transformed into the corresponding DPP **9** in 14% yield (Fig. 2).



Scheme 1 The synthesis of diketopyrrolopyrrole **3**.

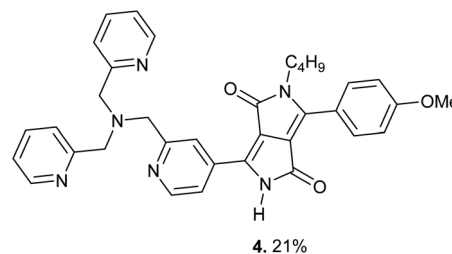
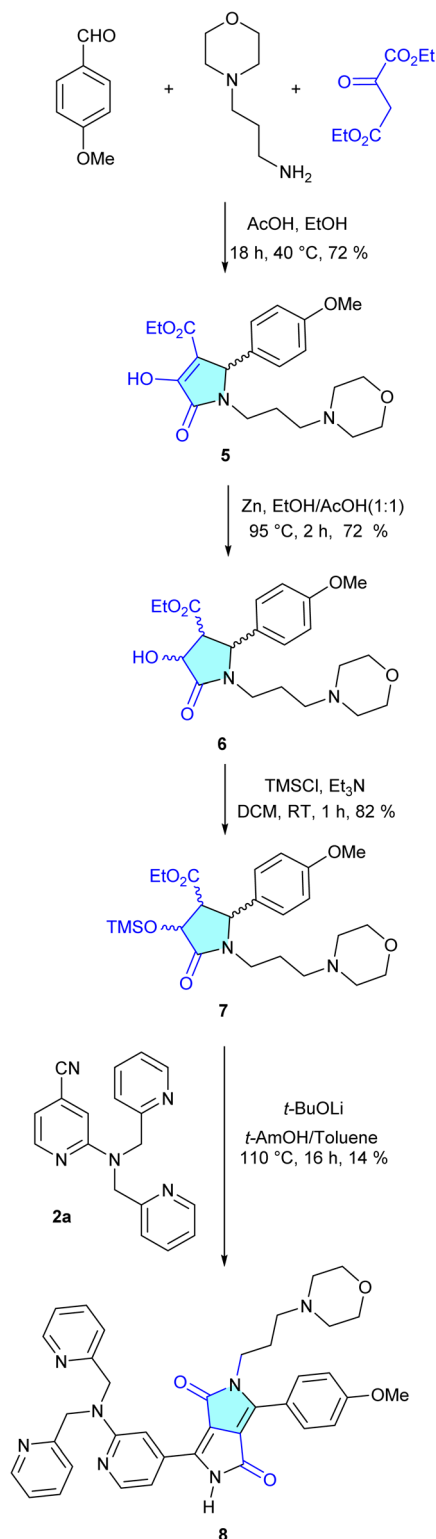


Fig. 1 The structure of DPP **4**.



In order to engineer the probe for mitochondria targeting, the fluorophore must be decorated with either a lipophilic triphenylphosphonium (TPP⁺) moiety²² or quaternary ammonium salt.²³ Hence, DPP 3 was transformed into DPP 10

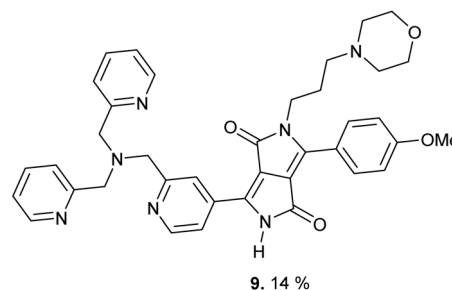
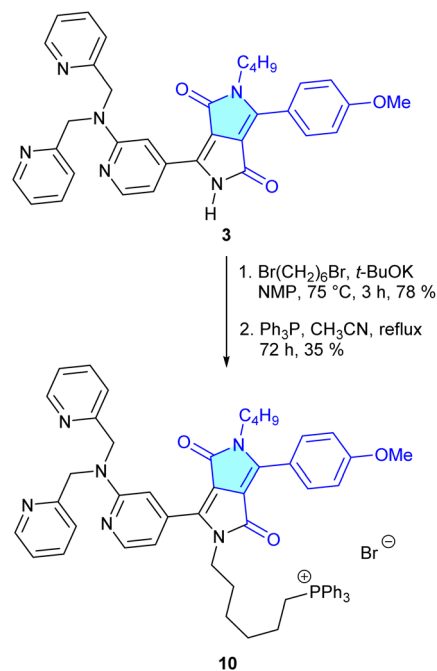


Fig. 2 The structure of DPP 9.



possessing a TPP⁺ unit, using a standard procedure,²² in 27% yield (Scheme 3).

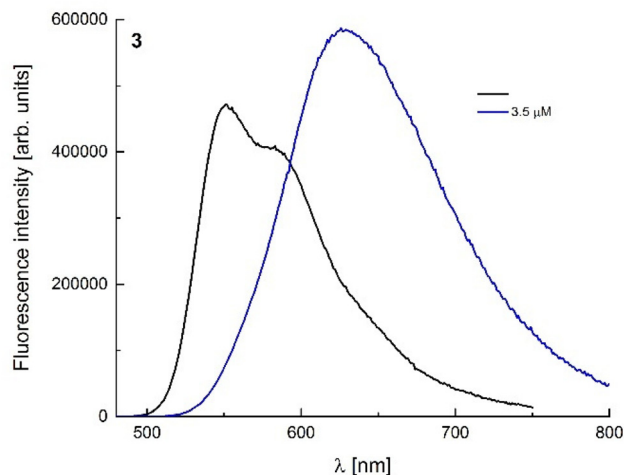
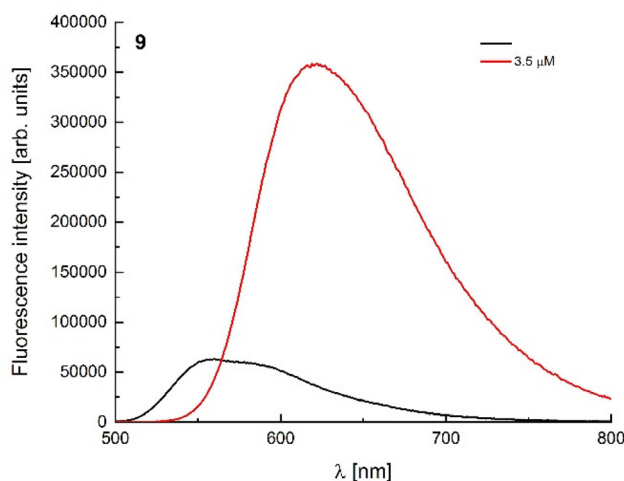
Photophysical studies

The photophysical properties of DPPs 3, 4 and 8–10 were investigated in CH₃CN. DPPs 3 and 4, possessing butyl chains at the N2 position, show the absorption (emission) maximum in the 490–500 (550–560) nm region, with associated fluorescence quantum yields (Φ_f) in the 40–60% range (Table 1, Fig. 3 and 4, and Fig. S1–S16 and S22–S66[†]). Unsurprisingly, DPPs 8 and 9 bearing the morpholine unit at the N2 position have essentially the same $\lambda_{\text{abs}}^{\text{max}}$ (490–500 nm) and $\lambda_{\text{em}}^{\text{max}}$ (550–560 nm) as DPPs 3 and 4. At the same time, however, the fluorescence quantum yields of 8 and 9 are significantly reduced (9–12%, see Table 1). Interestingly, the fluorescence quantum yields of DPPs 8 and 9 in the absence of zinc are ≈ 200 fold higher than those of previously reported analogous lysoDPP probes.¹⁴ DPP 10 possessing TPP⁺ functionalities exhibits $\lambda_{\text{abs}}^{\text{max}} = 474$ nm and

Table 1 Photophysical properties of DPPs in CH₃CN

DPP	$\lambda_{\text{abs}}^{\text{max}}$ /nm	$\lambda_{\text{em}}^{\text{max}}$ /nm	$\Phi_{\text{fl}}^{\text{a}}/\%$
3	499	552	40
4	497	559	56
8	500	551	9
9	500	559	12
10	474	554	33

^a Determined using rhodamine 6G in EtOH.

**Fig. 3** The effect of Zn(ClO₄)₂ addition on the emission spectra of DPP 3 measured in acetonitrile.**Fig. 4** The effect of Zn(ClO₄)₂ addition on the emission spectra of DPP 9 measured in acetonitrile. Legend specifies colors of lines.

$\lambda_{\text{em}}^{\text{max}} = 554$ nm with Φ_{fl} of 33%. Hypsochromic shifts of absorption for DPPs bearing the TPP⁺ unit have been observed previously.^{22e}

The behavior of the DPPs in the presence of Zn²⁺ and other cations depends on the structure of the diketopyrrolopyrrole.

In the family comprising DPPs 3, 4, and 8, the addition of Zn(II) perchlorate induces a significant, ≈ 80 nm, bathochromic shift of the emission (Fig. 3 and Table 2). An analogous shift occurs after protonation with PhSO₃H as well as in the presence of cadmium cations. On the other hand, the addition of Mg²⁺ and Ca²⁺ is accompanied by a very small hypsochromic shift of fluorescence, but it requires at least 100 equivalents of Mg(ClO₄)₂ or Ca(ClO₄)₂ to reach a noticeable level. The presence of cobalt(II) salt causes total quenching of the fluorescence due to metal-to-ligand electron transfer upon excitation.²⁴ These effects can be explained in the following way: pyridine (or 2-aminopyridine) directly linked with the DPP core participates in the complexation process and its electron-withdrawing capacity is enhanced by the coordination of a zinc cation (or interaction with H⁺). Consequently, the electron-deficiency of DPP increases, which enhances the ICT character of the excited state. Polar media stabilize such ICT excited states and decrease the energy gap with the ground state, inducing bathochromic shifts in the observed emission.

DPP 10 plays a key role in our strategy. It simultaneously possesses TPP⁺ as a mitochondrion targeting unit and an electronically conjugated zinc-coordinating ability. The fluorescence intensity of DPP 10 decreases in the presence of a large concentration of H⁺ (Fig. S61†), whereas it increases in the presence of both Cd²⁺ and Zn²⁺ (Table 2, Fig. S62 and S63†). An interesting effect has been observed for cadmium. The addition of small amounts of Cd(ClO₄)₂ has an effect analogous to zinc whereas a larger excess shifts the emission further bathochromically beyond 700 nm. DPP 9 shares this architecture and the effects are similar. In this case, the addition of a Brønsted acid causes an immense 140 nm bathochromic shift of the emission whereas the addition of zinc salts results in a much smaller 80 nm bathochromic shift accompanied by a 30-fold fluorescence enhancement. Again, the red-shift occurs in the presence of only one equivalent of the zinc(II) salt. The presence of cadmium has a similar effect.

For DPPs 3, 9 and 10, which were selected to be used in cell imaging studies, the water solubility was measured (see the ESI† for details). The solubilities of DPPs 9 and 10 in water are found to be 3 μM and 7 μM respectively (Fig. S67 and S68†). The water solubility of DPP 3 turned out to be below the detection limit.

The multivalent character of the studied DPPs that possess coordination sites of different affinity for Zn²⁺ affects both the complexation efficiency and the stoichiometry of the formed complexes. Titrations of dyes 3, 4 and 8–10 with Zn(ClO₄)₂ in acetonitrile were monitored by FL spectroscopy (Fig. S17–S21†).^{25–27} The data clearly show that complexation processes deviate substantially from the simple 1:1 equilibrium. The most pronounced differences are at the initial points of the titration experiments (<0.5 equiv. of Zn²⁺) and have a different spectroscopic fingerprint for different dyes. Most likely, the curves reflect the formation of complexes that contain a higher amount of dye per Zn²⁺, for example, the 2:1 complex, (dye)₂Zn²⁺, and engage only peripheral coordination sites. As the amount of Zn²⁺ increases, 1:1 complexes, (dye)Zn²⁺, start

Table 2 Changes of fluorescence of DPPs **3**, **4** and **8–10** measured in acetonitrile in the presence of 1 eq. of various salts

Dye	Zn(ClO ₄) ₂ (1 eq.)			PhSO ₃ H (1 eq.)			Cd(ClO ₄) ₂ (1 eq.)			Mg(ClO ₄) ₂ (1 eq.)		
	Enhancement of fluorescence	$\Phi_{fl}/\%$	λ_{em} (nm)	Enhancement of fluorescence	$\Phi_{fl}/\%$	λ_{em} (nm)	Enhancement of fluorescence	$\Phi_{fl}/\%$	λ_{em} (nm)	Enhancement of fluorescence	$\Phi_{fl}/\%$	λ_{em} (nm)
3	1.6	64	629	1.2	48	665	2.0	80	613	1.06	42	553
4	1.2	67	637	0.2	11	715	1.2	67	616	1.4	78	613
8	6.6	59	612	4.1	37	616	1.4	13	612	0.88	8	554
9	6.5	78	622	2.6	31	798	1.8	22	613	2.0	24	597
10	2.1	69	622	1.3	43	660	2.1	69	611	1.15	38	556

to form. For all cases except **8**, at 1 equiv. of added Zn²⁺, the maximum enhancement of the 620 nm band is reached. Due to the complex character of the equilibria, quantitative interpretation of the titration data was not achieved. However, despite the initial formation of complexes with a different stoichiometry, the plateau that is reached already at 1 equiv. of Zn²⁺ at μM concentration indicates that the K_a for the apparent 1 : 1 complex is high ($>10^6 \text{ M}^{-1}$). A notable exception is dye **8**, which, at a similar concentration, requires 100 equiv. of Zn²⁺ to reach an equilibrium, indicating a much lower K_a .

Computational studies

To obtain more details about the nature of the excited states involved in these probes, we used time-dependent density functional theory (TD-DFT) to explore the electronic structure of compounds **3** and **4**. First, for model (compact) systems we compared CC2 and TD-DFT results and found rather small differences, the TD-DFT approach yielding slightly too large transition energies (see the ESI† for details). Next, we considered the two probes in CH₃CN and modelled their absorption and emission spectra. The computed vertical absorption wavelengths were 446 nm (**3**) and 450 nm (**4**), whereas the corresponding vertical fluorescence wavelengths attained were 555 nm (**3**) and 561 nm (**4**). The corresponding 0–0 energies were 2.46 and 2.45 eV. The latter values can be directly compared to the experimental absorption/emission crossing points of 2.25 and 2.22 eV indicating a reasonable agreement with a slight blueshift of the theoretical values, as expected from the CC2 results. For these two dyes, the transitions correspond to the H–L excitation, with moderate ICT character. To further confirm this statement, frontier MOs for DPP **4** have been shown in the ESI.† Fig. 5 shows the density difference plots for the two systems and from these it can be seen that the lowest excited state involves mainly rearrangements on the DPP core, the amino moieties playing a minor role. Using Le Bahers' model,²⁸ we computed ICT distances of 1.86 and 2.02 Å, for **3** and **4**, respectively.

To simulate the complexation with the Zn²⁺ cation, we added the cation to the chelating group, completing the coordination sphere with explicit CH₃CN molecules so as to obtain a realistic architecture. The optimized structures are shown in Fig. S64,† whereas the corresponding density of different plots can be found in Fig. 6. The presence of the zinc cation clearly enhances the accepting character of the vicinal

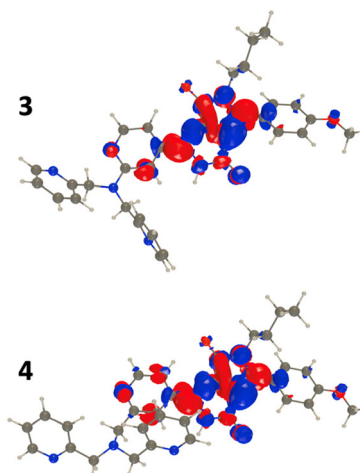


Fig. 5 Density difference plots for the model dyes **3** and **4**. The blue and red lobes indicate regions of decreased and increased density upon absorption, respectively. Contour threshold 1×10^{-3} .

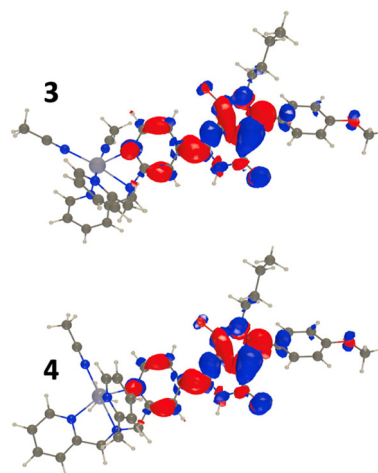


Fig. 6 Density difference plot for the model dyes of **3** and **4** with complexed Zn²⁺. See the caption of Fig. 5 for details.

pyridyl/phenyl substituent (mostly in red in Fig. 6), leading to an increased ICT with electron–hole distances of 2.57 and 2.60 Å, for **3** and **4**, respectively. Unsurprisingly, this increase of the ICT induces bathochromic shifts of the absorption (474

and 474 nm for **3** and **4**, respectively). For the fluorescence, the geometry relaxation becomes more important, and the theoretical vertical fluorescence after complexation is at 602 and 605 nm for **3** and **4**, respectively. For **3** and **4**, the change of emission energy upon complexation therefore corresponds to a *ca.* 50 nm redshift, which qualitatively fits the experimental findings (see Fig. 3), although a slightly smaller shift is obtained theoretically.

Imaging

DPPs **3**, **9** and **10** present a choice of dyes to be employed in fluorescence imaging studies. The presence of targeting functional groups leads to a different accumulation behavior in specific organelles in the cardiomyocyte H9C2 cells, as compared by colocalization experiments with the specific markers for individual organelles (Fig. 7–9).

We can conclude that DPP **10** with an attached triphenylphosphonium group (TPP⁺) accumulates preferentially in the mitochondria (Fig. 9). DPP **9** shows a preferential localization

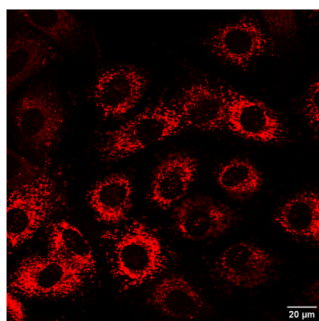


Fig. 7 Intracellular localization of DPP **3** as detected using confocal fluorescence microscopy.

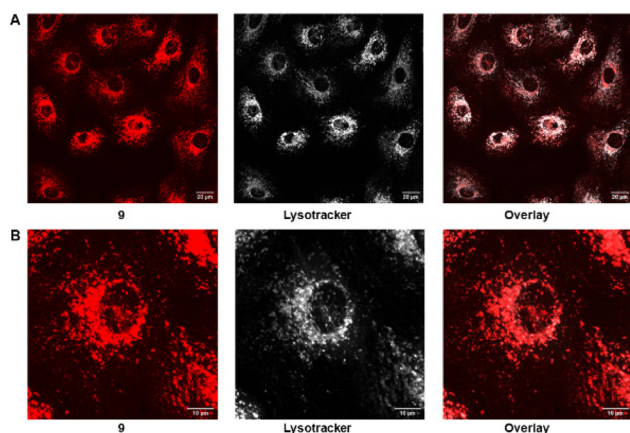


Fig. 8 Intracellular localization of DPP **9** as detected using confocal fluorescence microscopy. (A) The fluorescence of DPP **9** was recorded with 559 nm excitation, fluorescence of LysoTracker was recorded with 633 nm excitation. Overlay picture recorded simultaneously for two fluorophores in living H9C2 cells. (B) Pictures were recorded with higher magnification (3x) for a better resolution to see a single cell chosen from the above larger field of view for DPP **9**.

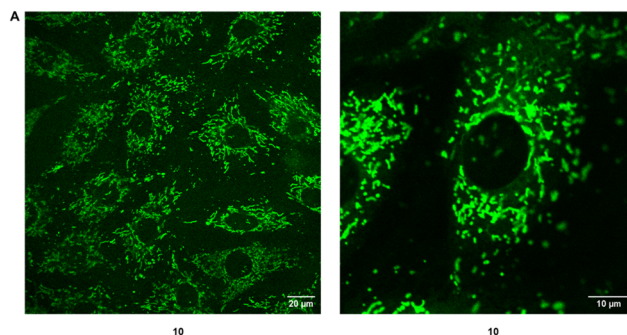


Fig. 9 Intracellular localization of DPP **10** as detected using confocal fluorescence microscopy. (A) The fluorescence of DPP **10** was recorded with 559 nm excitation in living H9C2 cells. (B) Pictures were recorded with higher magnification (3x) for a better resolution to see a single cell for DPP **10** dye accumulation.

in the lysosomes (Fig. 8) whereas the fluorescent probe **3** shows a more homogeneous distribution throughout the H9C2 lineage.

Conclusions

We have proved that the direct bridging of the diketopyrrolopyrrole chromophore with a zinc-recognition unit provides a highly sensitive probe for this cation switching the fluorescence from greenish-yellow to orange. These probes also react with Cd²⁺ but they are silent to other divalent cations of biological importance. Moreover, if the probe also possesses a morpholine unit, a marked 6-fold increase in the fluorescence intensity accompanies the bathochromic shift. The latter effect is specific to Zn²⁺. Coordination of the zinc cation to pyridine, which is electronically conjugated with the DPP core, enhances the ICT character of the lowest singlet excited state in polar media and its energy level drops closer to that of the ground state. Molecular engineering of these DPPs enables localization of them in either mitochondria or lysosomes. Installing all of the required substituents regulating all pivotal features, *i.e.*, the cation recognition unit, subcellular localization, solubility and donor–acceptor architecture, was only possible thanks to a previously-developed programmed synthesis of diketopyrrolopyrroles. These findings may serve as a blueprint for designing more efficient zinc probes.

Experimental

Synthetic procedures

All reagents and solvents were purchased from commercial sources and were used as received unless otherwise noted. Reagent grade solvents (CH₂Cl₂, hexanes) were distilled prior to use. Transformations with moisture- and oxygen-sensitive compounds were performed under a stream of argon. The reaction progress was monitored by means of thin-layer chromatography (TLC), which was performed on aluminum foil

plates, covered with silica gel 60 F254. Product purification was done by means of column chromatography with Kieselgel 60. The identity and purity of the prepared compounds were proved by ^1H NMR and ^{13}C NMR, as well as by mass spectrometry (*via* EI-MS or ESI-MS). HRMS (ESI-TOF) and HRMS (EI): double-focusing magnetic sector instruments with EBE geometry were utilized. NMR spectra were measured on 400 or 500 or 600 MHz instruments. Chemical shifts (δ , ppm) were determined with tetramethylsilane (TMS) as the internal reference; J values are given in Hz. All melting points for crystalline products were measured with an automated melting point apparatus and are given without correction. Pyrrolidinone 1 was obtained following the literature procedure.²⁰

General procedure for the synthesis of DPP derivatives

In a flame dried Schlenk flask, a mixture of appropriate nitrile (1 eq.) and lithium *tert*-butoxide (4 eq.) was heated to 110 °C under argon. To this solid mixture, *tert*-amyl alcohol (5 mL) was added in one portion followed by dropwise addition of pyrrolidinone 1 or 7 (1 eq.) dissolved in dry toluene (3 mL). The resulting dark solution was left stirring at this temperature overnight. After cooling to room temperature, the reaction mixture was diluted with water (100 mL) and extracted with DCM (100 mL), and subsequently washed once more with DCM (50 mL). The combined organic phases were dried over Na_2SO_4 , filtered and concentrated under vacuum. The resulting crude compound was subjected to chromatography on silica gel (DCM/MeOH = 9:1) and crystallized from DCM/*n*-hexanes to obtain the desired DPP product.

Optical measurements

UV/Vis absorption spectra were recorded on a PerkinElmer Lambda 35 Spectrometer. Fluorescence spectra were recorded on an FLS1000 from Edinburgh Instruments. All linear optical studies were performed with freshly prepared air-equilibrated solutions at room temperature (298 K). Acetonitrile was of spectrophotometric grade and was used without further purification. Quartz cells (10 mm) were used for the measurements of absorption and emission spectra. As a standard, Rh6G ($\Phi_{\text{fl}} = 0.94$ in EtOH) was used to determine fluorescence quantum yields.

First-principles calculations

All calculations were performed using the Gaussian16.A03 program.²⁹ The ground and excited state geometries were optimized at the PCM(ACN)³⁰ (TD-)M06-2X³¹/6-31+G(d) level, the vibrational frequencies were obtained at the exact same level of theory, and the total and transition energies were obtained at the PCM(cLR²,ACN)³²-TD-M06-2X/6-311+G(2d,p) level. Test calculations on model compounds (see the ESI†) performed with the CC2/aug-cc-pVTZ level revealed that the TD-DFT results are slightly blue-shifted.

Imaging

Cell culture conditions. The rat embryonic cardiomyoblast-derived H9C2 cell lines were cultured at 37 °C under a humidified

atmosphere containing 5% CO_2 in DMEM supplemented with 10% foetal bovine serum (FBS), 2 mM glutamine, 100 U ml^{-1} penicillin, and 100 $\mu\text{g ml}^{-1}$ streptomycin. **Fluorescence localization of diketopyrrolopyrrole-based zinc probes within the cells.** The cardiac H9C2 cells were loaded with fluorophores in DMEM supplemented with 10% FBS, 2 mM glutamine, 100 U ml^{-1} penicillin, and 100 $\mu\text{g ml}^{-1}$ streptomycin at 37 °C under a humidified atmosphere containing 5% CO_2 for 15 to 30 minutes with the diketopyrrolopyrrole-based zinc probe at the final concentration ranging from 200 to 500 nM. The final concentration of MitoTracker™ Green FM was 150 nM, and that of the lysosyme probe was 100 nM. The fluorophores were dissolved in DMSO. Before measurements, the incubation medium was replaced with FluoroBrite™ DMEM. The measurements were performed with an Olympus IX83 confocal microscope with the water objective 60x UPLSAPO 60XW. Registered data were transferred to ImageJ and analyzed for presentation.

Author contributions

Conceptualization: D.T.G., G.D.K.; investigation: G.D.K., M.B., A.W., O.O., M.Z.; supervision: D.T.G., A.S., D.J. V.I.V.; visualization: G.D.K., M.B., A.W.; writing – original draft: G.D.K., D.J., A.W.; writing – review & editing: D.T.G., M.B., A.S., D.J., V.I.V.

Conflicts of interest

There are no conflicts to declare.

Acknowledgements

This work was financially supported by the Foundation for Polish Science (TEAM POIR.04.04.00-00-3CF4/16-00). We also thank the National Science Centre, Poland, under the QuantERA programme, project 2017/25/Z/ST2/03038. DJ is indebted to the CCIPL mesocenter installed in Nantes for the very generous allocation of computational time. We also thank Dr Yevgen M. Poronik and Prof. Agnieszka Szumna for invaluable discussions. Imaging experiments were supported by the Nencki Institute of Experimental Biology, Polish Academy of Sciences.

References

- (a) M. D. Pluth, E. Tomat and S. J. Lippard, *Ann. Rev. Biochem.*, 2011, **80**, 333–355; (b) W. Maret, *Adv. Nutr.*, 2013, **41**, 82–91; (c) W. Maret, *Int. J. Mol. Sci.*, 2017, **18**, 2285–2296; (d) A. Krezel and W. Maret, *Arch. Biochem. Biophys.*, 2016, **611**, 3–19.
- A. S. Prasad, *Adv. Nutr.*, 2013, **4**, 176–190.
- (a) A. Atkinson, O. Khalimonchuk, P. Smith, H. Sabic, D. Eide and D. R. Winge, *J. Biol. Chem.*, 2010, **285**, 19450–

- 19459; (b) D. Rajapakse, T. Curtis, M. Chen and H. Xu, *Oxid. Med. Cell. Longevity*, 2017, 6926485; (c) S. L. Sensi, D. Ton-That, P. G. Sullivan, E. A. Jonas, K. R. Gee, L. K. Kaczmarek and J. H. Weiss, *Proc. Natl. Acad. Sci. U. S. A.*, 2003, **100**, 6157–6162; (d) J. J. Hwang, S.-J. Lee, T.-Y. Kim, J.-H. Cho and J.-Y. Koh, *J. Neurosci.*, 2008, **28**, 3114–3122.
- 4 J. P. Luzio, P. R. Pryor and N. Bright, *Nat. Rev. Mol. Cell Biol.*, 2007, **8**, 622–632.
- 5 (a) P. Ning, J. C. Jiang, L. C. Li, S. X. Wang, H. Z. Yu, Y. Feng, M. Z. Zhu, B. C. Zhang, H. Yin, Q. X. Guo and X. M. Meng, *Biosens. Bioelectron.*, 2016, **77**, 921–927; (b) M. L. Zastrow, R. J. Radford, W. Chyan, C. T. Anderson, D. Y. Zhang, A. Loas, T. Tzounopoulos and S. J. Lippard, *ACS Sens.*, 2016, **1**, 32–39; (c) K. Komatsu, Y. Urano, H. Kojima and T. Nagano, *J. Am. Chem. Soc.*, 2007, **129**, 13447–13454; (d) J. H. Lee, J. H. Lee, S. H. Jung, T. K. Hyun, M. Feng, J.-Y. Kim, J.-H. Lee, H. Lee, J. S. Kim, C. Kang, K.-Y. Kwon and J. H. Jung, *Chem. Commun.*, 2015, **51**, 7463–7465; (e) K. Sreenath, Z. Yuan, J. R. Allen, M. W. Davidson and L. Zhu, *Chem. – Eur. J.*, 2015, **21**, 867–874; (f) H. Z. Su, X. B. Chen and W. H. Fang, *Anal. Chem.*, 2014, **86**, 891–899.
- 6 (a) S. Zhu, J. Zhang, J. Janjanam, G. Vegesna, F.-T. Luo, A. Tiwari and H. Liu, *J. Mater. Chem. B*, 2013, **1**, 1722–1728; (b) L. Xue, G. Li, C. Yu and H. Jiang, *Chem. – Eur. J.*, 2012, **18**, 1050–1054; (c) G. Masanta, C. S. Lim, H. J. Kim, J. H. Han, H. M. Kim and B. R. Cho, *J. Am. Chem. Soc.*, 2011, **133**, 5698–5700; (d) S. Peng, Q. He, G. I. Vargas-Zúñiga, L. Qin, I. Hwang, S. K. Kim, N. J. Heo, C.-H. Lee, R. Dutta and J. L. Sessler, *Chem. Soc. Rev.*, 2020, **49**, 865–907; (e) A. Kanegae, Y. Takata, I. Takashima, S. Uchinomiya, R. Kawagoe, K. Usui, A. Yamashita, J. Wongkongkatap, M. Sugimoto and A. Ojida, *Commun. Chem.*, 2021, **4**, 104; (f) N. C. Lim and C. Brückner, *Chem. Commun.*, 2004, 1094–1095.
- 7 (a) L. Fang and M. Watinkson, *Chem. Sci.*, 2020, **11**, 11366–11379; (b) H. Zhu, J. Fan, J. Du and X. Peng, *Acc. Chem. Res.*, 2016, **49**, 2115–2126; (c) W. Xu, Z. Zeng, J.-H. Jiang, Y.-T. Chang and L. Yuan, *Angew. Chem., Int. Ed.*, 2016, **55**, 13658–13699; (d) S. Sumalekshmy and C. J. Fahrni, *Chem. Mater.*, 2011, **23**, 483–500; (e) K. P. Carter, A. M. Young and A. E. Palmer, *Chem. Rev.*, 2014, **114**, 4564–4601.
- 8 (a) D. G. Farnum, G. Mehta, G. G. I. Moore and F. P. Siegal, *Tetrahedron Lett.*, 1974, **29**, 2549–2552; (b) M. Grzybowski and D. T. Gryko, *Adv. Opt. Mater.*, 2015, **3**, 280–320; (c) M. Kaur and D. H. Choi, *Chem. Soc. Rev.*, 2015, **44**, 58–77; (d) W. Li, L. Wang, H. Tang and D. Cao, *Dyes Pigm.*, 2019, **162**, 934–950; (e) M. A. Auwalu and S. Cheng, *Chemosensors*, 2021, **9**, 44; (f) N. Luo, G. Zhang and Z. Liu, *Org. Chem. Front.*, 2021, **8**, 4560–4581.
- 9 (a) A. Kovalenko, C. Yumusak, P. Heinrichová, S. Stríteský, L. Fekete, M. Vala, M. Weiter, N. S. Sariciftci and J. Krajcovič, *J. Mater. Chem. C*, 2017, **5**, 4716–4723; (b) S. Luňák Jr., M. Weiter and M. Vala, *ChemPhysChem*, 2022, e202200252; (c) S. Shimizu, T. Iino, A. Saeki, S. Seki and N. Kobayashi, *Chem. – Eur. J.*, 2015, **21**, 2893–2904; (d) T. Marks, E. Daltrozzi and A. Zumbusch, *Chem. – Eur. J.*, 2014, **20**, 6494–6504; (e) G. M. Fischer, A. P. Ehlers, A. Zumbusch and E. Daltrozzi, *Angew. Chem., Int. Ed.*, 2007, **46**, 3750–3753; (f) A. Tang, C. Zhan, J. Yao and E. Zhou, *Adv. Mater.*, 2017, **29**, 1600013; (g) C. Zhao, Y. Guo, Y. Zhang, N. Yan, S. You and W. Li, *J. Mater. Chem. A*, 2019, **7**, 10174–10199; (h) A. Punzi, F. Nicoletta, G. Marzano, C. G. Fortuna, J. Dagar, T. M. Brown and G. M. Farinola, *Eur. J. Org. Chem.*, 2016, 3233–3242; (i) Y. Patil, T. Jadhav, B. Dhokale and R. Misra, *Asian J. Org. Chem.*, 2016, **5**, 1008–1914; (j) P. Josse, C. Dalinot, Y. Jiang, S. Dabos-Seignon, J. Roncali, P. Blanchard and C. Cabanetos, *J. Mater. Chem. A*, 2016, **4**, 250–256; (k) C. K. Lo and J. R. Reynolds, *Polymer*, 2016, **99**, 741–747; (l) M. Stolte, S. L. Suraru, P. Diemer, T. He, C. Burschka, U. Zschieschang, H. Klauk and F. Würthner, *Adv. Funct. Mater.*, 2016, **26**, 7415–7422.
- 10 (a) C. M. Mauck, P. E. Hartnett, E. A. Margulies, L. Ma, C. E. Miller, G. C. Schatz, T. J. Marks and M. R. Wasielewski, *J. Am. Chem. Soc.*, 2016, **138**, 11749–11761; (b) C. Ye, S. Mallick, M. Hertzog, M. Kowalewski and K. Börjesson, *J. Am. Chem. Soc.*, 2021, **143**(19), 7501–7508; (c) I. Papadopoulos, M. J. Álvaro-Martins, D. Molina, P. M. McCosker, P. A. Keller, T. Clark, Á. Sastre-Santos and D. M. Guldi, *Adv. Energy Mater.*, 2020, **10**, 2001496; (d) S. Masoomi-Godarzi, M. Liu, Y. Tachibana, L. Goerigk, K. P. Ghiggino, T. A. Smith and D. J. Jones, *Adv. Energy Mater.*, 2018, **8**, 1801720.
- 11 (a) Y. Lee, J. Y. Oh, W. Xu, O. Kim, T. R. Kim, J. Kang, Y. Kim, D. Son, J. B.-H. Tok, M. J. Park, Z. Bao and T.-W. Lee, *Sci. Adv.*, 2018, **4**, eaat7387; (b) K. Dhbaibi, L. Favereau, M. Srebro-Hooper, M. Jean, N. Vanthuyne, F. Zinna, B. Jamoussi, L. D. Bari, J. Autschbach and J. Crassous, *Chem. Sci.*, 2018, **9**, 735–742.
- 12 (a) Y. Qu, J. L. Hua and H. Tian, *Org. Lett.*, 2010, **12**, 3320–3323; (b) L. Deng, W. Wu and H. Guo, *J. Org. Chem.*, 2011, **76**, 9294–9304; (c) S. Lin, S. Liu, H. Zou, W. Zeng, L. Wang, R. Beuerman and D. Cao, *J. Polym. Sci., Part A: Polym. Chem.*, 2011, **49**, 3882–3889; (d) Y. H. Jeong, C. H. Lee and W. D. Jang, *Chem. – Asian J.*, 2012, **7**, 1562–1566; (e) Y. Qu, S. Y. Qu, L. Yang, J. L. Hua and D. H. Qu, *Sens. Actuators, B*, 2012, **173**, 225–233; (f) S. Schutting, S. M. Borisov and I. Klimant, *Anal. Chem.*, 2013, **85**, 3271–3279.
- 13 C. C. Du, S. B. Fu, X. L. Ren, X. H. Wang, Z. Wang, J. Zhou and H. Y. Wang, *New J. Chem.*, 2018, **42**, 3493–3502.
- 14 C. C. Du, S. B. Fu, X. H. Wang, A. C. Sedgwick, W. Zhen, M. Li, X. Li, J. Zhou, Z. Wang, H. Y. Wang and J. L. Sessler, *Chem. Sci.*, 2019, **10**, 5699–5704.
- 15 (a) Z. Liu, C. Zhang, Y. Chen, W. He and Z. Guo, *Chem. Commun.*, 2012, **48**, 8365–8367; (b) F. Qian, C. Zhang, Y. Zhang, W. He, X. Gao, P. Hu and Z. Guo, *J. Am. Chem. Soc.*, 2009, **131**, 1460–1468.
- 16 S. A. de Silva, A. Zavaleta, D. E. Baron, O. Allam, E. V. Isidor, N. Kashimura and J. M. Percapio, *Tetrahedron Lett.*, 1997, **38**, 2237–2240.

- 17 (a) G. J. Zhang, H. Y. Li, S. M. Bi, L. F. Song, Y. X. Lu, L. Zhang, J. J. Yua and L. M. Wang, *Analyst*, 2013, **138**, 6163–6170; (b) G. J. Zhang, S. M. Bi, L. F. Song, F. Wang, J. J. Yu and L. M. Wang, *Dyes Pigm.*, 2013, **99**, 779–786.
- 18 (a) S. Sumalekshmy, M. M. Henary, N. Siegel, P. V. Lawson, Y. Wu, K. Schmidt, J.-L. Bredas, J. W. Perry and C. J. Fahrni, *J. Am. Chem. Soc.*, 2007, **129**, 11888–11889; (b) F. Qian, C. Zhang, Y. Zhang, W. He, X. Gao, P. Hu and Z. Guo, *J. Am. Chem. Soc.*, 2009, **131**(4), 1460–1468.
- 19 X.-Y. Chen, J. Shi, Y.-M. Li, F.-L. Wang, X. Wu, Q.-X. Guo and L. Liu, *Org. Lett.*, 2009, **19**, 4426–4429.
- 20 M. Pieczykolan, B. Sadowski and D. T. Gryko, *Angew. Chem., Int. Ed.*, 2020, **59**, 7528–7535.
- 21 L. Wang, Y. Xiao, W. Tian and L. Deng, *J. Am. Chem. Soc.*, 2013, **135**, 2903–2906.
- 22 (a) Q. Hu, M. Gao, G. Feng and B. Liu, *Angew. Chem., Int. Ed.*, 2014, **53**, 14225–14229; (b) C. W. T. Leung, Y. Hong, S. Chen, E. Zhao, J. W. Y. Lam and B. Z. Tang, *J. Am. Chem. Soc.*, 2013, **135**, 62–65; (c) Roopa, N. Kumar, V. Bhalla and M. Kumar, *Chem. Commun.*, 2015, **51**, 15614–15628; (d) H. Ogasawara, Y. Tanaka, M. Taki and S. Yamaguchi, *Chem. Sci.*, 2021, **12**, 7902–7907; (e) G. D. Kumar, M. Banasiewicz, A. Wrzosek, R. P. Kampa, M. H. E. Bousquet, D. Kusy, A. Szewczyk and D. T. Gryko, *Chem. Commun.*, 2022, **58**, 4500–4503.
- 23 (a) W. Yang, P. S. Chan, M. S. Chan, K. F. Li, P. K. Lo, N. K. Mak, K. W. Cheah and M. S. Wong, *Chem. Commun.*, 2013, **49**, 3428–3430; (b) M. Grzybowski, E. Glodkowska-Mrowka, V. Hugues, W. Brutkowski, M. Blanchard-Desce and D. T. Gryko, *Chem. – Eur. J.*, 2015, **21**, 9101–9110; (c) S. Samanta, Y. He, A. Sharma, J. Kim, W. Pan, Z. Yang, J. Li, W. Yan, L. Liu, J. Qu and J. S. Kim, *Chem*, 2019, **5**, 1697–1726.
- 24 W. Chi, J. Chen, W. Liu, C. Wang, Q. Qi, Q. Qiao, T. M. Tan, K. Xiong, X. Liu, K. Kang, Y.-T. Chang, Z. Xu and X. Liu, *J. Am. Chem. Soc.*, 2020, **142**, 6777–6785.
- 25 F. Ulatowski, K. Dąbrowa, T. Bałakier and J. Jurczak, *J. Org. Chem.*, 2016, **81**, 1746–1756.
- 26 H. A. Benesi and J. H. Hildebrand, *J. Am. Chem. Soc.*, 1949, **71**, 2703.
- 27 S. Sumalekshmy, M. M. Henary, N. Siegel, P. V. Lawson, Y. Wu, K. Schmidt, J.-L. Bredas, J. W. Perry and C. J. Fahrni, *J. Am. Chem. Soc.*, 2007, **129**, 11888–11889.
- 28 T. Le Bahers, C. Adamo and I. Ciofini, *J. Chem. Theory Comput.*, 2011, **7**, 2498–2506.
- 29 J. Frisch, *et al.*, *Gaussian 16, Revision A.0.3*, Gaussian, Inc., Wallingford CT, 2016.
- 30 J. Tomasi, B. Mennucci and R. Cammi, *Chem. Rev.*, 2005, **105**, 2999–3093.
- 31 Y. Zhao and D. G. Truhlar, *Theor. Chem. Acc.*, 2008, **120**, 215–241.
- 32 C. A. Guido, A. Chrayteh, G. Scalmani, B. Mennucci and D. Jacquemin, *J. Chem. Theory Comput.*, 2021, **17**, 5155–5164.

Supporting Information

A sensitive zinc probe operating via enhancement of excited-state intramolecular charge transfer

G. Dinesh Kumar,^a Marzena Banasiewicz,^b Antoni Wrzosek,^c Omar O'Mari,^d Monika Zochowska,^c Valentine I. Vullev,^{*d} Denis Jacquemin,^{*e} Adam Szewczyk,^{*c} and Daniel T. Gryko^{*a}

^a Institute of Organic Chemistry, Polish Academy of Sciences, Kasprzaka 44/52, 01-224 Warsaw, Poland. E-mail: dtgryko@icho.edu.pl

^b Institute of Physics, Polish Academy of Sciences, Al. Lotników 32/46, 02-668 Warsaw, Poland.

^c Nencki Institute of Experimental Biology of Polish Academy of Sciences, Pasteur 3, 02-093 Warsaw, Poland. E-mail: a.szewczyk@nencki.gov.pl.

^d Department of Bioengineering, University of California, Riverside, 900 University Ave., Riverside, CA 92521, USA. Email: vullev@ucr.edu

^e CEISAM UMR 6230, CNRS, Université de Nantes, 44000 Nantes, France. E-mail: denis.Jacquemin@univ-nantes.fr

Table of contents

Section S1	General Information.....S2
Section S2	Experimental procedure.....S3
Section S3	Absorption and emission spectra.....S10
Section S4	Water solubility & binding constantsS40
Section S5	Imaging.....S42
Section S6	Theoretical calculations.....S43
Section S7	¹H & ¹³C- NMR and MS spectra.....S45
Section S8	References.....S73

Section S1: General Information

All reagents and solvents were purchased from commercial sources and were used as received unless otherwise noted. Reagent grade solvents (CH_2Cl_2 , hexanes) were distilled prior to use. Transformations with moisture- and oxygen-sensitive compounds were performed under a stream of argon. The reaction progress was monitored by means of thin-layer chromatography (TLC), which was performed on Kieselgel 60. The identity and purity of prepared compounds were proved by ^1H NMR and ^{13}C NMR as well as by mass spectrometry (via EI-MS or ESI-MS). HRMS (ESI-TOF) and HRMS (EI): double-focusing magnetic sector instruments with EBE geometry were utilized. NMR spectra were measured on 400 or 500 or 600 MHz instruments. Chemical shifts (δ , ppm) were determined with tetramethylsilane (TMS) as the internal reference; J values are given in Hz. All melting points for crystalline products were measured with an automated melting point apparatus and are given without correction.

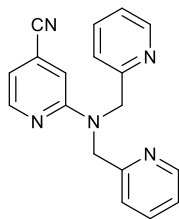
UV/Vis absorption spectra were recorded on a PerkinElmer Lambda 35 Spectrometer. Fluorescence spectra were recorded on a FLS1000 of Edinburgh Instruments. All linear optical studies were performed with freshly prepared air-equilibrated solutions at room temperature (298 K). Acetonitrile was spectrophotometric grade and was used without further purification. Quartz cells (10 mm) were used for the measurements of absorption and emission spectra. As a standard, Rh6G ($\Phi_{\text{fl}} = 0.94$ in EtOH) was used to determine fluorescence quantum yields.

Section S2: Experimental Procedure

All reagents and solvents were purchased from commercial sources and were used as received unless otherwise noted. Reagent grade solvents (DCM, hexanes) were distilled prior to use. Transformations with moisture- and oxygen-sensitive compounds were performed under a stream of argon. The reaction progress was monitored by means of thin-layer chromatography (TLC), which was performed on Kieselgel 60. The identity and purity of prepared compounds were proved by ^1H NMR and ^{13}C NMR as well as by mass spectrometry (via EI-MS or ESI-MS). HRMS (ESI-TOF) and HRMS (EI): double-focusing magnetic sector instruments with EBE geometry were utilized. NMR spectra were measured on 400 or 500 or 600 MHz instruments. Chemical shifts (δ , ppm) were determined with tetramethylsilane (TMS) as the internal reference; J values are given in Hz. All melting points for crystalline products were measured with an automated melting point apparatus and are given without correction. Pyrrolidone **1** was obtained following the literature procedure.¹

Synthesis of nitriles:

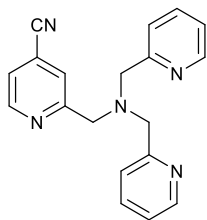
2-(bis(pyridin-2-ylmethyl)amino)isonicotinonitrile (**2a**)



2a

A mixture commercially available 2-fluoro-4-cyanopyridine (0.5 g, 4 mmol), di-(2-picolyl)amine (0.82 g, 4 mmol) in 5 ml of deoxygenated N,N-dimethylacetamide was heated to 130 °C under argon for overnight. Then reaction mixture was cooled to room temperature, diluted with water (100 mL) and extracted with EtOAc (2×100 mL). The organic phase dried over anhydrous Na_2SO_4 and filtered. The solvent was removed under reduced pressure and the resulting colorless oil was chromatographed on silica gel (hexane/EtOAc = 1: 1) to obtain desired product as colorless oil (1.06 g, 86%). ^1H NMR (500 MHz, CDCl_3) δ 8.56 (dd, J = 9.6 Hz, 2H), 8.27 (d, J = 11.2 Hz, 1H), 7.62 (dt, J = 3.4 Hz, 2H), 7.22-7.17 (m, 4H), 6.7 (dd, J = 8.0 Hz, 2H), 4.98 (s, 4H). ^{13}C NMR (126 MHz, CDCl_3) δ 158.2, 157.4, 149.6, 149.3, 136.8, 122.4, 121.4, 121.3, 117.4, 113.3, 108.5, 54.1. HRMS (ESI, m/z): $[\text{M}+\text{Na}]^+$ Calcd. for $\text{C}_{18}\text{H}_{15}\text{N}_5\text{Na}$: 324.3530; found, 324.3460.

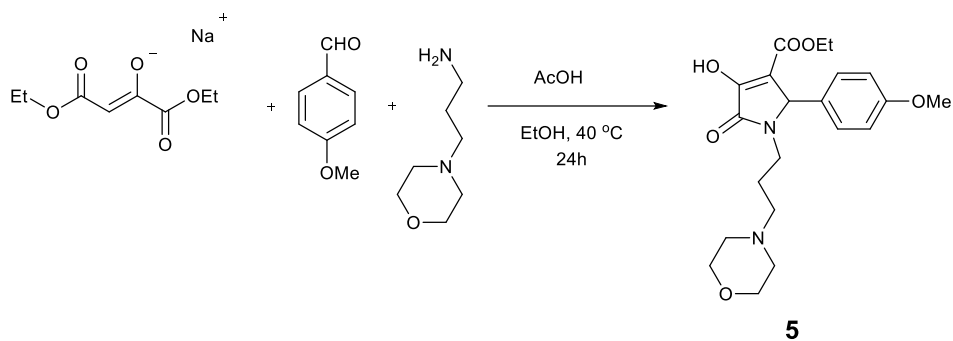
2-((bis(pyridin-2-ylmethyl)amino)methyl)isonicotinonitrile (**2b**)



2b

To a mixture of 2-Formylpyridine-4-carbonitrile (1 g, 7.5 mmol) and di-2-picolylamine (1.4 mL, 7.5 mmol) in 1,2-dichloroethane (20 mL), then $\text{NaBH}(\text{OAc})_3$ (2.1 g, 9.8 mmol) was added in portions. Then the reaction was stirred at room temperature for overnight, then reaction mixture was first acidified with 1N HCl to pH 4-5, followed by neutralized with 1N NaOH to pH 7-8. The organic phase was separated, and aqueous phase was extracted with DCM (2×100mL). The organic phases were combined and dried over Na_2SO_4 and the solvent was evaporated to give crude product which was purified by column chromatography using DCM/ CH_3OH (10:1) to obtain the desired product **2b** as a brown liquid (1.94 g, 82%). ^1H NMR (500 MHz, CDCl_3) δ 8.65 (d, $J = 5.1$ Hz, 1H), 8.52 (m, 2H), 7.85 (s, 1H), 7.65 (dt, $J = 7.6$ Hz, 2H), 7.49 (d, $J = 7.8$ Hz, 2H), 7.32 (dd, $J = 5.1$ Hz, 1H), 7.14 (m, 2H), 3.9 (s, 2H), 3.8(s, 4H). ^{13}C NMR (126 MHz, CDCl_3) δ 161.8, 158.6, 149.8, 149.3, 136.5, 124.6, 123.2, 123.1, 122.2, 120.1, 116.8, 60.5, 59.6. HRMS (ESI, m/z): $[\text{M}+\text{Na}]^+$ Calcd. for $\text{C}_{19}\text{H}_{17}\text{N}_5\text{Na}$: 338.1382; found, 338.1380.

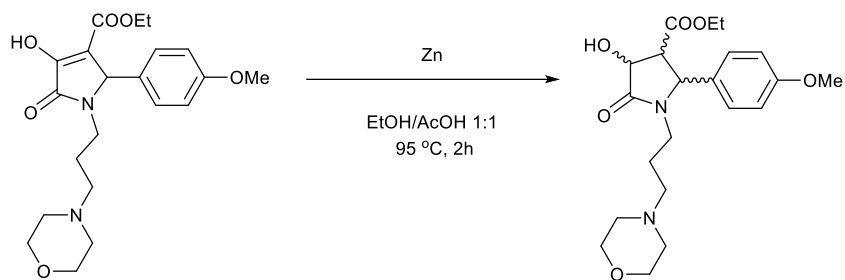
ethyl 4-hydroxy-2-(4-methoxyphenyl)-1-(3-morpholinopropyl)-5-oxo-2,5-dihydro-1H-pyrrole-3-carboxylate (5)



A 250 mL round bottom flask equipped with a magnetic stirring bar, was charged with ethanol (100 mL), 4-methoxy benzaldehyde (6.5 mL, 53 mmol) and (3-Aminopropyl)morpholine (7.8 mL, 53 mmol), reaction mixture was kept at room temperature, with constant stirring for 15 minutes. Next diethyl oxalacetate (10.0 g, 53 mmol) was added in one portion, followed by dropwise addition of acetic acid (6.1 mL, 106 mmol). Reaction mixture was heat up to 40 °C, and vigorously stirred overnight. Then reaction mixture was cooled to room temperature and diluted with water (200 mL), and extracted with DCM (200mL×2). Organic phase were dried over anhydrous Na_2SO_4 , filtered and concentrated in vacuo. Yellowish solid was recrystallized from EtOAc to obtain product **5** as white crystals (15.6 g, 72%); mp 171-172 °C. ^1H NMR (600 MHz, CDCl_3) δ 7.10 (d, $J = 8.6$ Hz, 2H), 6.86 (d, $J = 8.7$ Hz, 2H), 5.07 (s, 1H), 4.65 (bs, 2H), 4.14 (q, $J = 6.3$ Hz, 2H), 3.8 (s, 3H), 3.73-3.65 (m, 5H), 2.84-2.79 (m, 1H), 2.49 (s, 3H), 2.46-2.34 (m, 2H), 1.77 – 1.64 (m, 2H), 1.12 (t, $J = 7.1$ Hz, 3H); ^{13}C NMR (151 MHz, CDCl_3) δ 166.1, 165.1, 164.8, 159.8, 158.6, 128.9, 127.3, 114.1,

111.6, 66.4, 60.5, 55.7, 55.3, 53.2, 38.6, 24.4, 14.0. HRMS (ESI, m/z): $[M+H]^+$ Calcd. for $C_{21}H_{29}N_2O_6$: 405.2026; found, 405.2024.

ethyl 4-hydroxy-2-(4-methoxyphenyl)-1-(3-morpholinopropyl)-5-oxopyrrolidine-3-carboxylate (6)



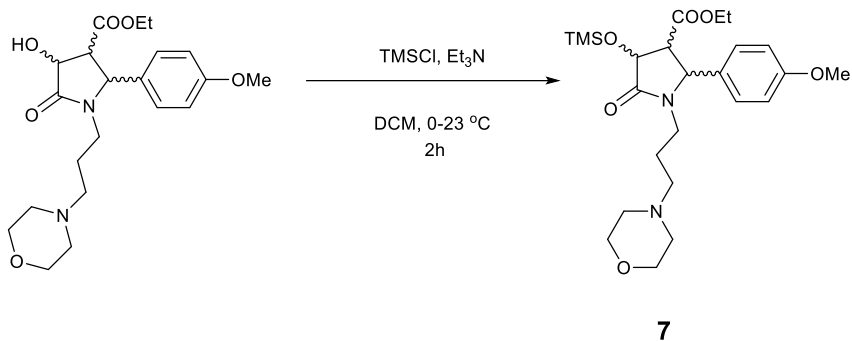
6

Compound **5** (15.0 g, 37.1 mmol) was dissolved in 150 mL mixture of EtOH/AcOH (1:1) and zinc powder (14.6 g, 222.5 mmol) was added and reaction mixture vigorously stirred at 95 °C for 1h. A second portion of zinc powder (14.6 g, 222.5 mmol) was added and stirring was continued at 95 °C until completion of the reaction. After cooling to room temperature reaction mixture was diluted with EtOAc (100 mL) the excess of zinc and the inorganic salts were filtered off. The filtrate was then diluted with water (150 mL). The aqueous layer was extracted with EtOAc (100 mL), and the combined organic phases were washed with saturated $NaHCO_3$ solution until neutral and finally dried over Na_2SO_4 , filtered and concentrated in vacuo to obtain liquid product **6** as mixture of diastereoisomers (10.8 g, 72%). Careful analysis of 1H NMR spectra of crude **6** showed the ratio 2:1 of major isomer **6** with the all-trans configuration in relation to the rest three minor compounds.

Crude compound (10.8 g, 31.9 mmol) was dissolved in dry EtOH (75 mL), freshly powdered K_2CO_3 (8.0 g, 79.7 mmol) was added in one portion. Reaction mixture was stirred at room temperature for 30 minutes. Next reaction mixture was diluted with EtOAc (100 mL) the excess of inorganic salts were filtered off. The filtrate was then washed with water (100 mL x 2), organic phase was dried over Na_2SO_4 , filtered and concentrated in vacuum to obtain yellowish liquid product (10.8 g, 99.5 %). 1H NMR spectra showed 10:1 ratio of major isomer **6a** with the all-trans configuration in relation to the rest two minor compounds.

1H NMR (500 MHz, $CDCl_3$) δ 7.22 (d, $J = 8.7$ Hz, 2H), 7.03 (bs, 4H), 6.91 (d, $J = 8.7$ Hz, 2H), 4.66 (dd, $J = 8.4, 7.9$ Hz, 2H), 4.14 (q, $J = 4.8$ Hz, 2H), 3.8 (s, 3H), 3.73-3.65 (m, 5H), 3.58-3.50 (m, 1H), 2.75-2.60 (m, 2H), 2.44 – 2.35 (m, 2H), 1.66-1.56 (m, 2H), 1.22 (t, $J = 7.1$ Hz, 3H); ^{13}C NMR (101 MHz, $CDCl_3$) δ 175.6, 173.5, 171.2, 160.0, 129.0, 114.4, 72.2, 65.9, 61.4, 60.9, 55.2, 52.6, 49.2, 38.7, 22.7, 21.4, 14.0. HRMS (ESI, m/z): $[M+H]^+$ Calcd. for $C_{21}H_{31}N_2O_6$: 407.2182; found, 407.2183.

ethyl 2-(4-methoxyphenyl)-1-(3-morpholinopropyl)-5-oxo-4-((trimethylsilyl)oxy)pyrrolidine-3-carboxylate (7)



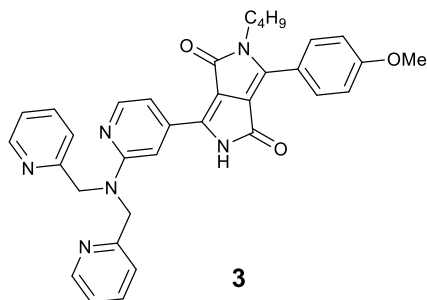
To cooled to ~ 0 °C solution of **6a** (7.0 g, 17.2 mmol) in dry DCM (100 mL), dry Et_3N (4.4 mL, 30.9 mmol) was added, next TMSCl (3.3 mL, 25.8 mmol) was added drop wise. After addition cooling bath was removed, and reaction mixture was allowed to reach room temperature and stirring was continued at room temperature for 1.5 h. Next reaction mixture was diluted with water (100 mL), phases were separated and organic phase was dried over anhydrous Na_2SO_4 , filtered and concentrated in vacuo gives brownish oil (6.8 g, 82%) of product **7** without chromatographic purification. ^1H NMR spectra showed 10:1 ratio of major isomer **7** with the all-trans configuration in relation to the rest two minor compounds, used for next reaction without further purification.

^1H NMR (600 MHz, CDCl_3) δ 7.13 (d, $J = 8.5$ Hz, 2H), 6.84 (d, $J = 8.7$ Hz, 2H), 4.55-4.49 (m, 2H), 4.10-4.06 (m, 2H), 3.75 (s, 3H), 3.56 (m, 6H), 2.91 (m, 1H), 2.62-2.58 (m, 1H), 2.22 (bs, 4H), 1.57-1.51 (m, 2H), 1.46-1.4 (m, 1H), 1.15 (t, $J = 7.2$ Hz, 3H), 0.15 (s, 9H). ^{13}C NMR (151 MHz, CDCl_3) δ 171.7, 171.6, 159.8, 129.7, 128.8, 114.3, 73.4, 66.8, 61.3, 60.5, 57.1, 55.9, 55.3, 53.5, 39.1, 23.5, 14.1, 1.9, 0.1. HRMS (ESI, m/z): $[\text{M}+\text{H}]^+$ Calcd. for $\text{C}_{24}\text{H}_{39}\text{N}_2\text{O}_6\text{Si}$: 479.2577; found, 479.2588.

General procedure for the synthesis of DPP derivatives

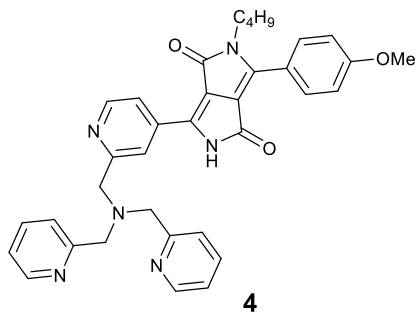
In flame dried Schlenk flask, a mixture of appropriate nitrile (1 eq.) and lithium *tert*-butoxide (4 eq.) was heated to 110 °C under argon. To this solid mixture, *tert*-amyl alcohol (5 mL) was added in one portion followed by dropwise addition of pyrrolidone **1** or **7** (1 eq.) dissolved in dry toluene (3 mL). The resulting dark solution was left to stir at this temperature for overnight. After cooling to room temperature reaction mixture was diluted with water (100 mL) and extracted with DCM (100 mL), water phase was one more time washed with DCM (50 mL). The combined organic phases were dried over Na_2SO_4 , filtered and concentrated in vacuum. The resulting crude compound was chromatographed on silica gel (DCM/MeOH = 9: 1) and crystallization from DCM/*n*-hexanes allowed to obtain the desired DPP product.

6-(2-(bis(pyridin-2-ylmethyl)amino)pyridin-4-yl)-2-butyl-3-(4-methoxyphenyl)-2,5-dihydropyrrolo[3,4-c]pyrrole-1,4-dione (**3**)



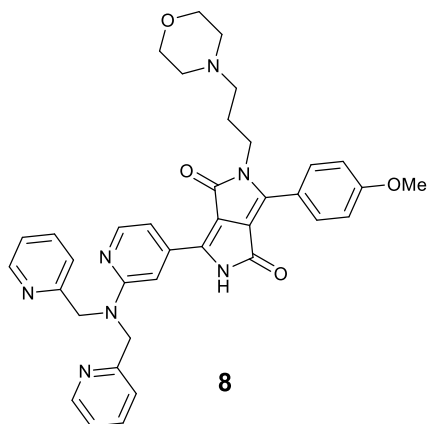
2-((bis(pyridin-2-ylmethyl)amino)isonicotinonitrile **2a** (1.5 g, 4.4 mmol), lithium *tert*-butoxide (1.42 g, 17.8mmol) and pyrrolidone **1** (1.82 g, 4.4 mmol) in combined solvent were used to obtain **3** as shiny red crystals (0.4 g, 21%); mp 217 °C. ¹H NMR (500 MHz, CDCl₃) δ 10.01 (s, 1H), 8.52 (s, 2H), 8.26 (d, *J* = 4.8 Hz, 1H), 7.80 (d, *J* = 7.8 Hz, 2H), 7.59-7.49 (m, 4H), 7.27 (s, 2H), 7.18 (s, 2H), 6.98 (d, *J* = 8.2 Hz, 2H), 5.03 (s, 4H), 3.82 (s, 3H), 3.77 (t, *J* = 7.5 Hz, 2H), 2.66 (br s, 2H), 1.57 (t, *J* = 6.8 Hz, 2H), 1.28 (q, *J* = 7.3 Hz, 2H), 0.87 (t, *J* = 7.3 Hz, 3H). ¹³C NMR (126 MHz, CDCl₃) δ 162.8, 162.7, 162.2, 158.7, 158.1, 150.3, 149.0, 148.9, 141.7, 136.9, 136.0, 130.9, 122.2, 121.7, 120.1, 114.4, 112.0, 110.1, 110.0, 103.3, 55.4, 53.6, 42.0, 31.4, 19.9, 13.6. HRMS (ESI, *m/z*): [M+H]⁺ Calcd. for C₃₄H₃₃N₆O₃: 573.2614; found, 573.2628.

6-((bis(pyridin-2-ylmethyl)amino)methyl)pyridin-4-yl)-2-butyl-3-(4-methoxyphenyl)-2,5-dihydropyrrolo[3,4-c]pyrrole-1,4-dione (4**)**



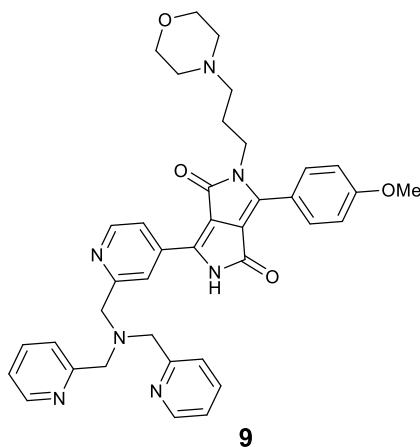
2-((bis(pyridin-2-ylmethyl)amino)methyl)isonicotinonitrile **2b** (0.5 g, 1.6 mmol), lithium *tert*-butoxide (0.5 g, 6.3 mmol) and pyrrolidone **1** (0.65 g, 1.6 mmol) in combined solvent were used to obtain **4** as shiny red crystals (0.19 g, 21%); mp 204 °C. ¹H NMR (600 MHz, CDCl₃) δ 10.3 (s, 1H), 8.99 (s, 1H), 8.78 (d, *J* = 4.0 Hz, 2H), 8.68 (d, *J* = 5.2 Hz, 1H), 8.40 (d, *J* = 4.3 Hz, 1H), 7.9 (d, *J* = 8.9 Hz, 2H), 7.59 (dt, *J* = 7.7 Hz, 2H), 7.41 (d, *J* = 7.7 Hz, 2H), 7.17 (dt, *J* = 5.7 Hz, 6.7 Hz, 2H), 7.09 (d, *J* = 8.8 Hz, 2H), 3.98 (s, 3H), 3.91 (d, *J* = 4.2 Hz, 6H), 3.87 (t, *J* = 7.8 Hz, 2H), 2.66 (br s, 1H), 1.67 (quint, *J* = 7.8 Hz, 2H), 1.33 (m, 2H), 0.91 (t, *J* = 7.0 Hz, 3H). ¹³C NMR (151 MHz, CDCl₃) δ 162.9, 162.4, 162.3, 160.9, 158.6, 150.5, 150.1, 149.5, 141.3, 136.6, 135.0, 130.9, 123.8, 122.5, 120.2, 119.9, 119.2, 114.5, 112.4, 110.3, 59.6, 59.4, 55.5, 42.1, 31.5, 20.0, 13.6. HRMS (ESI, *m/z*): [M+H]⁺ Calcd. for C₃₅H₃₅N₆O₃: 587.2757; found, 587.2781.

6-(2-(bis(pyridin-2-ylmethyl)amino)pyridin-4-yl)-3-(4-methoxyphenyl)-2-(3-morpholinopropyl)-2,5-dihydropyrrolo[3,4-c]pyrrole-1,4-dione (8)



2-(bis(pyridin-2-ylmethyl)amino)isonicotinonitrile **2a** (1.0 g, 3.3 mmol), lithium *tert*-butoxide (1.06 g, 13.2 mmol) and pyrrolidone **7** (1.58 g, 3.3 mmol) in combined solvent were used to obtain **8** as shiny red crystals (0.31 g, 15%); mp 230 °C. ¹H NMR (500 MHz, CDCl₃) δ 10.02 (s, 1H), 8.51 (d, *J* = 3.7 Hz, 2H), 8.29 (d, *J* = 5.2 Hz, 1H), 7.81 (d, *J* = 8.0 Hz, 2H), 7.57 (d, *J* = 7.2 Hz, 2H), 7.50 (d, *J* = 5.0 Hz, 2H), 7.23 (d, *J* = 7.7 Hz, 2H), 7.12 (d, *J* = 6.0 Hz, 2H), 6.98 (d, *J* = 8.5 Hz, 2H), 5.01 (s, 4H), 3.88 (d, *J* = 7.4 Hz, 2H), 3.81 (s, 3H), 3.58 (t, *J* = 4.0 Hz, 4H), 2.28 (bs, 6H), 1.75 (m, 2H). ¹³C NMR (126 MHz, CDCl₃) δ 162.8, 162.2, 159.0, 158.3, 150.0, 149.3, 149.2, 141.9, 136.6, 135.9, 130.9, 122.0, 121.4, 120.1, 114.4, 111.9, 110.1, 109.1, 103.1, 66.9, 59.9, 55.4, 53.6, 40.5, 26.9, 25.9. HRMS (ESI, *m/z*): [M+H]⁺ Calcd. for C₃₇H₃₈N₇O₄: 644.2985; found, 644.2988.

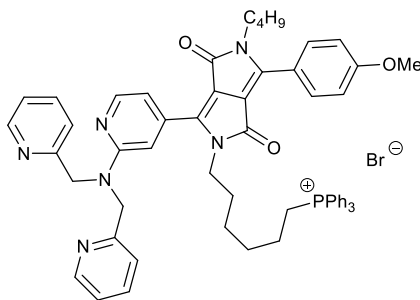
6-(2-((bis(pyridin-2-ylmethyl)amino)methyl)pyridin-4-yl)-3-(4-methoxyphenyl)-2-(3-morpholinopropyl)-2,5-dihydropyrrolo[3,4-c]pyrrole-1,4-dione (9)



2-((bis(pyridin-2-ylmethyl)amino)methyl)isonicotinonitrile **2b** (0.5 g, 1.6 mmol), lithium *tert*-butoxide (0.5 g, 6.3 mmol) and pyrrolidone **7** (0.76 g, 1.6 mmol) in combined solvent were used to obtain **9** as shiny red crystals (0.14 g, 14%); mp 194 °C. ¹H NMR (500 MHz, CDCl₃) δ 10.34 (s, 1H), 8.96 (s, 1H), 8.74 (d, *J* = 4.0 Hz, 2H), 8.66 (d, *J* = 5.0 Hz, 1H), 8.35 (d, *J* = 4.4 Hz, 1H), 7.88 (d, *J* = 8.9 Hz, 2H), 7.58 (td, *J* = 7.6,

2H), 7.40 (d, $J = 7.7$ Hz, 2H), 7.15 (td, $J = 5.5, 5.0, 6.6$ Hz, 2H), 7.03 (d, $J = 8.8$ Hz, 2H), 3.96 (m, 4H), 3.88 (d, $J = 7.9$ Hz, 7H), 3.61 (bs, 4H), 2.34 (bs, 6H), 1.84 (bs, 2H). ^{13}C NMR (126 MHz, CDCl_3) δ 162.9, 162.4, 162.3, 160.9, 158.6, 150.5, 149.9, 149.5, 141.5, 136.6, 134.9, 130.9, 123.8, 122.5, 120.1, 119.8, 119.3, 114.5, 112.3, 110.5, 66.7, 59.6, 59.4, 55.9, 55.5, 53.5, 45.8, 40.6, 25.9, 8.6. HRMS (ESI, m/z): $[\text{M}+\text{H}]^+$ Calcd. for $\text{C}_{38}\text{H}_{40}\text{N}_7\text{O}_4$: 658.3142; found, 658.3164.

Preparation of mitochondrial probe 10:



10

A suspension of DPP **3** (0.3 g, 0.52 mmol) and *t*-BuOK (0.15 g, 1.3 mmol) in dry NMP (10 mL) was stirred at 75 °C under argon atmosphere for 15 min. then 1,6-dibromohexane (0.25 mL, 1.6 mmol) was added and the mixture was stirred at 75 °C under argon for 3 h. After cooling to room temperature reaction mixture was diluted with water (100 mL) and extracted with DCM (100 mL), water phase was one more time washed with DCM (50 mL). The combined organic phases were dried over Na_2SO_4 , filtered and concentrated in vacuum. The product was purified by column chromatography over silica gel using a step gradient of MeOH in DCM as eluent (from 0% to 10%). Compound was obtained as an orange red semi solid (300 mg, 78%); HRMS (ESI, m/z): $[\text{M}+\text{Na}]^+$ Calcd. for $\text{C}_{40}\text{H}_{43}\text{BrN}_6\text{O}_3\text{Na}$: 757.2478; found, 757.2467.

Alkylated crude compound of **3** (300 mg, 0.41 mmol) and triphenylphosphine (1.06 g, 4.1 mmol) were added into a flask containing 5 mL of acetonitrile. The mixture was refluxed for 72 h. After removal of solvent in vacuo, the remaining solid was purified by column chromatography with gradient solvent from CH_2Cl_2 to $\text{CH}_2\text{Cl}_2/\text{MeOH}$ (v/v = 9/1). Compound **10** was obtained as orange-red crystals by recrystallization from diethyl ether (130 mg, 35%); mp 105 °C. ^1H NMR (600 MHz, CD_3CN): δ 8.9 (s, 2H), 8.8 (s, 1H), 8.35-8.26 (m, 4H), 8.03 (d, $J = 6.0$ Hz, 2H), 7.79-7.65 (m, 17H), 7.20 (d, $J = 9.6$ Hz, 2H), 6.99 (d, $J = 9.6$ Hz, 2H), 5.53 (s, 4H), 3.86 (s, 3H), 3.64 (t, $J = 7.8$ Hz, 4H), 3.4-3.2 (m, 6H), 1.39-1.27 (m, 8H), 0.88 (t, $J = 9.0$ Hz, 3H). ^{13}C NMR (126 MHz, CDCl_3) δ 162.2, 161.7, 158.6, 149.4, 148.7, 144.3, 137.0, 135.0, 133.7, 130.9, 130.3, 130.2, 122.2, 121.3, 118.8, 117.3, 114.3, 111.1, 108.2, 104.8, 65.3, 55.4, 54.5, 54.3, 41.2, 40.8, 31.0, 29.7, 28.5, 27.8, 25.2, 24.8, 21.9, 21.4, 19.5, 14.6, 12.9; HRMS (ESI, m/z): $[\text{M}+\text{H}]^+$ Calcd. for $\text{C}_{58}\text{H}_{58}\text{N}_6\text{O}_3\text{P}$: 917.4308; found, 917.4303.

Section S3: Absorption and emission spectra

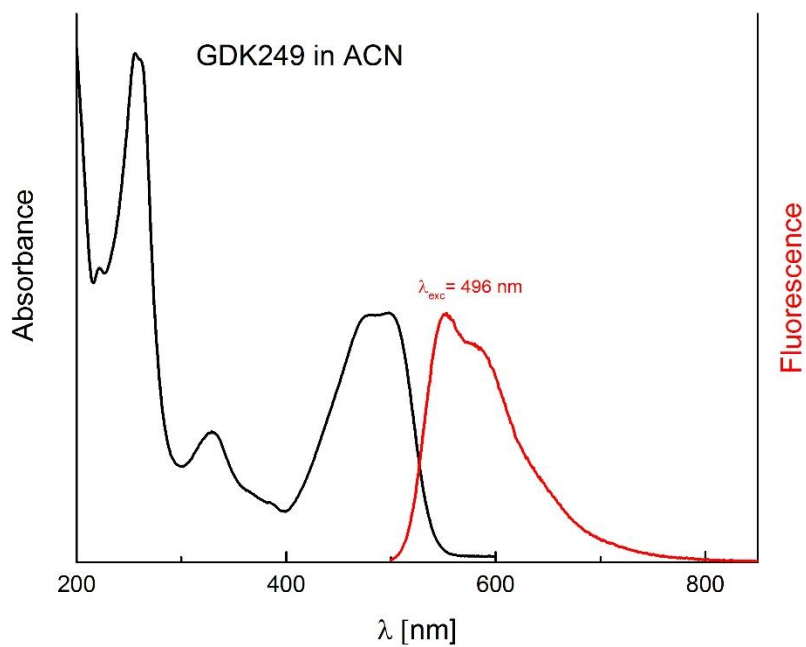


Fig. S1. The absorption and emission spectra of DPP 3 in CH_3CN .

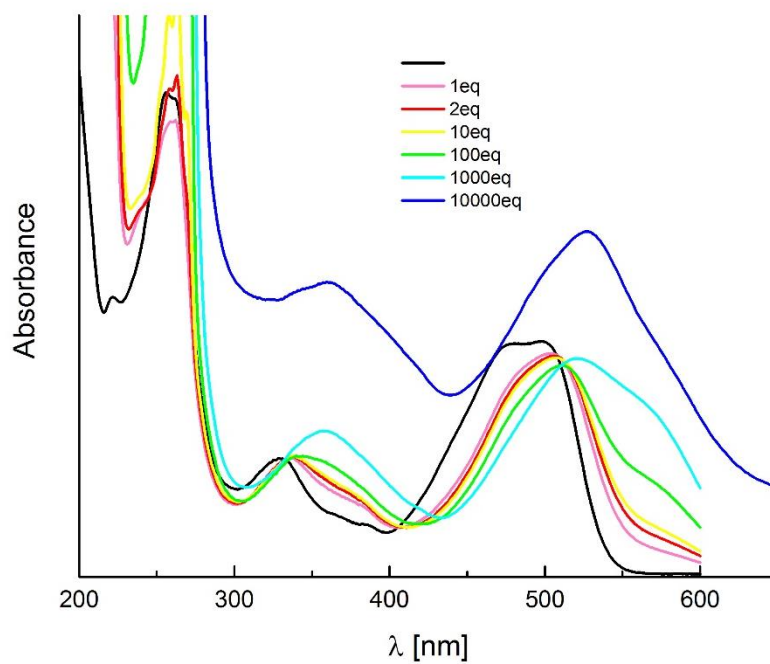


Fig. S2. The effect of PhSO_3H addition on the absorption spectra of DPP 3 measured in CH_3CN .

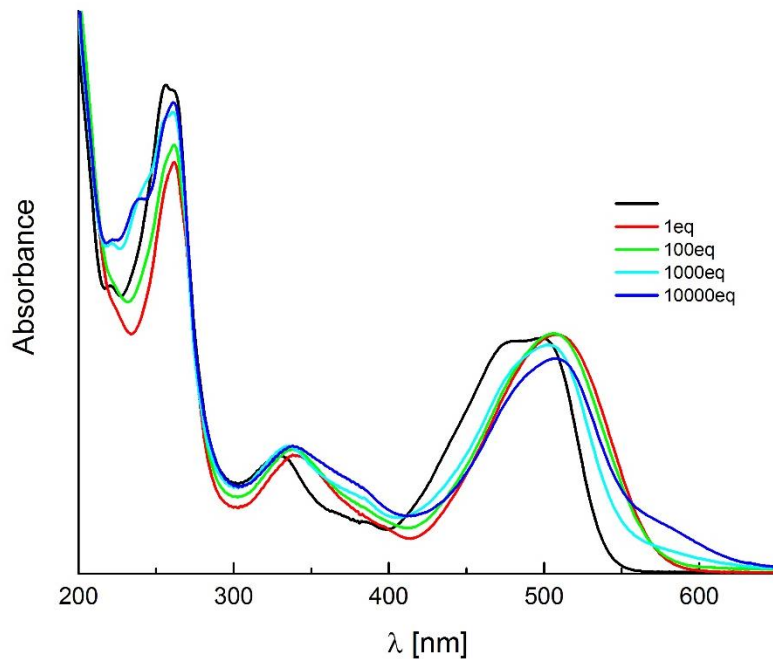


Fig. S3. The effect of cadmium perchlorate addition on the absorption spectra of DPP **3** measured in CH₃CN.

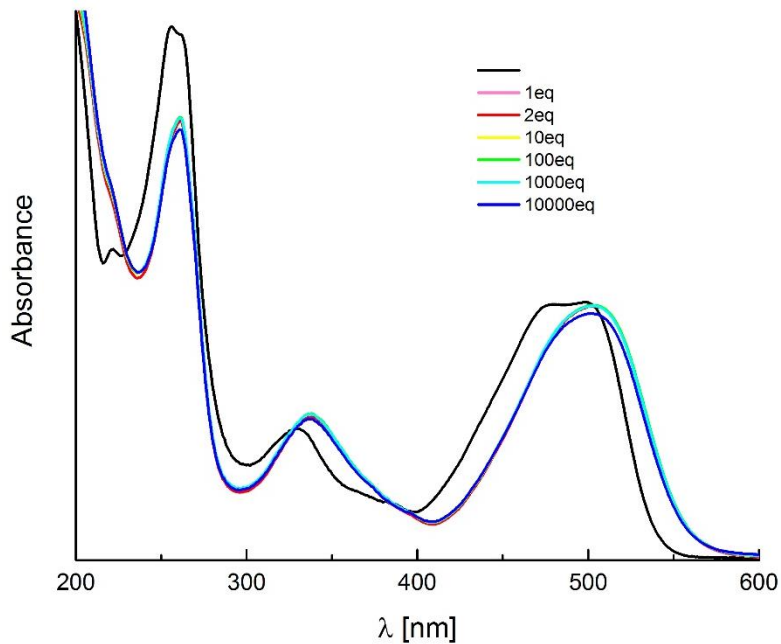


Fig. S4. The effect of zinc perchlorate addition on the absorption spectra of DPP **3** measured in CH₃CN.

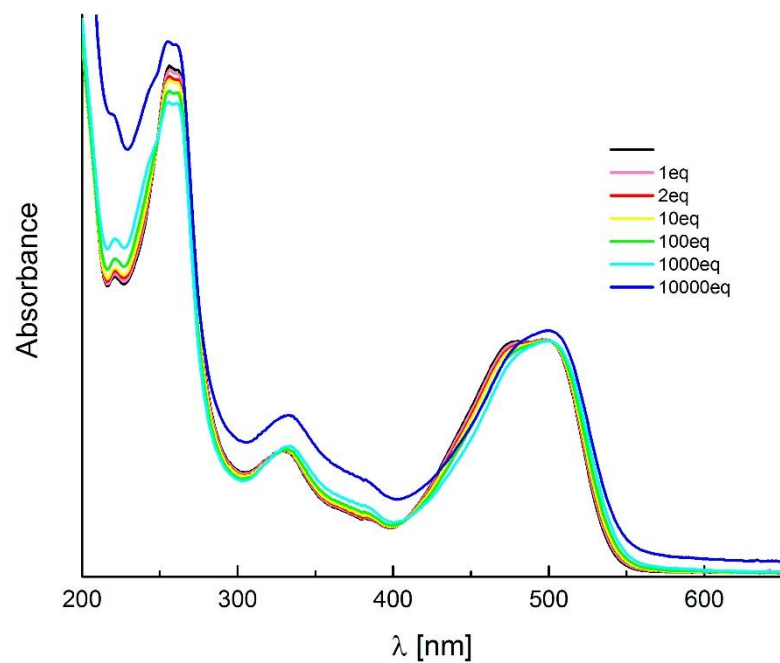


Fig. S5. The effect of magnesium perchlorate addition on the absorption spectra of DPP **3** measured in CH₃CN.

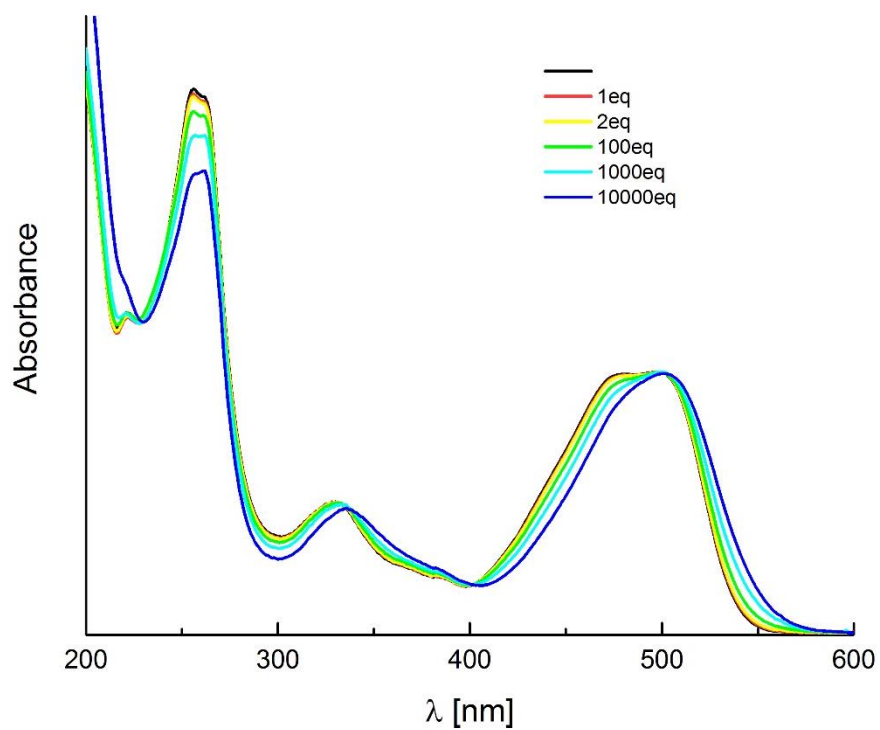


Fig. S6. The effect of calcium perchlorate addition on the absorption spectra of DPP **3** measured in CH₃CN.

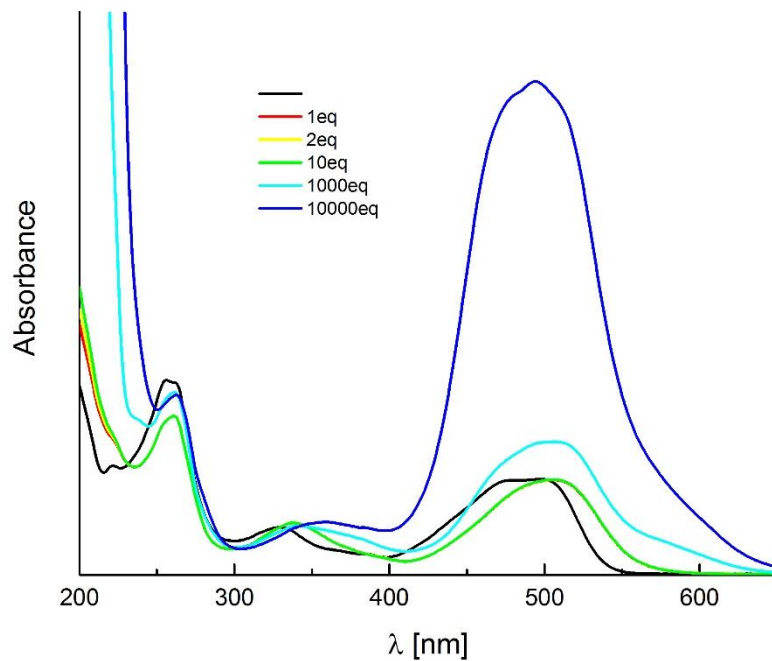


Fig. S7. The effect of cobalt perchlorate addition on the absorption spectra of DPP **3** measured in CH₃CN.

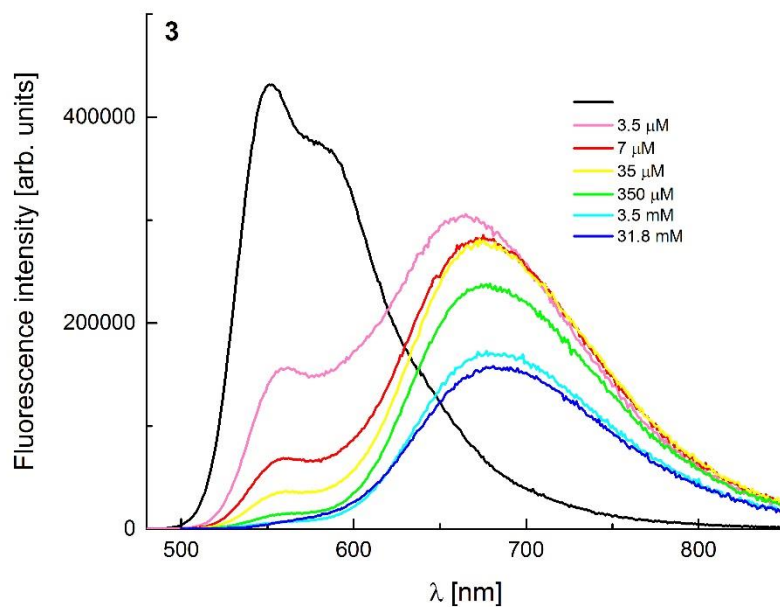


Fig. S8. The effect of PhSO₃H addition on the emission spectra of DPP **3** measured in CH₃CN.

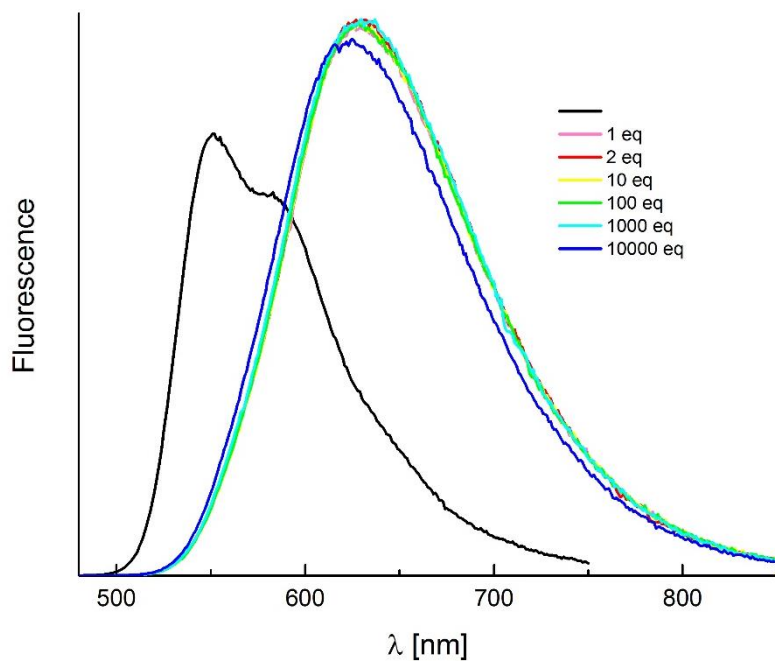


Fig. S9. The effect of zinc perchlorate addition on the emission spectra of DPP **3** measured in CH₃CN.

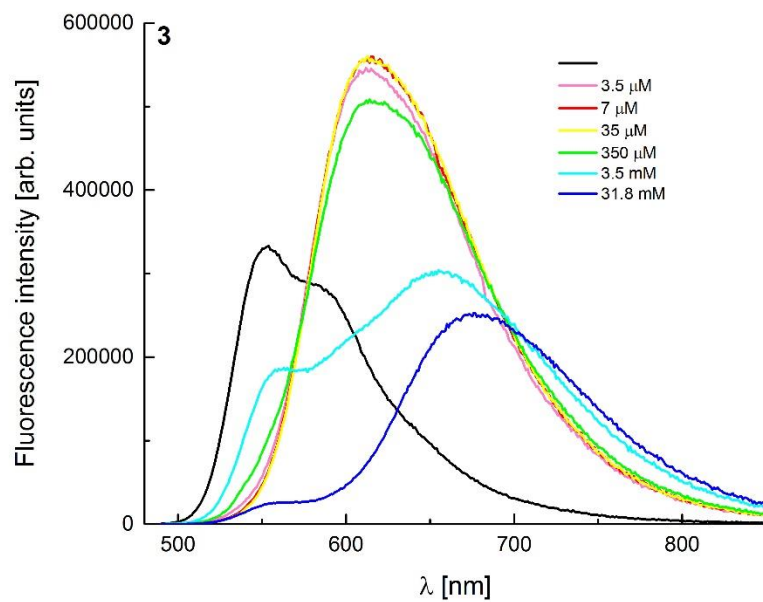


Fig. S10. The effect of cadmium perchlorate addition on the emission spectra of DPP **3** measured in CH₃CN.

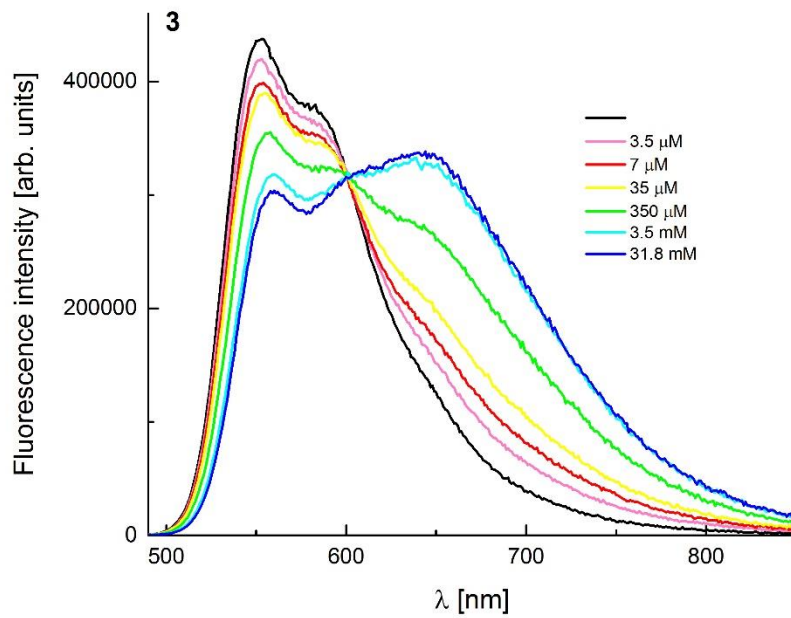


Fig. S11. The effect of magnesium perchlorate addition on the emission spectra of DPP 3 measured in CH_3CN .

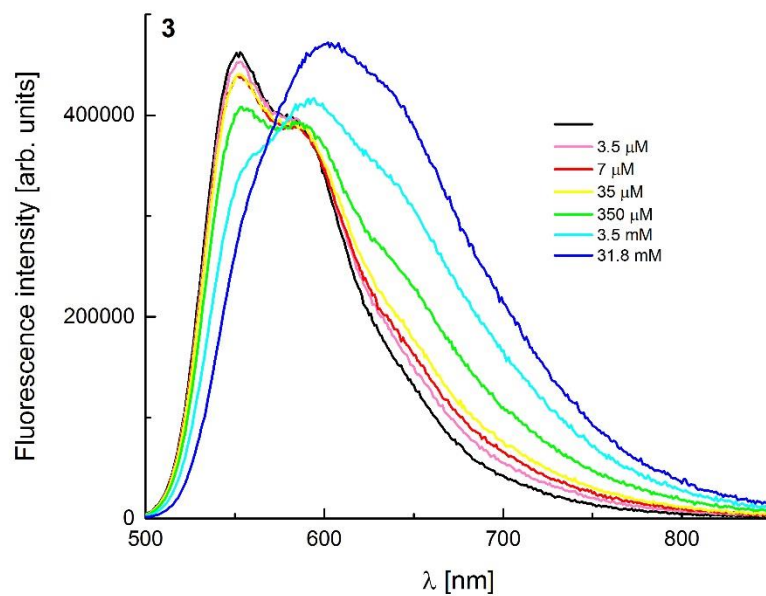


Fig. S12. The effect of calcium perchlorate addition on the emission spectra of DPP 3 measured in CH_3CN .

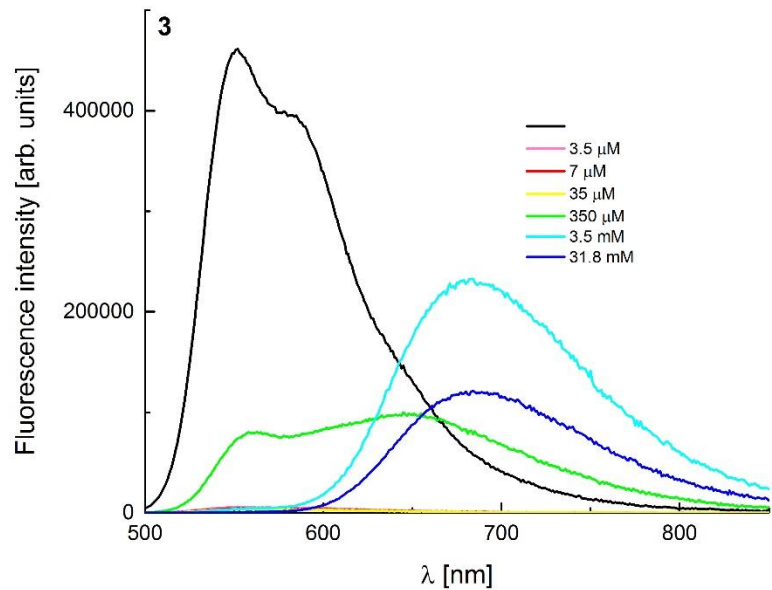


Fig. S13. The effect of cobalt perchlorate addition on the emission spectra of DPP 3 measured in CH₃CN.

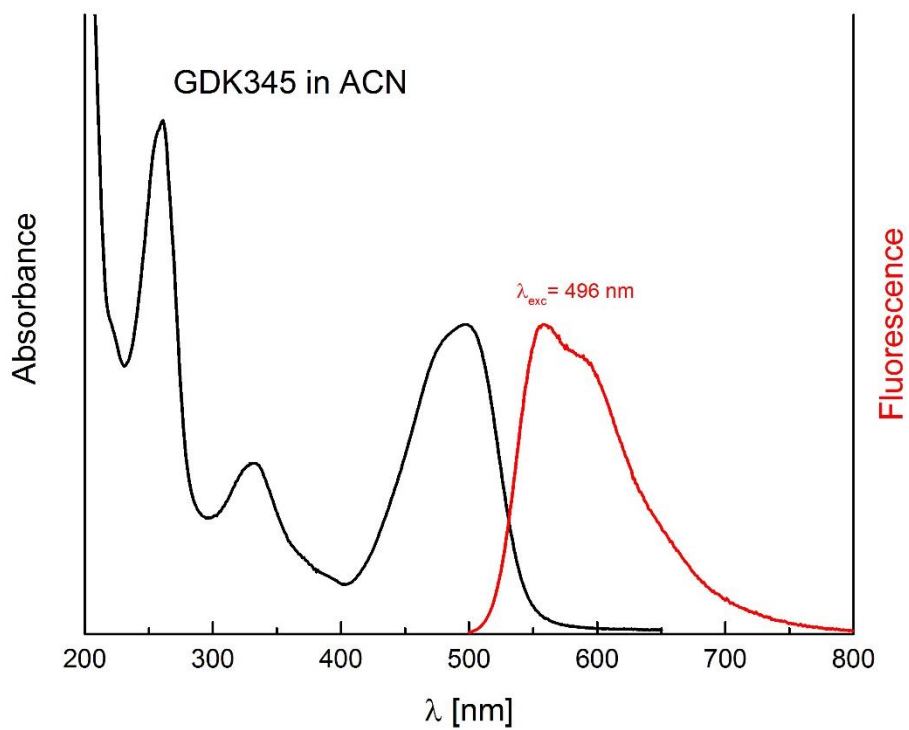


Fig. S14. The absorption and emission spectra of DPP 4 in CH₃CN.

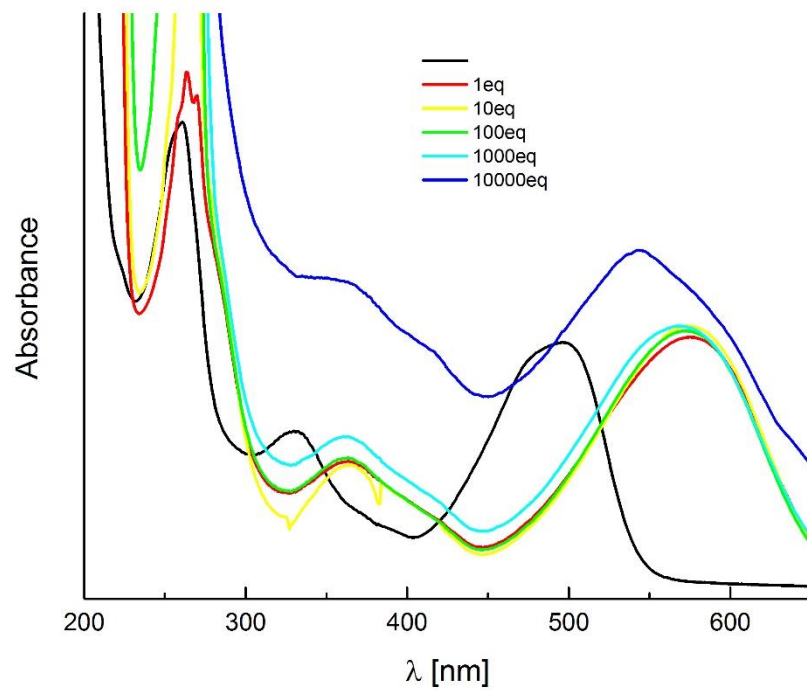


Fig. S15. The effect of PhSO₃H addition on the absorption spectra of DPP 4 measured in CH₃CN.

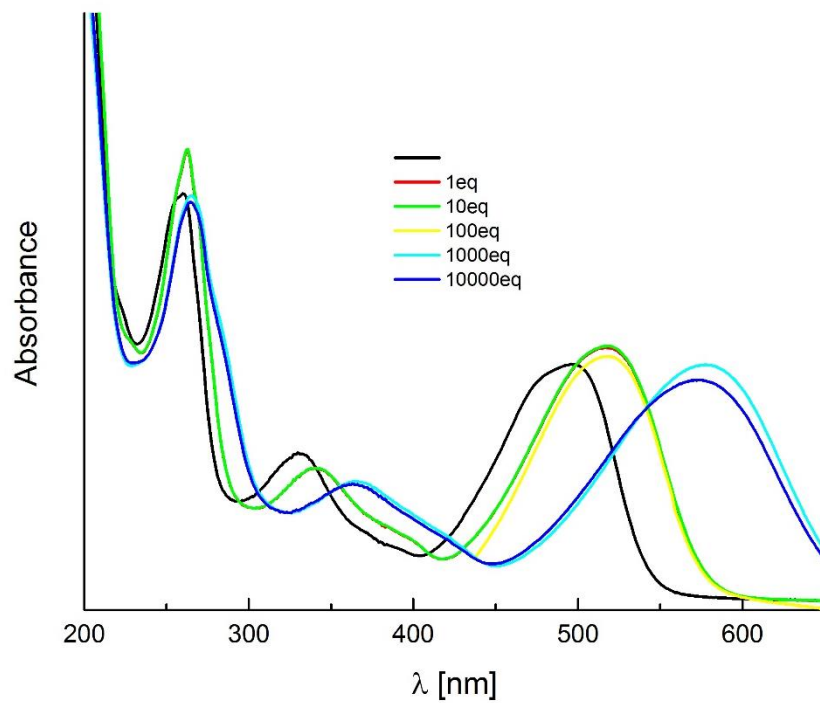


Fig. S16. The effect of cadmium perchlorate addition on the absorption spectra of DPP 4 measured in CH₃CN.

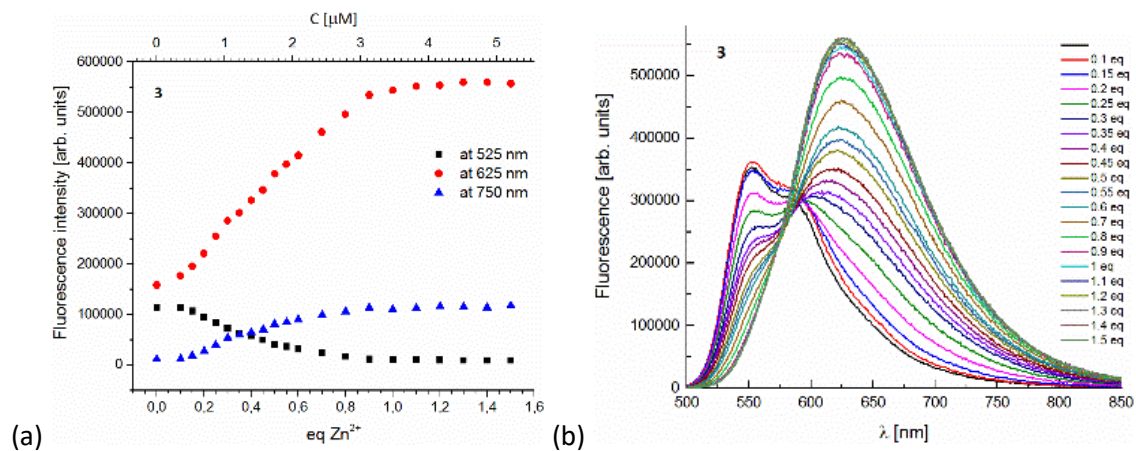


Fig S17. Fluorescence titration for compound 3. a: Titration curve; b: Fluorescence spectrum

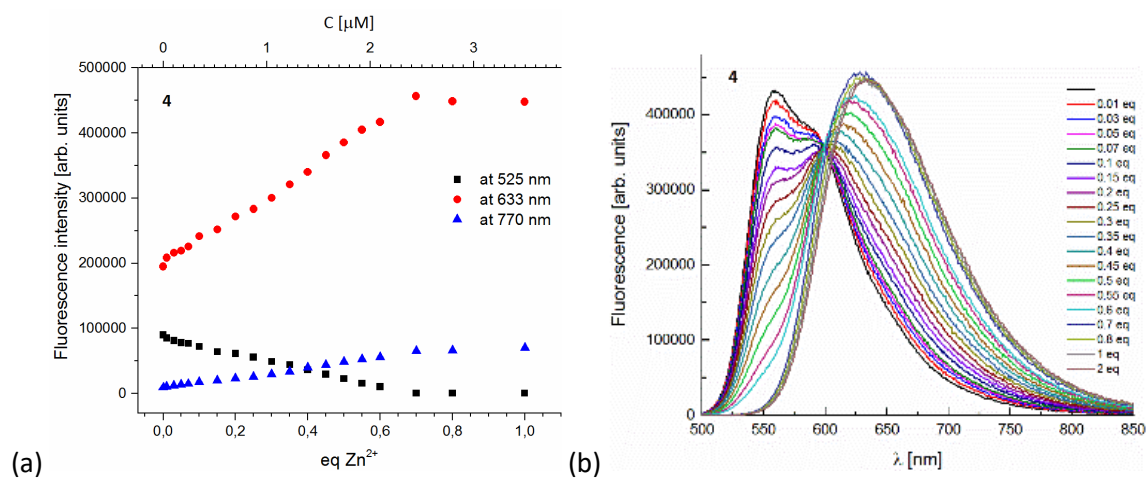


Fig S18. Fluorescence titration for compound 4. a: Titration curve; b: Fluorescence spectrum

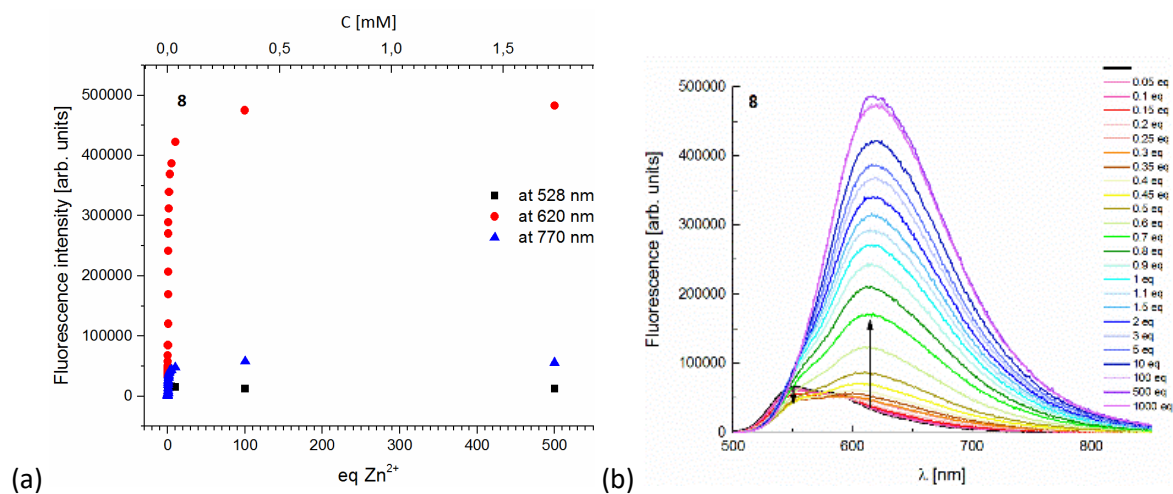


Fig S19. Fluorescence titration for compound 8. a: Titration curve; b: Fluorescence spectrum

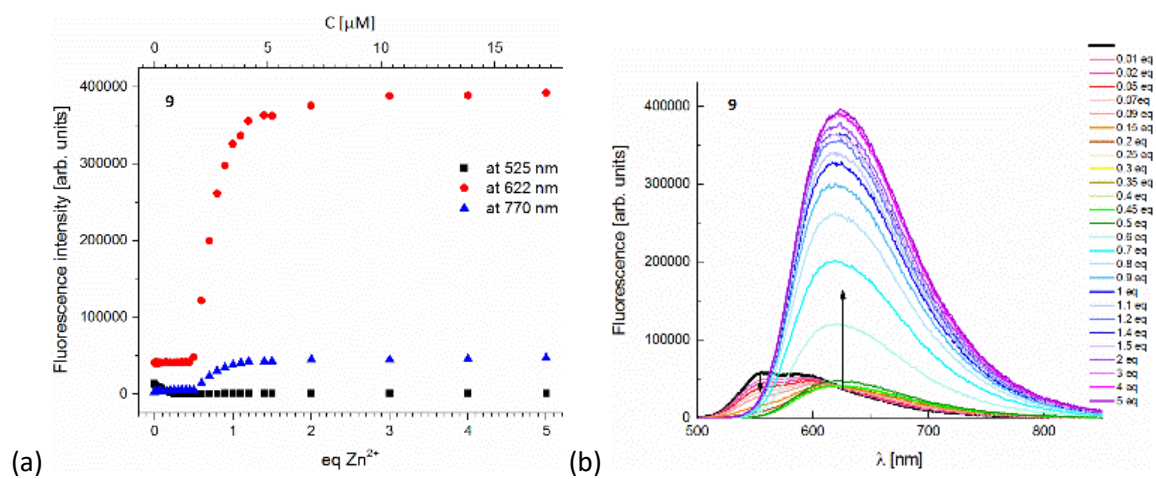


Fig S20. Fluorescence titration for compound **9**. a: Titration curve; b: Fluorescence spectrum

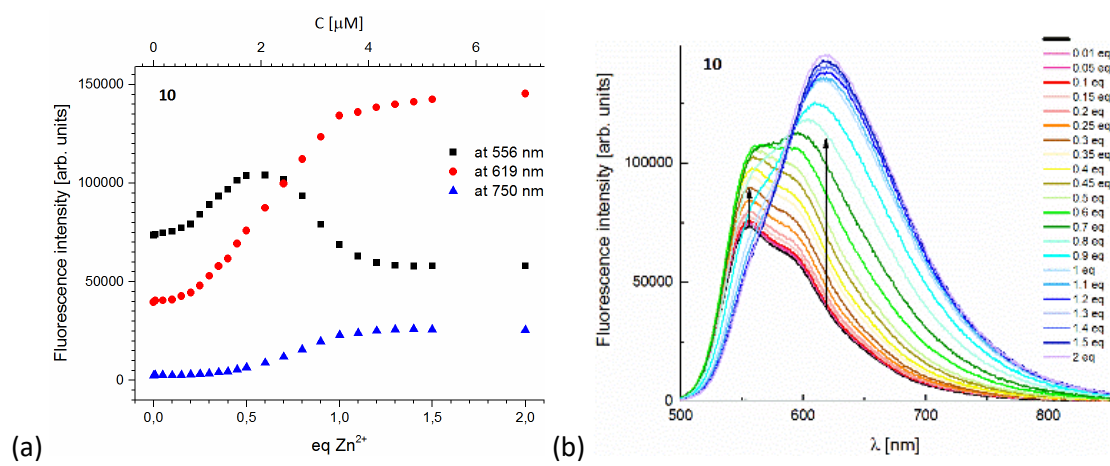


Fig S21. Fluorescence titration for compound **10**. a: Titration curve; b: Fluorescence spectrum

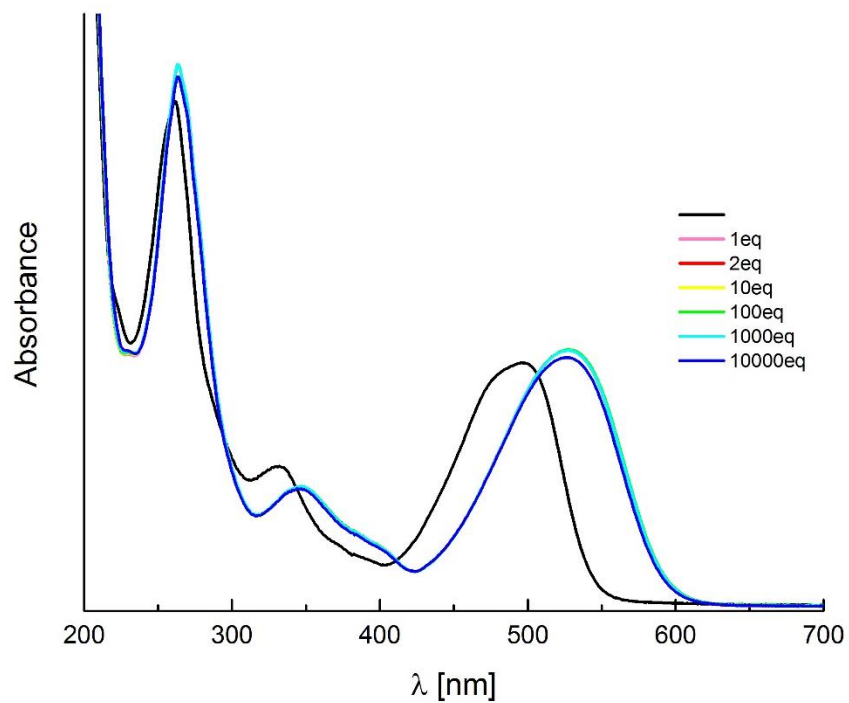


Fig. S22. The effect of zinc perchlorate addition on the absorption spectra of DPP 4 measured in CH₃CN.

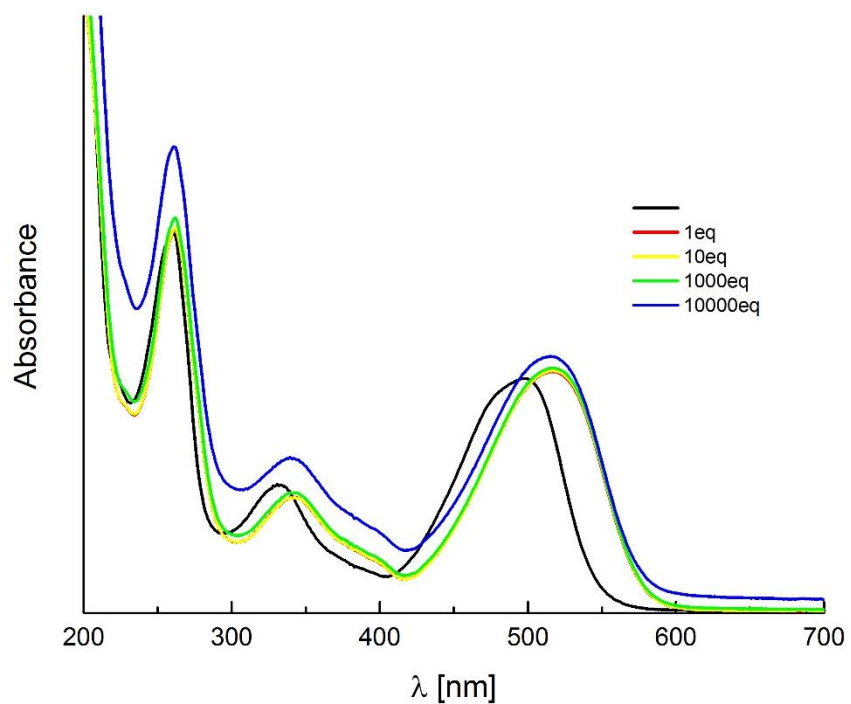


Fig. S23. The effect of magnesium perchlorate addition on the absorption spectra of DPP 4 measured in CH₃CN.

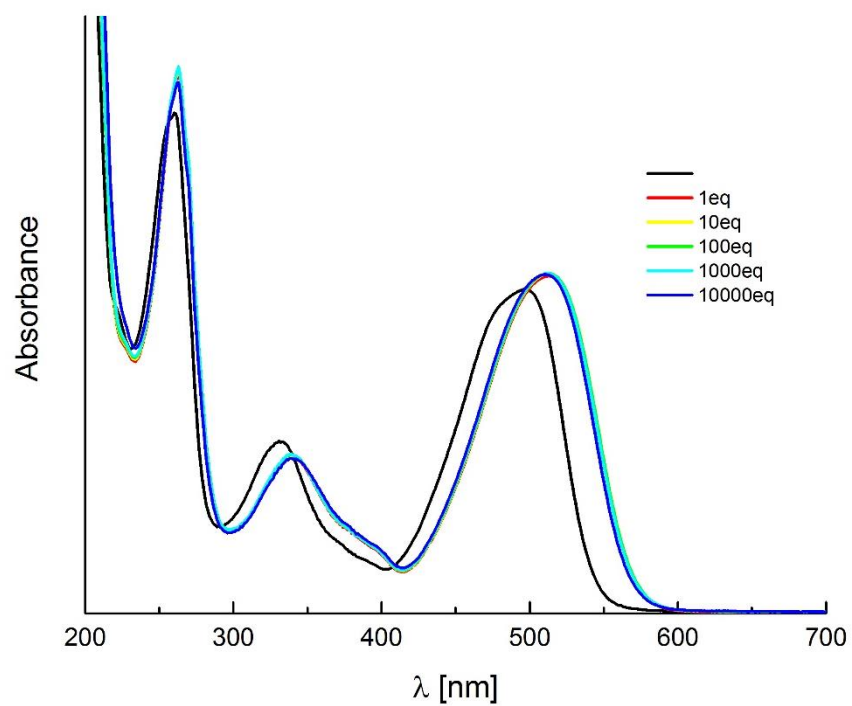


Fig. S24. The effect of calcium perchlorate addition on the absorption spectra of DPP 4 measured in CH₃CN.

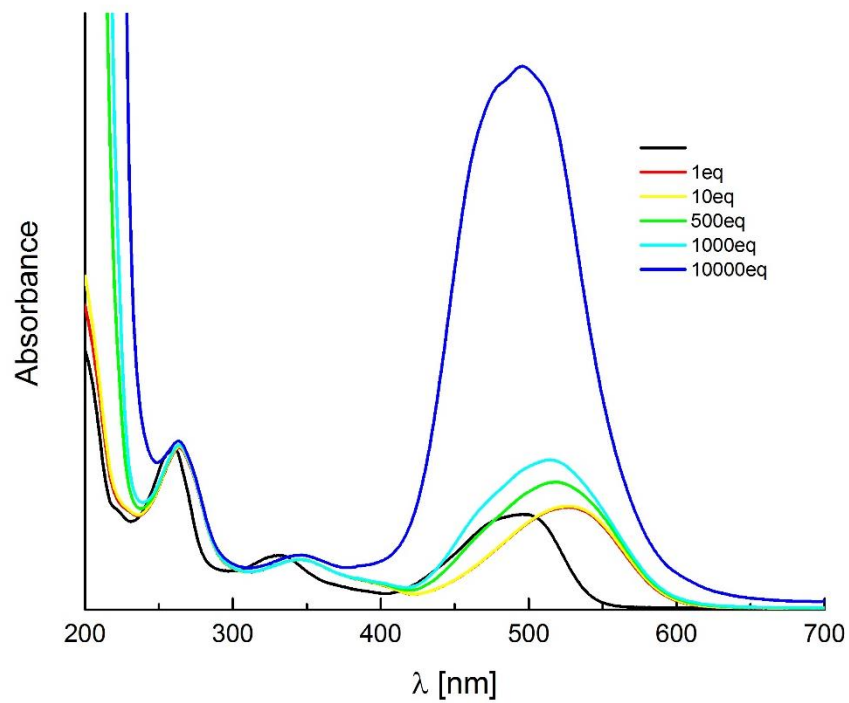


Fig. S25. The effect of cobalt perchlorate addition on the absorption spectra of DPP 4 measured in CH₃CN.

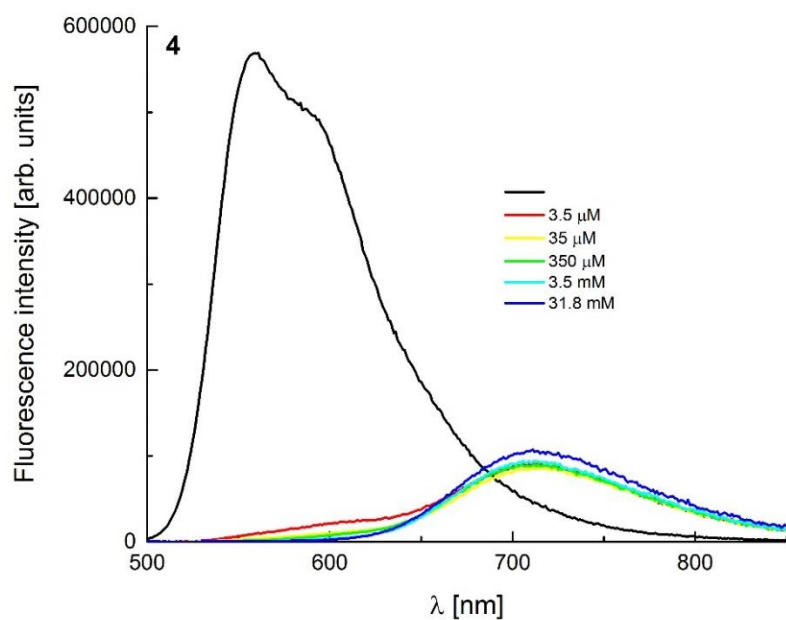


Fig. S26. The effect of PhSO₃H addition on the emission spectra of DPP 4 measured in CH₃CN.

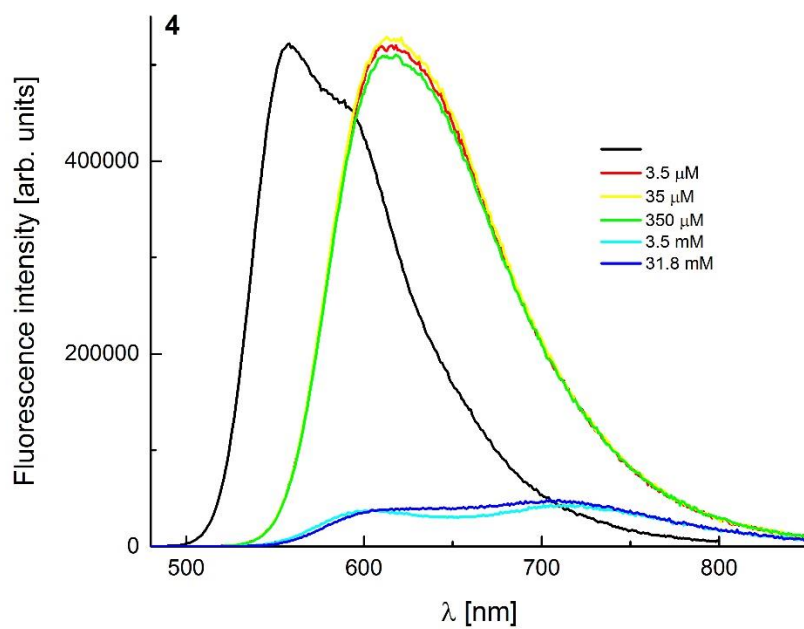


Fig. S27. The effect of cadmium perchlorate addition on the emission spectra of DPP 4 measured in CH₃CN.

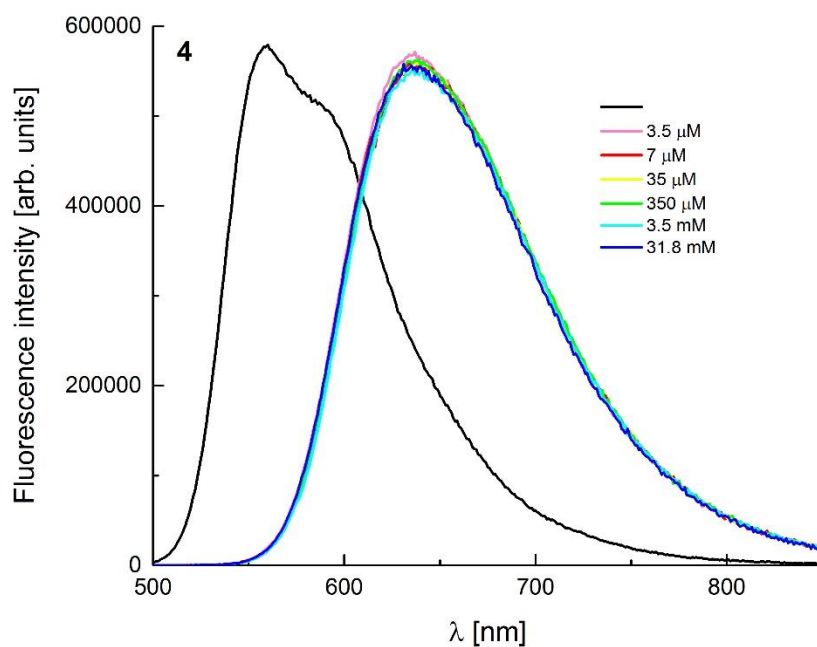


Fig. S28. The effect of zinc perchlorate addition on the emission spectra of DPP 4 measured in CH₃CN.

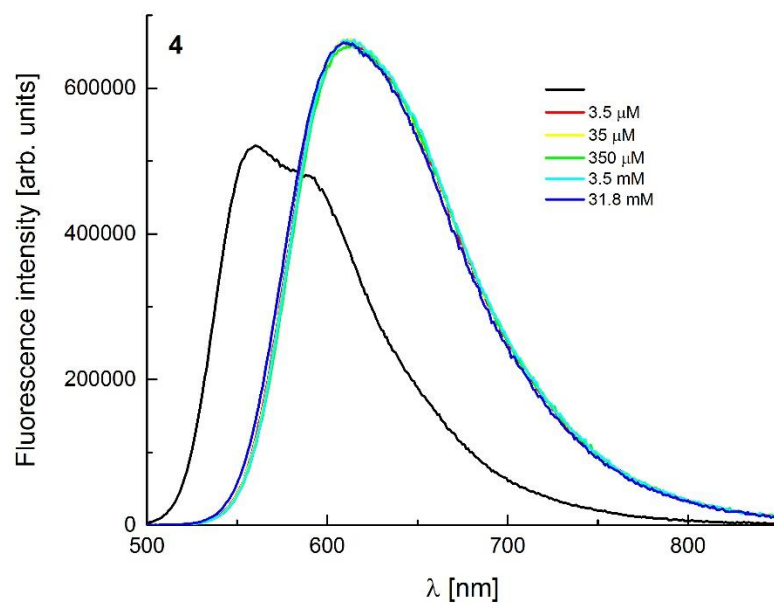


Fig. S29. The effect of magnesium perchlorate addition on the emission spectra of DPP 4 measured in CH₃CN.

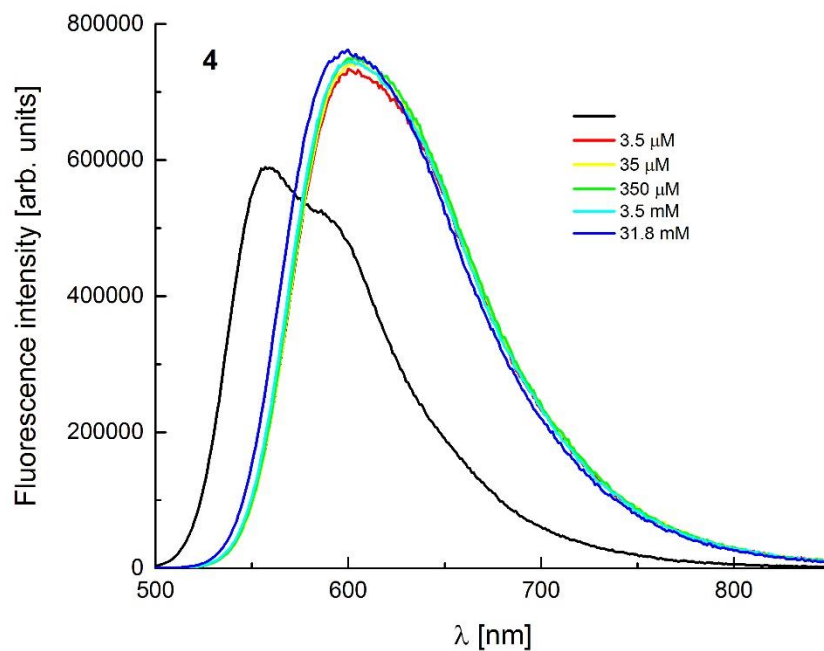


Fig. S30. The effect of calcium perchlorate addition on the emission spectra of DPP 4 measured in CH₃CN.

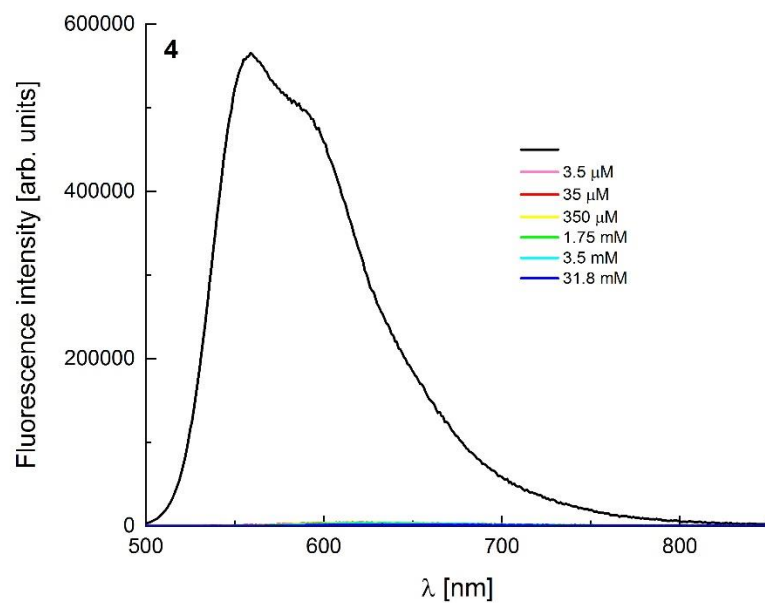


Fig. S31. The effect of cobalt perchlorate addition on the emission spectra of DPP 4 measured in CH₃CN.

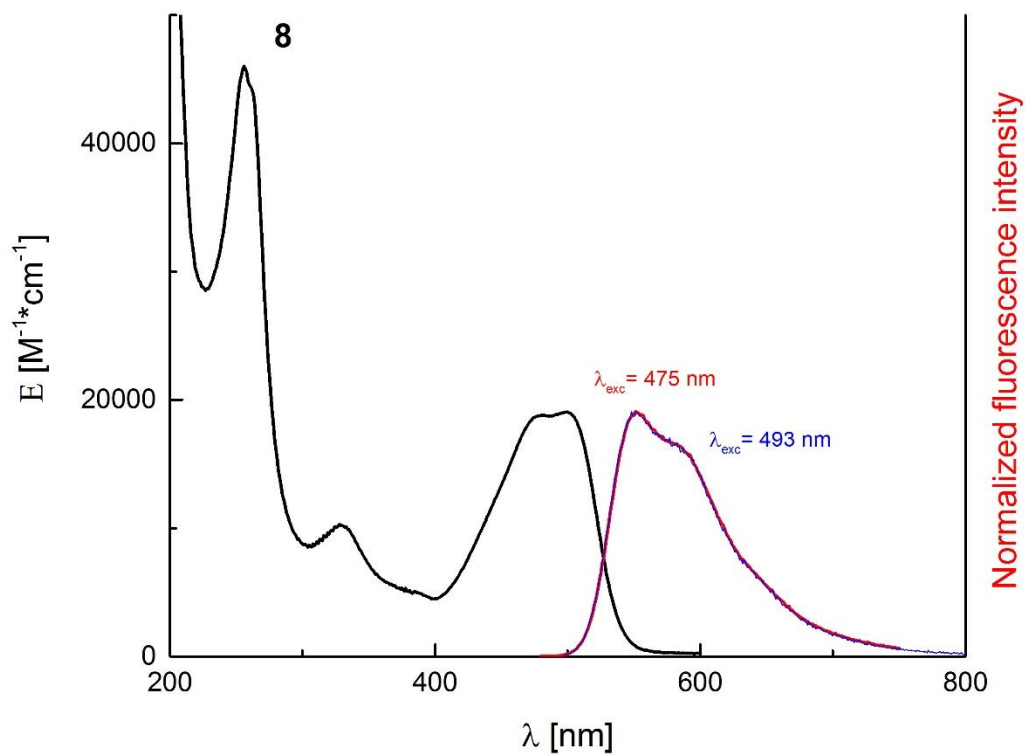


Fig. S32. The absorption and emission spectra of DPP **8** in CH₃CN.

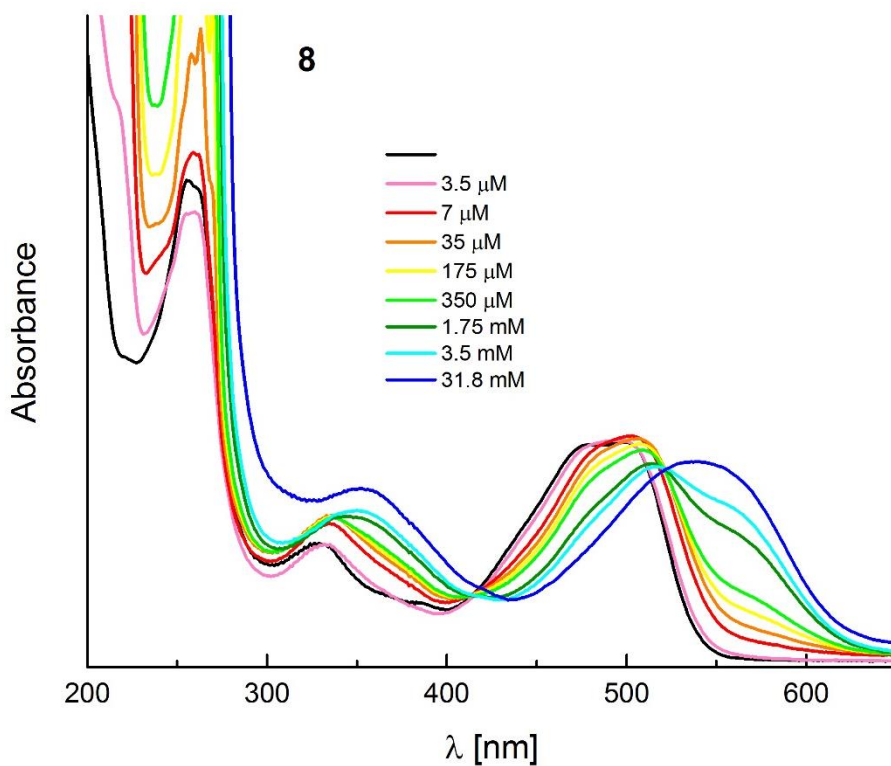


Fig. S33. The effect of PhSO₃H addition on the absorption spectra of DPP **8** measured in CH₃CN.

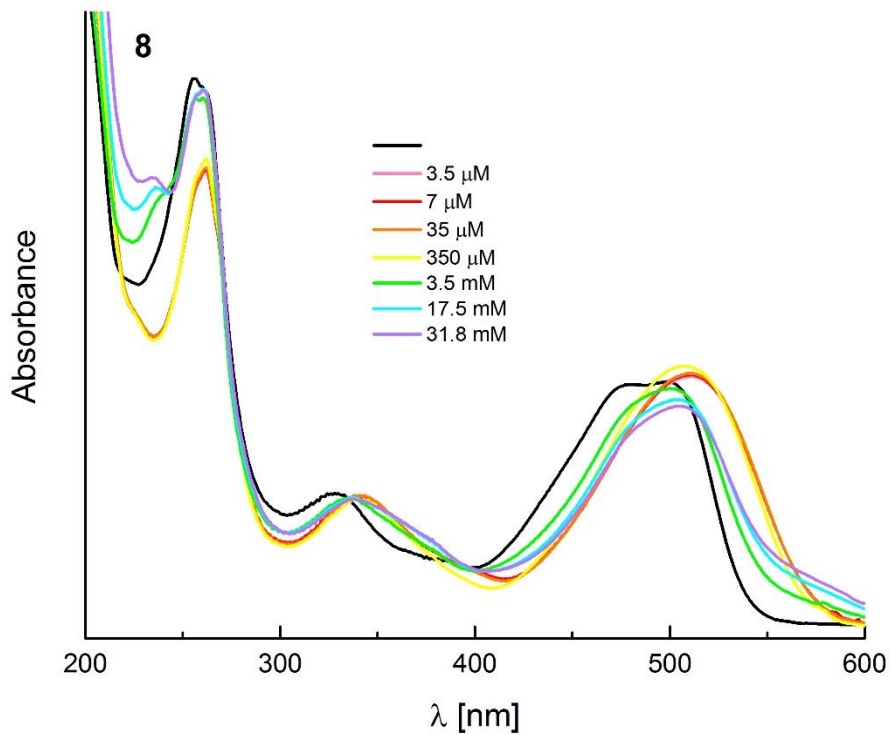


Fig. S34. The effect of cadmium perchlorate addition on the absorption spectra of DPP **8** measured in CH₃CN.

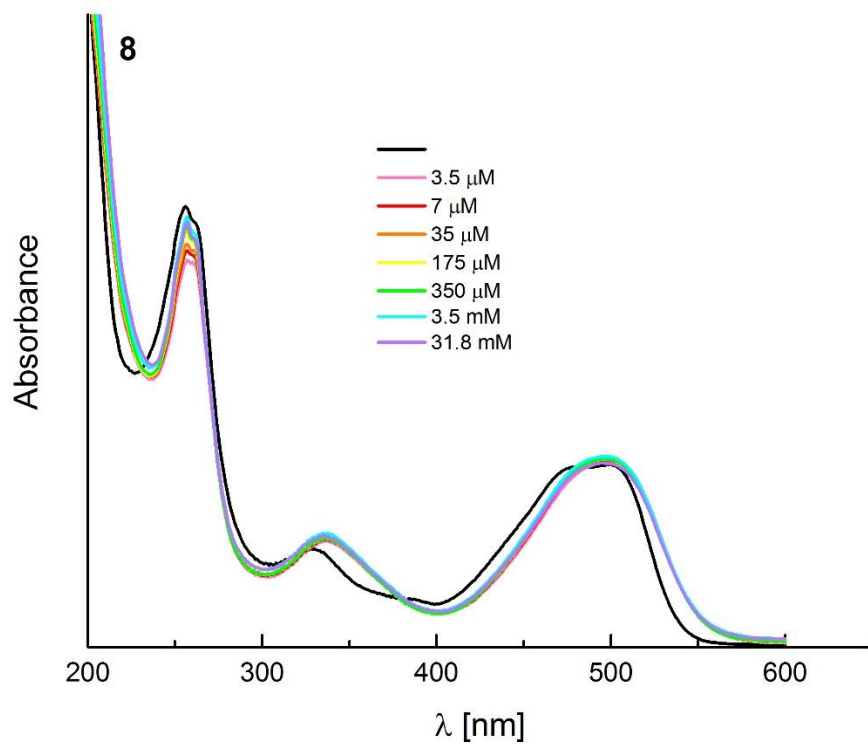


Fig. S35. The effect of zinc perchlorate addition on the absorption spectra of DPP **8** measured in CH₃CN.

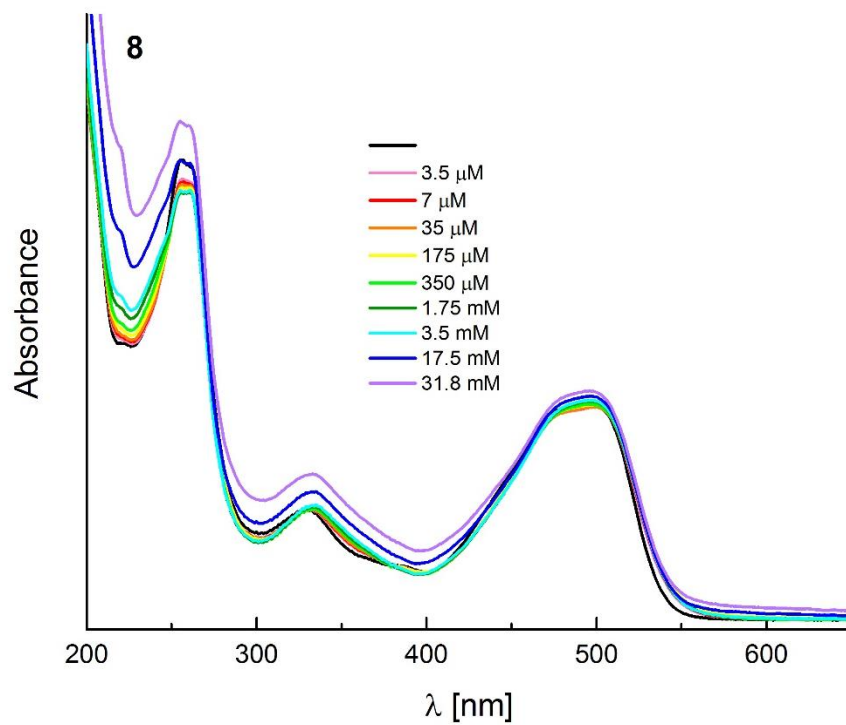


Fig. S36. The effect of magnesium perchlorate addition on the absorption spectra of DPP 8 measured in ACN.

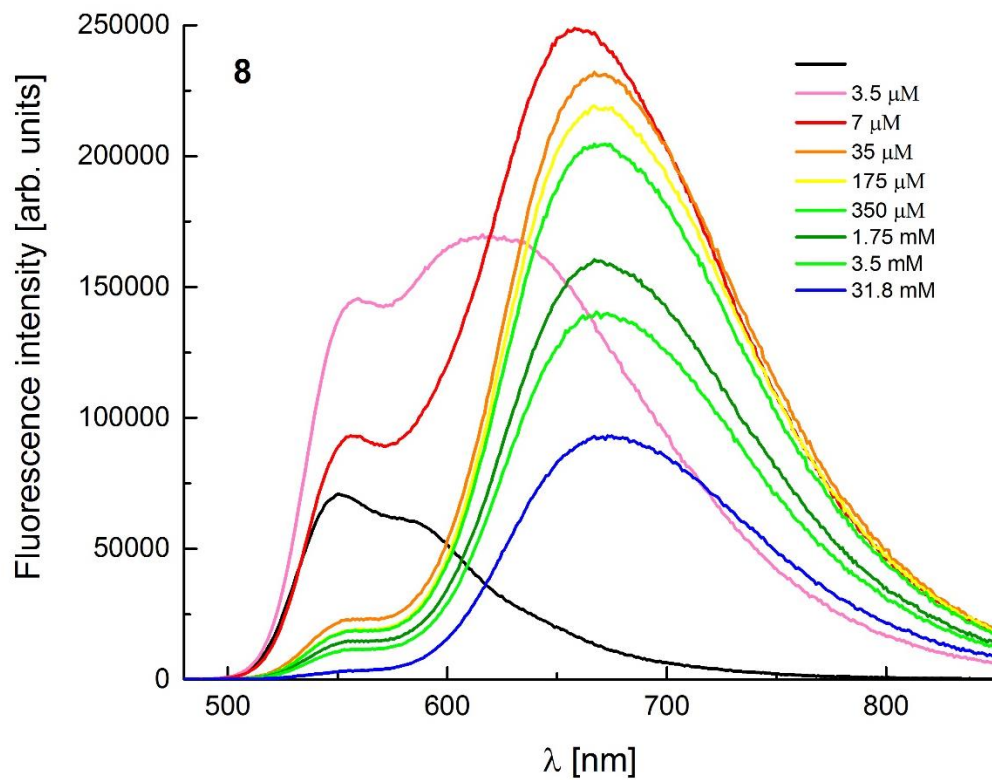


Fig. S37. The effect of PhSO_3H addition on the emission spectra of DPP 8 measured in CH_3CN .

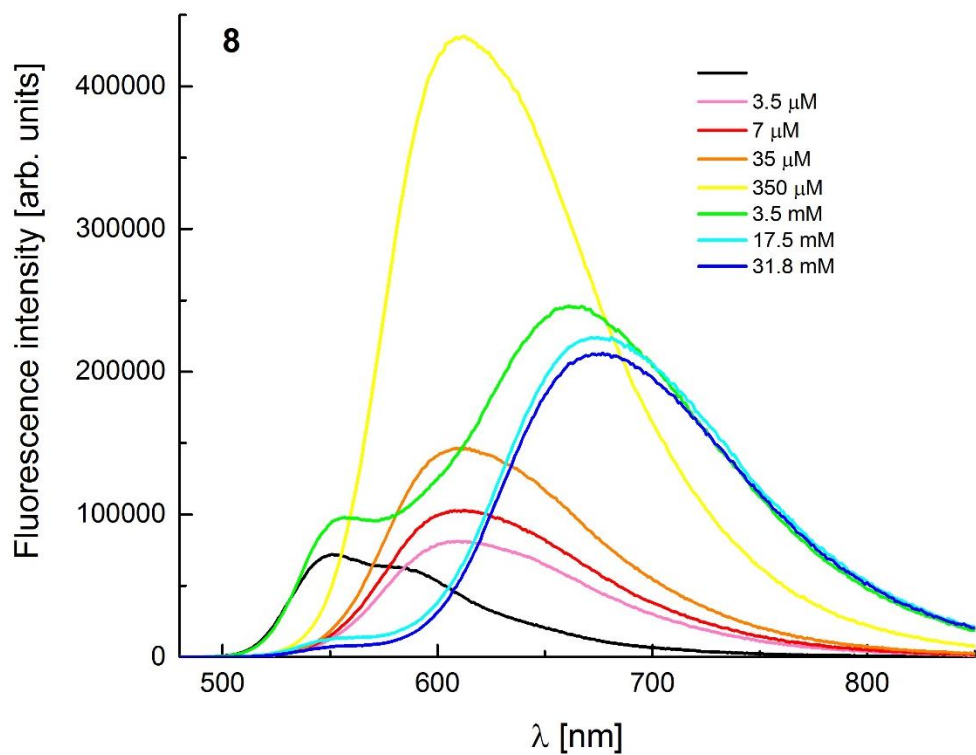


Fig. S38. The effect of cadmium perchlorate addition on the emission spectra of DPP **8** measured in CH₃CN.

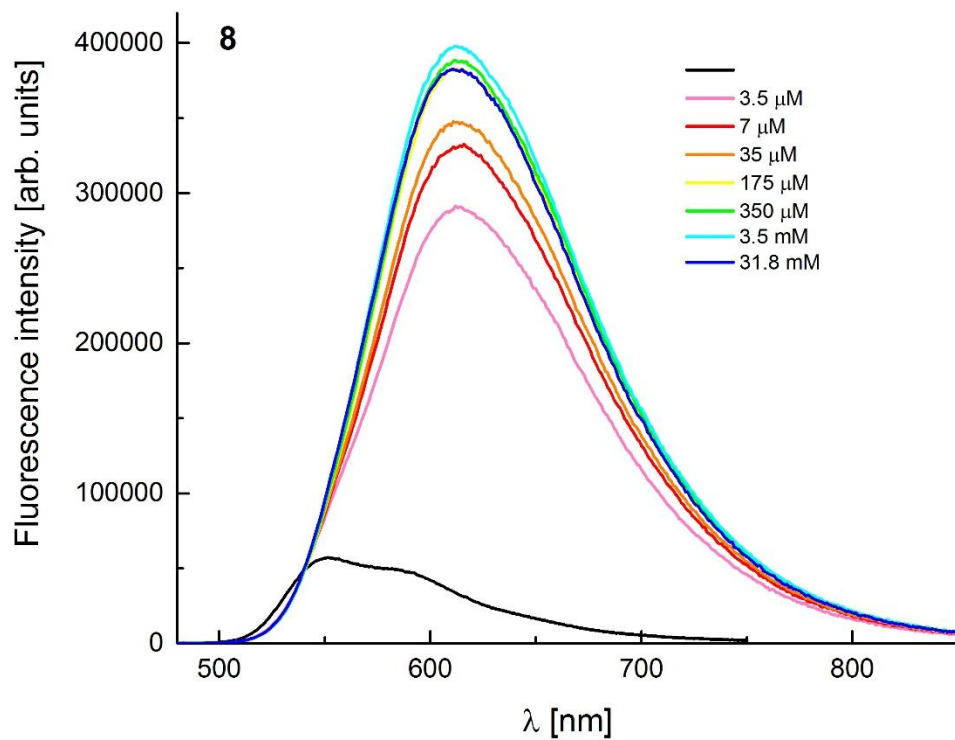


Fig. S39. The effect of zinc perchlorate addition on the emission spectra of DPP **8** measured in CH₃CN.

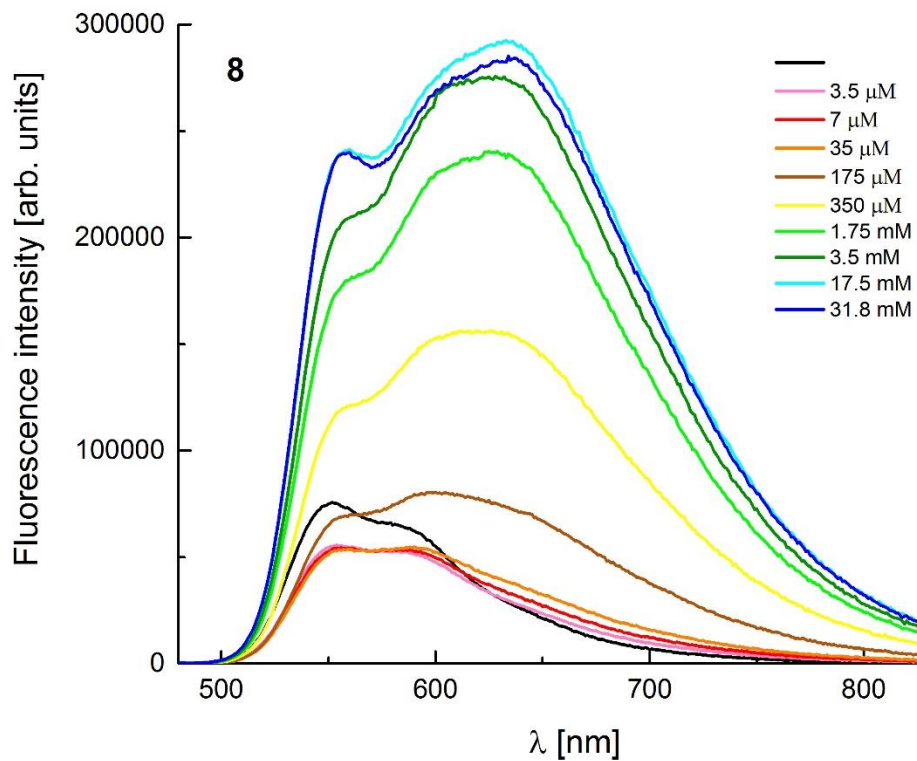


Fig. S40. The effect of magnesium perchlorate addition on the emission spectra of DPP 8 measured in CH₃CN.

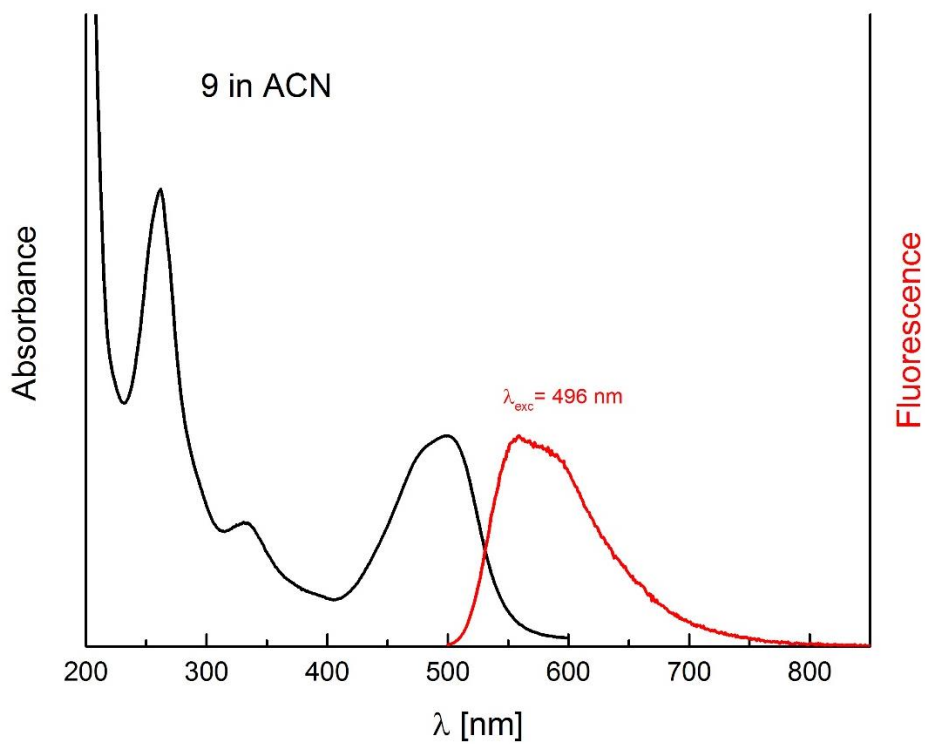


Fig. S41. The absorption and emission spectra of DPP 9 in CH₃CN.

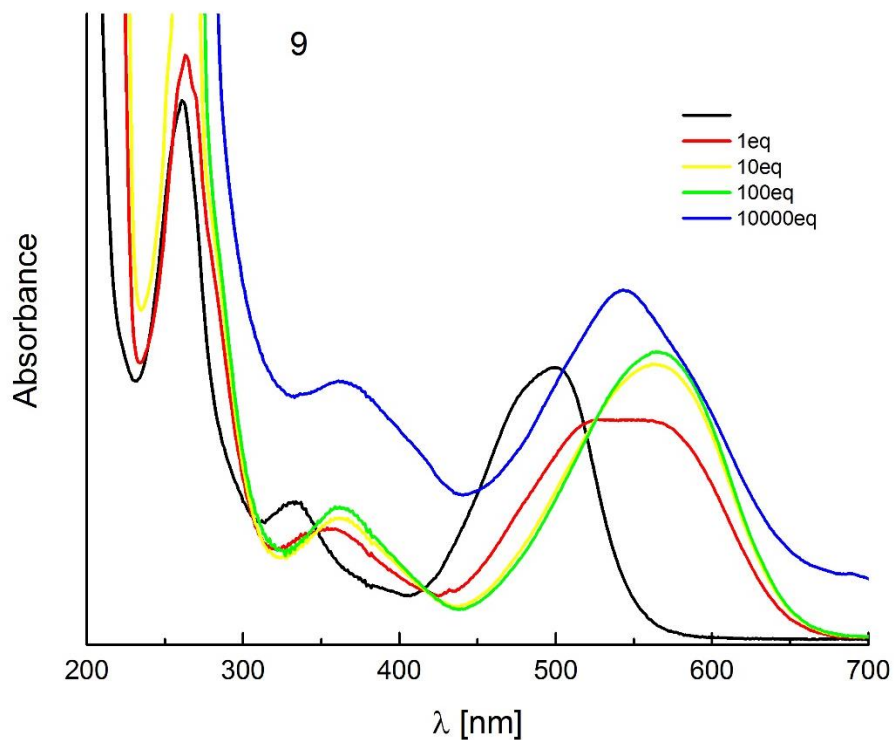


Fig. S42. The effect of PhSO₃H addition on the absorption spectra of DPP 9 measured in CH₃CN.

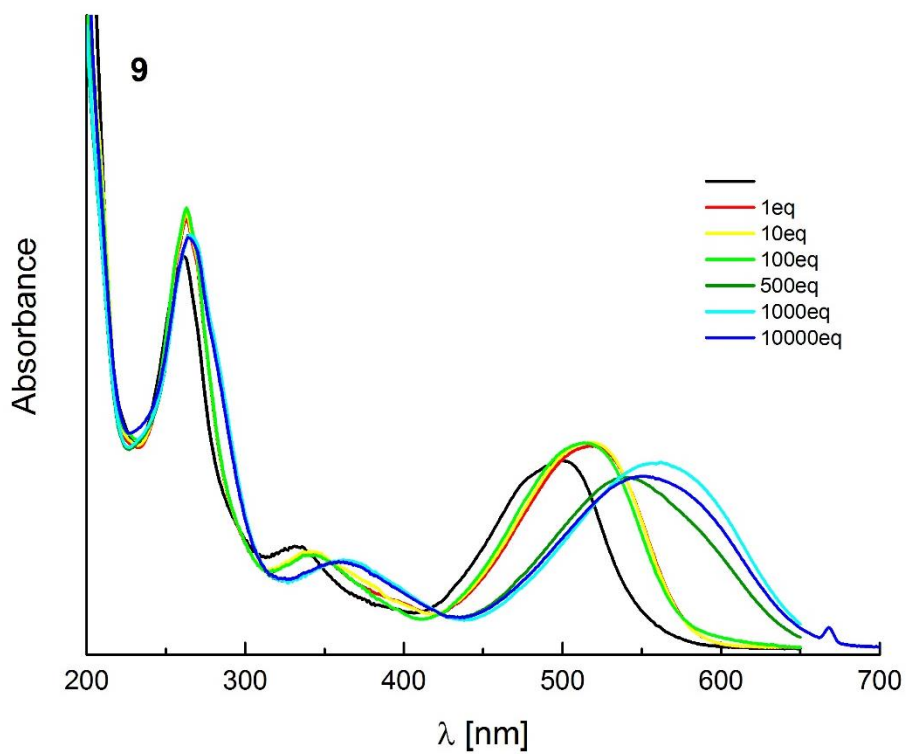


Fig. S43. The effect of cadmium perchlorate addition on the absorption spectra of DPP 9 measured in CH₃CN.

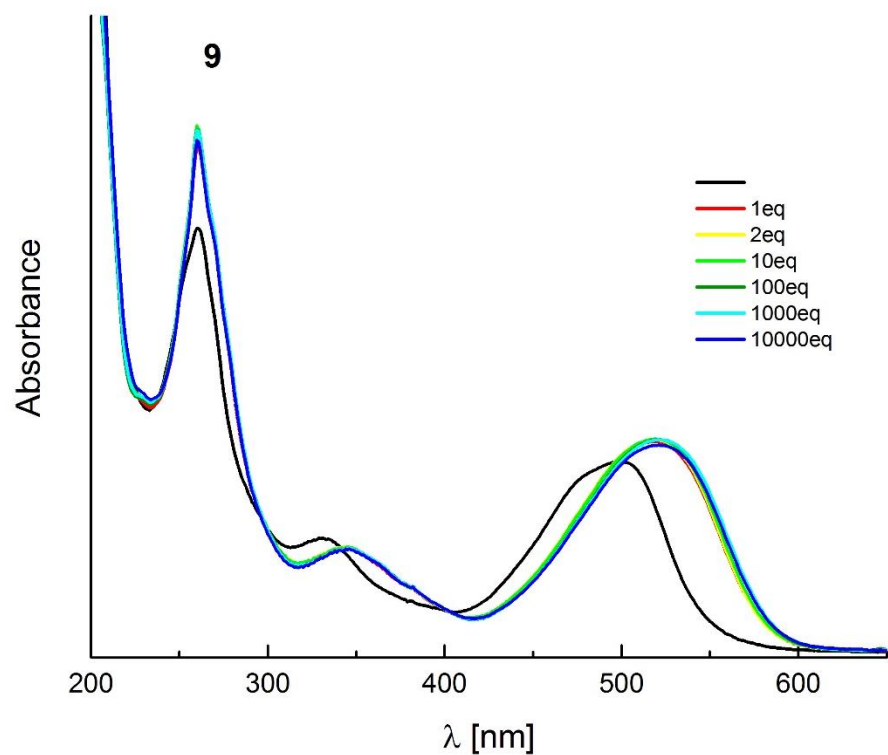


Fig. S44. The effect of zinc perchlorate addition on the absorption spectra of DPP **9** measured in CH₃CN.

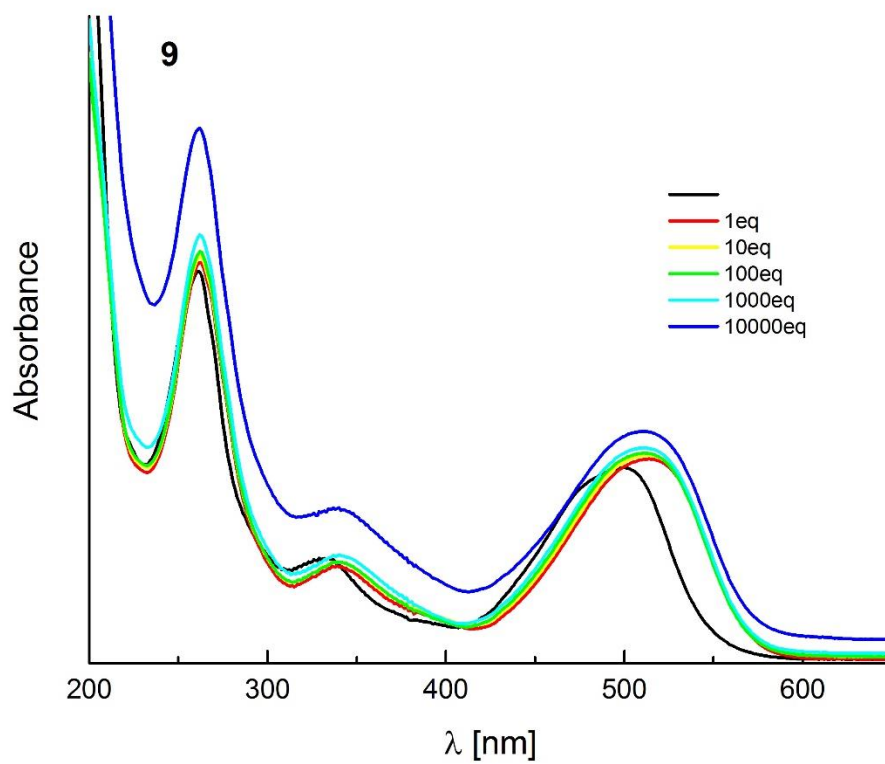


Fig. S45. The effect of magnesium perchlorate addition on the absorption spectra of DPP **9** measured in CH₃CN.

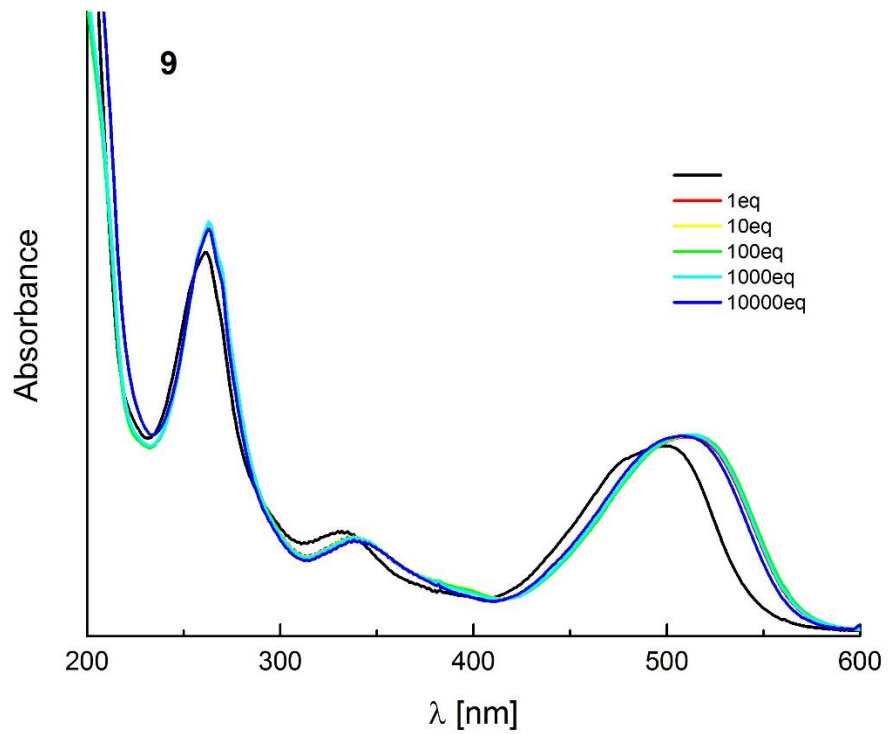


Fig. S46. The effect of calcium perchlorate addition on the absorption spectra of DPP **9** measured in CH₃CN.

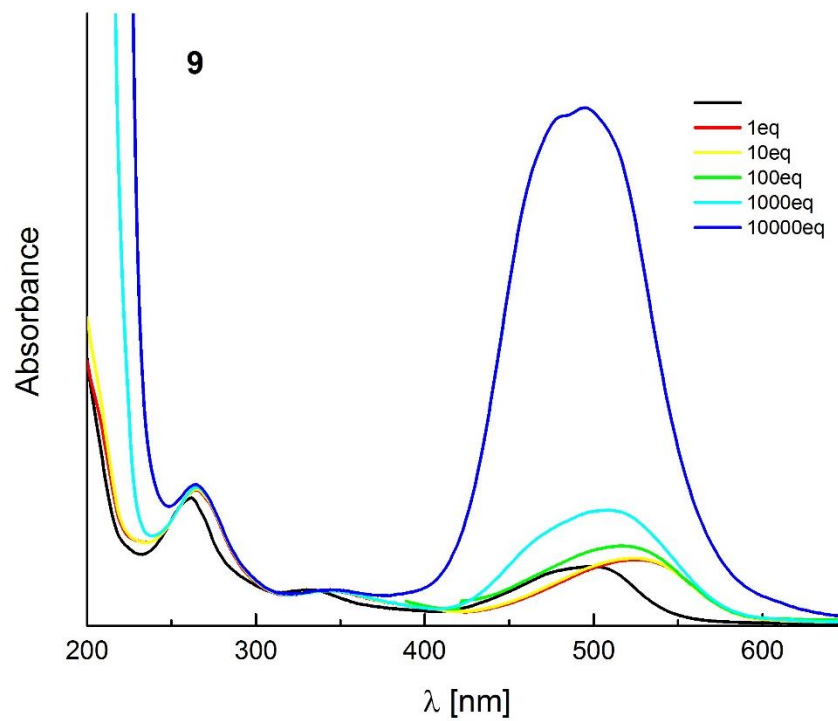


Fig. S47. The effect of cobalt perchlorate addition on the absorption spectra of DPP **9** measured in CH₃CN.

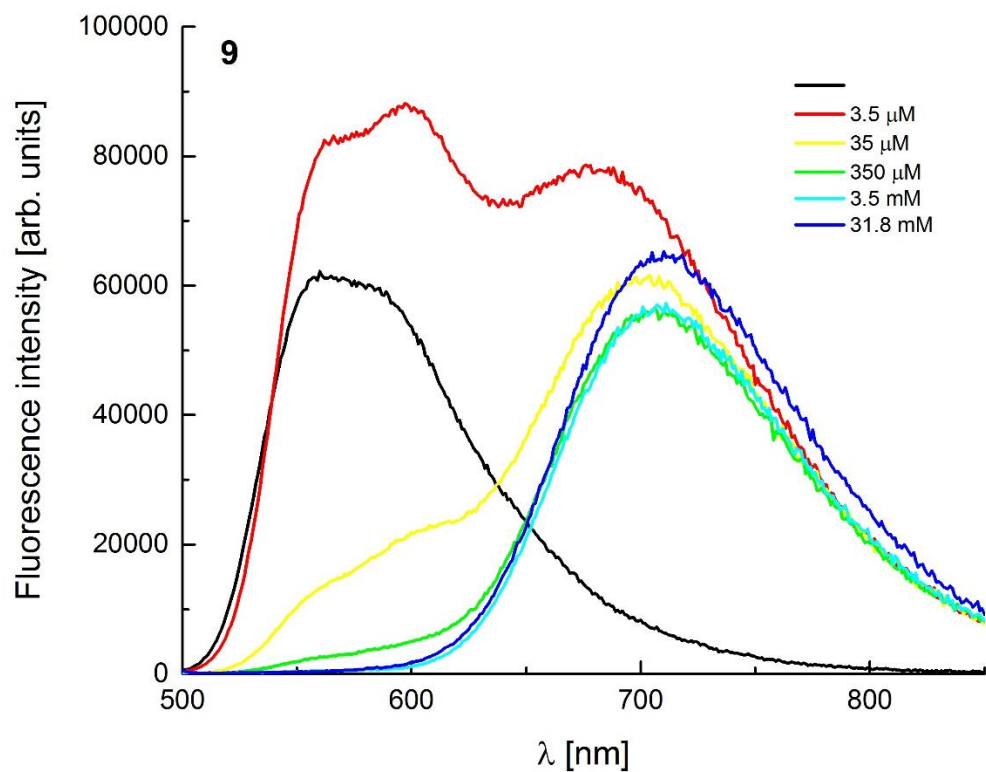


Fig. S48. The effect of PhSO₃H addition on the emission spectra of DPP 9 measured in CH₃CN.

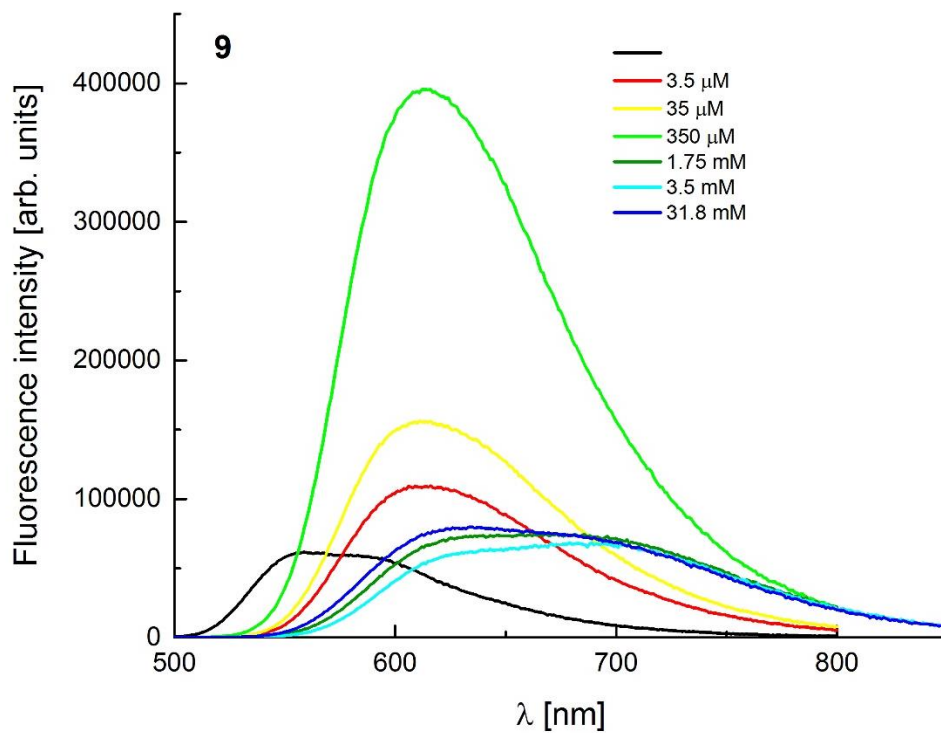


Fig. S49. The effect of cadmium perchlorate addition on the emission spectra of DPP 9 measured in CH₃CN.

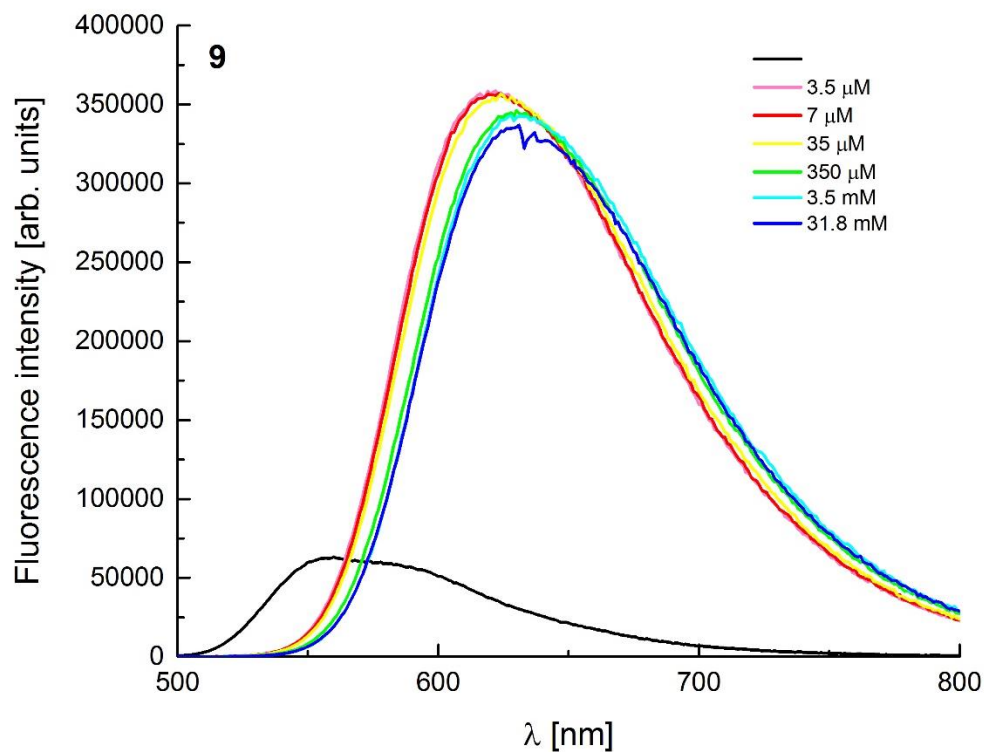


Fig. S50. The effect of zinc perchlorate addition on the emission spectra of DPP 9 measured in CH₃CN.

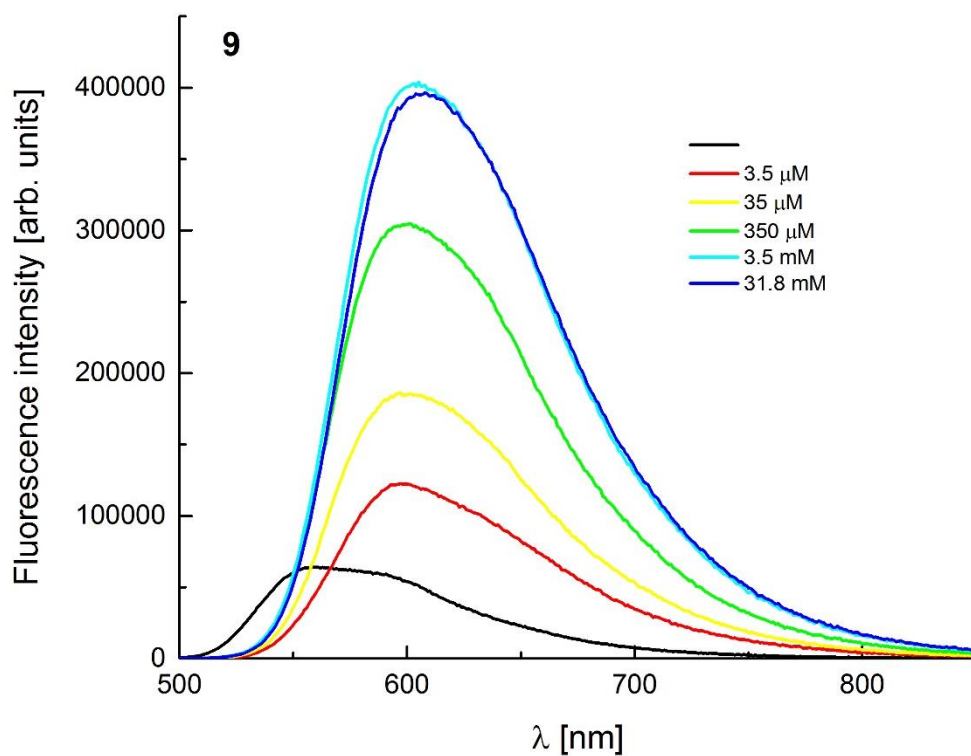


Fig. S51. The effect of magnesium perchlorate addition on the emission spectra of DPP 9 measured in CH₃CN.

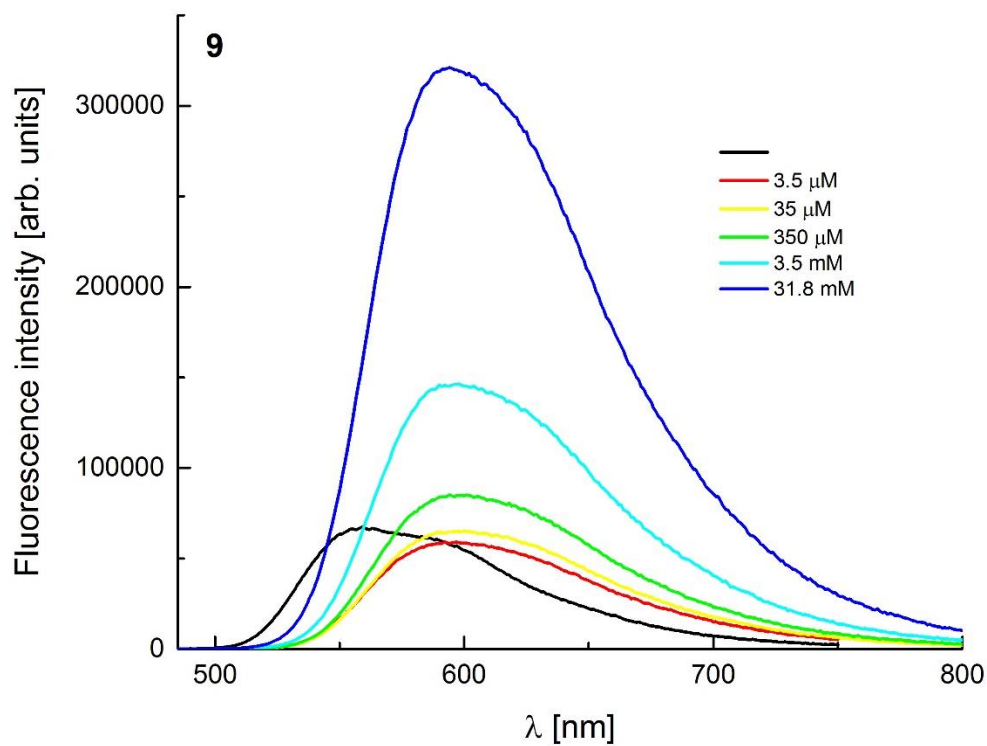


Fig. S52. The effect of calcium perchlorate addition on the emission spectra of DPP **9** measured in CH₃CN.

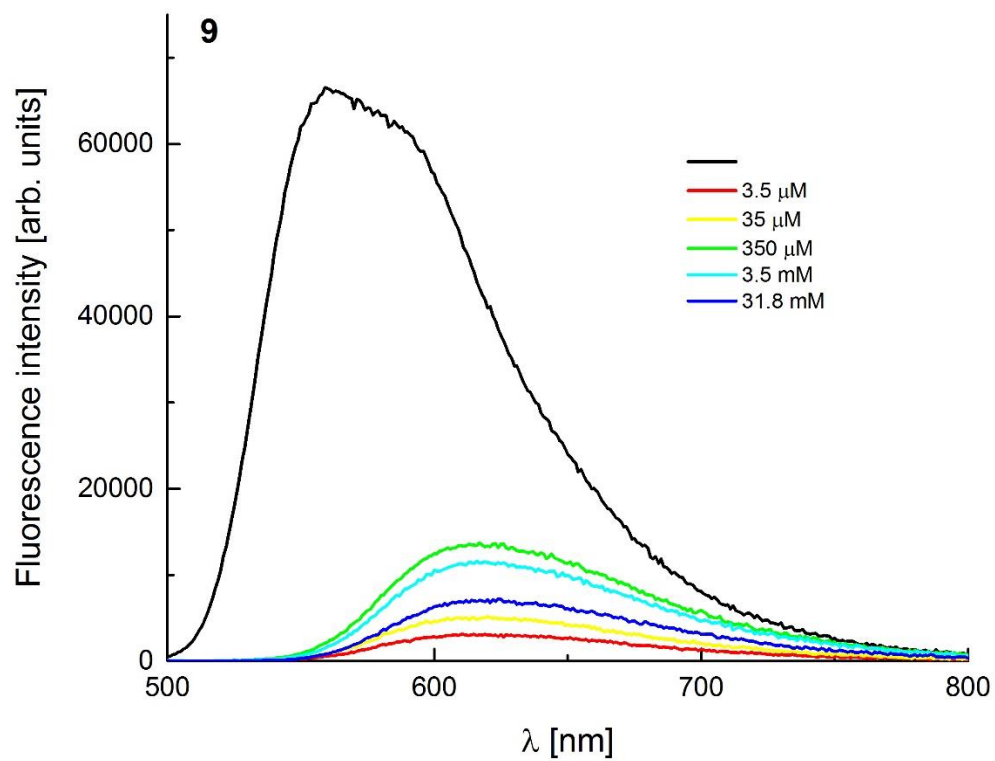


Fig. S53. The effect of cobalt perchlorate addition on the emission spectra of DPP **9** measured in CH₃CN.

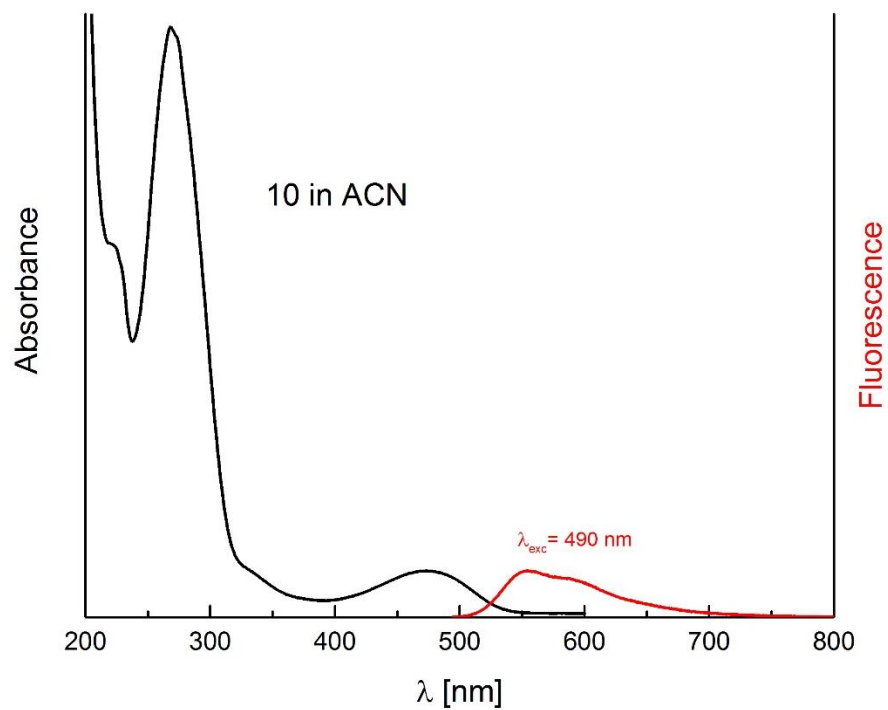


Fig. S54. The absorption and emission spectra of DPP **10** in CH_3CN .

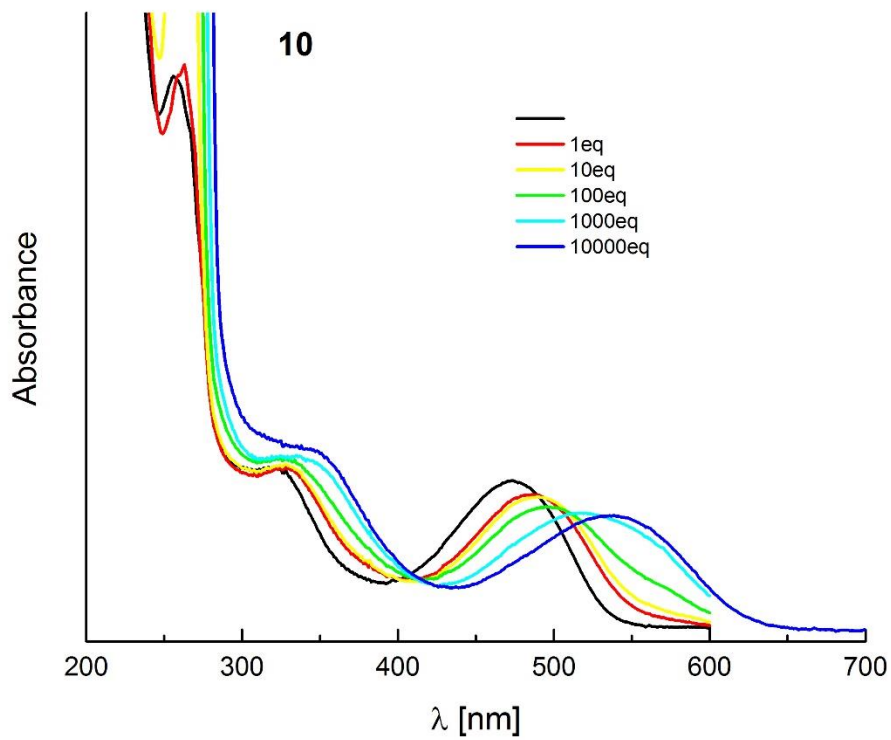


Fig. S55. The effect of PhSO_3H addition on the absorption spectra of DPP **10** measured in CH_3CN .

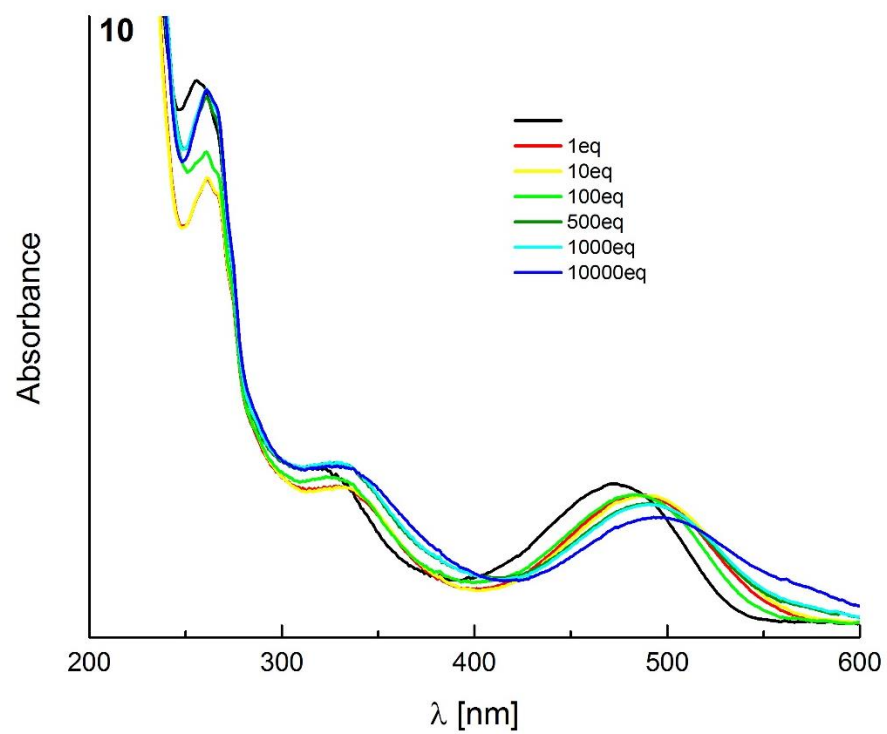


Fig. S56. The effect of cadmium perchlorate addition on the absorption spectra of DPP **10** measured in CH₃CN.

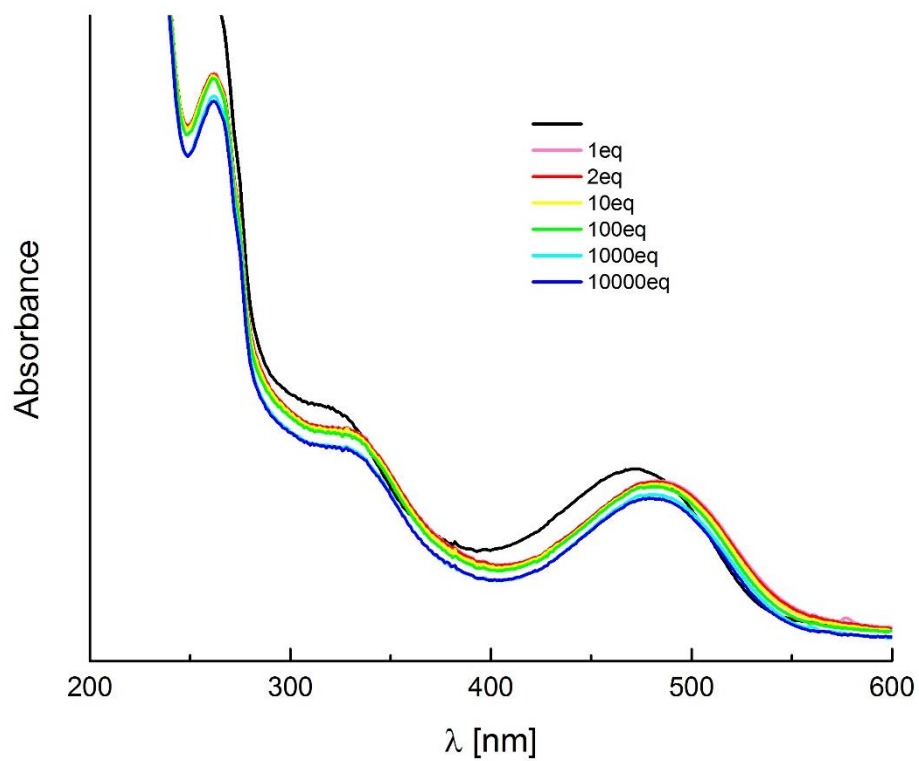


Fig. S57. The effect of zinc perchlorate addition on the absorption spectra of DPP **10** measured in CH₃CN.

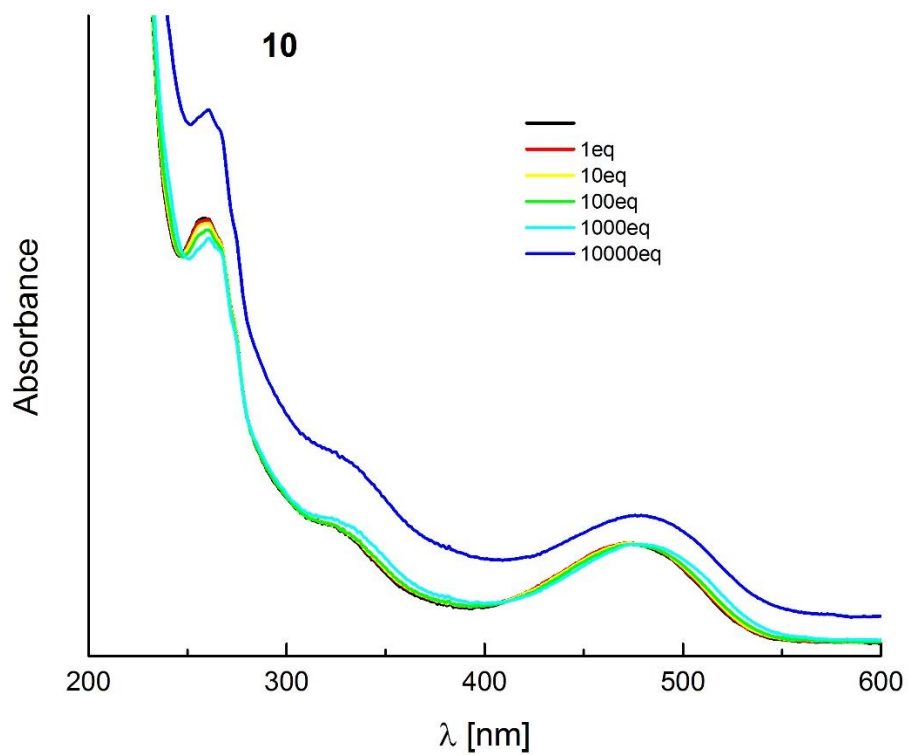


Fig. S58. The effect of magnesium perchlorate addition on the absorption spectra of DPP **10** measured in CH₃CN.

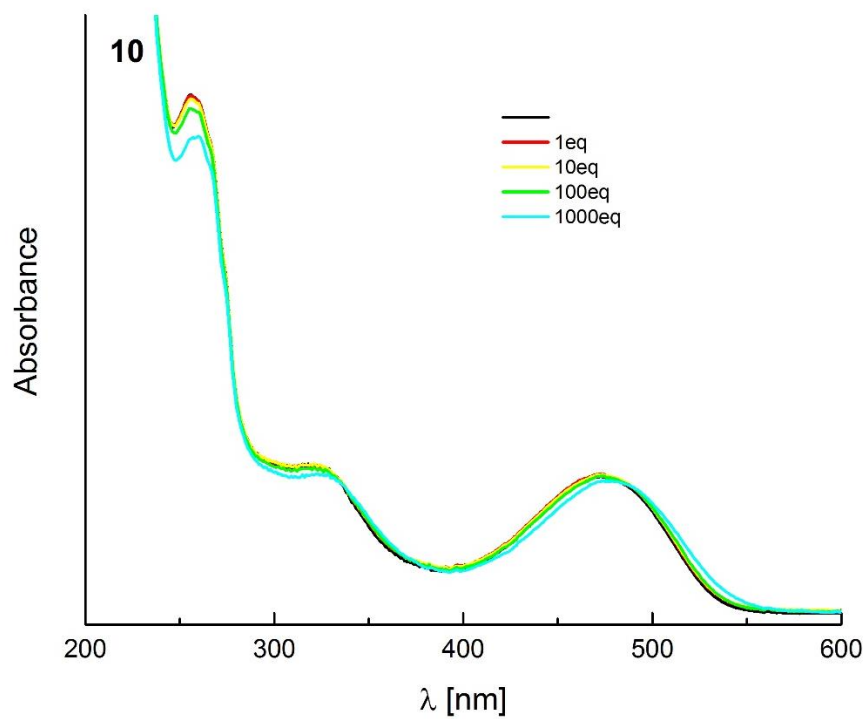


Fig. S59. The effect of calcium perchlorate addition on the absorption spectra of DPP **10** measured in CH₃CN.

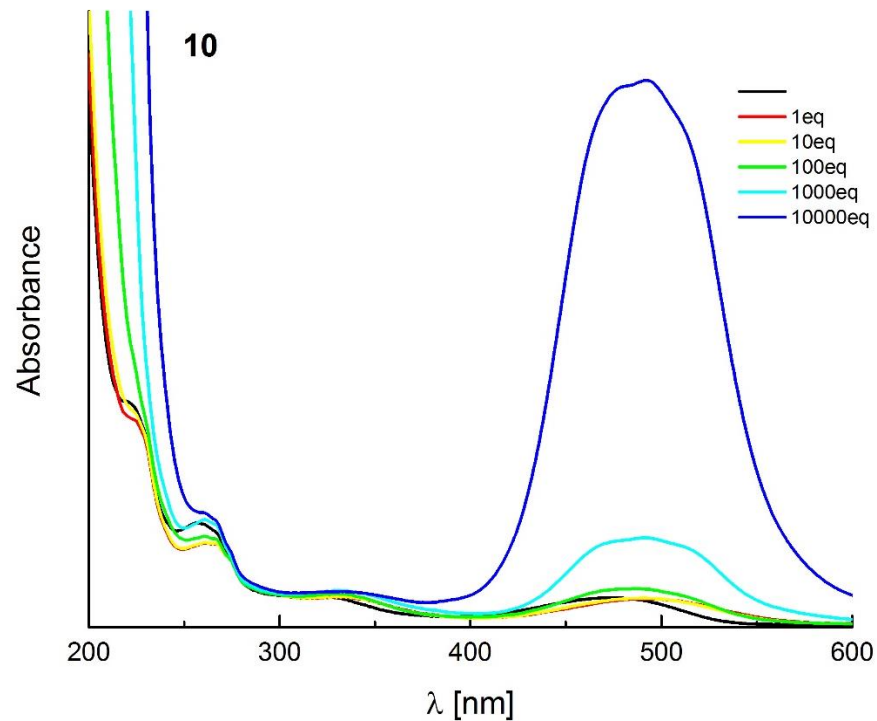


Fig. S60. The effect of cobalt perchlorate addition on the absorption spectra of DPP **10** measured in CH₃CN.

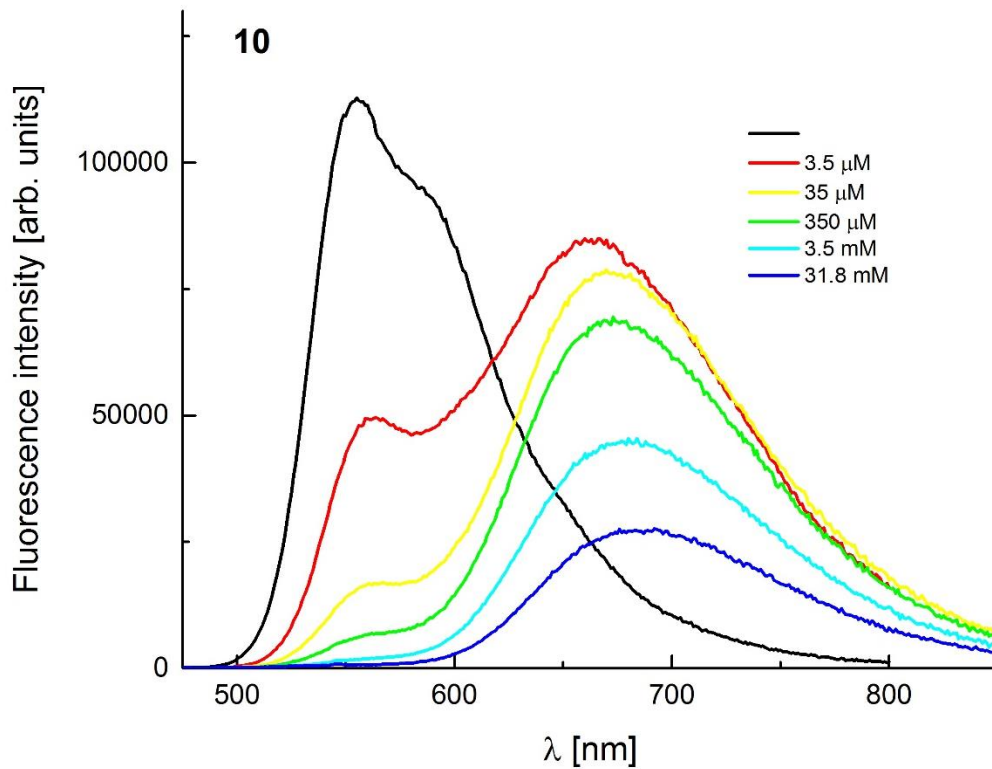


Fig. S61. The effect of PhSO₃H addition on the emission spectra of DPP **10** measured in CH₃CN.

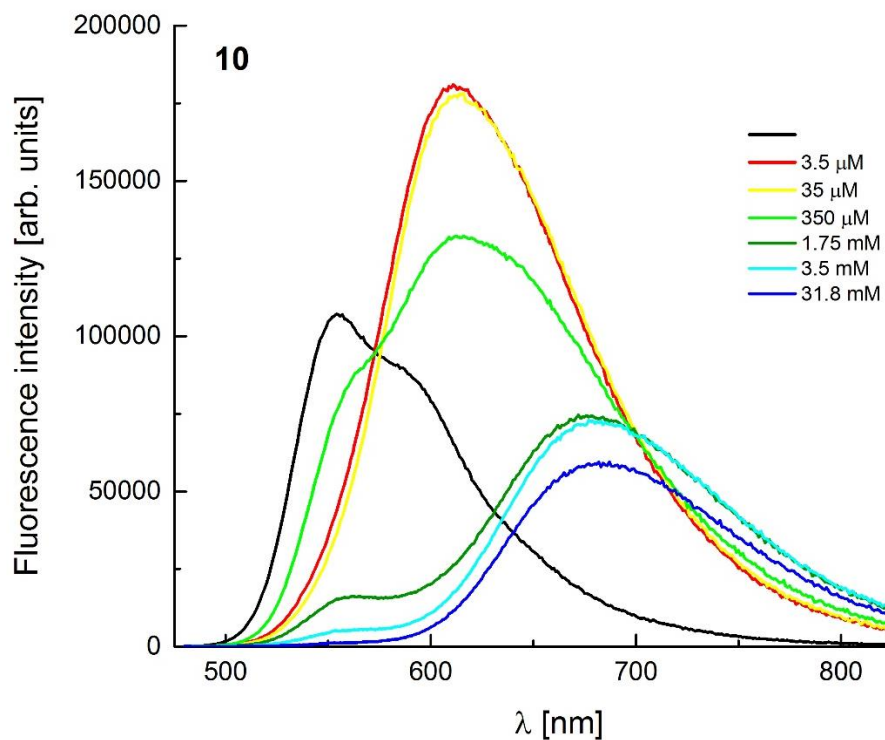


Fig. S62. The effect of cadmium perchlorate addition on the emission spectra of DPP **10** measured in CH_3CN .

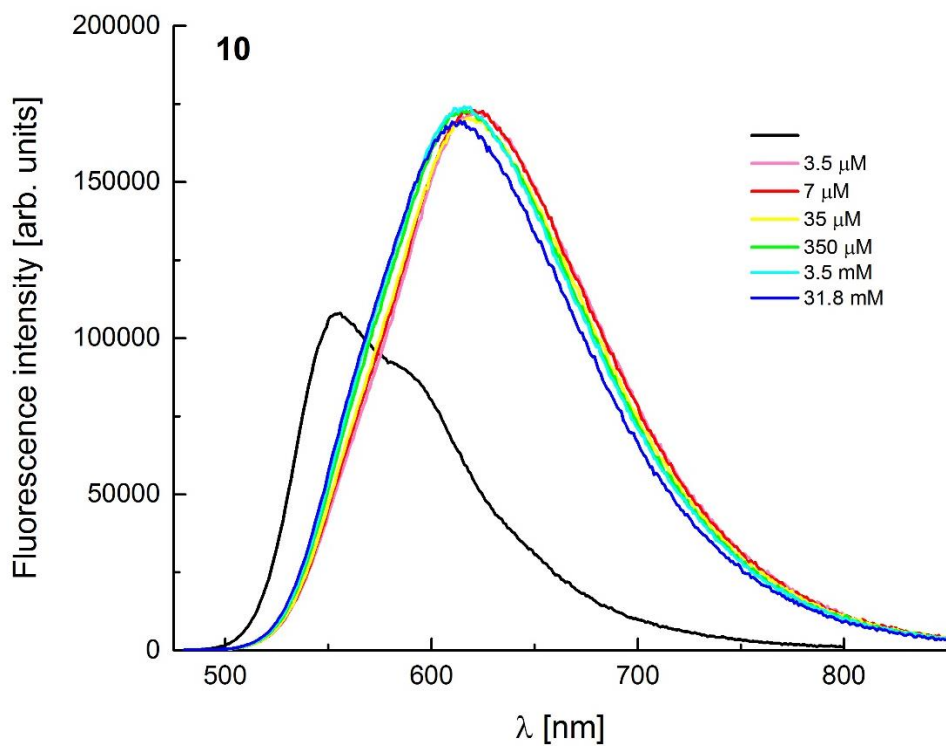


Fig. S63. The effect of zinc perchlorate addition on the emission spectra of DPP **10** measured in CH_3CN .

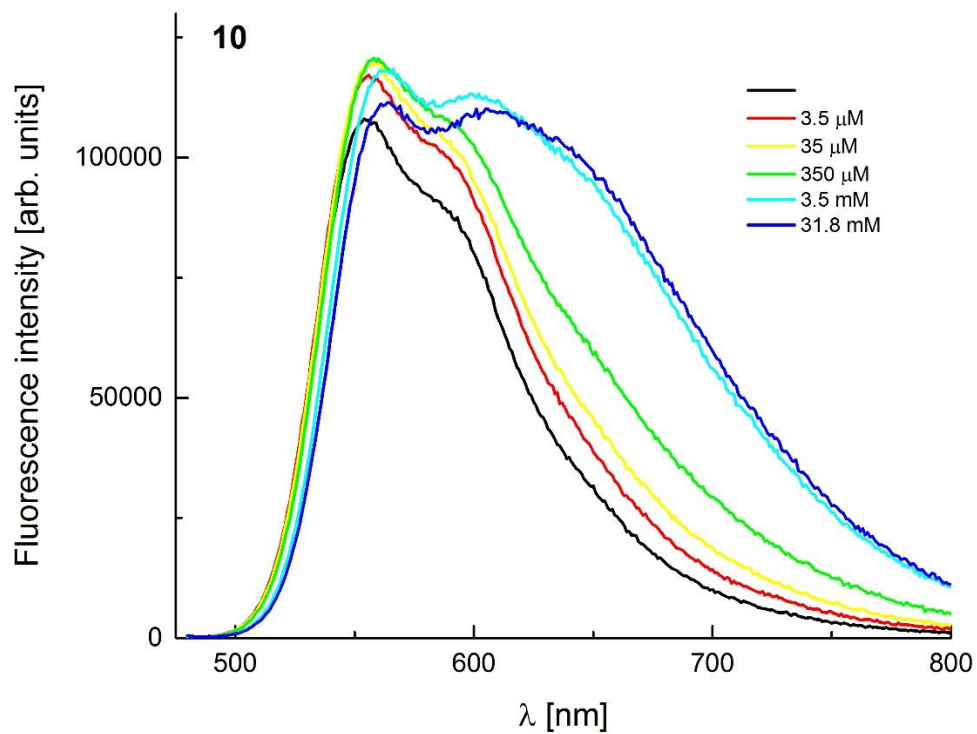


Fig. S64. The effect of magnesium perchlorate addition on the emission spectra of DPP **10** measured in CH_3CN .

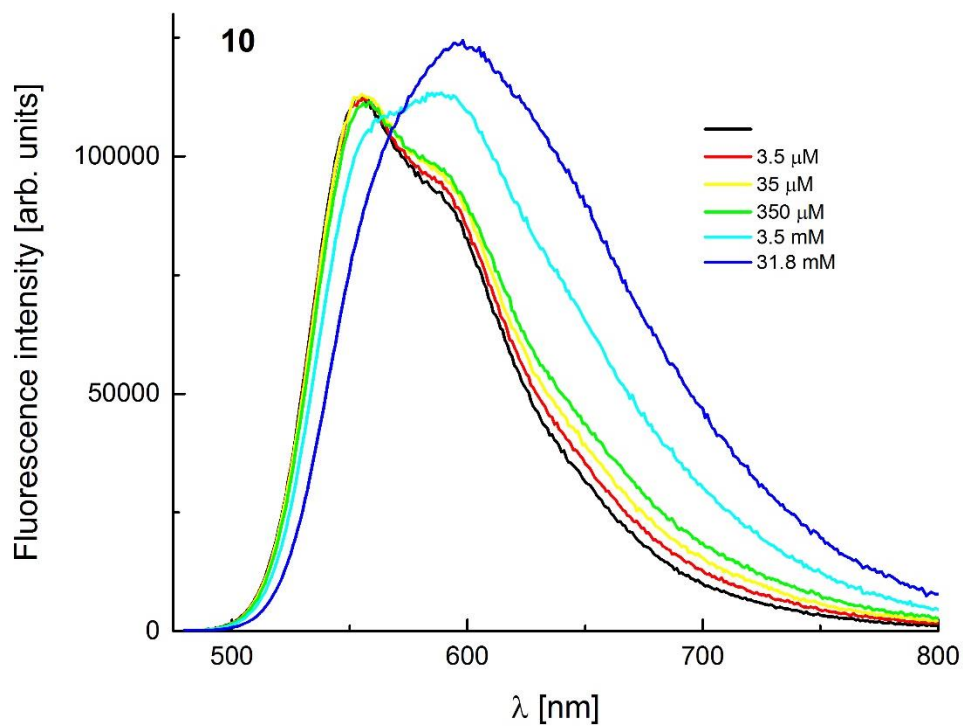


Fig. S65. The effect of calcium perchlorate addition on the emission spectra of DPP **10** measured in CH_3CN .

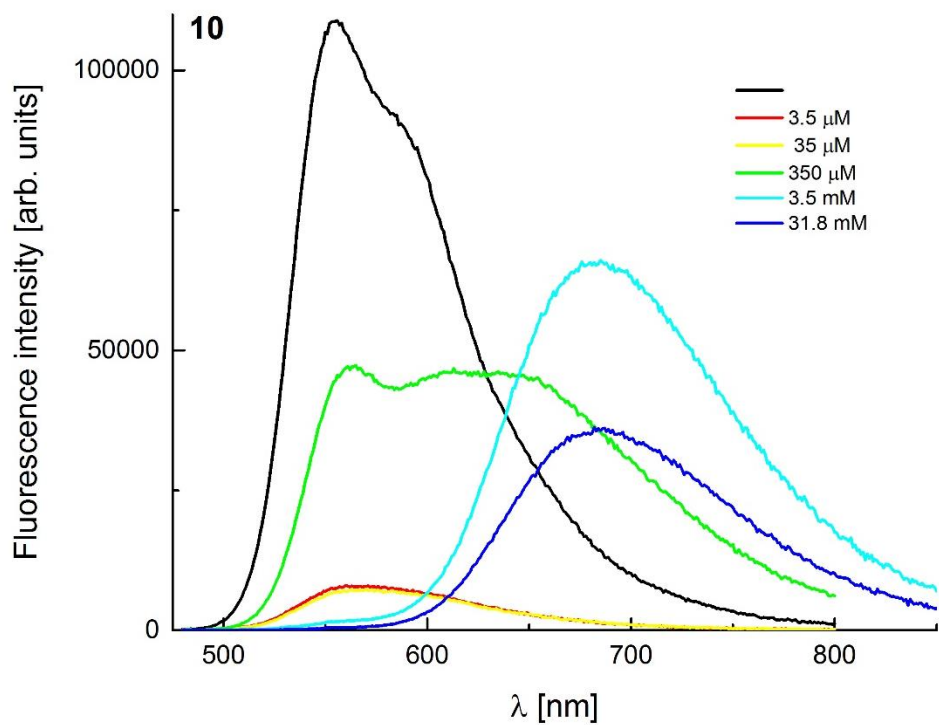


Fig. S66. The effect of cobalt perchlorate addition on the emission spectra of DPP 10 measured in CH₃CN.

Section S4: Water solubility and binding constants

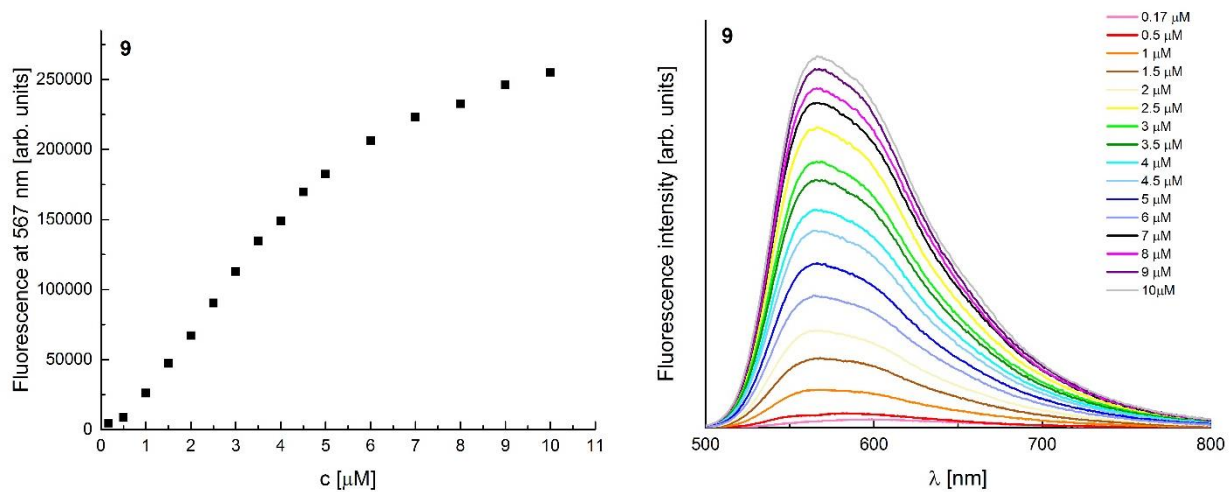


Fig. S67. Plot of fluorescence intensity against concentration of DPP 9 in water.

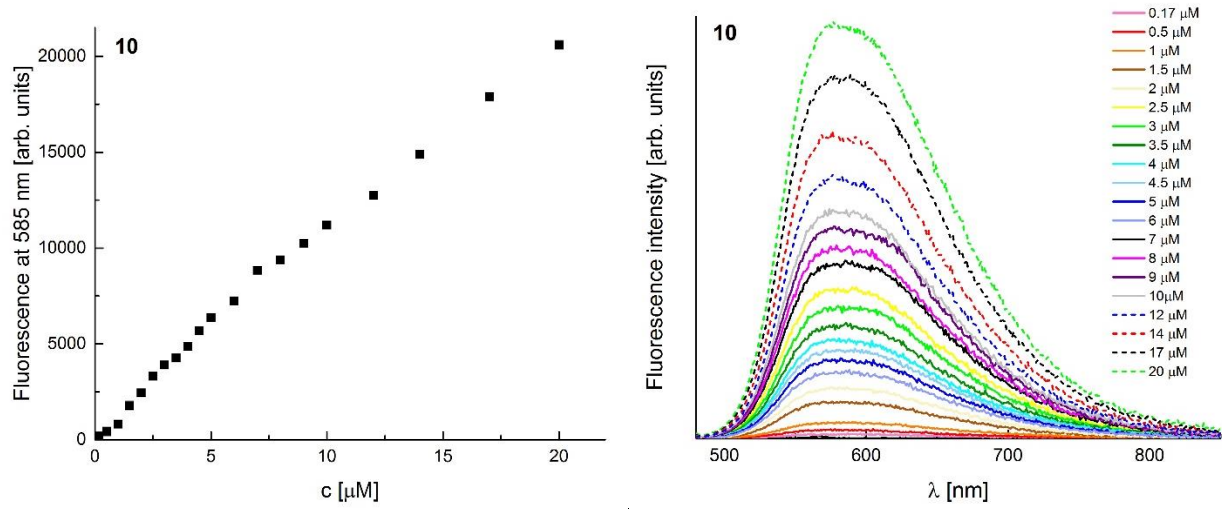


Fig. S68. Plot of fluorescence intensity against concentration of DPP **10** in water.

Section S5: Imaging

Cell culture conditions. The rat embryonic cardiomyoblast-derived H9C2 cell lines were cultured at 37°C in a humidified atmosphere containing 5% CO₂ in DMEM supplemented with 10% foetal bovine serum (FBS), 2 mM glutamine, 100 U/ml penicillin, and 100 µg/ml streptomycin.

Fluorescence localization of diketopyrrolopyrrole-based zinc probes within the cells. The cardiac H9C2 cells were loaded with fluorophores in DMEM medium supplemented with 10% FBS, 2 mM glutamine, 100 U/ml penicillin, and 100 µg/ml streptomycin at 37°C in a humidified atmosphere containing 5% CO₂ for 15 to 30 minutes with the diketopyrrolopyrrole-based zinc probe at the final concentration ranging from 200 to 500 nM. The final concentration of the MitoTracker™ Green FM was 150 nM, and Lysosyme probe was 100 nM. The fluorophores were dissolved in DMSO. Before measurements, the incubation medium was replaced with FluoroBrite™ DMEM. The measurements were performed with use of Olympus IX83 confocal microscope with the water objective 60x UPLSAPO 60XW. Registered data were transferred to the ImageJ and analyzed for presentation.

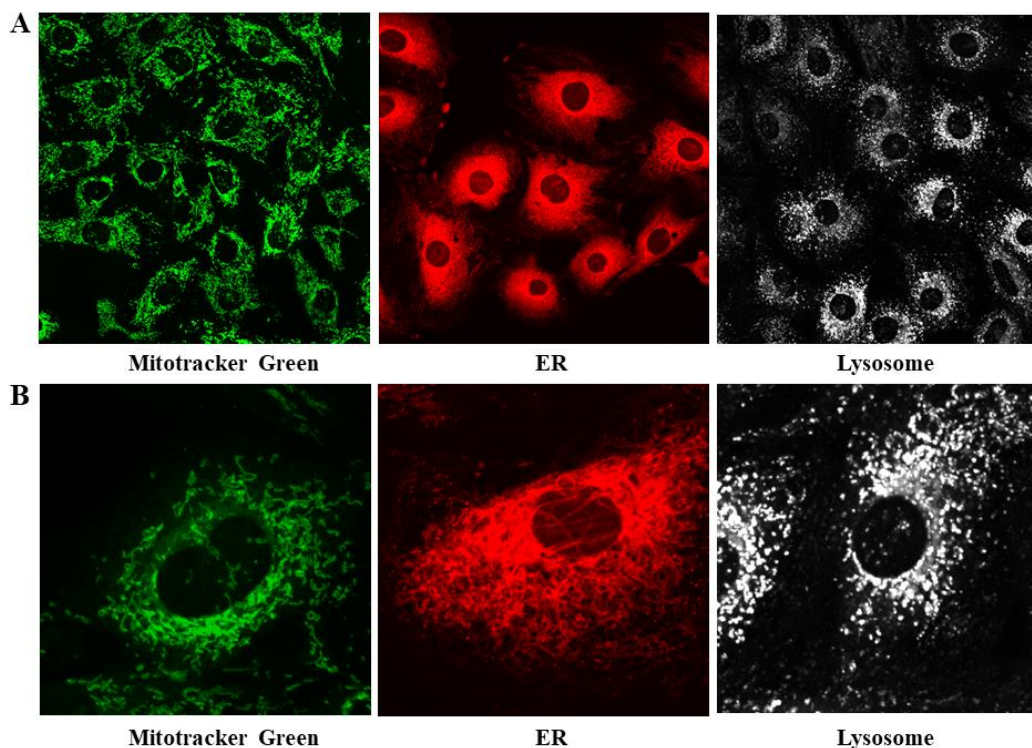


Fig. S69. Confocal imaging of the location of organellar fluorescent markers in H9C2 cells line. A. Localization of fluorescent markers for mitochondria (Mitotracker Green), endoplasmic reticulum (ER), and lysosomes, respectively, in H9C2 cells. B. Three-fold magnification of the selected Region of Interest (ROI), respectively for the individual fluorescent markers.

Section S6: Additional computational results

To ascertain the quality of the TD-DFT results, we have considered three smaller models of the investigated probes, denoted **M3**, and **M4** (see Fig. S64) for which CC2/*aug-cc-pVTZ* single point calculations were achievable.

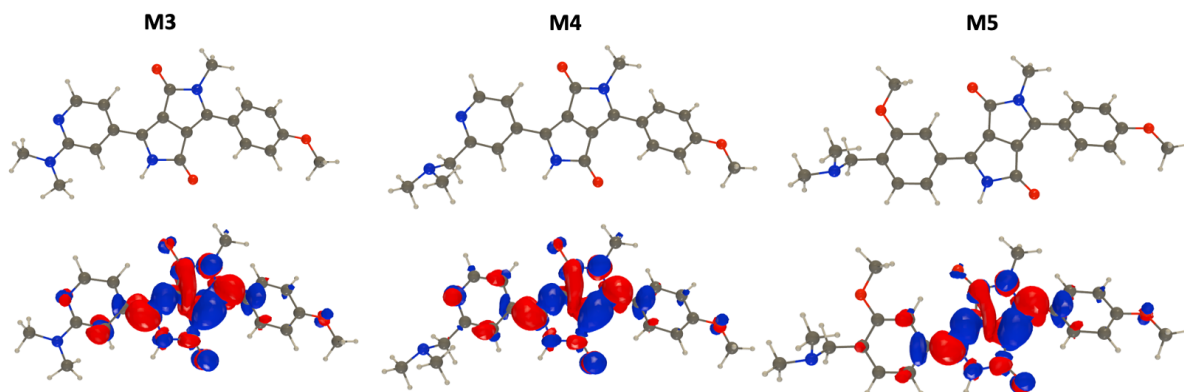


Fig. S70: Representation of the model probes used to test the reliability of the TD-DFT approach. We also provide the density difference plots (contour threshold: 0.001 au).

The cLR²-PCM-TD-DFT protocol returns vertical absorption at 452, 461, and 453 nm for **M3**, and **M4** respectively. When adding the difference between CC2/*aug-cc-pVTZ* and TD-DFT results computed in gas phase, the values are increases slightly to 464, 473, and 463 nm, respectively. For vertical fluorescence, the cLR²-PCM-TD-DFT values are 549, 557, and 542 nm, for for **M3**, and **M4**, respectively, whereas the CC2-corrected results are 552, 562, and 541 nm. Again, the values are very close and this hints that the selected functional is well suited for the systems under investigation.

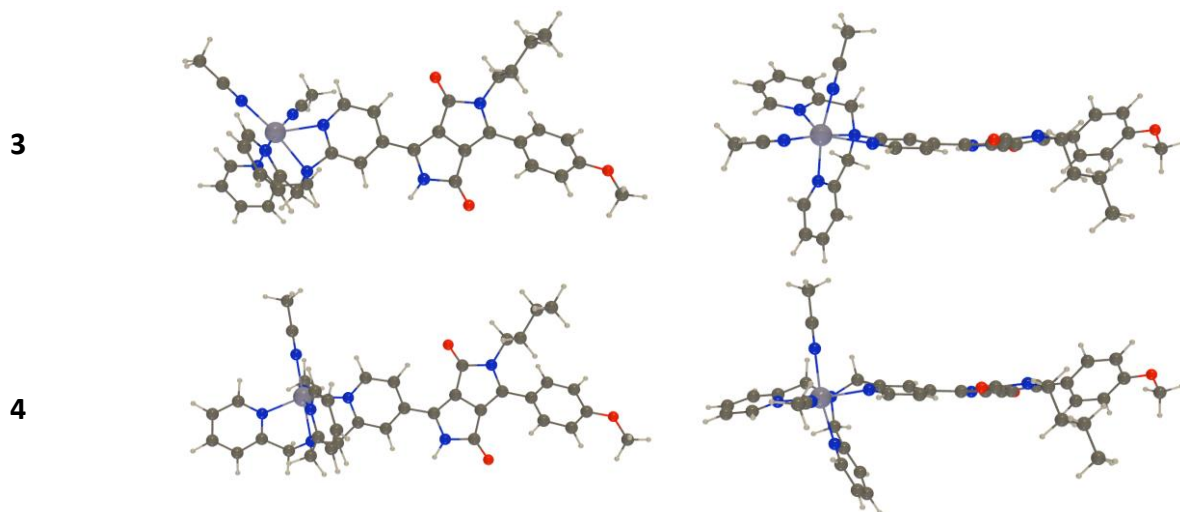
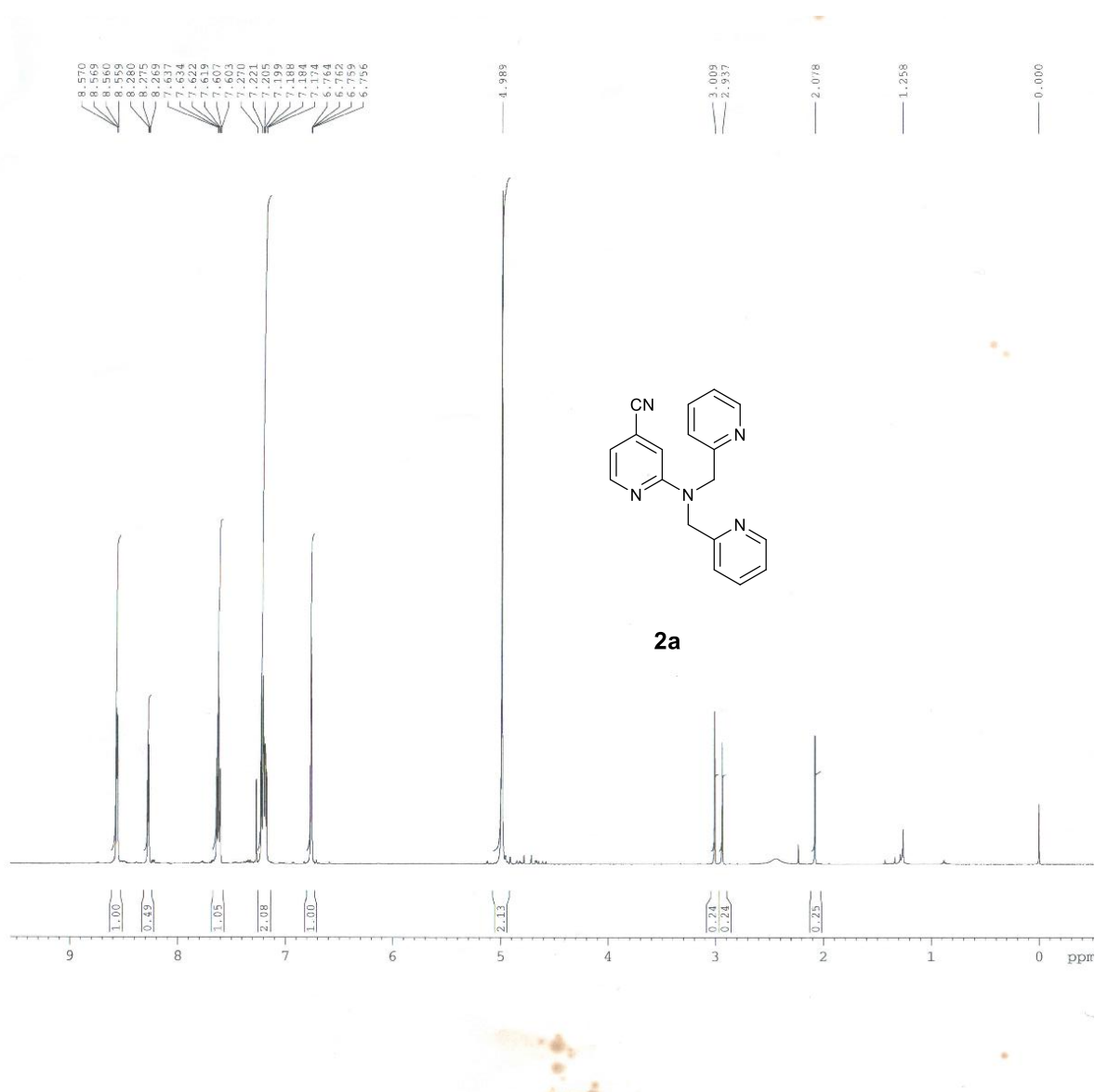
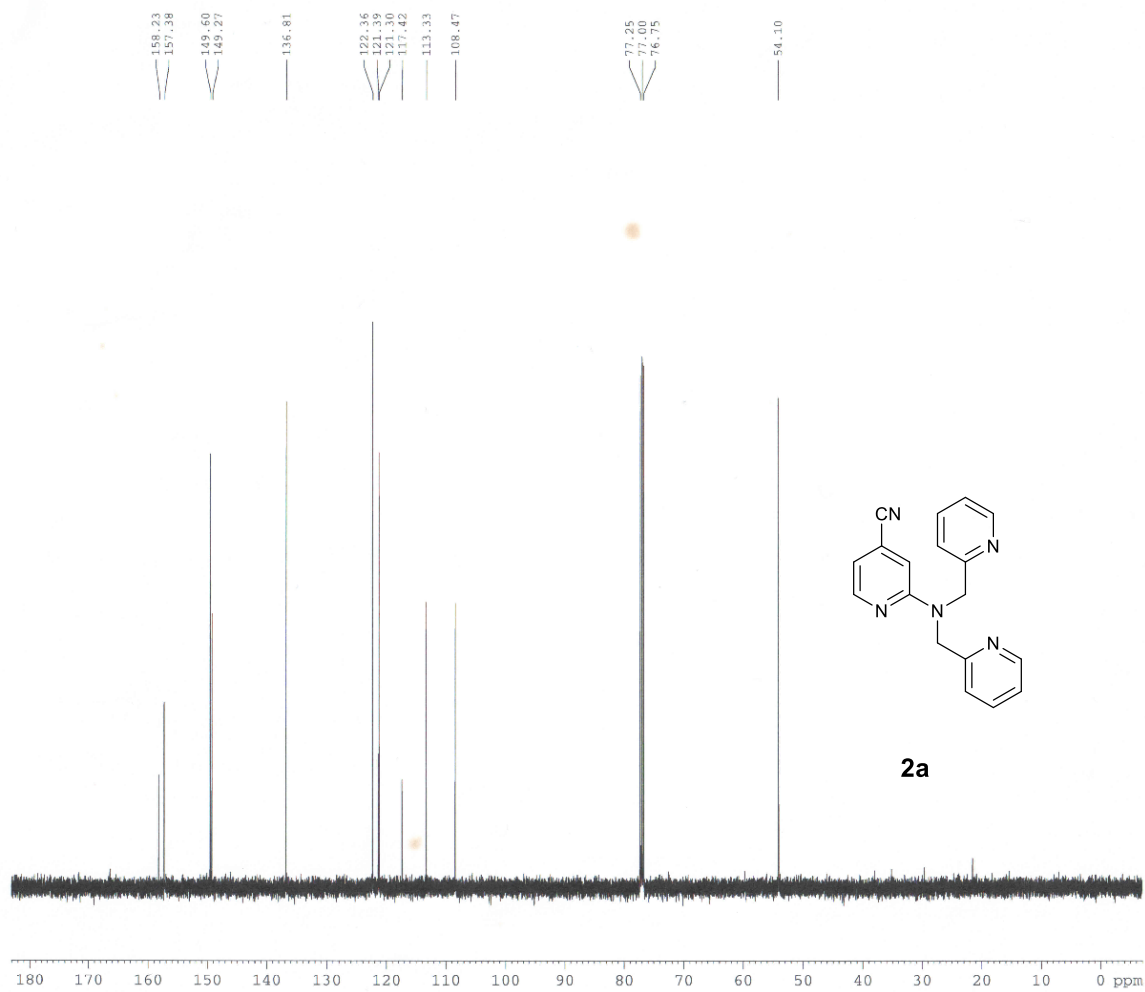


Fig. S71: Optimal geometries of the molecules **3**, **4** with a Zn²⁺ ion complexed and explicit ACN molecules added to complete the coordination sphere of the cation. Side (left) and top (right) views.

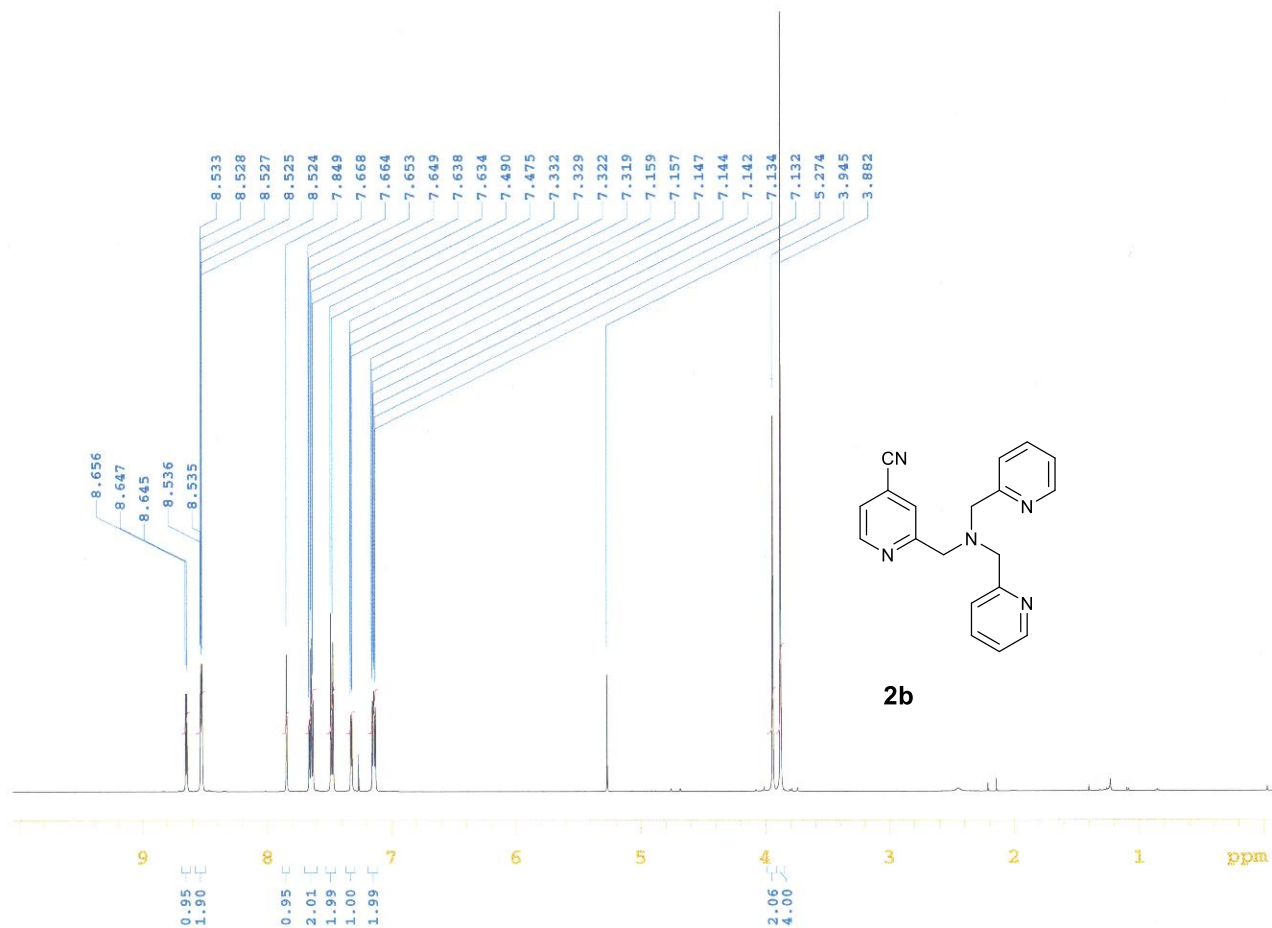
Section S7: ^1H , ^{13}C and HRMS spectra



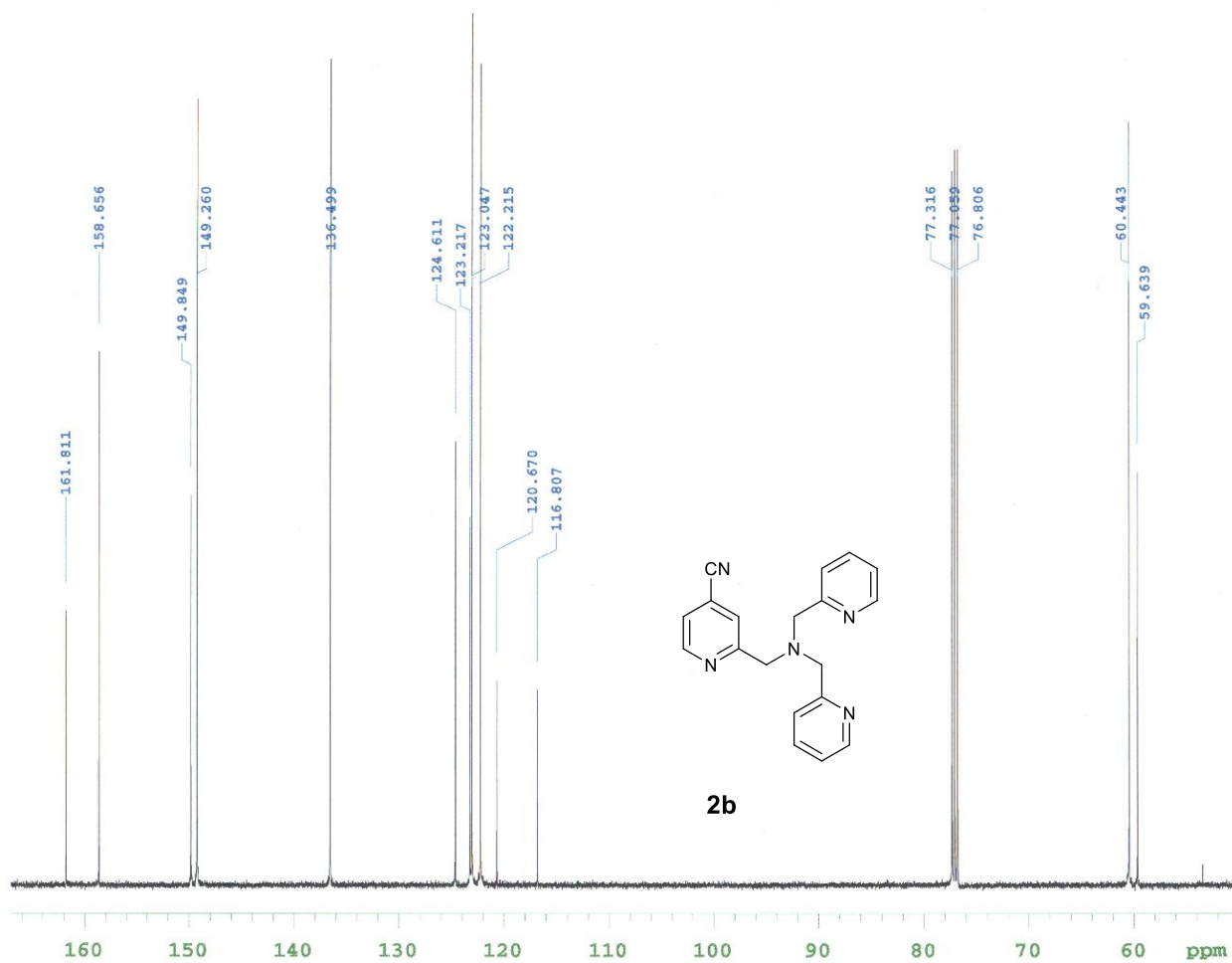
^1H -NMR spectra of **2a** in CDCl_3



^{13}C -NMR spectra of **2a** in CDCl_3



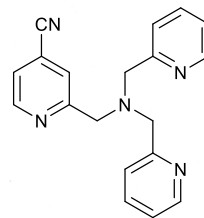
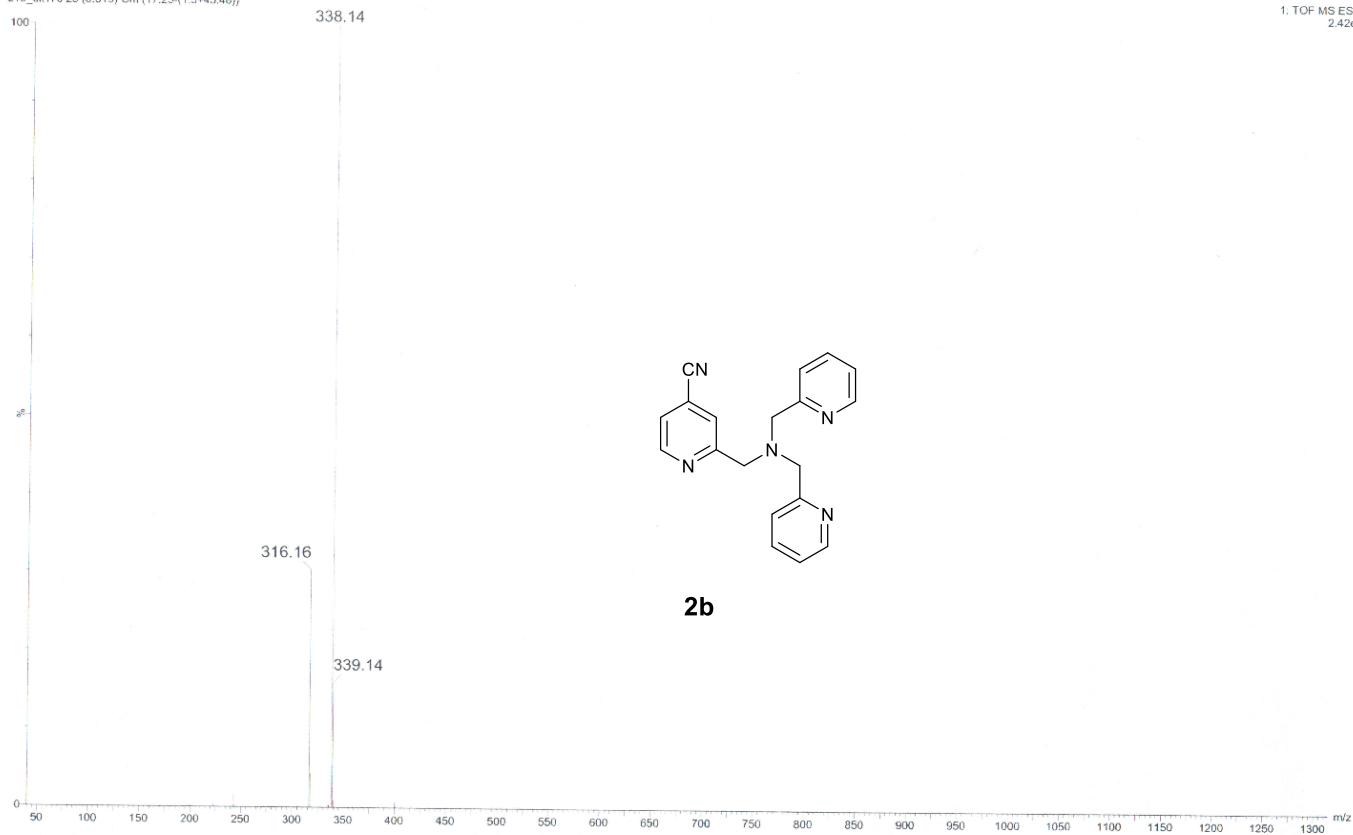
$^1\text{H-NMR}$ spectra of **2b** in CDCl_3



^{13}C -NMR spectra of **2b** in CDCl_3

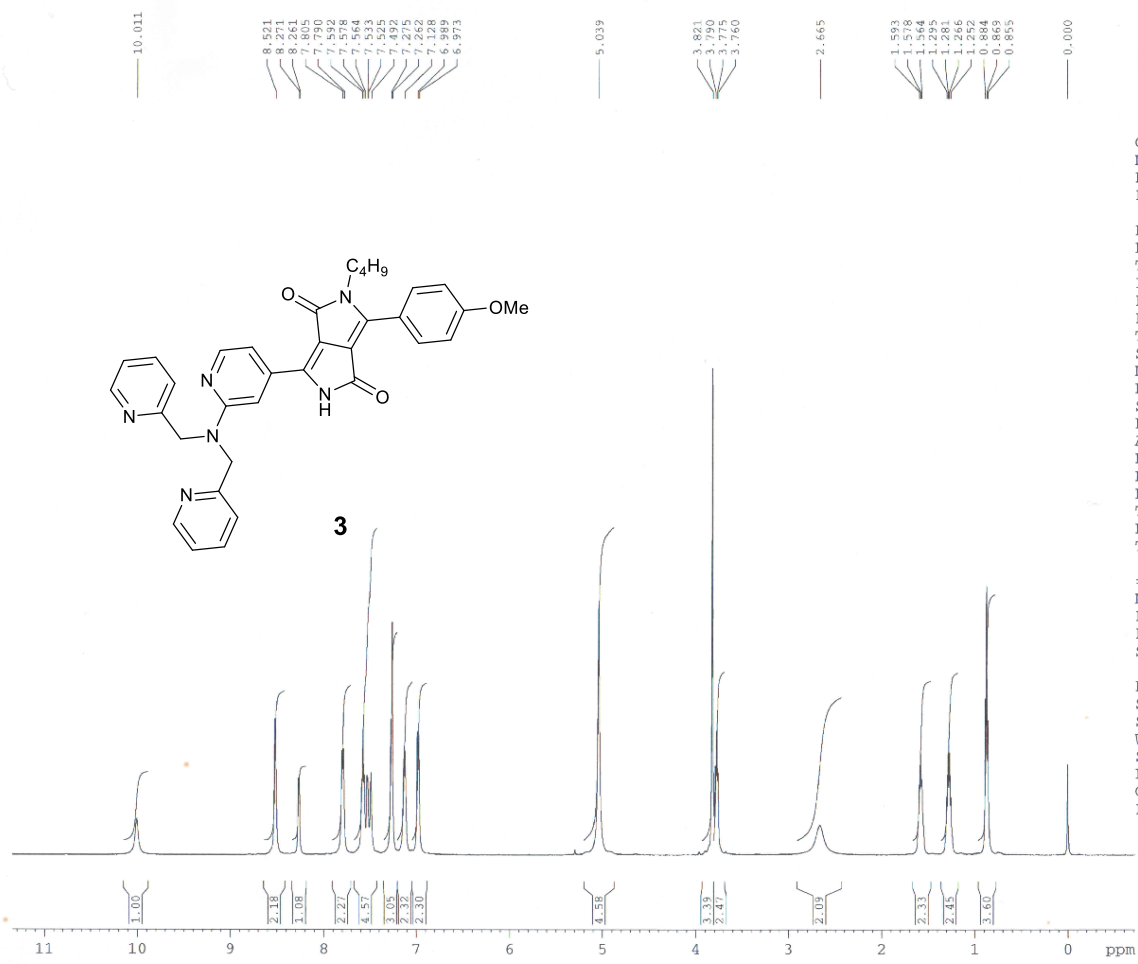
z10_dk176 25 (0.519) Cm (17.25-(1.3+45.48))

1. TOF MS ES+
2.4266

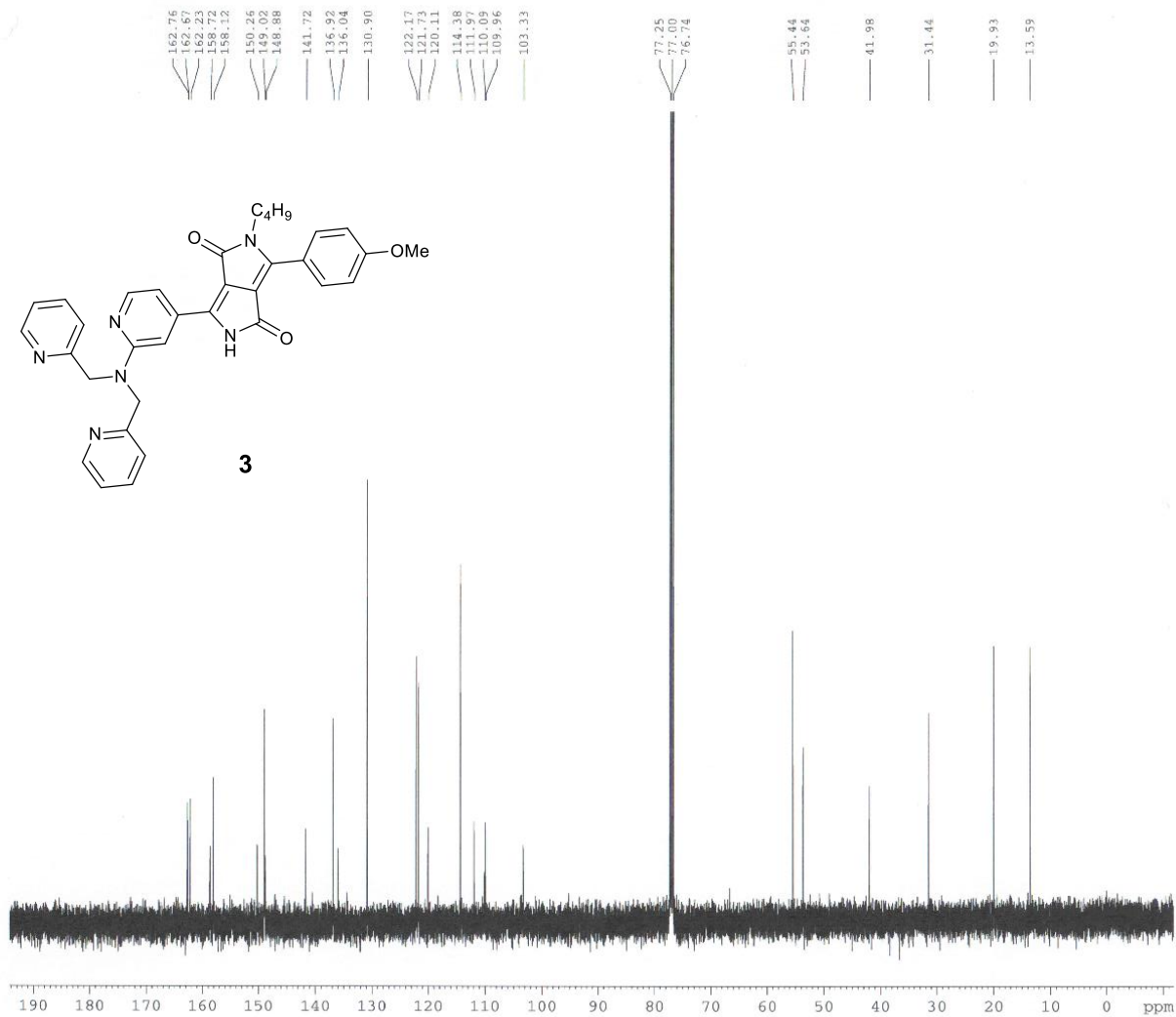


2b

HRMS (ESI, m/z) spectra of **2b**



¹H-NMR spectra of **3** in CDCl₃



¹³C-NMR spectra of **3** in CDCl₃

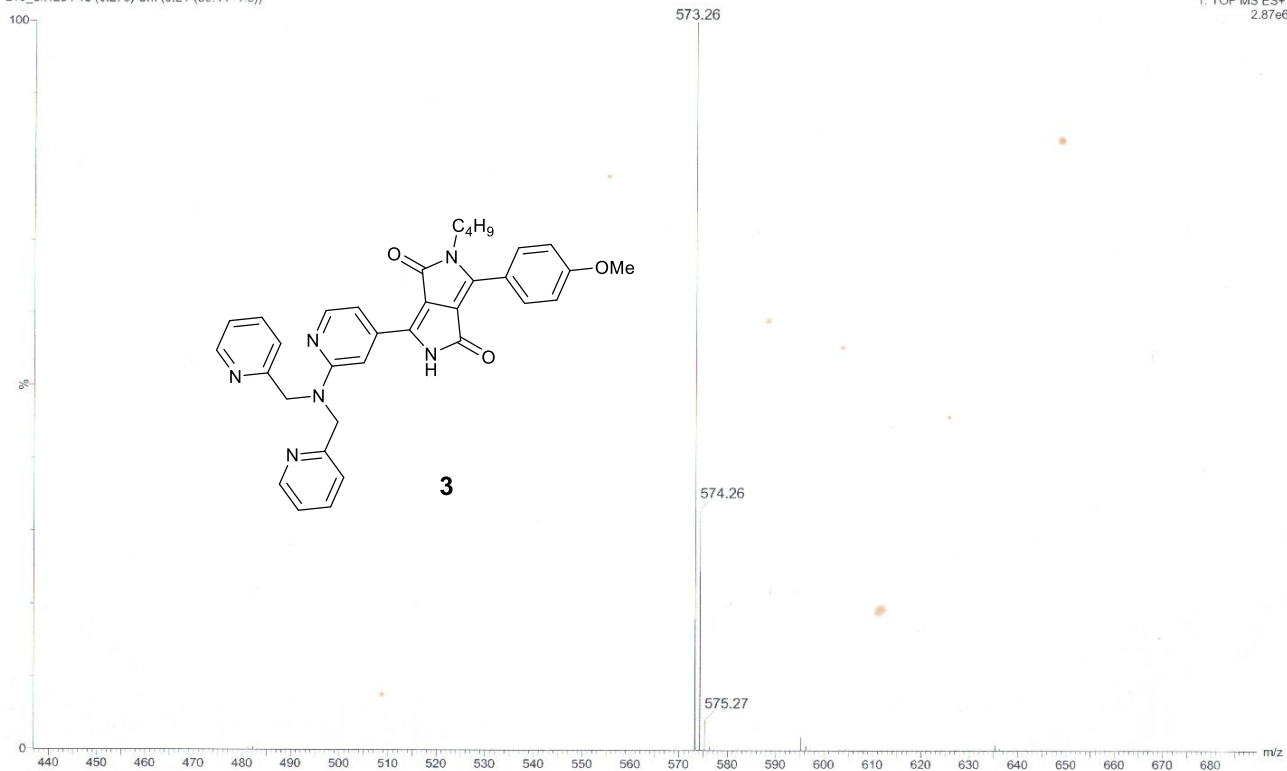
Elements Used:

C: 0-150 H: 0-150 N: 0-6 O: 0-3

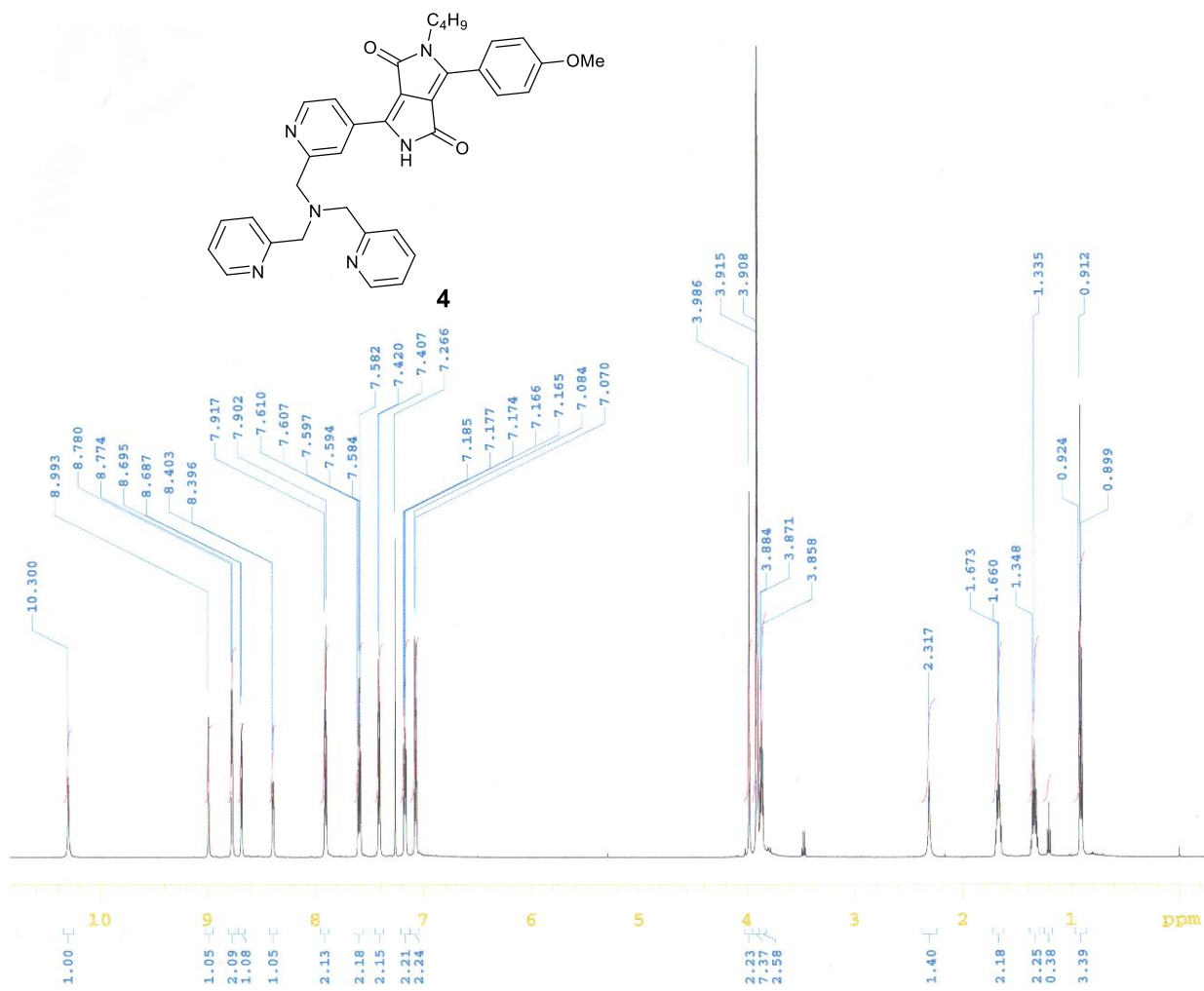
Mass	Calc. Mass	mDa	PPM	DBE	Formula	i-FIT	i-FIT Norm	Fit Conf %	C	H	N	O
573.2628	573.2614	1.4	2.4	21.5	C34 H33 N6 O3	583.7	0.013	98.75	34	33	6	3
	573.2654	-2.6	-4.5	25.5	C39 H33 N4 O	588.1	4.384	1.25	39	33	4	1

GDK-249

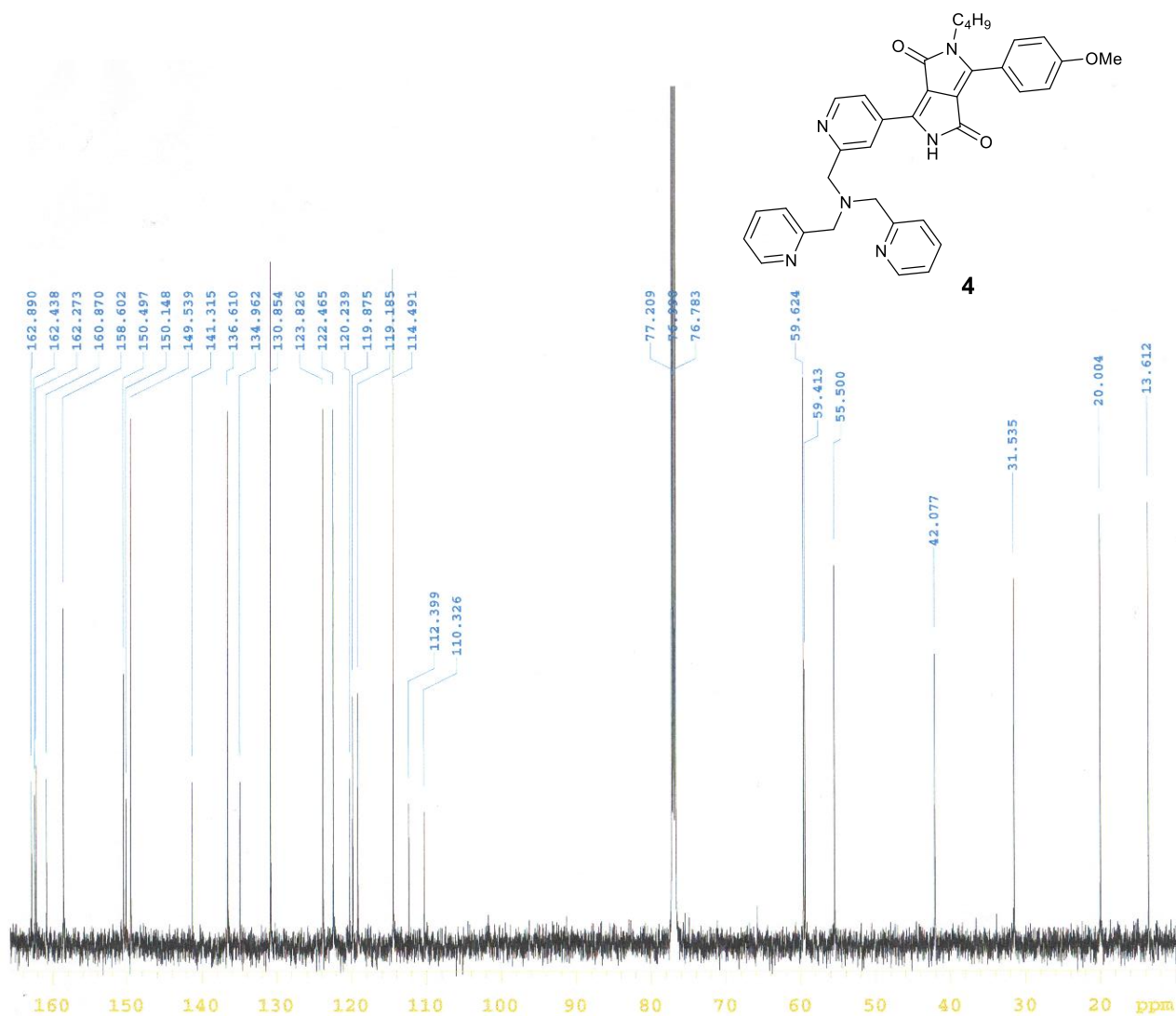
z10_dk1254 13 (0.276) Cm (9:21-(30:44+1:8))



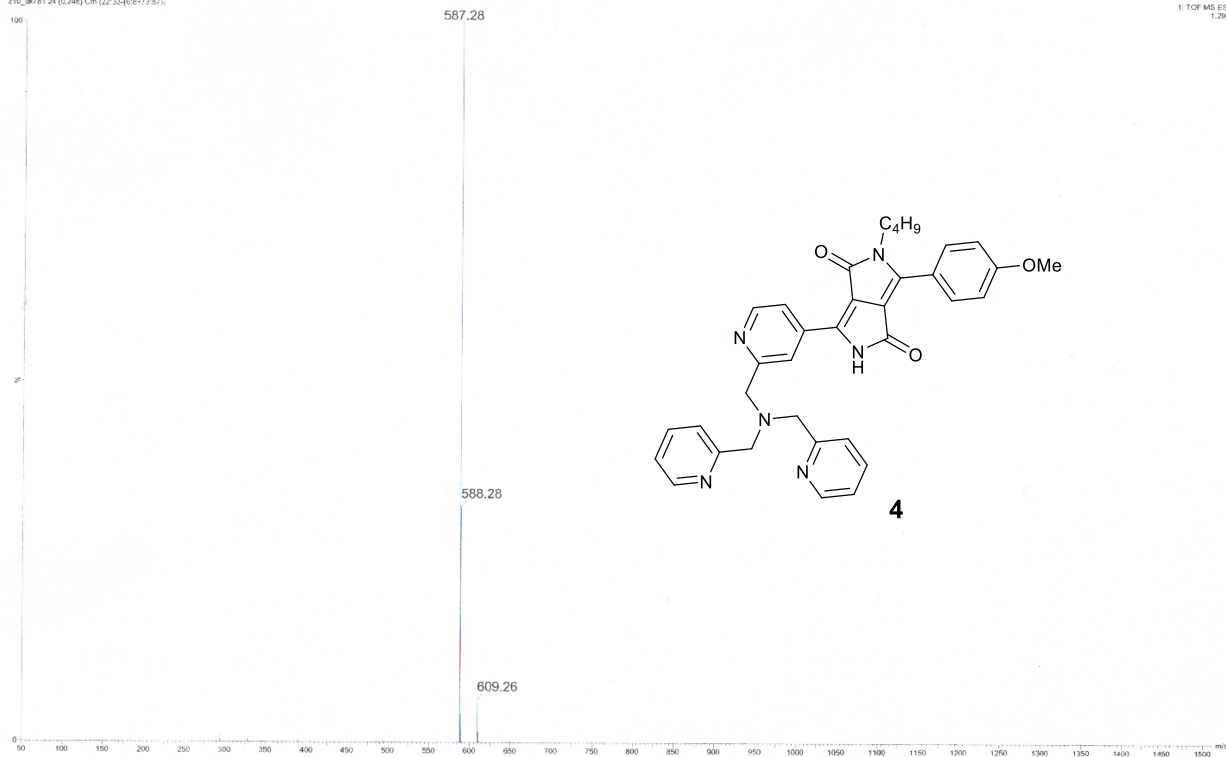
HRMS (ESI, m/z) spectra of **3**



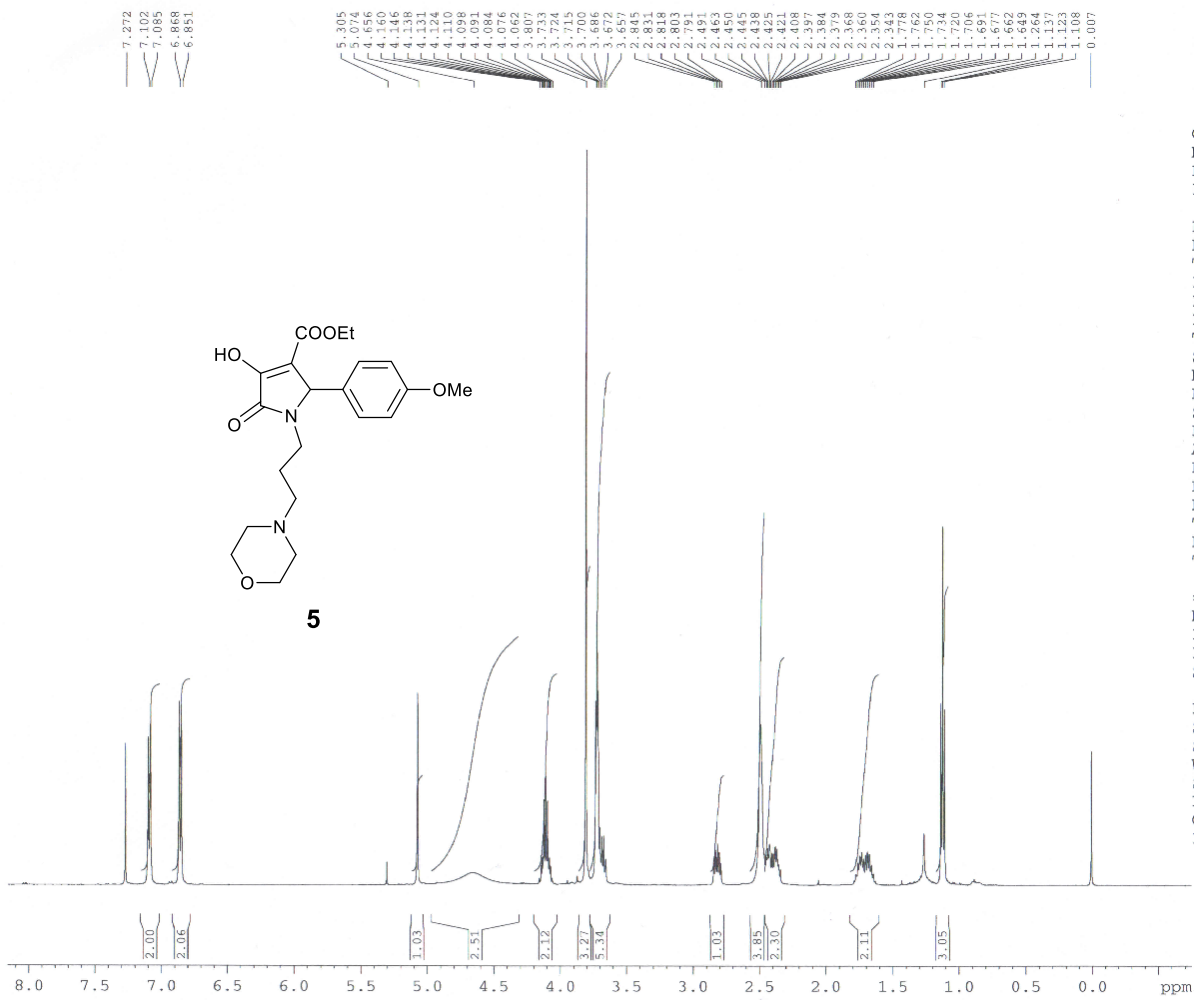
¹H-NMR spectra of **4** in CDCl₃



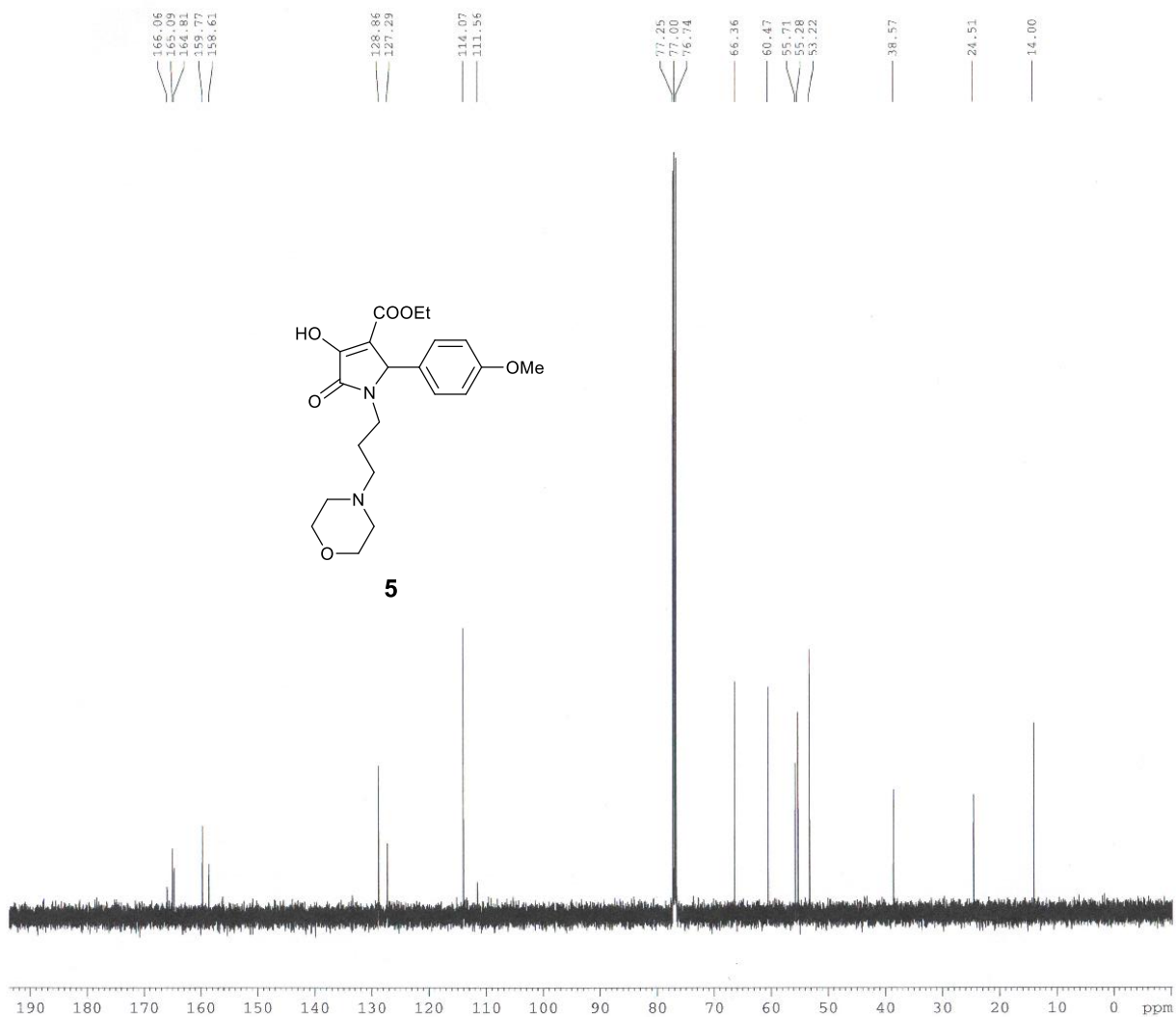
¹³C-NMR spectra of 4 in CDCl₃



HRMS (ESI, m/z) spectra of **4**



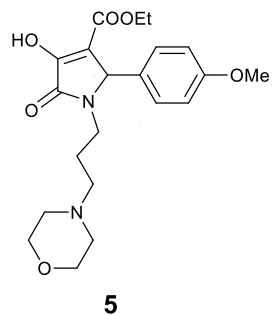
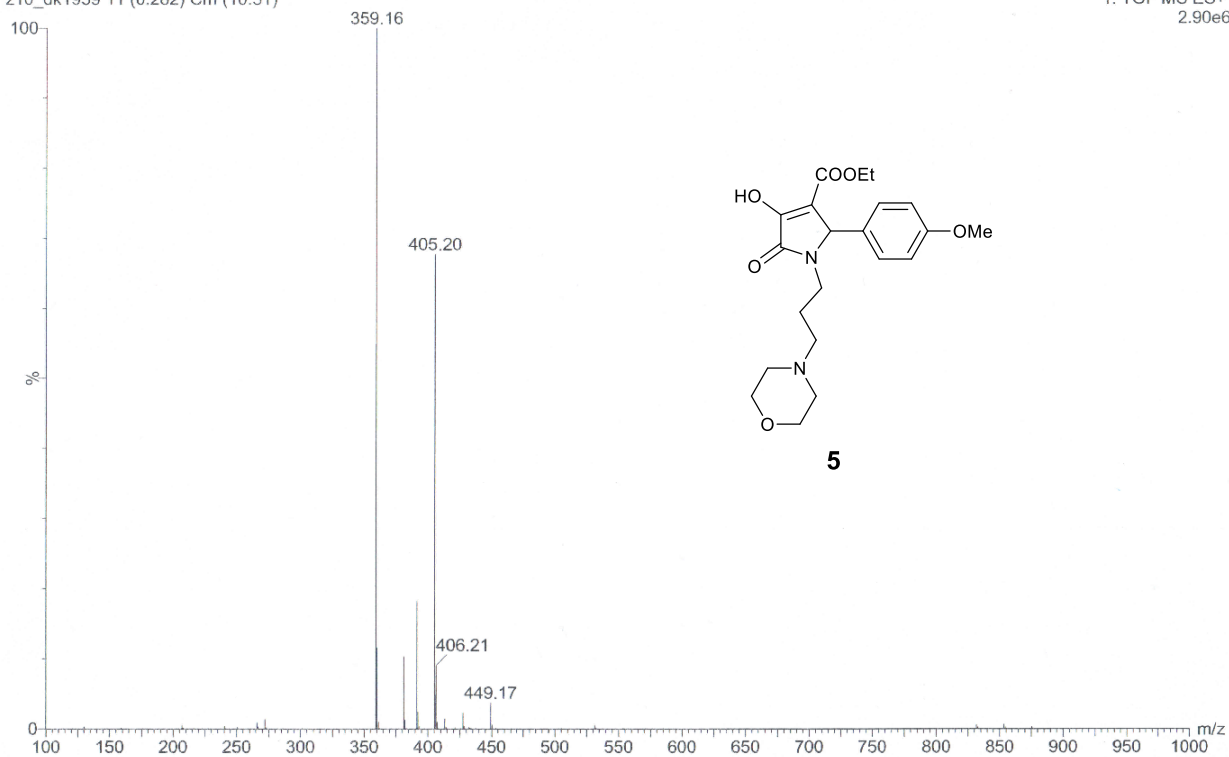
¹H-NMR spectra of **5** in CDCl₃



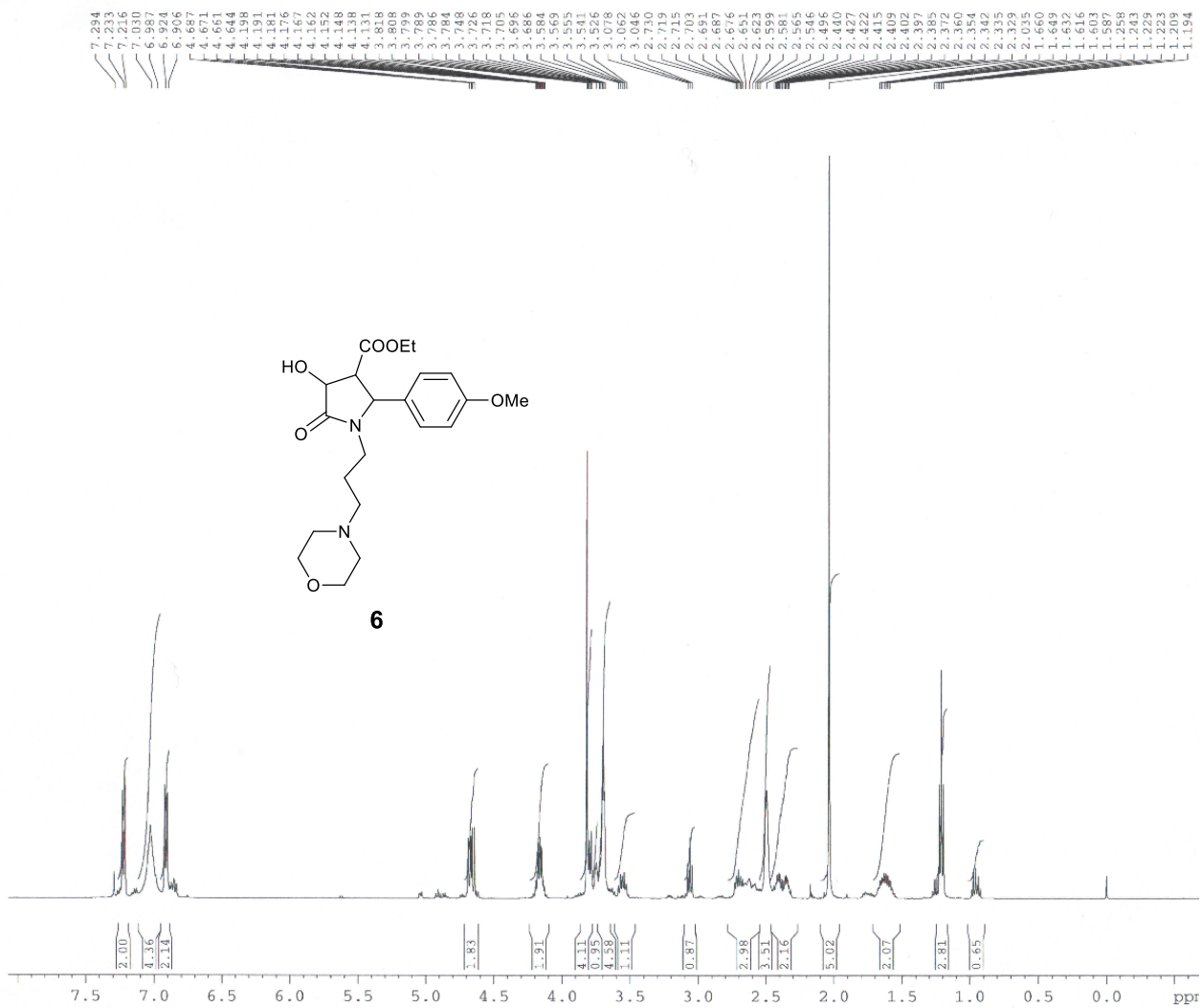
¹³C-NMR spectra of **5** in CDCl₃

SDR0303-10
z10_dk1959 11 (0.282) Cm (10:31)

1: TOF MS ES+
2.90e6



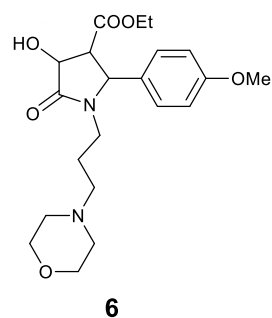
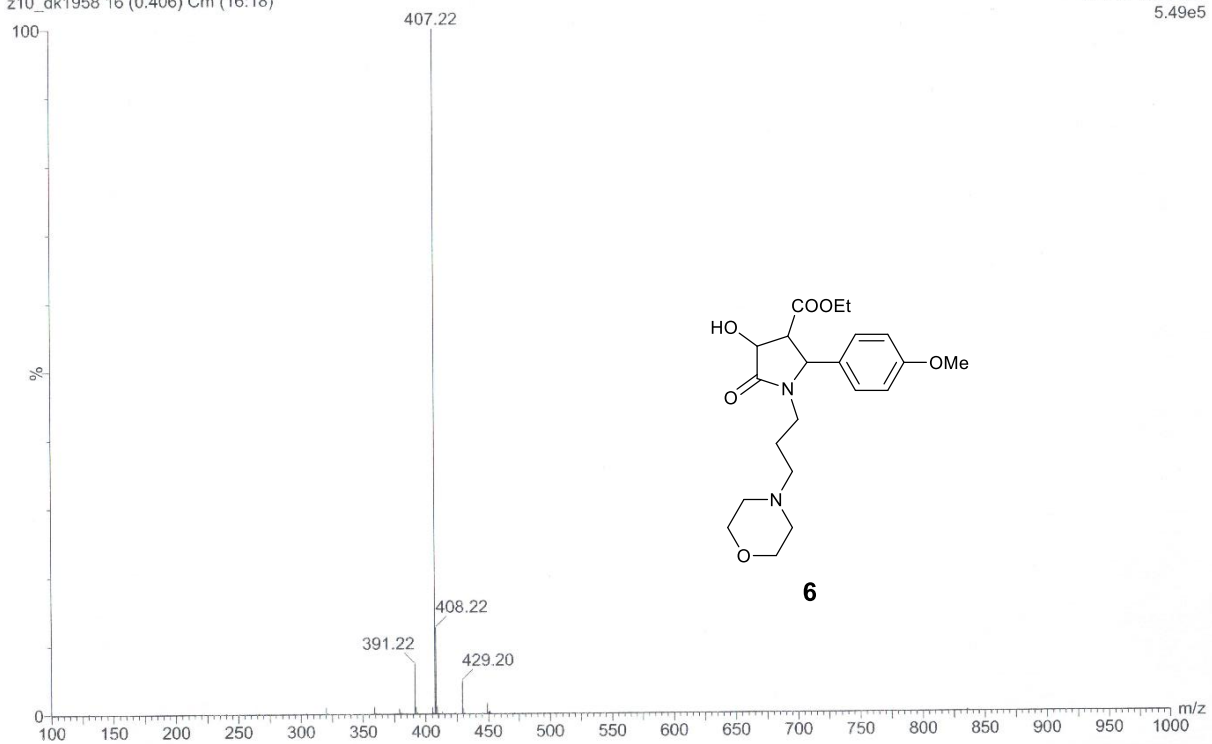
HRMS(ESI, m/z) spectra of 5



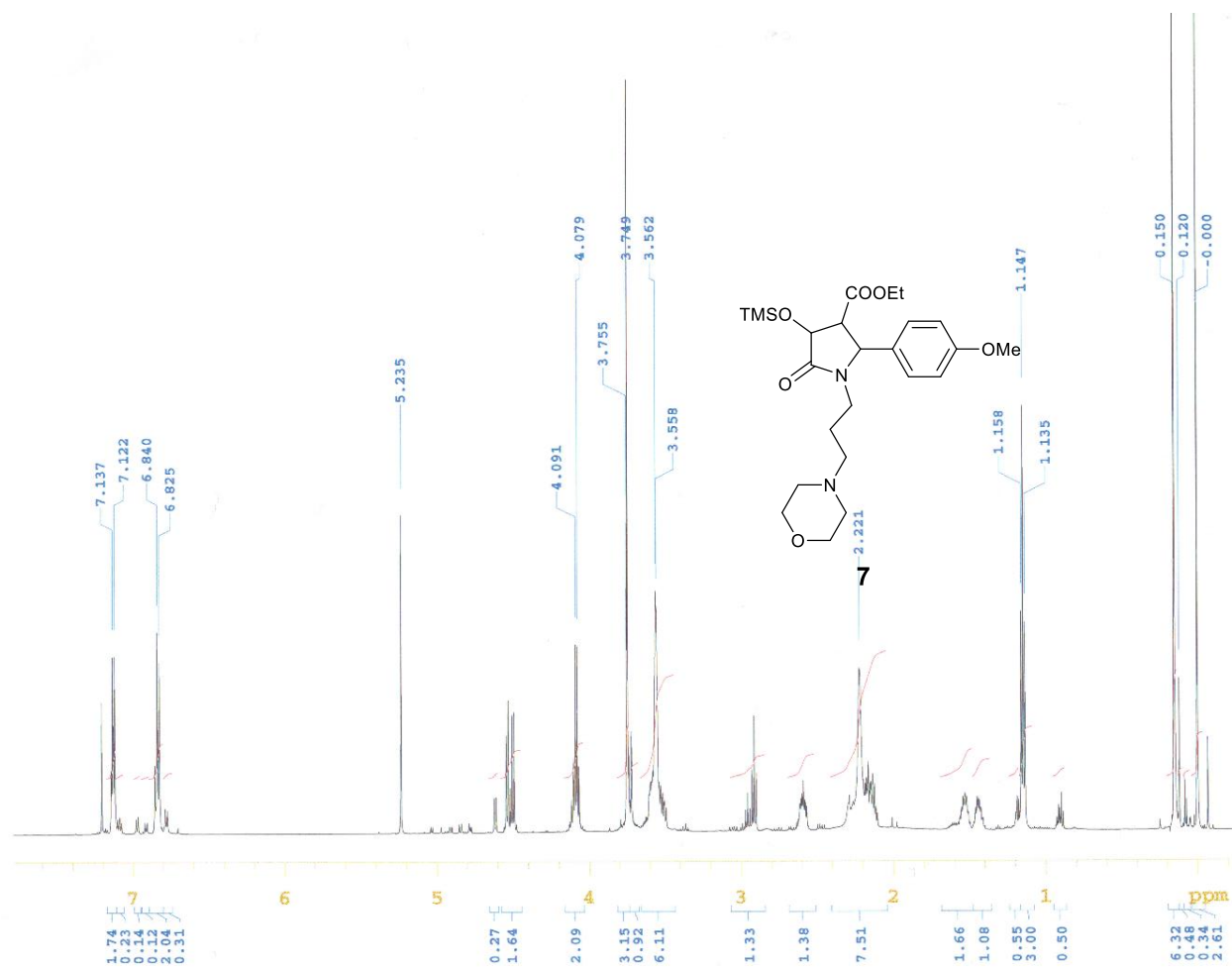
¹H-NMR spectra of **6** in CDCl₃

GDKU306-1U
z10_dk1958 16 (0.406) Cm (16:18)

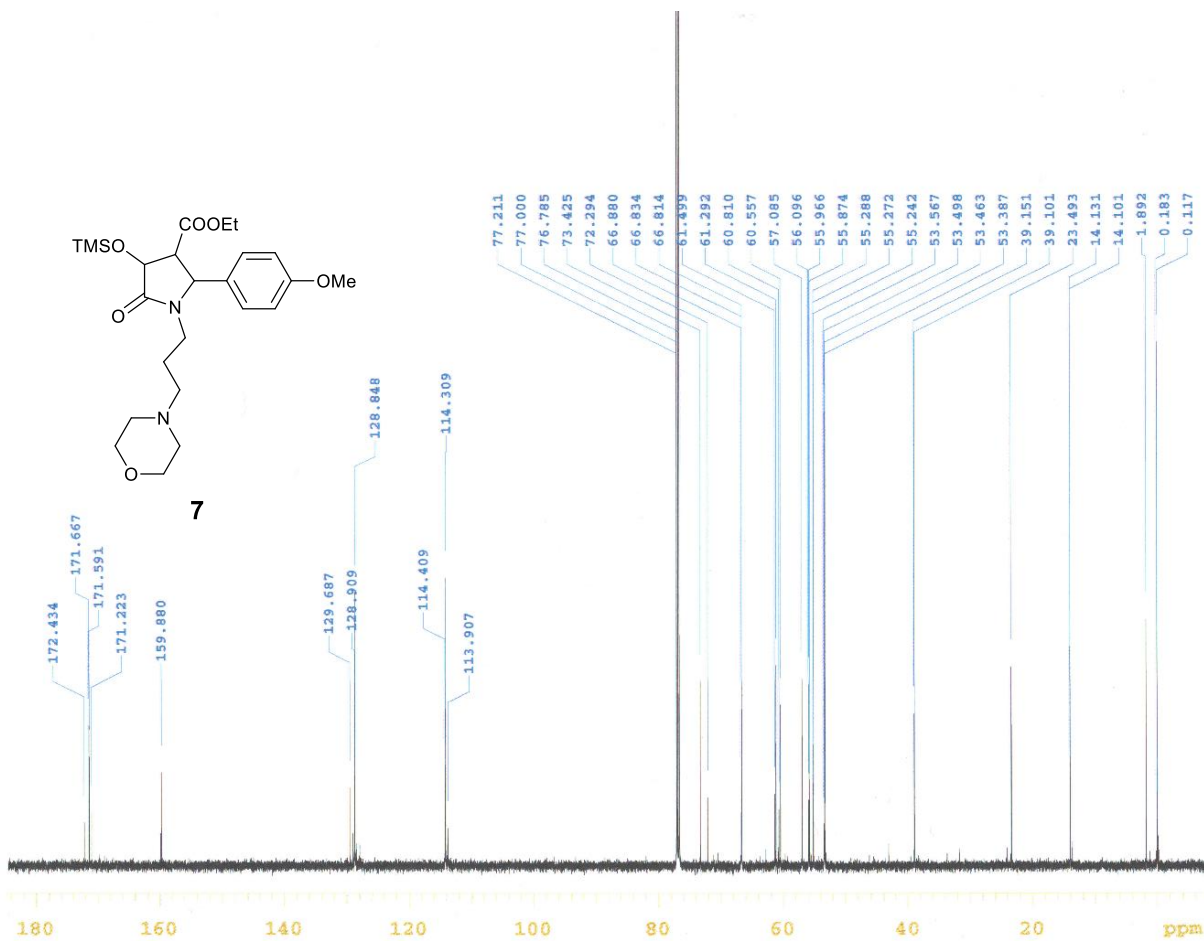
1: TOF MS ES+
5.49e5



HRMS (ESI, m/z) spectra of **6**



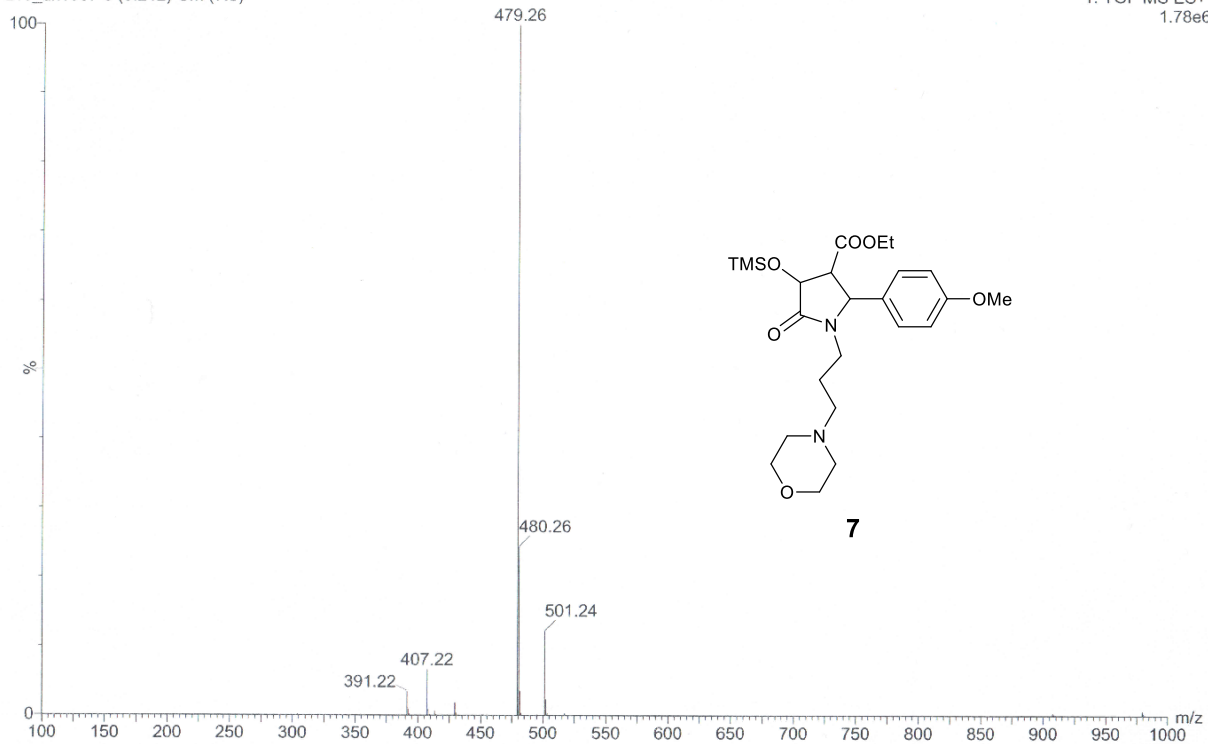
¹H-NMR spectra of **7** in CDCl₃



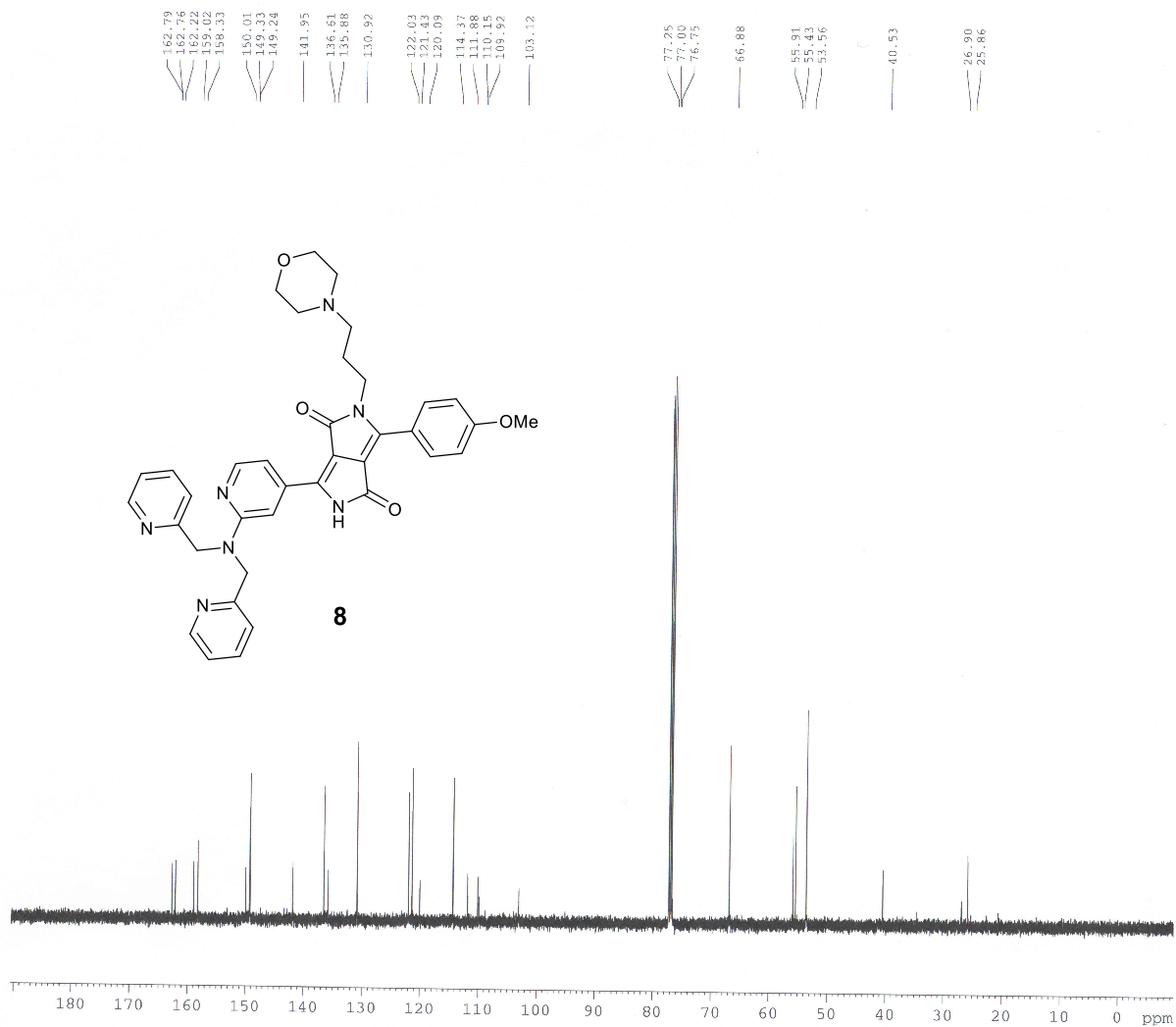
$^{13}\text{C-NMR}$ spectra of **7** in CDCl_3

z10_dk1957 8 (0.212) Cm (7:9)

1: TOF MS ES+
1.78e6



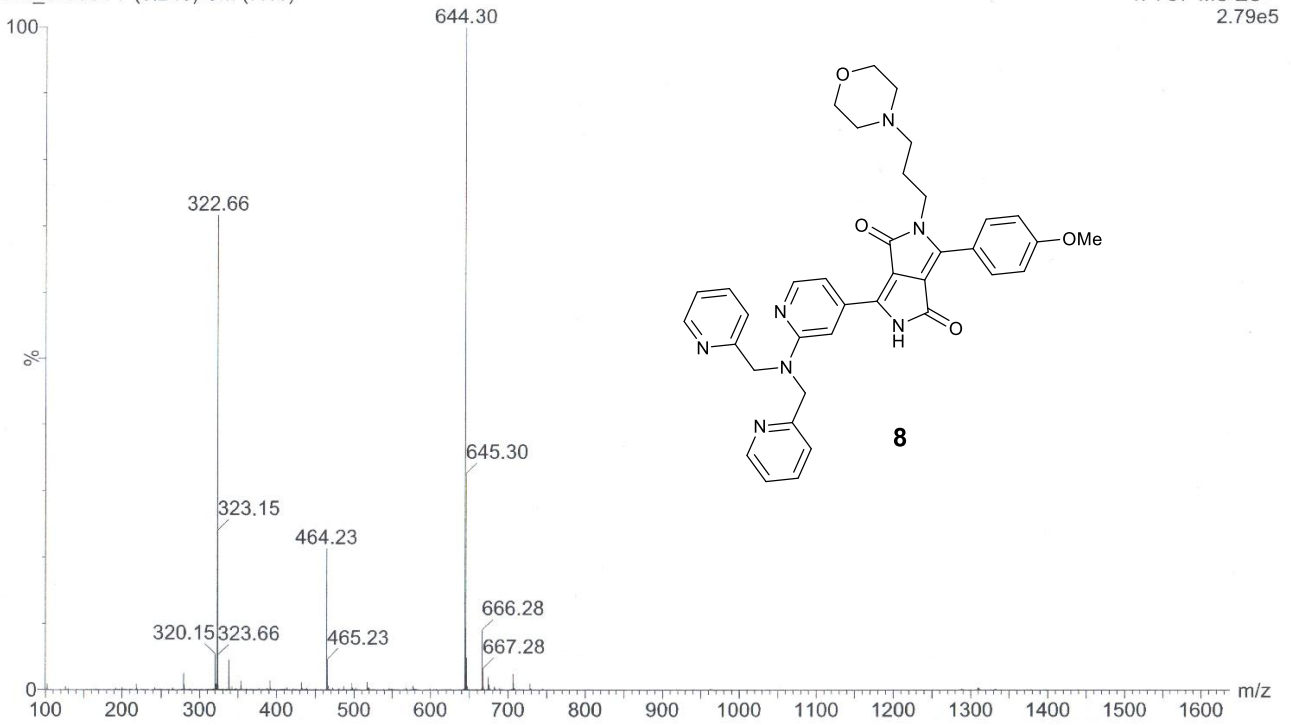
HRMS (ESI, m/z) spectra of **7**



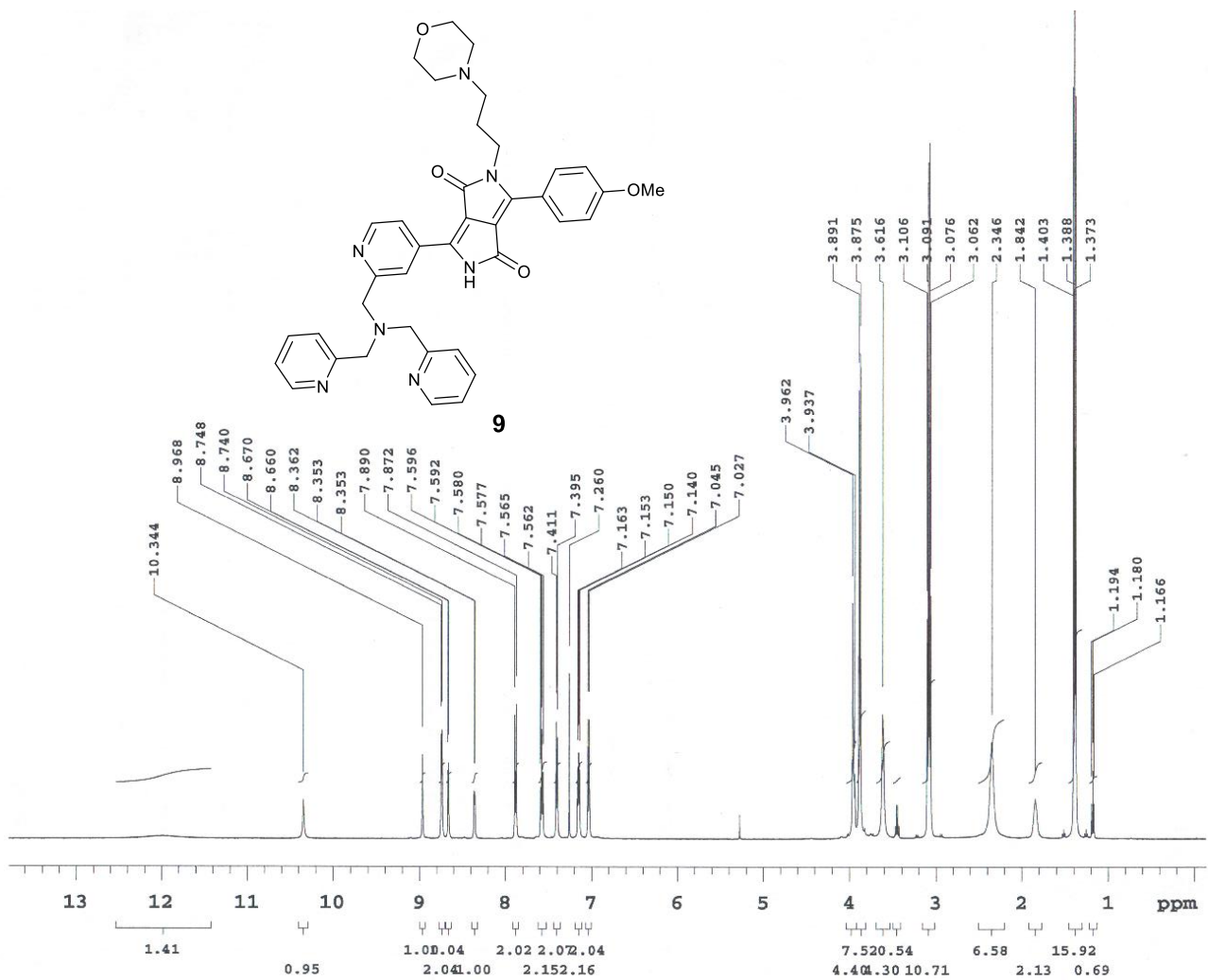
¹³C-NMR spectra of **8** in CDCl₃

z10_dk0504 7 (0.245) Cm (7:10)

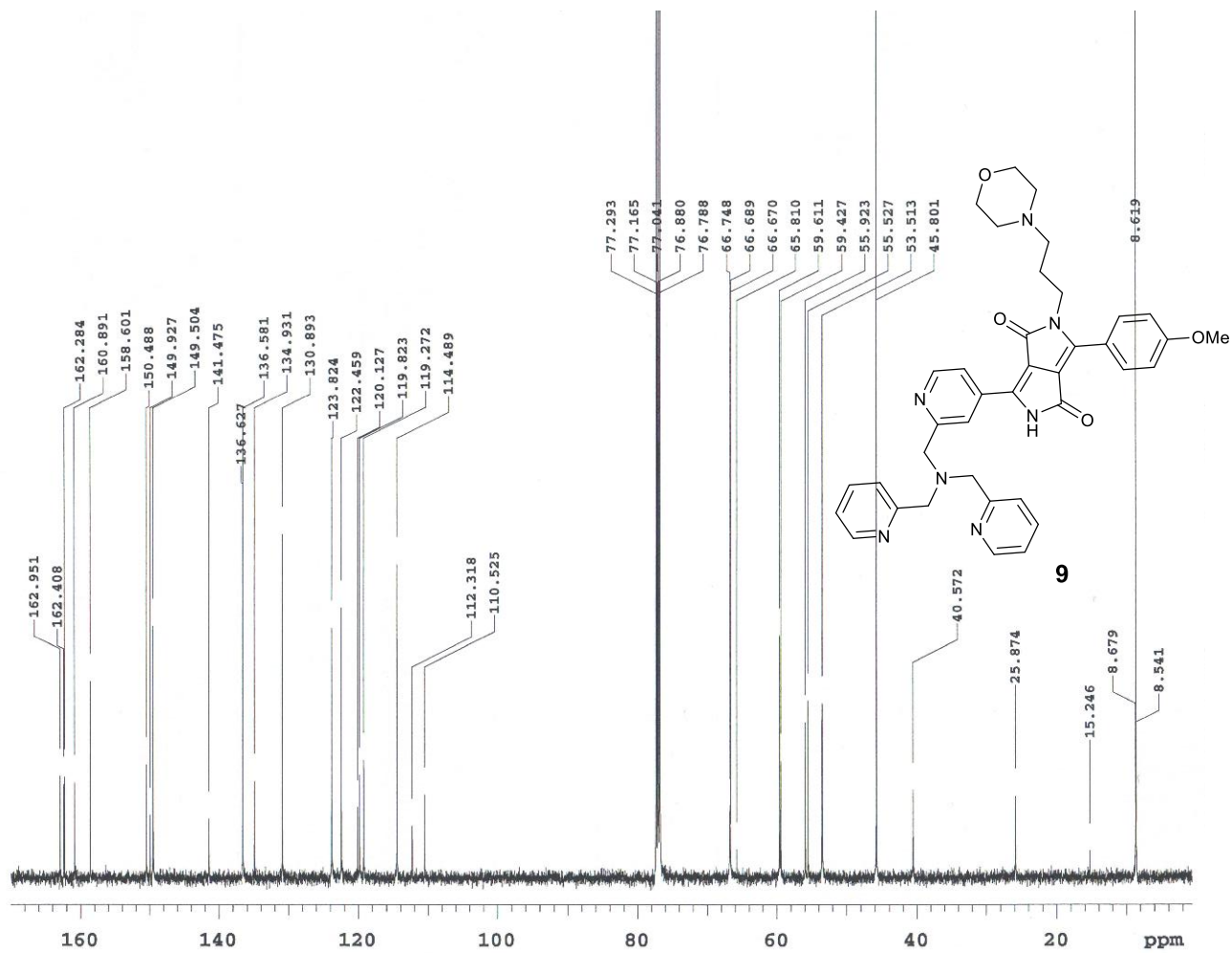
1: TOF MS ES+
2.79e5



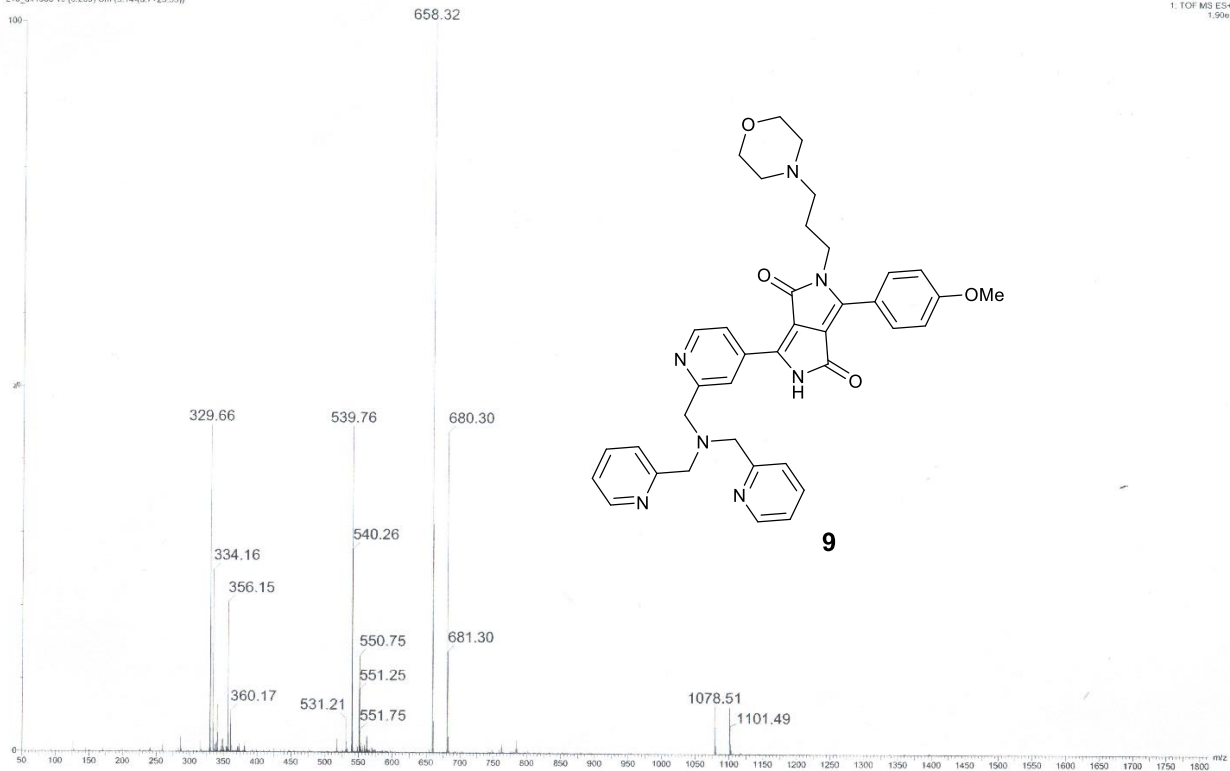
HRMS (ESI, m/z) spectra of **8**



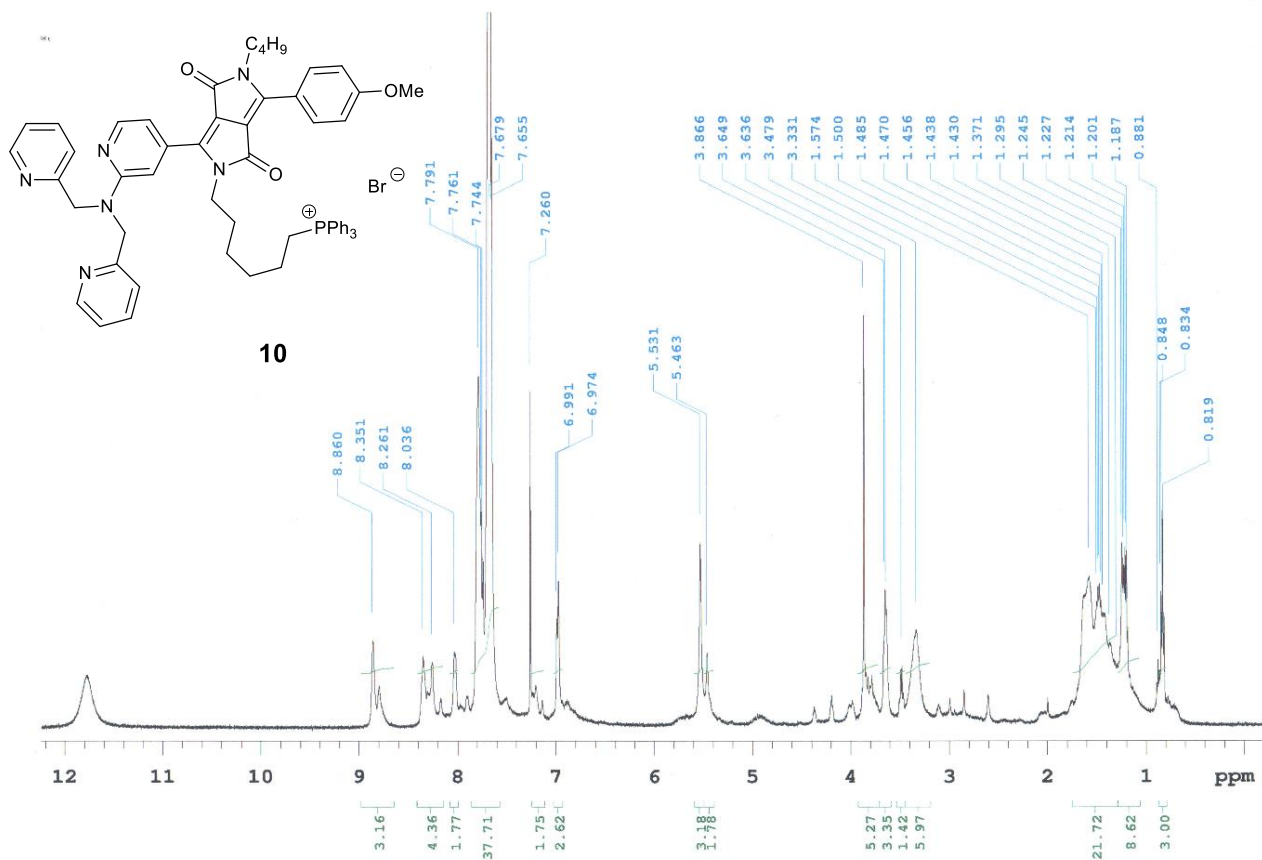
¹H-NMR spectra of **9** in CDCl₃



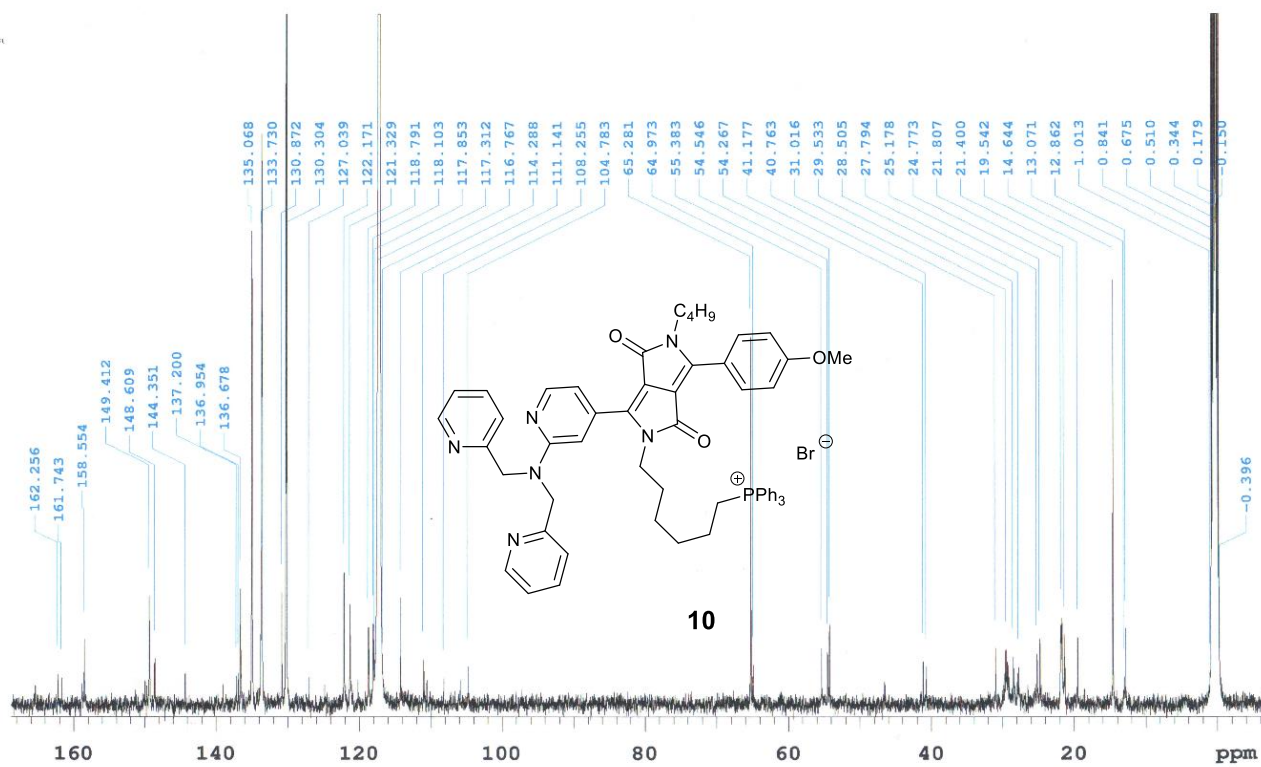
¹³C-NMR spectra of **9** in CDCl₃



HRMS (ESI, m/z) spectra of **9**



¹H-NMR spectra of **10** in CDCl₃



^{13}C -NMR spectra of **10** in $CDCl_3$

Section S8: References

1. M. Pieczykolan, B. Sadowski and D. T. Gryko, *Angew. Chem. Int. Ed.*, 2020, **59**, 7528-7535.

7. Declarations of the authors of publications



Instytut Chemii Organicznej, PAN
ul. Kasprzaka 44/52
01-224 Warszawa
Polska

Warszawa, 30.11.2022r.

I declare that my contribution to the following publications consisted of:

- > **G. Dinesh Kumar**, M. Banasiewicz, D. Jacquemin, D. T. Gryko, *Chem. Asian J.* **2021**, *16*, 355–362. „Switch-on Diketopyrrolopyrrole-Based Chemosensors for Cations Possessing Lewis Acid Character”.

Co-development of research concepts and interpretation of results. I developed and carried out the synthesis of nitrile substrates 2a-2h and transformed into final compounds 3-10 under developed conditions, which I subjected to a full chemical analysis. I participated in analyzing the photophysical properties and preparation of the manuscript.

- > **G. Dinesh Kumar**, M. Banasiewicz, A. Wrzosek, R. P. Kampa, M. H. E. Bousquet, D. Kusy, D. Jacquemin, A. Szewczyk, D. T. Gryko, *Chem. Commun.*, **2022**, *58*, 4500–4503. „Probing the flux of mitochondrial potassium using an azacrown-diketopyrrolopyrrole based highly sensitive probe”.

Co-development of research concepts and interpretation of results. I developed and carried out the synthesis of substrates S4, S5-7, and S13-16, used them for synthesis of final compounds S9-S11, S17, 1 and 2 under optimized Buchwald-Hartwig amination reaction conditions, which I subjected to a full chemical analysis. I wrote the first draft of the manuscript. I participated in analyzing the photophysical properties, biological imaging experiments and preparation of the final version of the manuscript.

- > **G. Dinesh Kumar**, M. Banasiewicz, A. Wrzosek, O. O’Mari, M. Zochowska, V. I. Vullev, D. Jacquemin, A. Szewczyk, D. T. Gryko, *Org. Biomol. Chem.*, **2022**, *20*, 7439–7447. „A sensitive zinc probe operating via enhancement of excited-state intramolecular charge transfer”.

Co-development of research concepts and interpretation of results. I developed and carried out the synthesis of substrates 2a-2b and 5-7, used them for synthesis of final compounds 3-4 and 8-10 under optimized conditions, which I subjected to a full chemical analysis I wrote the first draft of the manuscript. I participated in analyzing the photophysical properties, biological imaging experiments and preparation of the final version of the manuscript.

.....

Warsaw 24th November 2022.

I declare that my contribution to the following publications consisted of:

- > G. Dinesh Kumar, M. Banasiewicz, D. Jacquemin, D. T. Gryko, *Chem. Asian J.* **2021**, *16*, 355–362. „Switch-on Diketopyrrolopyrrole-Based Chemosensors for Cations Possessing Lewis Acid Character”.

Co-development of research concepts, interpretation of results and preparation of the final version of the manuscript.

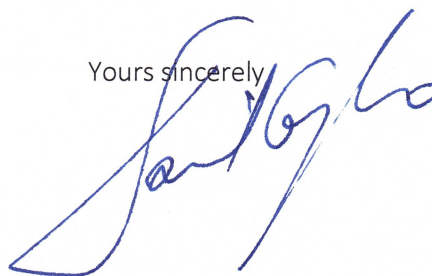
- > G. Dinesh Kumar, M. Banasiewicz, A. Wrzosek, R. P. Kampa, M. H. E. Bousquet, D. Kusy, D. Jacquemin, A. Szewczyk, D. T. Gryko, *Chem. Commun.*, **2022**, *58*, 4500–4503. „Probing the flux of mitochondrial potassium using an azacrown-diketopyrrolopyrrole based highly sensitive probe”.

Co-development of research concepts, interpretation of results and preparation of the final version of the manuscript.

- > G. Dinesh Kumar, M. Banasiewicz, A. Wrzosek, O. O’Mari, M. Zochowska, V. I. Vullev, D. Jacquemin, A. Szewczyk, D. T. Gryko, *Org. Biomol. Chem.*, **2022**, *20*, 7439–7447. „A sensitive zinc probe operating via enhancement of excited-state intramolecular charge transfer”.

Co-development of research concepts, interpretation of results and preparation of the final version of the manuscript.

Yours sincerely



Dr Marzena Banasiewicz
mbanas@ifpan.edu.pl
Instytut Fizyki PAN
Al. Lotników 32/46
02-668 Warsaw
Poland

Warsaw 26.09.2022

STATEMENT

I hereby declare that my contribution to the publications listed below is as follows:

1. G. Dinesh Kumar, M. Banasiewicz, D. Jacquemin, D. T. Gryko, *Chem. Asian J.* **2021**, *16*, 355–362. „Switch-on Diketopyrrolopyrrole-Based Chemosensors for Cations Possessing Lewis Acid Character”
2. G. Dinesh Kumar, M. Banasiewicz, A. Wrzosek, R. P. Kampa, M. H. E. Bousquet, D. Kusy, D. Jacquemin, A. Szewczyk, D. T. Gryko, *Chem. Commun.*, **2022**, *58*, 4500–4503. „Probing the flux of mitochondrial potassium using an azacrown-diketopyrrolopyrrole based highly sensitive probe”
3. G. Dinesh Kumar, M. Banasiewicz, A. Wrzosek, O. O’Mari, M. Zochowska, V. I. Vullev, D. Jacquemin, A. Szewczyk, D. T. Gryko, *Org. Biomol. Chem.*, **2022**, DOI: 10.1039/d2ob01296k. „A sensitive zinc probe operating via enhancement of excited-state intramolecular charge transfer”

I measured absorption and fluorescence spectra in solution of the studied compounds. I worked out these results in form of Tables and Figures. I was involved in editing process of the Manuscript.



Marzena Banasiewicz

Dr Rafał P. Kampa

Laboratory of Intracellular Ion Channels

Nencki Institute of Experimental Biology PAS

3 Pasteur St., 02-093 Warsaw, Poland

Warsaw, 19.09.2022

Hereby I would like to declare that my contribution to the publications:

1. **G. Dinesh Kumar**, M. Banasiewicz, A. Wrzosek, R. P. Kampa, M. H. E. Bousquet, D. Kusy, D. Jacquemin, A. Szewczyk, D. T. Gryko, *Chem. Commun.*, **2022**, 58, 4500–4503. „*Probing the flux of mitochondrial potassium using an azacrown-diketopyrrolopyrrole based highly sensitive probe*”

I participated in the measurement of cell survival in the presence of the studied dyes.

Rafał P. Kampa



Dr Monika Żochowska
Laboratory of Intracellular Ion Channels
Nencki Institute of Experimental Biology PAS
3 Pasteur St., 02-093 Warsaw, Poland

Warsaw, 19.09.2022

Hereby I would like to declare that my contribution to the publication:

G. Dinesh Kumar, M. Banasiewicz, A. Wrzosek, O. O'Mari, M. Zochowska, V. I. Vullev, D. Jacquemin, A. Szewczyk, D. T. Gryko, *Org. Biomol. Chem.*, **2022**, DOI: 10.1039/d2ob01296k. „*A sensitive zinc probe operating via enhancement of excited-state intramolecular charge transfer*”

I participated in the H9C2 cell culture for the confocal microscopy.

Monika Żochowska



Prof. dr hab. Adam Szewczyk
Laboratory of Intracellular Ion Channels
Nencki Institute of Experimental Biology PAS
3 Pasteur St., 02-093 Warsaw, Poland

Warsaw, 19.09.2022

Hereby I would like to declare that my contribution to the publications:

1. **G. Dinesh Kumar**, M. Banasiewicz, A. Wrzosek, R. P. Kampa, M. H. E. Bousquet, D. Kusy, D. Jacquemin, A. Szewczyk, D. T. Gryko, *Chem. Commun.*, **2022**, 58, 4500–4503. „*Probing the flux of mitochondrial potassium using an azacrown-diketopyrrolopyrrole based highly sensitive probe*”
2. **G. Dinesh Kumar**, M. Banasiewicz, A. Wrzosek, O. O’Mari, M. Zochowska, V. I. Vullev, D. Jacquemin, A. Szewczyk, D. T. Gryko, *Org. Biomol. Chem.*, **2022**, DOI: 10.1039/d2ob01296k. „*A sensitive zinc probe operating via enhancement of excited-state intramolecular charge transfer*”

I participated in the supervision, interpretation, and the discussion of confocal microscopy results..



Adam Szewczyk

Dr Antoni Wrzosek

Laboratory of Intracellular Ion Channels

Nencki Institute of Experimental Biology PAS

3 Pasteur St., 02-093 Warsaw, Poland

Warsaw, 19.09.2022

Hereby I would like to declare that my contribution to the publications:

1. **G. Dinesh Kumar**, M. Banasiewicz, A. Wrzosek, R. P. Kampa, M. H. E. Bousquet, D. Kusy, D. Jacquemin, A. Szewczyk, D. T. Gryko, *Chem. Commun.*, **2022**, 58, 4500–4503. „*Probing the flux of mitochondrial potassium using an azacrown-diketopyrrolopyrrole based highly sensitive probe*”
2. **G. Dinesh Kumar**, M. Banasiewicz, A. Wrzosek, O. O’Mari, M. Zochowska, V. I. Vullev, D. Jacquemin, A. Szewczyk, D. T. Gryko, *Org. Biomol. Chem.*, **2022**, DOI: 10.1039/d2ob01296k. „*A sensitive zinc probe operating via enhancement of excited-state intramolecular charge transfer*”

I participated in the measurement of confocal microscopy and the interpretation of the results.

Antoni Wrzosek



Prof. Denis Jacquemin
Denis.Jacquemin@univ-nantes.fr

Ref. **Contribution Letter**

Nantes, 19/09/2022

To whom it may concern,

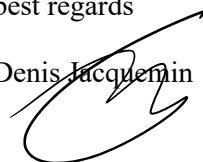
I hereby declare that my contribution to the publications below:

1. G. Dinesh Kumar, M. Banasiewicz, D. Jacquemin, D. T. Gryko, *Chem. Asian J.* 2021, *16*, 355–362. „*Switch-on Diketopyrrolopyrrole-Based Chemosensors for Cations Possessing Lewis Acid Character*”
2. G. Dinesh Kumar, M. Banasiewicz, A. Wrzosek, R. P. Kampa, M. H. E. Bousquet, D. Kusy, D. Jacquemin, A. Szewczyk, D. T. Gryko, *Chem. Commun.*, 2022, *58*, 4500–4503. „*Probing the flux of mitochondrial potassium using an azacrown-diketopyrrolopyrrole based highly sensitive probe*”
3. G. Dinesh Kumar, M. Banasiewicz, A. Wrzosek, O. O’Mari, M. Zochowska, V. I. Vullev, D. Jacquemin, A. Szewczyk, D. T. Gryko, *Org. Biomol. Chem.*, 2022, DOI: 10.1039/d2ob01296k. „*A sensitive zinc probe operating via enhancement of excited-state intramolecular charge transfer*”

I supervised the theoretical parts of this work and wrote the theoretical section of all manuscripts. For publications 1 and 3, I also performed all the DFT and TD-DFT calculations. In all contributions, I was involved in the proof checking of the full manuscript.

With best regards

Prof. Denis Jacquemin



Manon H.E. Bousquet
Manon.bousquet@unit-nantes.fr

Ref. Contribution Letter

Nantes, 19/09/2022

To whom it may concern,

I hereby declare that my contribution to the publications below:

1. G. Dinesh Kumar, M. Banasiewicz, A. Wrzosek, R. P. Kampa, M. H. E. Bousquet, D. Kusy, D. Jacquemin, A. Szewczyk, D. T. Gryko, *Chem. Commun.*, 2022, 58, 4500–4503. „*Probing the flux of mitochondrial potassium using an azacrown-diketopyrrolopyrrole based highly sensitive probe*”

I performed all theoretical calculations and contributed to analyze the related data.

With best regards

Manon H. E. Bousquet





Instytut Chemii Organicznej
Polskiej Akademii Nauk

Dr Damian Kusy
d.kusy@icho.edu.pl
Instytut Chemii Organicznej PAN
ul. Kasprzaka 44/52
01-224 Warszawa

Warszawa 25.11.2022r.

Oświadczenie

Oświadczam, że mój wkład w powstanie poniższej publikacji polegał na wykonaniu pomiarów fotostabilności badanych związków.

G. Dinesh Kumar, M. Banasiewicz, A. Wrzosek, R. P. Kampa, M. H. E. Bousquet, D. Kusy, D. Jacquemin, A. Szewczyk, D. T. Gryko, *Chem. Commun.*, **2022**, *58*, 4500–4503. „*Probing the flux of mitochondrial potassium using an azacrown-diketopyrrolopyrrole based highly sensitive probe*”


Damian Kusy

Omar O'Mari

ooma001@ucr.edu

Ref. **Contribution Letter**

O'Mari, 11/04/2022

To whom it may concern,

I hereby declare that my contribution to the publications below:

1. **G. Dinesh Kumar**, M. Banasiewicz, A. Wrzosek, O. O'Mari, M. Zochowska, V. I. Vullev, D. Jacquemin, A. Szewczyk, D. T. Gryko, *Org. Biomol. Chem.*, **2022**, DOI: 10.1039/d2ob01296k.
"A sensitive zinc probe operating via enhancement of excited-state intramolecular charge transfer"

I performed the initial "classic" charge transfer analysis.

With best regards

Omar O'Mari

University of California, Riverside

900 University Ave
Riverside , 92521
Ca, U.S.A.

UC RIVERSIDE



THE MARLAN AND ROSEMARY BOURNS
COLLEGE OF ENGINEERING

DEPARTMENT OF BIOENGINEERING
RIVERSIDE, CALIFORNIA 92521

phone: (951) 827-6239
fax: (951) 827-6416
e-mail: vullev@ucr.edu

November 10, 2022

To: Whom it may concern
From: Valentine I. Vullev
Re: Contribution to a publication in *Org. Biomol. Chem.*

Hereby I declare my contribution to the following publication:

G. Dinesh Kumar, M. Banasiewicz, A. Wrzosek, O. O'Mari, M. Zochowska, V. I. Vullev, D. Jacquemin, A. Szewczyk, D. T. Gryko, "A sensitive zinc probe operating via enhancement of excited-state intramolecular charge transfer," *Org. Biomol. Chem.* **2022**, *20*, 7439–7447.

My principal contribution involved supervising the charge-transfer studies for this project.

Sincerely yours,

A handwritten signature in black ink, appearing to read "V. I. Vullev".

Valentine I. Vullev
Professor of Bioengineering, Chemistry,
Biochemistry, and Materials Science and Engineering
Fulbright U.S. Scholar Fellow (2018 – 2019)